

Nuclear Measurements, Evaluations
and Applications (NEMEA-7)
Collaborative International Evaluated
Library Organisation (CIELO)

Workshop Proceedings
5-8 November 2013
Geel, Belgium

Unclassified

NEA/NSC/DOC(2014)13

Organisation de Coopération et de Développement Économiques
Organisation for Economic Co-operation and Development

29-Jul-2014

English - Or. English

NUCLEAR ENERGY AGENCY
NUCLEAR SCIENCE COMMITTEE

Cancels & replaces the same document of 28 July 2014

Nuclear Measurements, Evaluations and Applications (NEMEA-7) Collaborative International Evaluated Library Organisation (CIELO)

Workshop Proceedings

**5-8 November 2013
Geel, Belgium**

The complete original document is available in PDF FORMAT ONLY. Special NEA presentation agreed with the Documents Desk.

Emmeric Dupont
emmeric.dupont@oecd.org
+33 1 45 24 10 84

JT03360792

Complete document available on OLIS in its original format

This document and any map included herein are without prejudice to the status of or sovereignty over any territory, to the delimitation of international frontiers and boundaries and to the name of any territory, city or area.



NEA/NSC/DOC(2014)13
Unclassified

English - Or. English

Nuclear Science
NEA/NSC/DOC(2014)13

**Nuclear Measurements, Evaluations and Applications (NEMEA-7)
Collaborative International Evaluated Library Organisation (CIELO)**

Workshop Proceedings

5-8 November 2013
Geel, Belgium

© OECD 2014

NUCLEAR ENERGY AGENCY
ORGANISATION FOR ECONOMIC CO-OPERATION AND DEVELOPMENT

ORGANISATION FOR ECONOMIC CO-OPERATION AND DEVELOPMENT

The OECD is a unique forum where the governments of 34 democracies work together to address the economic, social and environmental challenges of globalisation. The OECD is also at the forefront of efforts to understand and to help governments respond to new developments and concerns, such as corporate governance, the information economy and the challenges of an ageing population. The Organisation provides a setting where governments can compare policy experiences, seek answers to common problems, identify good practice and work to co-ordinate domestic and international policies.

The OECD member countries are: Australia, Austria, Belgium, Canada, Chile, the Czech Republic, Denmark, Estonia, Finland, France, Germany, Greece, Hungary, Iceland, Ireland, Israel, Italy, Japan, Luxembourg, Mexico, the Netherlands, New Zealand, Norway, Poland, Portugal, the Republic of Korea, the Slovak Republic, Slovenia, Spain, Sweden, Switzerland, Turkey, the United Kingdom and the United States. The European Commission takes part in the work of the OECD.

OECD Publishing disseminates widely the results of the Organisation's statistics gathering and research on economic, social and environmental issues, as well as the conventions, guidelines and standards agreed by its members.

*This work is published on the responsibility of the OECD Secretary-General.
The opinions expressed and arguments employed herein do not necessarily reflect the official
views of the Organisation or of the governments of its member countries.*

NUCLEAR ENERGY AGENCY

The OECD Nuclear Energy Agency (NEA) was established on 1 February 1958. Current NEA membership consists of 31 countries: Australia, Austria, Belgium, Canada, the Czech Republic, Denmark, Finland, France, Germany, Greece, Hungary, Iceland, Ireland, Italy, Japan, Luxembourg, Mexico, the Netherlands, Norway, Poland, Portugal, the Republic of Korea, the Russian Federation, the Slovak Republic, Slovenia, Spain, Sweden, Switzerland, Turkey, the United Kingdom and the United States. The European Commission also takes part in the work of the Agency.

The mission of the NEA is:

- to assist its member countries in maintaining and further developing, through international co-operation, the scientific, technological and legal bases required for a safe, environmentally friendly and economical use of nuclear energy for peaceful purposes, as well as
- to provide authoritative assessments and to forge common understandings on key issues, as input to government decisions on nuclear energy policy and to broader OECD policy analyses in areas such as energy and sustainable development.

Specific areas of competence of the NEA include the safety and regulation of nuclear activities, radioactive waste management, radiological protection, nuclear science, economic and technical analyses of the nuclear fuel cycle, nuclear law and liability, and public information.

The NEA Data Bank provides nuclear data and computer program services for participating countries. In these and related tasks, the NEA works in close collaboration with the International Atomic Energy Agency in Vienna, with which it has a Co-operation Agreement, as well as with other international organisations in the nuclear field.

This document and any map included herein are without prejudice to the status of or sovereignty over any territory, to the delimitation of international frontiers and boundaries and to the name of any territory, city or area.

Corrigenda to OECD publications may be found online at: www.oecd.org/publishing/corrigenda.

© OECD 2014

You can copy, download or print OECD content for your own use, and you can include excerpts from OECD publications, databases and multimedia products in your own documents, presentations, blogs, websites and teaching materials, provided that suitable acknowledgment of the OECD as source and copyright owner is given. All requests for public or commercial use and translation rights should be submitted to rights@oecd.org. Requests for permission to photocopy portions of this material for public or commercial use shall be addressed directly to the Copyright Clearance Center (CCC) at info@copyright.com or the Centre français d'exploitation du droit de copie (CFC) contact@cfcopies.com.

Foreword

The 7th workshop on Nuclear Measurements, Evaluations and Applications (NEMEA) focused on international collaboration in nuclear data by hosting the kick-off meeting of the pilot project of the Collaborative International Evaluated Library Organisation (CIELO). CIELO aims at fostering nuclear data advances by using the joint expertise of the nuclear data community under the auspices of the OECD Nuclear Energy Agency.

The workshop aimed at status reviews of planned and completed contributions and related developments for the CIELO pilot isotopes (^1H , ^{16}O , ^{56}Fe , ^{235}U , ^{238}U and ^{239}Pu). The workshop further sought to facilitate in-depth discussions on nuclear data issues which are being addressed in the framework of European Commission projects like ERINDA, EUFRAT, ANDES and CHANDA.

Acknowledgements

The organisation of the NEMEA-7/CIELO workshop was supported by the Joint Research Centre of the European Commission, by the OECD Nuclear Energy Agency and by the Los Alamos National Laboratory.

Special thanks are due to the staff of the Institute for Reference Materials and Measurements and to workshop secretaries Carmen Cabanillas and Mira van de Lucht for the smooth organisation of a very successful and agreeable event.



Table of Contents

Executive Summary	9
¹H and ¹⁶O.....	11
Chair: T. Fukahori	
<i>G.M. Hale, M.W. Paris</i>	
Status and plans for ¹ H and ¹⁶ O evaluations by R-matrix analyses of the NN and ¹⁷ O systems	13
<i>S. Kopecky, A.J.M. Plompen</i>	
Low-energy scattering data for oxygen	23
<i>S. Kunieda, T. Kawano, M. Paris, G. Hale, K. Shibata, T. Fukahori</i>	
Estimation of neutron cross-sections for ¹⁶ O Up to 5.2 MeV through R-matrix analysis.....	33
<i>C.R. Lubitz, P.K. Romano, T.H. Trumbull, D.P. Barry</i>	
Evidence for a 3% error in the experimental and evaluated databases for the ¹⁶ O neutron scattering and total cross-sections	41
<i>P.K. Romano, C.R. Lubitz, T.H. Trumbull</i>	
Critical benchmark results for a modified ¹⁶ O evaluation	55
⁵⁶Fe.....	63
Chair: R. Jacqmin	
<i>M. Herman, A. Trkov, D. Brown</i>	
Fe isotope evaluation within the CIELO project	65
<i>O. Iwamoto, N. Iwamoto</i>	
Review of nuclear data of major actinides and ⁵⁶ Fe in JENDL-4.0.....	75
<i>J.R. Vanhoy, S.F. Hicks, B.R. Champine, B.P. Crider, E.A. Garza, S.L. Henderson, S.H. Liu, E.E. Peters, F.M. Prados-Estévez, M.T. McEllistrem, T.J. Ross, L.C. Sidwell, J.L. Steves, S.W. Yates</i>	
Differential cross-section measurements at the University of Kentucky – Adventures in analysis	85
<i>Y. Danon, Z. Blain, A. Daskalakis, B. McDermott, D. Williams, D. Barry, R. Block, T. Donovan, B. Epping, G. Leinweber, M. Rapp</i>	
CIELO-related nuclear data measurements at the Gaertner LINAC Center at RPI.....	95
The Big Three – ²³⁵U, ²³⁸U, ²³⁹Pu – Part 1	103
Chair: M.B. Chadwick	
<i>B. Morillon, P. Romain</i>	
BRC neutron evaluations of actinides with the TALYS code.....	105

<i>R. Capote, M. Sin, A. Trkov, M.W. Herman, D. Bernard, G. Noguère, A. Daskalakis, Y. Danon</i>	
Evaluation of neutron-induced reactions on ^{238}U nucleus.....	113
<i>T. Kawano, P. Talou, M.B. Chadwick</i>	
Status of ^{239}Pu evaluations.....	119
The Big Three – ^{235}U, ^{238}U, ^{239}Pu – Part 2	129
Chair: M. Herman	
<i>G. Noguère, L. Leal, P. Leconte, D. Bernard, O. Bouland, Y. Penelïau, C. De Saint Jean</i>	
New evaluation of the resolved and unresolved resonance range of ^{239}Pu	131
<i>A. Bacquias, C. Borcea, Ph. Dessagne, M. Kerveno, J.C. Drohé, N. Nankov, A.L. Negret, M. Nyman, A. Plompen, C. Rouki, G. Rudolf, M. Stanoiu, J.C. Thiry</i>	
^{235}U and ^{238}U (n,xn gamma) cross-sections	141
<i>T.J. Wright, F. Mingrone, J. Billowes, E. Berthoumieux, D. Cano-Ott, C. Guerrero, F. Gunsing, C. Massimi, E. Mendoza, P. Schillebeeckx, n_TOF collaboration</i>	
High-precision measurement of the $^{238}\text{U}(n,\gamma)$ cross-section at the n_TOF facility, CERN.....	149
<i>A. Wallner, R. Capote, M. Christl, L.K. Fifield, M. Hotchkis, A. Krasa, J. Lachner, J. Lippold, A. Plompen, V. Semkova, M. Srnecik, P. Steier, S. Tims, S. Winkler</i>	
Neutron-induced reactions on U and Th – A new approach via AMS	159
<i>I.J. Thompson, F.S. Dietrich, W.E. Ormand</i>	
Coupled-channels effects in optical potentials for deformed nuclei.....	169
<i>C. De Saint Jean, E. Privas, P. Archier, G. Noguère, O. Litaize, P. Leconte, D. Bernard</i>	
Evaluation of cross-section uncertainties using physical constraints for ^{238}U , ^{239}Pu	177
The Big Three – ^{235}U, ^{238}U, ^{239}Pu – Part 3	187
Chair: E. Bauge	
<i>O. Litaize, L. Berge, D. Regnier, O. Serot, Y. Penelïau, P. Archier, C. De Saint Jean</i>	
Investigation of prompt fission neutron and gamma spectra with their covariance matrices – Application to $^{239}\text{Pu}+n_{\text{th}}$, $^{238}\text{U}+n_{1.8\text{MeV}}$, $^{235}\text{U}+n_{\text{th}}$	189
<i>A. Oberstedt, R. Billnert, S. Oberstedt</i>	
Characteristics of prompt fission gamma-ray emission – Experimental results and predictions	199
<i>A. Sardet, T. Granier, B. Laurent, A. Oberstedt, C. Varignon</i>	
Preliminary results on $^{238}\text{U}(n,f)$ prompt fission neutron energy spectra at 2, 5.2 and 15 MeV measured using a p-terphenyl scintillator.....	211
<i>N. Kornilov, T. Massey, S. Grimes</i>	
Scintillation neutron detector with dynamic threshold	221
General Interest – Part 1	229
Chair: M. Dunn	
<i>H. Leeb, G. Schnabel, T. Srdinko</i>	
What is the proper evaluation method: Some basic considerations	231
<i>D. Brown, J. Hirdt, M. Herman</i>	
Data mining the EXFOR database.....	241

General Interest – Part 2	249
Chair: P. Schillebeeckx	
<i>C. Paradela, L. Audouin, I. Durán, E. Leal-Cidoncha, L.S. Leong, D. Tarrío, L. Tassan-Got, n_TOF Collaboration</i>	
Fission measurements at the n_TOF facility with a PPAC detection set-up	251
<i>P. Salvador-Castiñeira, F-J. Hambsch, T. Bryś, S. Oberstedt, C. Pretel, M. Vidali</i>	
Measurement of the neutron-induced fission cross-section of ^{240,242} Pu.....	257
<i>A. Stankovskiy, G. Van den Eynde, O. Cabellos, C.J. Díez, P. Schillebeeckx, J. Heyse</i>	
Sensitivity analysis of the nuclear data for MYRRHA reactor modelling.....	267
General Interest – Part 3	277
Chair: Z. Ge	
<i>L. Fiorito, C. Díez, O. Cabellos, A. Stankovskiy, G. Van den Eynde, P.E. Labeau</i>	
Application of a Bayesian/generalised least-squares method to generate correlations between independent neutron fission yield data	279
<i>E. Mitenkova, N. Novikov</i>	
Effect of fission yield libraries on the irradiated fuel composition in Monte Carlo depletion calculations	287
<i>T. Kooyman, N. Messaoudi</i>	
Comparative sensitivity study of some criticality safety benchmark experiments using JEFF-3.1.2, JEFF-3.2T and ENDF/B-VII.1.....	297
Appendix 1: Final Programme	305
Appendix 2: List of Participants	309

Executive Summary

The 7th workshop on Nuclear Measurements, Evaluations and Applications (NEMEA) provided an opportunity for the Collaborative International Evaluated Library Organisation (CIELO) to meet and advance its objectives to improve our understanding of neutron reactions on key isotopes that are especially important in nuclear applications, especially in the area of criticality safety and reactors.

CIELO is focusing initially on six nuclides: ^1H , ^{16}O , ^{56}Fe , $^{235,238}\text{U}$ and ^{239}Pu . These nuclides are important in the aforementioned applications, and despite decades of work many open questions remain to be solved. In some cases, the existing evaluations need improvement because the underlying experimental measurements are either lacking or contradictory. In other cases, nuclear theory work is needed to better advance predictions. In yet other cases, information from cross-section measurements is proving difficult to reconcile with information from integral nuclear criticality experiments or neutron shielding experiments.

It is worthwhile to briefly summarise the main challenges we face.

For oxygen, new work is needed to better define the total and elastic cross-sections at lower energies and neutron scattering angular distributions. An outstanding uncertainty in the (n,α) cross-section needs to be addressed, where various evaluations, calculations and data sets are discrepant by as much as 30% or more. This impacts nuclear criticality calculations involving solutions and oxides.

For iron, much work has been done to better understand the resonant nuclear reactions as well as higher energy reactions involved in inelastic and elastic scattering, which appear to impact nuclear criticality. This needs to be integrated into a new, higher fidelity evaluation, with the hope that improved integral simulations of neutronics result.

For ^{235}U , the biggest challenge to be faced is updating the evaluations to account for rather major changes in neutron capture, inspired by integral reactor observations and confirmed by recent cross-section measurements. Resolving different representations of inelastic scattering will likewise be important.

For ^{238}U , new resonance measurements are being integrated into new evaluations. Further, upgrades to the evaluations will better represent inelastic and elastic scattering and facilitate improved simulations of a wide range of nuclear integral measurements.

Updated inelastic scattering analyses are also needed for ^{239}Pu to resolve present uncertainties. New neutron capture measurements are coming online and will help better constrain this reaction, which is surprisingly poorly determined.

Considerable work is also being done for all of the actinides to better determine fission neutron spectra, multiplicities, and cross-sections, as well as fission gamma-ray data.

CIELO relies on the collaboration among several nuclear data projects across the world, some of them having different short-term objectives, but all of them working towards improving basic nuclear data. The papers at this workshop describe the work being done in more detail in the framework of these projects. The community's goal is to issue a first set of advances in our knowledge within about two years.

Mark Chadwick (LANL, CIELO Co-ordinator)
Arjan Plompen (JRC-IRMM)
Emmeric Dupont (OECD/NEA)

¹H and ¹⁶O

Chair: T. Fukahori

Status and plans for ¹H and ¹⁶O evaluations by R-matrix analyses of the N-N and ¹⁷O systems

Gerald M. Hale, Mark W. Paris

Theoretical Division, Los Alamos National Laboratory
Los Alamos, New Mexico, United States

Abstract

We discuss the current status of R-matrix analyses of the light-element reactions induced by neutrons on protons (¹H) and ¹⁶O. An analysis of the NN system at nucleon energies up to 30 MeV was used to provide the n-p standard cross-sections below 20 MeV for the IAEA/ENDF evaluation in 2005. A new analysis of the NN system is planned for the coming year, extending the energy range to at least 200 MeV, and including many different types of polarisation measurements. LANL R-matrix analyses of the ¹⁷O system have been used to provide n+¹⁶O cross-sections for several previous ENDF/B evaluations. Our recent work on this system, dating back to 2010, includes substantial new information about the α +¹³C reactions, including elastic scattering. Serious questions remain, however, about the low-energy n+¹⁶O scattering cross-section, and the normalisation of the ¹⁶O(n, α)¹³C cross-section. Mentioned also at the end is the problem of unreasonably small parameter uncertainties resulting from R-matrix analyses such as these that fit very large numbers of experimental data points.

Introduction

We will discuss in this paper the status of and planned future work at Los Alamos National Laboratory (LANL) on the two light nuclei considered as part of the CIELO set, ¹H and ¹⁶O. The work on hydrogen is being done as part of the international standard cross-section re-evaluation, and the work on oxygen is a continuation of a long history of R-matrix analyses of reactions in the ¹⁷O system that have been done at LANL. The discussion will begin with a brief introduction to the R-matrix formalism that is the framework for all the phenomenological light-element evaluation work done at Los Alamos, and to the Energy Dependent Analysis (EDA) code that is used there to perform the numerical calculations.

Following that we will describe the analysis of the nucleon-nucleon (N-N) system at energies up to 30 MeV that was used to provide the current n-p scattering and capture cross-sections that are in the Evaluated Nuclear Data File (ENDF/B). The scattering lengths and other low-energy data are in nearly perfect agreement with the best available measurements. We plan within the coming year to extend the N-N analysis to much higher energies, making use of the extensive database of cross-section and polarisation measurements that exists at energies below 250 MeV. The challenge will be to do the high-energy extension in such a way that the excellent fit we already have at lower energies is maintained, since changes in the distant-level R-matrix parameters will affect the whole energy range of the analysis.

There are two major issues with the current evaluation of the ¹⁶O cross-sections: one is that the low-energy scattering cross-sections are about 3% too high, and the other is the normalisation of the ¹⁶O(n,α)¹³C cross-section is uncertain to more than 30%. We will discuss recent R-matrix work on the reactions in the ¹⁷O system that appears to be making progress on resolving the first issue, but the second one seems to be more problematic, both from the theoretical and experimental perspective.

Finally, we will make some brief comments about the problem of the small calculated uncertainties (covariances) resulting from R-matrix analyses, and proceed to the conclusions of the paper.

R-matrix formalism and the EDA code

As has been pointed out at many nuclear data conferences, e.g. Hale (1993), R-matrix theory (Lane and Thomas, 1958) is the most useful framework for describing light-nuclear reactions, particularly those exhibiting resonance structure. Figure 1 is a schematic showing some of the R-matrix quantities discussed below, as well as the separation of co-ordinate space into an “interior” and “exterior” region, separated by the “channel surface”, and becoming at infinite cluster separations ($r_c \rightarrow \infty$) the “asymptotic” region.

Formally, the R-matrix elements can be expressed as projections on the channel-surface functions $|c\rangle$ of the Green’s function operator $G_B = (H + \mathcal{L}_B - E)^{-1}$. H is the total interaction hamiltonian when all the nucleons of the system are close together, E is the total c.m. energy, and:

$$\mathcal{L}_B = \sum_c |c\rangle \langle c| \left(\frac{\partial}{\partial r_c} r_c - B_c \right) \quad (1)$$

is the so-called “Bloch operator”. Its purpose is to make the combination $H + \mathcal{L}_B$ hermitian in the finite region bounded by the channel radii $r_c = a_c$, and to introduce the boundary values B_c of the logarithmic derivative at the channel surface, $\{r_c = a_c\}$. Then the solutions of the eigenvalue equation:

$$(H + \mathcal{L}_B - E_\lambda)|\lambda\rangle = 0 \quad (2)$$

form a complete, orthogonal set in the internal region ($r_c \leq a_c$), in terms of which the elements of the R-matrix take their familiar pole expansion:

$$R_{c'c} = \langle c'| G_B |c\rangle = \sum \frac{\langle c'|\lambda\rangle \langle \lambda|c\rangle}{E_\lambda - E} \quad (3)$$

The R-matrix thus parameterises through the real reduced-width amplitudes $\gamma_{c\lambda} = \langle c|\lambda\rangle$ and the eigenenergies E_λ the scattering wave functions at short distances, which are matched at the channel surface to their known asymptotic forms (see Figure 1) to determine the scattering amplitudes (S -matrix elements), from which any measured observable can be calculated.

The multi-channel R-matrix formalism has been implemented in the most general possible form in the Los Alamos code EDA (Dodder, Hale and Witte, n.d.). A flow chart of the code’s operation is shown in Figure 2. The code accommodates any number of two-body channels having particles with arbitrary spins, masses and charges. The formulation is relativistic, so that even zero-mass particles, such as photons, are treated correctly. General scattering observables for $2 \rightarrow 2$ processes are calculated using the Wolfenstein trace formalism (1956). Experimental data can be modified by the use of adjustable normalisations and energy shifts, and the calculations can fold in the effects of beam energy resolution/spread. A modified rank-one variable-metric search algorithm is used to find the local minima of the chi-squared surface, and to compute the parameter covariance matrix at the solution.

Figure 1: Schematic diagram showing the separation of co-ordinate space assumed in R-matrix theory, as well as definitions and properties of some of its relevant quantities

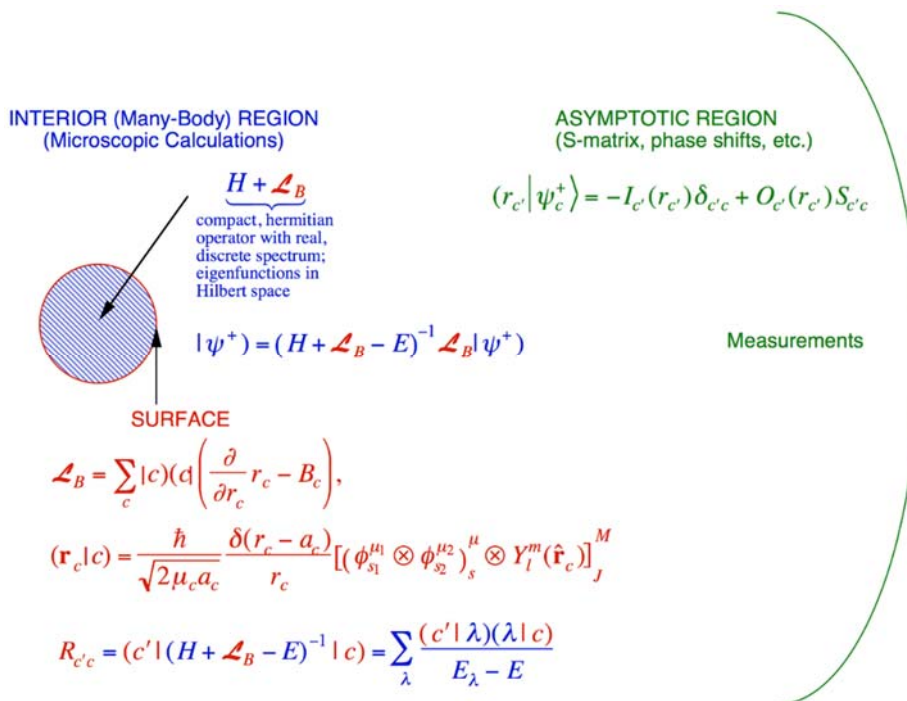
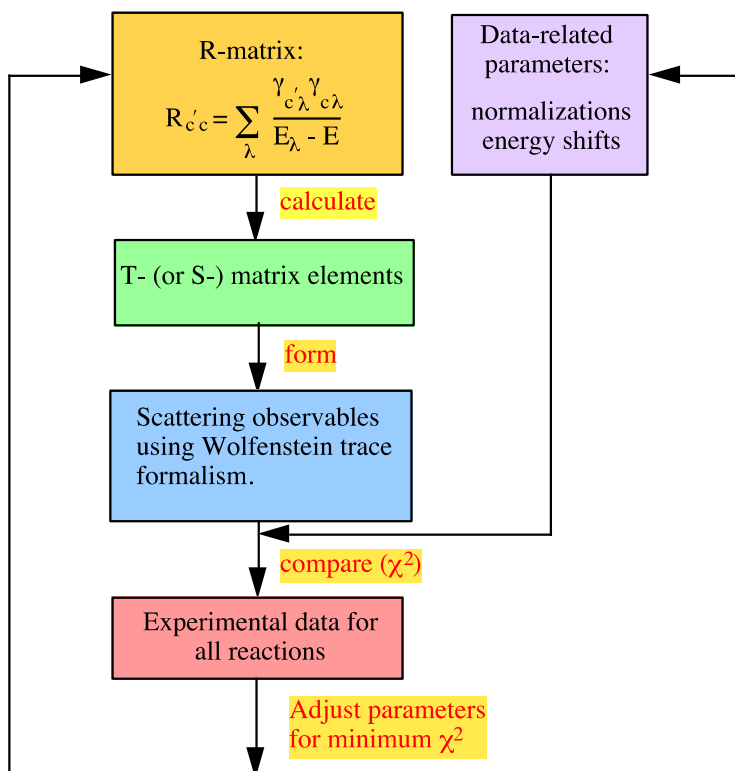


Figure 2: Schematic of the EDA code



N-N (¹H) analysis

A LANL R-matrix analysis of the N-N system at nucleon energies up to 30 MeV was used to provide the n-p (¹H) standard cross-sections below 20 MeV for the IAEA/ENDF evaluation in 2005. This analysis included data for p+p and n+p scattering, as well as for n+p capture and γ +d photo-disintegration. A very good fit (with a reduced chi-squared of 0.83) was obtained to all the experimental data (more than 5 000 points) included, with small uncertainties at low energies (see Table 1).

Table 1: Summary of the charge-independent N-N analysis at energies below 30 MeV

Channel	a_c (fm)	l_{max}
p+p	3.26	3
n+p	3.26	3
γ +d	40	1

Reaction	# Pts.	χ^2	Observable types
p(p,p)p	692	815	$\sigma(\theta)$, $A_y(p)$, $C_{x,x}$, $C_{y,y}$, $K_{x'}$, $K_{y'}$, $K_{z'}$
p(n,n)p	4 378	3 232	σ_T , $\sigma(\theta)$, $A_y(n)$, $C_{y,y}$, $K_{y'}$
p(n, γ)d	80	133	σ_{int} , $\sigma(\theta)$, $A_y(n)$
d(γ ,n)p	59	35	σ_{int} , $\sigma(\theta)$, $\Sigma(\gamma)$, $P_y(n)$
Norms.	129	72	
Total	5338	4 287	19

The spin-dependent n-p scattering lengths resulting from the analysis are $a_0 = 23.719(5)$ fm and $a_1 = 5.414(1)$ fm. These give the values:

$$\begin{aligned}
 a_c &= (3a_1 + a_0)/4 = -1.8693 \text{ fm} \\
 \sigma_{pol} &= (a_1^2 + a_0^2)/4 = -1.3332 \text{ b} \\
 \sigma_{sc} &= \pi(3a_1^2 + a_0^2) = 20.437 \text{ b}
 \end{aligned}
 \tag{4}$$

for the coherent scattering length, polarised cross-section, and scattering cross-section, respectively, near zero energy. The first two agree exactly with the experimental values (Schoen, 2003; Alfimenkov, *et al.*, 1967), while the zero-energy scattering cross-section agrees with the measurement of Houk (1971), but not with that of Dilg (1975). The scattering lengths derived from the phenomenological Argonne potential v_{18} (Wiringa, Stokes and Schiavilla, 1995) are $a_0 = -23.732$ and $a_1 = 5.419$ fm, in reasonable agreement with those from the R-matrix analysis.

The n-p total cross-sections are generally very well fit within their error bars at energies up to 40 MeV. However, two rather surprising observations are that many of those error bars are as large as 5%, and that the measurement of Cierjacks (1969), which has by far the smallest statistical uncertainties, shows a pronounced systematic deviation with energy from the calculation and from the trend of the other experiments. The other data are scattered rather uniformly about the calculated curve.

A new analysis of the N-N system is planned for the coming year, extending the energy range to at least 200 MeV. This will be a major undertaking, involving the addition of many new data sets, some of which are in the energy range of the existing analysis. Table 2 lists the types of observables that have been measured for nucleon-nucleon scattering in various energy ranges, according to a preliminary survey we have done using

Table 2: Types of experimental data available for the N-N system by energy range

0 < E < 30 MeV															
	$\sigma(\theta)$	P_{n000}	D_{n0n0}	K_{0nn0}	A_{00nn}	A_{00ss}	A_{00kk}	A_{00sk}	$C_{\ell m 00}$	$D_{s'0s0}$	$D_{k'0s0}$	$K_{0s's0}$	$D_{s'0k0}$	$D_{k'0k0}$	$K_{0s''k0}$
	$\sigma(\theta)$	P	D	D_T	A_{yy}	A_{xx}	A_{zz}	A_{zx}	C_{KP}	R	R_P	R_T	A	A_P	A_T
pp	363	70	8	0	7	4	0	0	0	8	0	0	5	0	0
np	243	231	0	3	31	0	0	0	0	0	0	0	0	0	0
30 MeV < E < 150 MeV															
	$\sigma(\theta)$	P_{n000}	D_{n0n0}	K_{0nn0}	A_{00nn}	A_{00ss}	A_{00kk}	A_{00sk}	$C_{\ell m 00}$	$D_{s'0s0}$	$D_{k'0s0}$	$K_{0s's0}$	$D_{s'0k0}$	$D_{k'0k0}$	$K_{0s''k0}$
	$\sigma(\theta)$	P	D	D_T	A_{yy}	A_{xx}	A_{zz}	A_{zx}	C_{KP}	R	R_P	R_T	A	A_P	A_T
pp	331	257	24	0	8	3	0	0	1	24	14	0	21	0	0
np	629	313	0	6	28	0	20	0	0	5	0	0	5	0	3
150 MeV < E < 250 MeV															
	$\sigma(\theta)$	P_{n000}	D_{n0n0}	K_{0nn0}	A_{00nn}	A_{00ss}	A_{00kk}	A_{00sk}	$C_{\ell m 00}$	$D_{s'0s0}$	$D_{k'0s0}$	$K_{0s's0}$	$D_{s'0k0}$	$D_{k'0k0}$	$K_{0s''k0}$
	$\sigma(\theta)$	P	D	D_T	A_{yy}	A_{xx}	A_{zz}	A_{zx}	C_{KP}	R	R_P	R_T	A	A_P	A_T
pp	60	203	28	8	96	96	39	96	0	23	11	0	20	5	0
np	456	164	5	13	39	0	2	0	0	0	0	7	0	0	7

Measured	Unp. beam/Unp. target	Pol. beam/Unp. target	Unp. beam/Pol. target	Pol. beam/Pol. target
Differential cross section	J_{0000}	A_{0000}	A_{000k}	A_{00ik}
Scatt. pol.	P_{p000}	D_{p0i0}	K_{p00k}	M_{p0ik}
Recoil pol.	P_{0q00}	K_{0qi0}	D_{0q0k}	N_{0qik}
Pol. correlations	C_{pq00}	C_{pqi0}	C_{pq0k}	C_{pqik}

the experimental database for hadronic scattering maintained on the Scattering Analysis Interactive Dial-in (SAID) system at George Washington University. Since the R-matrix parametrisation and kinematics used in the EDA code are relativistic, we do not anticipate any problem in principle with extending the range of the analysis to such high energies.

¹⁷O analysis

In 2010, a new R-matrix analysis of reactions in the ¹⁷O system was performed at energies below 7 MeV, which was intended to update the ¹⁶O evaluation for ENDF/B-VII.1. A rather good fit was obtained to most of the nearly 6 000 data points included in the analysis. However, since the scale of the ¹⁶O(n, α)¹³C cross-section obtained from the analysis disagreed by some 25% with that of recent measurements, it was decided to withhold the new evaluation and return to the previous version (VII.0), despite the fact that the newer evaluation appeared to perform equally well in integral data testing.

The channel configuration of the 2010 analysis and a summary of the data that were included are given in Table 3. A significant amount of new data was available for the α +¹³C reactions because they are of interest in astrophysics. Since there were sizeable variations in the normalisations of these data sets, especially for the ¹³C(α ,n)¹⁶O reaction,

Table 3: Summary of the ¹⁷O system analysis

Channel	a_c (fm)	l_{max}
n+ ¹⁶ O	4.3	4
α + ¹³ C	5.4	5

Reaction	Energy range	Data types	# data points
¹⁶ O(n,n) ¹⁶ O	$E_n = 0-7$ MeV	$\sigma_T, \sigma(\theta), P_n(\theta)$	2 718
¹⁶ O(n, α) ¹³ C	$E_n = 2.35-5$ MeV	$\sigma_{int}, \sigma(\theta), A_n(\theta)$	850
¹³ C(α ,n) ¹⁶ O	$E_a = 0-5.4$ MeV	σ_{int}	874
¹³ C(α , α) ¹³ C	$E_a = 2-5.7$ MeV	$\sigma(\theta)$	1 296
Total		8	5 738

the normalisations of most of the cross-sections included were allowed to go free (but constrained by their experimental errors) as search parameters. The fit to the total and integrated cross-sections for the $n+^{16}\text{O}$ reactions is shown in Figure 3. The total cross-section is shown on the left of the figure at energies below 2 MeV, and on the upper right at energies between 2 and 7 MeV, in the range where the $\alpha+^{13}\text{C}$ channel is open. The $^{13}\text{C}(\alpha,n)$ cross-section is shown at the bottom right of the figure such that the α -particle energy scale roughly matches that of the neutron energies on the total cross-section. One sees that the agreement with all the data shown is quite good. The $^{13}\text{C}(\alpha,n)^{16}\text{O}$ measurement shown is that of Bair and Haas (1973), reduced by 6%, and not by 20% as recommended in their note added in proof. This is shown in more detail in Figure 4, where the calculation is also compared with the recent data of Harissopoulos (2005), which are considerably lower in magnitude.

Finally, Figure 5 shows a comparison of the calculation with the low-energy S-factor data of several groups, including the recent measurement of Heil (2008). These data were not actually included in the fit, but as the plot shows, the magnitude of the calculation is quite consistent with their scale, and that of Drotleff. The shape of the calculation is most consistent with the data of Kellogg, but with a large re-normalisation factor.

Figure 3: Comparison of the calculated total and reaction cross-sections with experimental data

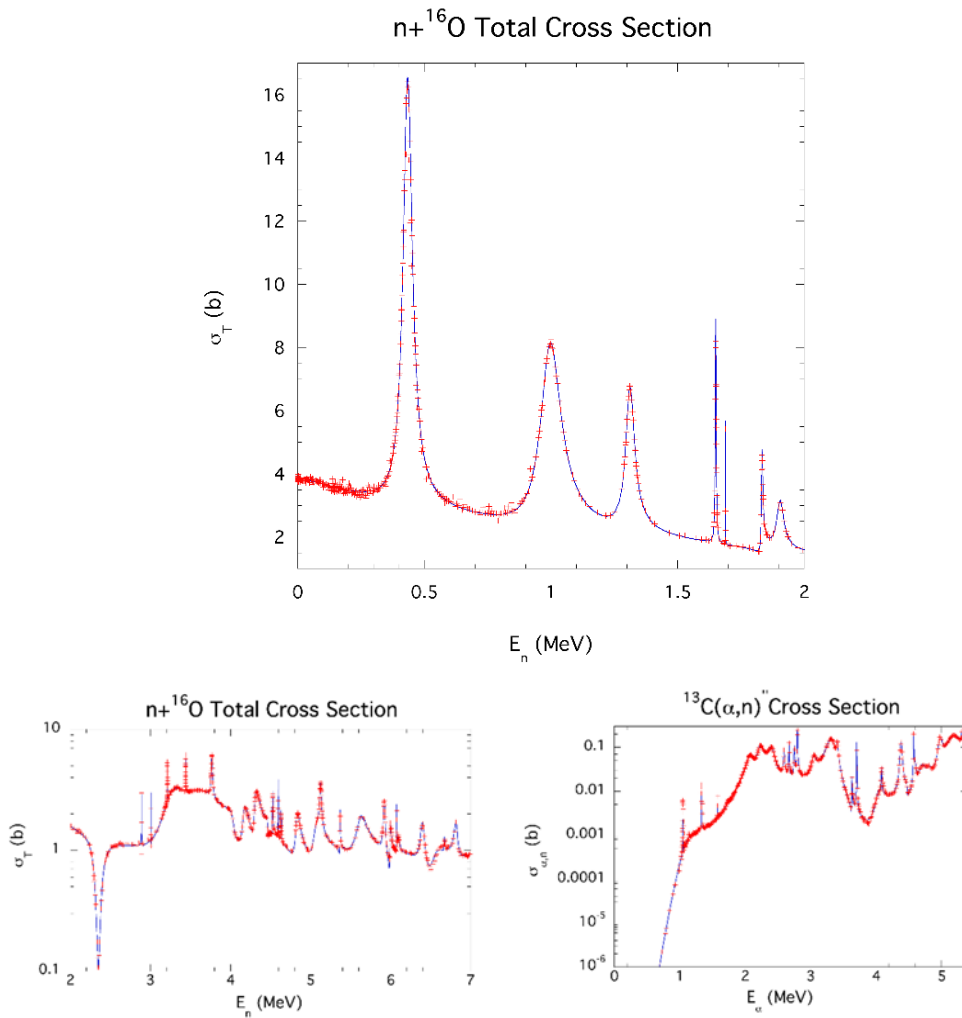


Figure 4: Comparison of the calculated ¹³C(α,n) cross-section with experimental data

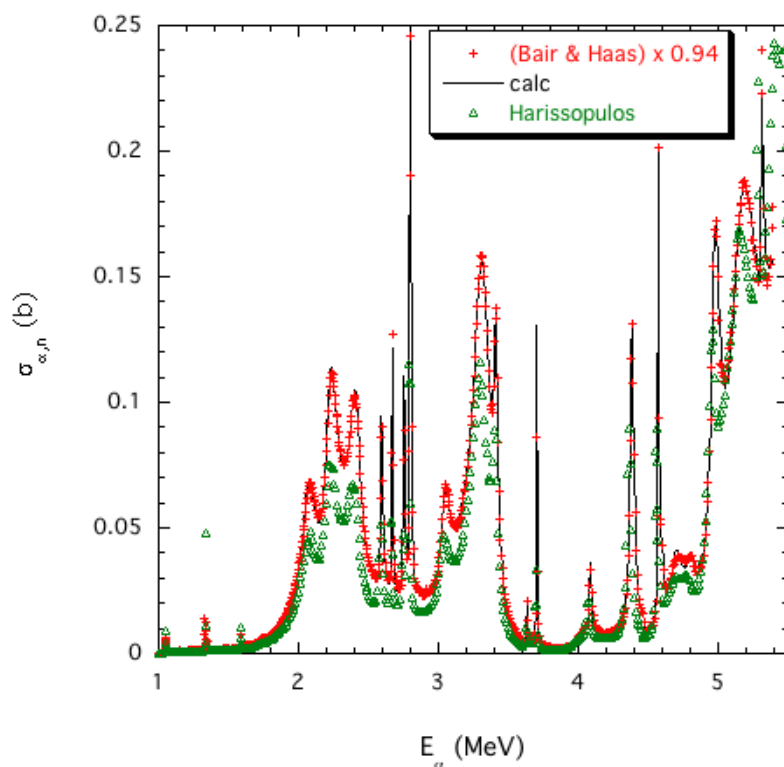
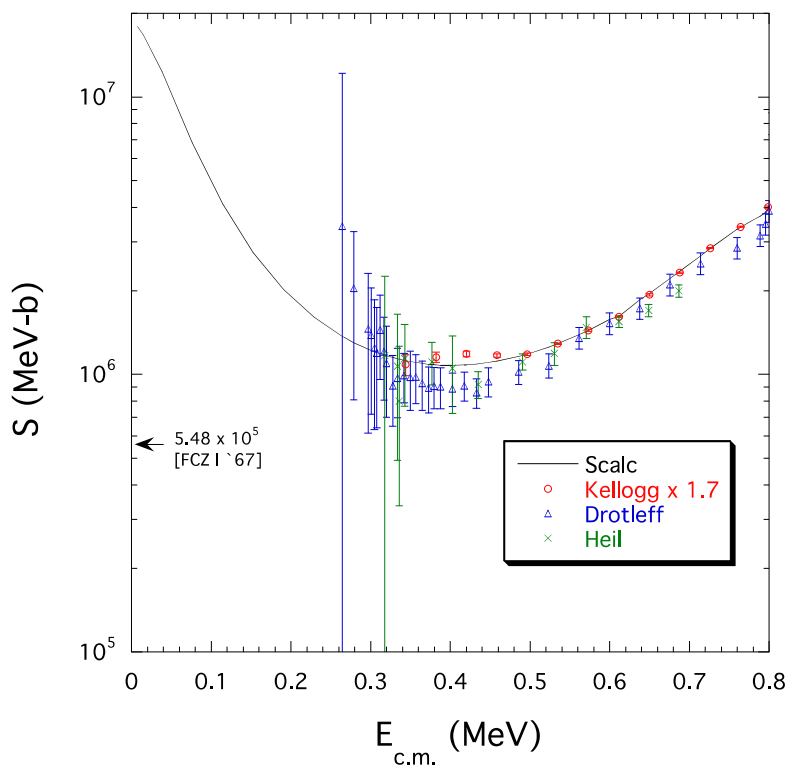


Figure 5: Comparison of the low-energy ¹³C(α,n) S-factor with experimental data



We plan to continue the analysis started in 2010 with new (n,α) data and with new and/or corrected low-energy $n+^{16}\text{O}$ scattering data as determined within the CIELO working group. That process has already begun with a new fit that includes low-energy scattering data based on measurements of the scattering lengths, and a correction to the Okhubo total cross-section measurement for the hydrogen content of the target. These changes have allowed the low-energy scattering cross-section to come down from nearly 3.9 b to about 3.8 b, which more closely approaches the unbroadened value Lubitz, *et al.* (2013) think it should have. The total cross-sections were also allowed to over-shoot in the peaks somewhat without a chi-square penalty, using an option in EDA that limits the χ^2 contribution of individual points. This allowed a further reduction of the calculated reaction cross-sections due to the unitary constraint that *anti-correlates* the behaviour of the total and reaction cross-sections for resonances above the threshold that have most of their width in the neutron channel. Thus, resolution-folding in the peaks of resonances appears to be an important element in connecting cross-section normalisations to the constraints imposed by using a unitary multi-channel theory used to fit the data.

Cross-section uncertainties

A long-standing puzzle in nuclear data evaluation has been that the parameter uncertainties, and thus the propagated cross-section uncertainties, from R-matrix analysis programs such as EDA, have been unreasonably small. This has necessitated in some cases scaling up the output uncertainties from the code by large empirical factors. One expects, of course, a $1/\sqrt{N}$ statistical reduction of the parameter uncertainties for a large sample size. However, for $(N \sim 5\,000)$ with 50-150 parameters, as is typical for these R-matrix analyses, this reduction gives uncertainties that are unreasonably small. Perhaps the answer is to use a proposal by Avni (1976) to use confidence levels, rather than standard errors, to determine parameter uncertainties. For small numbers of degrees of freedom, these prescriptions are almost the same, but they may diverge for larger values. We plan to devote further study to this perplexing problem.

Conclusions

The analyses described here are further examples of the extraordinary flexibility of R-matrix theory to describe both resonant (^{17}O) and non-resonant (N-N) reactions while upholding the fundamental properties of multi-channel nuclear scattering theory: causality, reciprocity (time-reversal invariance) and unitarity. The nucleon-nucleon data are quite well represented by the present analysis at energies below 30 MeV. The challenge for the next standards (and CIELO) evaluation will be to extend the energy range of the analysis to something like 250 MeV while maintaining the present quality of the fit at lower energies.

The LANL analysis of the ^{17}O system is presently in reasonably good shape at energies in the CIELO range. However, there are important issues to be settled, both experimentally and theoretically. One is the value and energy dependence of the $n+^{16}\text{O}$ scattering cross-section at low energies. The energy dependence given by the bound-state S-wave poles and the first P-wave resonance is consistent with most of the (unbroadened) measurements. In our most recent work, the value of the zero-energy cross-section has come down by 0.1 b to about 3.8 b. However, this reduction cannot hold over the whole energy range as Lubitz, *et al.* (2013) have argued, since a decrease in the total cross-section above the $\alpha+^{13}\text{C}$ threshold causes the (n,α) cross-section to increase, contradicting the preliminary normalisation of recent measurements. The effects of experimental resolution broadening and theoretical unitary constraints in the peaks of narrow resonances are intimately connected to the question of the normalisation of the cross-sections in this energy range.

Acknowledgements

This work has been supported mainly by the United States Department of Energy Nuclear Data and Nuclear Criticality Safety Programs.

References

- Alfimenkov, V.P. *et al.* (1967), "Choice of the Proper Set of Neutron-Deuteron Scattering Lengths from Experiments on Transmission of Polarized Neutrons Through a Polarized Deuteron Target", *Phys. Lett.*, 24B, pp. 151-153.
- Avni, Y. (1976), "Energy Spectra of X-ray Clusters of Galaxies", *Ap. J.*, 210, pp. 642-646.
- Bair, J.K. and F.X. Haas (1973), "Total Neutron Yield from the Reactions $^{13}\text{C}(\alpha,n)^{16}\text{O}$ and $^{17,18}\text{O}(\alpha,n)^{20,21}\text{Ne}$ ", *Phys. Rev. C*, 7, pp. 1356-1364.
- Cierjacks, S., *et al.* (1969), "High-Precision Measurement of the Total n-p Scattering Cross Section in the Energy Range 0.7-32 MeV", *Phys. Rev. Lett.*, 23, pp. 866-868.
- Dilg, W. (1975), "Measurement of the Neutron-Proton Total Cross Section at 132 eV", *Phys. Rev. C*, 11, pp. 103-109.
- Dodder, D.C., G.M. Hale and K. Witte (n.d.), *The Energy Dependent Analysis Code for Nuclear Reactions*, Los Alamos National Laboratory, Los Alamos, NM, unpublished.
- Hale, G.M. (1993), "Use of R-matrix Theory in Light Element Evaluations", *Proc. Int. Symp. on Nuclear Data Evaluation Methodology*, C.L. Dunford (ed.), Brookhaven National Laboratory, Upton NY, 12-16 October 1992, *World Scientific*, pp. 306-315.
- Harissopulos, S., *et al.* (2005), "Cross Section of the $^{13}\text{C}(\alpha,n)^{16}\text{O}$ Reaction: A Background for the Measurement of Geo-Neutrinos", *Phys. Rev. C*, 72, pp. 062801(R)-1-5.
- Heil, M., *et al.* (2008), "The $^{13}\text{C}(\alpha,n)$ Reaction and Its Role as a Neutron Source for the s Process", *Phys. Rev. C*, 78, pp. 025803-1-17.
- Houk, T.L. (1971), "Neutron-Proton Scattering Cross Section at a Few Electron Volts and Charge Independence", *Phys. Rev. C*, 3, pp. 1886-1903.
- Lane, A.M. and R.G. Thomas (1958), "R-matrix Theory of Nuclear Reactions", *Rev. Mod. Phys.*, 30, pp. 257-353.
- Lubitz, C.R., *et al.* (2013), "Evidence for a Three Percent Error in the Experimental and Evaluated Databases for the ^{16}O Neutron Scattering and Total Cross Sections", these proceedings.
- Schoen, K. *et al.* (2003), "Precision Neutron Interferometric Measurements and Updated Evaluations of the *n-p* and *n-d* Coherent Neutron Scattering Lengths", *Phys. Rev. C*, 67, pp. 044005-1-21.
- Wiringa, R.B., V.G.J. Stokes and R. Schiavilla (1995), "Accurate Nucleon-Nucleon Potential with Charge-Independence Breaking", *Phys. Rev. C*, 51, pp. 38-51.
- Wolfenstein, L. (1956), "Polarization of Fast Nucleons", *Ann. Rev. Nucl. Sci.*, 6, pp. 43-76.

Low-energy scattering data for oxygen

S. Kopecky, A.J.M. Plompen

EC-JRC Institute for Reference Materials and Measurements
Geel, Belgium

Abstract

A survey of literature data of the scattering lengths of oxygen is performed, and these values are compared to low-energy precise total cross-section data. To check the quality of the data and the correctness of the relation between coherent scattering lengths and low-energy total cross-sections the situation is examined first for carbon. A value and uncertainty for the coherent scattering length of oxygen is recommended for use in future evaluations of ¹⁶O. This coherent scattering length is fully consistent with the high-precision, low-energy total cross-section data. The consistency requires the use of a larger uncertainty than claimed in the most accurate cross-section papers. This larger uncertainty is nevertheless very small and well within the requirements of applications of this cross-section. The recommended value is $b_c(^{16}\text{O}) = 5.816 \pm 0.015$ fm and the associated total cross-section for the neutron-energy range 0.5 to 2 000 eV is 3.765 ± 0.025 b. The stated uncertainties are one standard deviation total uncertainty.

Introduction

In the literature a large number of high-precision experimental data for coherent scattering lengths exists (Sears, 1992; Rauch and Waschkowski, 2000; Dawidowski, *et al.*, 2013). For most of the available nuclei the quoted uncertainties are better than a few per cent, i.e. the accuracy is in most cases better than the values from conventional cross-section measurements using the transmission technique at time-of-flight facilities. Therefore it is worth investigating: *i)* how the quantities are derived to understand how reliable the quoted uncertainties are; *ii)* how coherent scattering lengths are related to high-precision measured total cross-section values. Below we first introduce these neutron optical measurements leading to accurate coherent scattering lengths. We then introduce the high-precision total cross-section measurements and discuss the relation between these two quantities. To illustrate what may be achieved carbon is discussed first. The ¹⁶O database is then presented and the consistency of the results is discussed in order to analyse what the best value for the coherent scattering length is and how it relates to the best total cross-section measurements at low energy. This discussion leads to the use of an uncertainty larger than would be obtained by weighted average. The final uncertainty is nevertheless small and the value and uncertainty should be a reference for any future evaluations of the ¹⁶O cross-section.

Neutron optical measurements

To determine the coherent scattering lengths, most of the experiments rely on either Fraunhofer diffraction (or small angle scattering), refraction, reflection or interferometry. All of the latter methods rely on dynamical scattering theory (Sears, 1982). The principal aim of the dynamical theory is the treatment of coherence between the incident neutron beam and the scattered neutron beam when the Bragg condition is not met for any of the lattice planes of the material. Such coherence is only possible if the wavelengths of the incident and scattered waves are the same. It therefore just concerns elastic scattering in this strict sense and any other scattering process that changes the wavelength leads to attenuation of the neutron beam and is treated as absorption along with actual neutron removal reactions.

Unlike the kinematic theory, which solves the scattering equation in Born approximation and therefore ignores the local field, the dynamical theory first derives the effective interaction potential and then solves the Schrödinger equation rigorously using appropriate boundary conditions. It is found that when Bragg's law is not satisfied for a crystal the coherent wave is the same as that in a homogeneous body of the same composition and density (Sears, 1982). The resulting theory closely resembles conventional optics. As in optics, the propagation of neutron waves through a medium is governed by a refractive index n which is given by:

$$n^2 - 1 = -N \frac{\lambda^2}{\pi} \left\{ \pm \left[b^2 - \left(\frac{\sigma_a}{2\lambda} \right)^2 \right]^{\frac{1}{2}} + i \frac{\sigma_a}{2\lambda} \right\}$$

with N the density of the sample (nuclei per unit volume), b the coherent scattering length, λ the wave length of the neutron and σ_a the absorption cross-section of the sample.

This relation is used to extract the coherent scattering length b from neutron optical experiments. As summarised in the review by Sears (1982), the accuracy of the above formula is higher than the experimental corrections and uncertainties involved in deriving the coherent scattering lengths.

It should be noted that in fact the term important for the refractive index is the coherent scattering length at zero momentum transfer or the forward scattering amplitude. For this reason terms like the neutron-electric scattering length can be excluded in the formula (Sears, 1982). Secondly, as the strict definition of coherence explained above is applicable, there is no role for the Doppler effect. The temperature of the sample is of minor concern and only impacts the determination of the sample density N during the measurement.

Neutron optical measurements used for accurate determinations of the coherent scattering length include gravity reflectometry, interferometry and prism deflection.

Reflectometry uses the fact that for most materials the refractive index is negative. For pure hydrogen it would be positive, but hydrogenous compounds may be found that have an overall negative refractive index. With a negative refractive index total reflection occurs for neutrons travelling through air upon incidence on a material under sufficiently small angles. The critical angle for total reflection can be determined precisely and from that the refractive index and hence the coherent scattering length follows. In a gravity reflectometer small angles are achieved by neutrons falling on a surface after a long flight path. The critical angle expressed as a critical height of drop turns out to be independent of the neutron wavelength. The method is therefore non-dispersive and as such allows very accurate determinations of the coherent scattering length (for the best cases a few times 10^{-4}).

In an interferometer a monochromatic neutron beam is first split in two and then recombined. Care is taken that the two beams travel the same geometrical distance. To determine a coherent scattering length of a material a sample is placed in one of the two neutron beams thereby creating a different optical path length for that branch of the interferometer. This results in a modification of the intensity of the beams extracted from the interferometer. By rotating the sample the path length through the sample is varied, leading to characteristic interference oscillations in the measured intensity which allow to determine the refractive index and thereby the coherent scattering length. The method is non-dispersive and competes in accuracy with the gravity reflectometer.

In prism deflection the angle of deflection of mono-energetic neutrons through a prism is measured. The method relies entirely on the accuracy with which angles may be measured both for the measurement of the deflection and for the determination of the neutron wavelength (distribution). The latter point is critical as the method is dispersive, in contrast with the other two techniques, and the refractive index varies quadratically with the wavelength. Accuracies similar to those of the gravity reflectometer and the interferometer were obtained.

Characteristic examples of these three techniques with the appropriate references are given below [see also Sears (1982)] in the discussion about the carbon and oxygen data. It should be stressed that these methods achieve their accuracy also because appropriate attention was paid to sample preparation and characterisation. In particular the sample purity, thickness and/or density need to be characterised accurately to draw full profit of the accuracy of the equipment that was used. In fact, the refractive index is linear in the atom density as it is linear in the coherent scattering length.

The scattering cross-section

To compare the coherent scattering length as derived with thermal neutrons with total cross-sections measured at higher energy, the relationship between scattering length and total cross-section has to be clear. Within the accuracies required for the present investigation the “total” coherent scattering length, as a function of the neutron energy can be given as (Sears, 1986):

$$b_c(E) = b_c \left(1 - \frac{k^2 a^2}{6} \right) - Z(1 - f(E))b_{ne}$$

with b_c the bound coherent scattering length, a the free scattering length, k the wave number of the relative motion of the system. This relation has been derived using the effective range approximation, with the effective range radius given by:

$$r_{eff} = \frac{2}{3}a; a = \frac{A}{A+1}b_c$$

This relation for the effective range is an approximation, which is used to indicate the expected behaviour. The detailed energy dependence requires an R-matrix analysis. The neutron-electron scattering length is $b_{ne} = -1.33 \cdot 10^{-3}$ fm (Kopecky), Z is the charge number and $f(E)$ is the atomic form factor. A simple description of the energy dependence of the form factor can be found in e.g. Sears (1986).

Finally, using the incoherent approximation, the coherent scattering cross-section can be written as:

$$\sigma_s = 4\pi b_c^2(E) \left(\frac{A}{A+1} \right)^2 \left(1 + \frac{k_b T_{eff}}{2AE} \right)$$

with T_{eff} the effective temperature (mean vibrational energy per degree of freedom), which depends on the various sample properties, such as temperature, phonon spectrum, etc. This approximation will in general be sufficiently accurate if $E \gg (k_b T_{eff}/2A)$, for most materials this condition will be reached already below 1 eV.

For the nuclei and energy range considered in this paper the absorption cross-section is very low and the total cross-section is equal to the scattering cross-section for all except very low energies. Furthermore for nuclei with spin zero the coherent scattering cross-section is the total scattering cross-section (here we only consider ¹²C and ¹⁶O).

Neutron total cross-sections are universally measured with the transmission technique. Using an appropriate neutron source a neutron beam is created by collimation. A detector is placed in the beam to measure the neutron flux of the beam C_{out} and the neutron flux when the neutron beam is attenuated by a sample of the material of interest C_{in} . The ratio of the two fluxes is the transmission factor which is expressed in terms of the material density ρ , its thickness t and the total cross $\sigma(E)$ section by:

$$T(E) = \frac{C_{in}}{C_{out}} = e^{-t\rho\sigma(E)}$$

The method is in principle absolute in the sense that it does not require any other cross-sections in its realisation and analysis. At white neutron sources with the time-of-flight technique cross-section accuracies in the per cent range are readily obtained. Several experimental corrections and effects are important for the accuracy of the technique, such as detector dead time, background count rates, the knowledge of sample thickness in terms of nuclides per area, the compensation for impurities in the sample.

Here, we want to highlight a limited number of high-accuracy total cross-section measurements. Most of these measurements make use of mono-energetic filtered beams to determine the total cross-section for a specific energy with a very low background. In particular, accuracies in the permille range were obtained for the cross-sections at these energies, about one order of magnitude more accurate than for the best conventional transmission data. Examples and the appropriate references are given in the sections below. The data by Houck are an exception.

Carbon

Before investigating the situation for oxygen, it is interesting to look into the data for a nucleus for which the cross-section is very well known: carbon.

In Table 1 a summary is given of coherent scattering lengths deduced from neutron optical measurements and from total cross-section measurements.

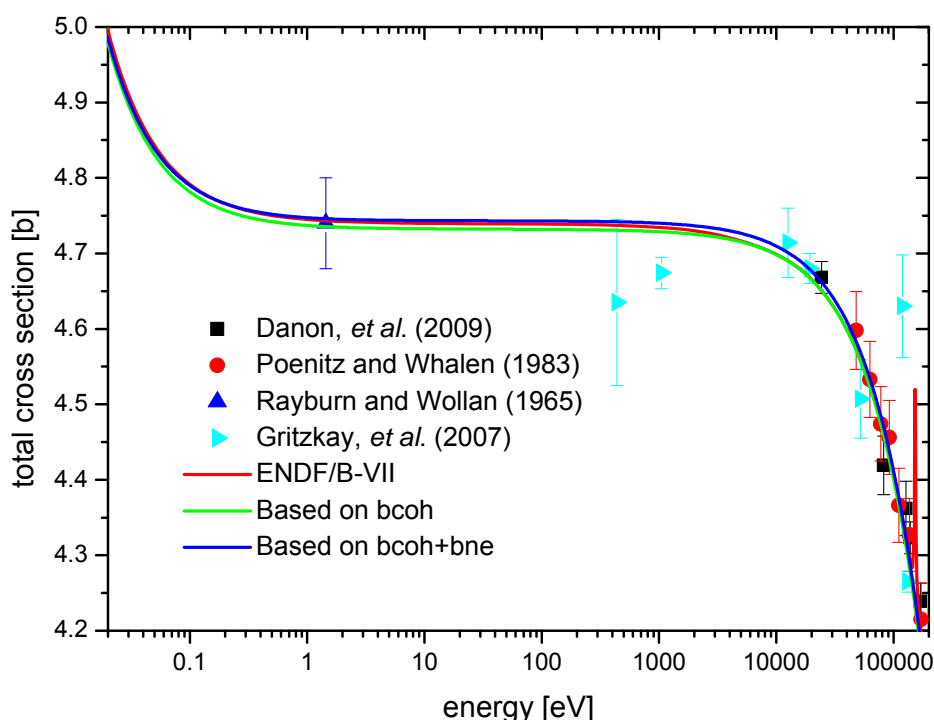
Table 1: The coherent scattering lengths for ¹²C as listed in the literature

b_c (fm)	$\sigma(b_c)$ (fm)	Method	Author(s)
6.6484	0.0013	Gravity reflectometer	Koester and Nistler (1975)
6.647	0.005	Interferometry	Freund, <i>et al.</i> (1981)
6.623	0.009	Transmission	Houck (1971)
6.660	0.006	Transmission	Dilg and Vonach (1971)

The agreement between the four values quoted in Table 1 is satisfactory, even if the spread of the values is larger than the given uncertainties. It can be concluded that, at least for the two transmission results, the uncertainty of the derived coherent scattering length should be multiplied by a factor of 2.

Using the most accurate value for the coherent scattering length (Sears, 1986), the total cross-section can be calculated using Eqs. (2-4). The results can then be compared to evaluated data files and experimental data. As can be seen in Figure 1 the agreement between available cross-section data in the literature and the cross-section derived from the coherent scattering lengths is very good; for the agreement between the calculated cross-section and the value given no ENDF/B-VII is of the order 10^{-3} over the whole energy range considered. Therefore the methodology suggested here can be applied for oxygen.

Figure 1: Comparison of carbon total cross-section data with the calculated total cross-section using the above formulas and the best value for the bound coherent scattering length



Oxygen

Neutron optical measurements

Table 2 lists the coherent scattering lengths that can be found in the literature, only considering the most accurate results. The two measurements are from two experimental groups, using two different measurement methods, one employing the Munich gravity reflectometer, the other prism deflection at NBS. Both measurements quote uncertainties of $\leq 10^{-3}$, but the values differ significantly outside their uncertainties.

Table 2: The most accurate determinations of the coherent scattering length of ¹⁶O

b_c (fm)	$\sigma(b_c)$ (fm)	Method	Author	Modified b_c (fm)
5.830	0.002	Prism deflection	Schneider (1976)	5.830
5.801	0.006	Gravity reflectometer	Nistler (1974)	5.804

As a first step in an attempt to resolve the differences, the most recent recommended values of scattering lengths used for deriving the oxygen quantities are used to recalculate the values, i.e. the measurements made use of oxygen containing compounds and had to compensate for the additional nuclei besides ¹⁶O in the sample.

The value of the coherent scattering length of oxygen was measured by Nistler (1974) by measuring the reflection of a variety of H₂O and D₂O mixtures, using the hydrogen coherent scattering length as input. The value for the hydrogen scattering length used $b_H = -3.740 \pm 0.003$ fm (Koester and Nistler, 1975) was derived by the same group, using the same technique of gravitational reflection measurements. The neutron optical properties of a variety of organic liquids had been measured, and a simultaneous analysis provided scattering lengths of H, C and Cl. The most accurate value of the carbon scattering length is due to that measurement. As we were able to demonstrate, for carbon a very good agreement between scattering lengths and cross-section measurements can be observed.

The best value for hydrogen that can be found in the literature is $b_H = -3.471 \pm 0.001$ fm (Schoen, 2003), a value compiled from the complete set of experimental data. When using this value for correcting the values quoted by Nistler (1974), the change to the coherent scattering length of oxygen is marginal (last column Table 1).

A similar observation can be made for the work of Schneider (1976). In that work the oxygen scattering length is derived using a value for the scattering length of Si as $b_{Si} = 4.1485 \pm 0.0008$ fm. Using the most accurate value in literature $b_{Si} = 4.15071 \pm 0.00022$ fm (Ioffe, 1998) the induced change in the deduced scattering length of oxygen is negligible and cannot explain the difference with the value of Nistler.

Therefore, even when using the most recent – or most accurate – values of the scattering lengths of the nuclei in the compounds used for determining the ¹⁶O scattering length, the discrepancy between the values of Nistler and Schneider cannot be resolved. Even checking the papers and the given numerical values in detail does not provide any satisfactory explanation of the differences, nor does this indicate which of the work groups was especially optimistic in the estimated uncertainties.

The natural compromise is therefore to adopt the average of the two experimental scattering lengths as the evaluated value and half the difference of the two as one standard deviation: $b_{(^{16}\text{O})} = 5.816 \pm 0.015$ fm. Despite the significant increase in uncertainty relative to the experiments the relative uncertainty of this compromise is still very good: 0.26%.

Below we check the consistency of this evaluated coherent scattering length with high-accuracy total cross-sections measured at 130, 1 970 and 23 500 eV.

Transmission measurements

Three very accurate cross-section measurements for single energies can be found in the literature (Dilg, Koester and Nistler, 1971; Koester, Waschowski and Meier, 1990; Block, *et al.* 1975). Each of these works used the filtered beam technique. Dilg, Koester and Nistler (1971) and Koester, Waschowski and Meier (1990) used resonance filtered beams at the Munich research reactor. For the measurements at 130 eV resonance scattering at Co was used (Dilg, Koester and Nistler, 1971), and for the 1970 eV resonance a combination of Cu and Se resonance scattering was employed (Koester, Waschowski and Meier, 1990). Block, *et al.* (1975) used a Fe filter at the Kyoto electron linac in combination with time-of-flight to obtain an accurate cross-section at 23 500 eV.

From the measured total cross-sections, scattering lengths of oxygen can be derived, using the above formulas. The given uncertainties only reflect the uncertainties of the cross-section measurements. Especially for the higher energy points the effective range correction will induce an additional component to the uncertainty. It should be noted

that for a light nucleus such as oxygen it is important to include the neutron-electron scattering in the analysis of the total cross-section data, as this scattering contributes approximately 0.01 fm to the scattering length at energies above 0.1 eV.

The value of Dilg, Koester and Nistler (1971) for ¹⁶O is derived from a measurement of SiO₂ by subtracting a measured value for the Si cross-section of 2.0442±0.0018 b. Using the latest, most accurate measurement of the coherent scattering length of natural Si (Ioffe, 1998), one finds a cross-section of 2.0385 b. Adopting this value instead of Dilg's value for Si, the extracted oxygen cross-section changes by approximately 0.1% to 3.764 b and the extracted coherent scattering length will change by 0.002 fm, a value smaller than the experimental uncertainty.

Koester, Waschkowski and Meier (1990) measured the total cross-section of Si and SiO₂ at 1 970 eV and the value of Si that was subtracted is 2.019 b. Using the scattering length of Ioffe, *et al.* [18], one can estimate the cross-section of Si at 1 970 eV to be 2.037 b, using the expressions given earlier. This will only slightly modify the extracted oxygen cross-section, in fact only a change within the experimental uncertainty is observed. The derived modified coherent scattering length is given in Table 3.

Table 3: Measured total cross-sections for ¹⁶O and their modification on the basis of corrections to the Si cross-section

Neutron energy (eV)	Reference	Measured SiO ₂ σ(b)	Extracted ¹⁶ O	Extracted ¹⁶ O b _c (fm)	Modified ¹⁶ O σ(b)	Modified ¹⁶ O b _c (fm)
130	Dilg, Koester and Nistler (1971)	9.566 (13)	3.761 (7)	5.803 (6)	3.764 (7)	5.805 (6)
1 970	Koester, Waschkowski and Meier (1990)	9.56 (5)	3.77 (3)	5.815 (30)	3.750 (30)	5.800 (30)
23 500	Block, <i>et al.</i> (1975)		3.736 (7)	5.820 (6)	n/a	n/a

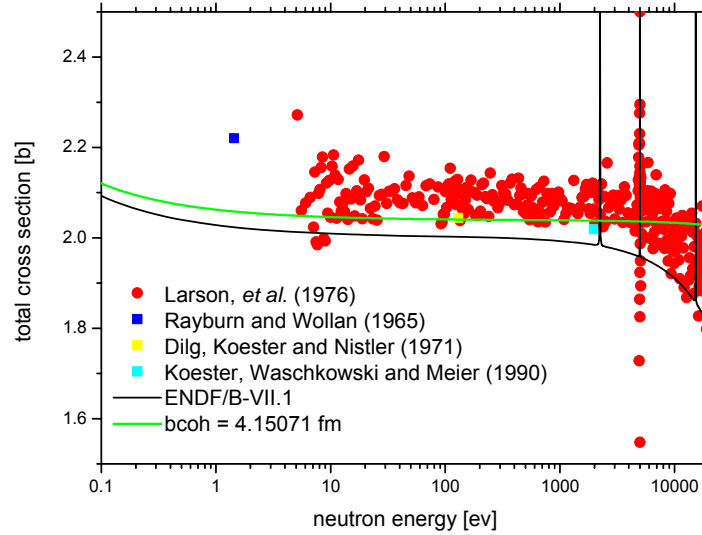
Block, *et al.* (1975), measured Be, Si, Al and their oxides. The value of the oxygen cross-section has then been derived as a mean of the difference of the elemental sample and the respective oxide sample. We refrain from trying to adjust the cross-section in this case, as the uncertainties connected with the correct energy dependence of the cross-section are too large, due to the high energy of the measurement.

It can be observed that the total cross-section of silicon, derived from the ENDF/B-VII.1 files of ²⁸Si, ²⁹Si and ³⁰Si is lower than the curve derived from the measured coherent scattering length, and the evaluation does not agree very well with the available experimental data. It should be noted that the systematic uncertainty quoted in Larson, *et al.* (1976) is 3% (not indicated in the plot), therefore the ENDF/B-VII.1 file will agree with that set of data within the quoted uncertainties. Even so, it is not understood why the evaluation does not match the data by Larson, *et al.* or even better: the value by Dilg, Koester and Nistler (1971). The deviation at energies above approximately 2 keV of the cross-section derived by Eqs. (2-4) from the experimental data is due to neglecting of the resonance contributions. This is easily fixed by a proper R-matrix analysis.

Conclusion

The cross-section points derived by transmission measurements are in agreement with the cross-sections calculated based on the coherent scattering length. This point already evident from Table 3 is highlighted in another way in Figure 2. This adds support to the suggestion given above to adopt the average of the two most accurate values of Schneider and Nistler as the evaluated ¹⁶O coherent scattering length and use half the spread of the two measured values for the uncertainty: $b_c(^{16}O) = 5.816 \pm 0.015$ fm.

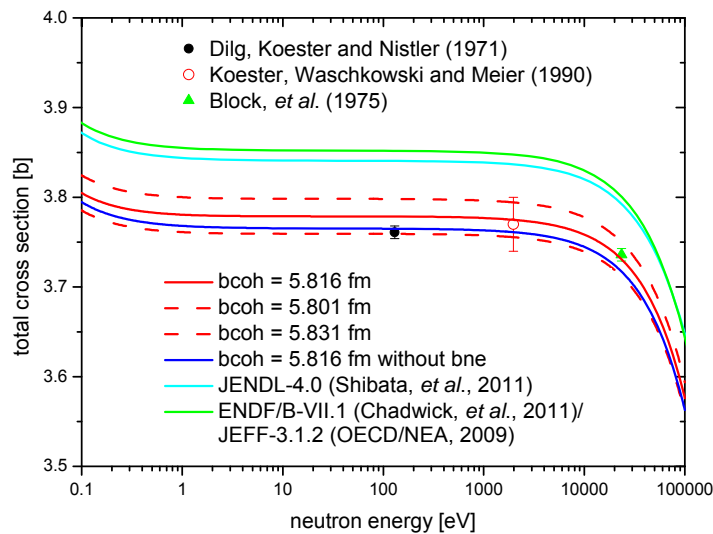
Figure 2: Measured total silicon cross-section, compared to ENDF/B-VII.1 and cross-section values derived with Eq. (4), with $b_{coh} = 4.15071$ fm and adding a $1/v$ capture contribution



Therefore a total scattering cross-section of 3.765 ± 0.025 b can be recommended for use in the energy range between 0.5 and 2 000 eV. To derive this value the neutron-electron scattering length had to be included, otherwise a difference of approximately 0.5% would be observed. The inclusion of the neutron-electron scattering length will introduce an energy dependence of the cross-section; this dependence can be neglected in the suggested energy range at present accuracy levels, but should be correctly accounted for outside that region.

Figure 3 also shows the need for modification of existing evaluations in the energy range considered here. We note that JENDL-3.3 (Shibata, *et al.*, 2002) (not shown in the figure) is nearly identical with the cross-section value recommended here. The total cross-section of ENDF/B-VII.1 (Chadwick, *et al.*, 2011) and JEFF-3.1.2 (OECD/NEA, 2009) are indistinguishable on the scale of Figure 3.

Figure 3: Comparison of the high-precision total cross-section data with the estimate based on the above formulas and the evaluated bound coherent scattering length



References

- Block, R., *et al.* (1975), "Precision Neutron Total Cross Section Measurements Near 24 keV", *J. Nucl. Sci. Techn.*, 12, 1.
- Chadwick, M.B., *et al.* (2011), "ENDF/B-VII.1 Nuclear Data for Science and Technology: Cross Sections, Covariances, Fission Product Yields and Decay Data", *Nucl. Data Sheets*, 112, 2887-2996.
- Danon, Y., *et al.* (2009), "Beryllium and Graphite High-Accuracy Total Cross-Section Measurements in the Energy Range from 24-900 keV", *Nuclear. Sci. and Eng.*, 161, 321.
- Dawidowski, K., *et al.* (2013), "Neutron Scattering Lengths and Cross Section", *Exp. Meth. Phys. Sci.*, 44, 471.
- Dilg, W. and H. Vonach (1971), "Präzise Messung der totalen Wirkungsquerschnitte von Wismut, Blei, Silizium und Kohlenstoff für 130 eV Neutronen", *Z. Naturforsch.*, 26a, 442.
- Dilg, W., L. Koester and W. Nistler (1971), "The Neutron-Deuteron Scattering Lengths", *Phys. Lett.*, 36 B, 208.
- Freund, A.K., *et al.* (1985), "Determination of the Coherent Scattering Length of Carbon Using Neutron Interferometry", *Nucl. Instrum. Meth. A*, 234, 394.
- Gritzky, O., *et al.* (2007), "The Total Neutron Cross Section for Natural Carbon in the Energy Range 1 to 148 keV", *Proc. of International Conference on Nuclear Data for Science and Technology*, O. Bersillon, *et al.* (eds.), p. 543.
- Houk, T.L. (1971), "Neutron-Proton Scattering Cross Section at a Few Electron Volts and Charge Independence", *Phys. Rev. C*, 3, 1886.
- Ioffe, A., *et al.* (1998), "Precision Neutron-Interferometric Measurements of the Coherent Neutron-Scattering Length in Silicon", *Phys. Rev. A*, 58, 1475.
- Koester, L. and W. Nistler (1975), "New Determination of the Neutron-Proton Scattering Amplitude and Precise Measurements of the Scattering Amplitudes on Carbon, Chlorine, Fluorine and Bromine", *Z. Physik A*, 272, 189.
- Koester, L., W. Waschkowski and J. Meier (1990), "Cross Sections for Neutron of 1 970 eV and Contributions to Fundamental Neutron Interactions", *Z. Physik A*, 337, 341.
- Kopecky, S., *et al.* (1997), "Neutron Charge Radius Determined from the Energy Dependence of the Transmission of Liquid ²⁰⁸Pb and ²⁰⁹Bi", *Phys. Rev. C*, 56, 2229.
- Larson, D.C., *et al.* (1976), *Measurement of the Neutron Total Cross Section of Silicon from 5 eV to 730 keV*, ORNL-TM-5618, Oak Ridge National Laboratory, Oak Ridge, TN.
- Nistler, W. (1974), "Messung der kohärenten Streuamplitude für die Neutron-Deuteron Wechselwirkung am Neutronenschwerkraftrefraktometer des FRM", *Z. Naturforsch.*, 29a, 1284.
- OECD/NEA (Organisation for Economic Co-operation and Development/Nuclear Energy Agency) (2009), *The JEFF-3.1.1 Nuclear Data Library*, JEFF Report 22, A. Santamarina, D. Bernard and Y. Rugama (eds.), OECD/NEA, Paris.

- Poenitz, W.P. and J.F. Whalen (1983), *Neutron Total Cross Section Measurements in the Energy Region from 47 keV to 20 MeV*, ANL/NDM-80.
- Rauch, H. and W. Waschkowski (2000), "Neutron Scattering Lengths", *Low-Energy Neutrons and Their Interaction with Nuclei and Matter 1*, Landolt-Bornstein, Chapter 6, Springer Verlag, Berlin.
- Rayburn, L.A. and E.O. Wollan (1965), "Total Neutron Cross Sections at 1.44 eV", *Nucl. Phys.*, 61, 381.
- Schneider, C.S. (1976), "Coherent Nuclear Scattering Amplitude of Germanium, Copper and Oxygen for Thermal Neutrons", *Acta Cryst. A*, 32, 375.
- Schoen, K., *et al.* (2003), "Precision Neutron Interferometric Measurements and Updated Evaluations of the n-p and n-d Coherent Neutron Scattering Lengths", *Phys. Rev. C*, 67, 044005.
- Sears, V.F. (1982), "Fundamental Aspects of Neutron Optics", *Phys. Reports*, 82, 1, and references therein.
- Sears, V.F. (1992), "Neutron Scattering Lengths and Cross Sections", *Neutron News*, 3, 26.
- Sears, V.F. (1986), "Electromagnetic Neutron-Atom Interactions", *Phys. Reports*, 141, 281, and references therein.
- Shibata, K., *et al.* (2002), "Japanese Evaluated Nuclear Data Library Version 3 Revision-3: JENDL-3.3", *J. Nucl. Sci. Technol.*, 39, 1125.
- Shibata, K., *et al.* (2011), "JENDL-4.0: A New Library for Nuclear Science and Engineering", *J. Nucl. Sci. Technol.*, 48 (1), 1-30.

Estimation of neutron cross-sections for ¹⁶O up to 5.2 MeV through R-matrix analysis

Satoshi Kunieda,^a Toshihiko Kawano,^b Mark Paris,^b
Gerry Hale,^b Keiichi Shibata,^a Tokio Fukahori^a

^aJapan Atomic Energy Agency,
Tokai-mura, Naka-gun, Ibaraki, Japan

^bLos Alamos National Laboratory,
Los Alamos, New Mexico, United States

Abstract

There are differences among experimental cross-sections for ¹⁶O, which make the evaluated data still uncertain. R-matrix is rigorous and straightforward to the quantum mechanical theory. We estimate the neutron cross-sections for ¹⁶O up to 5.2 MeV through R-matrix analysis. In this work, particular attention is paid to issues in the scale of (n,α) reaction cross-sections and hydrogen contents in some of the experimental total cross-sections. Our preliminary results suggest that those problems could be solved/reduced due to the physical constraints imposed by the theory.

Introduction

The differences among measured data make the evaluated cross-sections as yet uncertain, which consequently affects the integral calculation more or less. Oxygen is one of the important elements in a number of nuclear applications. However, all the nuclear data libraries in the world have issues to be solved as follows:

- There are systematic differences among the experimental ¹⁶O(n,α)¹³C or the inverse reaction cross-sections. The discrepancies reach up to about 30%, rendering the evaluated cross-sections as yet uncertain.
- There are ~3% differences among the experimental total cross-sections below 10 keV, which makes the present evaluations larger. The most probable reason is due to plausible amounts of hydrogen content remaining in some of the measurements, which consequently increases the evaluated values.
- There are increasing demands for giving uncertainties in evaluated cross-sections to estimate the margin of integral calculations. However, the evaluated values are low fidelity, which is based only on the experimental information.

The purpose of this study is to reduce/solve those issues as they are mutual concerns in the world. The R-matrix theory is rigorous and straightforward to the quantum mechanics, which brings physical constraints to the behaviour of cross-sections. We carry out multi-channel R-matrix analyses for ¹⁷O system – n+¹⁶O and α+¹³C to estimate both the neutron elastic-scattering and ¹⁶O(n,α)¹³C reaction cross-sections up to 5.2 MeV. The measured data we use are six sets of total cross-sections (Cierjacks, *et al.*, 1968, 1980;

Schrack, Schwartz and Heaton, 1972; Perey, Love and Kinney, 1972; Johnson, *et al.*, 1973; Ohkubo, 1987) and recent experimental data of $^{16}\text{O}(n,\alpha)^{13}\text{C}$ and $^{13}\text{C}(\alpha,n)^{16}\text{O}$ reaction cross-sections (Harissopoulos, *et al.*, 2005; Giorganis, *et al.*, 2007). Since there are differences among measured data, we also try to search for some experimental parameters as well as the R-matrix parameters in this analysis. We present preliminary results of cross-sections and uncertainty that are “physically” constrained by the theory.

A multi-channel R-matrix code (AMUR)

A multi-channel R-matrix code (AMUR) is now under development based on the formalism of Wigner-Eisenbud (1947). As long as we have enough information on the nuclear structure, the theory gives exact solutions without any approximation. The code is designed to calculate cross-sections not only for neutron but also charged-particle reactions. Although the photon channels are not yet included in the current version, the code can be applied to the analysis for light nuclei since the neutron radiative-capture cross-sections are negligible as in the order of micro-barn.

The code also has functions of the parameter search with the generalised least-square method based on the Bayes’ theorem. Therefore, the values of R-matrix parameter can be deduced from experimental cross-sections with covariance/uncertainty. Furthermore, if necessary, unknown experimental values such as renormalisation, possible background terms and even the resolution could be given as parameters to be searched for.

Analysis for ^{17}O system

Channels and theoretical parameters

The maximum neutron energy is set to 5.2 MeV to study a simple case. The threshold of the (n,α_0) reaction is about 2.4 MeV, and the other reactions are still closed up to 5.2 MeV. Therefore, we only consider two partitions in this R-matrix analysis, $n+^{16}\text{O}_{g.s.}$ and $\alpha+^{13}\text{C}_{g.s.}$. For the level assignments of the compound nucleus ^{17}O , we followed those given in the latest version of *Nuclear Data Sheets* except for a few levels. We considered the levels of $J = 1/2^{\pm}$, $3/2^{\pm}$, $5/2^{\pm}$ and $7/2^{\pm}$ which can be excited by the incoming partial waves of $l = 0$ to 4.

The R-matrix parameters to be searched for are the channel radii, reduced width amplitudes and the energy eigenvalues for each level in the compound nucleus ^{17}O . The contributions from the negative and distant levels are also treated as parameters, except for the levels $J = 5/2^{\pm}$ and $7/2^{\pm}$ in which the effect is found to be very small.

Experimental data used in this analysis

Table 1 lists the measured cross-sections preliminarily used in the parameter search. Those experimental data complement the energy range of our interests. We used six sets of total cross-sections that have been measured with the time-of-flight (TOF) method. They are given with a sufficiently fine resolution to separate the resonances. Especially, the experimental data of Cierjacks, *et al.* (1980) are given with very fine resolution, which identify even very small and/or narrow resonances.

Table 1: Experimental total cross-sections used in the parameter search

Reaction	Author(s)	Year	Lab	Adopted range
O(n,total)	Cierjacks, <i>et al.</i>	1968	KIT	0.5 MeV < E _n < 5.2 MeV
	Schrack, Schwartz and Heaton	1972	NBS	0.5 MeV < E _n < 5.2 MeV
	Perey, Love and Kinney	1972	ORNL	0.5 MeV < E _n < 5.2 MeV
	Johnson, <i>et al.</i>	1974	ORNL	50 keV < E _n < 5.2 MeV
	Cierjacks, <i>et al.</i>	1980	KIT	3.1 MeV < E _n < 5.2 MeV
¹⁶ O(n,total)	Ohkubo	1984	JAERI	1 keV < E _n < 940 keV
¹³ C(α,n) ¹⁶ O	Harissopulos, <i>et al.</i>	2005	RUB	E _{thre} < E _a < 3.5 MeV
¹⁶ O(n,α) ¹³ C	Giorginis, <i>et al.</i>	2007	IRMM	3.9 MeV < E _n < 5.2 MeV

Since experimental ¹⁶O(n,α)¹³C reaction cross-sections are limited, we analysed the ¹³C(α,n)¹⁶O reaction cross-sections recently measured by Harissopulos, *et al.* (2005). Since the measured data are given with a fine resolution over the corresponding energy range, they are very useful to deduce the parameter values for the alpha-particle channels. We also analysed measured ¹⁶O(n,α)¹³C reaction cross-sections of Giorginis, *et al.* (2007) although the number of data points are rather limited.

Experimental parameters

A number of efforts have been devoted to the uncertainty estimation in experimental studies. However, measurements for the same observable do not necessarily agree well. This suggests there could be unknown sources of uncertainty in each measurement, which consequently make the evaluated cross-sections still uncertain. It is expected that those issues should be solved/reduced through the R-matrix fit since the theory imposes unitarity constraints in the analysis. Hence, as described in the next paragraph, we introduced some experimental parameters in our fits to lead the cross-sections toward more reasonable values.

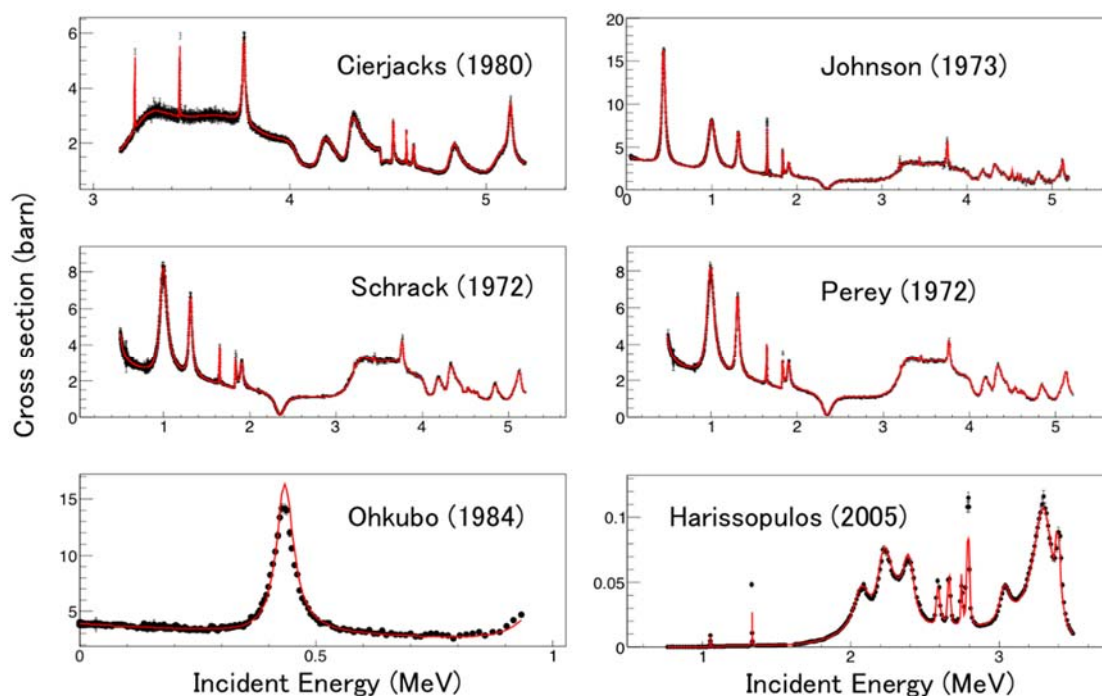
One of the issues in measurement could be, more or less, the normalisation, which would be a source of the systematic uncertainty. Indeed, there are systematic difference between previous (Bair and Haas, 1973) and recent (Harissopulos, *et al.*, 2005; Giorginis, *et al.*, 2007) measurements for (n,α) and/or (α,n) reaction cross-sections. The differences reach up to about 30%, which exceed the uncertainty given in the literature. In this analysis, we introduce a renormalisation factor for each measurement, and it is treated as a parameter to be searched for in the R-matrix fit.

There is an inconsistency between the total cross-section of Ohkubo (1987), Johnson, *et al.* (1973) and a number of very accurate experimental data below about 10 keV (Dilg, Koester and Nistler, 1971; Moxon, Endacott and Jolly, 1974; Block, *et al.*, 1975; Koester, Waschkowski and Meier, 1990). A plausible reason is because there is a small amount of hydrogen content in the experimental data of Ohkubo and Johnson, *et al.* Therefore, we tried to search for the effective hydrogen cross-sections in the measurements: the hydrogen cross-sections [taken from ENDF/B-VII.1 (Chadwick, *et al.*, 2011)] weighted by a scale parameter are added to the R-matrix calculations, where the scale parameter is determined in the fitting procedure.

Examples of results

All the theoretical and experimental parameters were deduced through simultaneous analysis to those measured data described above. In the fitting procedure, the calculations were broadened with the experimental resolution (preliminary, the resolution is treated as one of the parameters to be searched for if the information is missed/limited in the literature). We successfully fitted all the experimental cross-sections as plotted in Figure 1.

Figure 1: Examples of fitted results



Values of renormalisation

Table 2 lists renormalisation parameters obtained for each measurement. Those values were determined with very small uncertainty due to the unitarity constraint from the R-matrix theory. This suggests the analysis is nearly independent of systematic differences among the measurements. The renormalisation values we obtained are nearly equal to 1.0 for total cross-sections. However, the values were found to be about 1.5 both for the $^{13}\text{C}(\alpha, n)^{16}\text{O}$ and $^{16}\text{O}(n, \alpha)^{13}\text{C}$ measurements. Those values were guided by the measured total cross-sections since there were correlations between the different reactions. It should be noted that the estimated $^{13}\text{C}(\alpha, n)^{16}\text{O}$ cross-sections are consistent with the measured data of Bair and Haas (1973).

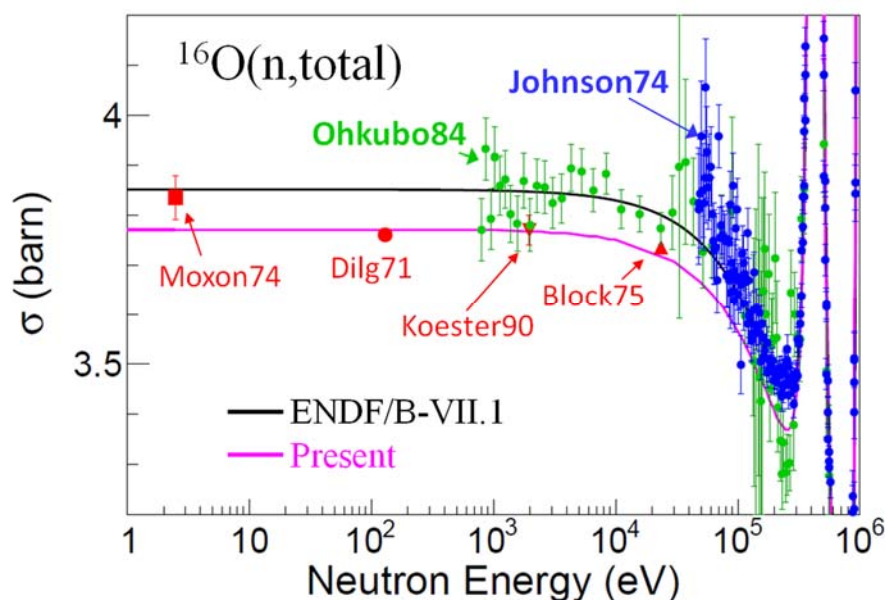
Hydrogen content in measurements

The values of ratio to the hydrogen cross-sections from ENDF/B-VII.1 was found to be $0.01665 \pm 6.02\%$ and $0.00988 \pm 8.38\%$ for experimental data of Ohkubo and Johnson, *et al.*, respectively. That means the corresponded plausible hydrogen contents could be 346 ± 21 (mb) and 205 ± 17 (mb). Figure 2 shows the calculated total cross-sections in a lower energy range with experimental data. If the plausible hydrogen content was not considered in R-matrix analysis, results overestimated experimental data of Dilg, Koester and Nistler (1971), Block, *et al.* (1975) and Koester, Waschowski and Meier (1990) by about 3% or

Table 2: Renormalisation parameters obtained for each measurement

Reaction	Measurement	Renormalisation to measurement
¹⁶ O(n,total)	Cierjacks, <i>et al.</i> (1968)	0.967 ± 0.15%
	Schrack, Schwartz and Heaton (1972)	0.982 ± 0.09%
	Perey, Love and Kinney (1972)	0.996 ± 0.09%
	Johnson, <i>et al.</i> (1973)	1.018 ± 0.09%
	Cierjacks, <i>et al.</i> (1980)	1.032 ± 0.35%
¹⁶ O(n,total)	Ohkubo (1987)	0.997 ± 0.02%
¹³ C(α,n) ¹⁶ O	Harissopulos, <i>et al.</i> (2005)	1.521 ± 1.14%
¹⁶ O(n,α) ¹³ C	Giorginis, <i>et al.</i> (2007)	1.487 ± 1.31%

Figure 2: Improved total cross-sections in a lower energy range



more as the value given in ENDF/B-VII.1. On the other hand, the situation is essentially improved if the credible hydrogen contents are considered in the R-matrix analysis as done in the present study.

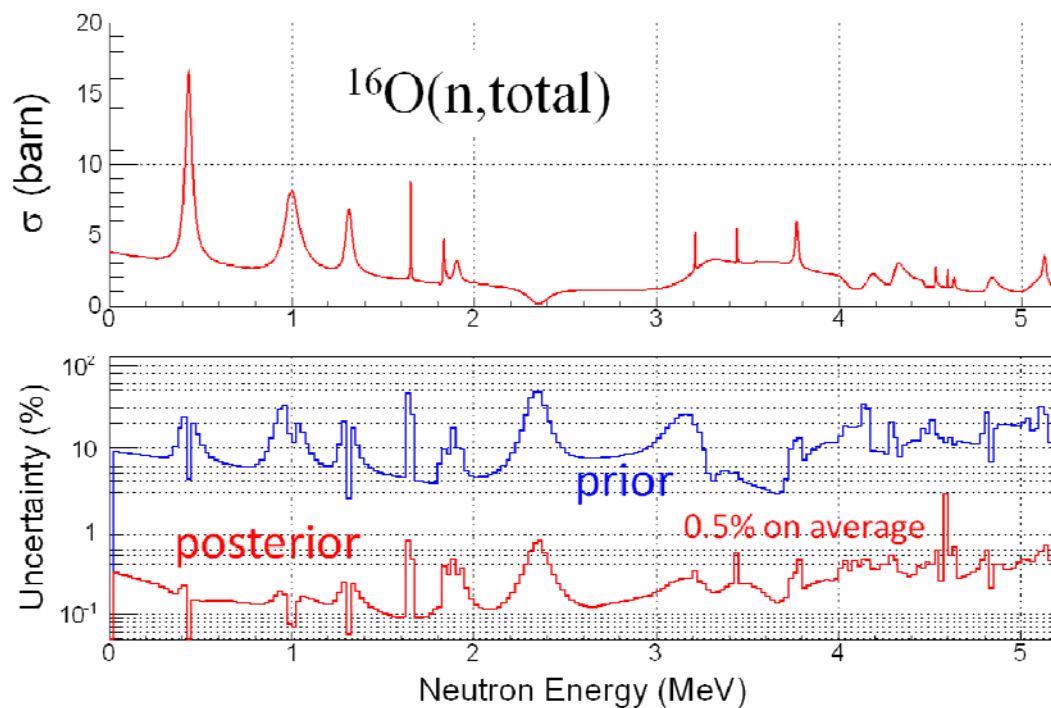
Uncertainty of cross-sections

As an example, the present total cross-section is illustrated with uncertainty in Figure 3. The uncertainty values we obtained surely reflect both the experimental and theoretical knowledge. The values obtained are 0.5% for total and 2.5% for ¹⁶O(n,α)¹³C cross-sections on average. They are lower than the difference among the measurements since the physical constraints have been imposed by R-matrix theory. However, the present results are still preliminary because only the uncertainties of theoretical parameters were propagated to those for cross-sections.

Preliminary conclusions

Neutron cross-sections were estimated with uncertainty for ¹⁶O below $E_n = 5.2$ MeV through R-matrix analysis to the measurements. We entrusted the unitarity constraints from the theory to estimate the absolute values of cross-sections. Plausible amounts of hydrogen in some of the experimental total cross-sections were also deduced. Our preliminary ¹³C(α ,n)¹⁶O and ¹⁶O(n, α)¹³C reaction cross-sections are larger than the recent experimental data by a factor of about 1.5, but the total cross-sections obtained were found to be consistent with a number of accurate measurements in the lower energy region. Further experimental studies and benchmark calculations should be carried out to make sure our results are reasonable.

Figure 3: Present total cross-sections with uncertainty



Acknowledgements

The authors would like to thank Dr. A. Plompen (IRMM) and Dr. C. Lubitz (KAPL), who provided very useful experimental knowledge. Author S.K. is also grateful to Dr. O. Iwamoto (JAEA) who gave valuable comments on this work.

References

- Bair, J.K. and F.X. Haas (1973), "Total Neutron Yield from the Reactions $^{13}\text{C}(\alpha, n)^{16}\text{O}$ and $^{17,18}\text{O}(\alpha, n)^{20,21}\text{Ne}$ ", *Phys. Rev. C*, 7, 1356.
- Block, R.C., *et al.* (1975), "Precision Neutron Total Cross Section Measurements Near 24 keV", *J. Nucl. Sci. Technol.*, 12, 1 (1975).
- Chadwick, M.B., *et al.* (2011), "ENDF/B-VII.1 Nuclear Data for Science and Technology: Cross Sections, Covariances, Fission Product Yields and Decay Data", *Nucl. Data Sheets*, 112, 2887.
- Cierjacks, S., *et al.* (1968), *High Resolution Total Neutron Cross-Sections Between 0.5 and 30 MeV*, Kernforschungszentrum Karlsruhe Reports, No. 1000.
- Cierjacks, S., *et al.* (1980), "High Precision Time-of-Flight Measurements of Neutron Resonance Energies in Carbon and Oxygen Between 3 and 30 MeV", *Nucl. Instr. Meth.*, 169, 185-198 (1980).
- Dilg, W., L. Koester and W. Nistler (1971), "The Neutron-Deuteron Scattering Lengths", *Phys. Lett. B*, 36, 208.
- Giorginis, G., *et al.* (2007), "The Cross Section of the $^{16}\text{O}(n, \alpha)^{13}\text{C}$ Reaction in the MeV Energy Range", *Conf. on Nucl. Data for Sci. and Technology*, Nice, France, Vol. 1, p. 525.
- Harissopulos, S., *et al.* (2005), "Cross Section of the $^{13}\text{C}(\alpha, n)^{16}\text{O}$ Reaction: A Background for the Measurement of Geo-Neutrinos", *Phys. Rev. C*, 72, 062801.
- Johnson, C.H., *et al.* (1973), *The $^{16}\text{O}+n$ Total Cross Section: Diagnostics and Refinements*, ORNL-4937, Oak Ridge National Laboratory, Oak Ridge, TN.
- Koester, L., W. Waschowski and J. Meier (1990), "Cross Sections for Neutrons of 1 970 eV and Contributions to Fundamental Neutron Interactions", *Z. Phys. A*, 337, 341 (1990).
- Moxon, M.C., D.A.J. Endacott and J.E. Jolly (1974), *Neutron Total Cross Section Measurements*, A.E.R.E. Harwell Reports, No. 20, p. 29, United Kingdom.
- Ohkubo, M. (1987), *Neutron Total Cross Section Measurements on Oxygen, Aluminum and Carbon Below 930 keV*, JAERI-M 86-193, JAERI, Japan.
- Perey, F.G., T.A. Love and W.E. Kinney (1972), *A Test of Neutron Total Cross-Section Evaluations from 0.2 to 20 MeV for C, O, Al, Si, Ca, Fe, and SiO₂*, Oak Ridge National Laboratory Reports, 4823, Oak Ridge, TN.
- Schrack, R.A., R.B. Schwartz and H.T. Heaton (1972), "Neutron Total Cross Sections for Oxygen and Calcium from .5 to 20 MeV", *Bulletin of the American Physical Society*, 17, 555.
- Wigner, E.P. and L. Eisenbud (1947), "Higher Angular Momenta and Long Range Interaction in Resonance Reactions", *Phys. Rev.*, 72, 29.

Evidence for a 3% error in the experimental and evaluated databases for the ¹⁶O neutron scattering and total cross-sections

C.R. Lubitz, P.K. Romano, T.H. Trumbull, D.P. Barry
Knolls Atomic Power Laboratory, Bechtel Marine Propulsion Corp.
Schenectady, NY, United States

Abstract

Kozier, et al. (2013) called attention to the fact that the ¹⁶O thermal scattering cross-section in most current evaluated libraries is ~3% above the long-standing coherent-scattering value of 3.761 barns as given in the Atlas of Neutron Resonances. In this paper we present evidence that this discrepancy is not only at 2 200 m/s but occurs in various high-energy experimental data sets. From there it found its way into most current evaluations, and 2 200 m/s is simply a "high visibility" point. Careful comparison between suspect experiments and high-precision experiments which do not have the error supports the idea that the former misinterpreted the room temperature thermal scattering cross-section as an "unbroadened" zero-Kelvin value. The ratio of those two numbers is 1.0315.

Introduction

The purpose of this paper is to provide evidence for the hypothesis that some very competent experimentalists and evaluators were insufficiently aware of the fact that the 2 200 m/s scattering cross-section for ¹⁶O is 3.15% higher at room temperature than it is at zero Kelvin. In 2012 Kozier, *et al.*, called attention to the fact that the thermal scattering cross-section in most current evaluated libraries is ~3% above the long-standing coherent-scattering value of 3.761 barns given in the *Atlas of Neutron Resonances* and we hypothesise that the 3% they discuss is the result of the temperature difference.

A detailed discussion would require more than the space allotted here, so we will just mention six reasons why such a situation could have arisen and gone unnoticed for more than forty years:

- Inspection of the unbroadened (0 K, free-atom, target-at-rest) cross-sections in any evaluated set of ¹⁶O cross-sections and their room-temperature (293.6 K) Doppler-broadened counterparts shows that above about 2 eV they are identical. You have to look carefully to see the low-energy tail.
- Inspection also shows that the 0 K scattering cross-section is constant at low energy, over several hundred eV at least. This is expected because there are no narrow ¹⁷O bound states (negative-energy resonances), or positive-energy resonances close enough to affect the cross-section. There are bound states which contribute to the low-energy cross-section but they are broad single-particle states whose positive energy tails vary observably only over much wider energy intervals.

Note: The low-energy scattering cross-section in ENDF/B-VI.8, VII.0 and VII.1, which was inserted into the LANL ENDF/B-VI.8 evaluation to correct a trend with

leakage (Caro, 1998) is an exception to the previous statement. Apparently the file which KAPL supplied to LANL inadvertently subtracted the capture cross-section from the scattering thereby causing it to decrease near zero energy instead of being flat. It also has a small rise of unknown origin to a peak of 3.852 at 31.855 eV which is unphysical. These errors carried over to JEFF-3.1, 3.1.1, 3.1.2, and GENDL-3.1 although JEFF-3.1.2 corrected the small rise. The errors have no technological significance but should be corrected.

- A Doppler-broadened constant cross-section is, e.g. Larson, *et al.* (1998):

$$\frac{\sigma_D(E)}{\sigma_0} = \left[\frac{1}{\sqrt{\pi x}} \right] \exp(-x^2) + \left(1 + \frac{1}{2x^2} \right) \operatorname{erf}(x) \quad (1)$$

with $x = \sqrt{EA/T}$; E = neutron energy in eV, A = mass ratio, T = temperature in eV.

At low energy, $\sigma_D(E)$ becomes “ $1/v$ ”. At 2 200 m/s and room temperature 293.6 K, $E = T = .0253$ eV and $x = \sqrt{A}$. Even for low A , the exponential is small and the error function is ~ 1.0 , so that:

$$\frac{\sigma_D(E)}{\sigma_0} = 1 + 1/2A$$

This is 1.0315 for ¹⁶O (Lubitz, 2008).

- Larson, *et al.* (1998) emphasised that the commonly-used high-energy form of the formula neglects the “small term” in the derivation and loses the low-energy rise. It is possible that a user of that broadening method, seeing a flat cross-section at thermal, would be unaware of the error, and taking a room temperature 2 200 m/s scattering cross-section from some evaluated data set, would unknowingly get a value 3.15% too high. Since the $1/v$ rise is gone above ~ 2 eV, the appropriate extrapolation of a high-energy scattering cross-section to thermal is flat, but to the 0 K value, not room temperature. An additional factor tending to obscure the extrapolation is that the total cross-section rises at 0 K because of capture, and that is invariant with temperature.
- Another unappreciated fact is that neutron optics measurements of the coherent scattering length give a 0 K value irrespective of the temperature of the sample or of its physical state. The implied coherent scattering cross-section obtained from the coherent scattering length, as described in the *Atlas*, or in Sears’ *Neutron Optics*, is therefore also a zero Kelvin quantity. The reason is that there is no momentum transfer at zero degrees, so $f(0)$ does not “sense” the target’s state, and hence is the same as if the target were at rest, i.e. at zero Kelvin from the standpoint of “ENDF cross-sections”.
- The thermal scattering cross-sections in the *Atlas* are mostly coherent and are therefore zero Kelvin values inconsistent with the 2 200 m/s reaction cross-sections, which are explicitly room temperature. Users believing that the ¹⁶O value in the *Atlas*, 3.761 b, would be measured in a room temperature transmission experiment at 2 200 m/s therefore have another route to a 3% error. The same comment applies to the *Standards* values for ¹H and ¹²C, which are also at 0 K, but $1/2A$ is larger and the difference is more difficult to overlook.

This investigation shows that the thermal scattering discrepancy pointed out by Kozier, *et al.* (2013), is not specific to that energy region. Cross-sections of 2 200 m/s are highly visible and the 3% was finally noticed, but it apparently found its way into the evaluations via high-energy data which were somehow “tied” to the thermal cross-section. Below we show some examples of these.

Five high-precision data points and one high-precision transmission measurement

To determine whether a given measurement or evaluation is off by 3% we need a set of values that are accurate. These are our candidates:

Schneider (1976) used prism refraction and subtracted the coherent scattering length of silicon from that of quartz (SiO₂) to get $B_{\text{coh}}(\text{O}) = 5.830(2)f$. This extremely small uncertainty has no explicit component for the fact that he measured the quartz and silicon in different experiments. His implied 0 K elastic cross-section is 3.7938 (0.0026) b and the .0253 eV total is 3.7940. An open item is to update this value to whatever B_{coh} of silicon is now.

Dilg, Koester and Nistler (1971) subtracted silicon from quartz transmission using a cobalt resonance to scatter the beam at 130 eV. They also measured the quartz and silicon in different experiments. Their value, 3.761 ± 0.007 (0.19%) is quoted in the *Atlas of Neutron Resonances*. However, ENDF/B-VII.1 silicon is 2% below their value so we quote them as 3.7831. Dilg's value of $\sigma_{\text{coh}}(\text{Si})$ was 2.0442 ± 0.0018 ; room temperature ENDF/B-VII.1 is 2.0021. This unforced update reduces the discrepancy with Schneider from 13 sigma to 4 and removes "transmission measurement support" for the *Atlas* optics value 3.7614. CIELO-O should arrange for an expert examination of the optics measurements which cluster around $B_{\text{coh}} = 5.08 f$ to see why they are so low. We also note that the 2% difference in silicon is very close to the Doppler ratio $1 + 1/2A$ for A~28. We would expect the silicon database to have the same problems as oxygen.

Koester, Waschkowski and Meier (1990) reported 3.77 ± 0.03 (0.8%) barns at 1 970 eV. They double-scattered a reactor beam from ⁶³Cu and ⁸⁰Se to get a filtered source of ~1 970 eV neutrons. Those were transmitted through silicon and quartz targets in the same apparatus. This eliminates the need to update their silicon cross-section, because the value they used cancels out when they subtract the silicon from the SiO₂. Because of the double scattering the intensity is low but their claimed uncertainty is still low by transmission standards.

Block, *et al.* (1975) subtracted iron-filtered transmission at 23.5 keV through Al₂O₃, SiO₂, Al and Si, therefore no update is needed. Their value, 3.736 ± 0.007 b is sometimes viewed as corroborating the low "optics" value, 3.761, but is actually lower because the cross-section has fallen between .0253 eV and 23.5 keV.

[Window] is a representative value for the bottom of the window at 2.35 MeV. It received a lot of attention because of its role in neutron leakage through air and water. We use the Cierjacks 1968 value, 103 ± 3 mb, but reduced to 100 because, as shown below, this data set is one we believe to be 3% too high.

Cierjacks (1980) is titled "high precision" and covers the range from 3 to 32 MeV. The liquid oxygen target eliminates the silicon uncertainty and because of its high cyclotron resolution it is widely used as an energy standard. Its unspecified normalisation to their earlier 1968 "thin sample" measurement has engendered some uncertainty in the evaluation community but we find that their EXFOR data are totally consistent with the above 5 "point" measurements, so that in combination they determine the total cross-section to about 0.5%. That does not mean they determine the true value to 0.5%. What it does mean is that any proposed cross-section which deviates from it should have some equally precise measurements to justify the difference.

The "A-B" adjustment procedure

The hypothesised error is that the room temperature 2 200 m/s cross-section was inadvertently used where the zero Kelvin value was appropriate. This could have resulted

either in a spurious multiplicative overestimate of ~3% at all energies in the experiment, or in a spurious additive constant background whose value would be about ~3% of the thermal value, ~4 barns or ~120 mb.

Either scenario would have led the experimentalists to search for unknown sources of additive background contamination, but another possibility would have been detector calibration errors that were multiplicative so for the adjusted cross-section we assumed $\sigma^{T'} = A\sigma^T + B$, where T stands for “to-be-adjusted” and A and B are unknown constants. The (so-called) “high-precision” set to which we adjust is σ^H . Of course, any data set can be “least-squares-adjusted” to any other one without regard for their accuracy.

The least-squares algorithm for A and B requires a common energy mesh for the two sets σ^T and σ^H so we insert the σ^H energy points into the σ^T energy mesh by interpolating in σ^T . Interpolating the other way, into σ^H , could alter the H-values. An unweighted chi-squared seems to work satisfactorily:

$$\chi^2 = \sum_j (\sigma_i^{T'} - \sigma_i^H)^2 = \sum_i (A\sigma_i^T + B - \sigma_i^H)^2 \quad (2)$$

The sum is over those H-points which are “overlapped” by T-points and can be interpolated. Solving the two linear equations:

$$\frac{\partial \chi^2}{\partial A} = 0; \quad \frac{\partial \chi^2}{\partial B} = 0$$

determines A and B. We use the RMS deviation between the “high-precision” file σ^H and the (interpolated) adjusted file $\sigma^{T'}$ as a figure of merit for the fit. The interpolated energies are not left in the adjusted set $\sigma^{T'}$ which remains on its original mesh but “looks like” σ^H to the extent that the transformation allows.

Since the hypothesised error, the use of a 3% high thermal cross-section, could result either in an inadvertent multiplication at 2 200 m/s by 1.0315 or in the addition of a constant, we can ask two questions:

- 1) “If you start from the value of the adjusted cross-section $\sigma^{T'}$ at 0.0253 eV, what purely multiplicative constant will give you back the raw unadjusted value?” The answer is:

$$\sigma^T / \sigma^{T'} = \frac{1}{A} (1 - B/\sigma^{T'})$$

with both cross-sections evaluated at 2 200 m/s and that “thermal ratio” is also interesting. The Sayer 2000 (“SA00”) (Sayer, *et al.*, 2000) evaluation exemplifies this situation.

- 2) “If you start from the value of the adjusted cross-section $\sigma^{T'}$ at energy E, what purely additive constant will give you back the raw unadjusted value?” The answer is:

$$\sigma^T - \sigma^{T'} = (A - 1)\sigma^T - B$$

The Cierjacks (1980) normalisation exemplifies this situation.

Testing the high-precision data set

To determine how consistent the “5 points” and Cierjacks 1980 (“CI80”) are with each other we started by comparing several modern evaluated ¹⁶O files. We found that when they were adjusted to each other the shapes were very similar, meaning that it did not matter much which one you started with. We selected Sayer 2000 (“SA00”) because their resonance parameters were included in the file we had and they claimed to have calculated angular distributions that matched KAPL’s in ENDF/B-VI.8, unchanged in VII.0 and VII.1.

Here are three comments about this evaluation, which we believe to be a high-quality effort adversely impacted by unrecognised errors in the experimental database:

- 1) It used a number of ORNL-measured data which were 3% high and renormalised CI80 up by 3.5%. Their resonance fit is excellent but 3% high.
- 2) It has the ENDF/B-VI.0 high Bair and Haas (n, α) data and the 3% high elastic/total, both of which we now believe to be wrong. Our adjustment says nothing about the scattering/(n, α) split above 3 MeV but fixes the total quite precisely.
- 3) In the resolved resonance region, 0.0 to 6.2 MeV, their 3.5%-increased CI80 data was “averaged” with the other data which they fit, and the same thing happened above 6.2 MeV where the fitting procedure and the “other data” were different and the averaging was therefore different. Implicit in that procedure is a “discontinuity” in the CI80 data at 6.2 MeV. That is consistent with normal evaluation procedures but in the present context, where we consider CI80 to be “correct”, it induces a “blip” in our adjusted SA00 data relative to EXFOR CI80. When we adjust the SA00 total cross-section to CI80 below and above 6.2 MeV the results differ by about 1%. This was only noticed late in the process and we plan to examine it more closely. It is implicit in the plots we show but 1% is difficult to see.

We then made two different adjusted files from SA00, one adjusted to the 5 points as a group (“SA00.5PTS”) and the other independently adjusted to CI80 (“SA00.SI80”). To deal with the preceding comment we used an adjustment of SA00 to the segment of CI80 between 3 MeV and 6.9 MeV, because, as shown below, it matches almost exactly the independent fit to the 5 points. Because it emphasises the resonance region, 6.9 MeV is reasonable.

Note: We found that changing the range of energies over which we fit the CI80 changed the values of A and B but these tended to cancel so that the overall result was about the same. Using 6.9 MeV gives A and B values close to the “5-point” values and therefore the greatest degree of consistency when we adjust other data sets to the combined high-precision set.

We found that SA00.5PTS and SA00.CI80 (3-6.9 MeV) were very close to each other and also matched the high-precision data very closely. It is important to keep in mind that this agreement is unforced. The five experimentalists worked independently, as did CI80. The evaluators mostly did not even fit the 5 points, and in some cases renormalised experimental input data.

Adjustment of the Sayer 2000 total cross-section to the five high-precision points “SA00.5PTS”

The results of this adjustment are:

- A = 0.9692, 1/A = 1.0318, B = 0.0017, b = 1.7 mb, RMS deviation = 6.5 mb;
- adjusted 2 200 m/s total cross-section = 3.7856;
- adjusted 2 200 m/s scattering cross-section = 3.7854 b;
- thermal (2 200 m/s) scattering cross-section ratio $\sigma^T/\sigma^{T'}$ = 3.9040/3.7854 = 1.0313.

Because Sayer 2000 was heavily weighted to 3% high measurements, the adjustment comes out almost entirely multiplicative with 1/A = 1.0318. The very small additive component, B = 1.7 mb, is in the “right direction” and the thermal ratio is 1.0313, even closer to the hypothesised value of 1.0315. The adjustment procedure is saying that the least-squares fit can be replicated very closely by applying the thermal ratio, 1.0313, to the entire evaluated set.

Adjustment of the Sayer 2000 total cross-section to Cierjacks 1980 from 3-32 MeV "SA00.CI80_3-32"

The results of this adjustment are:

- $A = 0.9576$, $1/A = 1.0443$, $B = 0.0421$, $b = 42.1$ mb, RMS deviation = 54.7 mb;
- adjusted 2 200 m/s total cross-section = 3.7808 b;
- adjusted 2 200 m/s scattering cross-section = 3.7806 b;
- thermal (2 200 m/s) scattering cross-section ratio $\sigma^T/\sigma^{T'} = 3.9040/3.7806 = 1.0326$.

The larger multiplicative reduction (4.43%) relative to the "5-point" value is offset by a larger additive increase (42.1 mb). The thermal ratio changes by only a tenth of a per cent, from 3.13% to 3.26%. We assume that CI80 is correct over its entire range, but that the Sayer adjustment is 1% or so high above the resonance region.

Adjustment of the Sayer 2000 total cross-section to Cierjacks 1980 from 3-6.9 MeV "SA00.CI80_3-6.9"

The results of this adjustment are:

- $A = 0.9683$, $1/A = 1.0327$, $B = 0.0038$, $b = 3.8$ mb, RMS deviation = 67.2 mb;
- adjusted 2 200 m/s total cross-section = 3.7844;
- adjusted 2 200 m/s scattering cross-section = 3.7842;
- thermal (2 200 m/s) scattering cross-section ratio $\sigma^T/\sigma^{T'} = 3.9040/3.7842 = 1.0317$.

Despite the different values of A and B in the two different CI80 adjustments the thermal ratios are very close. We adopted the 3-6.9 MeV values because A and B were so close to the 5-point fit above. Presumably the larger RMS deviation simply reflects the random fluctuations of the measured CI80 data relative to the "5-point" fit above. We believe that the ~1% difference between the two SI80 adjustments is due to the normal change in evaluation procedures at the top of the resolved resonance range.

How well do the 5-point fit and the CI80 fit agree?

Table 1 shows that the agreement is so close that either one can be used, and the consistency between CI80 and the five points is essentially perfect. Column 5 provides the percentage difference between the experimental values and the mean of the two fits. The large 1.25% at 3.5 MeV is discussed below. The Schneider experiment measured the scattering cross-section at zero energy. It is quoted in Table 1 as the equivalent 2 200 m/s value augmented by 0.2 mb of radiative capture. To repeat, this comparison shows that the evaluated SAYER 2000 total cross-section ("SA00"), adjusted two different ways, to *completely independent* experiments, gives almost identical results at six different "high-precision" points, confirming the consistency of the two "high-precision" data sets. The simplest interpretation is that the measurements were not only high-precision but also high-accuracy.

The large deviation in Table 1, 1.25% for the Cierjacks 1980 value, is related to the CI80 EXFOR value at 3.5 MeV, 2.9981 barns. Inspection of Figure 1, which shows the vicinity of 3.5 MeV, makes it clear that 2.9981 is not the average for that group of points. Our value, 2.9533, is the result of a quadratic fit to a run of about 80 points between 3.4 and 3.6 MeV and is a more believable local average.

When Sayer, *et al.* did their evaluation, they raised the Cierjacks 1980 data by 3.5%, increasing the 2.9981 to 3.1030. In the fitting process that was averaged with other data but only changed a little, to 3.0844. Our adjustment reduced that number by ~3.1% to the 2.9904 in Table 1. We believe that the CI80 data are accurate and when we eliminate all the questionable normalisations, the 1.25% in Table 1 will drop dramatically.

Table 1: Adjusting Sayer 2000 to either the five low-energy points or to Cierjacks 1980 gives almost identical results

Name of point, energy, value	Sayer 2000 5 points "SA00.5PTS"	Sayer 2000 CI80_3-6.9 "SA00.CI80_3-6.9_MEV"	Diff. MB	C/E %
Schneider – 0253 eV – 3.7940	3.7856	3.7844	-1.2	-0.32%
ENDF/B-VII.1 Dilg – 130 eV – 3.7831	3.7848	3.7839	-0.9	0.03%
Koester – 1 970 eV – 3.77	3.7805	3.7796	-0.9	0.27%
Block – 23 500 eV – 3.736	3.7310	3.7302	-0.8	-0.02%
Window – 2.35 MeV – 0.100	0.0996	0.1015	+1.9	0.55%
Cierjacks 1980 – 3.5 MeV – 2.9533	2.9907	2.9904	-0.3	1.25%

Figure 1: The Cierjacks 1980 point at 3.5 MeV (in red) and the ten nearest neighbours; the red point does not look like a local average

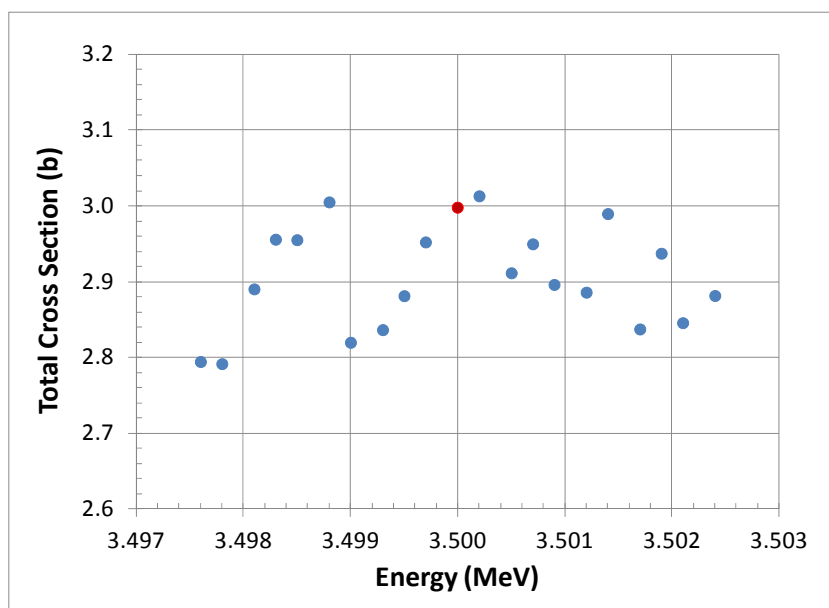
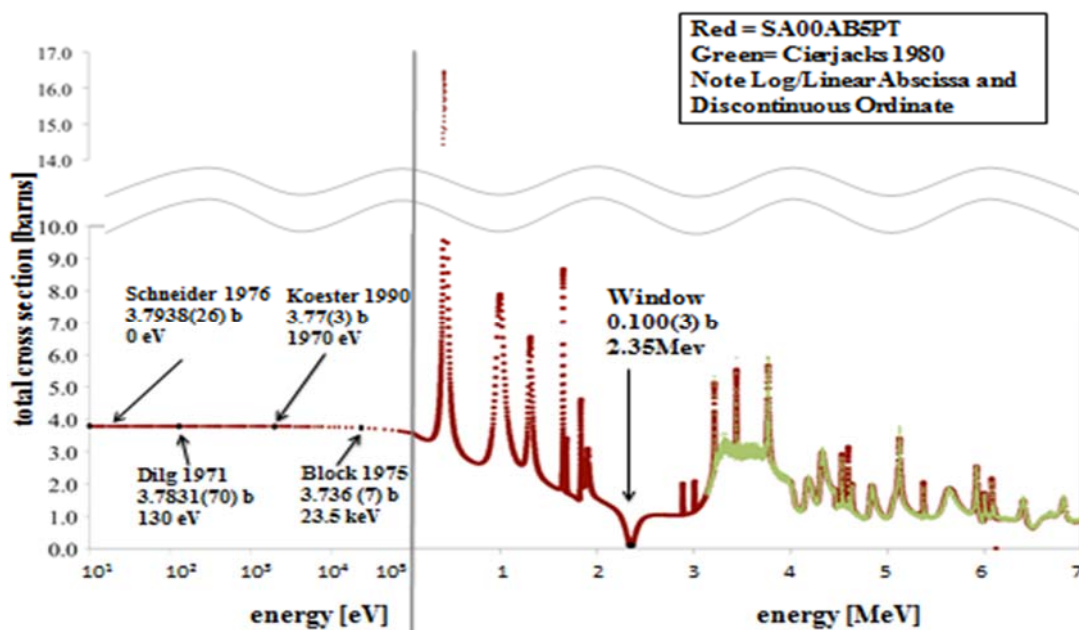


Figure 2 overlays the data described in Table 1: the five high-precision points, Cierjacks 1980 in green, and adjusted Sayer 2000 in red. At this scale the size of the dots is much larger than the actual differences. It is visual confirmation of the fact that a relatively simple renormalisation of Sayer 2000 makes it match all the precision data very accurately.

Figure 2: Shows that Cierjacks 1980 is consistent with the low-energy precision points



Normalisation of Cierjacks 1980 to Cierjacks 1968

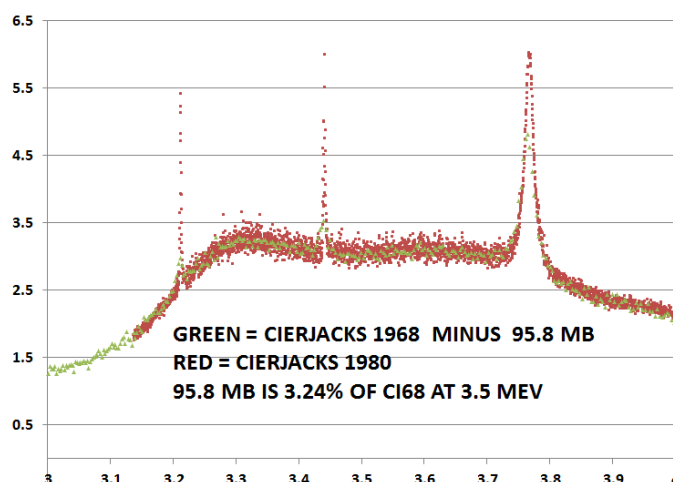
In their 1980 paper, Cierjacks, *et al.* say they had background problems fitting their data, possibly because they had measured the background and data on different days, so they “normalised to their 1968 data at 3.5 MeV”. They do not give any numbers, and because of the experimental fluctuations a comparison of their EXFOR data does not give much of a clue as to what they actually did.

We estimated the values of CI68 and CI80 at 3.5 MeV using least-squares quadratic fits from 3.4 to 3.6 MeV. Small blips in the experimental data prevented using the Sayer 2000 “shape” as for the 1.0 MeV resonance peak and for smoothing Ohkubo’s data (below). The CI68 quadratic is $y = 12\,178.01532 x^2 - 85\,792.42052 x + 154\,141.8751$ mb. At 3.5 MeV it is 3 049.1 mb. The CI80 quadratic is $y = 282\,971.6335 x^2 - 1\,977\,339.946 x + 3\,457\,240.563$ mb. At 3.5 MeV it is 2 953.3 mb. The ratio is 1.0324. The difference is 95.8 mb.

Our interpretation of those numbers is that both experiments agreed *very closely*. Somehow, the 1968 data were normalised multiplicatively to a room temperature total cross-section at 2 200 m/s. They knew something was wrong, because transmission experiments are not usually normalised and 3% would have been very large for an unexplained error. We believe that is why they did not publish the data. In 1980 Cierjacks did not normalise to thermal and was 3% below CI68. He ascribed it to a background problem in the CI80 data, and because background is additive, he presumably added the 3.5 MeV difference, 95.8 mb, as a flat increase to his data. He probably did the same kind of smoothing that we did in order to get values for normalisation.

To complicate the situation, we now believe that his 1980 EXFOR data are very accurate and are probably the original unnormalised data. Figure 3 overlays Cierjacks 1980 (red) and adjusted Cierjacks 1968 (green). The adjustment is a subtraction of 95.8 mb, which is 3.24% of CI68 at 3.5 MeV. That is probably what Cierjacks did in 1980, although it is the reverse of what he said, and the EXFOR data are also inconsistent with the paper. Although not shown here, the good agreement continues to higher energies.

Figure 3: The agreement between “fixed” CI68 and CI80 is excellent



Peak height analysis of the 1.0 MeV resonance in Cierjacks 1968

In evaluated files resonance peak heights are constrained by unitarity built into the R-matrix formalism, but that is not true of background-corrected experimental data. The observed height of a resonance is the sum of contributions from every channel. The peak shape itself is from the resonance’s own channel $c = (\alpha J \ell s)$ but its observed height depends on the height of the neighbouring resonance tails and on the combined potential scattering from every channel.

Above the (n, α) threshold the height is reduced by the alpha width but below it the radiative capture reduction is negligible and the unitary value is determined entirely by the resonance energy as $(J + 1/2)4\pi/k^2$. The resonance widths, the other resonance’s tails, and the other channels’ scattering radii may differ between evaluations, but the peak height in the resonant channel is determined solely by the energy.

In Sayer 2000 the height of the 1.0 MeV resonance is 8.147 b. In JENDL-4.0 its height is 8.201 b. The average of these two numbers, 8.174, is representative of unitary evaluated data. The CI68 value is 8.430 and the ratio is $8.430/8.174 = 1.0313$. The CI68 peak is 3.13% higher than a credible unitary limit, and that can only happen if a multiplicative normalisation was applied to the data. A conventional additive background error would be unlikely to match the 2 200 m/s Doppler ratio so precisely.

We determined the CI68 value, 8.430, using the same adjustment code we used for the cross-sections. The role of the “high-precision” points, σ^H , was played by the measured values in EXFOR CI68 between 0.98 and 1.02 MeV, the peak of the measured data. The data to be adjusted, σ^T , were the Sayer 2000 values over the same range, which presumably is an accurate representation of the shape. The adjusted file, σ^T , is therefore the smooth evaluated peak shape after being least-squares fitted to the experimental data.

The fact that the CI68 data are 3.24% above CI80 at 3.5 MeV (above) and 3.13% above the theoretical unitary limit at 1.0 MeV implies a multiplicative error, and the fact that it is 1.031 or 1.032 implicates the 2 200 m/s Doppler ratio.

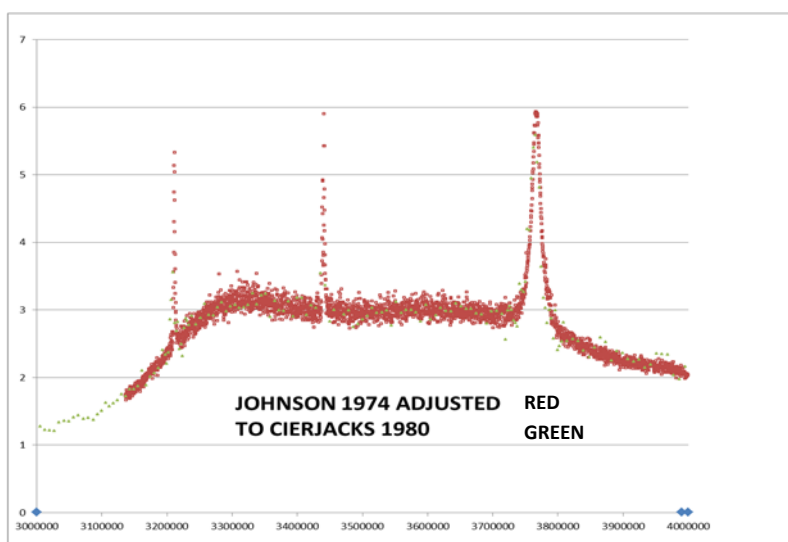
Adjustment of the Johnson 1974 total cross-section to Cierjacks 1980 from 3-6.9 MeV

A plot of JO74 against CI80 shows it to be high. Adjusting it to CI80 gives the interesting result: $A = 0.93972$, $1/A = 1.0641$, $B = 59.7$ mb, RMS deviation = 174 mb.

These numbers say that to make JO74 agree with CI80, reduce Johnson’s data by 6.4% and then add back 59.7 mb. The large RMS deviation is due to the fact that both sets are fluctuating experimental data so that interpolation into the CI80 energy mesh has a large random component.

We interpret these numbers as follows: in 1974 Johnson probably regarded the CI68 data as very accurate, not knowing that they were 3.2% high multiplicatively. In his effort to make his own data agree with them, he repeated the same error they made and got a file that was 3.2% higher than CI68, hence the 6.4% in $1/A$. That was obviously wrong and not knowing that he and they had erred multiplicatively he brought it back down additively, assuming that he had overestimated some background. In the absence of anything better, he reduced it by about 60 mb, which is 3% of the average cross-section, 2 barns, in that region. But not being sure of what was happening, he left the data unpublished. Figure 4 shows the result of adjusting JO74 to CI80.

Figure 4: The agreement between “fixed” JO74 and CI80 is excellent



Analysis of the Ohkubo 1985 total cross-section

The Ohkubo data are widely used because they cover a lower energy range than many other measurements, 791 eV to 9.35 keV. They are especially relevant because the ENDF/B-VI.0 thermal elastic value, 3.8883 b, “was almost entirely determined by fitting the Ohkubo data” (Hale, n.d.). Space does not permit a full discussion but here is a synopsis of our adjustments.

Ohkubo (1987) presented a linear fit to his low-energy data: $\sigma_t(E) = 3.85 - 2.0e-6 * E$ (eV). Our least-squares adjustment of that formula to the four lowest-energy precision points is mathematically equivalent to an unconstrained least-squares linear fit to the same four points and is $\sigma_t(E) = 3.7841 - 2.083e-6 * E$.

Since his fitted data were all above 2 eV, and the fit is flat down to zero energy, it describes unbroadened zero Kelvin cross-sections. The 1.7% difference in the fits at $E = 0$ could be water contamination but it does not matter, because the high-precision data which point to 3.7841 are consistent to $\sim 0.25\%$, so that changing that number would require experimental data of comparable accuracy.

Ohkubo (1987) ascribes his strong statistical fluctuations to aluminium resonances in the Al_2O_3 sample, and recognises that the thermal cross-section, 3.85 b, is high. “At very low energy ($E_n \approx 0$), σ_t is obtained to be 3.85 ± 0.06 barn in the present measurements. This value is 2.6% higher than the value 3.761 ± 0.006 barn measured by Koester, *et al.*, at thermal neutron energy.” These statements illustrate two of the points made in this paper:

- 1) The room temperature extrapolation to zero energy is flat, without the 3% rise he would have seen had he measured it below 2 eV.
- 2) The value 3.761 is quoted as a room temperature value, like the 3.85. The Dilg transmission experiment was indeed at room temperature, but the other measurements of 3.76 were optics measurements at zero Kelvin. In our opinion a high silicon cross-section lowered the Dilg oxygen value and we should attempt to understand why so many optics measurements clustered at the wrong low value while another group are higher.

Table 2 gives the values for the two fits at the four points. It shows that a straight line which brings the Ohkubo fit closer to the high-precision points by least-squares is *within a quarter of a per cent* of all four experiments.

Table 2: Comparison of two linear fits to the low-energy zero Kelvin total cross-section

Experiment			Raw OH85 linear fit			Adjusted OH85 linear fit*		
Name	Energy EV	Expt. (E) barns	Raw fit (C)	Ratio C/E - 1	Difference C-E MB	Adjusted fit (C)	Ratio C/E - 1	Difference C-E MB
Schneider	0.0253	3.7940	3.85	+1.5%	56.0	3.7841	-0.26%	-9.9
Dilg	130	3.7831	3.8497	+1.8%	66.6	3.7838	+0.02%	+0.7
Koester	1 970	3.77	3.8461	+2.0%	76.1	3.7800	+0.27%	+10.0
Block	23 500	3.736	3.8030	+1.8%	67.0	3.7351	-0.02%	-0.9

* This is identical to an unconstrained linear least-squares fit to the four points.

Adjustment of Ohkubo 1985 tabulated data to the high-precision measurements

An attempt to adjust the tabulated Ohkubo data to the two high-precision points which they overlapped, Koester and Block, failed because it requires interpolation of the high-precision points into the experimental data and that incurred large random errors. To smooth the Ohkubo data we adjusted the Sayer 2000 5-points (“SA00.5PTS”) data set to it. The array being adjusted is assumed to be an accurate, smooth representation of the cross-section and by fitting it to the fluctuating experimental data we obtain an accurately-smoothed representation of the latter. We call it SA00.5PTS.OH85.

In a second step we adjusted SA00.5PTS.OH85 back onto SA00.5PTS. This adjusts the Ohkubo data but with the fluctuations removed. We call it SA00.5PTS.OH85.5PTS. The last step is to apply the A and B coefficients from Step 2 to the raw Ohkubo data (“OH85”). Figure 5 overlays those adjusted Ohkubo data points (“OH85.ITERATED.4PTS”) with the accurate SA00.5PTS. The adjustment to Ohkubo’s data was to increase it multiplicatively by 11.4% and then subtract a uniform 520 mb. The very large multiplicative adjustment is saying that the peak should be higher relative to the smaller cross-sections and then bring it back down by half a barn says that overall the original fit was OK; 520 mb is close to 11%.

Figure 5: The agreement between “fixed” OH85 and adjusted SA00 is excellent

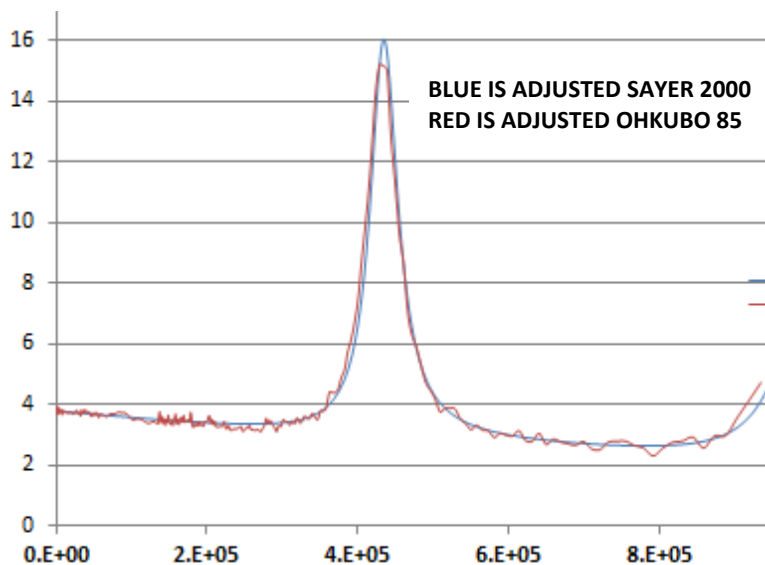
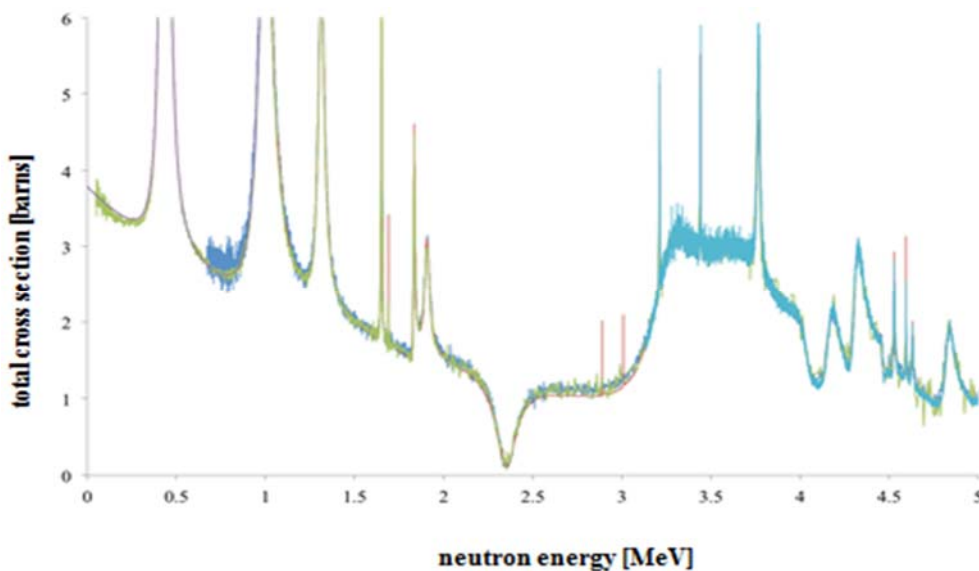


Figure 6: Four consistently adjusted cross-sections

Ohkubo (purple); Johnson (green); Cierjacks 68 (blue);
Sayer 2000 (orange); Cierjacks 1980 (EXFOR, aqua)

At low energy the Sayer 2000 (orange) curve is within a quarter of a per cent of the high-precision measurements



Conclusions

Based on the good agreement between evaluations and experiments when they are consistently adjusted to the high-precision points, it appears that the data were measured quite accurately but because of ordinary background and calibration problems, plus a little-recognised 3.15% difference between the room temperature 2 200 m/s scattering

and the zero Kelvin value (Lubitz, 2008), an error of that magnitude occurred in several high-quality measurements. They influenced other experimentalists which in turn affected the major evaluations.

While 3% in scattering is not negligible, it is small enough to have gone unnoticed for 44 years, from 1968 (Cierjacks) to 2012 (Kozier, *et al.*), despite the fact that it was 0 K in the *Atlas*, the *Standards* and all compendia of coherent scattering cross-sections, but room temperature in almost every major (0 K) evaluation starting with ENDF/B-VI.0. If that is the case, then the silicon cross-section is probably the largest remaining source of uncertainty in the low-energy oxygen cross-section. It would be reasonable to expect analogous “Doppler-errors” in silicon at the (1/2A) ~2% level.

References

- Block, R., *et al.* (1975), “Precision Neutron Total Cross-Section Measurements Near 24 keV”, *J. Nucl. Sci. Technol.*, 12 (1), pp. 1-11.
- Caro, E. (1998), “¹⁶O Neutron Cross Section Evaluation”, *Proc. Int. Conf. on the Physics of Nuclear Science and Technology*, Long Island, New York, 5-8 October.
- Cierjacks, S., *et al.* (1980), High Precision Time-of-Flight Measurements of Neutron Resonance Energies in Carbon and Oxygen Between 3 and 30 MeV”, *Nucl. Inst. & Methods*, 169, 185-198.
- Dilg, W., L. Koester and W. Nistler (1971), “The Neutron-Deuteron Scattering Lengths”, *Phys. Lett. B*, 36 (3), pp. 208-210.
- Hale, G. (n.d.), private communication.
- Koester, L., W. Waschowski and J. Meier (1990), “Cross Sections for Neutrons of 1 970 eV and Contributions to Fundamental Neutron Interactions”, *Z. Physik A*, 337, pp. 341-348.
- Kozier, K., *et al.* (2013), “Reactivity Impact of ¹⁶O Thermal Elastic-Scattering Nuclear Data for Some Numerical and Critical Benchmark Systems”, *Nucl. Technol.*, 183, pp. 473-483.
- Larson, N., *et al.* (1998), *Doppler Broadening Revisited*, ORNL/TM-13525, Oak Ridge National Laboratory, Oak Ridge, TN.
- Lubitz, C. (2008), “The Temperature of Coherent Scattering Cross Sections”, *Cross Section Evaluation Working Group 2008*.
- Ohkubo, M. (1987), *Neutron Total Cross Section Measurements on Oxygen*, JAERI-M 86-193, Japan Atomic Energy Research Institute (JAERI), Tokyo, Japan.
- Sayer, R., *et al.* (2000), “R-matrix Evaluation of ¹⁶O Neutron Cross Sections up to 6.3 MeV”, ORNL/TN-2000/212, Oak Ridge National Laboratory, Oak Ridge, TN.
- Schneider, C.S. (1976), “Coherent Nuclear Scattering Amplitudes of Germanium, Copper and Oxygen for Thermal Neutrons”, *Acta Cryst. A*, 32, pp. 375.

Critical benchmark results for a modified ¹⁶O evaluation

Paul K. Romano, Cecil R. Lubitz, Timothy H. Trumbull
Knolls Atomic Power Laboratory, Bechtel Marine Propulsion Corp.
Schenectady, NY, United States

Abstract

The effect of a uniform reduction in the elastic scattering cross-section for ¹⁶O on critical benchmarks is quantified and discussed. It is hypothesised that current evaluations for ¹⁶O systematically overestimate elastic scattering by about 3% due to a normalisation error in various experimental data. Selected critical benchmarks from the HEU-SOL-THERM (HST) series of the International Handbook of Evaluated Criticality Safety Benchmark Experiments were simulated using the MC21 Monte Carlo code. The benchmark results show that a decrease in the elastic scattering cross-section to agree with high-precision experimental measurements leads to higher leakage and lower benchmark eigenvalues. Additionally, a trend with the above-thermal leakage fraction was observed. The sensitivity of this trend to the first Legendre polynomial coefficient of the elastic scattering angular distribution was calculated. Based on the observed sensitivity, a 35% decrease in the first-order Legendre polynomial coefficient would be required to eliminate the trend with above-thermal leakage fraction.

Introduction

The majority of power reactors in the world use UO₂ or mixed-oxide fuel, leading many to believe that the cross-sections for ¹⁶O are known with great precision. On the contrary, there are a number of problems in the measured cross-section data for ¹⁶O. These problems are also present in the evaluated cross-section data that directly impact the results of transport simulations.

One of the major problems with ¹⁶O is that the elastic scattering cross-section in a number of evaluated libraries is not in agreement with high-precision experimental measurements (Chadwick, *et al.*, 2013). For example, the scattering cross-section in ENDF/B-VII.1 is approximately 3% higher than experimental values given in Dilg, Koester and Nistler (1971), Block, *et al.* (1975), Schneider (1976), and Koester, Waschkowski and Meier (1990). Very recently, it was demonstrated that the elastic scattering cross-section of ¹⁶O can have a large impact on the *k*-eigenvalue for solution thermal critical benchmarks (Kozier, *et al.*, 2013).

It has been hypothesised (Chadwick, *et al.*, 2013) that the cause of the discrepancy in the scattering cross-section is a normalisation of the room temperature transmission experiments to a room temperature 2 200 m/s total cross-section. At non-zero temperatures, a constant cross-section develops a 1/*v* rise at low energies. The increase in the cross-section at $E = kT$ for $T = 293.6$ K can be represented as $1 + 1/(2A)$ where *A* is the atomic weight ratio. For ¹⁶O, the increase is 3.15%, close to the amount that current

cross-section evaluations deviate from the high-precision measurements. If one experimental measurement was normalised incorrectly, it is possible that the incorrect normalisation propagated through to other measurements.

The objective of the present work is to quantify the effect of modifying a current evaluation for ¹⁶O with new cross-sections that agree with a set of high-precision measurements. The choice of the high-precision measurements and a full discussion of what changes may need to be made in order to develop a new evaluation are to be discussed at this workshop. This work merely aims to assess the impact of the most likely change to the ¹⁶O cross-section: a decrease in the elastic scattering cross-section by about 3%.

Results and analysis

The first half of the results demonstrates the change in eigenvalue in a selected set of benchmarks resulting from a decrease of the elastic scattering cross-section. The second half of the results focuses on trends of the eigenvalue with the above-thermal leakage fraction and the sensitivity of that trend with respect to the first moment of the elastic scattering angular distribution. All simulations were performed using the MC21 Monte Carlo Particle Transport Code (Griesheimer, *et al.*, 2013).

Cross-section sets

To obtain a decrease in the elastic scattering cross-section, a number of options were considered:

- 1) Use the ENDF/B-VII.1 data and decrease the elastic scattering to match the high-precision points.
- 2) Use a different evaluation that is closer to the high-precision points, e.g. JENDL-3.3.
- 3) Use a proposed R-matrix evaluation by Sayer, *et al.* (2000) and decrease elastic scattering to match the high-precision points. This evaluation was proposed but was never adopted by any of the major libraries.

The third option was adopted for the following reasons:

- 1) The scattering cross-section in the Sayer evaluation is almost exactly 3.15% above the high-precision measurements.
- 2) The Sayer evaluation has resonance parameters in MF=2 unlike, the other evaluations which represent the entire cross-section using MF=3.
- 3) The thermal scattering cross-section in the Sayer evaluation is constant at very low energy whereas the ENDF/B-VII.1 evaluation shows a slight dependence on energy which is puzzling.

The Sayer evaluation also has resonance energies and widths for the (n, α) channel. After that evaluation was completed, a 32% decrease in the (n, α) cross-section was made by Page in ENDF/B-VII.0 based on measured data by Harissopulos, *et al.* (2005). Without any changes, this means that the Sayer (n, α) cross-section will be approximately 32% too high below 6.12 MeV where the cross-sections are given by reconstructed resonances from MF=2. Above 6.12 MeV, the Sayer evaluation matches ENDF/B-VII.1.

The Sayer evaluation was processed with NJOY 2012 (MacFarlane, *et al.*, 2012) and NDEX (Sutton, *et al.*, 2007) to generate a cross-section file in the ND_LIBRARY format that is used by MC21. Two adjustments were made to the ¹⁶O point-wise cross-sections in the resulting ND_LIBRARY. The elastic scattering cross-section was reduced by 3.15%. Additionally, the (n, α) cross-section was reduced by 32% below 6.12 MeV and left unchanged above 6.12 MeV where it is the same as ENDF/B-VII.1.

Selected benchmark models

The MC21 simulations were based on 37 critical benchmarks from the HEU-SOL-THERM (HST) series of the *International Handbook of Evaluated Criticality Safety Benchmark Experiments* (OECD/NEA, 2010). The HST series was chosen for its sensitivity to the oxygen cross-sections and because they have been analysed in previous studies of ¹⁶O cross-sections (Caro, 1998). The following benchmark cases were used:

- HEU-SOL-THERM-001 Cases 1-10;
- HEU-SOL-THERM-009 Cases 1-4;
- HEU-SOL-THERM-010 Cases 1-4;
- HEU-SOL-THERM-011 Cases 1-2;
- HEU-SOL-THERM-012 Case 1;
- HEU-SOL-THERM-013 Cases 1-4;
- HEU-SOL-THERM-032 Case 1;
- HEU-SOL-THERM-042 Cases 1-8;
- HEU-SOL-THERM-043 Cases 1-3.

Comparison of ENDF/B-VII.1 and modified Sayer

Simulations of the 37 benchmarks were run in MC21, first with all cross-sections from ENDF/B-VII.1 and subsequently with all cross-sections other than ¹⁶O from ENDF/B-VII.1 and ¹⁶O from Sayer with the aforementioned modifications. All of the simulations used 100 000 neutrons per fission generation, 100 inactive generations and 1 000 active generations. By using 100 000 000 active histories, the 95% confidence intervals on all tallies are sufficiently small that any stochastic error can be neglected.

Table 1 shows the benchmark eigenvalue for each case and the ratio of the calculated eigenvalue from MC21 to the benchmark eigenvalue (C/E) for the ENDF/B-VII.1 and modified Sayer evaluations. The decreased elastic scattering cross-section in the Sayer evaluation causes an increase in the mean free path of neutrons and consequently higher leakage and a lower eigenvalue. The spectrum also becomes slightly harder as fewer neutrons reach thermal energies.

Table 1: Benchmark eigenvalues for selected critical benchmarks and C/E ratios for the ENDF/B-VII.1 and modified Sayer evaluations

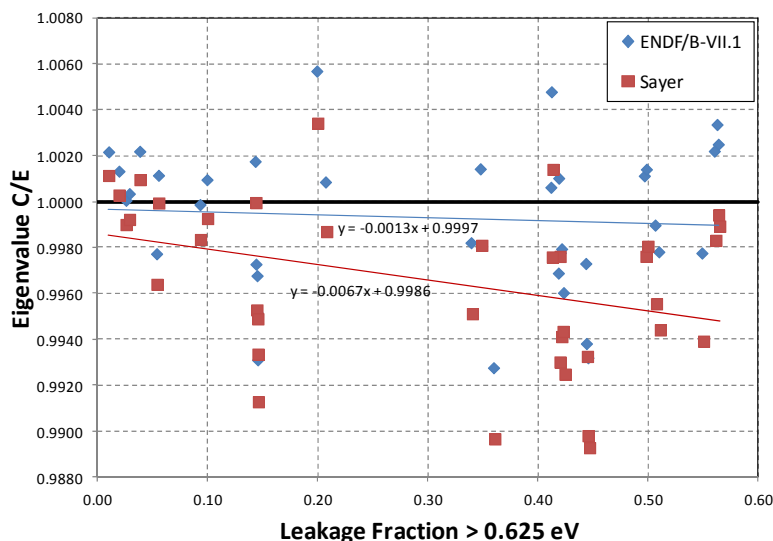
Case	Benchmark eigenvalue	ENDF/B-VII.1 C/E	Modified Sayer C/E
hst-001-01	1.00040	0.99777	0.99412
hst-001-02	1.00210	0.99382	0.98980
hst-001-03	1.00030	1.00102	0.99761
hst-001-04	1.00080	0.99730	0.99326
hst-001-05	1.00010	0.99821	0.99512
hst-001-06	1.00020	1.00143	0.99810
hst-001-07	1.00080	0.99688	0.99301
hst-001-08	0.99980	0.99794	0.99434
hst-001-09	1.00080	0.99320	0.98928
hst-001-10	0.99930	0.99276	0.98966

Table 1: Benchmark eigenvalues for selected critical benchmarks and C/E ratios for the ENDF/B-VII.1 and modified Sayer evaluations (*cont.*)

Case	Benchmark eigenvalue	ENDF/B-VII.1 C/E	Modified Sayer C/E
hst-009-01	0.99900	1.00335	0.99942
hst-009-02	1.00000	1.00250	0.99893
hst-009-03	1.00000	1.00220	0.99831
hst-009-04	0.99860	0.99776	0.99392
hst-010-01	1.00000	1.00112	0.99761
hst-010-02	1.00000	1.00141	0.99805
hst-010-03	1.00000	0.99897	0.99555
hst-010-04	0.99920	0.99781	0.99441
hst-011-01	1.00000	1.00478	1.00140
hst-011-02	1.00000	1.00062	0.99758
hst-012-01	0.99990	1.00085	0.99869
hst-013-01	1.00120	0.99727	0.99528
hst-013-02	1.00070	0.99677	0.99489
hst-013-03	1.00090	0.99311	0.99128
hst-013-04	1.00030	0.99516	0.99335
hst-032-01	1.00150	0.99773	0.99640
hst-042-01	0.99570	1.00096	0.99926
hst-042-01	0.99650	0.99987	0.99835
hst-042-01	0.99940	1.00114	0.99994
hst-042-01	1.00000	1.00219	1.00096
hst-042-01	1.00000	1.00006	0.99900
hst-042-01	1.00000	1.00034	0.99922
hst-042-01	1.00000	1.00132	1.00028
hst-042-01	1.00000	1.00216	1.00114
hst-043-01	0.99860	0.99603	0.99248
hst-043-02	0.99950	1.00568	1.00342
hst-043-03	0.99900	1.00175	0.99995

Previous work has shown that a trend in C/E with respect to leakage can be indicative of problems in the scattering angular distributions (Caro, 1998). Figure 1 shows the eigenvalue C/E for the ENDF/B-VII.1 and modified Sayer evaluations for each case simulated plotted as a function of the above thermal leakage fraction (ATLF). To be consistent with previous work, ATLF is defined in the models as net leakage from the fuel region at energies above 0.625 eV. We see that the lower elastic scattering cross-section in the modified Sayer evaluation has resulted in a decreasing trend with ATLF. The trend can be explained by the fact that the observed change in ATLF between the two evaluations was greater for cases where there is more net leakage, i.e., if the percentage change in leakage is the same for all cases, the cases that had higher leakage to begin with will experience a greater decrease in eigenvalue.

Figure 1: C/E ratios for ENDF/B-VII.1 and modified Sayer evaluations as a function of above thermal leakage fraction



Sensitivity to angular distributions

One possible means for removing the trend in C/E with the above thermal leakage fraction is to adjust the elastic scattering angular distribution. For ¹⁶O, the angular distribution is represented in both the ENDF/B-VII.1 and Sayer evaluations as a Legendre polynomial expansion of the cosine of the scattering angle in the centre-of-mass system. To assess the sensitivity of the leakage and hence the eigenvalue C/E to the angular distribution, the first-order Legendre polynomial coefficient was perturbed by +2% and -2% and all the benchmark cases were simulated again.

Figure 2 shows the eigenvalue C/E for the modified Sayer evaluation along with the cases that had a perturbed first-order Legendre polynomial coefficient. Since the first-order Legendre polynomial is proportional to the scattering cosine, this implies that a larger first-order coefficient will result in a more forward-peaked scattering distribution. Conversely, a smaller coefficient will result in a less forward-peaked scattering distribution. We see that the cases for which the coefficient was reduced results in less leakage and therefore a smaller trend with ATLF.

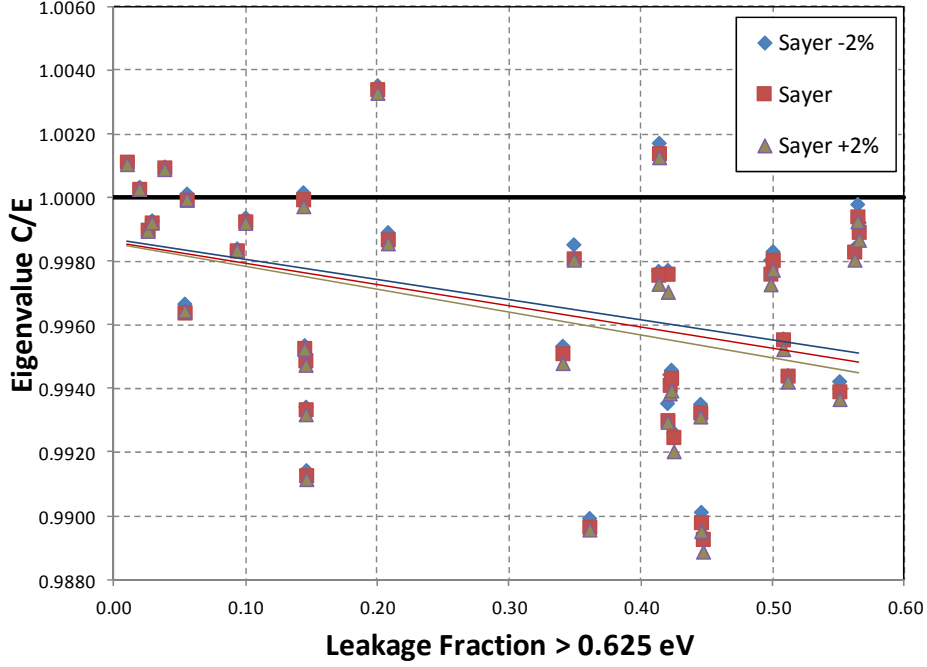
Based on the observed changes to the C/E ratios at different values of ATLF, we can develop an estimate of how much one would need to change the first-order coefficient in order to eliminate the trend with ATLF. Let us first express the expected eigenvalue as a first-order Taylor series expansion of the first-order Legendre polynomial coefficient, a_1 :

$$k\left(L, a_1 + \Delta a_1 = k(L, a_1) + \left.\frac{\partial k}{\partial a_1}\right|_L \Delta a_1\right) \tag{1}$$

where k is the expected eigenvalue, L is the ATLF, a_1 is the original coefficient of the first-order Legendre polynomial and Δa_1 is the change in the coefficient. To force the trend with ATLF to be flat, the expected eigenvalue at two different values of L must be equivalent:

$$k(L_1, a_1) + \left.\frac{\partial k}{\partial a_1}\right|_{L=L_1} \Delta a_1 = k(L_2, a_1) + \left.\frac{\partial k}{\partial a_1}\right|_{L=L_2} \Delta a_1 \tag{2}$$

Figure 2: C/E ratios for Sayer evaluation with and without perturbations to the elastic scattering angular distribution



The partial derivatives can be expressed by a finite difference approximation:

$$k(L_1, a_1) + \frac{k(L_1, a'_1) - k(L_1, a_1)}{a'_1 - a_1} \Delta a_1 = k(L_2, a_1) + \frac{k(L_2, a'_1) - k(L_2, a_1)}{a'_1 - a_1} \Delta a_1 \quad (3)$$

where a'_1 is the perturbed first-order Legendre polynomial coefficient. To remove the dependence on L , we can use the known linear regression fits:

$$\begin{aligned} k(L, a_1) &= k(0, a_1) + mL \\ k(L, a'_1) &= k(0, a'_1) + m'L \end{aligned} \quad (4)$$

where m and m' are the slopes of the linear regression fits to the unperturbed and perturbed cases, respectively. Substituting Eq. (4) in Eq. (3), rearranging terms, and solving for Δa_1 , we obtain:

$$\Delta a_1 = (a'_1 - a_1) \frac{m}{m - m'} \quad (5)$$

If we write the perturbed coefficient as $a'_1 = (1 + f)a_1$, we can then find the fractional change in a_1 required to remove the trend:

$$\frac{\Delta a_1}{a_1} = f \frac{m}{m - m'} \quad (6)$$

By using the slope of the linear regression fits in Based on the observed changes to the C/E ratios at different values of ATLF, we can develop an estimate of how much one would need to change the first-order coefficient in order to eliminate the trend with ATLF. Let us first express the expected eigenvalue as a first-order Taylor series expansion of the first-order Legendre polynomial coefficient, a_1 :

$$k\left(L, a_1 + \Delta a_1 = k(L, a_1) + \frac{\partial k}{\partial a_1}\bigg|_L \Delta a_1\right) \quad (1)$$

where k is the expected eigenvalue, L is the ATLF, a_1 is the original coefficient of the first-order Legendre polynomial and Δa_1 is the change in the coefficient. To force the trend with ATLF to be flat, the expected eigenvalue at two different values of L must be equivalent:

$$k(L_1, a_1) + \frac{\partial k}{\partial a_1}\bigg|_{L=L_1} \Delta a_1 = k(L_2, a_1) + \frac{\partial k}{\partial a_1}\bigg|_{L=L_2} \Delta a_1 \quad (2)$$

Figure 2, we find that:

$$\frac{\Delta a_1}{a_1} = -0.354 \quad (7)$$

which implies that a reduction of 35% in a_1 would remove the trend in ATLF under the assumption of a linear dependence on a_1 .

Conclusions

In this work, the effect of a uniform reduction in the elastic scattering cross-section of ¹⁶O has been quantified by simulating a selected set of criticality benchmark models using the MC21 Monte Carlo code. The simulation results show that the lower elastic scattering cross-section generally causes higher leakage and therefore a slightly harder spectrum and lower eigenvalues. Since the increase in leakage was observed to be roughly proportional to the overall leakage for a given problem, those benchmarks with higher leakage experienced a larger decrease in eigenvalue than those with less leakage, thus resulting in a decreasing trend with the above-thermal leakage fraction.

These results suggest that a decrease in the elastic scattering cross-section of ¹⁶O will likely need to be accompanied by other changes in order to obtain acceptable benchmark eigenvalue C/E ratios. One alternative for reducing or eliminating the trend of C/E with leakage is to modify the coefficients of the Legendre polynomial expansion of the elastic scattering angular distributions. A simple experiment was performed whereby the benchmark models were simulated again with the first-order Legendre polynomial coefficient perturbed by 2% to measure the sensitivity of the ATLF trend with respect to this coefficient. Based on an assumption of linearity, it was estimated that a 35% reduction in the first-order coefficient would be needed to remove the trend. This topic should be reassessed after a more realistic adjustment of the Sayer evaluation has been developed.

This study focused on the reactivity change in critical benchmarks from a 3.15% reduction of the entire elastic scattering cross-section. However, recent discussions in CIELO-O have clarified that any overestimation in the experimental resonance peaks will be eliminated by the unitarity requirements imposed by the R-matrix codes. This may reduce the size of the needed change in the first moment. Possible changes to the (n, α) cross-section and any changes to the ¹H and ^{235,238}U cross-sections through the CIELO collaboration (Chadwick, *et al.*, 2013) may also impact the benchmark eigenvalues.

References

- Block, R.C. *et al.* (1975), "Precision Neutron Total Cross-Section Measurements Near 24 keV", *J. Nucl. Sci. Technol.*, 12 (1), pp. 1-11.
- Caro, E. (1998), "¹⁶O Neutron Cross Section Evaluation", *Proc. Int. Conf. on the Physics of Nuclear Science and Technology*, Long Island, New York, 5-8 October.
- Chadwick, M.B., *et al.* (2013), "The CIELO Collaboration: Neutron Reactions on ¹H, ¹⁶O, ⁵⁶Fe, ^{235,238}U, and ²³⁹Pu", *Proc. Nuclear Data 2013*, New York City, New York, April.
- Dilg, W., L. Koester and W. Nistler (1971), "The Neutron-Deuteron Scattering Lengths", *Phys. Lett. B*, 36 (3), pp. 208-210.
- Griesheimer, D.P., *et al.* (2013), "MC21 v.6.0 – A Continuous-Energy Monte Carlo Particle Transport Code with Integrated Reactor Feedback Capabilities", *Proc. Joint Int. Conf. on Supercomputing in Nuclear Applications and Monte Carlo*, Paris, France, 27-31 October.
- Harissopulos, S., *et al.* (2005), "Cross Section of the ¹³C(α ,n)¹⁶O reaction: A Background for the Measurement of Geo-Neutrinos", *Phys. Rev. C*, 72, 062801, doi:10.1103/PhysRevC.72.062801.
- Koester, L., W. Waschkowski and J. Meier (1990), "Cross Sections for Neutrons of 1 970 eV and Contributions to Fundamental Neutron Interactions", *Z. Physik A*, 337, pp. 341-348.
- Kozier, K., *et al.* (2013), "Reactivity Impact of ¹⁶O Thermal Elastic-Scattering Nuclear Data for Some Numerical and Critical Benchmark Systems", *Nucl. Technol.*, 183, pp. 473-483.
- MacFarLane, R.E., *et al.* (2012), *The NJOY Nuclear Data Processing System, Version 2012*, LA-UR-12-27079, Los Alamos National Laboratory, Los Alamos, NM.
- OECD/NEA (Organisation for Economic Co-operation and Development/Nuclear Energy Agency) (2010), *International Handbook of Evaluated Criticality Safety Benchmark Experiments*, NEA/NSC/DOC(95)03, OECD/NEA, Paris.
- Sayer, R.O., *et al.* (2000), *R-Matrix Evaluation of ¹⁶O Neutron Cross Sections up to 6.3 MeV*, ORNL/TN-2000/212, Oak Ridge National Laboratory, Oak Ridge, TN.
- Schneider, C.S. (1976), "Coherent Nuclear Scattering Amplitudes of Germanium, Copper and Oxygen for Thermal Neutrons", *Acta Cryst. A*, 32, pp. 375.
- Sutton, T.M. *et al.* (2007), "The MC21 Monte Carlo Transport Code", *Proc. Joint International Topical Meeting on Mathematics & Computation in Supercomputing in Nuclear Applications*, Monterey, California, 15-19 April.

^{56}Fe

Chair: R. Jacqmin

Fe isotope evaluation within the CIELO project

M. Herman,^a A. Trkov,^b D. Brown^a

^aNational Nuclear Data Center, Brookhaven National Laboratory
Upton, NY, United States

^bJozef Stefan Institute, Ljubljana, Slovenia

Abstract

The plans for a new set of nuclear data evaluations for iron isotopes are outlined. They include a review of existing evaluations, comparison with the available experimental data and discussion of the concerns raised by the applications community. The new evaluations will take advantage of the expanded resources that will become available within the CIELO project and benefit from recent or revised experimental data and more detailed analysis of the uncertainties and correlations among different experiments. The focus will be on ⁵⁶Fe due to its dominant abundance. Modelling of neutron-induced reactions will exploit recent advances in application of nuclear reaction theory. Particular attention will be dedicated to the cross-section fluctuations that in the total cross-section persist up to about 10 MeV and to elastic and inelastic angular distributions. The possibility of extending the resonance region beyond the first inelastic threshold will be investigated, including an attempt to derive elastic angular distributions from the resonances. The full covariance matrix will be provided for all major cross-sections in the fast neutron energy range. Since iron is an important structural and shielding material in nuclear applications, there exist a large number of potentially useful integral benchmarks for data validation. In this preliminary phase a number of benchmarks have been identified. In the Radiation Shielding and Dosimetry Experiments Database (SINBAD) there are several shielding experiments that include significant amounts of iron and many others which include iron as a secondary material. In addition to the shielding reaction rate and spectra benchmarks, many of which are interesting due to different neutron spectra, geometrical configurations, amounts of iron present, etc., criticality safety benchmarks for the ICSBEP database can provide complementary information on the iron cross-sections due to different sensitivity profiles.

Introduction

The plans for a new set of nuclear data evaluations for the isotopes of iron are outlined. They include a review of existing evaluations, comparison with the available experimental data and discussion of the concerns raised by the applications community. The new evaluations will take advantage of the expanded resources that will become available within the CIELO project. New evaluation will benefit from recent or revised experimental data and more detailed analysis of the uncertainties and correlations among different experiments. The focus will be on ⁵⁶Fe due to its dominant abundance.

Comparison of existing evaluations

Evaluations for ⁵⁶Fe exist in all major libraries. All of them were started more than 20 years ago and were subsequently updated. It should be noted that most of the evaluations are totally independent and only ROSFOND makes use of JEFF evaluations for some reaction channels (e.g. total). All major files include covariances for cross-sections and angular distributions (MF=33,34).

The current ENDF/B-VII.1 (Chadwick, *et al.*, 2011) file originated in 1991 with evaluation by Fu, Perey, Hetrick, and Perey using TNG code up to 20 MeV. In 1996 Chadwick, Young and Koning extended this evaluation up to 200 MeV using the GNASH code and taking into account coupled channels (CC) and pre-equilibrium (PE) mechanisms. Additional changes were effected in 2000, 2004 and 2011.

The JEFF-3.1 (Koning, *et al.*, 2011) evaluation stems from the EFF-3.0 library and dates back to 1990. There have been, however, substantial updates in 1998 and 2009. The former concerned energies below 20 MeV and consisted of implementing the Geel high-resolution data and adding double-differential cross-sections resulting from MSC+MSD calculations with the EMPIRE code (Herman, *et al.*, 2007). In 2009 Koning, Hilaire and Duijvestijn extended the energy range from 20 to 200 MeV with TALYS calculations using OM+DWBA+HF+PE mechanisms.

The roots of the JENDL-4.0 (Shibata, *et al.*, 2011) evaluation go back to 1987 but it has been modified several times with the last update in 2010. The cross-sections up to 20 MeV were evaluated by Iijma, Yamakoshi, Shibata, and Igarasi using the POD, OPTMAN (Soukhovitski, *et al.*, n.d.), GNASH and CASTHY codes, taking into account the CC+HF+PE reaction mechanisms. This evaluation also makes use of the Geel high-resolution data.

Figures 1-5 compare cross-sections in the three above-mentioned libraries, as well as those in the Russian ROSFOND library, with experimental data for the major reactions channels in the fast energy range. There is good agreement among all the libraries for the total cross-sections, which is not surprising taking into account the wealth of experimental data available in the literature (also including those taken on the natural samples that are not shown on the plots). Somewhat larger discrepancies occur for the elastic channel, most likely due to treating the elastic as a sort of buffer for ensuring that partial cross-sections sum up to the total. One notes very strong fluctuations in both channels that extend up to 10 MeV. Similar scale fluctuations are also observed for the total inelastic and inelastic scattering to the first excited level (Figure 2). We note, however, that these fluctuation patterns do not follow those observed in the total and elastic cross-sections, which excludes using the recipe that is sometimes applied of scaling all cross-sections equally to match the fluctuations in the total. Figure 3 (left) shows that the three evaluations use different energy resolution to describe the fluctuations. JEFF-3.1 is the most detailed, while ENDF/B-VII.1 and JENDL-4.0 employ coarser resolution broadening. It is not clear whether this difference is relevant for applications. However, averaged inelastic cross-sections from the three evaluations differ considerably, especially close to the threshold. These differences might be partially responsible for different performance of the evaluations in integral testing.

Figure 3 (right) shows striking difference in modelling the inelastic scattering in various evaluations. Clearly, JENDL and ENDF predict strong direct contribution to the inelastic scattering to the fourth level, while JEFF either ignores it or estimates it much lower (JENDL and ENDF also differ in their estimate of the direct effect). JEFF-3.1 evaluation includes fluctuations that were imposed on the cross-sections by propagating fluctuations of the total cross-sections to the remaining reaction channels. This approach has no experimental support and might not be valid.

Figure 1: Total cross-sections for incident neutrons on ^{56}Fe in ENDF/B-VII.1, JEFF-3.1 and JENDL-4.0 libraries compared with experimental data

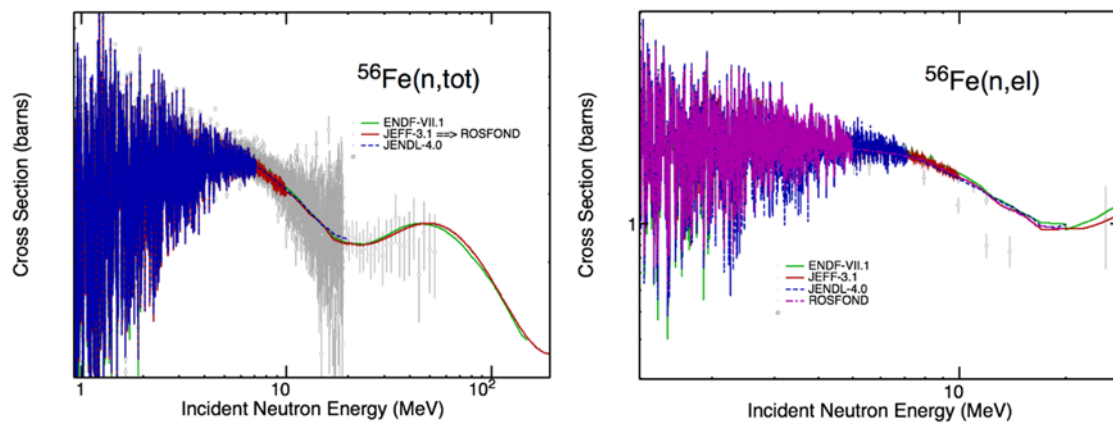


Figure 2: Inelastic cross-sections for neutron scattering on ^{56}Fe in ENDF/B-VII.1, JEFF-3.1 and JENDL-4.0 libraries compared with experimental data

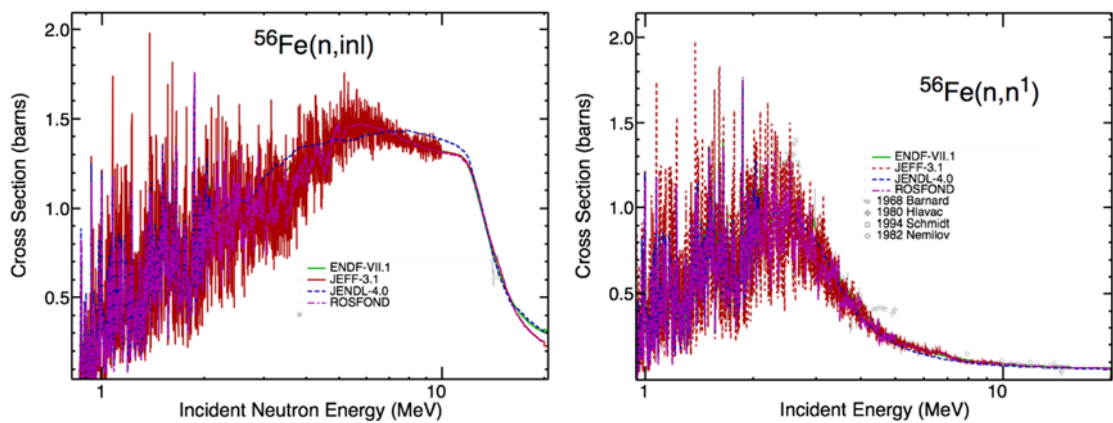


Figure 3: Details of the inelastic neutron scattering to the first level in ^{56}Fe (left) and comparison of inelastic scattering to the fourth level in ENDF/B-VII.1, JEFF-3.1 and JENDL-4.0 libraries (right)

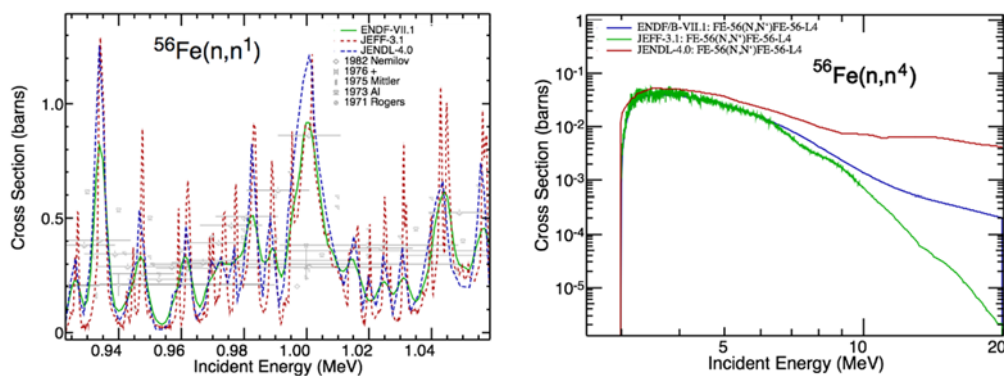


Figure 4 (left) shows fairly good agreement between all evaluations for the (n,p) reaction on ^{56}Fe , although some differences can be noted on the rising slope of the excitation function between 8 and 12 MeV. The $^{56}\text{Fe}(n,p)$ is a dosimetry reaction and very often used as a reference (standard) reaction in activation measurements. Therefore, it has to be evaluated very carefully. Fortunately, there is a very recent evaluation by Zolotarev (2013), which we intend to adopt for CIELO. In case of the (n, α) reaction there is not enough data to constrain evaluations [see Figure 4 (right)]. In these circumstances agreement among existing evaluations is quite good. All three agree perfectly at 15 MeV. Below this energy JEFF-3.1 and JENDL-4.0 follow the somewhat unusual straight-line shape of the (n,p) reaction, while ENDF adopts a shape more typical of the model calculations.

Figure 4: Comparison of $^{56}\text{Fe}(n,p)$ (left) and $^{56}\text{Fe}(n,\alpha)$ (right) cross-sections in ENDF/B-VII.1, JEFF-3.1 and JENDL-4.0 libraries

Experimental data are available for $^{56}\text{Fe}(n,p)$

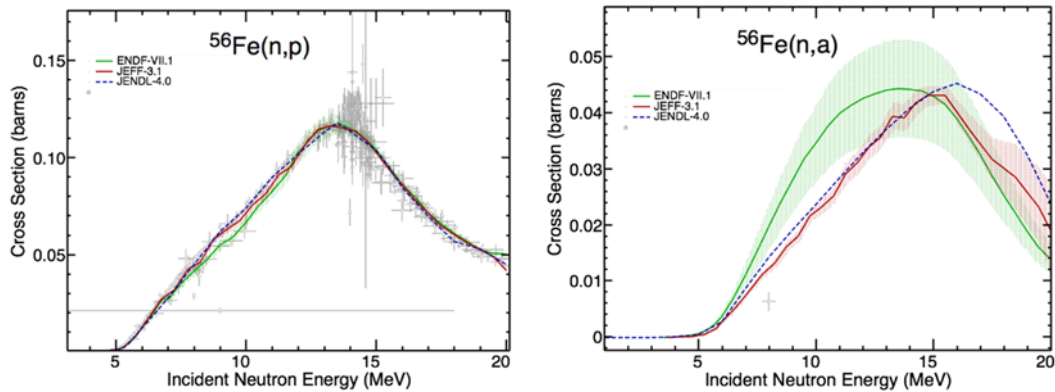
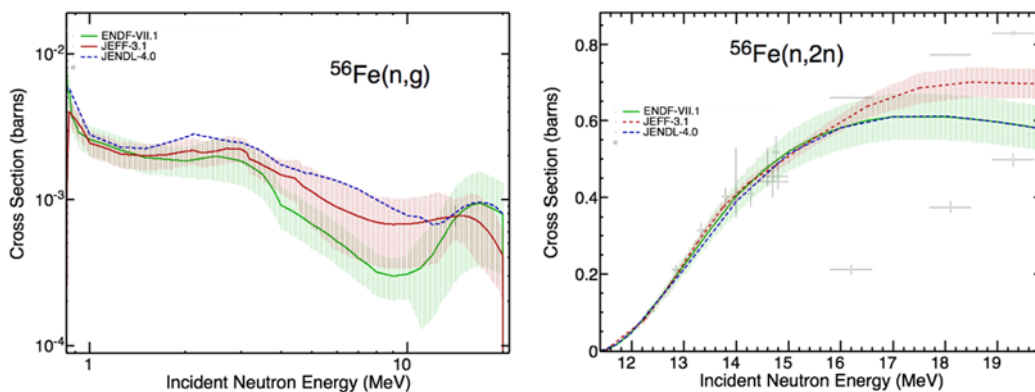


Figure 5 (left) compares capture reaction cross-sections in the three libraries. Again, taking into account that there are no experimental data and that capture in the fast neutron range is very small, agreement among the evaluations is fair, e.g. ENDF/B-VII.1 and JENDL-4.0 agree within their uncertainty bands in the whole energy range. Generally good agreement is also observed for the (n,2n) reaction cross-sections [Figure 5 (right)]. All evaluations agree very well up to 16 MeV, being constrained by experimental data between 13 and 15 MeV. Above 16 MeV JENDL and ENDF/B are practically identical while JEFF runs higher, but even then all nearly agree within their uncertainty bands.

Figure 5: Comparison of $^{56}\text{Fe}(n,\gamma)$ (left) and $^{56}\text{Fe}(n,2n)$ (right) cross-sections in ENDF/B-VII.1, JEFF-3.1 and JENDL-4.0 libraries

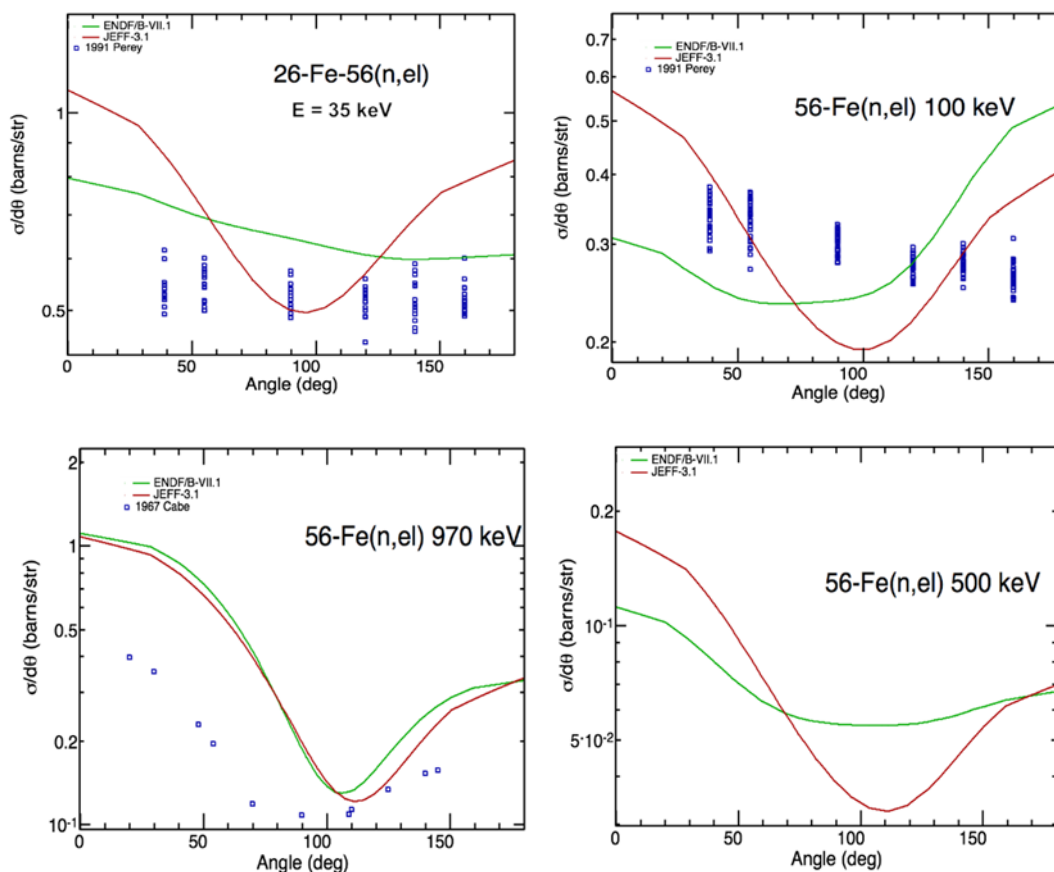
Experimental data are available for $^{56}\text{Fe}(n,2n)$



Recently, a lot of attention has been paid to elastic and inelastic angular distributions since, in the past, their impact on the integral performance of the evaluations has not been properly recognised. Our current understanding is that eventual deficiencies in angular distributions were compensated with other observables (usually cross-sections) to improve integral performance of the evaluation and that these changes were not always justified by the underlying physics. Figure 6 compares elastic angular distributions for ENDF/B-VII.1 and JEFF-3.1 with the experimental data. One notes that for incident energies up to 500 keV ENDF/B and JEFF evaluations differ considerably. Neither actually reproduces the experimental data and both seem to have fundamental deficiencies. JEFF appears to be too anisotropic at two lower energies (35 and 100 keV), while ENDF/B shows unphysical backward asymmetry at 100 keV. A strong difference in shape between the two evaluations persists at 500 keV and only close to 1 MeV do both evaluations come to fair agreement with each other, but not with the experimental data. Improving elastic and inelastic angular distributions will be one of the major challenges in the CIELO evaluation.

Figure 6: Angular distributions for elastic scattering of neutrons from ^{56}Fe at 35, 100, 500 and 970 keV incident energies (clockwise); results from the ENDF/B-VII.1 and JEFF-3.1 libraries are compared

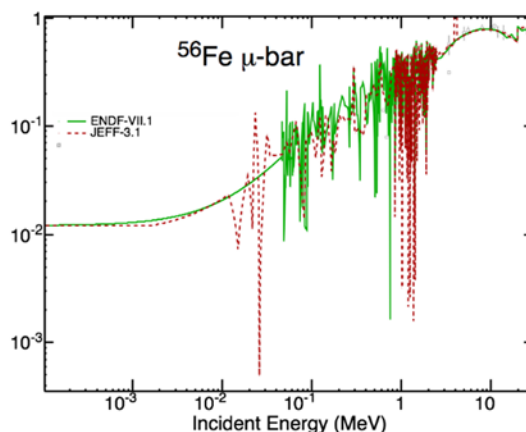
Experimental data at 35 and 100 keV were measured on a very dense energy grid and multiple incident energies appear on the same plot



Additional guidance regarding angular distributions comes from the so-called “mu-bar” quantity, which adopts $l=1$ coefficient in the Legendre polynomial expansion of the elastic angular distribution in the lab system as a measure of the elastic anisotropy. Figure 7 shows energy dependence of the mu-bar for ENDF/B-VII.1 and JEFF-3.1 compared to the experimental data. Both evaluations agree well above 2 MeV and in this energy

Figure 7: Comparison of μ -bars for ⁵⁶Fe in ENDF/B-VII.1 and JEFF-3.1 evaluations

Experimental data available above 2 MeV are in good agreement with both evaluations



range they both describe existing experimental data for ⁵⁶Fe. Below 2 MeV JEFF and ENDF/B reveal distinct fluctuations that appear to be very little correlated (if at all) between the two evaluations. There are no ⁵⁶Fe data to support these fluctuations but there is a strong evidence for the fluctuations in the measurements on natural iron. Preliminary analysis of these fluctuations has been performed, but it is premature to discuss the results here.

Status of experimental data

All of the stable isotopes of iron must be considered, namely ^{54,56-48}Fe as they constitute naturally occurring iron. In addition, ⁵⁵Fe must be considered, as it is a compound nucleus encountered in reactions on ⁵⁴Fe and ⁵⁶Fe. A preliminary search of the EXFOR database revealed the following number of SubEntries containing pertinent neutron-induced reaction data:

- ⁵⁴Fe: 419 subentries including five evaluations;
- ⁵⁵Fe: 2 subentries including one evaluation;
- ⁵⁶Fe: 636 subentries including seven evaluations;
- ⁵⁷Fe: 85 subentries including three evaluations;
- ⁵⁸Fe: 72 subentries including two evaluations;
- ^{nat}Fe: 918 subentries including one evaluation.

Each subentry contains one or more data sets and not all of this data is useful either for data fitting or for post-fitting validation. In particular, we cannot use the following data:

- polarisation data;
- ill-defined spectrum-averaged data including any sets marked with FIS or SPA (resonance integral and Maxwellian averaged data are acceptable);
- evaluated data including data marked with RECOM, EVAL, DERIV as well as all subentries with accession numbers beginning with the letter "V";
- quasi-evaluated data as this data required a model for data interpretation, including data marked with CN and SEQ;

- atomic data, marked with BA or FA;
- thermal neutron scattering data, marked with THS, COH or INC;
- kerma factors, marked with KER;
- deep inelastic scattering data (this is high energy, well above the 20 MeV limit we are considering), marked with DI.

Partial cross-section data (marked with PAR), data with poorly or inconsistently defined reactions (marked with INL, NON, SCT or ABS), coupled data (e.g. ratio data) and isotope/particle production data is usable for data validation, but not for fitting. Table 1 summarises the number of distinct sets that can be used in the iron evaluations.

Table 1: Number of EXFOR data sets that can be used for fitting in the resonance region, fitting in the fast region and for validation

	Resonance	Fast	Validation
⁵⁴ Fe	101 sets	161 sets	137 sets
⁵⁵ Fe	0 sets	0 sets	0 sets
⁵⁶ Fe	223 sets	134 sets	313 sets
⁵⁷ Fe	89 sets	23 sets	13 sets
⁵⁸ Fe	50 sets	23 sets	17 sets
^{nat} Fe	38 sets	327 sets	511 sets

It will take some time to examine each set to determine its practical usability. Nevertheless, the work of sorting out and using the resonance data has already begun (Leal, 2014). In addition, the data in the fast energy region can be extracted automatically.

Modelling fast neutron range

The evaluation of the fast neutron range will exploit recent advances in modelling nuclear reactions along with latest experimental results. The existing experimental database will be reviewed in order to select the most representative set of high quality experiments in close collaboration with the experimentalists. We plan to utilise the recent possibility of renormalising old experiments to the updated values of the standards, which is expected to improve the consistency of the experimental database. Such an updated set of measurements will be used to constrain model calculations by searching for the most adequate reaction models and corresponding optimal vector of model parameters. The technique of energy-dependent fine tuning will be invoked to correct possible model deficiencies and minimise their effect on the final evaluation.

Compared to previous evaluations we are in a position to take advantage of better physics and a more reliable set of model parameters. One of the most important novelties will be usage of the coupled-channels soft-rotor model for the incident and binary outgoing channels, with the potential that has been made available by Capote. In the preliminary calculations this potential proved to be superior to any “classical” potentials employed in previous evaluations. Use of the Engelbrecht-Weidenmueller transformation is also being considered, to account for interference between direct and compound nucleus mechanisms,

The pre-equilibrium emission treatment will take advantage of an array of available models, including quantum mechanical MSD+MSC for the inelastic channel, exciton model for the charge exchange and gamma channels and Iwamoto-Harada mechanism

for emission of clusters. If we decide to extend the evaluation above 20 MeV the HMS model will be used in the high-energy part of the evaluation to account for multiple pre-equilibrium emission.

Nuclear level densities, along with the optical model potential, are the most critical ingredients of statistical model calculations. Our pilot studies indicate that for ⁵⁶Fe, which is two nucleons away from the neutron and proton shell closures, the best results are obtained with microscopic level densities. To this end, we are going to investigate a possibility of using sophisticated quantum Monte Carlo method, which has been developed recently by Nakada and Alhassid (1997) and Mukherjee and Alhassid (2012). It has been demonstrated that such level densities provide a very good description of experimental level densities in the mass region close to iron.

Particular attention will be dedicated to the cross-section fluctuations that in the total cross-section persist up to about 10 MeV and to elastic and inelastic angular distributions. Recently we have developed a technique to modulate compound elastic and absorption cross-sections in such a way as to reproduce both the cross-section fluctuations and mu-bars. We may also take advantage of the resonance region extending beyond the first inelastic threshold to describe fluctuations and derive elastic angular distributions directly from the resonances. This approach would be preferable but it needs to be proved that it can provide acceptable reproduction of the experimental mu-bars.

The full covariance matrix will be provided for the resonance region and for all major cross-sections in the fast neutron energy range. Cross-correlations among different reaction channels will also be attempted, as these, if significant, may affect the uncertainties of transport calculations and data adjustment.

Benchmarking

In any modern evaluation, the analysis of suitable benchmarks is an integral part of the evaluation process. Since iron is an important structural and shielding material in nuclear applications, there exist a large number of potentially useful integral benchmarks for data validation. In this preliminary phase a number of benchmarks have been identified. In the Radiation Shielding and Dosimetry Experiments Database (SINBAD), the recently re-evaluated EURACOS-Fe and ASPIS experiments are not of benchmark quality. However, in the same database, there are several other shielding experiments that include iron, such as the Karlsruhe Iron Sphere, Wuerenlingen Iron Benchmark (PROTEUS), ORNL TSF Iron Broomstick, ORNL TSF Stainless Steel Broomstick, ORNL Neutron Transport Through Iron and SS, University of Illinois Iron Sphere (²⁵²Cf, D-T), University of Tokyo-YAYOI Iron Slab, NAIÁDE 1 Iron Benchmark (60 cm), Osaka Iron Sphere (OKTAVIAN), FNG-SS Shield, TUD Iron Slab Experiment, IPPE Iron Shells, ORNL 14-MeV Neutron SS/Borated Poly Slab, and many others, which include iron as a secondary material.

In addition to the shielding reaction rate and spectra benchmarks, many of which are interesting due to different neutron spectra, geometrical configurations, amounts of iron present, etc., criticality safety benchmarks for the ICSBEP database can provide complementary information on the iron cross-sections due to different sensitivity profiles. A lot of benchmarks use iron or steel as a reflector material, steel as cladding, iron as neutron absorbing material, separation material or shielding material. However, one should not jump to conclusions when discrepancies arise. For example, the ICSBEP benchmark PU-MET-INTER-002 (commonly known as ZPR-6/10) from ANL is a notorious outlier that is considered sensitive to iron since it has stainless steel in the core as well as in the axial and radial reflectors. With ENDF/B-VII.0 data the discrepancy in k_{eff} was nearly 3%. The new ⁵⁵Mn evaluation in ENDF/B-VII.1 reduced the discrepancy by about 1%, but the remaining discrepancy is still very large. Cumulative reaction rate integrals are very useful for identifying nuclides and energy ranges that contribute most strongly to absorption. They are defined as:

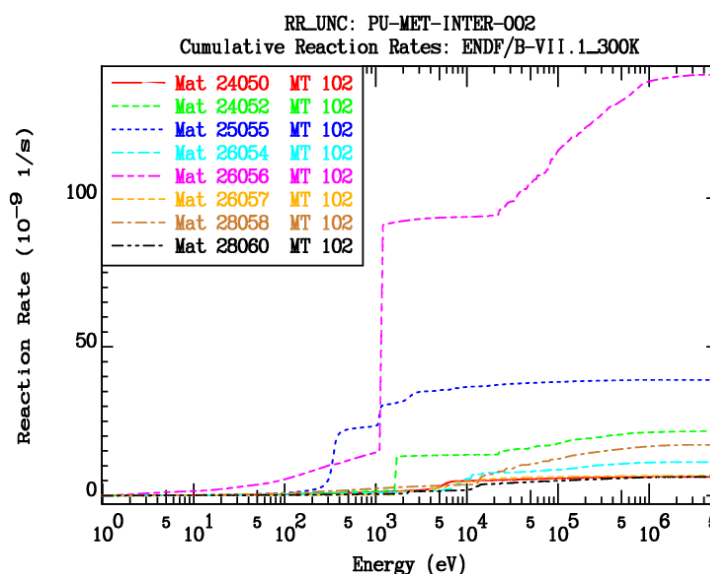
$$R = \int_0^E n\sigma(E)\phi(E)dE$$

where n is the number density, σ is the cross-section and ϕ is the neutron spectrum at the location of irradiation.

Figure 8 shows the cumulative capture reaction rate integrals of the nuclides of structural materials that show the highest contributions to capture. The main conclusion is that sensitivities to minor constituents must be established and the analysis should not be limited to the cross-sections alone, but also to the angular distributions and the neutron emission spectra.

Experiments were performed at RPI in which the neutron yields as a function of energy at a number of distinct angles were measured for a target in a quasi-monoenergetic neutron beam. Unfortunately the experimental data have not yet been released.

Figure 8: Cumulative capture reaction rate integrals of the nuclides of structural materials that show the highest contributions to capture



Acknowledgements

This work was sponsored by the Office of Nuclear Physics, Office of Science, United States Department of Energy under contract No. DE-AC02-98CH10886 with Brookhaven Science Associates.

References

- Chadwick, M.B., *et al.* (2011), "ENDF/B-VII.1 Nuclear Data for Science and Technology: Cross Sections, Covariances, Fission Product Yields and Decay Data", *Nuclear Data Sheets*, 112, p. 2887.
- Herman, M., *et al.* (2007), "EMPIRE: Nuclear Reaction Model Code System for Data Evaluation", *Nucl. Data Sheets*, 108, pp. 2655-2715.
- Koning, A.J., S. Hilaire and M.C. Duijvestijn (2008), "TALYS-1.0", *Proceedings of the International Conference on Nuclear Data for Science and Technology (ND2007)*, Nice, France, 22-27 April 2007, O. Bersillon, *et al.* (eds.), EDP Sciences, pp. 211-214.
- Koning, A.J., *et al.* (2011), "Status of the JEFF Nuclear Data Library", *J. Korean Phys. Soc.*, 59, No. 2, 1057.
- Leal, L. (2014), these proceedings.
- Mukherjee, A. and Y. Alhassid (2012), "Odd-Particle Systems in the Shell Model Monte Carlo: Circumventing a Sign Problem", *Phys. Rev. Lett.*, 109, p. 032503.
- Nakada, H. and Y. Alhassid (1997), "Total and Parity-Projected Level Densities Iron-Region Nuclei in the Auxiliary Fields Monte Carlo Shell Model", *Phys. Rev. Lett.*, 79, p. 2939.
- Shibata, K., *et al.* (2011), "JENDL-4.0: A New Library for Nuclear Science and Engineering", *J. Nucl. Sci. Technol.*, 48, p. 1.
- Soukhovitski, E., *et al.* (n.d.), Technical Report, JAERI-Data/Code 2004-002, Japan Atomic Energy Research Institute (unpublished).
- Young, P.G., E.D. Arthur and M.B. Chadwick (1998), "Comprehensive Nuclear Model Calculations: Theory and Use of the GNASH Code", *Proceedings of the Workshop on Nuclear Reaction Data and Nuclear Reactors (ICTP)*, Trieste, Italy, 15 April-17 May 1996, A. Gandini and G. Reffo (eds.), World Scientific Publ. Co., Singapore, pp. 227-404.
- Zolotarev, K.I. and P.K. Zolotarev (2013), *Evaluation of Some (n,n') , (n,γ) , (n,p) , $(n,2n)$ and $(n,3n)$ Reaction Excitation Functions for Fission and Fusion Reactor Dosimetry Applications*, Report INDC(NDS)-0657, IAEA, Vienna, Austria.

Review of nuclear data of major actinides and ^{56}Fe in JENDL-4.0

Osamu Iwamoto, Nobuyuki Iwamoto

Nuclear Data Center, Nuclear Science and Engineering Directorate
Japan Atomic Energy Agency
Ibaraki, Japan

Abstract

JENDL-4.0 was released in 2010. Most of the actinide data were revised from JENDL-3.3, especially at the fast energy region, using the newly developed CCONE code. Fission cross-sections of major actinides were determined using the least-squares method and the SOK code, taking available experimental data into account. In the resonance region around 1 keV for ^{235}U , capture cross-sections were reduced to improve integral benchmark tests. The reduction was confirmed by Jandel, et al. during a later experiment at Los Alamos. For ^{56}Fe , cross-sections of inelastic scattering and angular distributions of elastic scattering were revised from JENDL-3.3. Evaluation methods and comparisons with experimental data and other evaluated data will be reviewed.

Introduction

JENDL-4.0 was released in 2010 (Shibata, *et al.*, 2011). The revision from JENDL-3.3 (Shibata, *et al.*, 2002) was mainly focused on fission products and minor actinides. It is intended to improve reliability for applications such as innovative reactors, high burn-up use and MOX fuel reactors. To increase the reliability of evaluation for MA and FP, two theoretical nuclear reaction model codes, CCONE (Iwamoto, 2007) and POD (Ichihara, *et al.*, 2007) had been developed. All of the actinide data were reviewed and most were revised, based on available experimental data. Other significant progress of JENDL-4.0 was an increase of covariance data which were evaluated for all cross-sections, angular distributions and fission neutron spectra of all actinides.

Major actinide

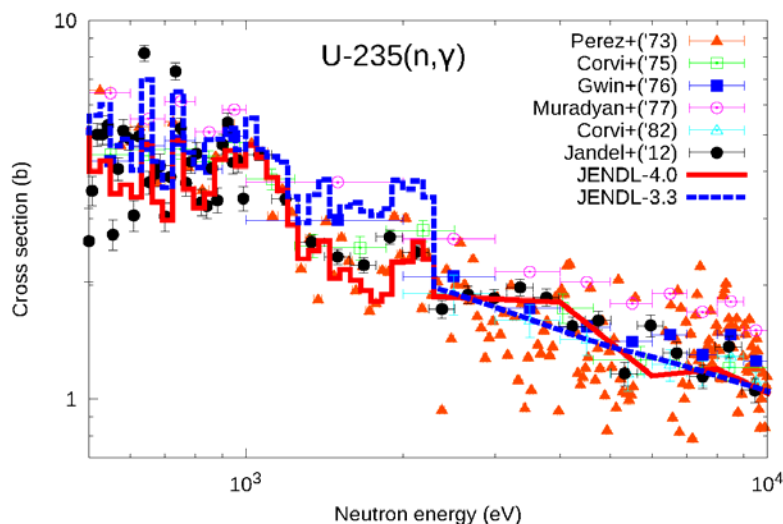
Resonance region

JENDL-4.0 adopted the resolved resonance parameters of SAMMY analyses carried out by Leal, *et al.* (1999), Derrien, *et al.* (2009) and Derrien, *et al.* (2007) for ^{235}U , ^{238}U and ^{239}Pu , respectively. The parameters of ^{235}U were also adopted by all of the recent nuclear data libraries of JENDL-3.3, ENDF/B-VII.1 (Chadwick, *et al.*, 2011), JEFF-3.1 (Koning, *et al.*, 2006), CENDL-3.1 (Ge, *et al.*, 2011) and ROSFOND-2010 (ABBN, n.d.). However, in JENDL-4.0 the upper limit of the original resolved resonance region 2.25 keV was lowered to 500 eV and modified point-wise cross-sections were given between 500 eV to 2.25 keV to recover the worsened integral benchmark results for some uranium-fuelled fast reactors, which would be arisen by changing the resonance parameter of JENDL-3.3 from JENDL-3.2. According

to the sensitivity analyses of the integral test, the capture cross-section would be overestimated around 1 keV and a gap of evaluated cross-section appearing at 2.25 keV in JENDL-3.3 should be decreased. The data recently measured by Jandel, *et al.* (2012) support JENDL-4.0 in that energy region. Evaluations of JENDL-4.0 and JENDL-3.3 are compared with experimental data in Figure 1.

Figure 1: ^{235}U neutron capture cross-section

JENDL-4.0 and JENDL-3.0 are shown by group-wise cross-section below 2.25 keV



Fast energy region

Fission cross-section

The fission cross-sections of major actinides were evaluated by the least-squares method using measured cross-sections and ratio data simultaneously using the SOK code (Kawano, *et al.*, 2000). The carefully checked 124 experimental data sets were included in the analysis. As well as the best-estimated cross-section, covariance data were deduced at the same time. By taking account of scatter of the experimental data, the obtained standard deviation was multiplied by a factor of 2. The ^{235}U fission cross-section ratios of various evaluations to JENDL-4.0 are shown in Figure 2. Above 0.1 MeV, the evaluated result of ^{235}U cross-sections agrees with the other evaluations. However, below 0.1 MeV, deviations from JENDL-4.0 become larger than the uncertainty.

Evaluation by CCONE code

With the exception of fission cross-sections, most of the data in the fast neutron region were evaluated by theoretical model calculation with the CCONE code. It had been developed for the JENDL-4.0 by integrating several nuclear reaction models such as coupled-channel optical model, distorted wave born approximation, pre-equilibrium two-component exciton model and the Hauser-Feshbach-Moldauer statistical model. The model parameters were determined to fit the experimental data, and their uncertainties were also deduced to evaluated covariance data by the least-squares method using the KALMAN code system (Kawano and Shibata, 1997) with available measured data. The covariance data, for which experimental data were scarce, were also evaluated using the parameter uncertainties. Figure 3 compares ratios of inelastic scattering cross-sections to JENDL-4.0 for ^{238}U and ^{239}Pu . For ^{238}U the cross-sections agree among evaluations within the uncertainty except for the lower and upper edge region. The ^{239}Pu cross-sections were in poor agreement especially with JEFF-3.1.1 (=RUSFOND-2010) and CENDL-3.1 evaluations.

Figure 2: Ratio of ^{235}U fission cross-section of various evaluations to JENDL-4.0

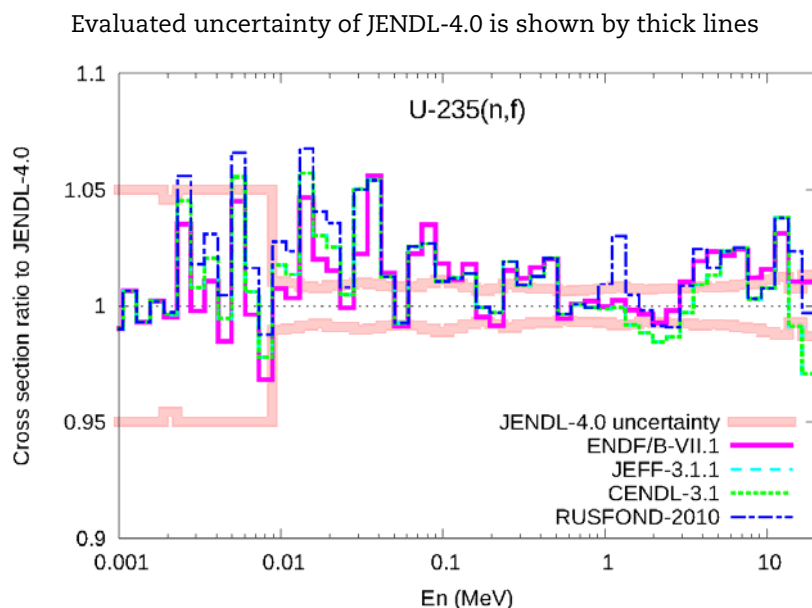
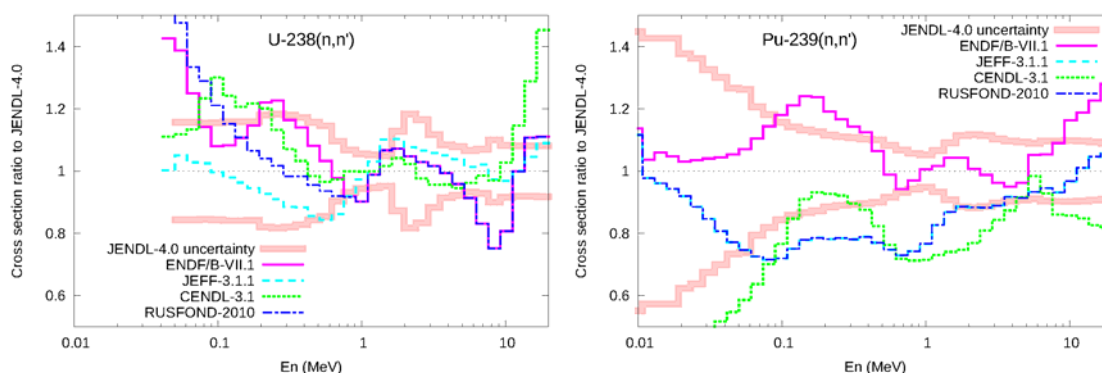


Figure 3: Ratio of inelastic scattering cross-section of various evaluations to JENDL-4.0 for ^{238}U (left) and ^{239}Pu (right)

Evaluated uncertainty of JENDL-4.0 was shown by thick lines

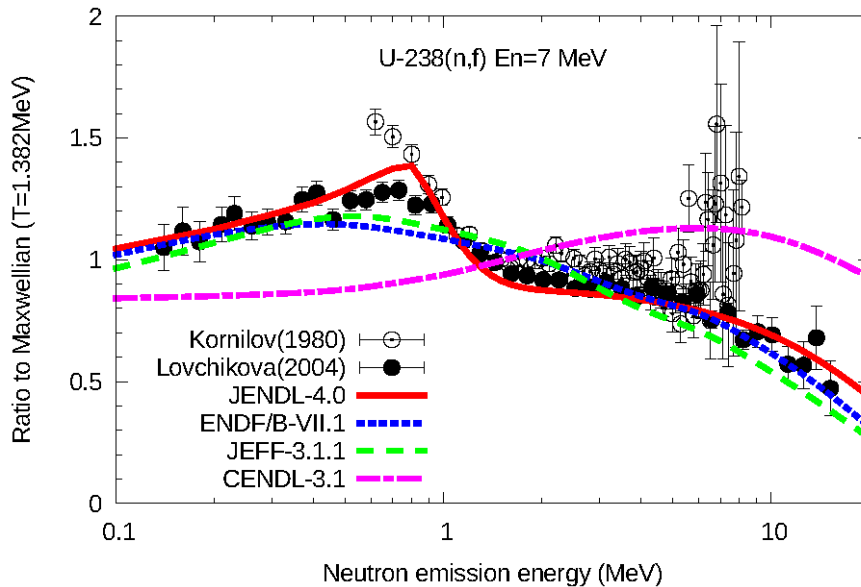


Prompt fission neutron spectra

The prompt fission neutron spectra were calculated based on the Madland-Nix model. Below the second chance fission threshold, the method combined with multimodal random-neck rupture of the fission process was applied to JENDL-3.3 evaluation of ^{235}U and ^{239}Pu (Ohsawa, 2001). Evaluation of ^{238}U was performed for JENDL-3.2. JENDL-4.0 adopted those values below the neutron incident energy around 5 MeV. Above the threshold energy of the second chance fission, the fission spectra were calculated incorporating the pre-equilibrium statistical model calculations by CCONE code. The pre-scission neutron spectra and average excitation energies leading to fission were deduced from the calculations done for the cross-section evaluation. The average excitation energies were adapted to the fission spectra systematics (Iwamoto, 2008) to estimate post-scission neutron spectra. The fission spectrum for ^{238}U at 7 MeV is shown in Figure 4. JENDL-4.0 agrees well with the experimental data. The bump around the neutron emission energy at 0.8 MeV could be due to the pre-scission neutrons that are taken into account in JENDL-4.0.

Figure 4: Prompt fission neutron spectrum for ²³⁸U at neutron incident energy 7 MeV

The spectra are shown by ratios to Maxwellian at T = 1.382 MeV



Iron-56

Total and elastic scattering cross-sections

A small part of nuclear data on ⁵⁶Fe was modified from JENDL-3.3. The neutron energy range for ⁵⁶Fe data in JENDL-4.0 is from 10⁻⁵eV to 20 MeV, while ENDF/B-VII.1 and JEFF-3.1.2 (OECD/NEA, 2012) cover much wider energy ranges up to 150 and 200 MeV, respectively. In the resolved resonance region the Reich-Moore formula was used with resolved resonance parameters which are given up to 850 keV. The parameters were taken from Froehner's evaluation in JEF-2. The detailed measurement of total cross-section for natural Fe shows resonance-like structure above 850 keV. JENDL-3.3 (and also JENDL-4.0) followed the fine structure data, and the total cross-section on ⁵⁶Fe was generated by subtracting the contributions of the other isotopes, and thus it still has resonance features as shown in Figure 5 (left). The angular distributions are important for the criticalities of fast reactors with iron reflectors. The Legendre coefficients of angular distribution for elastically scattered neutrons were revised in the JEDNL-4.0 evaluation using fine structure data measured by Perey, *et al.* (1991) in the range of 40 to 850 keV and by Kinney and McConnell (1976) in the range of 850 keV to 2.5 MeV. Model calculation was done by POD in the energies above 2.5 MeV. Figure 5 (right) shows that JENDL-4.0 has stronger forward peaking than the others above 2.5 MeV. The comparisons of angular distributions in different neutron energies are made with experimental data and evaluated libraries in Figure 6. JENDL-4.0 exhibits reasonable agreement with experimental data, except for the distributions at the most backward angles in higher energies.

Inelastic scattering cross-sections

The cross-sections of inelastic scattering to the first excited level (846 keV) below 2.1 MeV and to the second and third excited levels (2 085 and 2 657 keV, respectively) in the whole energy range were newly evaluated by POD and coupled-channel optical model calculations. The JENDL-3.3 evaluation was adopted below 2.1 MeV where the data were obtained from high resolution data of Voss, *et al.* (1971) by taking account of gamma-ray

Figure 5: Total cross-section in a resonance-like region (left) and first-order Legendre coefficients of elastic scattering angular distribution (right)

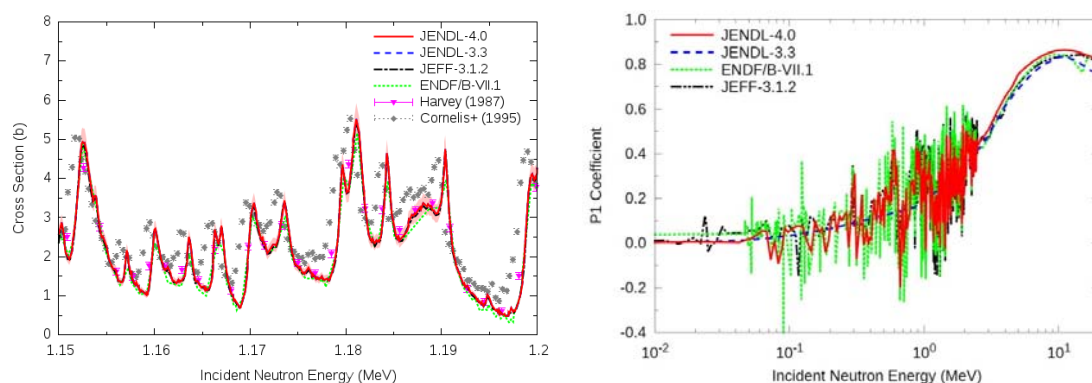
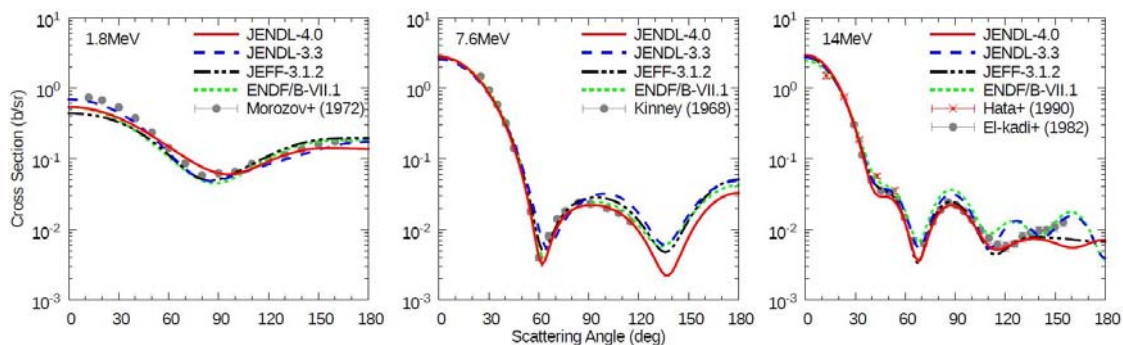


Figure 6: Elastic scattering angular distributions



angular distributions (Smith, 1976). These revisions for JENDL-4.0 were based on a shielding benchmark test. Figure 7 shows the $^{56}\text{Fe}(n,n_1)$ and $^{56}\text{Fe}(n,n_2)$ inelastic scattering cross-sections with uncertainties in comparison with experimental data and the other libraries. The $^{56}\text{Fe}(n,n_1)$ cross-section above 7 MeV in JENDL-4.0 is somewhat small relative to experimental data. The uncertainty, however, is reasonable, compared to the measured data and even to JENDL-3.3. On the other hand, comparing with available experimental data, the $^{56}\text{Fe}(n,n_2)$ cross-section in JENDL-4.0 is large below 4 MeV and small above 4 MeV, but the evaluated uncertainties still cover the experimental data. Figure 8 compares the angular distributions of inelastic scattering to the first and second excited levels with measured data and those of the evaluated libraries. The Legendre coefficients for inelastic scattering in JENDL-4.0 remain unchanged from those of JENDL-3.3. Consequently, the difference derives from each cross-section. The diversity of the measured angular distributions is relatively large, and thus we cannot judge which libraries are better to reproduce the experimental data. Much experimental effort is needed to increase the accuracy of nuclear data for the inelastic scattering angular distributions.

(n,p) and $(n,2n)$ reaction cross-sections

Figure 9 shows the (n,p) and $(n,2n)$ reaction cross-sections. The (n,p) reaction has been used as a monitor for measurements by the activation method. The cross-section in JENDL-4.0 was basically taken from JENDL-2 released in 1984 (Kikuchi, *et al.*, 1985), but at the evaluation of JENDL-3 (Shibata, *et al.*, 1990) it was revised by considering the data of Smith and Meadow (1975) below 7 MeV and Ikeda, *et al.* (1988) between 13 and 16 MeV. Covariance was based on the experimental data, and the uncertainty is 5 to 7%. The $(n,2n)$ reaction cross-section in JENDL-4.0 was very similar to that in ENDF/B-VII.1. This is due

Figure 7: Cross-sections of inelastic scattering to the first and second excited levels

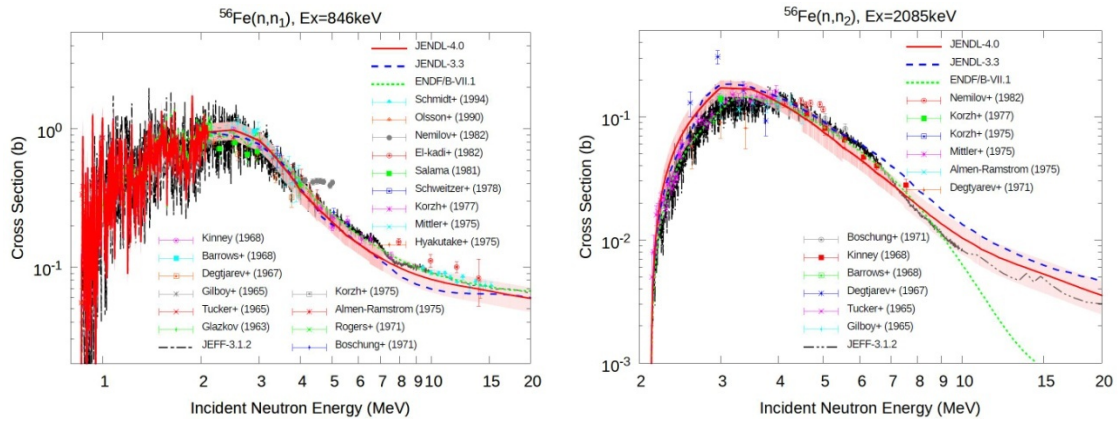


Figure 8: Angular distributions of inelastic scattering to the first and second excited levels

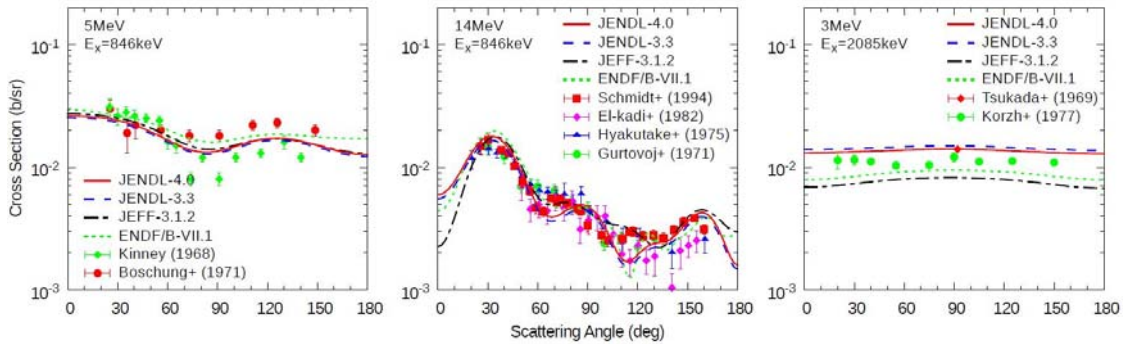
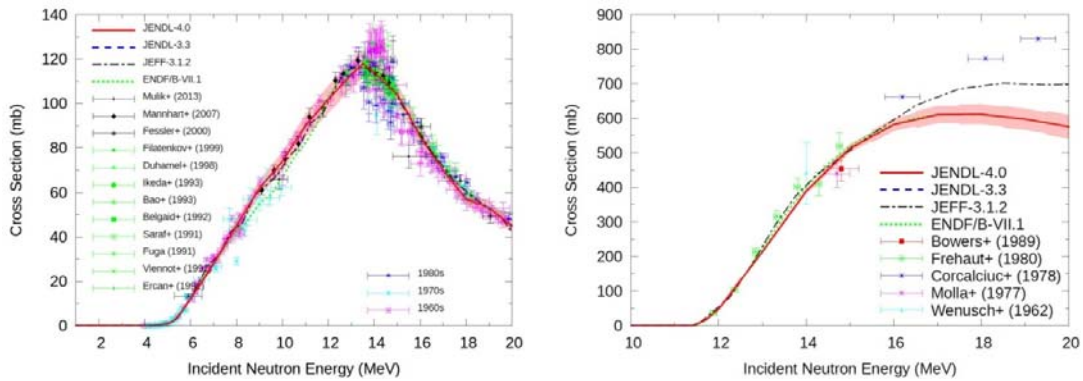


Figure 9: (n,p) and (n,2n) reaction cross-sections

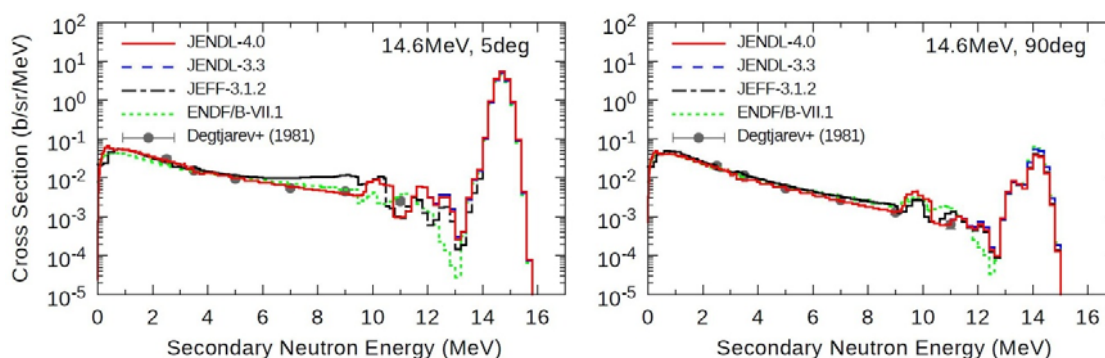


to the use of the same input parameter. The cross-section above 15 MeV is somewhat uncertain due to the lack of measured data. The covariance data were evaluated by KALMAN, considering the data measured by Frehaut, *et al.* (1980), Corcalciuc, *et al.* (1978), and Wenusch and Vonach (1962). The uncertainty derived from the covariance of model parameters was 2.4 to 6% with increasing energy above 15 MeV.

Neutron emission double differential cross-sections

Double differential cross-sections for neutron emissions at 14.6 MeV incident energy and at 5 and 90° were compared with experimental data and the evaluated libraries in Figure 10. Since the re-evaluation for JENDL-4.0 was very limited, the difference between JENDL-3.3 and JENDL-4.0 is only seen in regions related to elastic and inelastic scattering components. The non-negligible differences among evaluated libraries especially at the most forward and backward (not shown) angles were found in the secondary neutron energy range where inelastic scattering components are important.

Figure 10: Neutron emission double differential cross-sections



Acknowledgements

The authors are grateful to the members of Nuclear Data Center and the Japanese Nuclear Data Committee for their various contributions to the development of JENDL-4.0.

References

- ABBN (ABBN Laboratory) (n.d.), "Data Files and Substantiations", webpage on ABBN website, ABBN Laboratory, Department of Nuclear Power Plants, accessed 28 May 2011, www.ippe.ru/podr/abbn/english/libr/rosfond.php.
- Chadwick, M.B., *et al.* (2011), "ENDF/B-VII.1 Nuclear Data for Science and Technology: Cross Sections, Covariances, Fission Product Yields and Decay Data", *Nucl. Data Sheets*, 112 [12], pp. 2887-2996.
- Corcalciuc, V., *et al.* (1978), "A Study of the Neutron Induced Reactions for ^{19}F , ^{56}Fe and ^{59}Co in the Energy Interval 16 to 22 MeV", *Nucl. Phys. A*, 307 [3], pp. 445-471.
- Derrien, H., *et al.* (2007), " ^{239}Pu Neutron Resonance Parameters Revisited and Covariance Matrix in the Neutron Energy Range from Thermal to 2.5 keV", *Proc. of Int. Conference on Nuclear Data for Science and Technology*, Nice, France, 22-27 April 2007, article No. 176, CEA, EDP Sciences.

- Derrien, H., *et al.* (2009), “R-Matrix Analysis of ^{238}U High-Resolution Neutron Transmissions and Capture Cross Sections in the Energy Range 0 to 20 keV”, *J. Nucl. Sci. Eng.*, 161 [2], pp. 131-159.
- Frehaut, J., *et al.* (1980), “Status of (n,2n) Cross Section Measurements at Bruyères-le-Châtel”, INDC(USA)-84 (1), pp. 399-412.
- Ge, Z.G., *et al.* (2011), “The Updated Version of Chinese Evaluated Nuclear Data Library (CENDL-3.1)”, *J. Korean Phys. Soc.*, 59 [2], pp. 1052-1056.
- Ichihara, A., *et al.* (2007), *Program POD; A Computer Code to Calculate Cross Sections for Neutron-Induced Nuclear Reactions*, JAEA-Data/Code 2007-012, Japan Atomic Energy Agency.
- Ikeda, Y., *et al.* (1988), *Activation Cross Section Measurements for Fusion Reactor Structural Materials at Neutron Energy from 13.3 to 15.0 MeV Using FNS Facility*, JAERI-1312, Japan Atomic Energy Research Institute.
- Iwamoto, O. (2007), “Development of a Comprehensive Code for Nuclear Data Evaluation, CCONE, and Validation Using Neutron-Induced Cross Sections for Uranium Isotopes”, *J. Nucl. Sci. Technol.*, 44 [5], pp. 687-697.
- Iwamoto, O. (2008), “Systematics of Prompt Fission Neutron Spectra”, *J. Nucl. Sci. Technol.*, 45 [9], pp. 910-919.
- Jandel, M., *et al.* (2012), “New Precision Measurements of the $^{235}\text{U}(n,\gamma)$ Cross Section”, *Phys. Rev. Lett.*, 109, 202506 [5 pages].
- Kawano, T. and K. Shibata (1997), *Covariance Evaluation System*, JAERI-Data/Code 97-093, Japan Atomic Energy Research Institute.
- Kawano, T., *et al.* (2000), *Evaluation of Fission Cross Section and Covariances for ^{233}U , ^{235}U , ^{238}U , ^{239}Pu , ^{240}Pu , and ^{241}Pu* , JAERI-Research 2000-004, Japan Atomic Energy Research Institute.
- Kikuchi, Y., *et al.* (1985), “Second Version of Japanese Evaluated Nuclear Data Library (JENDL-2)”, *J. Nucl. Sci. Technol.*, 22 [8], pp. 593-603.
- Kinney, W.E. and J.W. McConnell (1976), “High Resolution Neutron Scattering Experiments at ORELA”, *Proc. Int. Conf. Interactions of Neutrons with Nuclei*, Lowell, p. 1319.
- Koning, A., *et al.* (2006), “The JEFF-3.1 Nuclear Data Library”, *JEFF Report 21*, NEA No. 6190, OECD/NEA, Paris.
- Leal, L.C., *et al.* (1999), “R-Matrix Analysis of ^{235}U Neutron Transmission and Cross-Section Measurements in the 0- to 2.25-keV Energy Range”, *J. Nucl. Sci. Eng.*, 131 [2], pp. 230-253.
- OECD/NEA (Organisation for Economic Co-operation and Development/Nuclear Energy Agency) (2012), “JEFF-3.1.2 – Neutron Data”, webpage on OECD/NEA Data Bank website, OECD/NEA, Paris, accessed 28 May 2014, www.oecd-nea.org/dbforms/data/eva/evatapes/jeff_31/JEFF312.
- Ohsawa, T. (2001), *New Evaluation of Prompt Neutron Spectra of ^{235}U and ^{239}Pu for JENDL-3.3*, JAERI-Conf 2001-006, pp. 157-159, Japan Atomic Energy Research Institute.
- Perey, C.M., *et al.* (1991), “ ^{56}Fe and ^{60}Ni Resonance Parameters”, *Conf. on Nucl. Data for Sci. and Technol.*, Juelich, pp. 41-44.
- Shibata, K., *et al.* (1990), *Japanese Evaluated Nuclear Data Library, Version-3, – JENDL-3*, JAERI-1319, Japan Atomic Energy Research Institute.
- Shibata, K., *et al.* (2002), “Japanese Evaluated Nuclear Data Library Version 3 Revision-3: JENDL-3.3”, *J. Nucl. Sci. Technol.*, 39 [11], pp. 1125-1136.

- Shibata, K., *et al.* (2011), "JENDL-4.0: A New Library for Nuclear Science and Engineering", *J. Nucl. Sci. Technol.*, 48 [1], pp. 1-30.
- Smith, D.L. (1976), *Fast-Neutron Gamma-Ray Production from Elemental Iron: $E_n \leq 2$ MeV*, ANL/NDM-20, Argonne National Laboratory, Argonne, IL.
- Smith, D.L. and J.W. Meadows (1975), "Cross-Section Measurement of (n,p) Reactions for ^{27}Al , $^{46,47,48}\text{Ti}$, $^{54,56}\text{Fe}$, ^{58}Ni , ^{59}Co and ^{64}Zn from Near Threshold to 10 MeV", *Nucl. Sci. Eng.*, 58, pp. 314-320.
- Voss, F., *et al.* (1971), "Measurement of High Resolution G-ray Production Cross Sections in Inelastic Neutron Scattering on Al and Fe between 0.8 and 13 MeV", *Proc. Third Conf. on Neutron Cross Sections and Technology*, Knoxville, TN, pp. 218-226.
- Wenusch, R. and H. Vonach (1962), "(n,2n) Cross-Section Measurements on ^{55}Mn , ^{59}Co , ^{52}Cr , ^{56}Fe and ^{68}Zn for 14 MeV Neutrons", *Oesterr. Akad. Wiss., Math-Naturw. Kl., Anzeiger*, 99, p. 1.

Differential cross-section measurements at the University of Kentucky – Adventures in analysis

J.R. Vanhoy,^a S.F. Hicks,^b B.R. Champine,^c B.P. Crider,^d
 E.A. Garza,^a S.L. Henderson,^b S.H. Liu,^d E.E. Peters,^d F.M. Prados-Estévez,^d
 M.T. McEllistrem,^d T.J. Ross,^d L.C. Sidwell,^b J.L. Steves,^a S.W. Yates^d
^aDept. of Physics, United States Naval Academy, Annapolis, Maryland, United States
^bDept. of Physics, University of Dallas, Irving, Texas, United States
^cDept. of Physics & Nuclear Engineering, United States Military Academy,
 West Point, New York, United States
^dDepts. of Chemistry and Physics & Astronomy, University of Kentucky,
 Lexington, Kentucky, United States

Abstract

Elastic and inelastic neutron scattering cross-sections are determined at the University of Kentucky Accelerator Laboratory (UKAL)¹ using time-of-flight techniques at incident energies in the fast neutron region. Measurements have been completed for scattering from ²³Na and for the ²³Na(n,n'γ) reaction; similar measurements are in progress for ⁵⁴Fe. Commencing in the summer of 2014, measurements will address ⁵⁶Fe. An overview of the facilities and instrumentation at UKAL is given, and our measurement and analysis procedures are outlined. Of particular concern are portions of the analysis which limit the accuracy and precision of the measurements. We briefly examine detector efficiencies derived from the ³H(p,n) cross-sections, attenuation and multiple scattering corrections, and neutron and γ-ray cross-sections standardisations.

Introduction and recent measurements

The main component of the applied science programme at the University of Kentucky Accelerator Laboratory (UKAL) is the measurement of neutron elastic and inelastic scattering differential cross-sections important for fission reactor applications, particularly on structural materials like ^{54,56}Fe and coolants like ²³Na. A major goal of this experimental programme is to verify the accuracy of evaluated cross-sections available for nuclei of interest in the nuclear data libraries such as ENDF, JENDL and JEFF. These evaluations are based on existing experimental cross-sections which are often sparse in the fast neutron energy region and often have uncertainties that are larger than desired or are not well documented.

The laboratory has facilities for the production and detection of neutrons in the fast neutron region – a region that is important for both pure and applied nuclear physics. The laboratory features a 7 MV HVEC CN Van de Graaff with an rf ion source and terminal bunching system that is capable of delivering microamperes of pulsed ion beams, bunched

1. www.pa.uky.edu/accelerator.

to a time spread of ~ 1 ns FWHM, onto the neutron production target. Quasi-monoenergetic fluences of fast neutrons are produced with the $^3\text{H}(p,n)$, $^2\text{H}(d,n)$ or $^3\text{H}(d,n)$ reactions in a gas cell or the $^7\text{Li}(p,n)$ reaction with an evaporated target.

Scattering samples are hung in the neutron fluence about 7 cm from the centre of the production target and are usually right-circular cylinders containing 0.1-0.5 mole of the enriched isotope of interest. One or more polyethylene samples of similar geometry are used for absolute normalisation.

Neutrons scattered from the sample are detected with a C_6D_6 scintillation detector using neutron TOF techniques. The well-shielded detector is mounted on a carriage rotatable about the centre of the scattering sample between angles of 0° - 150° relative to the incident beam direction. Flight paths between 2-4 m are used in most measurements, and pulse-shape discrimination is used to eliminate γ -ray events in the detector.

De-excitation γ -rays are detected using a HPGe detector that is surrounded by a BGO Compton-suppression annulus. The detector is mounted on the same rotatable carriage used for neutron detection, although the flight path used for γ -ray detection is typically about 1.2 m. Unwanted neutron events in the HPGe detector are rejected using TOF techniques. Gamma-ray angular distributions are typically performed from 30° - 150° and γ -ray excitation function measurements are performed at 125° .

A three-year project measuring (n,n) and (n,n') differential cross-sections and angle-integrated $(n,n'\gamma)$ cross-sections for scattering from ^{23}Na was recently completed. The agreement between these new data and the evaluated data is mixed. Angle-integrated $^{23}\text{Na}(n,n_0)$ cross-sections agree rather well with the ENDF/B-VII.1 (Larson, *et al.*, 2011) and JENDL-4.0 (Shibata, *et al.*, 2002) evaluations, while the JEFF-3.1.2 (Fort, *et al.*, 2005; Santimarina, *et al.*, 2009) values are significantly higher than experimental data. For inelastic scattering, the angle-integrated cross-sections are better described by the JENDL evaluation, whereas evaluated cross-sections from ENDF are about 15% too large and from JEFF are about 15% too small relative to these new measurements. We observed significant deviations in the shapes of the measured differential cross-sections from the inelastic levels, especially at forward and back angles where direct coupling can play a significant role in the scattering due to deformation in this mass region (Durell, *et al.*, 1972).

Measurements of $^{54}\text{Fe}(n,n)$ and $^{54}\text{Fe}(n,n'\gamma)$ cross-sections began in June 2013 and will continue through May 2014. Preliminary evaluation of elastic and inelastic scattering from ^{54}Fe reveals significant deviations between evaluated data and scattering from inelastic levels, but reasonably good agreement for elastic scattering. The analysis of the ^{54}Fe data continues. An analogous set of experiments will be performed on ^{56}Fe beginning in June 2014 to compare scattering from these two isotopes of Fe.

Adventures in analysis

Differential cross-sections are extracted from neutron time-of-flight data by standard techniques described by Hicks, *et al.* (1989, 1990, 1994). Relative cross-sections are converted to absolute cross-sections by comparison to the neutron scattering standard $^1\text{H}(n,n)$ cross-sections (Carlson, *et al.*, 2009; Hale, 2006).

Gamma-ray production cross-sections and angle-integrated (n,n') cross-sections are extracted from γ -ray excitation function data measured at a 125° scattering angle. The technique is described by Vanhoy, *et al.* (1992). Cross-section standardisation is typically done by comparison to the ENDF values for $^{56}\text{Fe}(n,n')$ (Chadwick, *et al.*, 2006).

The desired uncertainties for both the ^{23}Na and the $^{54,56}\text{Fe}$ cross-sections are on the order of 10% or less (Aliberti, *et al.*, 2004, 2006). However, the goal of the programme is to determine absolute cross-sections with as much precision and accuracy as possible within the limitation of the challenging experiments and analysis involved with neutron

production and detection. Many contributors to uncertainties in cross-sections are easily controlled, for example, counting statistics and dead time, but other contributors such as source reaction uncertainties are outside the scope of these current measurements. We consider three issues which limit performance in the following subsections.

Ambiguities in neutron detection efficiency

The general energy dependence of the main neutron detector efficiency is describable analytically (Drosg, 1972; Kellerman and Langkau, 1971). Different mechanisms, however, such as sub-threshold pulse pile-up and sub-MeV thresholds complicate the evaluation of the energy dependence of the neutron detection efficiency. Above $E_n = 4.4$ MeV, carbon inelastic scattering further complicates detector response evaluation (Kellerman and Langkau, 1971). Rather than attempting to model the detector efficiency with Monte Carlo simulations or closed-form expressions, it is measured experimentally for these (n,n) and (n,n') experiments by measuring the angular distribution of the source neutrons.

The detector carriage is positioned to rotate about a point directly under the centre of the gas cell with the main detector looking directly at the cell's centre. The relative neutron detector efficiency as a function of E_n is defined as:

$$eff(E_n) = \frac{Y_{Main}(\theta_{lab})}{Y_{FM} \left(\frac{d\sigma}{d\Omega_{Tpn}}(\theta_{lab}) \right)} \quad (1)$$

where $Y_{Main}(\theta)$ is main detector yield of source neutrons at lab angle θ , Y_{FM} is the forward monitor yield for the measurement at angle θ and $d\sigma/d\Omega_{Tpn}$ is the ${}^3\text{H}(p,n)$ cross-section at angle θ . The forward monitor is a scintillation detector used for relative normalisation by detecting source neutrons from a fixed location in the laboratory. Uncertainties in the ${}^3\text{H}(p,n)$ cross-sections are the largest contributing factors to the $eff(E_n)$ and one of the biggest contributors to the overall uncertainties in the neutron scattering cross-sections.

Existing $d\sigma/d\Omega_{Tpn}$ cross-sections can be taken from three recommended sources: *i)* Liskien and Paulsen (LP) (1973); *ii)* the DROSG-2000 program series (2003); *iii)* the evaluated ENDF database (ENDF) (Hale, 2006). LP and DROSG values are based on ${}^3\text{H}(p,n)$ experimental measurements, where the data exist. Absolute uncertainties in LP and DROSG cross-sections are given as ~3%. LP values are an evaluation of information available as of December 1972. DROSG values contain updated information current as of January 2000. ENDF values are produced through the nuclear data evaluation process on the ${}^4\text{He}$ compound nucleus system, the description of which is constrained by many types of experimental measurements (Brune, *et al.*, 1999; Drosg, 1980; Hoffman and Hale, 1997, 2008). Absolute uncertainties in ENDF appear to be ~5%.

Two comparisons of the differential cross-sections from these references are shown in Figures 1 and 2, along with % differences between LP and Drosg and between ENDF and Drosg cross-sections in red and blue, respectively, in the lower panels. Variations of $\pm 10\%$ are observed, with the largest differences observed at forward and back angles.

Efficiency curves utilised during the analysis of the $E_n = 4.0$ data sets are shown in Figure 3. The downturn in the ENDF curve above $E_n = 3.5$ MeV is not compatible with the anticipated detector response.

Absolute cross-sections are not impacted by the overall scale of the C_6D_6 efficiency, but they are sensitive to the energy dependence because the scattered neutron energies change considerably as a function of scattering sample and detection angle. The deviations shown in Figure 3 are the worst case observed in the ${}^{23}\text{Na}$ data sets. Below $E_p = 4.0$ MeV, there is no basis to choose one set of cross-sections (LP, Drosg or ENDF) over the other. Above $E_p = 4.0$ MeV, however, the LP and Drosg descriptions provide an energy dependence which more closely matches the anticipated shape of the C_6D_6 detector efficiency.

Figure 1: T(p,n) cross-section comparison at $E_p = 4.0$ MeV

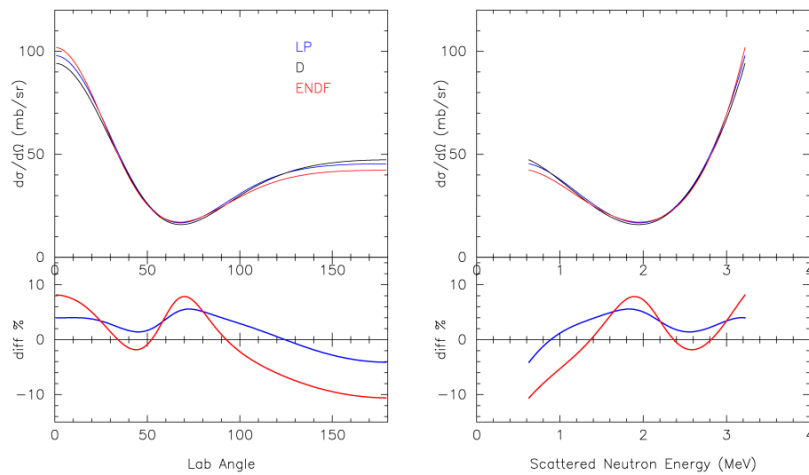


Figure 2: T(p,n) cross-section at $E_p = 5.0$ MeV

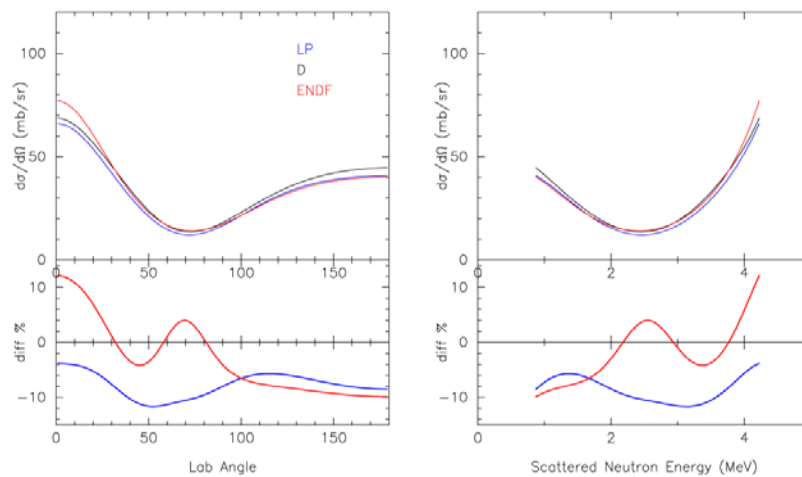
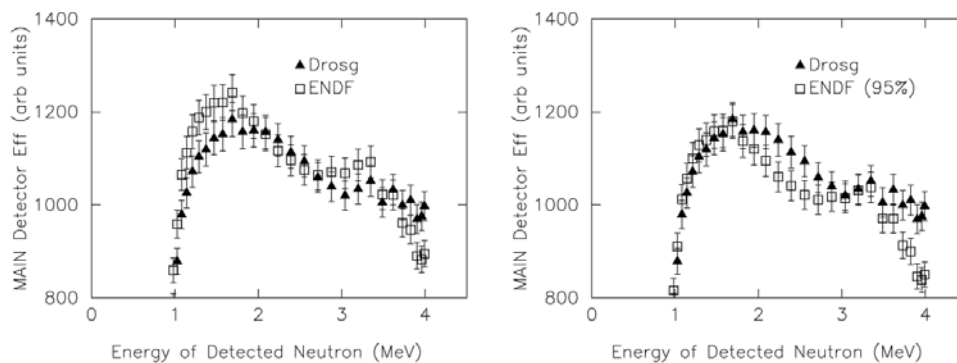


Figure 3: Comparison of efficiency curves calculated with ENDF and Drogg T(p,n) cross-sections

In the right-hand figure, the ENDF curve has been rescaled to accentuate the differences. Our technique does not require the absolute detector efficiency, but the energy variation is important.



Challenges in normalising (n,n'γ) cross-sections

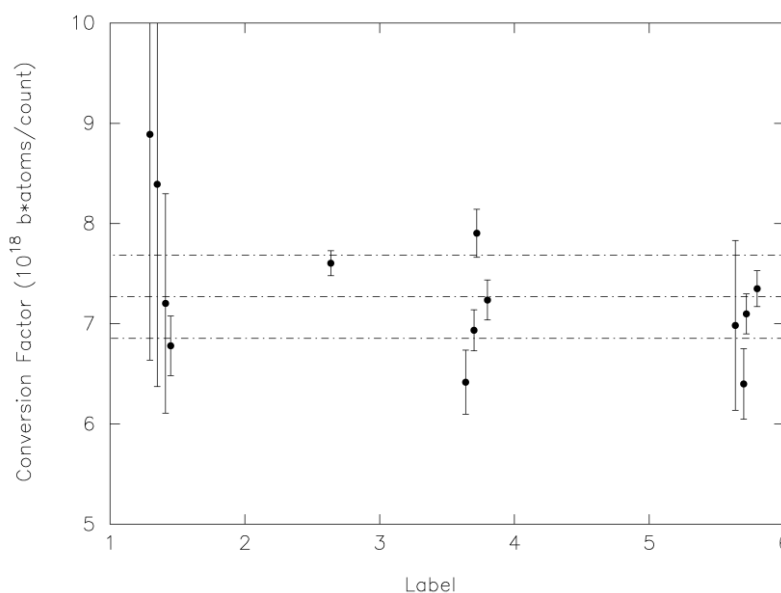
For the ²³Na(n,n'γ) measurements, we chose to make a comparison to the ⁵⁶Fe(n,n) inelastic cross-sections from the ENDF evaluation (Chadwick, *et al.*, 2006). The ⁵⁶Fe inelastic cross-sections are not considered an absolute standard, but are one of the better known choices and span a large energy range. The conversion of yield for the *i*th γ-ray to cross-section $\sigma_{Na,\gamma-ray i}$ is performed by forming a ratio to the ⁵⁶Fe cross-section as in:

$$\sigma_{Na,\gamma-ray i} = \frac{Na \text{ Corrected Yield}_{\gamma-ray i}}{N_{Na}} \cdot \left\langle \frac{br_{j \text{ transition } k} \bar{\sigma}_{Fe,level j}}{Fe \text{ Corrected Yield}_{j \text{ transition } k} / N_{Fe}} \right\rangle \quad (2)$$

Yields have been corrected for HPGe detector efficiency, neutron and γ-ray attenuation in the sample, and neutron multiple scattering in the sample. The symbols *N* are the number of atoms in the indicated sample. The numerator inside ⟨...⟩, $br_{jk} \bar{\sigma}_j$, is the γ-ray production cross-section for transition *k*. It is calculated from the inelastic scattering cross-section and the branching ratio. Subscript *j* denotes the particular final state in the ⁵⁶Fe(n,n) reaction. Subscripts *k* and *i* refer to particular γ-ray transitions. The symbol $\bar{\sigma}_{Fe,level j}$ denotes the energy-averaged level cross-section for ⁵⁶Fe(n,n) – averaged over the incident neutron energy spread across the sample. The symbol *br* denotes the branching ratio for transition *k* of level *j*. To obtain a reliable value for the averaging bracket ⟨...⟩ we considered 13 measurements of $br_{jk} \bar{\sigma}_j$ derived from four *j*-levels at eight incident neutron energies. The levels and energies chosen are free from γ-ray feeding effects. These 13 points are shown in Figure 4 below. The points are distributed on the horizontal axis by a label constructed as “(Level *j*). (2 * *E_n*)”. Thus cross-sections for the ⁵⁶Fe levels *j* = 1, 2, 3, and 5 were utilised.

Figure 4: Values used in determining the conversion factor, ⟨...⟩, for the ²³Na measurements

Lines represent the weighted average and its uncertainty



The bars on each point in Figure 4 are the root-mean-square variations in the ENDF ⁵⁶Fe cross-sections over the energy-averaging interval and dominate the uncertainty in determining ⟨...⟩. The best value of the conversion factor was calculated as:

$$\bar{x} = \frac{\sum w_i x_i}{\sum w_i} \quad \sigma^2 \approx \frac{N \sum w_i (x_i - \bar{x})^2}{(N-1) \sum w_i} \quad (3)$$

where x_i is the value of the point and w_i is $1/\sigma_i^2$, with σ_i the rms variation in the ⁵⁶Fe cross-section over the averaging interval. This method was thought to give the most realistic estimate for the conversion factor and its uncertainty.

The procedure discussed above produced excellent agreement with γ -ray production cross-sections recently measured by Rouki, *et al.* (2012) at the GELINA facility.

The UKAL group began ⁵⁴Fe measurements in June 2013 and will begin ⁵⁶Fe measurements in June 2014. In these cases, it is not appropriate to use previous ⁵⁶Fe γ -ray production cross-sections to perform the cross-section conversion. Because no other single high quality γ -ray production cross-section exists for the $E_n = 1$ to 5 MeV region, we intend to employ a set of targets to determine the conversion factor ⟨...⟩, among which are ⁴⁸Ti, ²⁷Al, ⁵²Cr, ¹²C, ²⁸Si and ⁵¹V.

Attenuation and multiple scattering corrections

Attenuation and multiple scattering corrections are accomplished with the code MULCAT, developed at the University of Kentucky (Velkey, *et al.*, 1975; Lilley, 1980). The code performs iterative Monte Carlo calculations, taking as input the normalised experimental angular distribution as determined from the data analysis, first for scattering from hydrogen in the polyethylene sample. The magnitudes of the corrections are then known. The Kentucky group has years of experience with MULCAT on medium-mass single-element samples (Hicks, *et al.*, 1987; Hicks and McEllistrem, 1987, 1988; Mirzza, *et al.*, 1985).

In comparing results to CSISRS data and ENDF model calculations, there is suspicion that the code produces slightly higher differential cross-sections at forward angles and slightly deeper minima. This suspicion is difficult to evaluate because the data tend to originate in the late 1960s and early 1970s and the ability to evaluate data corrections was severely limited at that time. Information obtained from the ENDF databases are model calculations and not always directly related to data.

To evaluate the performance, a consistency-check technique is adopted. A modelling experiment is designed using MCNPX to describe the experimental set-up. Starting from the ENDF databases, neutrons are scattered from a cylindrical carbon target and counted in a large array of detectors. The counts throughout the detector array are converted into a perturbed “measured cross-section”. This “measured cross-section” is then fed through MULCAT to generate the unperturbed cross-section. If all goes well, this unperturbed cross-section should be identical to the original ENDF database values.

Our first attempt at the consistency check uses the differential cross-section of $E_n = 4.0$ MeV neutrons on ¹²C.

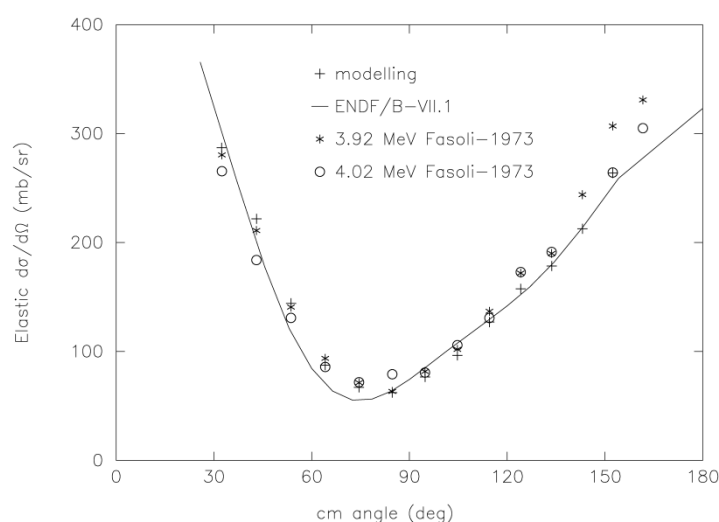
Figure 5 reveals that the agreement is adequate for a first attempt and that MULCAT is likely to perform much better than its own Monte Carlo-predicted calculational uncertainties (~10-13%). Differences at angles greater than 90° are < 4%. The significant differences occur in the region 50°-90° and are as large as 23%. These differences may be due to our first approximations relating to the beam uniformity and divergence:

- The MCNPX beam was assumed to uniformly illuminate the $\pm 8.2^\circ$ sample size.
- To convert detector counts to cross-section, the beam was assumed to be planar, not divergent as from the actual gas cell.
- MULCAT uses a realistic Liskien and Paulsen beam profile and includes the actual gas cell dimensions – this is a different treatment than the MCNPX calculation.

To learn more about the sensitivity of results to the geometric details, the next steps are to:

- construct a realistic MCNPX neutron source description using the IRMM code NeuSDesc (Birgersson and Lövestam, 2009);
- improve the MCNPX result statistics;
- improve our conversion of detector counts \rightarrow cross-section.

Figure 5: Preliminary MCNPX-MULCAT consistency check



Summary

Analysis of neutron scattering data is an adventure. Many corrections are required and the analysis utilises information from many other data sets and model calculations. Exploring and understanding the limitations of the foundational information is important for controlling the accuracy of the cross-section results. We have considered the limitations in neutron detection efficiency, the normalisation of $(n,n'\gamma)$ cross-sections, and attenuation and multiple scattering corrections.

Acknowledgements

Research at the University of Kentucky Accelerator Laboratory is supported by grants from the United States Department of Energy-Nuclear Energy Universities Program, the United States National Science Foundation, the DTRA Nuclear Science and Engineering Research Center, the USNA James Kinnear Fellowship and the Cowan Physics Fund at the University of Dallas.

References

- Aliberti, G., *et al.* (2004), "Impact of Nuclear Data Uncertainties on Transmutation of Actinides in Accelerator-Driven Assemblies", *Nuclear Science and Engineering*, 146, p. 13.
- Aliberti, G., *et al.* (2006), "Nuclear Data Sensitivity, Uncertainty and Target Accuracy Assessment for Future Nuclear Systems", *Annals of Nuclear Energy*, 33, pp. 700-733.
- Birgersson, E. and G. Lövestam (2009), *NeuSDesc – Neutron Source Description Software Manual*, EUR 23794 EN, available at: http://irmm.jrc.ec.europa.eu/about_IRMM/laboratories/Pages/the_van_de_graaff_laboratory.aspx.
- Brune, C.R., *et al.* (1999), "Total Cross Section of the ${}^3\text{H}(p,n){}^3\text{He}$ Reaction from Threshold to 4.5 MeV", arXiv:nucl-ex/9902010v1.
- Carlson, A.D., *et al.* (2009), "International Evaluation of Neutron Cross Section Standards", *Nucl. Data Sheets*, 110, pp. 3215-3324.
- Chadwick, M.B., *et al.* (2006), *ENDF/V-III.1 ${}^{56}\text{Fe}(n,n)$ Reaction Evaluation*, evaluation of September 1996, distribution of December 2006, available at www.nndc.bnl.gov/sigma.
- Drosg, M. (1972), "Accurate Measurement of the Counting Efficiency of a NE-213 Neutron Detector Between 2 and 26 MeV", *Nucl. Instrum. Meth.*, 105, pp. 573-584.
- Drosg, M. (1980), *The ${}^3\text{H}(p,n){}^3\text{He}$ Differential Cross Sections Below 5 MeV and the $n\text{-}{}^3\text{He}$ Cross Sections*, LA-8215-MS, UC-34c.
- Drosg, M. (2003), *Drosg-2000: Neutron Source Reactions*, IAEA-NDS-87 Rev. 8, and *Codes DROSG-2000 of the IAEA Version 2.21*.
- Durell, J.L., *et al.* (1972), "Lifetimes and Decay Modes of Energy Levels in ${}^{23}\text{Na}$, ${}^{26}\text{Mg}$ and ${}^{26}\text{Al}$ ", *J. Phys. A*, 5, pp. 302-317.
- Fasoli, U., *et al.* (1973), "Neutron-Carbon Interaction: Total and Elastic Scattering Differential Cross Sections and Phase Shift Analysis, 2.1 to 4.7 MeV", *Nucl. Phys. A*, 205, pp. 305-320.
- Fort, E., *et al.* (2005), *JEFF-3.1.2 Data Evaluation for ${}^{23}\text{Na}$* , and updates through May 2005.
- Hale, G.M. (2006), *ENDF/V-II.1 ${}^1\text{H}(n,n)$ Reaction Evaluation*, evaluation of October 2005, distribution of December 2006, available at www.nndc.bnl.gov/sigma.
- Hicks, S.E., *et al.* (1987), "Influence of Nuclear Dynamics on Neutron Scattering from ${}^{194}\text{Pt}$ ", *Phys. Rev. C*, 36, pp. 73-82.
- Hicks, S.E., *et al.* (1989), "Nuclear Dynamics of ${}^{192}\text{Os}$ as Probed in Neutron Scattering", *Phys. Rev. C*, 40, pp. 2509-2519.
- Hicks, S.E. and M.T. McEllistrem (1987), "Ground State Reorientation Effects in Elastic Scattering Cross Sections", *Nucl. Phys. A*, 468, pp. 372-380.
- Hicks, S.E. and M.T. McEllistrem (1988), "Energy Dependence of the Mean-Field Potential for Neutron Scattering from ${}^{190,192}\text{Os}$ and ${}^{194,196}\text{Pt}$ ", *Phys. Rev. C*, 37, pp. 1787-1790.

- Hicks, S.F., *et al.* (1990), "Collective Doorway Configurations in ^{49}Ca Through Neutron Scattering on ^{48}Ca ", *Phys. Rev. C*, 41, pp. 2560-2570.
- Hicks, S.F., *et al.* (1994), "Neutron Scattering Cross Sections for $^{204,206}\text{Pb}$ and Neutron and Proton Amplitudes of E2 and E3 Excitations", *Phys. Rev. C*, 49, pp. 103-115.
- Hoffman, H.M. and G.M. Hale (1997), "Microscopic Calculation of the ^4He System", *Nucl. Phys. A*, 613, pp. 69-106.
- Hoffman, H.M. and G.M. Hale (2008), " ^4He Experiments Can Serve as a Database for Determining the Three-Nucleon Force", *Phys. Rev. C*, 77, 044002.
- Kellerman, H.J. and R. Langkau (1971), "Neutron Detection Efficiency of the Liquid Scintillator NE 214 in the MeV Range", *Nucl. Instrum. Meth.*, 94, pp. 137-140.
- Larson, D.C., *et al.* (2011), *ENDF/B-VII.1 Data Evaluation for ^{23}Na 1977*, and updates through December 2011, available at www.nndc.bnl.gov/sigma.
- Lilley, J.R. (1980), *MULCAT-BRC, A Monte Carlo Neutron and Gamma-Ray Multiple Scattering Correction Program*, Internal Service de Physique et Techniques Nucléaire, Centre d'Études de Bruyères-le-Châtel, Report P2N/934/80.
- Liskien, H. and A. Paulsen (1973), "Neutron Production Cross Sections and Energies for the Reactions $\text{T}(p,n)^3\text{He}$, $\text{D}(d,n)^3\text{He}$, and $\text{T}(d,n)^4\text{He}$ ", *Nuclear Data Tables*, 11, pp. 569-619.
- Mirzza, M.C., *et al.* (1985), "Collective Excitations of ^{194}Pt in Low Energy Neutron Scattering", *Phys. Rev. C*, 32, pp. 1488-1495.
- Rouki, C., *et al.* (2012), "High Resolution Measurement of Neutron Inelastic Scattering Cross-Sections for ^{23}Na ", *Nucl. Instrum. Meth. A*, 672, pp. 82-93.
- Santamarina, A., *et al.* (2009), "JEFF-3.1.1 Nuclear Data Library", *JEFF Report 22*, OECD/NEA, Paris, available at www.nndc.bnl.gov/sigma.
- Shibata, K., *et al.* (2002), *JENDL Data Evaluation for ^{23}Na* , and updates through March 2002, available at www.nndc.bnl.gov/sigma.
- Velkey, D.E., *et al.* (1975), "Sample-Size Effects in Neutron Scattering Studied with Analytic and Monte Carlo Methods", *Nucl. Instrum. Meth.*, 129 pp. 231-239.
- Vanhoy, J.R., *et al.* (1992), "Neutron and Proton Dynamics of ^{48}Ca Levels and γ -Ray Decays from Neutron Inelastic Scattering", *Phys. Rev. C*, 45, pp. 1628-1643.

CIELO-related nuclear data measurements at the Gaertner LINAC Center at RPI

Y. Danon,^a Z. Blain,^a A. Daskalakis,^a B. McDermott,^a D. Williams,^a
D. Barry,^b R. Block,^b T. Donovan,^b B. Epping,^b G. Leinweber,^b M. Rapp^b

^aGaertner LINAC Center, Rensselaer Polytechnic Institute
Troy, NY, United States

^bBechtel Marine Propulsion Corporation, Knolls Atomic Power Laboratory
Schenectady, NY, United States

Abstract

The Gaertner LINAC Center at Rensselaer Polytechnic Institute (RPI) has been conducting neutron-induced transmission, scattering, capture and fission measurements on materials that are relevant to the Collaborative International Evaluated Library Organization (CIELO). Fission and capture measurements of ^{235}U in the resonance region were performed with the RPI multiplicity detector. Grouping the data in the energy range of 1 000 eV to 1 500 eV supports a capture cross-section that is lower than ENDF/B-VII.1 and closer to JENDL-4.0. Neutron scattering measurements have been made with incident energy range from 0.5 MeV to 20 MeV for ^{56}Fe and ^{238}U . For back-angle scattering the new data for ^{238}U show discrepancies from ENDF/B-VII.1 and are in better agreement with the JENDL-4.0 evaluation. High-energy resolution transmission of ^{56}Fe was measured in the energy range from 0.5 to 20 MeV and shows good agreement with the evaluations and previous measurements with a lower uncertainty above 4 MeV. Methods and results from these experiments will be discussed.

Introduction

The Gaertner LINAC Center at Rensselaer Polytechnic Institute (RPI) has been conducting nuclear data research since its inception in 1961 (Gaertner, Yeater and Fullwood, 1961). The centre houses a 60 MeV pulsed electron accelerator that can deliver a maximum beam power of about 10 KW. The centre includes several neutron production targets and detection systems that are located in different flight paths at 15 m, 25 m, 30 m, 45 m, 100 m and 250 m. Recent measurements include neutron transmission, capture, scattering and prompt fission neutron spectrum. The facility also houses a lead slowing-down spectrometer that is used for fission, (n, α) cross-section measurements for samples with small cross-sections or small mass (Thompson, *et al.*, 2012) and for measurements of fission fragment mass and energy distributions (Romano, *et al.*, 2010).

Some of the measurements that were recently completed or are still in progress include materials that are of interest to the Collaborative International Evaluated Library Organization (CIELO) and can thus contribute new data to the evaluation process. Recent relevant activity includes neutron scattering from ^{56}Fe and ^{238}U , neutron capture measurements of ^{235}U , neutron transmission measurements of ^{56}Fe and fission neutron distributions for ^{238}U .

Neutron scattering measurements for ²³⁸U and ⁵⁶Fe

A neutron scattering system based on an array of eight EJ-301 liquid scintillators was used to measure neutron scattering in the energy range from 0.5 MeV to 20 MeV (Saglione, *et al.*, 2010; Barry, *et al.*, 2013). The sample is located at a distance of 30.07 ± 0.02 m from the pulsed neutron source and the detectors are located at a distance of 0.50 ± 0.01 m. Two detectors were kept at each scattering angle and the measured angles were 27, 45, 60, 77, 112, 130, 153 and 156 degrees relative to the neutron beam direction. The detector data is collected by digitisers and processed into a time-of-flight (TOF) spectrum. The neutron flux shape incident on the sample was measured using a ²³⁵U fission chamber and was corrected for transmission through all the materials in the beam path. The EJ-301 detection efficiency as a function of energy was measured by placing the detectors in the neutron beam (at the sample position) and using a low intensity beam. Using this measurement and the known flux shape, the energy dependence of the neutron detection efficiency was obtained for each of the eight detectors.

Data analysis includes pulse shape discrimination (PSD) to reduce contributions from gammas. Because PSD can result in 1-2% false neutron detection (gammas that were mistakenly detected as neutrons), and the gamma emission from inelastic scattering and fission in the ²³⁸U sample was relatively high, an additional gamma rejection method was developed. In this method the fraction of false neutrons resulting from the PSD classification method was measured as a function of the gamma pulse area using several gamma sources. For the scattering measured data, the product of this fraction with the number of PSD classified gammas provides an estimate of the false neutrons. This method reduces the contribution to the neutron count from false neutrons to less than 0.005%.

The measured data was compared to detailed MCNP simulations that included the pulsed neutron source energy spectrum, the neutron pulse width and the energy dependent neutron detection efficiency. All the materials in the neutron beam path including 1.9 cm natural U filter, aluminium and water in the target structure, and Mylar vacuum windows were also included in the simulation. The simulations were done using several evaluated cross-section libraries to determine which evaluation fits the data best. To verify the experimental procedures and the quality of the simulations a 7-cm thick graphite sample was always measured in the same experiment by cycling between the sample, the graphite sample and no sample (a background component).

Neutron scattering from ²³⁸U

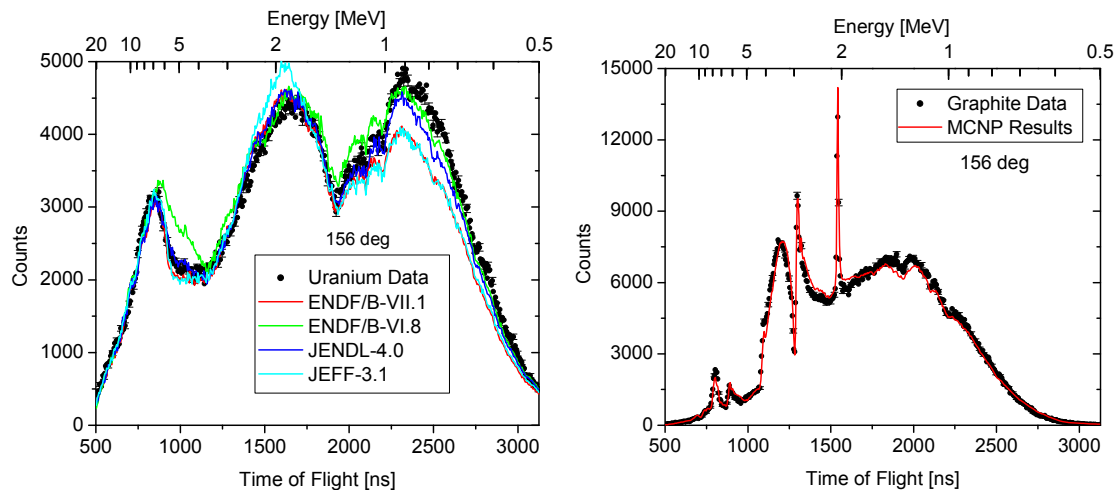
A cylindrical sample containing depleted uranium (0.2% ²³⁵U) with thickness of 0.979 ± 0.002 cm, diameter of 7.618 ± 0.002 cm, and mass 841.08 ± 0.02 g was used in this experiment. Preliminary results were given in Daskalakis, *et al.* (2012); however, they did not include the newly developed pulse rejection method which resulted in reduction of the experimental data near time-of-flight of 1 000 ns.

Examples of the experimental data and the MCNP simulations for backscattering to an angle of 156° are shown in Figure 1 for both ²³⁸U and graphite. The graphite data is used to quantify the systematics of uncertainties under the assumption that the ENDF/B-VII.1 evaluation of graphite is perfect. For ²³⁸U the evaluation which fits the experimental data best when using a χ^2 measure is JENDL-4.0.

Neutron scattering for ⁵⁶Fe

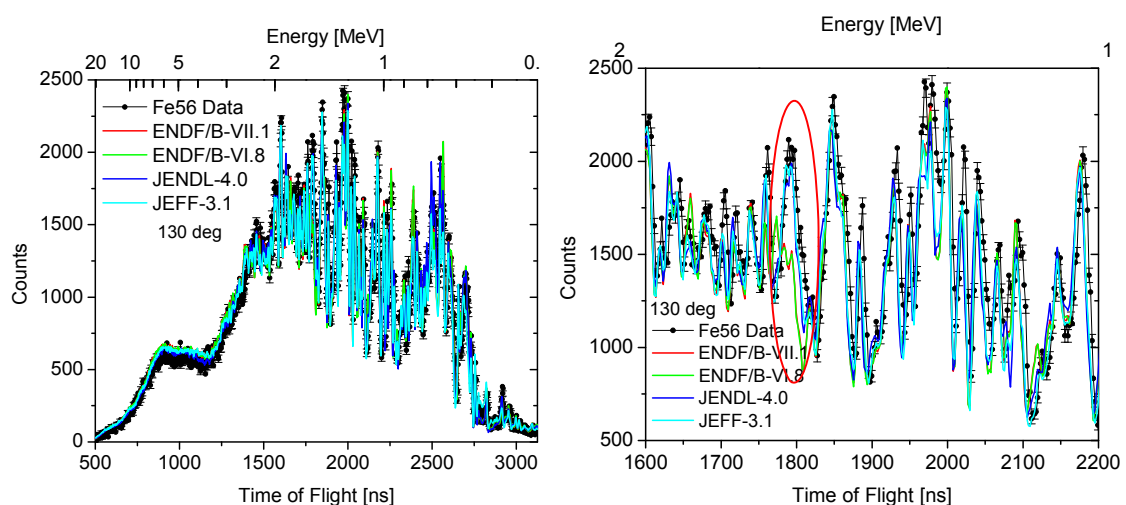
Similar measurements were completed with an ⁵⁶Fe sample (99.87% ⁵⁶Fe). The sample was square with approximate dimension of 7.70 cm × 15.25 cm × 3.23 cm thick and mass of 2951.0 ± 0.5 g.

Figure 1: Measured ^{238}U scattering compared with several MCNP simulations of the experimental system (right); measured graphite scattering compared with simulation using the ENDF/B-VII.1 evaluation (left)



The data analysis and simulation methodology were identical to the ^{238}U analysis. The experimental data and simulations with several evaluations are shown in Figure 2 for a scattering angle of 130° . Figure 2 serves as an example of the available measured data and how it can be used to benchmark different cross-section evaluations. The energy resolution is sufficient to resolve ^{56}Fe resonance structure up to 2 MeV. The right plot in Figure 2 shows a zoomed window which highlights a region where ENDF evaluations do not match the data as well as the JENDL-4.0 and JEFF-3.1 evaluations. This type of comparison provides an indication of energy regions where improvements in elastic or inelastic scattering are needed. The data analysis discriminates neutrons with energy below 0.5 MeV, for ^{56}Fe , where the first inelastic state is at 847 keV; this implies that below incident energy of about 1.35 MeV the system records only elastic scattering. Increasing the threshold during the data analysis allows measuring elastic scattering to higher energy and to enable separation of elastic from inelastic scattering. Overall the evaluation which fits the experimental data best when using a χ^2 measure is JEFF-3.1.

Figure 2: Measured ^{56}Fe scattering compared with several MCNP simulations of the experimental system (left); zoom in the region between 1-2 MeV (right)

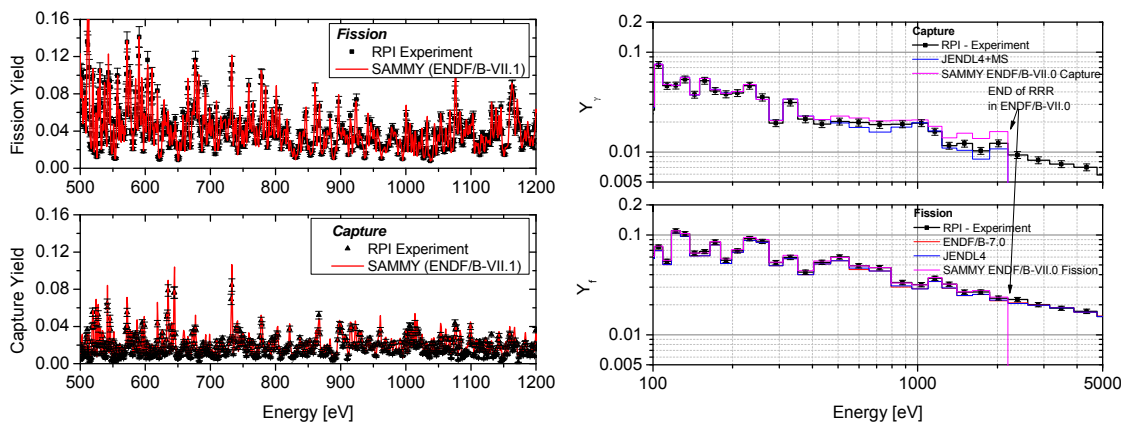


Simultaneous fission and capture measurements of ^{235}U

A method for simultaneous measurement of fission and capture was developed at RPI by utilising the RPI multiplicity detector (Williams, *et al.*, 2013) located on a 25.5 m flight path. The method uses the gammas emitted from capture and fission to measure both interactions without the need for a fission chamber. This enables the use of a larger sample (20 g, 93.33% ^{235}U). The high gamma detection efficiency of the multiplicity detector and its segmentation enable the use of the total energy deposition and multiplicity to separate fission from capture. The basic principle is that an event with total gamma energy deposition above the neutron binding energy of ^{235}U can only come from fission (or background) and below this energy it is a mix of fission and capture. Once the fission yield of the sample was measured, a normalisation procedure with two known resonances at low energy was used to find the fraction of fission that should be subtracted from the spectrum with total energy below the binding energy. For measurements in the energy range of 0.01-20 eV the thermal point and the 11.7 eV resonance were used for normalisation and for higher energy measurements the resonances at 11.7 eV and 19.0 eV were used, more details are given in Williams, *et al.* (2013). Additional correction was applied to the data to reduce contributions from scattered neutrons that were captured in the detector. Because of their high energy, the contribution from fission neutron was negligible. The outcome of this process was fission and capture yields with uncertainties in the range 5-8%.

The results are shown in Figure 3 with SAMMY calculations of the capture and fission yields. The left plot shows high resolution data in the energy range where differences between ENDF and JENDL exist. The right plot is the grouped yield which provides a better indication of the lower capture cross-section that was found compared to the ENDF/B-VII.0 evaluation. The resolved resonance region (RRR) for the JENDL-4 evaluations ends at 500 eV, which does not allow inclusion of SAMMY multiple scattering calculations above this energy. Instead the plotted curve was generated by a simple single collision yield calculation. The multiple scattering contributions were estimated based on the difference between a SAMMY calculation using ENDF/B-VII.0 and a simple first collision calculation of the capture yield using the ENDF/B-VII.0 cross-section. As expected the fission yields calculated from both evaluations are in very good agreement with the RPI experimental data. There is also good agreement between the evaluations and the experiment for capture yield below 500 eV. Above 500 eV the experimental capture yield is lower than ENDF/B-VII.0 and closer to JENDL-4.0.

Figure 3: Measured fission and capture yields of ^{235}U shown with SAMMY calculations using ENDF/B-VII.0 parameters (left); the grouped yields together with the ENDF/B-VII.0 and JENDL 4.0 evaluations (right)

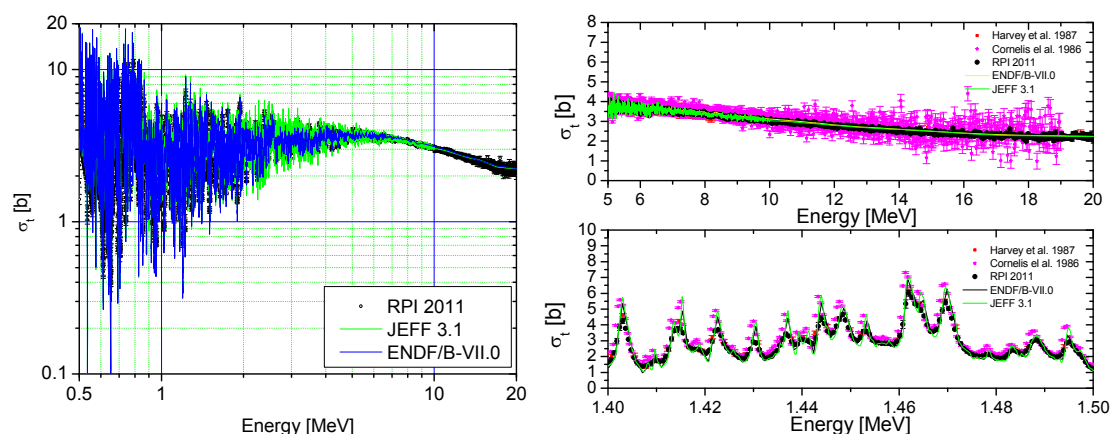


Transmission of ^{56}Fe

Transmission of metallic ^{56}Fe samples (99.87% ^{56}Fe) with thickness of about 3.22 cm and 7.69 cm were measured at a 250 m flight path using 12.7 cm thick large area modular liquid scintillator detector (EJ-301) [8]. This transmission set-up is useful for the energy range from 0.5-20 MeV and has a signal to background ratio of about 250 at 2 MeV. The transmission data for the two samples was converted into cross-section and the weighted average is shown in Figure 4 together with other experimental data and the ENDF/B-VII.1 evaluations.

Overall the RPI experimental data and the ENDF evaluations are in very good agreement. Above 5 MeV the RPI data has low uncertainty compared to previous measurements. This data can be used for further improvement of the resonance evaluation of ^{56}Fe and to improve the cross-section at the higher energy region above 5 MeV. Since two sample thicknesses were measured, a correction of the average cross-section for resolution broadening (Fröhner, *et al.*, 1996) can be accurately done for energies above the resolved resonance region.

Figure 4: Measured ^{56}Fe cross-section and calculations using the ENDF/B-VII.0 and JENDL-4.0 evaluations (left); a zoomed plot showing the low (bottom right) and the high (top right) energy regions is shown in the right plot compared to several other data sets and evaluations



Prompt fission neutron measurement

A system for measurement of prompt fission neutron spectra was developed based on a double time-of-flight measurement (Blain, Daskalakis and Danon, 2013). The sample was located about 30 m from the pulsed neutron source, liquid (EJ-301) and plastic (EJ-204) scintillator detectors were used to measure the fission neutron and were placed about 0.5 m from the sample. A fission tag was generated using four BaF_2 detectors that were in close proximity to the sample. The gamma tag method allows fast timing and also enables the use of larger samples. The system was first tested using a ^{252}Cf fission chamber where the gamma tagging method was compared to the more commonly used fission tagging method. In order to calculate the fission spectrum from the measured spectra the neutron detection efficiency was determined with the SCINFUL code (ORNL, 1988). For the case of EJ-301 it was found the SCINFUL code results were in good agreement with measurement of the energy dependent efficiency described above.

Results from ^{252}Cf were given in Blain, Daskalakis and Danon (2013) and are in good agreement with the evaluations. The system is currently being used for measurements on a ^{238}U sample.

Conclusions

The experimental programme at the Gaertner LINAC Center at Rensselaer Polytechnic Institute performed several measurements of ^{235,238}U and ⁵⁶Fe which are relevant to the CIELO project. The experiments include fast neutron scattering from ⁵⁶Fe and ²³⁸U, fast neutron transmission through ⁵⁶Fe and capture and fission yields of ²³⁵U. The scattering data provide a benchmark for new evaluations that will be performed during the CIELO project. The ⁵⁶Fe transmission data and ²³⁵U capture yield data can be used to improve the evaluated cross-sections. A system for measurement of prompt fission neutron spectra using the gamma tagging method was developed and demonstrated for ²⁵²Cf; measurements on ²³⁸U are in progress.

Acknowledgements

The authors would like to acknowledge the help and dedication of the RPI LINAC staff: Peter Brand, Mathew Gray, Martin Strock and Azeddine Kerdoun.

References

- Barry, D.P., *et al.* (2013), "Quasi-Differential Neutron Scattering in Zirconium from 0.5 MeV to 20 MeV", *Nuclear Science and Engineering*, 174, 188-201.
- Blain, E., A. Daskalakis and Y. Danon (2013), "Measurement of Fission Neutron Spectrum and Multiplicity Using a Gamma Tag Double Time-of-Flight Setup", *Proceedings of the International Nuclear Data Conference for Science and Technology (ND-2013)*, Upton, NY, 4-8 March.
- Daskalakis, A.M., *et al.* (2012), "Quasi-Differential Neutron Scattering Measurements of ²³⁸U", *Transactions of the American Nuclear Society*, Vol. 107, pp. 634-636, San Diego, CA, 11-15 November.
- Fröhner, F.H., *et al.* (1996), *Cross-Section Fluctuations and Self-Shielding Effects in the Unresolved Resonance Region*, NEA/WPEC-15, OECD/NEA, Paris.
- Gaertner, E.R., M.L. Yeater and R.R. Fullwood (1961), "Rensselaer Polytechnic Institute Linac Facility," *Proceedings of Symposium on Neutron Physics*, RPI, May.
- ORNL (Oak Ridge National Laboratory) (1988), *Scintillator Full Response to Neutron Detection (SCINFUL)*, PSR-0267, ORNL, Oak Ridge, TN.
- Rapp, M.J., *et al.* (2012), "Beryllium and Graphite Neutron Total Cross Section Measurements from 0.4 to 20 MeV", *Nuclear Science and Engineering*, Vol. 172, No. 3, pp. 268-277.
- Romano, C., *et al.* (2010), "Fission Fragment Mass and Energy Distributions as a Function of Neutron Energy Measured in a Lead Slowing Down Spectrometer", *Phys. Rev. C*, 81, 014607.
- Saglione, F.J., *et al.* (2010), "A System for Differential Neutron Scattering Experiments in the Energy Range from 0.5 to 20 MeV", *Nuclear Instruments and Methods in Physics Research*, Section A, Vol. 620, Nos. 2-3, pp. 401-409.

Thompson, J.T., *et al.* (2012), "Measurement of (n, α) Reactions on ^{147}Sm and ^{149}Sm Using a Lead Slowing-Down Spectrometer", *Nuclear Instruments and Methods in Physics Research*, Section A, Vol. 673, pp. 16-21.

Williams, David, *et al.* (2013), "New Measurement of the Neutron Capture Cross Section of ^{235}U Below 5 keV", *Proceedings of the International Nuclear Data Conference for Science and Technology (ND-2013)*, Upton, NY, 4-8 March.

The Big Three: ^{235}U , ^{238}U , ^{239}Pu – Part 1

Chair: M.B. Chadwick

BRC neutron evaluations of actinides with the TALYS code

B. Morillon, P. Romain
CEA/DAM/DIF
Arpajon, France

Abstract

We briefly report here part of the list of problems to overcome in order to build evaluations as predictive as possible for simulation of criticality benchmarks. Dispersive potential, large coupling scheme and neutron inelastic scattering are the most crucial points of this list of problems. Different tools to distinguish differences between evaluations are also presented.

Introduction

Although the various major actinide neutron evaluations from different libraries (ENDF/B-VII, JENDL-4.0, CENDL-3.1, BROND/ROSFOND, JEFF-3.1) reach an increasingly impressive quality with respect to the reproduction of many criticality benchmarks, significant differences between these evaluations, for certain reaction channels, are nevertheless evidence of compensating errors (Plompen, *et al.*, 2012; Chadwick, *et al.*, 2014) behind that perfect agreement between simulation and experiment.

Because it is also the most difficult to measure, while the other channels are more easily and widely measured, the inelastic channel remains the channel for which the maximum of uncertainty remains, both experimentally and theoretically.

Common nuclear reaction modelling

In their design most evaluations use the same chain of nested models starting with the optical model, which should preferably use a dispersive potential (Figures 1 and 2). However the determination of the optical potential is not the ultimate goal in order to reach the criteria required to build a “good evaluation”. Indeed, the dimension of the coupling scheme also proves to be essential. A sufficiently large coupling scheme can then converge to the “right” reaction cross-section relative to a selected optical potential.

As can be verified in Figures 2 and 3, the dimension of the coupling scheme, as the inclusion of dispersive terms in the optical potential have a clear influence on the calculation of the capture, fission and inelastic cross-sections. Fission cross-sections seems the most sensitive.

Figure 1: Impact of the coupling scheme's dimension on the s-wave neutron transmission coefficients (left); impact of the coupling scheme's dimension on the total and compound nucleus formation cross-sections (right)

The wide blue + yellow dashed curves correspond to the non-dispersive Souhovitiskii (2004) potential using the largest coupling scheme as for the red curve

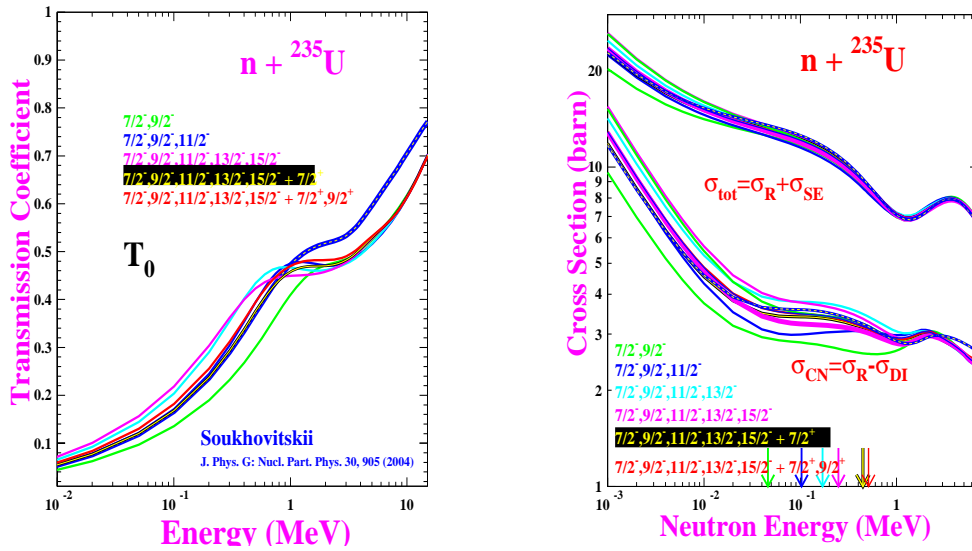


Figure 2: Impact of the coupling scheme's dimension on the capture cross-section (left); impact of the coupling scheme's dimension on the fission cross-section (right)

The wide blue + yellow dashed curves correspond to the non-dispersive Souhovitiskii (2004) potential using the largest coupling scheme as for the red curve

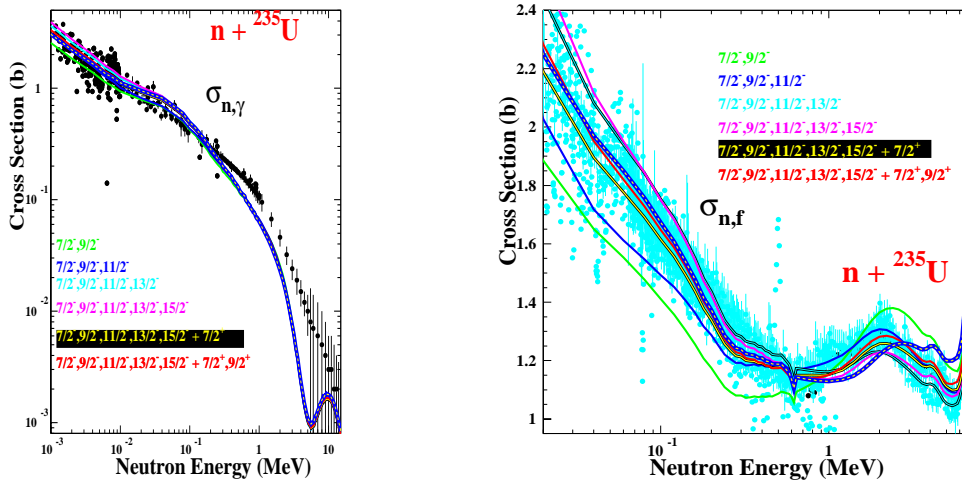
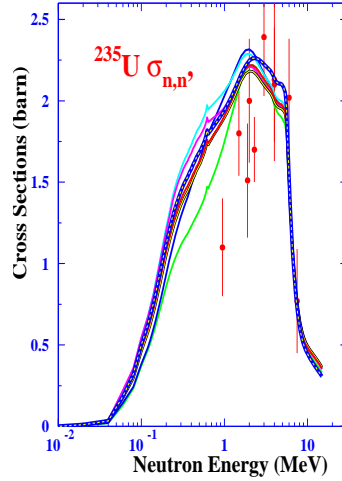


Figure 3: Impact of the coupling scheme's dimension on the inelastic cross-section

The wide blue + yellow dashed curve corresponds to the non-dispersive Soukhovitskii (2004) potential using the largest coupling scheme as for the red curve



Comparison tools

Dalitz plots

Even if for the first modelling phase (optical model), the different evaluations satisfy more or less to the same criteria (dispersive + large coupling scheme), differences nevertheless remain between them. One way to appreciate these differences is to represent these evaluations on a Dalitz (1954) plot.

In fact, for energies below the (n,2n) threshold, we can write:

$$\sigma_R = \sigma_{CE} + \sigma_{n,n'} + \sigma_{n,\gamma} + \sigma_{n,f}$$

and finally:

$$\begin{aligned} \sigma_R - \sigma_{CE} = \sigma_{n,n'} + \sigma_{n,\gamma} + \sigma_{n,f} = \sigma_{non-el} &\Leftrightarrow 1 = \frac{\sigma_{n,n'}}{\sigma_{non-el}} + \frac{\sigma_{n,\gamma}}{\sigma_{non-el}} + \frac{\sigma_{n,f}}{\sigma_{non-el}} \\ &\Leftrightarrow 1 = P_{n,n'}^{non-el} + P_{n,\gamma}^{non-el} + P_{n,f}^{non-el} \end{aligned}$$

which defines the probabilities of each non-elastic process occurring in this energy range. The interest is that these probabilities can directly be deduced from evaluated files as follows:

$$\sigma_{non-el} = MF_3MT_4 + MF_3MT_{102} + MF_3MT_{18} \Leftrightarrow 1 = \frac{MF_3MT_4}{\sigma_{non-el}} + \frac{MF_3MT_{102}}{\sigma_{non-el}} + \frac{MF_3MT_{18}}{\sigma_{non-el}}$$

The Dalitz plot uses the fact that for any point M , inside an equilateral triangle, the sum of its distances MH , MK , ML (Figure 4) respectively to each side of this equilateral triangle equals the height h of this triangle: $MH + MK + ML = h$, so when assuming: $MH = P_{n,f}^{non-el}$, $MK = P_{n,n'}^{non-el}$ and $ML = P_{n,\gamma}^{non-el}$ and $h = 1$, each set $(E, \sigma_{n,n'}(E), \sigma_{n,\gamma}(E), \sigma_{n,f}(E))$ of an evaluated file can be represented by a corresponding point inside an equilateral triangle of unitary height. Finally an evaluated file will display a path inside this triangle (Figure 4).

For ^{235}U , the differences between the path describing the ENDF/B-VII evaluation and this one describing our calculation [named TALYS1.4 (Koning, *et al.*, 2008)] show easily in this Dalitz representation that the probabilities $P_{n,n'}^{non-el} = MK$ and $P_{n,\gamma}^{non-el} = ML$ related to our calculation are higher than those of the ENDF/B-VII evaluation, conversely to the fission probability $P_{n,f}^{non-el} = MH$ [while our fission cross-section is greater than that of ENDF/B-VII on this energy range (10-100 keV), this latter probability is lower for our calculation only because our non-elastic cross-section σ_{non-el} is higher (Figure 5)]. Finally, to be comparable to the ENDF/B-VII simulation results on critical experiments, we were forced to leave the “entirely from modelling” way and adjust our capture cross-section in order to better simulate some precise critical benchmarks (BIGTEN, JEMINA for example). Now we will call BRC this “modified” evaluation to distinguish it with the TALYS-1.4 case (“entirely from modelling”).

Figure 4: Dalitz plots for the ENDF/B-VII and TALYS-1.4 evaluations (left); zoom on the upper part of the Dalitz plots (right)

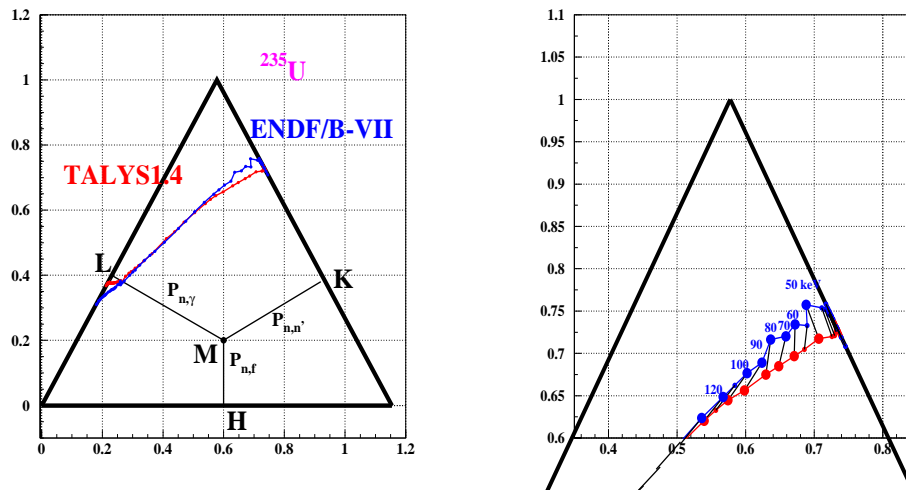
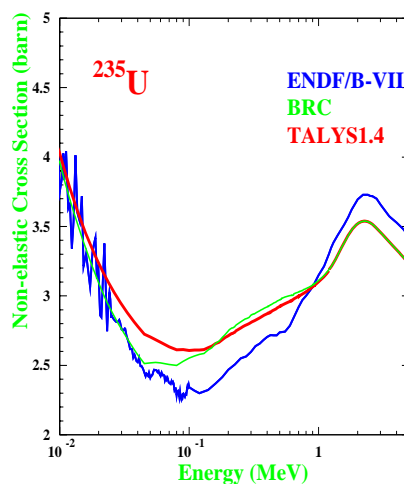


Figure 5: Non-elastic cross-sections for the ENDF/B-VII, BRC and TALYS-1.4 evaluations



Shannon theorem

Another compact way to represent evaluations is to use the Shannon theorem. Consider a situation in which N random events can occur with probabilities:

$$P_m (m = 1, 2, \dots, N), \left(\sum_m P_m = 1 \right)$$

Shannon (1948) showed that the lack of information associated with this probability set $\{P_m\}$ is given by:

$$H(\{P_m\}) = - \sum_m P_m \text{Log}_2 P_m$$

In our case, we will define the lack of information related to the various accessible non-elastic processes, when an actinide nucleus A is bombarded by neutrons of energy lower than the $(n,2n)$ emission threshold, as:

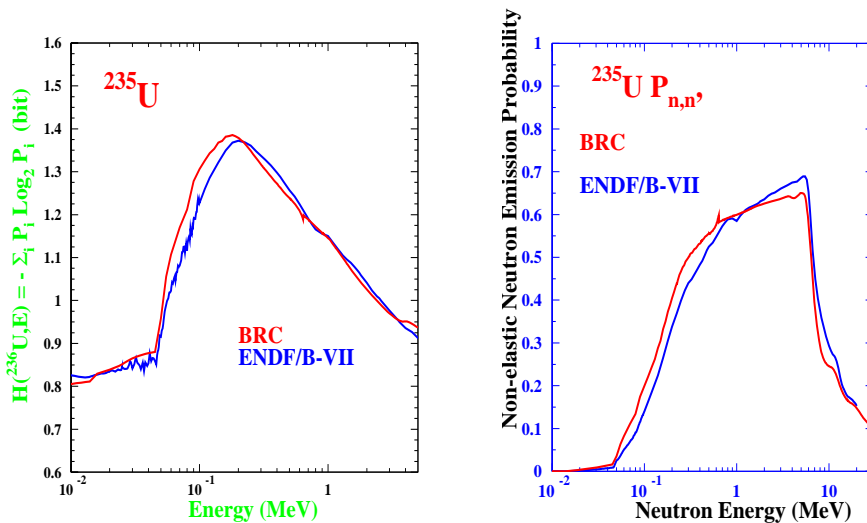
$$H(A, E) = -P_{n,n'}^{\text{non-el}} \text{Log}_2 P_{n,n'}^{\text{non-el}} - P_{n,\gamma}^{\text{non-el}} \text{Log}_2 P_{n,\gamma}^{\text{non-el}} - P_{n,f}^{\text{non-el}} \text{Log}_2 P_{n,f}^{\text{non-el}}$$

A simple picture to understand this entity is to consider a non-fissile nucleus such as ²³⁸U and incident neutrons with energy lower than the first inelastic energy threshold (10 keV, for example). In that case $P_{n,n'}^{\text{non-el}} = 0$, $P_{n,\gamma}^{\text{non-el}} \approx 0$ and $P_{n,f}^{\text{non-el}} \approx 1$ where it comes: $H(A, E) \approx 0$, which means that no information is missing *a priori*, or the outcome is almost certain: most of the time there will be a neutronic capture.

By this interpretation in terms of lack of information, the closer are the evaluations, the closer are their probabilities (for the different non-elastic processes) and therefore the nearer are their Shannon entropy $H(A, E)$.

In Figure 6 (left), for incident neutron energies between 50 keV and 200 keV, it appears that the outcome of the non-elastic processes for the ²³⁵U nucleus bombarded by neutrons, is more uncertain for the BRC evaluation than for the ENDF/B-VII evaluation. This is due to the fact that the inelastic process is higher with the BRC evaluation (Figure 6 right).

Figure 6: Lack of information on the non-elastic processes for the ENDF/B-VII and BRC evaluations (left); non-elastic neutron emission probability for the ENDF/B-VII and BRC evaluations (right)

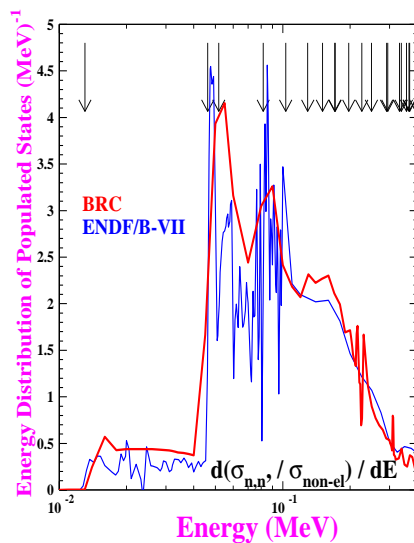


However, this is not because the outcome of the non-elastic processes is more certain with the ENDF/B-VII evaluation that this last is “better” and vice versa for the BRC evaluation.

At this stage it is also useful to compare the energy derivative $\frac{dP_{n,n'}^{non-el}}{dE}$ of the neutron inelastic emission probabilities. Indeed (Romain, 2012), this quantity permits to access to the populated states in the target nucleus by inelastic neutron scattering.

For the ENDF/B-VII evaluation (Figure 7), the surplus of “non-physical” peaks (non-physical meaning that they do not correspond to populated discrete states of the target nucleus) comes from the oscillations on the non-elastic cross-section (Figure 5), due to the extension of the unresolved resonances range (URR). The extension of the URR well beyond the inelastic thresholds of the first states of the target can be problematic. Indeed, in the usual modelling of this UR energy range, the direct inelastic component is omitted. If for some nucleus, this direct contribution can be a problem, for the ^{235}U nucleus up to 100 keV it remains partly negligible and can then be omitted without too great consequences for simulations of criticality benchmarks.

Figure 7: Energy distributions of the populated states of the ^{235}U by non-elastic processes for the ENDF/B-VII and BRC evaluations



Conclusion or what should be done?

- OMP:
 - Dispersive potential.
 - Choice of the coupling scheme (as large as possible).
- URR:
 - How to take into account the DI component when URR is extended too high in energy?

- Inelastic cross-sections:
 - Pseudo-states have to be incorporated in the evaluation in order to better agree with Baba's experiments (Baba, *et al.*, 1990).
 - Which approach to treat them?
 - As a consequence of the uncertainty around the inelastic cross-section, new measurements (when possible) of this last one should be undertaken!
- PFNS:
 - Pre-fission neutron spectra have to be included.
- Standard cross-sections:
 - For the ^{235}U nucleus, the replacement of the fission cross-section (calculated in a fully consistent way with those of all the other open channels) by the standard fission cross-section inevitably leads to a readjustment of some cross-sections, in order to compensate for the differences between these two sets of fission cross-sections. But through this readjustment, is it the beginning of an unintentional compensation or not?

Finally, would it be possible to eliminate all compensating errors?

Acknowledgements

We would like to thank H. Duarte for his help in the elaboration of these evaluated files.

References

- Baba, M., *et al.* (1990), *J. Nucl. Sci. Technol.*, 27, pp. 601-616.
- Chadwick, M.B., *et al.* (2014) "The CIELO Collaboration: Neutron Reactions on ^1H , ^{16}O , ^{56}Fe , $^{235,238}\text{U}$, and ^{239}Pu ", *Nuclear Data Sheets*, forthcoming.
- Dalitz, R.H. (1954), "Decay of τ Mesons of Known Charge", *Phys. Rev.*, 94, pp. 1046-1051.
- Koning, A.J., *et al.* (2008), "TALYS-1.0", *Proceedings of the International Conference on Nuclear Data for Science and Technology*, Nice, France, 22-27 April 2007, O. Bersillon, *et al.* (eds.), EDP Sciences, pp. 211-214.
- Plompen, A., *et al.* (2012), *Inelastic Scattering and Capture Cross-Section Data of Major Actinides in the Fast Neutron Region*, INDC(NDS)-0597, pp. 7-41, IAEA, Vienna.
- Romain, P., *et al.* (2012), "Examining Barrier Distributions and, in Extension, Energy Derivative of Probabilities for Surrogate Experiments", *Phys. Rev. C*, 85, pp. 044603-1-044603-11.
- Shannon, C.E. (1948), "A Mathematical Theory of Communication", *Bell Syst. Tech. J.*, 27, pp. 397-423 and pp. 623-656.
- Soukhovitskii, E.Sh., *et al.* (2004), "Global Coupled-Channel Optical Potential for Nucleon-Actinide Interaction from 1 keV to 200 MeV", *J. Phys. G: Nucl. Part. Phys.*, 30, pp. 905-920.

Evaluation of neutron-induced reactions on ^{238}U nucleus

R. Capote,^a M. Sin,^b A. Trkov,^{a,c} M.W. Herman,^d
D. Bernard,^e G. Noguère,^e A. Daskalakis,^f Y. Danon^f

^aNAPC-Nuclear Data Section, International Atomic Energy Agency (IAEA), Vienna, Austria

^bNuclear Physics Department, University of Bucharest, Bucharest, Romania

^cJozef Stefan Institute, Ljubljana, Slovenia

^dNational Nuclear Data Center, Brookhaven National Laboratory, Upton, NY, United States

^eSPRC/LEPh, Commissariat à l'Énergie Atomique (CEA) Cadarache,
Saint-Paul-lez-Durance, France

^fGaerttner LINAC Center, Rensselaer Polytechnic Institute, Troy, NY, United States

Abstract

Advanced modelling of neutron-induced reactions on ^{238}U nucleus using the EMPIRE system is aimed at improving our knowledge of the neutron scattering leading to better nuclear data for nuclear power applications. Capture and fission channels in $n + ^{238}\text{U}$ reaction are well constrained by available experimental data and IAEA neutron standard evaluations allowing to focus on the impact of elastic and inelastic scattering in evaluated cross-sections. The reaction model includes: i) a new rotational-vibrational dispersive optical model that couples the low-lying collective bands of vibrational character observed in even-even actinides; ii) the Engelbrecht-Weidenmüller transformation allowing inclusion of compound-direct interference effects enhanced by a dispersive treatment of the optical model potential; iii) a multi-humped fission barrier with absorption in the secondary well described within the optical model for fission. Impact of the advanced modelling on inelastic scattering cross-section and corresponding uncertainties is being assessed both by comparison with selected microscopic experimental data and integral criticality benchmarks including measured reaction rates (e.g. FLATTOP, JEMIMA, BIGTEN, MASURCA, PROFIL and PROFIL-2). Additionally, neutron scattering yields on ^{238}U measured accurately at RPI by the time-of-flight technique at 29° , 60° , 112° and 153° have been used as a further constraint on the incident energy dependence of elastic and inelastic scattering of neutrons. Benchmark calculations provided feedback to improve the reaction modelling. The improvement of scattering cross-sections in existing libraries is discussed.

Introduction

^{238}U is a major component of nuclear fuel in commercial power reactors (more than 90% of nuclear fuel composition), therefore its nuclear data are one of the most important sources of uncertainty of the neutron transport calculations in the reactor core. An IAEA Technical Meeting on “Inelastic Scattering and Capture Cross-Section Data of Major Actinides in the Fast Neutron Region” was recently held at IAEA headquarters in Vienna, Austria to review the status of nuclear data libraries and to evaluate what advances in nuclear modelling and measurement technique may improve our knowledge of these cross-sections (Plompen, Kawano and Capote, 2011). Attendees at this IAEA meeting

concluded “that advances in modelling are substantial, and that significant improvement can be made in reducing modelling uncertainties for capture and inelastic scattering.” (Plompen, Kawano and Capote, 2011) Tight target uncertainties in the fast neutron region on the capture and inelastic scattering data for major actinides were also derived from advanced reactor sensitivity studies in the WPEC SG-26 (OECD/NEA, 2008), motivating new evaluation efforts.

Some of the authors have recently submitted for publication two extensive papers on the “Physics of Neutron Interactions with ^{238}U ” (Capote, *et al.*, 2014b), and on “Elastic and Inelastic Scattering of Neutrons on ^{238}U Nucleus” (Capote, *et al.*, 2014a). We recommend those references as a detailed technical description of the evaluation work undertaken so far. In the next section we will briefly discuss the current status, problems and outlook.

Nuclear reaction modelling and differential data

The most prominent features of the nuclear reaction modelling employed in the current work (Capote, *et al.*, 2014a, 2014b) are:

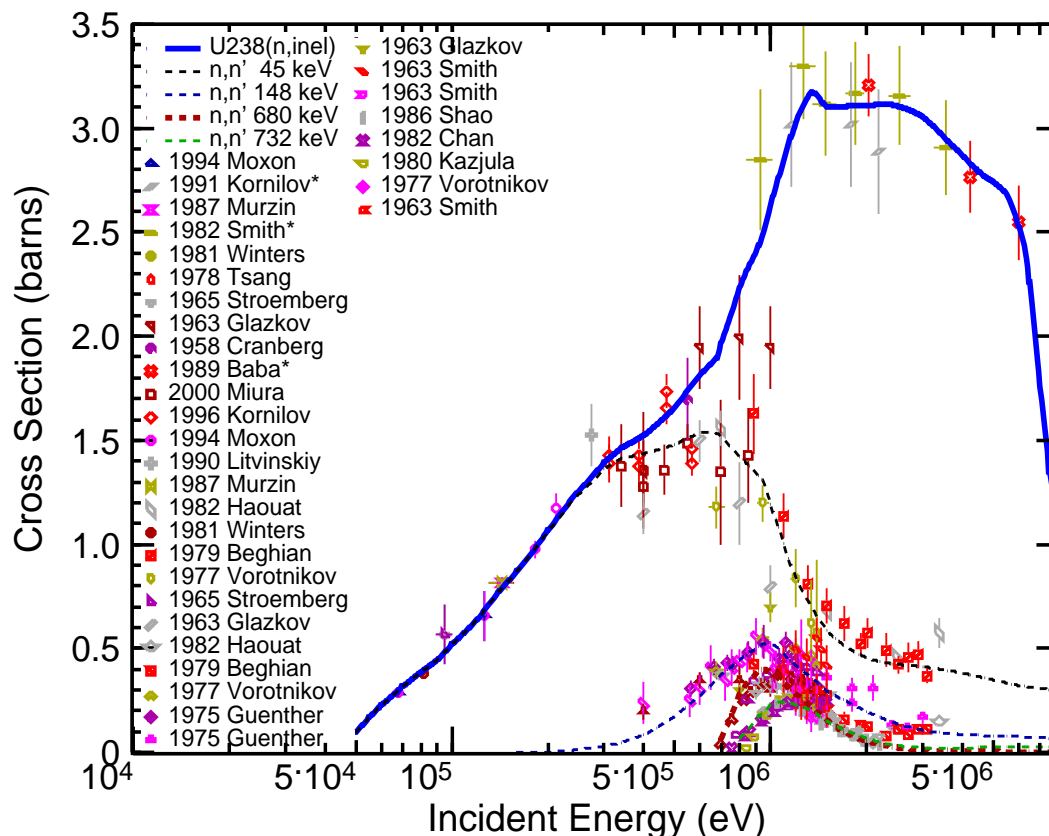
- 1) A new dispersive optical model that couples multiple collective bands of the ^{238}U nucleus (Quesada, *et al.*, 2013, 2014). Such coupling allows describing the direct neutron scattering on collective levels up to around 1.3 MeV of incident neutron energy.
- 2) The statistical model description of $^{238}\text{U}(n,f)$ and $^{238}\text{U}(n,\gamma)$ that reproduce standards' cross-section evaluation (Badikov, *et al.*, 2008; Carlson, *et al.*, 2009) as this is considered our best model-independent knowledge of those cross-sections.
- 3) The key components of the statistical reaction theory used to achieve 2), namely the optical model for fission (Sin, *et al.*, 2006; Sin and Capote, 2008), the anisotropic compound-elastic scattering (Capote, *et al.*, 2014a, 2014b), and the interference between the direct and compound reactions as predicted by Moldauer (1975).

The employed statistical reaction theory allowed for a concurrent description of the statistical decay leading to the fission, capture and neutron emission. The latest iteration of the neutron inelastic scattering cross-section on ^{238}U nucleus [file IAEA u238-ib33 (Capote, *et al.*, 2014a)] is shown in Figure 1. Compared to the evaluated nuclear data libraries [e.g. see Figure 3 of Capote, *et al.* (2014b)] the new evaluation is closer to the experimental data and ENDF-B/VII.1 (Chadwick, *et al.*, 2012) below 600 keV, and is higher than all other evaluations up to 1 MeV. The latter behaviour is due to the contribution of the direct excitation of multiple coupled collective bands (i.e. due to the new optical model) (Quesada, *et al.*, 2013, 2014). The previous iteration [file IAEA u238-ib25 (Capote, *et al.*, 2014b)] overestimated existing differential data for neutron energies between 3-7 MeV [as shown in Figure 3 in Capote, *et al.* (2014b)]. We received additional feedback from CEA benchmark calculations that indicated lower inelastic cross-section in that energy region, therefore the inelastic scattering cross-sections above 3 MeV were decreased when going from the b25 to the b33 version.

Quasi-differential measurements

A very useful and interesting experiment has been performed at RPI by Danon and co-workers (Danon, *et al.*, 2012; Daskalakis, *et al.*, n.d.), where scattered neutrons were measured at different angles by a time-of-flight technique in a white incident neutron spectrum extending from 500 keV up to approximately 20 MeV. The measured neutron yields featured contributions from both scattering and fission neutrons, which were not disentangled. The measured neutron yield at 153° backward angle on ^{238}U target was in disagreement both with ENDF-B/VII.1 (Chadwick, *et al.*, 2012) and JEFF-3.1 (Koning, *et al.*, 2006) evaluations [see Figure 6 of Capote, *et al.* (2014b)]. JENDL-4 (Shibata, *et al.*, 2011) and

Figure 1: Calculated $^{238}\text{U}(n,n')$ total inelastic (solid blue) and $^{238}\text{U}(n,n')$ inelastic scattering to several excited levels (dashed lines) versus selected experimental data from the EXFOR database (NRDC, n.d.)



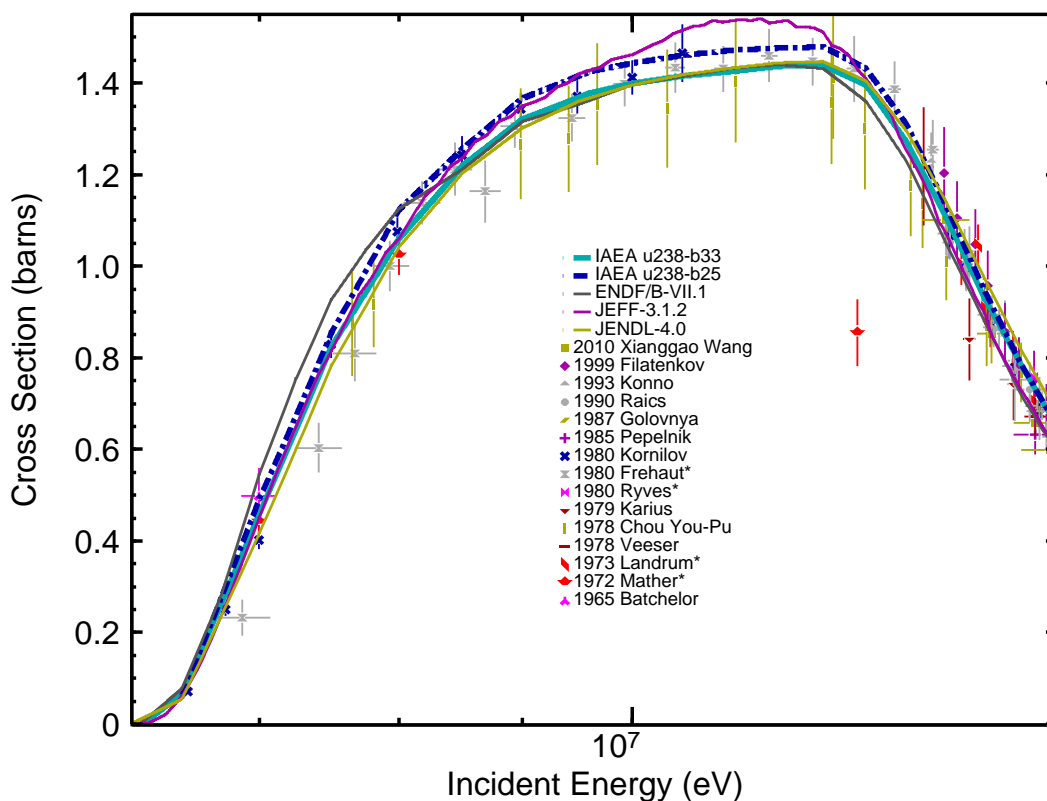
both IAEA evaluations (files u238-b25 and u238-b33) performed well at this angle (Capote, *et al.*, 2014b; Daskalakis, *et al.*, n.d.). Further improvements may be achieved by considering yield data measured at other angles together with available MCNP model of the experiment.

Integral benchmarks

Benchmark experiments are measurements of integral parameters that can be accurately modelled by computation with very few assumptions and approximations. We used ICSBEP criticality benchmarks (OECD/NEA, 2006) as an additional constraint to improve IAEA evaluations b25 (Capote, *et al.*, 2014b) and b33 (Capote, *et al.*, 2014a) (e.g. Flattop-25, Flattop-Pu, BigTen and JEMIMA critical assemblies). Additionally, our CEA collaborators considered fast neutron benchmarks, where selected reaction rates were measured [e.g. the PROFIL-2 experiment in the PHENIX reactor (D'Angelo and Cleri, 1990; Tommasi and Coulon, 1993)]. The agreement of F8/F5 and $^{238}\text{U}(n,\gamma)$ spectral indexes with measured data was very good for IAEA evaluations (both b25 and b33), an evidence of the quality of standards' evaluations (Badikov, *et al.* 2008; Carlson, *et al.*, 2009). On the other side, we found discrepancies for the $^{238}\text{U}(n,2n)$ spectral index. The calculated to measured $^{238}\text{U}(n,2n)$ value in PROFIL-2 experiment was equal to 1 with 2.8% uncertainty while the file u238-b25 (Capote, *et al.*, 2014b) produced a value of 0.952 and the latest file u238-b33 produced a value of 0.934 (Capote, *et al.*, 2014a).

The $^{238}\text{U}(n,2n)$ index was the only one that worsened when comparing u238-b25 and u238-b33 evaluations. Following integral indications, we compared calculated $^{238}\text{U}(n,2n)$ excitation functions vs. a comprehensive set of measured differential experimental data in Figure 2. From the figure, we can see that the IAEA u238-b33 evaluation is lower than the u238-b25 file in the whole energy range, thus confirming post-irradiation experiment results from the PROFIL-2 integral experiment. In the 14 MeV region, the JENDL-4 evaluation agrees with IAEA evaluations, being higher than ENDF-B/VII.1 and JEFF-3.1 results. This is interesting as there should be enough high quality activation measurements at 14-15 MeV to define evaluated data with small uncertainty; unfortunately this energy region is not relevant for reactor applications. In the region of the maximum of the $(n,2n)$ excitation function from 9-12 MeV of the neutron incident energy we observe a relatively large spread of evaluated results with the JEFF-3.1.2 evaluation being the highest, and the IAEA u238-b25 file the second highest. However, in the most important region for reactor applications, from the reaction threshold up to 9 MeV we see that ENDF/B-VII.1 library is the highest, being outside the already corrected differential data by Frehaut, *et al.* We plan to address these discrepancies in the next iteration; we expect the optimum evaluated $^{238}\text{U}(n,2n)$ cross-sections to be slightly higher than the IAEA u238-b25 evaluation, but with a very similar shape.

Figure 2: Evaluated $^{238}\text{U}(n,2n)$ cross-sections including new IAEA b25 (thick solid cyan) and b33 (dash-dotted) files compared with selected experimental data from EXFOR database (NRDC, n.d.)



Conclusions

Advanced modelling of neutron-induced reactions on ^{238}U target has been carried out to improve our knowledge of the neutron scattering cross-sections on this extremely important material for nuclear power applications. Current IAEA evaluations provide a very good starting point for the ^{238}U evaluation to be produced within the CIELO project.

References

- Badikov, S., *et al.* (2008), *International Evaluation of Neutron Cross-Section Standards*, STI/PUB/1291, IAEA, Vienna.
- Capote, R., *et al.* (2014a), “Elastic and Inelastic Scattering of Neutrons on ^{238}U Nucleus”, *Proc. CNR*13*, Maresias, Brazil, 7-11 October 2013, *EPJ Web of Conferences*, 69, 00008.
- Capote, R., *et al.* (2014b), “Physics of Neutron Interactions with ^{238}U : New Developments and Challenges”, *Proc. ND2013*, New York, United States, 4-8 March 2013, *Nucl. Data Sheets*, 118, 26-31.
- Carlson, A.D., *et al.* (2009), *Nucl. Data Sheets*, 110, 3215.
- Chadwick, M.B., *et al.* (2012), *Nucl. Data Sheets*, 112, 2887.
- D’Angelo, A. and F. Cleri (1990), “Analysis of Sample and Fuel Pin Irradiation Experiments in Phénix for Basic Nuclear Data Validation”, *Nucl. Sci. & Eng.*, 105, 244-255.
- Danon, Y., *et al.* (2012), presentation at *Int. Workshop on Elastic and Inelastic Scattering (WINS-2012)*, Boston, MA, United States 17-19 September 2012.
- Daskalakis, A.M., *et al.* (n.d.), “Quasi-Differential Neutron Scattering from ^{238}U from 0.5 to 20 MeV”, to be submitted to *Ann. Nucl. Engin.*
- Koning, A.J. *et al.* (2006), “The JEFF-3.1 Nuclear Data Library”, *JEFF Report 21*, NEA No. 6190, OECD/NEA, Paris, France.
- Moldauer, P.A., *Phys. Rev. C*, 12, 744 (1975).
- NRDC (International Network of Nuclear Reaction Data Centres) (n.d.), *EXchange FORmat Database (EXFOR)*, www-nds.iaea.org/exfor.
- OECD/NEA (Organisation for Economic Co-operation and Development/Nuclear Energy Agency) (2006), *International Handbook of Evaluated Criticality Safety Benchmark Experiments*, Technical Report NEA/NSC/DOC(95)03, Nuclear Science Committee, OECD/NEA, Paris, France.
- OECD/NEA (2008), *Uncertainty and Target Accuracy Assessment for Innovative Systems Using Recent Covariance Data Evaluations*, NEA/WPEC-26, M. Salvatores (co-ordinator), WPEC, OECD/NEA, Paris, France, ISBN 978-92-64-99053-1.
- Plompen, A., T. Kawano and R. Capote (eds.) (2011), *Technical Meeting on Inelastic Scattering and Capture Cross Section Data of Major Actinides in the Fast Neutron Region*, IAEA(NDS)-0597, International Atomic Energy Agency, Vienna, Austria.
- Quesada, J.M., *et al.* (2013), *EPJ Web of Conf.*, 42, 02005.
- Quesada, J.M., *et al.* (2014), *Nucl. Data Sheets*, 118, 270-272.

Shibata, K., *et al.* (2011), *J. Nucl. Sci. Technol.*, 48, 1.

Sin, M., *et al.* (2006), *Phys. Rev. C*, 74, 014608.

Sin, M. and R. Capote (2008), *Phys. Rev. C*, 77, 054601.

Tommasi, J. and P. Coulon (1993), "PHENIX Experiment Facilities for Fission Product Destruction and Actinide Burning", *Global '93: Future Nuclear Systems – Emerging Fuel Cycles and Waste Disposal Options*, Seattle, WA, United States, 12-17 September 1993, accessed 1 June 2014, www.iaea.org/inis/collection/NCLCollectionStore/_Public/25/010/25010974.pdf.

Status of ^{239}Pu evaluations

Toshihiko Kawano, Patrick Talou, Mark B. Chadwick
Los Alamos National Laboratory
Los Alamos, NM, United States

Abstract

This paper summarises the current status of nuclear data evaluations for $n+^{239}\text{Pu}$. The nuclear data we address include fission, capture, scattering cross-sections, as well as the prompt fission neutron energy spectrum, which has large sensitivities to the criticality benchmark testing. The evaluated nuclear data files currently available for ^{239}Pu are compared, and the source of differences in the cross-sections are discussed. Some open questions on the statistical model calculations for deformed systems are also given.

Introduction

Nuclear reaction data of ^{239}Pu , which is one of the most important major actinides, play an essential role in many nuclear applications, and significant efforts have been devoted to produce a high quality data file that better agrees with both differential and integral measurements available. In this sense the ^{239}Pu file in the nuclear data libraries such as ENDF, JENDL, JEFF, CENDL and ROSFOND, substantially characterises the library itself for nuclear energy applications. Therefore knowledge of the details of current nuclear data files provides important information for the development of future international co-operative nuclear data file. In this paper we look into the evaluated ^{239}Pu files in the major nuclear data libraries and discuss the key issues to be resolved in the international file. We take the most recent evaluation of ^{239}Pu in each library, namely CENDL-3.1, ENDF/B-VII.1, JEFF-3.1.2 and JENDL-4.0 unless the release number is explicitly stated otherwise. Since the ^{239}Pu data in ROSFOND is basically the same as JEFF-3.1.2, we drop this library from our comparison.

Summary of evaluated files

Here we give a brief summary of each ^{239}Pu file. Since the information given below is basically extracted from the comment section in the files, some ambiguities/errors may exist. The resonance history will be given in a different section.

The CENDL-3.1 file was carried over from CENDL-2.1, evaluated in 1990. The evaluation is based on both experimental data and model calculations with the FUP1 code.

ENDF/B-VII.1 is the same as ENDF/B-VII.0, evaluated in 2006, except for the delayed neutron data. The evaluation is based on ECIS and GNASH calculations. Special care was taken with the (n,2n) cross-section, which was evaluated by combining the LANSCE GEANIE prompt gamma-ray measurement and the GNASH calculation. The IAEA standards evaluation for fission cross-section was incorporated.

JEFF-3.1.2 is a minor upgrade of JEFF-3.0 that was released in 2006. The actual evaluation year is not given. The evaluation is based on ECIS and GNASH.

JENDL-4.0 is based on the CCONE code calculation in 2007. A simultaneous evaluation was performed for the fission cross-section.

Resolved resonance region

There are several different resolved resonance parameter sets stored in the files. ENDF adopts the Reich-Moore resonance parameters evaluated by Derrien and Nakagawa, which originally appeared in JENDL-3.2. The resolved resonance region is divided into three energy regions, 0-1 keV, 1-2 keV and 2-2.5 keV. In CENDL the comment section says the resonance parameters are the same as JENDL-3. However, the energy range is different; the source is unknown. In 2007 the updated parameters, in which the three energy regions were combined into one, were reported by Derrien. JENDL has this resonance parameter set.

Starting with the resonance parameters in ENDF, JEFF inserted a tiny negative resonance at -0.02 eV for better agreement with some integral benchmark tests. This tweak modifies the slope of fission and capture cross-section near the thermal energy, leaving the thermal cross-sections unchanged. This effort has been taken over by WPEC Subgroup 34 “Co-ordinated Evaluation of ^{239}Pu in the Resonance Region” for producing better resonance parameter sets, and benchmark testing of the new parameter set is under way.

Fast energy region

Fission cross-section

The fission cross-sections in the fast energy range (above the resolved resonance region) are given by either unresolved resonance parameters in MF=2 (up to 30 keV), or by the point-wise cross-section in MF=3. To compare the fission cross-sections we first processed the files with NJOY to generate a 640 energy group cross-section in the SAND-II group structure, and they are given in Figure 1. CENDL is not shown here because it says the unresolved resonance parameters are identical to those in JENDL-3. The ENDF fission cross-sections in the 1-2 keV region are unexpectedly larger than JENDL and JEFF, though still in the resolved resonance region. This was due to a background cross-section given in MF=3. Above 2.5 keV ENDF and JEFF adopt the same unresolved resonance parameters, hence they are identical.

Capture cross-section

Figure 2 compares the evaluated capture cross-sections in the fast energy region with some experimental data found in the EXFOR database. The evaluated cross-sections agree well up to 20 keV and they start deviating with up to 20% difference around 100 keV. Since the available experimental data are few and scattered, new experiments are needed to fill this gap. With the DANCE detector at LANSCE, LANL measured the capture cross-section up to 1 keV, and they will be able to provide new capture data in the higher energy region in the near future.

Inelastic scattering cross-section

^{239}Pu has the first excited state at 7.9 keV, and this relatively low threshold energy of inelastic scattering channel competes with the fission and capture reactions in the fast energy range. It is well known that there are significant differences in the evaluated inelastic scattering cross-sections among the nuclear data libraries, although these files

Figure 1: Fission cross-sections represented in the 640 energy group structure

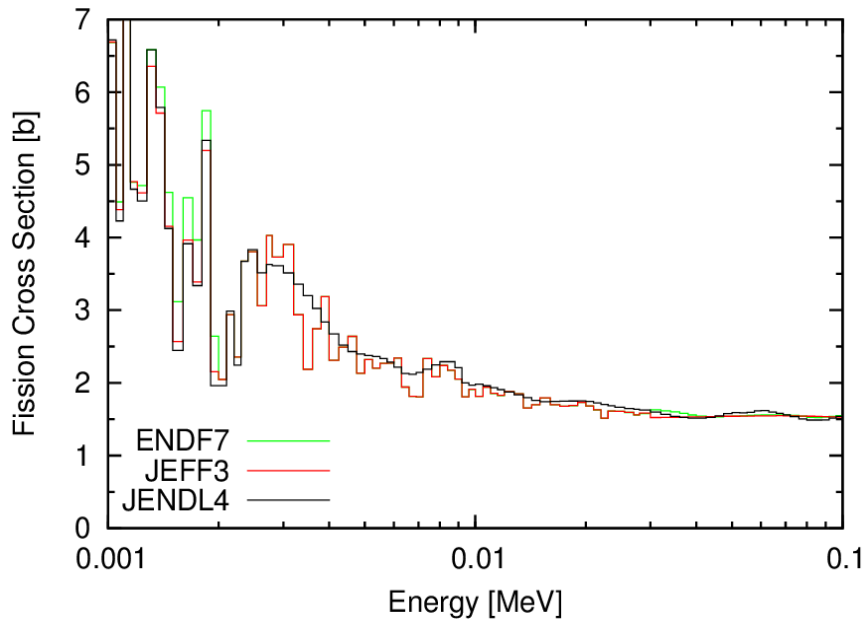
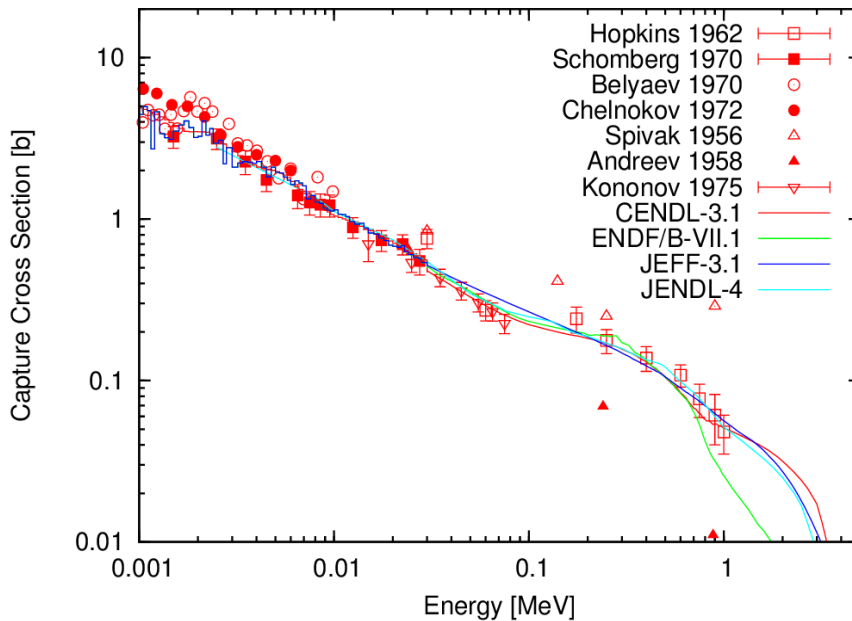


Figure 2: Capture cross-sections in the 1 keV to 5 MeV range



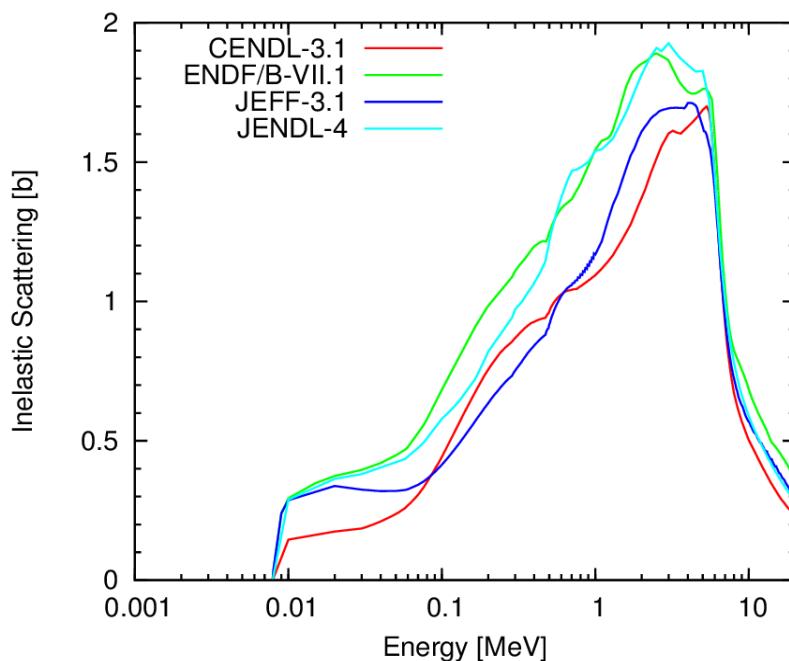
work equally well for calculating k_{eff} of Jezebel. This is discussed in the IAEA technical report (Plompen, Kawano and Capote, 2012) in detail, and Figure 3 gives the comparison of the total inelastic scattering cross-sections in the different libraries. Since the second excited state energy is 57 keV, and the cross-section to the second level is not so large up to 100 keV, the difference in the fast energy range, seen in Figure 3, is mainly due to the cross-section to the first excited state. It is clear that the difference in the inelastic channel is compensated by other nuclear data such as the elastic scattering cross-section in the integral benchmark testing.

Because there is no direct measurement of the angle-integrated inelastic scattering cross-section data, the evaluation of the inelastic scattering relies significantly on the statistical Hauser-Feshbach model calculation, and the following items should be investigated carefully:

- optical model potential that determines the total compound formation cross-section, as care must be taken for the coupling scheme as well as the treatment of weakly coupled states;
- competing channel cross-sections (fission and capture), which should be consistent with available experimental data;
- width fluctuation model, which re-distributes the total compound formation cross-section into individual channels.

We revisited the third item of the width fluctuation by the numerical simulation for the Gaussian Orthogonal Ensemble, and it was confirmed that the current modellings adopted in various Hauser-Feshbach codes do not produce such a large difference in the calculated cross-section. We plan to extend this by including the strongly coupled channels.

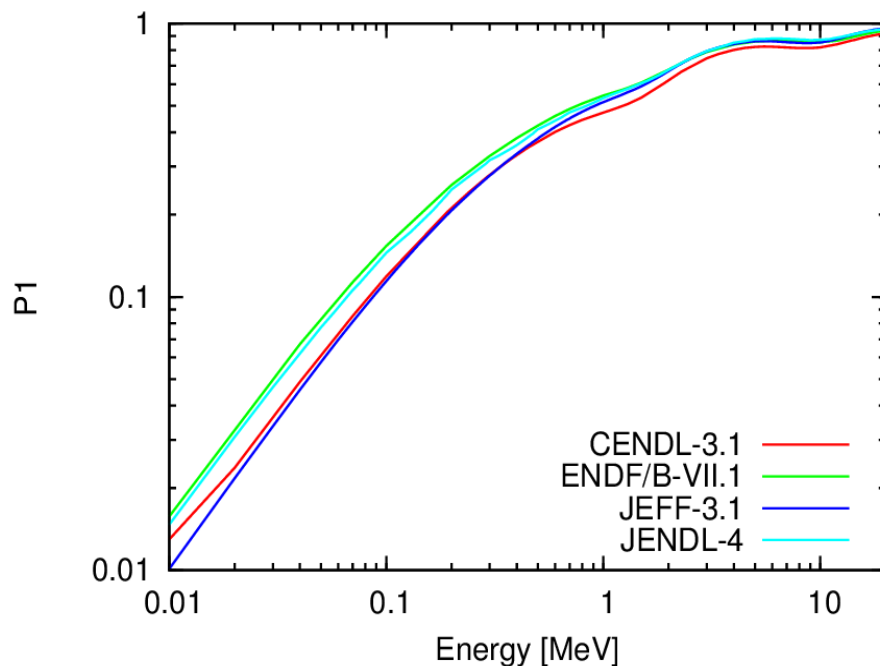
Figure 3: Comparison of total inelastic scattering cross-sections



Anisotropy of elastic scattering

Radiation transport simulations for the fast neutron systems are sensitive not only to the scattering cross-sections but also to the elastic scattering angular distributions, especially for the small systems which have large neutron leakage. The most important nuclear data are the $L=1$ component P_1 for the Legendre expansion of elastic scattering angular distributions. Figure 4 shows the evaluated P_1 in the libraries as a function of incident neutron energies. Since JEFF gives the angular distributions in a tabulated format, we fitted them by the Legendre polynomial. The actual values at 100 keV are: 0.15 for ENDF and JENDL, 0.11 for CENDL and JEFF. This difference is also one of the sources of compensation in calculating the k_{eff} of Jezebel.

Figure 4: L=1 components of elastic scattering angular distributions



The scattering angular distribution above the resolved resonance region is solely evaluated by the model calculations, since there is no scattering measurement in this energy region. The model calculation involves both the optical model part that gives the shape elastic scattering, and the statistical model part that gives the compound elastic contribution. The sensitivities of model parameters, as well as the modelling itself such as the number of coupled states, to the calculated anisotropy can be large. For example, it is known that the coupled-channels calculation depends on how many coupled levels are included (Dietrich, Thompson and Kawano, 2011). We performed simple calculations for ^{239}Pu with CoH_3 and obtained P_1 at 100 keV ranging from 0.12 to 0.18 depending on the number of coupled levels, from 3 to 7. The variation due to the coupling scheme roughly covers the differences among the libraries.

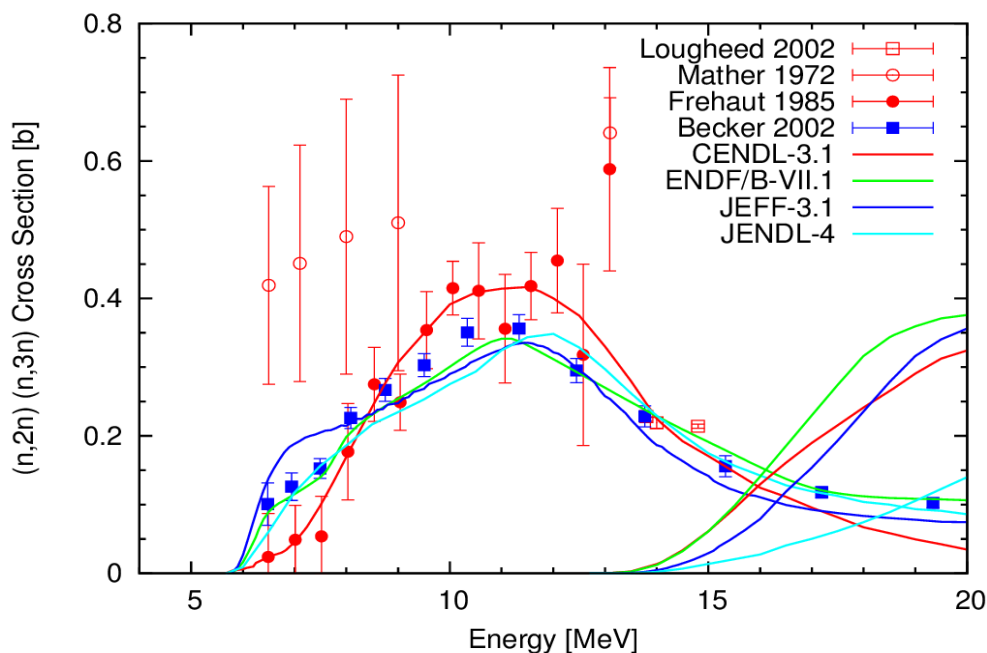
Above fast energy region

Fission cross-section

The fission cross-sections in the libraries agree within at most 5% above the unresolved resonance range (30 keV). The CENDL, ENDF and JENDL evaluations are based on the least-squares fitting to the experimental data, so that the difference comes from the selected experiments as well as estimated covariance data. JEFF adopted the Hauser-Feshbach model calculation in which available experimental data were fitted simultaneously.

(n,2n) and (n,3n) cross-section

Figure 5 shows the comparison of (n,2n) and (n,3n) reaction cross-sections in CENDL, ENDF, JEFF and JENDL. These evaluations are based on both the Hauser-Feshbach calculations and the available experimental data. Note that the experimental data of Frehaut are the original points, not corrected as known.

Figure 5: Comparison of (n,2n) and (n,3n) reaction cross-sections

In this energy region, the elastic scattering cross-section is basically equal to the shape elastic scattering calculated with the optical model, and the capture cross-section is negligible. Therefore the compound formation cross-section is distributed into the multi-chance fission, inelastic scattering, (n,2n) and (n,3n) channels. In this sense these channel cross-sections are correlated with each other, and the evaluation should be performed in a consistent way in order to avoid unphysical shape in excitation functions. Even if the fission cross-sections are evaluated by the direct fitting to the experimental data, the model calculations are required to reproduce the fission channel to a reasonable extent for evaluating the (n,2n) and (n,3n) channels.

Average number of neutrons per fission

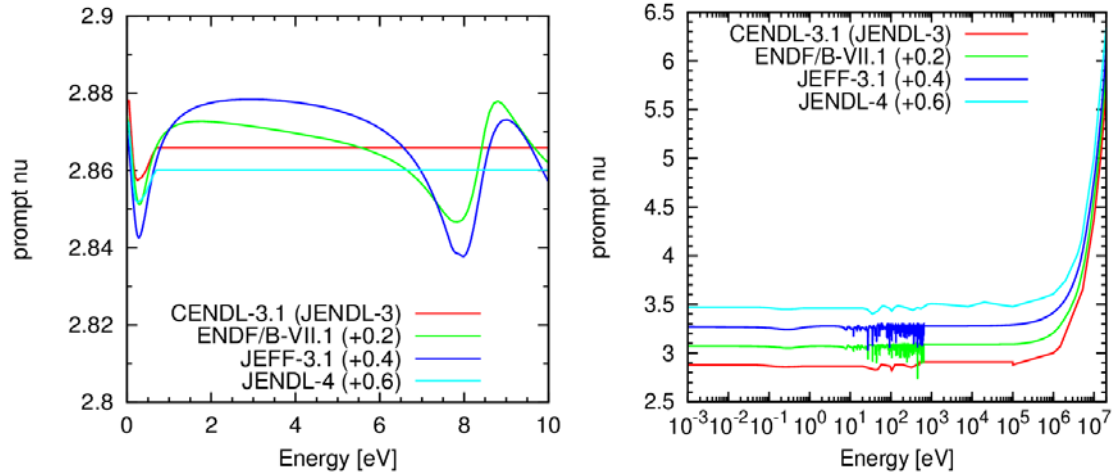
There is a large resolved resonance at 0.3 eV, which modifies the average number of prompt neutrons per fission (ν_p). All libraries consider this by representing it in an energy-dependent way. This is shown in Figure 5. Note that CENDL adopted JENDL-3 ν_p . JEFF and ENDF include strong fluctuation in the resolved resonance region, while JENDL-4 smoothed this out. The thermal values in each library are 0.2878 in CENDL (JENDL-3), 2.873 in ENDF, 2.868 in JEFF and 2.782 in JENDL-4. Because of the dip at 0.3 eV, comparison of the thermal values may also require consideration of the slope in the thermal region, even if the thermal values in the different libraries are consistent with each other.

The thermal values for delayed neutrons in the libraries agree within 5%. JENDL has the low-side value of 0.00622, and JEFF is at the high side of 0.0065. ENDF is between JENDL and JEFF.

There was a WPEC Subgroup 6 “Delayed Neutron Data” where an eight time-group representation was recommended instead of the traditional six-group. JEFF is the only library that adopts the eight-group structure for the delayed neutron. All other libraries retained the six-group structure.

Figure 5: Average number of prompt fission neutrons per fission as a function of neutron incident energies in the eV energy region (left) and in the entire energy range (right)

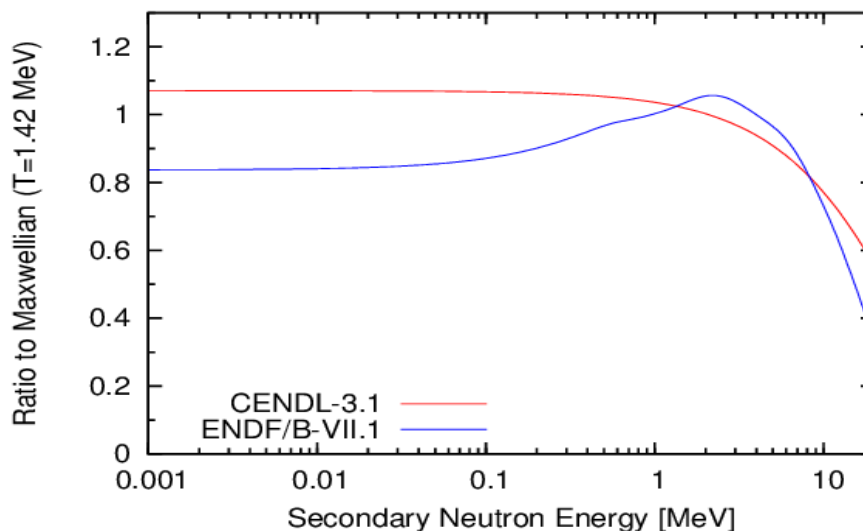
Note that each curve has an offset shown in the figures



Prompt fission neutron energy spectrum

Although the evaluations of prompt fission neutron spectrum for the thermal neutron-induced reaction are independent, they are based on the so-called Madland-Nix model (or Los Alamos model). CENDL is an exception – this looks a Maxwellian with a temperature of 1.37 MeV. ENDF, JENDL and JEFF might have different model parameters together with some modifications to the original Madland-Nix model, the differences among them are surprisingly small and hard to see in a plot. We plot the spectra in ENDF and CENDL only in Figure 6, which is shown as a ratio to the Maxwellian with a temperature of 1.42 MeV.

Figure 6: Prompt fission neutron spectra at the thermal energy as a ratio to the Maxwellian of $T = 1.47$ MeV



Recently WPEC Subgroup 34 proposed a new set of resolved resonance parameters. They note that indeed these new resonance parameters improve several thermal neutron integral benchmark tests, but we should keep in mind that the calculations of integral quantities also depend on both the prompt fission neutron spectrum and the average number of prompt neutrons at the thermal energy. These quantities are strongly coupled in the neutron transport calculations.

At the higher incident neutron energies, though they are less sensitive to the fission energy applications, different treatments of pre-fission neutron that evaporates from a compound nucleus before scission modify the shape of the spectrum. This calculation involves a complicated exclusive neutron emission calculation in the Hauser-Feshbach model, and only JENDL-4 considers the pre-fission neutrons carefully at this moment. The other libraries include the effect of pre-fission neutrons by correcting the available excitation energy for fission in the residual nucleus. A better modelling for the pre-fission neutron is under way at the IAEA co-ordinated research project on the prompt fission neutron spectrum, where they plan to re-evaluate the spectrum data for major actinides.

Another important direction of the fission neutron study is the sequential decay of fission fragments by the Monte Carlo technique (Becker, *et al.*, 2013; Vogt, *et al.*, 2009). This method allows us to calculate not only the neutron energy spectra but also other observables such as prompt gamma-ray energy spectra, number of neutrons as a function of fragment mass, correlation between emitted particles and so on. The downside of this method is that this requires a more detailed description of fission phenomenon, for example the excitation energy shared by two fission fragments and their spin and parity distributions. The Madland-Nix model calculation is still practical for the actual data evaluations. However, the Monte Carlo approach that is fitted to different observables provides us confidence in our fission spectrum modelling.

Conclusion

We have reviewed the evaluated nuclear data of ^{239}Pu in several libraries – CENDL, ENDF, JEFF and JENDL – and compared them with each other. The comparisons include the cross-sections of fission, capture, inelastic scattering, (n,2n), and (n,3n), as well as the elastic scattering angular distribution, the average number of prompt and delayed neutrons and the prompt fission neutron energy spectrum.

Acknowledgements

This work was carried out under the auspices of the National Nuclear Security Administration of the United States Department of Energy at Los Alamos National Laboratory under contract No. DE-AC52-06NA25396.

References

- Becker, B., *et al.* (2013), “Monte Carlo Hauser-Feshbach Predictions of Prompt Fission Gamma-Rays: Application to $n_{\text{th}}+^{235}\text{U}$, $n_{\text{th}}+^{239}\text{Pu}$, and ^{252}Cf (sf)”, *Phys. Rev. C*, 87, 014617.
- Dietrich, F., I. Thompson and T. Kawano (2011), “Target-Set Dependence of Cross Sections for Reactions on Statically Deformed Nuclei”, *Phys. Rev. C*, 85, 044611.
- Plompen, A., T. Kawano and R. Capote, (2012), *Summary Report on Technical Meeting on Inelastic Scattering and Capture Cross-Section Data of Major Actinides in the Fast Neutron Region*, INDC(NDS)-0597, IAEA, Vienna.
- Vogt, R., *et al.* (2009), “Event-By-Event Study of Prompt Neutrons from $^{239}\text{Pu}(n,f)$ ”, *Phys. Rev. C*, 80 044611.

The Big Three: ^{235}U , ^{238}U , ^{239}Pu – Part 2

Chair: M. Herman

New evaluation of the resolved and unresolved resonance range of ^{239}Pu

G. Noguère,^a L. Leal,^b P. Leconte,^a D. Bernard,^a
O. Bouland,^a Y. Penelieu,^a C. De Saint Jean^a

^aCommissariat à l'Énergie Atomique (CEA), DEN Cadarache
Saint-Paul-lez-Durance, France

^bOak Ridge National Laboratory, Oak Ridge, TN, United States

Abstract

This paper summarises the work performed on the ^{239}Pu resonance evaluation in the frame of the NEA/WPEC Subgroup 34 started in 2010. The aim of this subgroup was to produce a new evaluation of the resolved resonance range (RRR). Other topics were investigated. The resonance parameter covariance matrix (RPCM) was produced using the CONRAD code's marginalisation procedure. The unresolved resonance range was studied with the optical and statistical model codes ECIS and TALYS from 2.5 keV to 40 keV. The $(n,\gamma f)$ process was revisited to study the channel spin dependence of the neutron multiplicity $\nu p(E)$ as recommended in the JEFF-3.1.1 library. Various descriptions of the prompt fission neutron spectra (PFNS) were tested with fast, intermediate and thermal benchmarks. The RRR and RPCM produced in the frame of this subgroup were converted in ENDF-6 format and included in Files 2 and 32 of the latest version of the European library JEFF-32.

Introduction

The United States and European libraries have adopted the same evaluation for the ^{239}Pu resonance region, largely based on work from ORNL and CEA. In data testing for ENDF/B-VII.0, a general overprediction of Pu-SOL-THERMAL assemblies was noted, with an overprediction of typically about 0.5%.

Two efforts of recent years should be mentioned. First, the ^{239}Pu thermal energy range was improved in JEFF-3.1.1 for reducing the aforementioned discrepancies. Second, at ORNL, Derrien and Leal have developed a new set of resonance parameters that have been incorporated into the ENDF/A for testing. This most recent evaluation is more consistent with the cross-section resonance data and believed by the evaluators to be the best representation of these data to date. Nonetheless, this new evaluation does not improve the poor integral performance of the ENDF/B-VII.0 file. The goal of the NEA/WPEC Subgroup 34 was to bring together the experts in the OECD/NEA community to investigate if a new evaluation can be developed that both uses the most accurate cross-section data with nuclear theory constraints, and also better models the relevant integral criticality data. Results produced in the frame of this collaboration can be found elsewhere (Leal, *et al.*, 2012, 2013; Noguère, *et al.*, 2012a, 2012b, Kahler, *et al.*, 2012; Penelieu, *et al.*, 2013).

This paper is structured as follows. The neutron resonance shape analysis performed with the SAMMY code are first presented, followed by a discussion of the resonance parameter covariance matrix obtained with the CONRAD code's marginalisation procedure.

The evaluation work done using the ECIS and TALYS codes in the unresolved resonance range (URR) is then described. The remaining discussion is devoted to the $(n,\gamma f)$ process and its implications for the description of the neutron multiplicity in the resonance range.

Analysis of the resonance range

A new analysis was motivated by three inconsistent descriptions of the resolved resonance range adopted in the United States, European and Japanese libraries. The first problem was the separation of the resonance range in three distinct sets of resonance parameters in JEFF-3.1.1 and ENDF/B-71. Figure 1 shows the limits of each energy range (1 keV, 2 keV and 2.5 keV). External levels were added to avoid cross-section mismatch at the energy boundaries. The second problem is illustrated in Figure 2. In the original evaluated file in ENDF-6 format, a pseudo background cross-section was used to correct the fission cross-section between 1 keV and 2.5 keV. This background is not used in JEFF-3.1.1. Finally, the low-energy range of the ^{239}Pu evaluation available in JEFF was modified to improve the calculations of the reactivity temperature coefficient (RTC) in EOLE experiments (Figure 3).

Figure 1: ^{239}Pu resonance range described with three distinct sets of resonance parameters

The energy limits are 1 keV, 2 keV and 2.5 keV

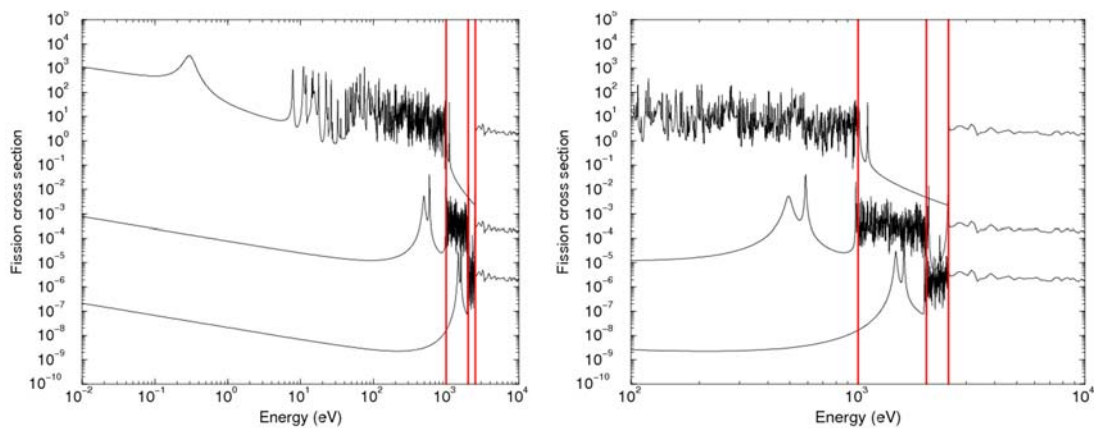


Figure 2: Comparison of the ^{239}Pu fission cross-section from JEFF and ENDF/B

No background cross-section was included in JEFF between 1 keV and 2 keV

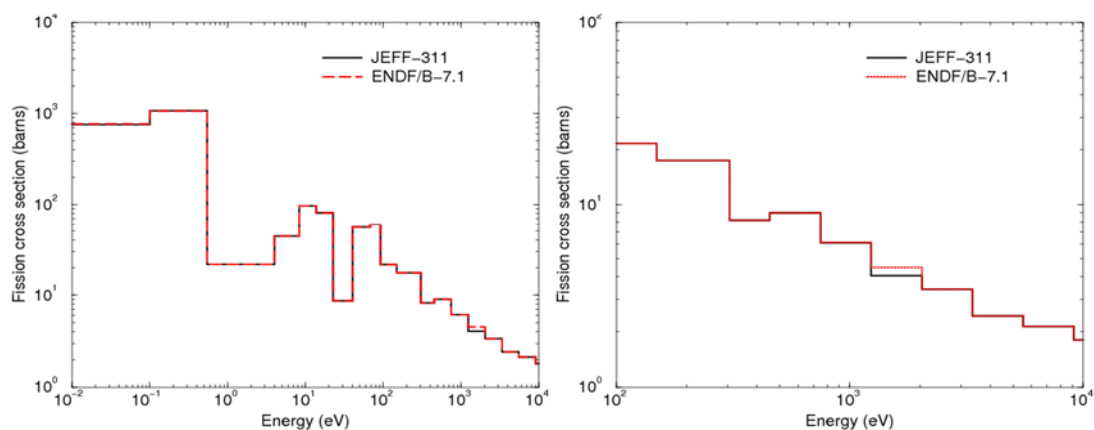
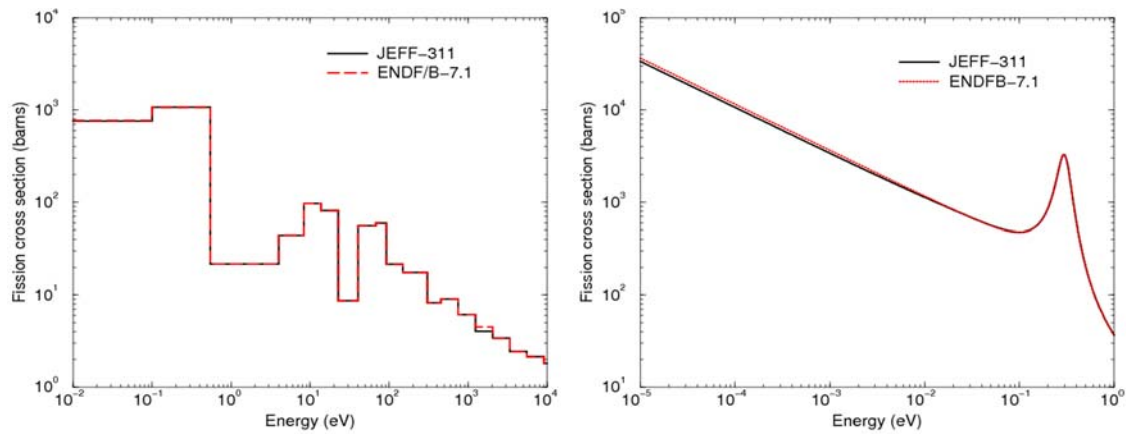


Figure 3: Modification of the low-energy range of ^{239}Pu to improve the calculations of the reactivity temperature coefficient in EOLE experiments



Source: Bernard, *et al.* (2007).

As a consequence, the ^{239}Pu evaluation in ENDF/B-71 is based on the older evaluation performed at ORNL with three energy ranges (Derrien, 1993; Derrien, *et al.*, 1990). In JENDF-4, the resonance range is based on the work of Derrien, *et al.* (2007) in which the RRR is described with a single set of resonance parameters up to 2.5 keV. The JEFF-3.1.1 library is equivalent to ENDF/B-71 with a slight modification on the low-energy range (Bernard, *et al.*, 2007). The aim of the evaluation work was to produce a single set of resonance parameters, such as JENDL-4, which gives integral trends as good as those obtained with JEFF-3.1.1.

This goal was achieved through the NEA/WPEC Subgroup 34. Table 1 lists the data sets used to establish a new set of resonance parameters with the SAMMY code. The thermal values and integral quantities are summarised in Table 2.

Table 1: Experimental data set used in the SAMMY code to produce a new set of ^{239}Pu resonance parameters up to 2.5 keV

Reference	Energy range (eV)	Facility	Measurement
Bollinger, <i>et al.</i> (1956)	0.01-1.0	Chopper	Total cross-section
Gwin, <i>et al.</i> (1971)	0.01-0.5	ORELA	Fission and absorption at 25.6 m
Gwin, <i>et al.</i> (1976)	1.0-100.0	ORELA	Fission and absorption at 40.0 m
Gwin, <i>et al.</i> (1984)	0.01-20.0	ORELA	Fission at 8 m
Weston, <i>et al.</i> (1984)	9.0-2 500.0	ORELA	Fission at 18.9 m
Weston, <i>et al.</i> (1988)	100.0-2 500.0	ORELA	Fission at 86 m
Weston, <i>et al.</i> (1993)	0.02-40.0	ORELA	Fission at 18.9 m
Wagemans, <i>et al.</i> (1988)	0.002-20.0	GELINA	Fission at 8 m
Wagemans, <i>et al.</i> (1993)	0.01-1 000.0	GELINA	Fission at 8 m
Harvey, <i>et al.</i> (1985)	0.7-30.0	ORELA	Transmission at 18 m
Harvey, <i>et al.</i> (1985)	30.0-2 500.0	ORELA	Transmission at 80 m

Table 2: Thermal values and integral quantities compiled in the *Atlas*, recommended in the ENDF libraries and found with the new ^{239}Pu evaluation

Quantity	<i>Atlas</i>	ENDF/B-VII.1 (JEFF-3.1)	JEFF-3.1.1	WPEC SG34
σ_γ	269.3±2.9	270.6	272.7	270.1
σ_f	748.1±2.0	747.7	747.08	747.2
g_f	1.0553±0.0013	1.054	1.050	1.052
g_a	1.077±0.003	1.078	1.075	1.077
$\bar{\nu}$	2.879±0.006	2.873	2.873	2.873
l_γ	180±20	181.4	181.5	180.1
l_f	303±10	302.6	303.6	309.1

Detailed explanations on the evaluation work can be found elsewhere (Noguère, *et al.*, 2012a). An independent work performed with the CONRAD code has confirmed the consistent description of the capture, fission and total cross-sections in the low-energy range (Figure 4). Final cross-sections are in good agreement with those of JEFF-3.1.1 (Figure 5). The resonance parameters were included in the latest version of the European library JEFF-3.2.

Various integral tests were performed to investigate the performances of the new evaluation. Oscillation measurements carried out in the MINERVE facility of the CEA Cadarache (CERES programme) suggest a K1 value close to $1\,163.9 \pm 15.0$ barns (Leconte, *et al.*, 2014). This result is in excellent agreement with the K1 value of 1 161 barns obtained with the new ^{239}Pu evaluation.

Production of the resonance parameter covariance matrix

The resonance parameter covariance matrix (RPCM) was produced by using the marginalisation procedure of the CONRAD code (Habert, *et al.*, 2010). In order to overcome problems related to storage and processing of large RPCM, a neutron width selection was

Figure 4: Comparison of the capture, fission and total cross-sections reconstructed with the SAMMY and CONRAD codes

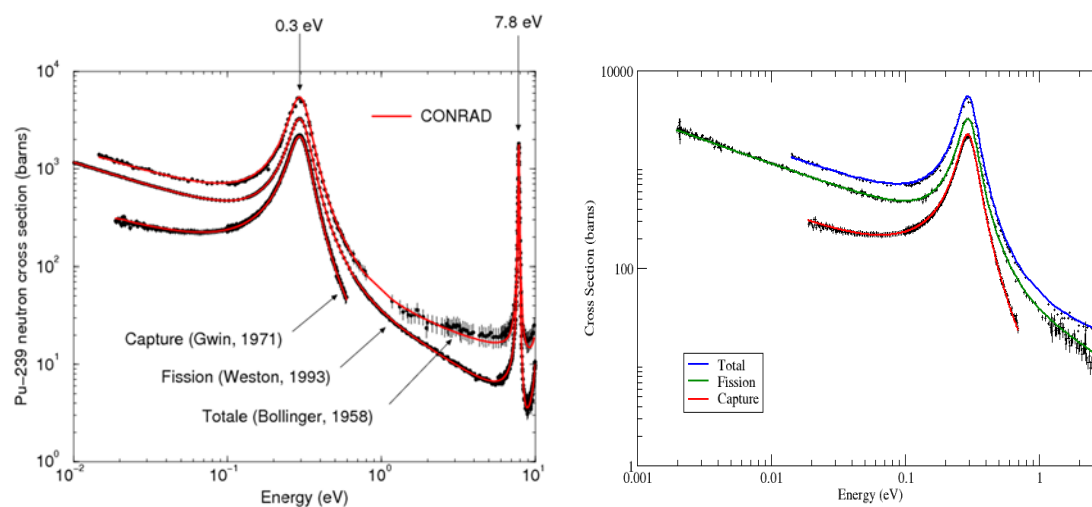
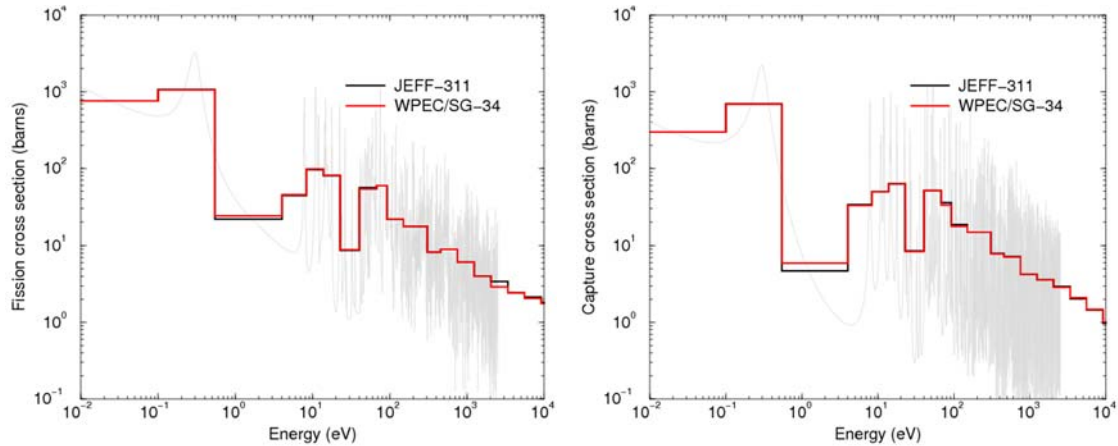
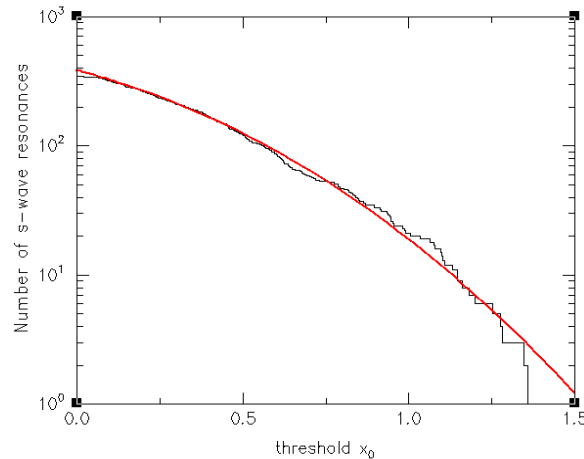


Figure 5: Comparison of the cross-sections reconstructed with the resonance parameters of JEFF-3.1.1 and WPEC SG34



applied to reduce the size of the resonance parameter set. The selection principle relies on properties of the cumulative Porter-Thomas integral distribution (Figure 6). An s-wave resonance is included in the marginalisation procedure if its reduced neutron width amplitude is larger than a threshold x_0 . The latter threshold should fulfil the conditions $\sigma_{\gamma,g}(x_0 = 0) \approx \sigma_{\gamma,g}(x_0 > 0)$ for capture and $\sigma_{f,g}(x_0 = 0) \approx \sigma_{f,g}(x_0 > 0)$ for fission in a given broad energy group g .

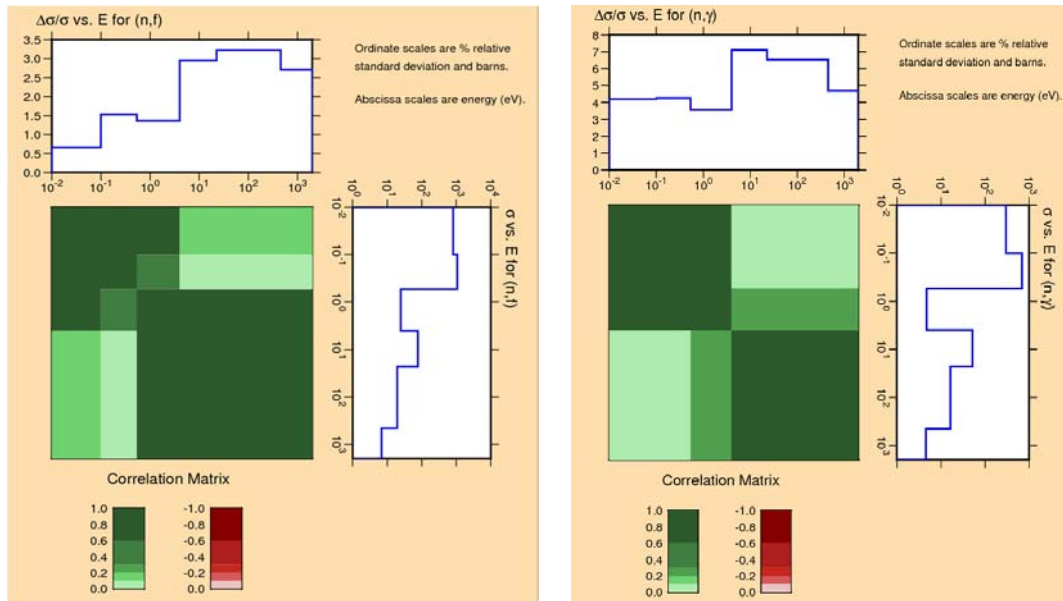
Figure 6: Cumulative Porter-Thomas integral distribution calculated from the neutron widths of the s-wave resonances below 1 keV



The energy domain was divided into three energy ranges to cover the thermal range, the first resonance at 0.3 eV and the resonance integral above 0.5 eV. Results obtained with the CONRAD code are shown in Figure 7. In the RRR, relative uncertainties for the fission and capture cross-sections remain below 3.0% and 7.0%, respectively. The systematic uncertainties are the dominant components of the final uncertainties. Therefore, the simple structures observed in the correlation matrices follow the main experimental data chosen as reference for the evaluation work (Table 1). The present results were included in File 32 (ENDF-6 format) of the latest European library JEFF-3.2.

In order to avoid the artificial use of such a neutron width selection, it is recommended to consider the AGS format developed at the IRMM as a concise method for storing and communicating large resonance parameter covariance matrices (Schillebeckx, *et al.*, 2012).

Figure 7: Relative uncertainties and correlation matrices for the ^{239}Pu fission and capture cross-sections below 2.5 keV

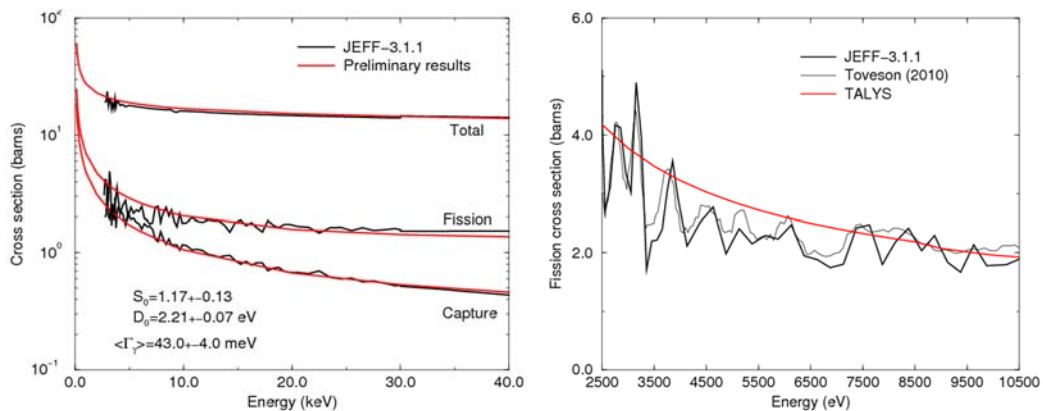


Analysis of the unresolved resonance range

Works performed in the framework of NEA/WPEC Subgroup 32 (entitled “Unresolved Resonance Treatment for Cross-Section and Covariance Representation”) have pointed out an inconsistent treatment of the ^{239}Pu unresolved resonance range between the processing systems NJOY and CALENDAR. Discrepancies between TRIPOLI (probability table from CALENDAR) and MCNP (probability tables from NJOY) calculations on a simple fast benchmark were close to 200 pcm. This problem was simply solved by using the flag LSSF=1 of the ENDF-6 format.

The remaining problem is the description of the observed large fluctuations in the unresolved resonance range (below 4 keV). The right-hand plot of Figure 8 indicates that these fluctuations exist in JEFF-3.1.1 and in the data of Tovesson, *et al.* (2010). Therefore, they are not of statistical origin.

Figure 8: Capture, fission and total cross-sections calculated with the ECIS and TALYS codes by using average resonance parameters established from the statistical analysis of the resolved resonance parameters



For the calculations of the self-shielding factors, a descriptive URR model is needed. The FITACS option of the SAMMY code and the recent URR option implemented in the TALYS code are able to establish a set of average resonance parameters consistent with the observed fluctuations. However, a new fission cross-section measurement in the URR is needed to get a better description of the rapid fluctuations of the cross-section.

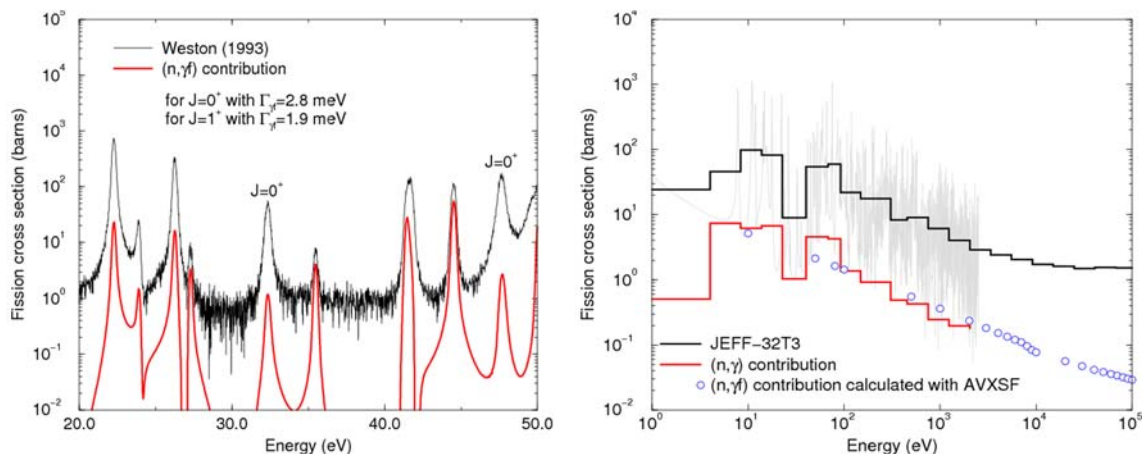
Investigation of the two-step $(n,\gamma f)$ process

The $(n,\gamma f)$ process was introduced by Lynn in 1959. The formal description of such a two-step process was published in 1965. The existence of the $(n,\gamma f)$ reaction is still a topic of discussion because direct measurements are not possible.

We assume that the observed fission is the sum of the one-step (or “direct”) fission and of the two-step $(n,\gamma f)$ reaction. The contribution of the two-step process can be deduced from the Reich-Moore parameters by introducing additional J-dependent partial widths $\Gamma_{\gamma f}$. Due to the numerous gamma decay possibilities before fission, the partial width of the $(n,\gamma f)$ reaction is often assumed constant over a wide energy range.

Figure 9 shows the contribution of this reaction in the resolved resonance range and in the continuum part. Below 2.5 keV, $\Gamma_{\gamma f} = 2.8 \pm 9.2$ meV for $J=0^+$ and $\Gamma_{\gamma f} = 1.9 \pm 0.8$ meV are used for $J=1^+$. The AVXSf calculations (Bouland, *et al.*, 2013) are in good agreement with the average contribution obtained in the resonance range. This study confirms the non-negligible contribution of the $(n,\gamma f)$ reaction for small s-wave resonances having $J=1^+$ (one partially open channel). For future evaluation works on ^{239}Pu , it would be worth including the partial width $\Gamma_{\gamma f}$ in the evaluated data file.

Figure 9: Comparison of the ^{239}Pu fission cross-section and of the $(n,\gamma f)$ reaction deduced from the resonance parameters established in the frame of the NEA/WPEC SG34 and calculated with the AVXSf code



Study of the channel spin dependence of $\nu p(E)$

Large fluctuations of the neutron multiplicity were measured in the resonance range. According to the spin assignment, the observed fluctuations are stronger for resonances having $J=1^+$. The latter channel is characterised by an average fission width of 30 meV, while for $J=0^+$ (two open channels), the average fission width is close to 2 eV. The $(n,\gamma f)$ reaction was introduced to explain such channel spin-dependent fluctuations.

In the present work, a phenomenological decomposition of the neutron multiplicity is used (Fort, *et al.*, 1988). Two fission widths Γ_f and $\Gamma_{\gamma f}$ were introduced for each channel $J=0$ and $J=1$. The neutron multiplicity can be expressed as follows:

$$\nu_p(E) \approx \sum_{i=1}^4 \nu_i P_i(E)$$

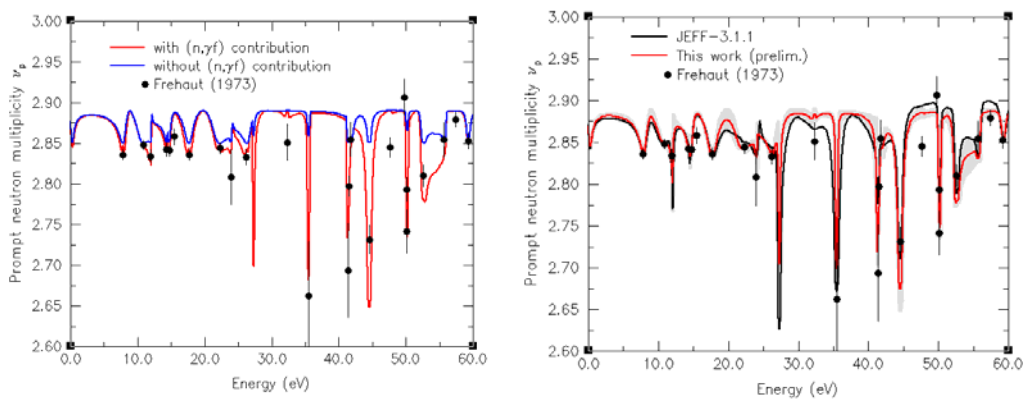
in which the probabilities P_i are given by:

$$P_i(E) = \frac{\sigma_i(E)}{\sigma_{(n,f)}(E) + \sigma_{(n,\gamma f)}(E)}$$

where $\sigma_i(E)$ represents the partial fission cross-sections for each channel. Final results are shown in Figure 10. The left-hand plot compares the magnitude of the neutron multiplicity with and without the contribution of the two-step $(n,\gamma f)$ process. Without the $(n,\gamma f)$ contribution, the phenomenological description of the neutron multiplicity fails to reproduce the large fluctuations observed for resonances with $J=1$. For $J=0$, the contribution of the $(n,\gamma f)$ reaction is negligible compare to the magnitude of the average fission width.

Figure 10: Neutron multiplicities calculated with and without the $(n,\gamma f)$ process

The resonance parameters established in the framework of NEA/WPEC SG34 provide $\nu_p(E)$ values in good agreement with JEFF-3.1.1



Conclusions

The evaluation work performed on ^{239}Pu in the framework of NEA/WPEC SG34 is completed. The final report will be made available via the NEA website. The resonance parameters and the corresponding covariance matrix are included in the latest version of the European library JEFF-3.2.

This collaborative effort allows to point out few missing experimental data. New measurements of the total cross-section (around 0.3 eV), of the fluctuations of the fission cross-section (in the unresolved resonance range below 5 keV) and of the neutron multiplicity (in the resonance range) are needed for future evaluations. For the capture cross-section, various experimental set-ups are under development.

From the evaluation point of view, it will be needed to include in the future evaluated file a set of J -dependent partial widths for the $(n,\gamma f)$ reaction. These additional partial widths will allow to perform on-the-fly calculations of $\nu_p(E)$ in the resolved and unresolved resonance range. As briefly explained in this document, the description of the structures observed in the fission cross-section (between 2.5 keV and 5 keV) is also a crucial issue for the calculation of reliable self-shielding factors.

References

- Bernard, D., *et al.* (2007), *Int. Conf. on Nuclear Data for Science and Engineering*, Nice, France.
- Bouland, O., *et al.* (2013), *Phys. Rev. C*, 88, 054612.
- Derrien, H. (1993), *J. Nucl. Sci. Technol.*, 30, 845.
- Derrien, H., *et al.* (1990), *Nucl. Sci. Eng.*, 106, 434.
- Derrien, H., *et al.* (2007), *Int. Conf. on Nuclear Data for Science and Engineering*, Nice, France.
- Fort, E., *et al.* (1988), *Nucl. Sci. Eng.*, 99, 375.
- Habert, B., *et al.* (2010), *Nucl. Sci. Eng.*, 166, 276.
- Kahler, A.C., *et al.* (2012), *3rd Int. Workshop on Nuclear Data Evaluation for Reactor Applications*, Aix-en-Provence, France.
- Leal, L., *et al.* (2012), “ ^{239}Pu Resonance Evaluation”, JEFFDOC-1432.
- Leal, L., *et al.* (2013), *Int. Conf. on Nuclear Data for Science and Engineering*, New York, United States.
- Leconte, P., *et al.*, *PHYSOR 2014*, submitted.
- Lynn, E., *et al.* (1965), *Phys. Lett.*, 18, 31.
- Noguère, G., *et al.* (2012a), “Improved MOX Fuel Calculations Using New Pu and Am Evaluations”, JEFFDOC-1481.
- Noguère, G., *et al.* (2012b), *3rd Int. Workshop on Nuclear Data Evaluation for Reactor Applications*, Aix-en-Provence, France.
- Peneliau, Y., *et al.* (2013), *Int. Conf. on Nuclear Data for Science and Engineering*, New York, United States.
- Schillebeckx, P., *et al.* (2012), *Nucl. Data Sheets*, 113, 3054.
- Tovesson, F., *et al.* (2010), *Nucl. Sci. Eng.*, 165, 224.

^{235}U and ^{238}U (n,xn gamma) cross-sections

A. Bacquias,^a C. Borcea,^b Ph. Dessagne,^a M. Kerveno,^a J.C. Drohé,^c N. Nankov,^c
A.L. Negret,^b M. Nyman,^c A. Plompen,^c C. Rouki,^c G. Rudolf,^a M. Stanoiu,^c J.C. Thiry^a

^aInstitut Pluridisciplinaire Hubert Curien, Université de Strasbourg, CNRS/IN2P3
Strasbourg, France

^bNational Institute of Physics and Nuclear Engineering “Horia Hulubei” (IFIN-HH)
Bucharest, Magurele, Romania

^cInstitute for Reference Materials and Measurements, Geel, Belgium

Abstract

The (n,n') and (n,2n) are important processes in the energy domain of fission neutrons, but the cross-sections suffer from large uncertainties, not compatible with the objectives fixed for future and advanced nuclear reactors. This paper presents our experimental effort to improve ^{235}U and ^{238}U (n,xn γ) cross-section data. The experiments were performed at the GELINA facility (Belgium), which provides a pulsed (800 Hz) neutron beam covering a wide energy spectrum (from a few eV to about 20 MeV). The GRAPhEME set-up is designed for prompt gamma spectroscopy and time-of-flight measurement. The analysis methods are presented. Already published results on ^{235}U are shown, as well as results on ^{238}U . The interpretation and discussion rely on the comparison with TALYS and EMPIRE predictions.

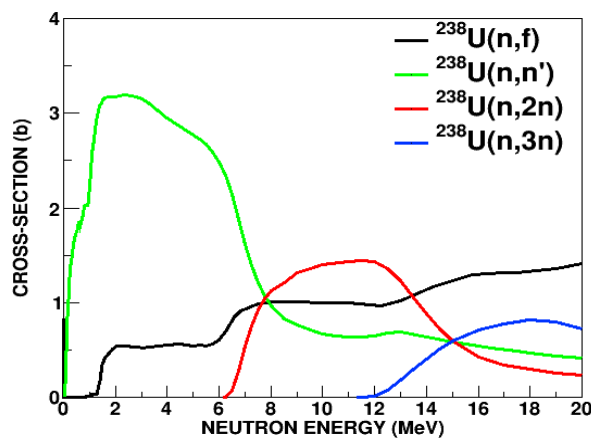
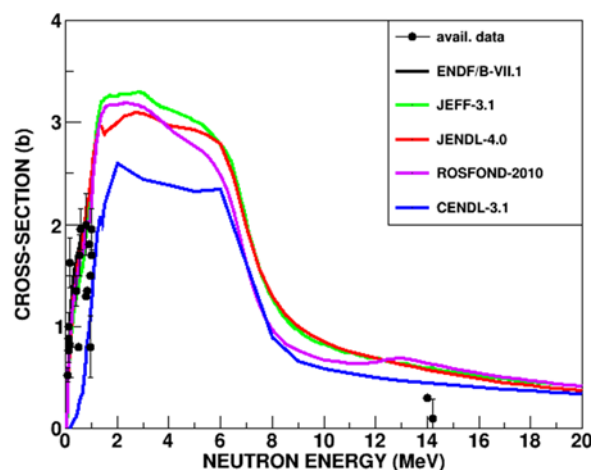
Introduction

In the present context of studies for future and advanced systems, (n,xn) reactions are very important. Figure 1 is a plot of the cross-sections of several neutron-induced reactions on ^{238}U , as evaluated by ENDF/B-VII as a function of neutron incident energy. It shows that (n,n') and (n,2n) reactions dominate fission over a broad energy range, from 45 keV up to 14 MeV. The importance of such processes makes their precise quantification a must for applications, and justifies afferent entries in the OECD/NEA High-Priority Request List (OECD/NEA, n.d.).

Few experimental measurements of the total inelastic cross-section exist, and they cover a limited range of incident neutron energy (below 1 MeV, and at 14 and 14.2 MeV). This situation offers few constraints for the evaluations, so that they disagree among themselves up to 20%, especially in the region of the maximum, between 1 and 5 MeV (see Figure 2).

This is obviously a problem in view of modern constraints on the design of nuclear reactors. The corresponding entry in the HPRL recommends a much better precision on this total inelastic cross-section, from about 4-20%, depending on the system.

Bernard, *et al.* (2013) at CEA Cadarache surveyed the impact of the evaluated inelastic cross-sections (as given in JEFF-3.1.1) on contemporary systems and/or benchmarks. They performed Monte Carlo simulations with the code TRIPOLI-4 to investigate the offset between calculated and experimental reactor features such as criticality k_{eff} , the delayed

Figure 1: Evaluated n-induced cross-sections on ^{238}U Figure 2: Experimental data and evaluations of the $^{238}\text{U}(n,n')$ cross-section

neutron ratio β_{eff} , and the radial power profile. As an example, the offset on the latter can be as large as several per cent for large reactor cores (PWR-N4). This confirms that the total cross-section is poorly known. These studies also showed that partial cross-sections ($n,n'\gamma$) should be measured and their uncertainties reduced, especially between 1 and 5 MeV incident neutron energy, for they contribute to a great extent to this situation.

In addition, ($n,xn\gamma$) cross-section measurements provide exclusive information on nuclear structure, and, as we will see in the “results” section, possibly selective knowledge on certain reaction mechanisms. They could therefore impose strong constraints on theoretical models.

Experimental set-up GRAPhEME and methods

The experiments were performed at JRC-IRMM, using a 30 metre flight-path of the GELINA facility. The “white” neutron beam was pulsed at 800 Hz. The energy spectrum of neutrons reaching our set-up typically ranged from a few keV (after some filtration to cut off low-energy neutrons) up to above 20 MeV. The flux was monitored as a function of time using a fission chamber (FC), based on a $^{235}\text{UF}_4$ deposit inside an ionisation chamber. The incident neutron energy was determined through the time-of-flight method.

A set of four planar high-purity germanium (HPGe) detectors was surrounding the target sample (typically a metallic disc about 200 μm thick and 5-10 cm in diameter, held between aluminium foils). All detectors (HPGe and FC) were connected to a digital data acquisition system TNT-2, so that time-of-flight and energy information was coded at the rate of 100 MHz. The HPGe were set by pairs at angles of 110° and 150° corresponding to zeroes of Legendre polynomial P_4 , so that the Gauss quadrature could be applied to obtain the angle-integrated cross-section (Brune, 2002).

The comparison of the gamma energy spectrum before the arrival of neutrons and the one in the presence of neutrons allows for the identification of reaction rays. The number of counts was extracted using standard analysis tools (background fit and subtraction, integration or fit of the peak, using ROOT or gf3 software depending on the complexity of the peak's shape).

Given the objectives of precision, we carefully determined uncertainty sources. The main contributions to uncertainty were the number of detected photons and the number of incident neutrons. Depending on the transition and the domain of incident neutron energy, these uncertainties sit between 1 and 20%. The efficiencies of the HPGe detectors were determined with calibrated source measurements and simulations (GEANT4 and MCNPX). The neutron losses between the fission chamber and the germaniums were quantified by MCNPX simulations. The neutron-induced fission cross-sections for the flux measurement were inherited from ENDF/B-VII.1; the uncertainties in this energy range are of the order or below 1%. The deposit inside the fission chamber is very well known, bringing the uncertainty on the number of nuclei of ^{235}U in the FC below 0.5%. The efficiency of the FC was precisely measured using in-beam calibration at PTB Braunschweig. For the experiments performed on uranium isotopes, the samples of highly enriched ^{235}U and of natural uranium were characterised very precisely by the target laboratory at IRMM (see Table 1 for details).

Table 1: Uranium samples properties

Isotope	Purity (at.%)	Mass (g)	Diameter (cm)	Thickness (mm)
^{235}U	93.20(3)	37.43(1)	12.004(4)	0.211(6)
^{238}U	99.17(1)	10.6175(1)	7.016(3)	0.181(6)

Several challenges came up during data acquisition and analysis, but remedies could be administrated when needed. The treatment of weakly observed gamma transitions (due to low cross-section, limited detection efficiency or high internal conversion coefficient) required high statistics accumulation. At the rate of 800 Hz, we gathered in both experiments over 1 200 hours of effective beam time, with data acquisition spreading over several months. This magnified some instabilities in the electronic chain of the HPGe, so that a continuous gain correction was eventually needed to take the best part of our detectors. Another type of deviation has been seen on the time-of-flight determination for low-amplitude signals in the germanium counters. This problem consisted of a gamma-energy dependent time shift towards larger ToF, i.e. lower incident neutron energies. This was suspected to affect transitions below 200 keV. A large amount of data was acquired with dedicated settings to address this problem; the shift was precisely measured. It resulted in a time correction only for the two lowest gamma transitions, namely the 45 keV ($2+$ to $0+$) and 103 keV ($4+$ to $2+$). Another point is the effective density of the target materials. As can be inferred from the figures in Table 1, neither of the samples used in our experiments reached the nominal density of metallic uranium. This was taken as a proof of oxidation. MCNPX simulations have been performed using different choices of oxide (UO_2 , U_3O_8 or a combination of both) layers on the surface of the samples, to investigate the different gamma self-absorption compared to pure metallic samples with their apparent density. The subsequent uncertainty contribution was

quantified and included in published data on ^{235}U (Kerveno, *et al.*, 2013). Re-characterisation of the natural uranium target has recently been pursued, using transmission as well as dimensions measurements before and after surface polishing.

Results

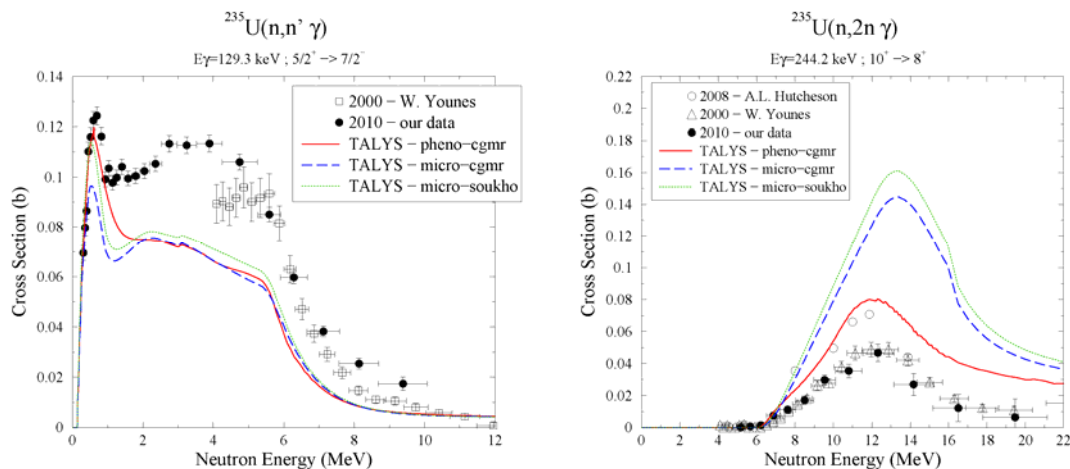
The case of ^{235}U

The sample of ^{235}U -enriched metallic uranium has been precisely characterised by the target laboratory of JRC-IRMM. The purity, mass and dimensions are reported in Table 1. Data were accumulated over an integrated effective beam time of 1 400 hours (this duration is obtained multiplying the stored number of beam pulses by the frequency of said pulses). The main difficulty in the analysis of ^{235}U rises from both the intrinsic radioactivity of the sample and gamma transitions in the fission products produced by the (n,f) process. Some of these rays occur at the same photon energy than inelastic or (n,2n) reaction rays, yielding in a superimposition of several peaks in the gamma-energy spectrum. The deconvolution of the different contributions was not always possible.

As is detailed in Kerveno, *et al.* (2013), the cross-section for one (n,n'g) could be produced, corresponding to the $5/2^+ \rightarrow 7/2^-$ (g.s.) transition in ^{235}U . The analysis of (n,2ng) transitions in the residual nucleus ^{234}U proved to be more accessible, and three cross-sections could be extracted, namely the $6^+ \rightarrow 4^+$ (152.7 keV), the $8^+ \rightarrow 6^+$ (200.9 keV) and the $10^+ \rightarrow 8^+$ (244.2 keV).

The comparison with other data sets – Younes, *et al.* (2000) in (n,n') and Younes, *et al.* (2000) and Hutcheson (2008) in (n,2n) – works rather well (see Figure 3). The same cannot be said about theoretical calculations performed by Romain (CEA Bruyères-le-Château) using different optical models and inputs in the TALYS code (Koning, Hilaire and Duijvestijn, 2008). Difficulties in reproducing the data have risen. The maximum of the cross-section for the (n,n'g) is correctly described, but some mechanisms seem missing or underestimated, yielding to a cross-section shape (as a function of incident neutron energy) rather different from data points. The theoretical predictions are in better shape for (n,2ng) cross-sections, but their magnitude seems systematically overestimated, and more so when increasing the energy (and spin) of the parent level in the ground state band. Among the three tested approaches, the phenomenological one gives the best results for now (Kerveno, *et al.*, 2013).

Figure 3: One $^{235}\text{U}(n,n'g)$ and one $^{235}\text{U}(n,2ng)$ cross-section



The case of ^{238}U

The sample of metallic natural uranium had a chemical purity of 99.9% and the natural isotopic composition (99.27% of ^{238}U), leading to an effective atomic composition of 99.17%, as given in Table 1. Data were accumulated over an integrated effective beam time of 1 211 hours. The sample being much less radioactive, and ^{238}U being much less subject to neutron-induced fission than ^{235}U in the neutron energy range considered in this work, many transitions could be analysed. Four (n,3ng), three (n,2ng) and 36 (n,n'g) cross-sections have been obtained as a function of incident neutron energy. The complete list is given in Figure 4. Some typical examples are given in the following (Figure 5). It is to be noted that the present cross-sections reflect the observation of gamma de-excitation, and are free of any corrections to account for internal conversion. Other experimental data were back-corrected for comparison using Hager-Seltzer conversion coefficients (HSICC), the only available values at the time the former data sets were published.

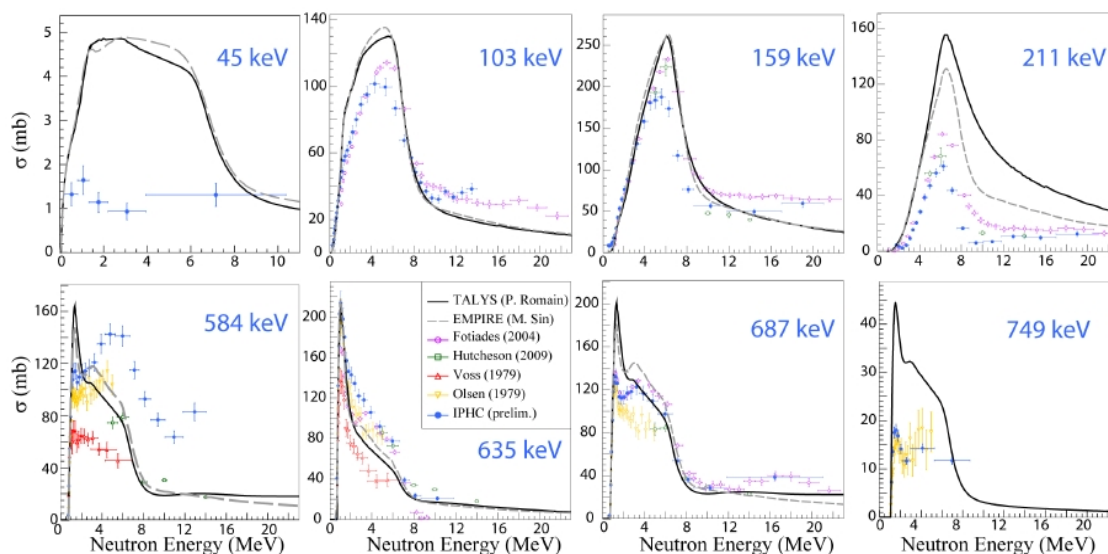
Figure 4: List of analysed gamma transitions with the ^{238}U sample

Table 1: List of treated (n,xn γ) on ^{238}U

E_{γ} (keV)	Reaction	Ei (J π)	Ef (J π)
44.915	(n,n')	44.915 (2+)	0 (0+)
103.5	(n,n')	148.38 (4+)	44.915 (2+)
104.2	(n,3n) ^{236}U	149.5 (4+)	45.2 (2+)
106.3 ^a	(n,2n) $^{237}\text{U}^a$	162.3 (9/2+)	56.3 (5/2+)
148.567	(n,2n) ^{237}U	159.962 (5/2+)	11.393 (3/2+)
155	(n,2n) ^{237}U	317.3 (13/2+)	162.3 (9/2+)
158.8	(n,n')	307.18 (6+)	148.38 (4+)
160.3	(n,3n) ^{236}U	309.8 (6+)	149.5 (4+)
211	(n,n')	518.1 (8+)	307.18 (6+)
212.46	(n,3n) ^{236}U	522.3 (8+)	309.8 (6+)
218.1	(n,n')	950.1 (2-)	731.93 (3-)
251.2	(n,n')	930.6 (1-)	680.11 (1-)
257.8	(n,n')	775.9 (10+)	518.1 (8+)
270.1	(n,n')	950.1 (2-)	680.11 (1-)
436.9	(n,n')	1168.88 (3-)	731.93 (3-)
448.1	(n,n')	1128.8 (2-)	680.11 (1-)
519.46	(n,n')	826.64 (5-)	307.18 (6+)
583.55	(n,n')	731.93 (3-)	148.38 (4+)
635.19	(n,n')	680.11 (1-)	44.915 (2+)
642.3	(n,3n) ^{236}U	687.6 (1-)	45.2 (2+)
678.3	(n,n')	826.64 (5-)	148.38 (4+)
679.96	(n,n')	680.11 (1-)	0 (0+)
686.99	(n,n')	731.93 (3-)	44.915 (2+)
749.2	(n,n')	1056.38 (4+)	307.18 (6+)
818.06	(n,n')	966.13 (2+)	148.38 (4+)
849.4	(n,n')	997.58 (3-)	148.38 (4+)
882.3	(n,n')	927.21 (0+)	44.915 (2+)
885.46	(n,n')	930.6 (1-)	44.915 (2+)
888.9	(n,n')	1037.25 (2+)	143.38 (4+)
905.5	(n,n')	950.1 (2-)	44.915 (2+)
921.19	(n,n')	966.13 (2+)	44.915 (2+)
952.65	(n,n')	997.58 (3-)	44.915 (2+)
957.3	(n,n')	1105.71 (3+)	148.38 (4+)
966.9	(n,n')	966.13 (2+)	0 (0+)
992.32	(n,n')	1037.25 (2+)	44.915 (2+)
1015	(n,n')sum	1060.27 (2+)	44.915 (2+)
		1059.66 (3+)	44.915 (2+)
		1163 (?)	148.38 (4+)
		... and 1014.5 in ^{27}Al	
1020	(n,n')sum	1167.99 (4+)	148.39 (4+)
		1168.88 (3-)	148.39 (4+)
1037.3	(n,n')	1037.25 (2+)	0 (0+)
1060.3	(n,n')sum	1060.27 (2+)	0 (0+)
		1105.71 (3+)	44.915 (2+)
1084.08	(n,n')sum	1128.84 (2-)	44.915 (2+)
		1232 (5+)	148.38 (4+)
1123	(n,n')	1168.88 (3-)	44.915 (2+)
1179.3	(n,n')	1223.78 (2+)	44.915 (2+)
1278.8	(n,n')	1278.54 (2+)	0 (0+)

^a Observed, but not referenced in NNDC website.

Figure 5: Selection of measured $^{238}\text{U}(n,n'g)$ cross-sections compared to other experimental data, TALYS and EMPIRE code predictions

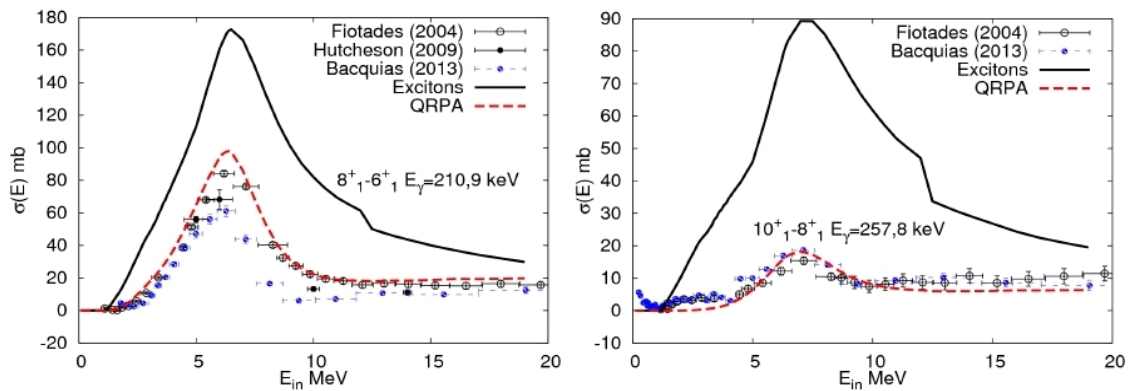


As can be seen from Figure 5, the data sets [present work and Fotiades, *et al.* (2004), Hutcheson, *et al.* (2009), Voss, *et al.* (1976) and Olsen, *et al.*, (1979)] agree rather well between themselves on most transitions, at least compared to the discrepancies that have been met with theoretical calculations performed with nuclear reaction codes [Romain with TALYS (Koning, Hilaire and Duijvestijn, 2008) and Sin (IFIN-HH, Bucharest) with EMPIRE (Herman, *et al.*, 2007)]. No general trend may be drawn from Figure 5. On some cases, models agree within a few per cent with data. This is the case for example with the 687 keV (3- to 2+) transition) beyond 3 MeV of incident neutron energy. On some transitions, the shape is better reproduced by EMPIRE (second rise of the cross-section after a first maximum, itself generally overestimated by models). The situation is problematic for the de-excitation of the first level (2+) by a gamma of 45 keV. Predictions overshoot the present data by a factor three. The experimental observation of this transition by photon detection is demanding and definitive conclusions on the results may not yet be formed. Meanwhile, the 211 keV transition between 8+ and 6+ levels of the main band, more experimentally accessible, suffers from overestimation by roughly a factor of two, depending on the code. This serves as an argument to underline the possible refinements missing in the present versions of the model calculations. The authors bear in mind that such models are constantly evolving. Recent inclusion of a QRPA model (Dupuis, *et al.*, 2012) instead of the excitons model (by default) in the TALYS code has been implemented by Dupuis (CEA Bruyères-le-Châtel). Available results on the 211 keV (8+ to 6+) as well as the 257 keV (10+ to 8+) transitions are presented in Figure 6. Although this constitutes preliminary work, the trend seems to be towards a reduction of predicted cross-sections at high spin (at least in the main band), which favours a better reproduction of available data, including the present work.

Conclusion and outlook

The analysis of ^{235}U data and their comparison with TALYS calculations revealed that a model can reproduce total fission, (n,n') and (n,2n) cross-sections to a reasonable extent (in the limit of available data), as is the case for the phenomenological approach, and yet display serious difficulties in reproducing partial cross-sections. Shapes are inherited from various mechanisms, which set at different incident neutron energies; our data may carry specific information on the processes at play in these reactions. In this view, our

Figure 6: Experimental data and TALYS predictions for two gamma transitions in ^{238}U : default excitons vs. QRPA model



large and coherent data set on ^{238}U constitutes a precious library of cases, stimulating further interaction with theoreticians. First progress may arise from (re)measurements of branching ratios, as was proposed by our collaboration in the frame of the CHANDA project. Theoretical efforts feature the description of collective effects, adopted level densities, populated spin distributions, etc.

Such discussions may profit from new data of similar richness currently under analysis, on each natural isotope of tungsten (182, 183, 184 and 186), as well as on ^{232}Th . Further measurements are planned on ^{233}U for the (n,2n) cross-section determination, of importance for radioprotection in future Th/U systems.

Acknowledgements

The authors wish to thank the team of the GELINA facility for the preparation of the neutron beam and for their strong support, and thank the team of the target laboratory for the precise characterisation of the samples.

This work was partly supported by PACEN/GEDEPEON and the European Commission within the 6th Framework Programme through I3-EFNUDAT (EURATOM contract No. 036434) and NUDAME (contract No. FP6-516487), and within the 7th Framework Programme through EUFRAT (EURATOM contract No. FP7-211499) and ANDES (EURATOM contract No. FP7-249671).

References

- Bernard, D., *et al.* (2013), “ANDES Deliverable 3.8”, *Final ANDES Meeting*, Hôtel Métropole, Brussels, Belgium.
- Brune, C.R. (2002), “Gaussian Quadrature Applied to Experimental Gamma-Ray Yields”, *Nuclear Instrumentation and Methods in Physics A*, 493, pp. 106-110.

- Dupuis, M., *et al.* (2012), “Impact of Collective Excitations on Direct Pre-equilibrium Emission: Axially-Symmetric Deformed Nuclei”, *13th Int. Conf. on Nuclear Reaction Mechanisms*, CERN-Proceedings-2012-002, p. 95.
- Fotiades, N., *et al.* (2004), “Measurements and Calculations of $^{238}\text{U}(n,\text{x}\gamma)$ Partial Gamma-Ray Cross-Sections”, *Physical Review C*, 69, p. 024601.
- Herman, M., *et al.* (2007), “EMPIRE: Nuclear Reaction Model Code System for Data Evaluation”, *Nucl. Data Sheets*, 108, pp. 2655-2715.
- Hutcheson, A.L. (2008), “Neutron-Induced Partial Gamma-Ray Cross-Section Measurements on Uranium”, Ph.D. Thesis, Duke University.
- Hutcheson, A.L., *et al.* (2009), “Cross-Sections for $^{238}\text{U}(n,n'\gamma)$ and $^{238}\text{U}(n,2n\gamma)$ Reactions at Incident Neutron Energies Between 5 and 14 MeV”, *Physical Review C*, 80, p. 014603.
- Kerveno, M., *et al.* (2013), “Measurement of $^{235}\text{U}(n,n'\gamma)$ and $^{235}\text{U}(n,2n\gamma)$ Reaction Cross-Sections”, *Physical Review C*, 87, p. 024609.
- Koning, A., S. Hilaire and M. Duijvestijn (2008), “TALYS-1.0”, *Proc. of the International Conference on Nuclear Data for Science and Technology (ND2007)*, EDP Sciences, pp. 211-214.
- OECD/NEA (Organisation for Economic Co-operation and Development/Nuclear Energy Agency) (n.d.), “NEA Nuclear Data High Priority Request List”, accessed 2 June 2014, OECD/NEA, Paris, www.oecd-nea.org/dbdata/hprl.
- Olsen, D., *et al.* (1979), “Measurement of $^{238}\text{U}(n,n'\gamma)^{238}\text{U}^*$ Cross Sections”, *Conference on Nuclear Cross Sections for Technology*, NBS Special Publ., 594, p. 677.
- Voss, F., *et al.* (1976), *Gamma-Ray Production Cross Section in Inelastic Neutron Scattering on ^{238}U* , Kernforschungszentrum Karlsruhe Reports, No. 2379.
- Younes, W., *et al.* (2000), *The $^{235}\text{U}(n,2n(\gamma))$ Yrast Partial Gamma-Ray Cross Sections: A Report on the 1998-1999 GEANIE Data and Analysis Techniques*, UCRL-ID-140313, Lawrence Livermore National Laboratory (LLNL), Livermore, CA, United States.

High-precision measurement of the $^{238}\text{U}(n,\gamma)$ cross-section at the n_TOF facility, CERN

Tobias James Wright,^a Federica Mingrone,^b Jon Billowes,^a Eric Berthoumieux,^c
Daniel Cano-Ott,^d Carlos Guerrero,^{e,f} Frank Gunsing,^c Cristian Massimi,^b
Emilio Mendoza,^d P. Schillebeeckx,^g n_TOF collaboration

^aThe University of Manchester, School of Physics and Astronomy
Manchester, United Kingdom

^bDipartimento di Fisica e Astronomia – Università di Bologna/
Istituto Nazionale di Fisica Nucleare, Bologna, Italy

^cCommissariat à l'Énergie Atomique (CEA) Saclay, Gif-sur-Yvette, France

^dCIEMAT, Nuclear Innovation Unit, Madrid, Spain

^eEuropean Organization for Nuclear Research (CERN), Meyrin, Switzerland

^fUniversidad de Sevilla, Seville, Spain

^gEuropean Commission JRC, Institute for Reference Materials and Measurements
Geel, Belgium

Abstract

A new experiment to measure the $^{238}\text{U}(n,\gamma)$ cross-section has been carried out at the CERN n_TOF facility within the ANDES project. Two complementary detection systems have been used: two low neutron sensitivity C_6D_6 detectors and the Total Absorption Calorimeter (TAC) comprising 40 BaF_2 scintillators. High quality data has been obtained up to 10 keV with the TAC and up to a higher neutron energy unresolved region with the C_6D_6 . All the steps in the measurements and the subsequent data analysis are dealt with in depth, aiming for overall 2-3% accuracy per detection system.

Introduction

New concepts for nuclear systems are being explored to improve the sustainability of nuclear energy that appears in the EU SET-Plan (EC, n.d.) as an unavoidable component in the mix for energy generation. Despite many previous measurements, challenges still exist within the present level of basic nuclear data knowledge, as shown in the case of ^{238}U . The OECD/NEA High Priority Request List and WPEC SG26 report (OECD/NEA, n.d., 2008) state the need for a reduction in the uncertainty of the $^{238}\text{U}(n,\gamma)$ cross-section to 1-2% in the neutron energy range between 22 eV and 25 keV. Measurements have been performed at both the n_TOF (Guerrero, *et al.*, 2013) facility and the GELINA (Ene, *et al.*, 2010) facility, using two contrasting detection systems to reduce any systematics from a single measurement. The measurements performed at the n_TOF facility will be presented in this contribution.

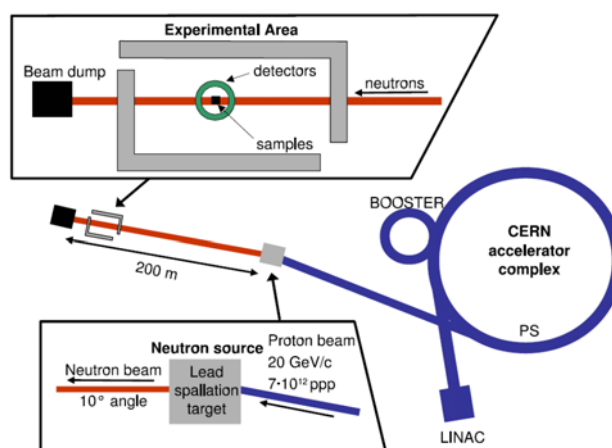
Experimental set-up

The n_TOF Facility at CERN

At the n_TOF facility (Guerrero, *et al.*, 2013) neutrons are generated in spallation reactions by a pulsed 20 GeV/c proton beam impinging on a lead block (see Figure 1), which is surrounded by 5 cm of water and borated water which serves as a coolant and as a moderator of the originally fast neutron spectrum. The resulting white neutron beam ranges from thermal energies to 1 GeV with a nearly isoethargic flux dependence up to 100 keV. The neutrons travel through an evacuated beam line to the experimental area at a distance of 185 m from the spallation target, where the sample and the detectors are placed.

Figure 1: Layout of the n_TOF facility within the CERN accelerator complex

20 GeV/c protons are sent to the n_TOF lead spallation target in bunches of 7×10^{12} protons. The experimental hall is located near the end of the 200 m long neutron beam line.



The n_TOF experimental programme includes measurements of fission cross-sections performed with parallel plate avalanche counters (PPAC) and MicroMegas (MGAS) detectors, and of capture cross-sections studied either with total energy detectors C_6D_6 or with the TAC. An overview of the n_TOF facility and the various measuring devices is given in Guerrero, *et al.* (2013). One of the main features of the experimental set-up at n_TOF is the fully digitised data acquisition system, which is described in detail in Abbondanno, *et al.* (2005).

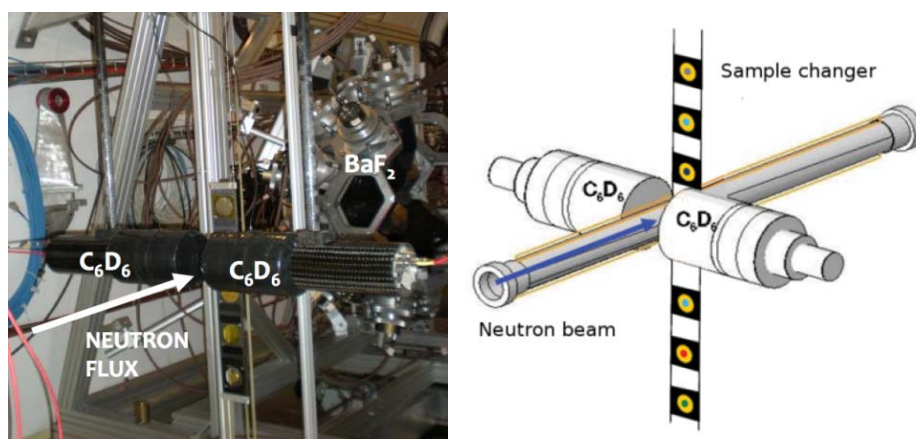
Samples

The ^{238}U sample was provided by the EC-JRC-IRMM, where an isotopic analysis was undertaken in 1984. It is an extremely pure, 6.125(2) grams approximately rectangular ($53.90 \times 30.30 \text{ mm}^2$) sample which contains <1 ppm of ^{234}U , ~ 11 ppm ^{235}U and <1 ppm ^{236}U . It is a wide sample, which with perfect alignment covers 97% of the n_TOF neutron beam. The sample was encased in ~ 60 microns of aluminium foil and ~ 75 microns of Kapton, so as to comply with CERN's radioprotection regulations. As well as measuring ^{238}U , it was necessary to perform some auxiliary measurements to accurately characterise any backgrounds that were present. For the TAC measurement, these samples were ^{197}Au , no sample or canning present and $^{\text{nat}}\text{C}$. For the C_6D_6 measurement these samples were no sample present, Al + Kapton (sample canning), $^{\text{nat}}\text{C}$ and $^{\text{nat}}\text{Pb}$. For the C_6D_6 detection set-up ^{197}Au , $^{\text{nat}}\text{Fe}$ and $^{\text{nat}}\text{Ag}$ samples were measured to validate the analysis procedure. Further details of the sample properties can be found in Schillebeeckx, *et al.* (n.d.).

C_6D_6 set-up

The measurement was carried out using two C_6D_6 liquid scintillators, placed opposite each other at 90° with respect to the beam, 9 cm upstream from the sample: one commercial BICRON and one custom made [Forschungszentrum Karlsruhe (FZK)] (Plag, *et al.*, 2003). Both the detectors and the geometry are optimised to have a very low sensitivity to scattered neutrons and a very low solid angle in order to apply the total energy detection method, which requires that the total detection efficiency for a capture event turns out to be proportional only to the total energy released in the event itself. To achieve this proportionality, only one γ -ray per cascade is detected and the pulse height weighting technique (PHWT) (Abbondanno, *et al.*, 2004) is exploited, which utilises the assumption that it is always possible to find a function of the pulse height $W(E)$ that, once convoluted with the pulse distribution from capture events, gives as a result the total radiative energy.

Figure 2: The C_6D_6 detection system in the experimental area (left) and modelled for simulations (right)

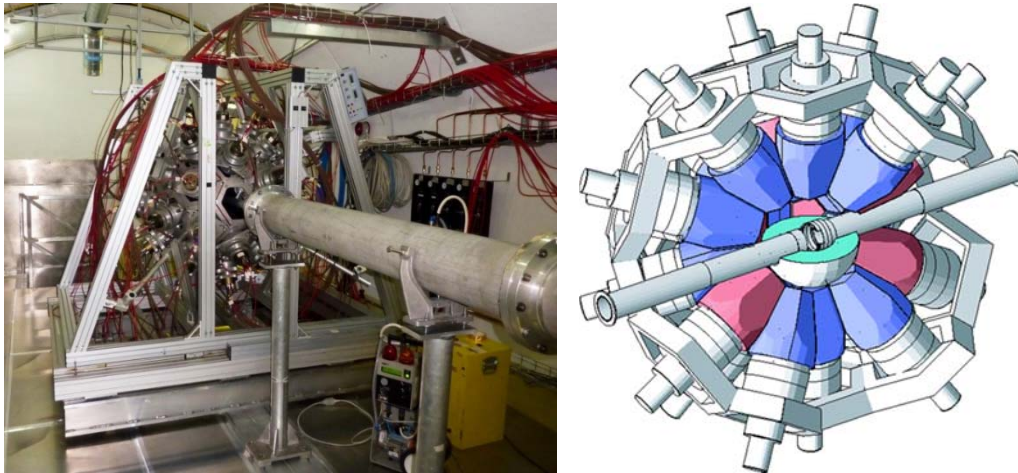


TAC set-up

The Total Absorption Calorimeter (TAC) (Guerrero, *et al.*, 2009) is a segmented 4π detector array made of 40 BaF_2 crystals specifically designed for measuring neutron capture cross-section measurements at the n_TOF facility. The large solid angle coverage and high efficiency for detecting gamma rays means the TAC can reach an almost 100% efficiency for detecting capture cascades. It has been used in many previous measurements to accurately measure capture cross-sections from small mass actinides (Massimi, *et al.*, 2010; Guerrero, *et al.*, 2012a) and recently has been shown to work in combination with a fission detector to measure fission and capture cross-sections simultaneously using a tagging technique (Guerrero, *et al.*, 2012b). The TAC features excellent time resolution (~ 0.6 ns signal rise time), reasonable energy resolution ($\sim 12\%$ at 1.8 MeV) and strong background rejection capabilities using analysis conditions in the crystal multiplicity (m_{cr}) and the deposited energy (E_{sum}).

To reduce the background induced from neutrons scattered at the sample, each crystal is surrounded by a ^{10}B loaded (16% in mass) carbon fibre capsule and a borated polyethylene neutron absorber surrounds the sample. The neutron absorber material was carefully selected to minimise the background due to scattered neutrons using Monte Carlo simulation software, Geant4 (Agostinelli, *et al.*, 2003). A detailed description of the TAC can be found in Guerrero, *et al.* (2009).

Figure 3: The TAC detection system in the experimental area (left) and modelled for simulations (right)



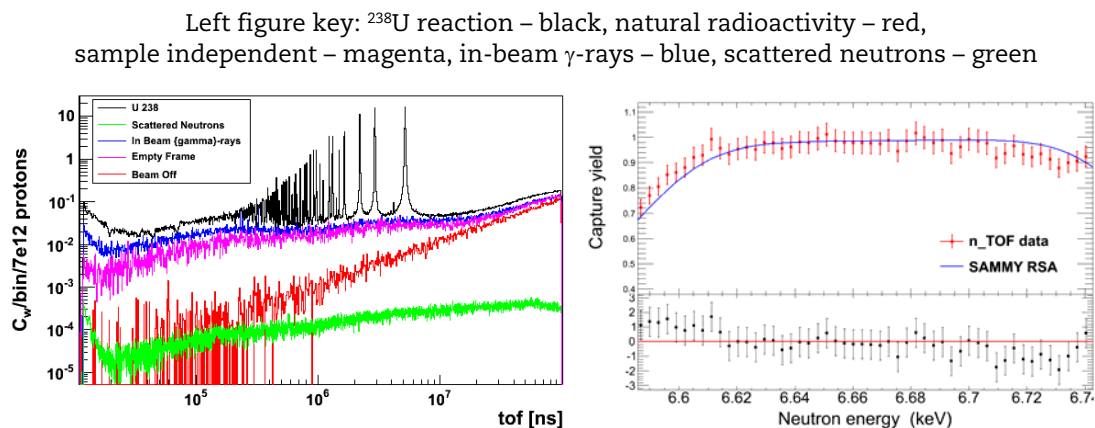
Data analysis: RAW data to capture yield

For both measurements the raw TOF spectra were converted into neutron energy by the use of well-known ^{238}U resonance energies.

C_6D_6 analysis

The required proportionality between the γ -ray efficiency and total radiative energy released in a capture event is achieved with the PHWT. To calculate the weighting functions, the precise knowledge of the detector response as a function of energy is required, which is obtained from very detailed Monte Carlos simulations using Geant4 (Agostinelli, *et al.*, 2003). The detectors were calibrated in energy by three calibration sources (^{137}Cs , ^{88}Y and Am-Be). Furthermore, the stability of the neutron flux and detector gain was monitored to ensure only wholly accurate data was taken. In Figure 4 the time of flight spectra are shown for ^{238}U and the main backgrounds. It is seen that the uranium radioactivity dominates for long flight times, i.e. at low neutron energies, while for energies above 100 keV, the main background contribution is due to in-beam γ -rays. The background related to scattered neutrons is negligible as expected for the C_6D_6 detection set-up.

Figure 4: Weighted counts for the $^{238}\text{U}(n,\gamma)$ reaction with all the main background components (left); the first saturated resonance of ^{238}U fitted with SAMMY (right)



The observable in-neutron capture cross-section measurements is the capture yield $Y_{(n,\gamma)}$ i.e. the number of capture reactions occurred per incident neutron, which is defined from measurable quantities as:

$$Y_{(n,\gamma)}(E_n) = \frac{C_W(E_n) - B_W(E_n)}{N_{BIF} \cdot \varepsilon_{n,\gamma} \cdot \varphi_n(E_n)} \quad (1)$$

where $C_W(E_n)$ and $B_W(E_n)$ are the total and background counts per pulse, weighted by the same weighting functions, N_{BIF} (beam interception factor) is the fraction of the beam intercepted by the sample, $\varepsilon_{n,\gamma}$ is the efficiency for detecting capture cascades and $\varphi_n(E_n)$ is the neutron flux per pulse. The neutron flux at n_TOF has been well characterised using different detection systems and reactions of known cross-sections, as discussed in Guerrero, *et al.* (2013). The values of N_{BIF} and $\varepsilon_{n,\gamma}$ are difficult to calculate accurately and usually dominate the overall uncertainty of capture cross-section measurements. In order to avoid this, in this particular measurement the thickness of the ²³⁸U sample has been chosen in such a way that in the first three resonances all the neutrons arriving at the sample undergo at least one interaction, thus being saturated at their peaks. Moreover, for the first resonance the neutron width is much smaller compared with the radiation width. Under this condition, $Y_{(n,\gamma)}$ becomes constant and close to one, therefore the product $N_{BIF}\varepsilon_{n,\gamma}$ is determined by comparing the measured yield with the expected one at the saturated region of the first resonance. The resonance analysis code SAMMY (Larson, 2008) has been used to calculate the expected capture yield and the fit can be seen in Figure 4. It has been shown that this saturated resonance method can be used to determine the normalisation with an uncertainty of less than 1%, as discussed in Schillebeeckx, *et al.* (2012). Further details of this analysis can be found in Mingrone, *et al.* (2014).

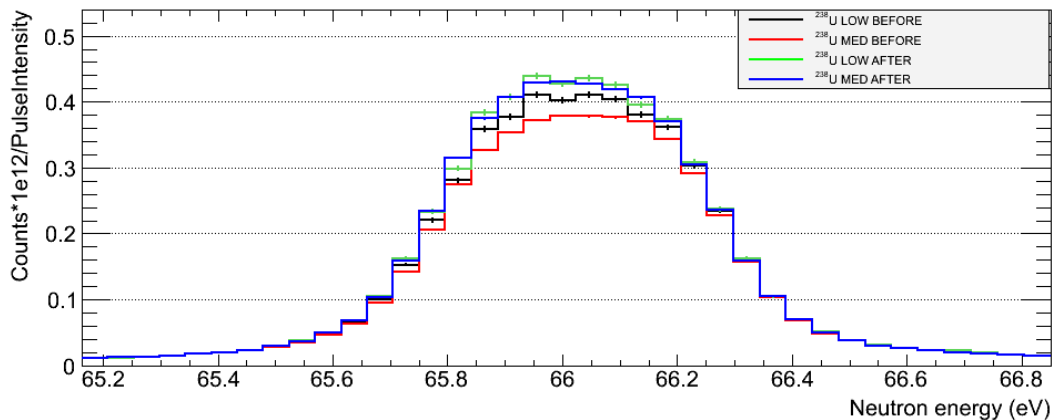
TAC analysis

The TAC was calibrated in energy with three γ -ray sources (¹³⁷Cs, ⁸⁸Y and Am-Be). Furthermore, the two simultaneous γ -rays of ⁸⁸Y were used to calibrate the 40 crystals in time, which allows a coincidence window of 20 ns to be used. One of the advantages of the TAC is that the signal to background ratio can be optimised by putting a constraint on the multiplicity and total deposited energy. For this measurement, the optimal conditions were found to be $m_{cr} \geq 2$ and $2.5 < E_{sum} < 5.75$ MeV. This specifically allows the rejection of the 478 keV and 2.2 MeV γ -rays originating from the ¹⁰B(n, α) γ and ¹H(n, γ) reactions respectively.

Similar backgrounds are present within the TAC as the C₆D₆, however some additional effects must be taken into account. Firstly, the TAC has higher neutron sensitivity, therefore the background originating from neutrons scattered by the sample must be taken into account. This background is particularly problematic, as it follows the same resonant structure as the ²³⁸U(n, γ) cross-section. This is done using the measurement of a ^{nat}C sample, which can be considered a pure neutron scatterer. In the TAC deposited energy spectra, one assumes any counts above the neutron separation energy of ²³⁸U ($S_n \sim 4.9$ MeV) are from scattered neutrons. By scaling the experimental counts in this region to that of the carbon spectra, one retrieves an estimation of the neutron scattering background. Further information can be found in (Guerrero, *et al.*, 2009).

Due to the TAC's high efficiency and the large sample size, dead time and pile-up effects influence the results. To correct for this, a novel dead time correction method has been applied (Mendoza, *et al.*, n.d.; Guerrero, *et al.*, n.d.). To validate the correction, two different beam intensities were taken (low $\sim 0.6 \cdot 10^{12}$ protons per pulse and med $\sim 1.1 \cdot 10^{12}$ protons per pulse) which subsequently gave different counting rates. As is shown in Figure 5, before the correction is applied counts are being lost due to dead time and pile-up when a higher count rate is present, however after application the two data sets agree within 1%. Furthermore, the asymmetrical shape of the 66.02 eV resonance due to

Figure 5: Illustration of the effect of dead time in the TAC data



pile-up changes after application of the correction. The capture yield is subsequently calculated following the same procedure as for the C_6D_6 . Further details of this analysis can be found in Wright, *et al.* (2014).

Results and uncertainties

The following plots show the capture yields from each detection system in different neutron energy regions.

Figure 6: Experimental capture yield Y_{exp} of a ^{238}U sample with an areal density of $9.56 \cdot 10^{-4}$ at/b resulting from measurements at n_TOF with the C_6D_6 detectors

Experimental data are compared with the corresponding theoretical yield Y_{cal} derived with SAMMY using the parameters of Derrien, *et al.* (2005).

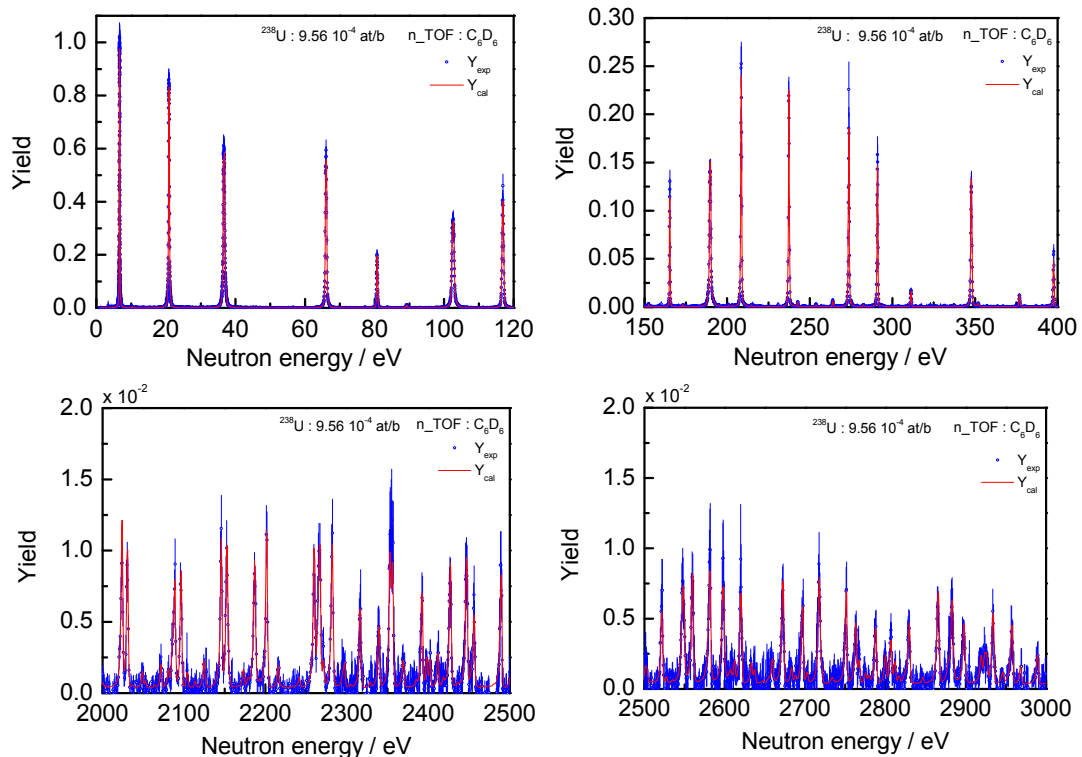
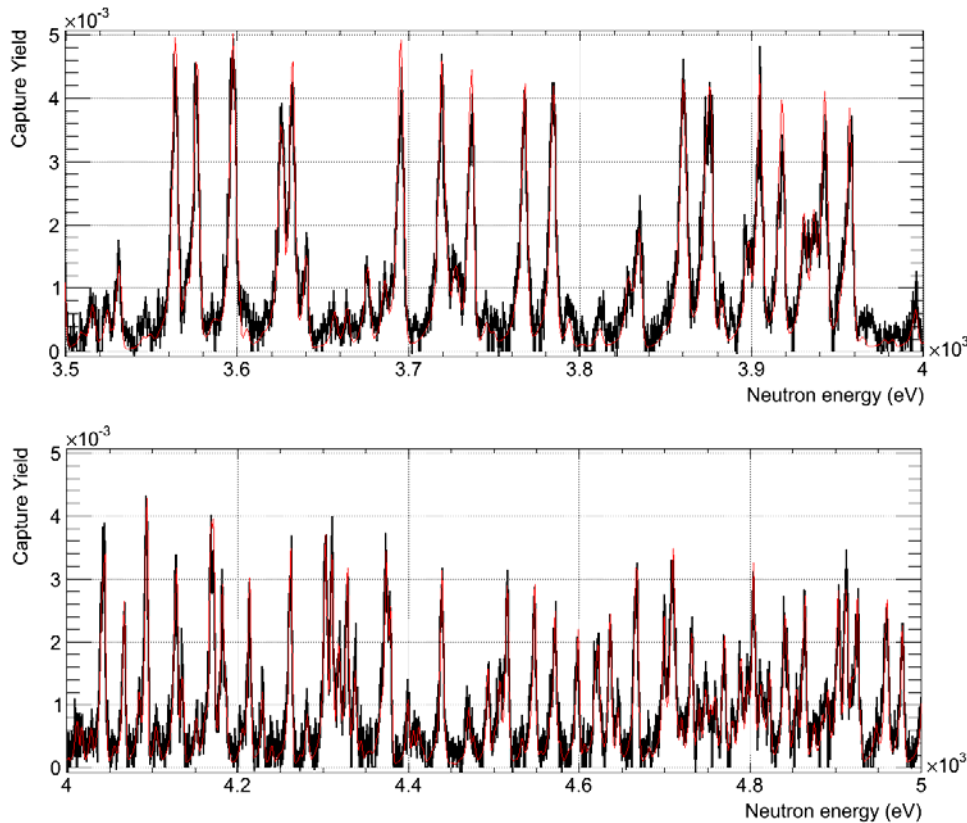


Figure 7: Experimental capture yield Y_{exp} of a ^{238}U sample with an areal density of $9.56 \cdot 10^{-4}$ at/b resulting from measurements at n_TOF with the TAC

Experimental data are compared with the corresponding theoretical yield Y_{cal} derived with SAMMY using the parameters of Derrien, *et al.* (2005)



The two data sets complement each other, as better statistics are obtained with the TAC but with an upper limit in neutron energy of 10 keV. As above this energy range, the TAC is saturated by the so-called γ -flash and the cross-section can be analysed as unresolved through the C_6D_6 detection system, allowing the statistical error to be kept to a minimum. For a detailed description of the uncertainties within the two measurements, see Schillebeeckx, *et al.* (n.d.). It is believed that by taking care of all the sources of systematic error in the best way, the final uncertainty of the yield will be of the order 2-3% for each measurement. This is on the limit of what is possible from a time-of-flight cross-section measurement facility.

Summary, conclusions and outlook

In summary, a new measurement of the $^{238}\text{U}(n,\gamma)$ cross-section has been successfully completed at the n_TOF facility, CERN. Two separate capture yields have been extracted which allow an analysis of resolved resonances up to 10 keV, and an unresolved cross-section analysis above this. All backgrounds have been dealt with utmost care, and the resulting uncertainties have been minimised and quantified. An initial comparison with the current evaluations suggest that a good agreement is seen, but there are significant differences of individual resonances therefore this new data set should prove extremely useful in any future $^{238}\text{U}(n,\gamma)$ evaluation. A detailed resonance analysis evaluation will be performed in the immediate future, where any true differences from the evaluations will be quantified.

Acknowledgements

The authors would like to acknowledge financial support from the EC FP7 ANDES project, the Nuclear Decommissioning Agency (UK) and would like to thank the JRC-IRMM for providing the high-quality sample.

References

- Abbondanno, U., *et al.* (2004), “New Experimental Validation of the Pulse Height Weighting Technique for Capture Cross-Section Measurements”, *Nucl. Instr. and Meth. A*, 521, 454.
- Abbondanno, U., *et al.* (2005), “The Data Acquisition System of the Neutron Time-of-Flight Facility n_TOF at CERN”, *Nucl. Instr. and Meth. A*, 538, 692-702.
- Agostinelli, S., *et al.* (2003), “Geant4 – A Simulation Toolkit”, *Nucl. Instrum. and Meth. A*, 506, 250-303.
- Derrien, H., *et al.* (2005), *Neutron Resonance Parameters and Calculated Cross Sections from Reich-Moore Analysis of Experimental Data in the Neutron Energy Range from 0 to 20 keV*, ORNL/TM-2005/241, Oak Ridge National Laboratory, Oak Ridge, TN, United States.
- EC (European Commission) (n.d.), “SET-Plan – European Strategic Energy Technology Plan”, EC, Brussels/Luxembourg, accessed 12 June 2014, http://ec.europa.eu/energy/technology/set_plan/set_plan_en.htm.
- Ene, D., *et al.* (2010), “Global Characterisation of the GELINA Facility for High-Resolution Neutron Time-of-Flight Measurements by Monte Carlo Simulations”, *Nucl. Instrum. Meth. A*, 618, 54-68.
- Guerrero, C., *et al.* (n.d.), “A Monte Carlo Based Pile-up and Dead-Time Correction Method for Measurements in Coincidence with Detector Arrays”, *Nucl. Instrum. and Meth. A*, in preparation.
- Guerrero, C., *et al.* (2009), “The n_TOF Total Absorption Calorimeter for Neutron Capture Measurements at CERN”, *Nucl. Instrum. and Meth. A*, 608, 424-433.
- Guerrero, C., *et al.* (2012a), “Measurement and Resonance Analysis of the ^{237}Np Neutron Capture Cross Section”, *Phys. Rev. C*, 85, 044616.
- Guerrero, C., *et al.* (2012b), “Simultaneous Measurement of Neutron-Induced Capture and Fission Reactions at CERN”, *Eur. Phys. J. A*, 48, 29.
- Guerrero, C., *et al.* (2013), “Performance of the Neutron Time-of-Flight Facility n_TOF at CERN”, *Eur. Phys. J. A*, 49, 27.
- Larson, N.M. (2008), *Updated Users Guide for SAMMY: Multilevel R-Matrix Fits to Neutron Data Using Bayes' Equations*, ORNL/TM-9179/R8 and ENDF-364/R2, Oak Ridge National Laboratory, Oak Ridge, TN, United States.
- Massimi, C., *et al.* (2010), “ $^{197}\text{Au}(n,\gamma)$ Cross Section in the Resonance Region”, *Phys. Rev. C*, 81, 044616.

- Mendoza, E., *et al.* (n.d.), “Pulse Pile-Up and Dead-Time Correction Methods Applied to the Digitised Signals of a Segmented BaF_2 Total Absorption Calorimeter Used in (n,γ) Cross Section Measurements”, *Nucl. Instrum. and Meth. A*, in preparation.
- Mingrone, F., *et al.* (2014), “Measurement of the ^{238}U Radiative Capture Cross Section with C_6D_6 at the CERN n_TOF Facility”, accepted for publication in *Nucl. Data Sheets*.
- OECD/NEA (Organisation for Economic Co-operation and Development/Nuclear Energy Agency) (n.d.), “NEA High Priority Request List”, OECD/NEA, Paris, accessed 2 June 2014, www.oecd-nea.org/dbdata/hprl/index.html.
- OECD/NEA (2008), *Uncertainty and Target Accuracy Assessment for Innovative Systems Using Recent Covariance Data Evaluations*, Working Party on International Nuclear Data Evaluation Co-operation, Subgroup 26 Report, OECD/NEA, Paris, ISBN 978-92-64-99053-1.
- Plag, R., *et al.* (2003), “An Optimized C_6D_6 Detector for Studies of Resonance-Dominated (n,γ) Cross-Sections”, *Nucl. Instr. Meth. Phys. Res. A*, 496, 425.
- Schillebeeckx, P., *et al.* (n.d.), *Final Report of the ^{238}U Total and Radiative Neutron Capture Cross Section Measurements at IRMM and n_TOF*, ANDES Deliverable 1.8 of Work Package 1, Task 1.2.
- Schillebeeckx, P., *et al.* (2012), “Determination of Resonance Parameters and Their Covariances from Neutron Induced Reaction Cross Section Data”, *Nucl. Data Sheets*, 113, 3054-3100.
- Wright, T., *et al.* (2014), “High-Precision Measurement of the $^{238}\text{U}(n,\gamma)$ Cross Section with the Total Absorption Calorimeter (TAC) at n_TOF, CERN”, accepted for publication in *Nucl. Data Sheets*, 113.

Neutron-induced reactions on U and Th – A new approach via AMS

A. Wallner,^{a,b} R. Capote,^c M. Christl,^d L.K. Fifield,^a M. Hotchkis,^e A. Krasa,^f J. Lachner,^{b,d}
J. Lippold,^g A. Plompen,^f V. Semkova,^c M. Srncik,^a P. Steier,^b S. Tims,^a S. Winkler^b

^aDepartment of Nuclear Physics, Australian National University, Canberra, Australia

^bVERA, Faculty of Physics, University of Vienna, Austria

^cNAPC Nuclear Data Section, International Atomic Energy Agency, Vienna, Austria

^dLaboratory of Ion Beam Physics, Dept. of Physics, ETH Zurich, Switzerland

^eAustralian Nuclear Science and Technology Organisation, Sydney, Australia

^fEuropean Commission, Joint Research Centre, IRMM, Geel, Belgium

^gInst. f. Umweltphysik, Ruprecht-Karls-Univ. Heidelberg, Heidelberg, Germany

Abstract

Recent studies exhibit discrepancies at keV and MeV energies between major nuclear data libraries for $^{238}\text{U}(n,\gamma)$, $^{232}\text{Th}(n,\gamma)$ and also for (n,xn) reactions. We have extended our initial (n,γ) measurements on $^{235,238}\text{U}$ to higher neutron energies and to additional reaction channels. Neutron-induced reactions on ^{232}Th and ^{238}U were measured by a combination of the activation technique and atom counting of the reaction products using accelerator mass spectrometry (AMS). Natural thorium and uranium samples were activated with quasi-monoenergetic neutrons at IRMM. Neutron capture data were produced for neutron energies between 0.5 and 5 MeV. Fast neutron-induced reactions were studied in the energy range from 17 to 22 MeV. Preliminary data indicate a fair agreement with data libraries; however at the lower band of existing data. This approach represents a complementary method to on-line particle detection techniques and also to conventional decay counting.

Introduction

Cross-sections for neutron-induced reactions are a basic nuclear property and accurate knowledge of nuclear data is crucial for many applications, in particular for nuclear technology. Advanced future reactor concepts are based on fast and epithermal energy regimes where nuclear data information is limited or discrepant, mainly because only a small number of facilities can produce appropriate neutrons for such studies. Thus, high demand exists to confirm previous measurements or to produce new nuclear data for this energy region. Here we focus on nuclear reactions leading to long-lived reaction products in the actinide mass region, in particular Th and U. Existing data for neutron-induced reactions on U and Th have been measured via detection of the prompt radiation, by the activation technique and by detection of emitted particles (Jandel, *et al.*, 2012; Guerrero, *et al.*, 2012). A major difficulty in these experiments is, however, the discrimination against the strong γ -background (e.g. from the competing fission channel) or unfavourable decay schemes. Until recently, no measurements have been performed for such reactions applying the technique of accelerator mass spectrometry (AMS) (Wallner, *et al.*, 2011, 2014; Wang, *et al.*, 2013). Indeed AMS was applied in the “early days”

of AMS in the late 1970s for a nuclear reaction study [²⁶Mg(p,n)] (Paul, *et al.*, 1980), though it took some 25 years (2005) until it became more widely used for studying some nuclear reactions of relevance to nuclear astrophysics (Nassar, *et al.*, 2005; Wallner, 2010).

Long-lived radionuclides are difficult to measure in standard activation experiments due to their low activities. This shortcoming can be overcome by using mass spectrometric techniques for measuring directly the number of produced radionuclides rather than their decay: AMS is an atom-counting technique, thus is independent of the half-life of the nuclide counted. It is usually applied in quantifying long-lived radionuclides ($T_{1/2} > \text{years}$) where decay counting is limited due to low decay rates. Such long-lived nuclides might be either the direct product of a reaction, or a decay product of a directly produced short-lived nuclide.

Figure 1: Chart of the nuclides relevant for neutron-induced reactions on Th and U

Excerpt from Karlsruhe Chart of the Nuclides (Magill, Pfennig and Galy, 2009)

Np 231 48.8 m	Np 232 14.7 m	Np 233 36.2 m	Np 234 4.4 d	Np 235 396.1 d	Np 236 223 h	Np 237 2.144 · 10 ⁶ a	Np 238 2.117 d	Np 239 2.355 d	Np 240 7.22 m
U 230 20.8 d	U 231 4.2 d	U 232 68.9 a	U 233 1.592 · 10 ⁵ a	U 234 0.0054 a	U 235 0.7204 a	U 236 230 m	U 237 6.75 d	U 238 99.2742 a	U 239 23.5 m
Pa 229 1.50 d	Pa 230 17.4 d	Pa 231 3.276 · 10 ⁴ a	Pa 232 1.31 d	Pa 233 27.0 d	Pa 234 1.47 m	Pa 235 24.2 m	Pa 236 9.1 m	Pa 237 8.7 m	Pa 238 2.3 m
Th 228 1.913 a	Th 229 7880 a	Th 230 7.54 · 10 ⁴ a	Th 231 25.5 h	Th 232 100 a	Th 233 22.3 m	Th 234 24.10 d	Th 235 7.1 m	Th 236 37.5 m	Th 237 5.0 m
Ac 227 21.773 a	Ac 228 6.13 h	Ac 229 62.7 m	Ac 230 122 s	Ac 231 7.5 m	Ac 232 119 s	Ac 233 145 s	Ac 234 44 s	146	
Ra 226 1600 a	Ra 227 42.2 m	Ra 228 5.75 a	Ra 229 4.0 m	Ra 230 93 m	Ra 231 103 s	Ra 232 4.2 m	Ra 233 30 s	Ra 234 30 s	

The main advantage of AMS (Synal, 2013; Kutschera, 2013) compared to other mass spectrometric techniques is the use of particle accelerators. This additional accelerator, coupled to two mass spectrometers (low-energy and high-energy component), completely suppresses any molecular interference and for a few cases isobaric interference is excluded as well, and hence highest sensitivities are obtained. A disadvantage is that AMS may require elaborate sample preparation and is a costly technique and, like all mass spectrometric techniques, it is sample-destructive.

One important feature is that AMS detection depends on different systematic uncertainties compared to standard techniques (Wallner, *et al.*, 2012). Neglecting radioactive decay, the isotope ratio $N_{\text{product}}/N_{\text{target}}$ generated in an activation experiment is directly related to the cross-section for a specific reaction and to the neutron fluence Φ [see Eq. (1)]. Depending on the cross-section value, isotope ratios between 10^{-10} and 10^{-15} are typically produced in such activations:

$$\sigma_{\text{exp}} = \frac{N_{\text{product}}}{N_{\text{target}}} \times \frac{1}{\Phi} \quad (1)$$

For example, assuming a cross-section of 100 mbarn and exposing a sample to a neutron fluence of $10^{13} \text{ n cm}^{-2}$ results in an isotope ratio of 10^{-12} . This combination of activation and AMS allows the production of data with typical uncertainties between 2 and 10% largely depending on the isotope of interest (Wallner, 2010).

Recent AMS studies on ^{232}Th and ^{238}U

We have extended our initial neutron capture measurements on $^{235,238}\text{U}$ (Wallner, *et al.*, 2011, 2014) to higher neutron energies and to additional reaction channels. These measurements were performed through the transnational access activities offered within the framework of the European EUFRAT programme (EC, n.d.a). Importantly, utilising different neutron-producing reactions in combination with four independent AMS facilities allowed us to study in detail potential systematic uncertainties hidden in such measurements.

Natural uranium and thorium samples were exposed to neutrons of energies between 0.5 and 21 MeV at IRMM (Semkova, *et al.*, 2009) utilising three different neutron-generating reactions. A proton or deuteron beam of a few μA intensity, accelerated by a Van de Graaff accelerator, bombarded a deuterium or tritium target: neutrons with mean energies of 0.5, 1.0 and 2.1 MeV were produced via the (T,p) reaction; and with mean energies of 2.1 and 5 MeV via the (d,d) reaction, thus data at 2.1 MeV could be deduced from two independent irradiations. Higher neutron energies between 13 and 21 MeV were available via the (d,T) reaction (see Tables 1 and 3).

The longer-lived nuclides produced in these irradiations were subsequently quantified by AMS at different laboratories: the VERA laboratory, University of Vienna (Steier, *et al.*, 2010); ETH Zurich (Christl, *et al.*, 2013); ANSTO, Sydney (Hotchkis, *et al.*, 2013); and HIAF at the ANU, Canberra (Fifield, *et al.*, 2010). Most AMS measurements are now finished and data evaluation is in progress. Some preliminary data are given below for two cases: *j*) $^{232}\text{Th}(n,2n)$ in the energy range from 17.5 to 22 MeV; *ii*) neutron capture on ^{232}Th and ^{238}U for energies between 0.5 and 5 MeV.

Table 1: Summary of recent IRMM irradiations with subsequent AMS studies in the mass range from W to U (EUFRAT programme)

Experiment	Reaction studied	Energy (MeV)	AMS facility
I	$^{204}\text{Pb}(n,3n)^{2029}\text{Pb}$	18/20.5	VERA (Wallner, <i>et al.</i> , 2013)
IIa, IIb	$^{232}\text{Th}(n,2n)^{231}\text{Th}$	17.55/18.8/20.05/22.0	VERA/ETH/ANSTO
IIa, IIb	$^{232}\text{Th}(n,4n)^{229}\text{Th}$	17.55/18.8/20.05/22.0	VERA/ETH
IIa, IIb	$^{232}\text{Th}(n,\alpha)^{229}\text{Ra} \rightarrow ^{229}\text{Th}$	17.55/18.8/20.05/22.0	VERA/ETH
IIa, IIb	$^{238}\text{U}(n,3n)^{236}\text{U}$	17.55/18.8/20.05/22.0	VERA
III	$^{232}\text{Th}(n,\gamma)^{233}\text{Th}$	0.5/1/2.1/2.1/5	ANU
III	$^{238}\text{U}(n,\gamma)^{239}\text{U}$	0.5/1/2.1/2.1/5	ANU
IV	$^{186}\text{W}(n,n\alpha)^{182}\text{Hf}$	21	ANU – in progress

$^{232}\text{Th}(n,x)$ and $^{238}\text{U}(n,x)$ – Irradiations with fast neutrons at IRMM

A particular feature of the U and Th isotopes are the low (n,2n) and (n,3n) thresholds. Even the (n,4n) reaction could be studied. For instance (n,3n) channels are open below 12 MeV neutron energy. In addition, (n, α) reactions have no reaction threshold at all. While plenty of experimental data exist for the $^{238}\text{U}(n,2n)$ reaction, above 15 MeV only a limited number of data points is available, and no data exist above 19 MeV. The $^{238}\text{U}(n,3n)$ reaction exhibits discrepancies between JEFF-3.1 (Koning, *et al.*, 2011) and ENDF/B-VII (Chadwick, *et al.*, 2011; Shibata, *et al.*, 2011), and above 15 MeV only one experiment has been performed so far. In general, knowledge for ^{232}Th is practically limited to (n,2n), and even for that reaction there are large discrepancies around 14 MeV neutron energy. Like

$^{232}\text{Th}(n,4n)$, the reaction $^{232}\text{Th}(n,\alpha)^{229}\text{Ra}$ leads to the production of the longer-lived ^{229}Th isotope. Both reactions can be measured directly via the isotope ratio $^{229}\text{Th}/^{232}\text{Th}$. Due to the expected very small cross-sections (μbarn to mbarn) in case of the (n,α) reaction, quite low isotope ratios were expected from such irradiations.

From the theoretical point of view, the dominant mechanism of $(n,2n)$ emission in actinides above 16 MeV incident neutron energies is the pre-equilibrium or direct interaction of neutrons with target nuclei. An accurate measurement of multiple neutron emission above 16 MeV thus allows for a much better understanding of the pre-equilibrium emission in heavy nuclei. Within this project we aimed to demonstrate the potential of AMS for such fast neutron-induced reactions on Th and U, which will also allow exploring the limits for other isotopes and reactions in this mass region.

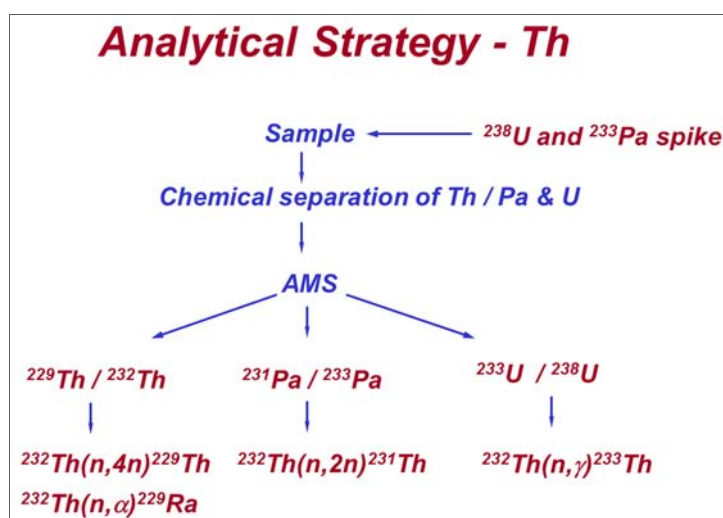
We used natural thorium and uranium samples that were found to be low in their natural content of the potential nuclear reaction products: for U the same sample material was available that was previously utilised for our initial $^{235}\text{U}(n,\gamma)$ and $^{238}\text{U}(n,\gamma)$ measurements [IRMM BC0206-1 (Verbruggen, *et al.*, 2007)], kindly provided by St. Richter from IRMM (low in ^{236}U and ^{233}U). Similarly, commercial ThO material from Merck was found suitable; i.e. the content of ^{229}Th , ^{231}Pa and ^{233}U was below the detection limit.

Owing to the high sensitivity of AMS these measurements require small sample masses of typically 30 mg. Two sample activations of 50 and 150 hours, respectively, were performed at IRMM with two pellets each of thorium-oxide and uranium-oxide. Simultaneous irradiations at two different angles relative to the incoming deuteron beam resulted in different neutron energies. Neutrons with energies of 17.55 and 20.05 MeV; and 18.8 and 22 MeV, respectively, were generated via the $\text{T}(d,n)^4\text{He}$ reaction. Taking the typical neutron flux at IRMM of $2 \times 10^7 \text{ s}^{-1}$, an irradiation time of 150 hours and e.g. a cross-section of 1 barn for the $^{238}\text{U}(n,3n)$ reaction, we calculate [Eq. (1)] a conversion ratio $^{236}\text{U}/^{238}\text{U}$ of $\sim 1 \times 10^{-11}$. Experience on the AMS performance for heavy isotopes at VERA (Steier, *et al.*, 2010, 2013), in particular for $^{235}\text{U}(n,\gamma)$ measurements (Wallner, *et al.*, 2014) has shown that isotope ratios of about 10^{-11} are required in order to obtain good quantitative results. Measurements on ^{236}U showed a background of $\approx 10^{-12}$ at the VERA facility, limited mainly by interference from the neighbouring mass ^{235}U . Based on existing experience with previous AMS measurements in that mass range, we may achieve an overall cross-section uncertainty of the order of $\sim 5\%$.

The longer-lived nuclides produced in these irradiations with fast neutrons, namely ^{229}Th , ^{231}Pa , ^{233}U and ^{236}U , were measured at VERA (3 MV AMS facility) (Steier, *et al.*, 2010), at ETH Zurich (0.6 MV) (Christl, *et al.*, 2013) and ANSTO (10 MV) (Hotchkis, *et al.*, 2013) (see Table 1). They all have dedicated actinide measurement set-ups with low interfering background. To this end, a beam switching mode was used to sequentially measure both the count rate of the radionuclide of interest (i.e. ^{229}Th or ^{236}U) and the current of the stable ions (e.g. ^{232}Th or ^{238}U).

Sample chemistry was required for the thorium and uranium samples after the neutron activations. The Th-oxide and U-oxide pellets were dissolved and the various reaction products were extracted via column chemistry. The case for ThO is shown in Figure 2; after dissolution the sample was spiked with a well-known amount of ^{233}Pa and ^{238}U . The ^{233}Pa is isolated from a parent solution of ^{237}Np , and the time between this isolation and the chemical separation of the desired isotopes is kept to a minimum to minimise any ^{233}U contribution that could arise from the addition of the ^{233}Pa spike. ^{231}Pa [decay product of ^{231}Th from $^{232}\text{Th}(n,2n)$] was separated together with the ^{233}Pa spike; similarly, ^{233}U (the decay product of ^{233}Th) was extracted together with ^{238}U . Finally, the Th fraction containing the bulk ^{232}Th as well as the reaction product ^{229}Th was available. In all cases oxide powder (Th, Pa and U) was produced, mixed with iron and silver and pressed into sample holders for the subsequent AMS measurements.

Figure 2: Sample preparation and chemical separation of the reaction products for AMS as exemplified for the case of fast-neutron induced reactions on Th



Some preliminary data are listed in Table 2. The AMS data are given in arbitrary units (a.u.); the measured quantity was $^{231}\text{Pa}/^{233}\text{Pa}$, with ^{233}Pa (27 days half-life) derived from the spike added during sample preparation. A good agreement was found between the different AMS laboratories. Our preliminary data indicate cross-sections at the lower end of the band of values suggested by nuclear data libraries.

Table 2: Preliminary data for $^{232}\text{Th}(n,2n)$ from neutron irradiations at IRMM and AMS measurements at VERA (Vienna), ETH (Zurich) and ANSTO (Sydney)

E_n (MeV)	AMS-VERA (a.u.)	AMS-ETH (a.u.)	AMS-ANSTO (a.u.)	AMS (barn)	Evaluations (barn)
17.55	1.6 ± 0.3	1.5 ± 0.2	1.65 ± 0.3	0.20	0.3-0.5
18.80	2.9 ± 0.3	3.0 ± 0.2	2.9 ± 0.3	--	0.25-0.45
20.05	29 ± 2	32 ± 1.2	24 ± 5	0.18	0.2-0.4
22.00	2.2 ± 0.2	2.0 ± 0.2	2.2 ± 0.2	--	~0.2

$^{232}\text{Th}(n,\gamma)$ and $^{238}\text{U}(n,\gamma)$: 0.5-5 MeV neutrons produced at IRMM

The low neutron capture cross-sections for MeV neutron energies make activation and direct measurements difficult and only very limited experimental data are available so far. Such lack of data is reflected in large discrepancies between major data libraries. Within the European EFNUDAT programme (2007), the capture cross-sections of ^{235}U and ^{238}U were determined for broad neutron energy distributions peaking around 30 keV and 426 keV (Ratynski and Käppeler, 1988). Within the EUFRAT scheme we have extended such measurements to higher neutron energies, with the lowest neutron energy at 500 keV, which connects directly to the previous measurements. We activated natural uranium and thorium samples at four different energies with neutrons between 0.5 and 5 MeV energy.

Activations at IRMM were conducted two times for ~5 days (three and two stacks of U/Th pellets, respectively). Again, different neutron energies were achieved with simultaneous irradiations at different angles relative to the incoming proton and deuteron beam, respectively. With neutron fluences between 0.5 and 10×10^{12} n cm⁻², we obtained isotope ratios $^{233}\text{Th}/^{232}\text{Th}$ and $^{239}\text{U}/^{238}\text{U}$ between 7×10^{-14} and 1×10^{-12} .

After the activation, the number of nuclides produced via neutron capture on ^{232}Th (^{233}Th) and ^{238}U (^{239}U) was quantified by AMS through their decay products ^{233}U and ^{239}Pu , respectively. Here we used the AMS system at the Heavy Ion Accelerator Facility (HIAF) at the Australian National University (ANU) (Fifield, *et al.*, 2010). This set-up is based on a 15 MV tandem accelerator (14 UD pelletron). In combination with a unique 6 m time-of-flight path isotopic interference is strongly suppressed in the AMS measurement. Actinide AMS was developed at the ANU and is also routinely applied in a variety of environmental applications.

After the activations the thorium-oxide and uranium-oxide samples were ground to a homogenous powder and split into two sub-samples each. A ^{238}U (^{242}Pu) (EC, n.d.b, n.d.c) spike was added to the Th (U) fractions. The material was dissolved completely and the bulk Th (U) was separated from the ^{233}U and ^{238}U (^{239}Pu and ^{242}Pu) using a UTEVA resin for column separation. The U and Pu fractions were mixed with Fe (for co-precipitation), converted to oxide powder and finally pressed into Al sample holders for the AMS measurements. $^{233}\text{U}/^{238}\text{U}$ reference materials as well as a series of blank samples were produced in the same way for comparison in the AMS measurements.

In case of ^{233}U ["decay product" of ^{233}Th from $^{232}\text{Th}(n,\gamma)$] ^{232}Th background did not pose any limiting interference because ^{233}U was separated by the chemistry prior to the AMS measurements. Similarly, the quantification of ^{239}Pu was done relative to a well-known spike of ^{242}Pu (IRMM-085), after separation from the bulk U material.

Some preliminary data are listed in Table 3. These values do not yet include all AMS measurements. Cross-sections for five neutron energies (with 2.1 MeV twice) will eventually be available from these measurements. Listed also is a value for $^{238}\text{U}(n,\gamma)$ from an independent activation utilising a different activation set-up at KIT (Ratynski and Käppeler, 1988) and the AMS set-up at VERA (Wallner, *et al.*, 2014). Our 0.52 MeV data point connects directly to that experiment. Note the values listed from the nuclear data library [e.g. ENDF (Chadwick, *et al.*, 2011)] are point values and do not take into account the broader neutron energy distributions in the experiment. The overall cross-section uncertainty is expected to be of the order of 5-10%.

Table 3: Preliminary data for $^{232}\text{Th}(n,\gamma)$ and $^{238}\text{U}(n,\gamma)$ from irradiations at IRMM and AMS measurements at the ANU

E_n (MeV)	Neutron production	Th(n, γ) (mbarn)	ENDF-Th (mbarn)	U(n, γ) (mbarn)	ENDF-U (mbarn)	AMS/ENDF – Th	AMS/ENDF – U
0.46*	$^7\text{Li}(p,n)^7\text{Be}$	–		108 ± 4	109		1.00 ± 0.03
0.52	$\text{T}(p,n)^3\text{He}$	172	153	123	110	1.12	1.12
1.0	$\text{T}(p,n)^3\text{He}$	118	136	108	128	0.87	0.85
2.1	$\text{T}(p,n)^3\text{He}$	59	68	42	43	0.86	0.97
2.1	$\text{D}(d,n)^3\text{He}$	~40	68	40	43	~0.59	0.92
5.0	$\text{D}(d,n)^3\text{He}$	~10	2.8	6	2.1	~3.5	3

* For comparison an independent result from a sample activation at KIT utilising the Van de Graaff accelerator and the $^7\text{Li}(p,n)$ reaction for neutron production is shown as well (Ratynski and Käppeler, 1988; Käppeler, *et al.*, 2011).

Summary and outlook

This method of cross-section measurements, i.e. combining sample activation with subsequent AMS measurement, has the advantage that the involved systematic uncertainties are in no way correlated with the uncertainties inherent e.g. to the TOF technique or the incomplete knowledge of the decay pattern. Limitations of this method

(if neutron fluence and energy spectra are well known) are either the background in the spectra of the particle detector or counting statistics due to the low number of nuclides in the sample.

These two cases are illustrated in Figure 3. The first case, i.e. background from interfering nuclides is the limiting quantity, is exemplified for the case of $^{235}\text{U}(n,\gamma)^{236}\text{U}$: AMS facilities with the highest sensitivity for ^{236}U detection (e.g. ANU, VERA, ETH) demonstrate a detection limit of $^{236}\text{U}/^{238}\text{U} < 3 \times 10^{-12}$. This ratio converts to $^{236}\text{U}/^{235}\text{U} \approx 4 \times 10^{-10}$ (natural uranium); assuming a neutron capture cross-section of 150 mbarn for a neutron energy of 500 keV, we calculate the required neutron fluence [Eq. (1)] being $\approx 3 \times 10^{15} \text{ n cm}^{-2}$.

Figure 3: Limitations of our method are exemplified for Case I, $^{235}\text{U}(n,\gamma)$, requiring a minimum isotope ratio and for Case II, $^{238}\text{U}(n,\gamma)$, requiring a minimum number of reaction products (e.g. ^{239}Pu), i.e. a minimum mass

Examples - limitations

(I): limitation due to background in the AMS measurement → isotope ratio

example: $^{235}\text{U}(n,\gamma)^{236}\text{U}$; $E_n = 500 \text{ keV}$, $\sigma = 150 \text{ mb}$

$$^{236}\text{U}/^{238}\text{U} = 3 \times 10^{-12} \text{ (limit in AMS)}$$

$$^{236}\text{U}/^{235}\text{U} = 4 \times 10^{-10}$$

$$\phi = 3 \times 10^{15} \text{ n cm}^{-2}$$

(II): limitation due to statistics in the AMS measurement → sample mass

example: $^{238}\text{U}(n,\gamma)^{239}\text{U} \rightarrow (0.5 \text{ h}) \rightarrow ^{239}\text{Np} \rightarrow (2.4 \text{ d}) \rightarrow ^{239}\text{Pu}$ ($t_{1/2} = 24 \text{ 000 a}$)
+ extraction of ^{239}Pu from U-bulk

$$N_{239} = 10^7 \text{ ! (required for AMS counting} \rightarrow \approx 10^3 \text{ detected)}$$

$$\sigma \times \phi = 100 \text{ mbarn} \times 10^{14} \text{ n cm}^{-2}$$

$$= 10^{-11}$$

$$m_{238} = N_{239} \times A/N_A / \sigma \phi$$

$$= 0.4 \text{ mg material required}$$

For the second case the total number of produced nuclides defines the final precision of the data. If the reaction product decays to another element (e.g. ^{239}U decays via ^{239}Np to ^{239}Pu , see Figure 1), this decay product can be separated from the bulk material (e.g. uranium). Thus interference from neighbouring isotopes in the particle detector (Case I) is strongly reduced and usually the measurement is limited by counting statistics or the reproducibility of AMS. Assuming a typical overall measurement efficiency between 10^{-3} and 10^{-4} (fraction of counted radionuclides vs. the total number of radionuclides in the sample), the number of produced radionuclides has to be of the order of 10^6 to 10^7 atoms, to generate data with an uncertainty of 3% (i.e. 1 000 particles registered in the detector). For the case of $^{238}\text{U}(n,\gamma)^{239}\text{U}$, we require 10^7 atoms of ^{239}U produced in an activation experiment. For a neutron energy of 500 keV the capture cross-section is about 100 mbarn. Using a fluence value of $1 \times 10^{14} \text{ n cm}^{-2}$ [1/30 of the above value for $^{235}\text{U}(n,\gamma)$, Case I] results in an isotope ratio $^{239}\text{U}/^{238}\text{U} = ^{239}\text{Pu}/^{238}\text{U} = 1 \times 10^{-11}$. Because we separate ^{239}Pu from the bulk uranium, ^{238}U is expected not to interfere in AMS. The total number of ^{239}Pu produced in the irradiation is proportional to the sample mass. If we require at least 10^7 ^{239}Pu nuclei generated, we can calculate a minimum number of ^{238}U atoms in the sample, i.e. a minimum mass of uranium to be activated: hence we calculate $\approx 0.4 \text{ mg}$ of ^{238}U is required. Similar calculations can be done for the other isotopes in the actinide region. Thus, for some cases this type of measurement can be performed with very small samples. In the future, new powerful neutron irradiation facilities, e.g. FRANZ (Käppeler, *et al.*, 2011; Ratzinger, *et al.*, 2010) and SARAF (Weissman, *et al.*, 2010), will provide new opportunities for such measurements, which might allow to use μg -size samples.

Acknowledgements

We acknowledge support from the European EUFRAT programme. We want to thank S. Richter from IRMM for providing valuable material with low ^{236}U content required for the $^{238}\text{U}(n,\gamma)$ measurements.

References

- Chadwick, M.B., *et al.* (2011), *Nucl. Data Sheets*, 112, 2887.
- Christl, M., *et al.* (2013), *Nucl. Instrum. Meth. B*, 294, 29.
- EC (European Commission) (n.d.a), “EUFRAT – European Facility for Nuclear Reaction and Decay Data Measurements”, webpage on EC/Joint Research Center website, EC, Brussels/Luxembourg, last updated 2 June 2014, accessed 16 June, 2014, <https://ec.europa.eu/jrc/eufrat>.
- EC (n.d.b), “IRMM-058, Uranium-233 Spike, Nitrate Solution”, information available from “Reference Materials (RM)” webpage on JRC/IRMM website, EC, Brussels/Luxembourg, last updated 30 April 2014, accessed 17 June 2014, <https://ec.europa.eu/jrc/en/reference-materials>.
- EC (n.d.c), “IRMM-085, Plutonium-242 Spike, Nitrate Solution”, information available from “Reference Materials (RM)” webpage on JRC/IRMM website, EC, Brussels/Luxembourg, last updated 30 April 2014, accessed 17 June 2014, <https://ec.europa.eu/jrc/en/reference-materials>.
- EFNUDAT (2007), “The EFNUDAT Project”, webpage on EFNUDAT website, accessed 16 June 2014, www.efnudat.eu.
- Fifield, K., *et al.* (2010), *Nucl. Instr. and Meth. B*, 268, 858.
- Guerrero, C., *et al.* (The n_TOF collaboration) (2012), *Eur. Phys. J. A*, 48, 29.
- Hotchkis, M.A.C., *et al.* (2013), *Nucl. Instr. and Meth. B*, 294, doi:10.1016/j.nimb.2012.01.019.
- Jandel, M., *et al.* (2012), *Phys. Rev. Lett.*, 109, 202506.
- Käppeler, F., *et al.* (2011), *Rev. Mod. Phys.*, 83, 157.
- Koning, A.J., *et al.* (2011), *J. of the Korean Physical Society*, 59, 1057, accessed 2 June 2014, www.oecd-nea.org/dbforms/data/eva/evatapes/jeff_31/JEFF312.
- Kutschera, W. (2013), “Applications of Accelerator Mass Spectrometry”, *100 Years of Mass Spectrometry*, K. Blaum, Y. Litvinov (eds.), *Int. J. Mass Spectrom.*, 349-350, 203-218.
- Magill, J., G. Pfennig and J. Galy (2009), *Karlsruhe Nuklidkarte*, 7th Edition 2006, revised printing November 2009.
- Nassar, H., *et al.* (2005), *Phys. Rev. Lett.*, 94, 092504.
- Paul, M., *et al.* (1980), *Phys. Lett.*, 94B, 303.
- Ratynski, W. and F. Käppeler (1988), *Phys. Rec. C*, 37, 595.

- Ratzinger, U., *et al.* (2010), *Proceedings of IPAC'10*, Kyoto, Japan, 23-28 May, MOPEC059.
- Semkova, V., *et al.* (2009), *PRC*, 80, 024610.
- Shibata, K., *et al.* (2011), *J. Nucl. Sci. Technol.*, 48, 1; and Ge, Z.G., *et al.* (2011), "The Updated Version of Chinese Evaluated Nuclear Data Library (CENDL-3.1)", *J. of the Korean Physical Society*, 59, 1052.
- Steier, P., *et al.* (2010), *Nucl. Instrum. Meth. B*, 268, 1045.
- Steier, P., *et al.* (2013), *Nucl. Instrum. Meth. B*, 294, 160.
- Synal, H-A. (2013), "Developments in Accelerator mass Spectrometry", *100 Years of Mass Spectrometry*, K. Blaum, Y. Litvinov (eds.), *Int. J. Mass Spectrom.*, 349-350, 192-202.
- Verbruggen, A., *et al.* (2007), *Preparation and Certification of IRMM-075*, Report EUR 22924 EN, Belgium.
- Wallner, A. (2010), *Nucl. Instrum. Methods B*, 268 1277.
- Wallner, A., *et al.* (2011), *J. Korean Phys. Soc.*, 59, 1410.
- Wallner, A., *et al.* (2012), *Eur. Phys. J. Web of Conf.*, 35, 01003.
- Wallner, A., *et al.* (2013), *Nucl. Instr. and Meth. B*, 294, 374.
- Wallner, A., *et al.* (2014), submitted for publication.
- Wang, X., *et al.* (2013), *Phys. Rev. C*, 87, 014612.
- Weissman, L., *et al.* (2010), *Proceedings of Linac 2010*, Tsukuba, Japan, 12-17 September, WE102.

Coupled-channels effects in optical potentials for deformed nuclei

I.J. Thompson, F.S. Dietrich, W.E. Ormand
Lawrence Livermore National Laboratory
Livermore, CA, United States

Abstract

Coupled-channels calculations for neutron scattering on actinide nuclei have recently been shown to need more excited states for convergence than was previously believed. The poor convergence shows up especially when calculating the total and the compound-nucleus production cross-sections below 1 or 2 MeV incident neutron energy. Since it is exactly the compound-nucleus production cross-sections which enter into Hauser-Feshbach models for many applications, we find that previous optical potentials of Soukhovitskii and of Dietrich (FLAP 2.2) are not sufficiently converged. We report on using a modified version of the Koning and Delaroche optical potential as a bare potential within coupled channels calculations. Changes to the surface imaginary strength and its diffuseness are sufficient to provide competitive fits to ^{232}Th and ^{238}U total, elastic and inelastic cross-sections. There remain systematic reductions in the compound-nucleus production cross-section compared with Soukhovitskii (2004), indicating that further work is needed to properly extract the compound-nucleus production cross-sections and their uncertainties.

Introduction

In many nuclear applications we want the cross-sections for the production of compound-nucleus (CN) states when neutrons are incident on rotational nuclei. This cross-section, also known as the fusion or absorption cross-section, is needed for the rotational nuclei which are particularly common in the rare earth and actinide regions, as it enters into Hauser-Feshbach models for many applications. In some hot astrophysical environments we also need the equivalent cross-sections for nuclei in initial excited states. We have recently (Dietrich, *et al.*, 2012) investigated the coupled-channels calculation of these cross-sections. The results of these investigations require us to reassess the extraction of optical potentials from fitting scattering data. Here we focus on neutrons + ^{238}U scattering, with the longer-term aim of generating a regional optical potential for actinide nuclei, all of which have large static deformations.

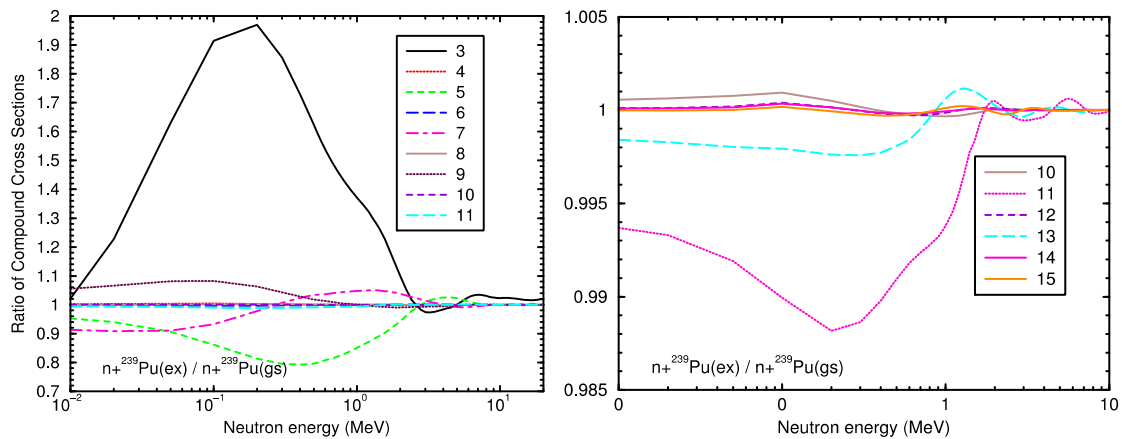
Convergence issues for rotational nuclei

Coupled-channels calculations for neutron scattering on actinide nuclei were found to need more excited states for convergence than was previously believed (Dietrich, *et al.*, 2012). The poor convergence shows up especially when calculating the total and the compound-nucleus production cross-sections below 1 or 2 MeV incident neutron energy. We first discovered this when trying to predict the CN cross-sections (σ_{CN}) for neutrons

incident on excited states in ^{239}Pu , following the earlier results in Kawano (2009). We found the ratios of excited-state to ground-state cross-sections shown in Figure 1, and were astonished by the large fluctuations of the results with increasing the number s of levels in the coupled channels sets. We define s by $s = 3$ for the ground state and two excited states, for example. Calculations with $s = 3$ (commonly used in applications!) give this ratio nearly to 2.0 (Figure 1, left), whereas converged results (Figure 1, right) differ from unity only by 0.03%.

Figure 1: Ratio of CN cross-sections for initial excited to initial ground states, with neutrons incident on ^{239}Pu

The lines are for different sizes of coupled-channels sets.
The right figure is an enlargement for 11 to 15 coupled levels.



We conclude in general that even-even nuclei (in their $K=0$ bands) require coupled-channels sets of $s = 6$ levels, whereas even-odd nuclei (with half-integer K bands) require up to 12 levels for accuracy. This is particularly critical in the fast neutron energy range between 0.1 and 1 MeV incident energy.

Validity of the adiabatic limit, and validity of the “fictitious even-even model”

The adiabatic limit is to set to zero the excitation energies E^* for all the states in a rotational band: $E^* = 0$. This is equivalent to having a large (infinite actually) moment of inertia of target, or, equivalently, that the target then does not rotate during the neutron scattering time. (Dietrich, *et al.*, 2012) proved that then the σ_{CN} is the average over all nuclear orientations of the CN production for each orientation, and that this applies for all nuclei (even or odd; any K).

Our numerical tests show that the adiabatic approximation is rather accurate, and moreover still at neutron energies much less than the typically excited inelastic energies. Figure 2 shows that deviations from adiabaticity in the total and elastic cross-sections are at most 0.4%, for both ^{238}U and ^{235}U . The exceptionally small values of these (converged!) deviations imply a good validity of spectator approximation for target spins. The compound-nucleus production is then independent of both ground-state spin I and of band-head projection K .

Furthermore, we can predict any transition $I \rightarrow I'$ from knowing all $0 \rightarrow L$ transitions. Barrett (1964) developed the partial-wave theory for adiabatic scattering on axially symmetric deformed nuclei. From his Eq. (15) we can prove that the scattering amplitude $f_{IM' \cdot IM}^K(\theta)$ for an arbitrary transition in a rotational band with band-head projection K is

simply given in terms of the scattering amplitudes $f_{IM',00}^K(\theta)$ from the (possibly fictitious) even-even nucleus with the same physical potentials and deformations:

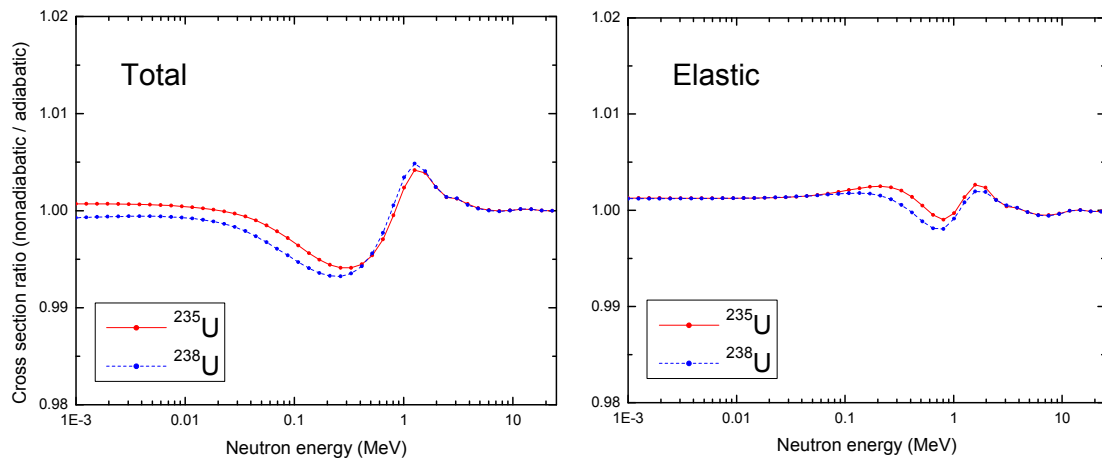
$$f_{IM',IM}^K(\theta) = \sum_L \langle IK, L0 | IK \rangle \langle IM, LM' - M | IM' \rangle f_{LM'-M,00}^0(\theta)$$

From this result we can then easily derive the relation between the cross-sections:

$$\frac{d\sigma(I \rightarrow I')}{d\Omega} = \sum_L |\langle IK, L0 | IK \rangle|^2 \frac{d\sigma(0 \rightarrow L)}{d\Omega}$$

that was given in Lagrange (1982) but without proof. Furthermore, it is now accurate to average transmission coefficients over target spins (with m -state-count weighting), as is already commonly done in applications.

Figure 2: For total (left) and CN cross-sections (right), the ratio of non-adiabatic to adiabatic scattering of neutrons on ²³⁵U (red lines) and ²³⁸U (blue lines)

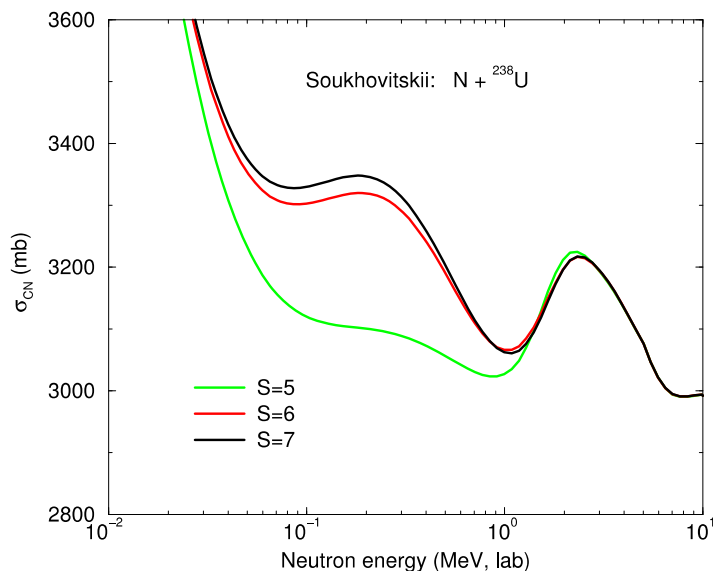


Previously used rotational models and optical potentials for neutrons

In the widely-used Hauser-Feshbach code TALYS (Koning, 2011), the default calculations are $\text{maxrot} = 2$. This input parameter is the number of levels in addition to the ground state ($s = \text{maxrot} + 1$), making $s = 3$. The FLAP 2.2 actinide potential was fitted with $s = 3$. Comparing these numbers with our convergence conclusions above indicates a clear need to re-run practical calculations, and *also* re-evaluate the fitting of the optical potentials themselves.

The Soukhovitskii, *et al.* (2004) optical potential has been a standard for actinide potentials for many purposes. They fitted their potentials using what they called “saturated coupling” of $\text{maxrot} = 4$ ($s = 5$). These $s = 5$ calculations are indeed converged for most observables: mainly σ_{TOT} , $\sigma_{\text{el}}(\theta)$, and $\sigma_{\text{inel}}(\theta)$. *However*, as we see in Figure 3, they are *not* fully converged for absorption (the CN production cross-section σ_{CN}). Recent improvements to the Soukhovitskii (2004) potential have included satisfying dispersion relations (Capote, 2008), including off-diagonal isospin terms (Quesada, 2007), and including additional side bands (Quesada, 2013), but the differences in the CN cross-sections between $s = 5$ and $s = 7$ calculations still remain (Capote, n.d.). The combination of all these facts shows the need for a general re-examination of the determination of CN cross-sections on the basis of other experimental scattering observables.

Figure 3: Compound-nucleus production cross-sections for neutrons incident on ^{238}U , using the Soukhovitskii (2004) potential with different numbers of levels included in the coupled channel set



A new optical potential fit for actinide nuclei

We have therefore sought to improve the FLAP 2.2 regional actinide optical potential from Frank Dietrich (Escher, 2010), where the potential parameters are piecewise linear functions of neutron energy. Soukhovitskii (2004) used analytic functions for his energy dependence, but these are not so easy to adjust in the various energy regions. In order to have a fitted optical potential that is suitably independent of those two potentials, after some trials we found it satisfactory to use a modified version of the Koning and Delaroche optical potential (Koning, 2003). That potential was fitted to mainly spherical nuclei of mass numbers below $A = 209$, so some changes must be expected when that global form is extrapolated up to $A = 232\text{--}242$, and also when it becomes a bare potential within a coupled-channels set.

We therefore start with a deformed Koning-Delaroche global potential, as does Nobre (2013) for rare earth targets. Our research showed that small changes to the surface imaginary strength and its diffuseness are sufficient to give competitive fits to ^{232}Th and ^{238}U total, elastic and inelastic cross-sections. The first task is to fit ^{238}U , the results for which we show in these proceedings. Further reports will examine the fits for ^{232}Th , and then other actinides. We call the result the “FLAP 3.0” parameter set.

Figures 4-7 show neutron + ^{238}U scattering; the blue line is Soukhovitskii (2004), and the green line is also Soukhovitskii (2004) but with Koning’s (2003) simplified formula for Fermi energies. We use rotational deformations $\beta_2 = 0.223$, $\beta_4 = 0.056$. The red lines are our new FLAP 3.0, using $\beta_2 = 0.213$, $\beta_4 = 0.043$ from a re-analysis of inelastic cross-sections. The two Soukhovitskii curves need to be shown, because our desire for keeping the same piecewise linear parameters for all actinides means that we need a simplified treatment of the low-energy cut-off of the imaginary potential. The absorptive part is designed to go to zero quadratically as the scattering energy approaches the Fermi energy.

Figure 4 shows the elastic angular distribution for neutrons scattered from ^{238}U at 14.2 MeV, and Figure 5 shows similar elastic distributions for a range of incident neutron energies from 4.5-10 MeV. At all energies the new FLAP 3.0 scattering distributions are as

good as those from the Soukhovitskii (2004) potential, or better. Figure 6 shows on top the total cross-sections, and below the CN production cross-sections. There is still a possible shortcoming in our FLAP 3.0 potential for scattering between 3-6 MeV, as this energy range has proved to be recalcitrant in our attempts to improve the fit to the data.

What is most interesting are systematic reductions in the lower-left plot in Figure 6 for the compound-nucleus production cross-section compared with Soukhovitskii in the energy range 0.06-2 MeV. This discrepancy arises apparently because of multiple minima in the goodness-of-fit when searching for parameters, and was found only because we use a parameter search that is essentially independent of that leading to the Soukhovitskii (2004) parameterisation. This discrepancy indicates definitively that further work is needed to properly determine the uncertainties of the extracted compound-nucleus production cross-sections, and thus to see exactly how well they are in fact constrained by presently available scattering data.

Figure 7 shows the fitting of the low-energy neutron resonance parameters: the s - and p -wave strength functions S_0 and S_1 , as well as the “potential scattering radius” R' . We can see the effects of the different treatments in the blue line and green line treatments of the Soukhovitskii cut-off of the imaginary potential at low energies. The Fermi energy in the blue symbols gives a significantly better fit to the s -wave S_0 parameter. This difference can also be seen in the lower left plot of Figure 6, with the different trends of the CN cross-section below 0.03 MeV neutron scattering energy.

Figure 4: Elastic scattering angular distributions of neutrons on ^{238}U at 14.2 MeV incident energy

The blue and green curves use the Soukhovitskii optical potential as explained in the text, and the red curve is the new FLAP 3.0 fit; the data are from Guanran (1984) and Hansen (1986)

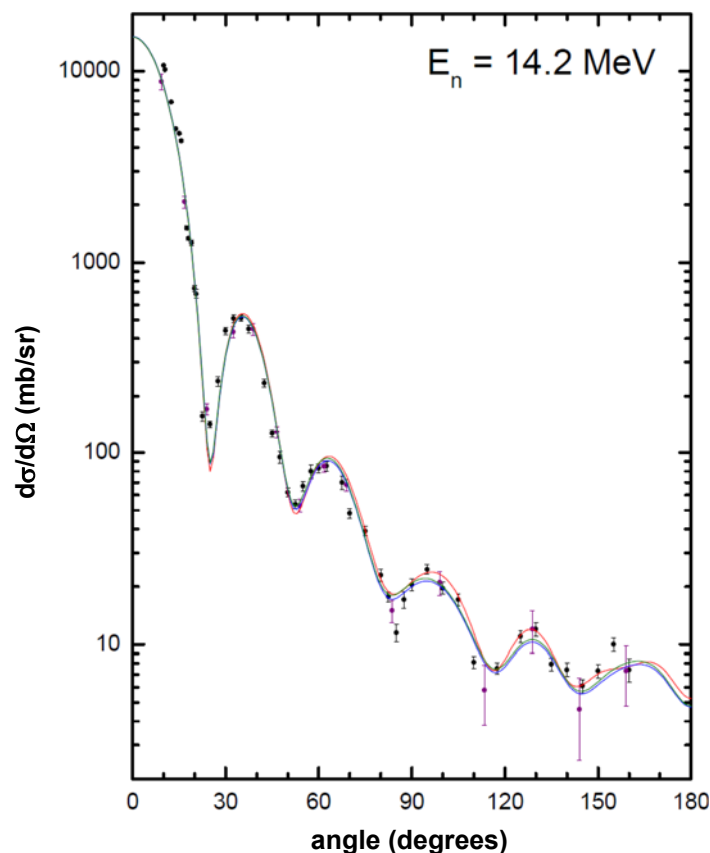


Figure 5: Elastic scattering for $n + ^{238}\text{U}$ at incident energies from 4.5-10 MeV

The lines have the same significance as in the previous figure; the data are from Smith (1996)

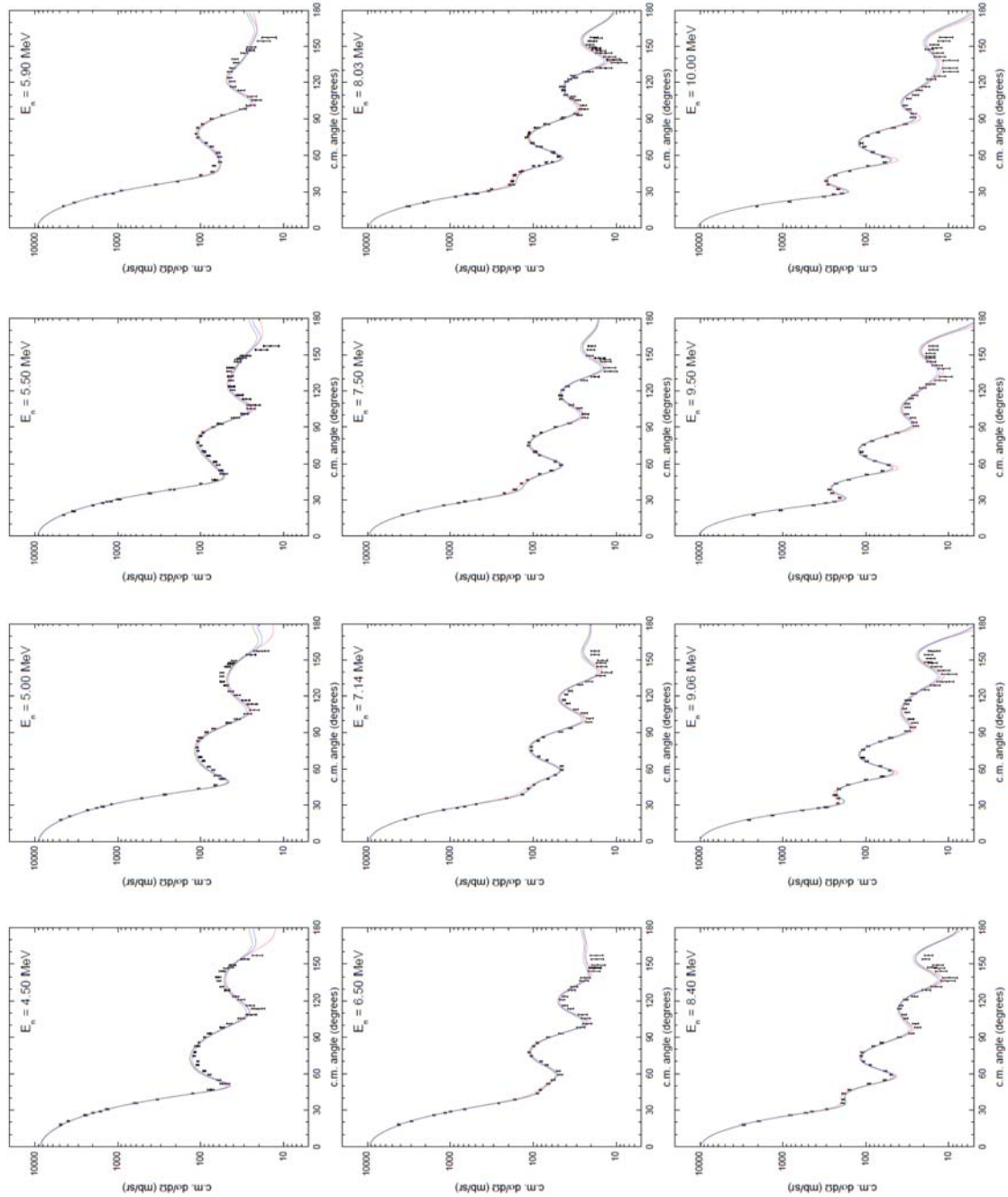


Figure 6: Total (upper) and CN production (lower) cross-sections for $n + ^{238}\text{U}$ scattering

The left plots show 0.01-10 MeV, whereas the right plots show the results for incident energies from 1-200 MeV with an expanded vertical scale; the data are from Poenitz (1981, 1983) and Abfalterer (2001)

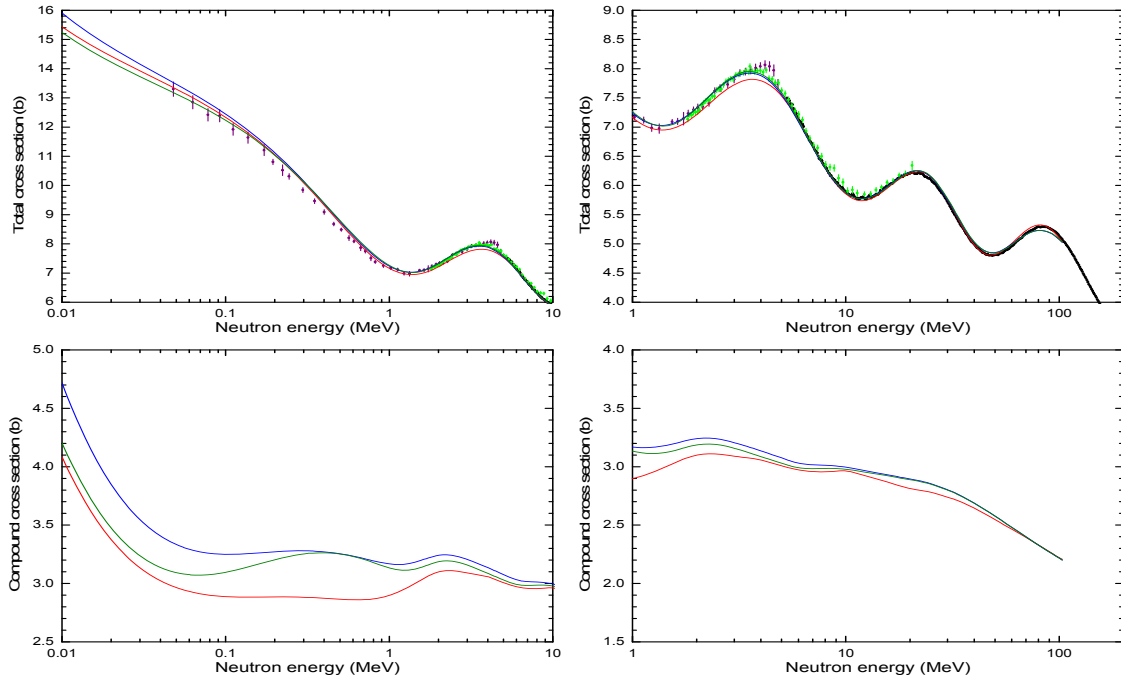
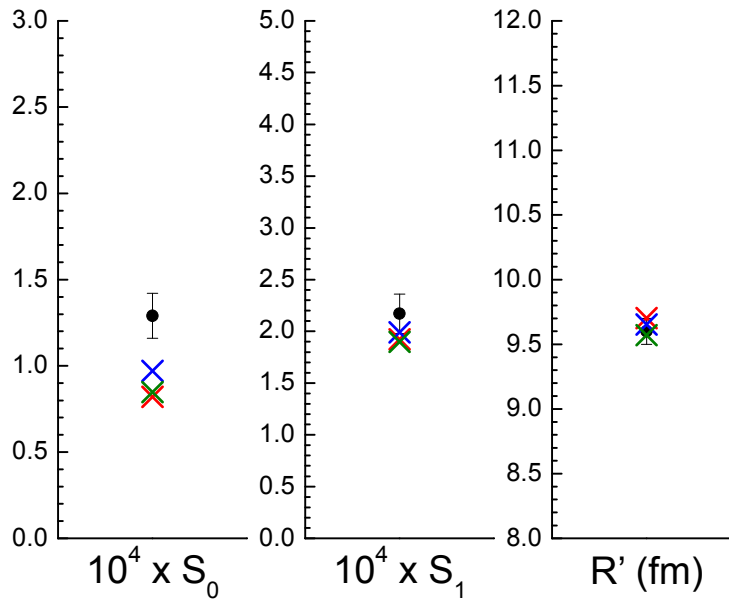


Figure 7: Neutron strength functions describing low-energy $n + ^{238}\text{U}$ scattering

S_0 and S_1 are (respectively) the s- and p-wave strength functions, and R' is the potential scattering radius; the data are from Mughabghab (2006)



Conclusions

We need to pay good attention to the convergence of inelastic scattering in rotational models. We bring to general attention the considerable uncertainties in extraction of CN production cross-sections from other observables. To help in this programme of research, we have developed and presented a new actinide potential (FLAP 3.0) that is independent of the fit of Soukhovitskii (2004). Furthermore, when using the new potentials, we may well benefit from the good physical accuracy of adiabatic model for rotational excitations, as well as from the use of the “fictitious even-even model” when faced with the onerous numerical task of calculating rotational excitation cross-sections for odd nuclei with over 12 levels constituting the coupled-channels set, as needed for converged results.

Acknowledgements

This work was done under the auspices of the United States Department of Energy by Lawrence Livermore National Laboratory under contract No. DE-AC52-07NA27344.

References

- Abfalterer, W.P., *et al.* (2001), *Phys. Rev. C*, 63, 044608 (2001).
- Barrett, R.C. (1964), *Nucl. Phys.*, 51, 27.
- Capote, R. (n.d.), private communication.
- Capote, R., *et al.* (2008), *J. Nucl. Sci. Tech.*, 45, 333.
- Dietrich, F.S., T. Kawano and I.J. Thompson (2012), *Phys. Rev. C*, 85, 044611.
- Escher, J.E. and F.S. Dietrich (2010), *Phys. Rev. C*, 81, 024612 (FLAP 2.2 in Appendix A).
- Koning, A.J. and J-P. Delaroche (2003), *Nucl. Phys. A*, 713, 231 (2003).
- Koning, A.J., S. Hilaire and M.C. Duijvestijn (2011), *TALYS 1.4*, www.talys.eu.
- Guanran, S., *et al.* (1984), *Chinese J. Nucl. Phys.*, 6, 193.
- Kawano, T., *et al.* (2009), *Phys. Rev. C*, 80, 024611.
- Hansen, L.F., *et al.* (1986), *Phys. Rev. C*, 34, 2075.
- Lagrange, Ch., O. Bersillon and D.G. Madland (1983), *Nucl. Sci. Eng.*, 83, 396.
- Mughabghab, S.F. (2006), *Atlas of Neutron Resonances*, 5th edition, Elsevier, Amsterdam.
- Nobre, G.P.A., *et al.* (2013), arXiv:1311.1735 [nucl-th].
- Poenitz, W.P., J.F. Whalen and A.B. Smith (1981), *Nucl. Sci. Eng.*, 78, 333.
- Poenitz, W.P. and J.F. Whalen (1983), ANL/NDM-80, ANL, Argonne, IL, United States.
- Quesada, J.M., *et al.* (2007), *Phys. Rev. C*, 76, 057602.
- Quesada, J.M., *et al.* (2013), *EPJ Web of Conferences*, 42, 02005.
- Smith, A.B. and S. Chiba (1996), *Ann. Nucl. Energy*, 23, 459.
- Soukhovitskii, E.S., *et al.* (2004), *J. Phys. G*, 30, 904.

Evaluation of cross-section uncertainties using physical constraints for ^{238}U , ^{239}Pu

Cyrille De Saint Jean, Edwin Privas, Pascal Archier,
Gilles Noguère, Olivier Litaize, Pierre Leconte, David Bernard
Commissariat à l'Énergie Atomique (CEA), DEN-Cadarache
Saint-Paul-lez-Durance, France

Abstract

Neutron-induced reactions between 0 eV and 20 MeV are based on various physical properties such as nuclear reaction models, microscopic and integral measurements. Most of the time, the evaluation work is done independently between the resolved resonance range and the continuum, giving rise to mismatches for the cross-sections, larger uncertainties on boundary and no cross-correlation between high-energy domain and resonance range. In addition the use of integral experiment is sometimes only related to central values (evaluation is “working fine” on a dedicated set of benchmarks) and reductions of uncertainties are not straightforward on cross-sections themselves: working fine could be mathematically reflected by a reduced uncertainty. As the CIELO initiative is to bring experts in each field to propose/discuss these matters, after having presented the status of ^{238}U and ^{239}Pu cross-sections covariances evaluation (for JEFF-3.2 as well as the WPEC SG34 subgroup), this paper will present several methodologies that may be used to avoid such effects on covariances. A first idea based on the use of experiments overlapping two energy domains appeared in the near past. It was reviewed and extended to the use of systematic uncertainties (normalisation for example) and for integral experiments as well. In addition, we propose a methodology taking into account physical constraints on an overlapping energy domain where both nuclear reaction models are used (continuity of both cross-sections and derivatives for example). The use of Lagrange multiplier (related to these constraints) in a classical generalised least square procedure will be exposed. Some academic examples will then be presented for both point-wise and multi-group cross-sections to present the methodologies. In addition, new results for ^{239}Pu will be presented on resonance range and higher energies to reduce capture and fission cross-section uncertainties by using integral experiments (JEZEBEL experiment as well as the CERES programme).

Introduction

This paper will present the status of our work on the big three covariance evaluations for JEFF-3.2 and for WPEC SG34. This work is meant to be shared within the CIELO project.

In neutron-induced reactions between 0 eV and 20 MeV, knowledge of cross-sections is based:

- for experimentalists on the finest microscopic experiments and smartest integral experiments – related issues are then systematic uncertainty;
- for theoreticians on the knowledge of nuclear reaction models (resonance parameters, optical models, fission barrier, average width...) – related issues are then use of systematics and a proper parameter uncertainty evaluation.

Thus, a general problem arises during the evaluation of cross-sections. The evaluation work may be done independently between the resolved resonance range, the unresolved resonance range and the continuum. Several inconsistencies could be detected such as mismatches at the boundaries for punctual cross-section or larger uncertainties on boundary and no cross-correlations between the high-energy domain and the resonance range. In addition, good overall integral behaviours with deviations among evaluation compensating effects were seen on major isotopes (Morillon, *et al.*, 2012). Uncertainties must reflect the lack of knowledge, inconsistencies as well as advances. One solution is to add physical constraints.

In these energy ranges, the knowledge of neutron-induced cross-section is based on microscopic and integral experiments as well as nuclear reaction models. Model parameters, necessary ingredients of nuclear reaction models, are not always predicted by theory. The key point of any parameter estimation (resonance parameters, optical models, fission barrier, average width, multi-group cross-sections...) is to add physical constraints to properly find the most physical values. These constraints are present in traditional evaluation microscopic experiments and to some extent integral experiments, in conjunction with theoretical considerations.

In this paper we will explain and generalise these physical constraints by presenting methodologies that may be used for avoiding inconsistent effects.

First, we will present a general mathematical framework related to Bayesian parameter estimations.

Covariance in CIELO

In principle, all CIELO participants could share all models, parameters, files and experiments (microscopic and integral). In previous WPEC subgroups this was not necessarily the case.

In the resolved and unresolved resonance range, various past WPEC subgroups (^{238}U , ^{239}Pu , etc.) shared among participants resonance parameters, microscopic measurements, some integral experiments (“public”) and the related experimental knowledge. Tests of advances in additional integral experiments (“restricted”) were done to ensure additional validation. Thus, covariance evaluations on the shared information could be performed and compared.

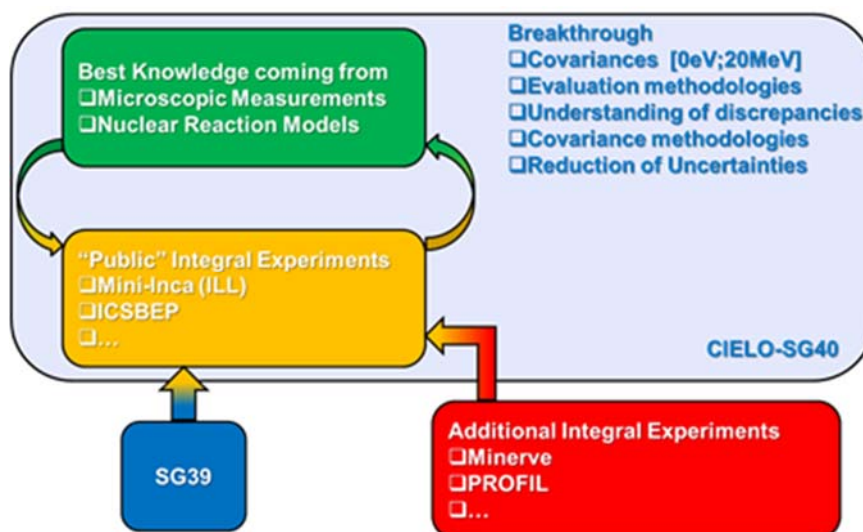
In the continuum, questions arise about nuclear reaction models (and their related parameters). It was not usual to share this information. Mainly, methodologies, microscopic and public integral experiments were shared. As for uncertainty evaluation (as well as the evaluation itself) the shared part is crucial, as one has to think of finding new ways to treat the uncertainties of models (sharing 1 000 evaluations could be a solution?) if no parameters are discussed.

Nevertheless, in both cases, CIELO should allow a step forward.

Strategy for JEFF authors in CIELO for the big three isotopes

Figure 1 illustrates the strategy proposed and chosen by authors to evaluate nuclear data covariances of the big three isotopes.

Figure 1: Authors' strategy for covariances in CIELO



The main idea is to work sequentially by first doing the covariance analysis with the best knowledge coming from microscopic experiments and models, then use the result as an *a priori* for additional data assimilation by taking into account dedicated integral experiments (ICSBEP mainly). The latter could be done in conjunction with the WPEC SG39 subgroup. Further work can be proposed on additional “restricted” experiments that cannot be shared among CIELO participants: in our case it could be oscillations experiments taking place in the Minerve reactor or irradiation experiments of small actinide samples in Phénix (PROFIL experiments).

General mathematical description

To implement physical constraints, one has to use some mathematical treatment of experiments and models: the art of the evaluation. In our case, it is based on a Bayesian approach (Bayes, 1763) which allows the treatment and data assimilation of microscopic and integral experiments in the same mathematical framework.

$$p(\bar{x}|\bar{y}, U) = \frac{p(\bar{x}|U) \cdot p(\bar{y}|\bar{x}, U)}{\int d\bar{x} \cdot p(\bar{x}|U) \cdot p(\bar{y}|\bar{x}, U)}$$

where p is the probability density function and U represents the “background” or “prior” information from which the prior knowledge of \bar{x} is assumed. U is supposed independent of \bar{y} . In this framework, the denominator is just a normalisation constant.

A data assimilation procedure can be seen as an estimation of the first two moments of the posterior density probability of a set of parameters \bar{x} knowing an *a priori* information on these parameters and a likelihood which gives the probability density function of observing a data set knowing \bar{x} . \bar{y} can be microscopic and/or integral experimental data sets.

One major problem is thus the proper uncertainty propagation of all sources of uncertainties coming from these measurements: statistical as well as systematic uncertainties arising during the data reduction process (normalisation, background reduction) introducing sometimes long-range correlations (Frohner, 1997). Furthermore, uncertainties related to the experimental conditions (isotopic concentration, effective temperature) should also be treated properly. Various additional mathematical techniques

were developed to properly take into account these kinds of problems (De Saint Jean, *et al.*, 2009; Habert, *et al.*, 2010; Noguère, *et al.*, 2008). They are based on the concept of Bayesian marginalisation which allows integrating nuisance parameter distribution into model parameters. Estimated uncertainties on cross-sections with this type of methodology exhibit high correlation as a function of energy (De Saint Jean, *et al.*, 2012).

^{239}Pu covariance matrices

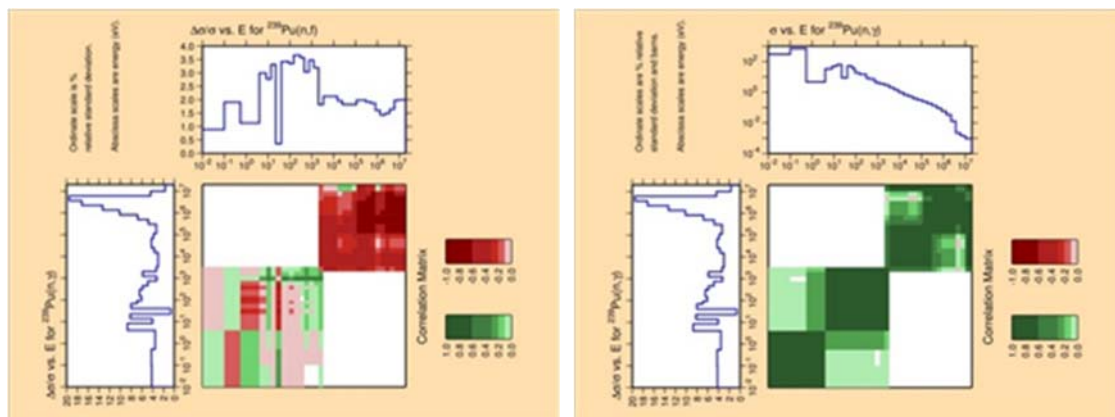
Figure 2 shows some covariance matrices for capture and fission cross-sections obtained for this isotope.

The resolved resonance range was divided in three energy ranges to account for the thermal cross-section, the first resonance around 0.3 eV and the resonance integral ($E > 0.5$ eV). Final uncertainties are dominated by normalisation accuracy introduced in the marginalisation procedure (0.5-3% for the fission cross-section and 4-9% for the capture cross-section). A neutron width selection based on the truncated Porter-Thomas integral distribution was performed to produce a “manageable” large covariance matrix. The marginalisation procedure indeed creates highly correlated cross-sections. These covariances were proposed in the framework of WPEC Subgroup 34.

In the continuum range, construction of an *a priori* based on JEFF-3.2 cross-sections was made. With this evaluation, a covariance analysis was made using systematic uncertainties on fission and capture cross-sections, based on *International Evaluation of Neutron Cross-section Standards*, a CRP report by Carlson, *et al.* Figure 2 exhibits the obtained correlations and uncertainties.

Improvements and ongoing works are scheduled by using additional microscopic experiments, as well as “public” integral nuclear data oriented experiments.

Figure 2: Fission/capture (left) and capture/capture (right) ^{239}Pu cross-sections correlations as a function of energy from 0 eV to 20 MeV



^{238}U covariance matrices

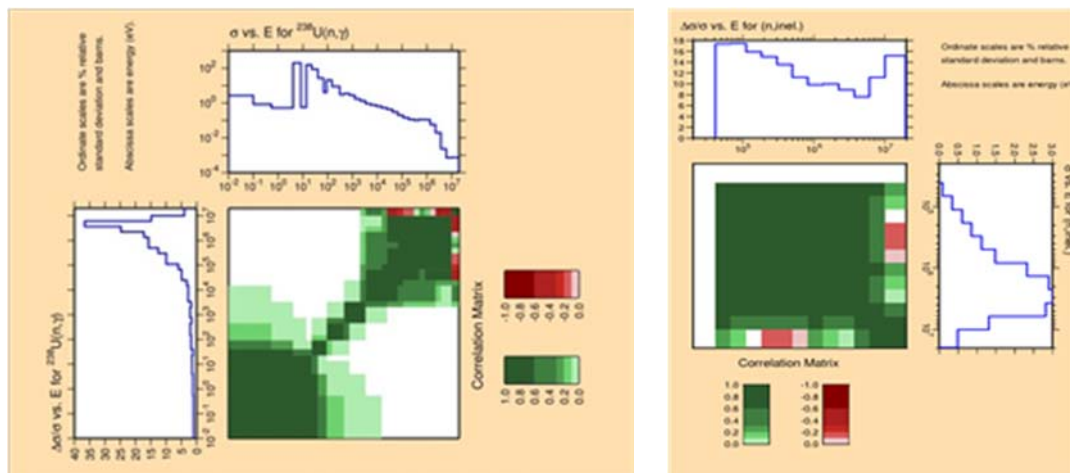
Figure 3 shows some correlations matrices and uncertainties for capture and inelastic cross-sections obtained for this isotope.

The work done so far on the resolved resonance range is based on the interpretation of microscopic experiments [mainly Harvey (1988) transmission data]. Systematic uncertainties were taken into account via a marginalisation procedure. Covariances on resonance parameters as well as cross-sections were proposed to JEFF-3.2. Improvements

for future work include adding as many as possible microscopic experiments [especially Macklin, *et al.* (1988) capture data] and looking for dedicated integral experiments. One can notice on Figure 3 that the thermal range as well as the first ^{238}U resonance are very well known (around 1%) and that the uncertainty is increasing with energy to about 2.5% at the end of the resolved range (around 3 keV).

In the continuum range, as for ^{239}Pu an *a priori* evaluation was proposed, sticking to JEFF-3.1.1. Systematic microscopic uncertainties were used. Figure 3 shows the result of this evaluation of covariances on the total inelastic ^{238}U cross-sections. It shows an uncertainty between 10-20%. This level of uncertainties was proved to be of major impact for reactors [pressurised water reactors as well as fast reactors (Archier, *et al.*, 2012)]. Future work will be focused on evaluating uncertainties for the JEFF-3.2 new high-energy range evaluation.

Figure 3: Uncertainties and correlation matrix capture cross-section (left) and for total inelastic cross-section of ^{238}U (right)



Intermediate conclusions for CIELO

First of all, one major conclusion is related to the fact that the resolved resonance range and the continuum range were evaluated separately, which is creating block diagonal matrices. The unavailability of cross-correlation between the thermal, epithermal and fast energy range should be looked for as they are of major impact on reactor applications.

Concerning ^{238}U , one can see that a major effort should be made to precisely evaluate and to reduce the inelastic cross-section uncertainties. Microscopic as well as dedicated integral experiments are necessary to reduce them. In addition, as scheduled by CIELO, improvements on the evaluation itself are foreseen.

Concerning, ^{239}Pu , mainly the capture at low- and high-energy ranges as well as the capture-to-fission ratio should be investigated to reduce uncertainties.

The ^{235}U capture cross-section was pointed out in the past in the intermediate energy range as to be especially and carefully looked for.

In addition, even though not treated in this paper, additional important nuclear data should be investigated such as angular distributions, PFNS, nu-bar and other isotopes should be properly evaluated regarding their uncertainties: O, Fe, thermal data...

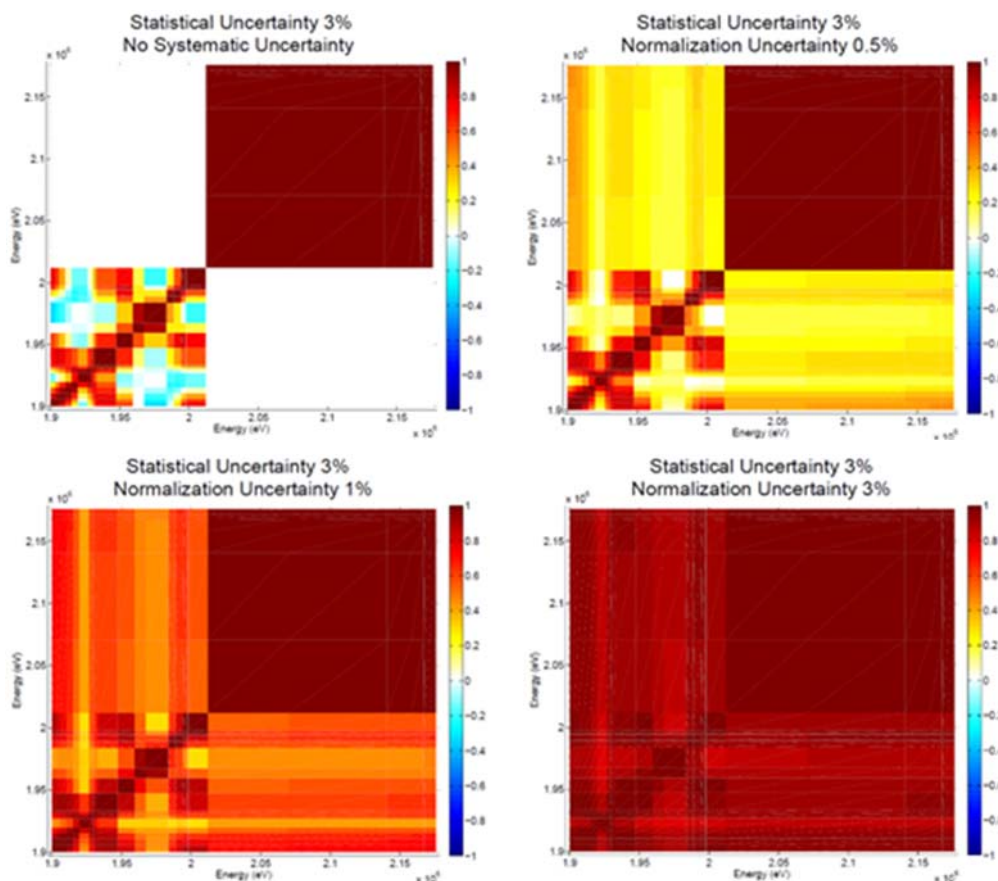
A general conclusion is that even for well-known isotopes, new microscopic/integral experiments are very much wanted with a finer estimation of systematic uncertainties

(normalisation and background issues), with measurements in the unresolved resonance range and with finer angular distribution. These advances in measurements should also be done in conjunction with advances in the theoretical models (adding microscopic ingredient to have less “free” parameters).

What additional physical constraints could be used?

Methodologies to treat systematic experimental uncertainty were given in the past to avoid unrealistic low parameters uncertainties (De Saint Jean, *et al.*, 2009; Habert, *et al.*, 2010; Noguère, *et al.*, 2008) at the end of the evaluation but with only one nuclear reaction model. In this paper we refer to the previous work of De Saint Jean, *et al.* (2014), which consists of using experiments with systematic uncertainties whose energy range can be simulated by several nuclear reaction models. In De Saint Jean, *et al.* (2014), an example on sodium inelastic cross-section is given to highlight the effect of experimental normalisation uncertainty on two models (R-matrix and optical). As can be seen in Figure 4, the effect of normalisation is to create correlations between evaluated cross-sections even with two different models as long as they are compared to the same experiment with systematic uncertainties. It is quite straightforward to understand that no cross-correlations between energy domains would appear if only statistical uncertainties are treated.

Figure 4: Impact on inelastic cross-section correlations of different normalisation uncertainties (from 0.5 to 3%)



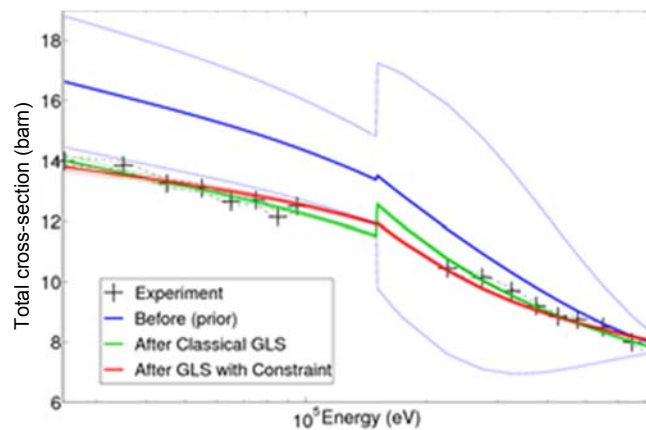
Source: De Saint Jean, *et al.* (2014).

A first true covariance evaluation was made on sodium for JEFF-3.2 taking into account systematic uncertainties on several models (Archier, *et al.*, 2014).

In De Saint Jean, *et al.* (2014), a new proposal based on the use of Lagrange multipliers to impose physical constraints on nuclear reactions models (or on cross-sections) was proposed as well as the related mathematical framework. Academic examples were treated at that time on ^{238}U .

Figure 5 shows that adding this constraint allows ensuring continuity on average cross-sections. Furthermore, cross-correlation were created between the two energy domains calculated by two different nuclear reaction models.

Figure 5: Adjustment of the total cross-section of ^{238}U with classical generalised least square and generalised least square with constraint



Source: De Saint Jean, *et al.* (2014).

Work will be done in the future to use both methodologies (systematic uncertainties and Lagrange multipliers with two models) for $^{235,238}\text{U}$ and ^{239}Pu .

A last, more usual, physical constraint used in the evaluation is to use integral experiment during the evaluation process (De Saint Jean, *et al.*, 2011).

One can see in Figures 6 and 7 that using the Jezebel integral experiment in the evaluation will reduce not only uncertainties in the fission cross-section (by a factor 2) but also will reduce *a priori* high correlations in the high-energy range. The result of this

Figure 6: ^{239}Pu cross-sections correlations: microscopic experiment only *a priori* (left) and taking into account Jezebel integral experiment (right)

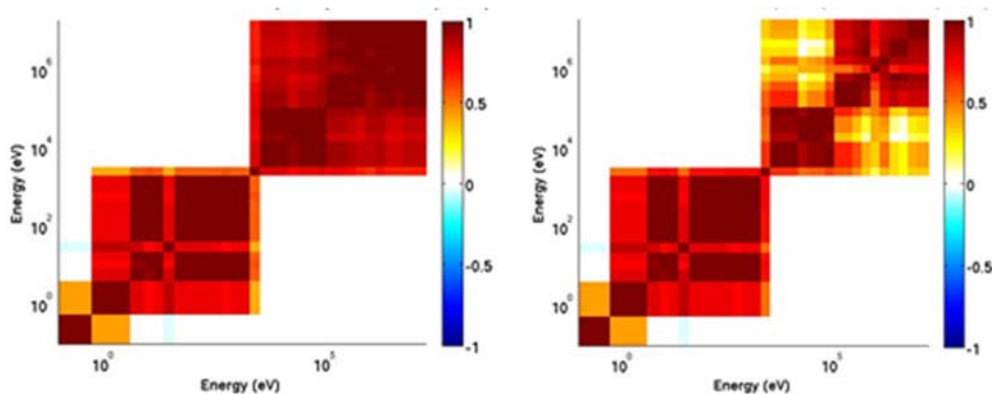
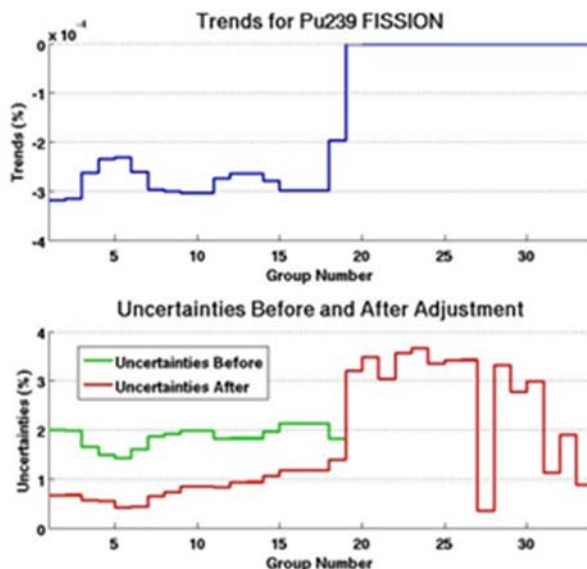


Figure 7: ^{239}Pu fission cross-section uncertainties

Green is microscopic experiment only *a priori* and red corresponds to an additional data assimilation of the Jezebel integral experiment

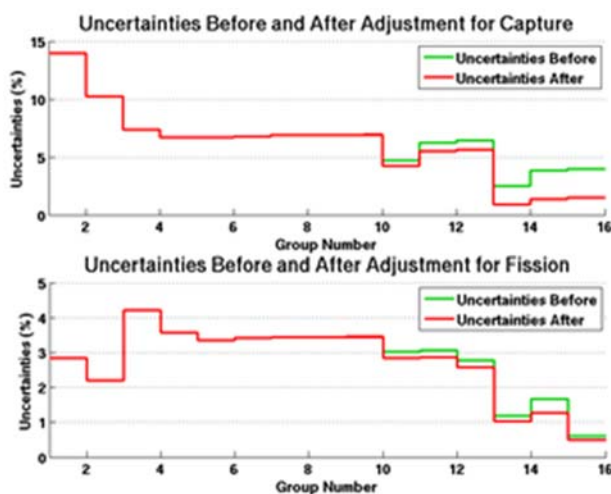


double reduction is to lower drastically integral parameters uncertainties such as k_{eff} . The use of this new matrix on a sodium fast reactor was giving a reduction of ^{239}Pu fission cross-section contribution by a factor of 2.5 on the related k_{eff} . The uncertainty reduction for SFR is less important because the SFR neutron flux is shared between the unresolved resonance range (not impacted by Jezebel) and the fast range (Jezebel range).

The same integral data assimilation was tested in the CERES programme in DIMPLe (Marshall, *et al.*, 1990) and Minerve in the thermal and epithermal range. A potential reduction of a factor 2-3 of the ^{239}Pu capture cross-section uncertainties in the thermal range was pointed out by this study, as can be seen in Figure 8. Further investigation is needed to determine firm conclusions.

Figure 8: ^{239}Pu cross-section uncertainties

Green is microscopic experiment only *a priori* and red corresponds to an additional data assimilation of the CERES integral experiments



General conclusions

Cross-section covariance evaluations were done on ^{238}U and ^{239}Pu . The matrices obtained exhibit high correlation in the studied energy range and no cross-correlation between the resonance and continuum range. Major advances could be made within the CIELO WPEC subgroup.

Additional physical constraints were proposed to take these cross-correlations into account (Lagrange multipliers + systematic uncertainties on several models) as well as trying to reduce the already evaluated covariances (integral experiments).

The first methods to create cross-correlations seem very promising but not straightforward to use: the choice of parameters to be included is very important and difficulties arise if they are not well chosen, if boundaries are not well chosen and if model defects are present. Work is ongoing to propose additional constraints by using some common nuclear reaction model parameters between nuclear reaction models such as effective radius, average width, etc.

The second proposition based on the use of integral measurements could give major uncertainty reduction as well as less correlated matrices. Nevertheless, the choice of integral experiments is crucial to disentangle nuclear data sensitivities and difficulty arises if parameters are not well chosen or forgotten (PFNS, angular distributions, etc.) and if spurious integral experiments (as for microscopic ones) with hidden errors are used. In addition, if one uses a whole series of ICSBEP measurements, it may be important to properly estimate correlations between these series of experiments. Unrealistic uncertainty reduction could appear if not.

References

- Archier, P., *et al.* (2012), “Nuclear Data Uncertainty Propagation For Neutronic Key Parameters of CEA’s SFR-V2b and CFV Sodium Fast Reactor Designs”, *PHYSOR 2012 – Advances in Reactor Physics*, Knoxville, TN, United States, 15-20 April 2012, on CD-ROM, American Nuclear Society, LaGrange Park, IL.
- Archier, P., *et al.* (2014), “New JEFF-3.2 Sodium Neutron Induced Cross-Sections Evaluation from 0 to 20 MeV”, *Nucl. Data Sheets*, 115.
- Bayes, Rev. T. (1763), “An Essay Toward Solving a Problem in the Doctrine of Chances”, *Philos. Trans. R. Soc. London*, 53, pp. 370-418.
- De Saint Jean, C., *et al.* (2009), “A Monte Carlo Approach of Nuclear Model Parameters Uncertainties Propagation”, *Nucl. Sci. Eng.*, 161, 363.
- De Saint Jean, C., *et al.* (2011), “Uncertainty Evaluation of Nuclear Reaction Model Parameters Using Integral and Microscopic Measurements with the CONRAD Code”, *Journal of the Korean Physical Society*, 59, 1276-1279.
- De Saint Jean, C., *et al.* (2012), “Estimation of Multi-Group Cross Section Covariances for $^{235,238}\text{U}$, ^{239}Pu , ^{241}Am , ^{56}Fe , ^{23}Na and ^{27}Al ”, *PHYSOR 2012 – Advances in Reactor Physics*, Knoxville, TN, United States, 15-20 April 2012, on CD-ROM, American Nuclear Society, LaGrange Park, IL.

- De Saint Jean, C., *et al.* (2014), “Estimation of Nuclear Reaction Model Parameter Covariances and the Related Neutron Induced Cross Sections with Physical Constraints”, *Nucl. Data Sheets*, 115.
- Frohner, F.H. (1997), “Assigning Uncertainties to Scientific Data”, *Nuc. Sci. Eng.*, 126, 1.
- Habert, B., *et al.* (2010), “Retroactive Generation of Covariance Matrix of Nuclear Model Parameters Using Marginalization Techniques”, *Nucl. Sci. Eng.*, 166, 276-287.
- Harvey, J.A., *et al.* (1988), “High Resolution Neutron Transmission Measurements on ^{235}U , ^{239}Pu and ^{238}U ”, *International Conference on Nuclear Data for Science and Technology*, Mito, Japan, 30 May-3 June 1988.
- Macklin, R.L., *et al.* (1988), “High Energy Resolution Measurement of the ^{238}U Neutron Capture Yield in the Energy Region Between 1 and 100 keV”, *International Conference on Nuclear Data for Science and Technology*, Mito, Japan, 30 May-3 June 1988.
- Marshall, J., *et al.* (1990), “Irradiated Fuel Measurements in DIMPLE”, *Proceedings of PHYSOR 90*, Marseille, France.
- Morillon, B., *et al.* (2012), “CEA-2012: New Uranium and Plutonium Evaluations, Benchmarking”, JEFF-DOC 1485, OECD/NEA, Paris.
- Noguère, G., *et al.* (2008), “Assessment and Propagation of the ^{237}Np Nuclear Data Uncertainties in Integral Calculations by Monte Carlo Technique”, *Nucl. Sci. Eng.*, 160, 108.

The Big Three ^{235}U , ^{238}U , ^{239}Pu – Part 3

Chair: E. Bauge

Investigation of prompt fission neutron and gamma spectra with their covariance matrices – Application to $^{239}\text{Pu}+n_{\text{th}}$, $^{238}\text{U}+n_{1.8\text{MeV}}$, $^{235}\text{U}+n_{\text{th}}$

Olivier Litaize, Léonie Berge, David Regnier, Olivier Serot,
Yannick Penelieu, Pascal Archier, Cyrille De Saint Jean
Commissariat à l'Énergie Atomique (CEA), DEN, Cadarache
Saint-Paul-lez-Durance, France

Abstract

Prompt fission neutron and gamma spectra as well as multiplicities are important for nuclear heating purpose. A recent tool, FIFRELIN, has been developed at Cadarache for simulating the de-excitation of the fission fragments (FF) in order to generate the quantities mentioned above within a single code. The input data required by the code are the pre-neutron mass and kinetic energy distributions. These distributions come from experiments. Additional models are used to sample the charge, spin and parity of the fragments. The excitation energy sharing between two complementary fragments has been detailed in previous works. When the FF characteristics are sampled (A , Z , KE , J , π) the de-excitation process can start.

The first scheme is based on Weisskopf statistical theory for neutron emission and level density plus strength functions for gamma emission. The neutron emission is performed before the gamma emission (uncoupled scheme). The second one is a Hauser-Feshbach like scheme based on neutron and gamma transmission coefficients (neutron and gamma emissions are coupled). The whole simulation allows the estimation of fission observables such as prompt fission neutron and gamma spectra as well as multiplicities but also distributions of all fission-related quantities. Various thermal, fast and spontaneous fissioning systems have been studied.

In addition, a coupling algorithm between FIFRELIN and the CONRAD nuclear data evaluation code has been initiated in order to generate covariance matrices related to prompt fission spectra.

Introduction

Prompt fission neutron and gamma spectra as well as multiplicities are important for nuclear heating purpose. A recent tool, FIFRELIN (Litaize and Serot, 2010), has been developed at Cadarache for simulating the de-excitation of the fission fragments (FF) in order to generate fission observables (such as the quantities mentioned above) within a single code. Another tool, CONRAD, is dedicated to the evaluation of nuclear data and associated covariance matrices (De Saint Jean, *et al.*, 2007). Prompt fission neutron spectrum (PFNS) models such as Maxwell, Watt (1952) or Madland-Nix (1982) have been implemented in CONRAD in order to estimate the covariance matrices. This paper is

decomposed in two parts: the first one is dedicated to the prompt fission neutron and gamma spectra calculated from a Monte Carlo simulation of the fission fragment de-excitation using FIFRELIN. The decay can be calculated within a Weisskopf (1937) or a Hauser-Feshbach (1952) approach. The second part is dedicated to the calculation of the variance-covariance matrices performed with CONRAD. A coupling scheme was initiated between the two codes but we only present here the covariance matrices obtained from the well-known analytical PFNS models mentioned above.

Prompt fission spectra

The Monte Carlo simulation of fission fragment de-excitation starts with sampling the initial characteristics of the fission fragments before neutron emission: mass A , kinetic energy KE , nuclear charge Z , spin J and parity π . Mass and kinetic energies are usually sampled from experimental data and other characteristics are sampled from models (Litaize and Serot, 2010). The excitation energy sharing between the two complementary fragments is performed through a aT^2 relation using the Ignatyuk prescription for the level density parameter (accounting for shell corrections and pairing energy) and a mass dependent temperature ratio law ($R_T(A) = T_L/T_H$) where T_L stands for the temperature of the light fragments group and T_H for the heavy fragments group. A rotating liquid drop model is used in this work to estimate the rotational part of energy coming from collective excitations. This rotational energy is subtracted from the total excitation energy before partitioning the intrinsic excitation energy on the complementary fragments.

The de-excitation can be simulated with a Weisskopf (1937) theory based model for neutrons down to a spin dependent energy limit $E_{\text{lim}}^*(J)$. Under this limit, a Dicebox approach (Becvar, 1998) is used for gamma emission using different kinds of level density models such as Constant Temperature Model (CTM), Composite Gilbert Cameron Model (CGCM) or Hartree-Fock-Bogoliubov Model (HFB) and gamma strength function models such as Standard Lorentzian (SLO), Generalized Lorentzian (GLO), Enhanced Generalized Lorentzian (EGLO) or Hartree-Fock-Bogoliubov Model (HFB). The parameters involved in these models come from the RIPL-3 nuclear data parameter library (Capote, *et al.*, 2009). A second model is based on a Hauser-Feshbach formalism (1952) allowing to take into account the spin dependence of the various nuclear levels involved in a whole neutron and gamma coupled cascade. Neutron transmission coefficients are calculated through the Talys-1.4 code (Koning, Hilaire and Duijvestijn, 2007) using different optical model parameters and the gamma transmission coefficients are calculated as in the first scheme. This last model has been recently implemented in the FIFRELIN code (Regnier, 2013) and preliminary results can be found in Regnier, Litaize and Serot (2013a, 2013b), Litaize, Regnier and Serot (2013), and Serot, Litaize and Regnier (2013). The major gain of this algorithm is to take into account the competition between neutron and gamma emission with a better accuracy than with a Weisskopf model.

Finally, there are five parameters that can be considered as free inside the code: the minimum and maximum temperature ratio: R_T^{min} and R_T^{max} , the fraction of rigid spheroid moment of inertia k_{rig} involved in the calculation of the rotational energy and the average spin cut-off parameters for light and heavy fragments $\langle\sigma_L\rangle$ and $\langle\sigma_H\rangle$ used in the initial fission fragment spin distribution.

These parameters are chosen to reproduce some selected total average fission observables (“target” fission observables). Most of the time, these targets are the total average prompt neutron multiplicity for light and heavy fragments $\langle\nu_L\rangle$ and $\langle\nu_H\rangle$. When a good agreement with experimental results is achieved for these total average target observables, the set of selected parameters is used to study all the other fission observables (distributions, correlations, neutron and gamma spectra, multiplicities as a function of mass, kinetic energy, charge and so on). The preliminary results for the thermal fission of ^{235}U , the fast fission of ^{238}U and the thermal fission of ^{239}Pu are presented hereafter.

Figure 1 shows a recent calculation of the prompt fission neutron spectrum (PFNS) of thermal neutron-induced fission of ^{235}U (Regnier, 2013). The ratio to a Maxwellian is compared with experimental data from Starostov, Semenov and Nefedov (1981), Starostov, Nefedov and Boytzov (1983), Lajtai, *et al.* (1985), Yufeng (1989), and Hamsch and Kornilov (n.d.). The impact of the level density model and optical model potentials was reported in Regnier, Litaize and Serot (2013b). The selected models for the level density is the Composite Gilbert Cameron Model (CGCM) (1965) and a Koning-Delaroche (KD) (2003) parameterisation is used for the optical model potential for neutron transmission coefficients. The selected model for E1 gamma strength function is the Enhanced Generalized Lorentzian model (EGLO). The calculated spectrum is harder than measured spectra. There is room for improvement, in the optical model potential parameters for instance.

Figure 1: Ratio to a Maxwellian ($T = 1.35$ MeV) of the $^{235}\text{U}+n_{\text{th}}$ PFNS

Comparison between different experimental data (Starostov, Semenov and Nefedov, 1981; Starostov, Nefedov and Boytzov, 1983; Lajtai, *et al.*, 1985; Yufeng, 1989; Hamsch and Kornilov, n.d.) and the FIFRELIN calculation (Regnier, 2013)

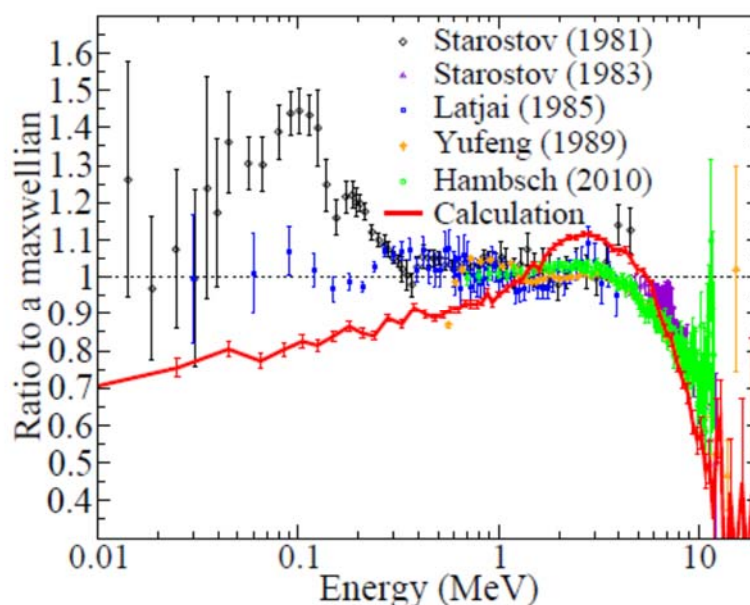


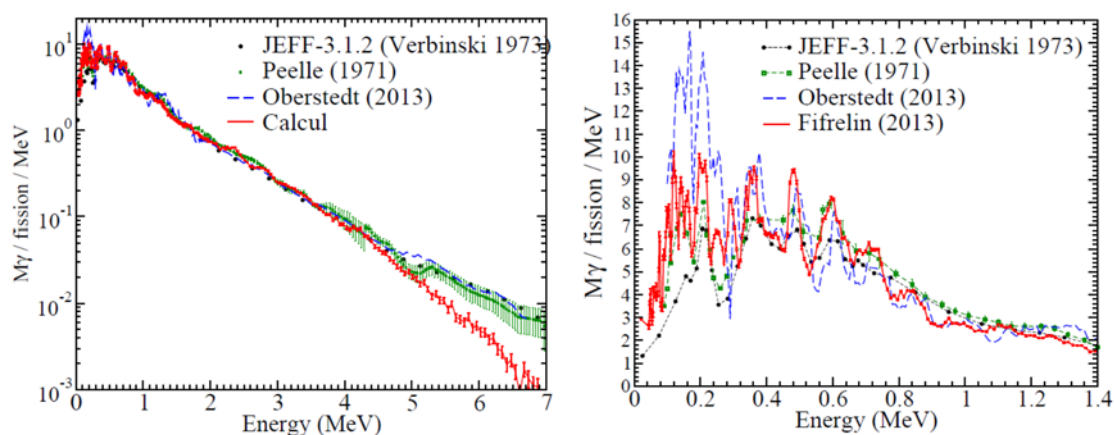
Figure 2 shows a recent calculation of the prompt fission gamma spectrum (PFGS) of thermal neutron-induced fission of ^{235}U (Regnier, 2013). The result is compared with experimental data from Peelle and Maienschein (1971) and Oberstedt, *et al.* (2013) and with the JEFF-3.1.2 nuclear data evaluation file. The impact of the level density and gamma strength function models was reported in (Regnier, Litaize and Serot, 2013b). Because the nuclear level scheme is a composite scheme based on experimental data from the RIPL3 database and reconstructed levels and transition probabilities from models, the structures observed at low energies can be reproduced with a good agreement, except below 300 keV, especially in the ^{235}U case.

Figure 3 shows a calculation of the PFNS of fast neutron-induced fission of ^{238}U at 1.8 MeV (Litaize, *et al.*, 2013). The result obtained with FIFRELIN using the Weisskopf and Hauser-Feshbach approaches is compared with evaluated nuclear data files. Different values of the five model parameters mentioned in the previous section were tested and the trend is always the same: the Weisskopf approach leads to a softer spectrum compared to a Hauser-Feshbach approach.

Figure 2: Prompt fission gamma spectrum for $^{235}\text{U}+n_{\text{th}}$

Comparison between Peelle data (1971), Oberstedt data (2013) and FIFRELIN calculation (Regnier, 2013)

Left: whole energy range. Right: low-energy range highlighting the capability of the code to reproduce the structures except below 300 keV (in the particular case of ^{235}U) if compared with the data of Oberstedt, *et al.*

**Figure 3: PFNS for $^{238}\text{U}+n_{1.8\text{MeV}}$**

Spectra calculated within a Weisskopf approach are systematically softer than those calculated with a Hauser-Feshbach approach. The result from nuclear data evaluation files is lying in between.

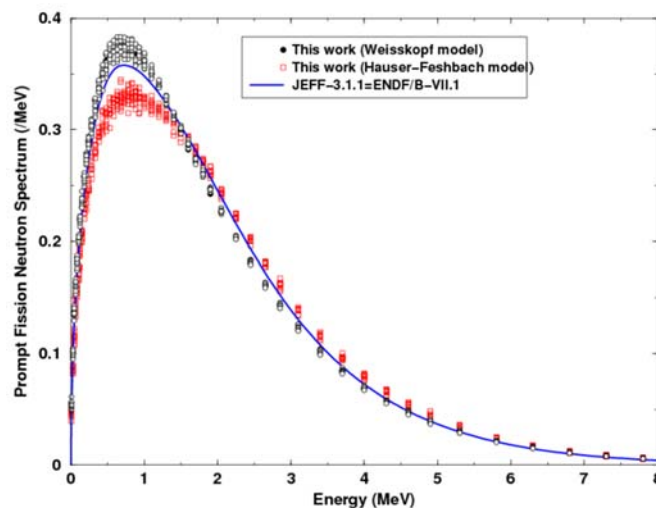


Figure 4 shows a recent calculation of the PFNS of thermal neutron-induced fission of ^{239}Pu (Regnier, 2013). The ratio to a Maxwellian is compared with experimental data from Starostov, Semenov and Nefedov (1981), Starostov, Nefedov and Boytzov (1983), Lajtai, *et al.* (1985), and Nefedov, Starostov and Boytzov (1983). The impact of the level density model and optical model potentials was reported in Regnier (2013).

Figure 5 shows a recent calculation of the PFGS of thermal neutron-induced fission of ^{239}Pu (Regnier, 2013). The result is compared with experimental data from Verbinski, *et al.* (Verbinski, Weber and Sund, 1973). The impact of the level density and gamma strength

Figure 4: Ratio to a Maxwellian ($T = 1.38$ MeV) of the prompt fission neutron spectrum for $^{239}\text{Pu}+n_{\text{th}}$

Comparison between different experimental data (Starostov, Semenov and Nefedov, 1981; Starostov, Nefedov and Boytzov, 1983; Lajtai, *et al.*, 1985; Nefedov, Starostov and Boytzov, 1983) and the FIFRELIN calculation (Regnier, 2013)

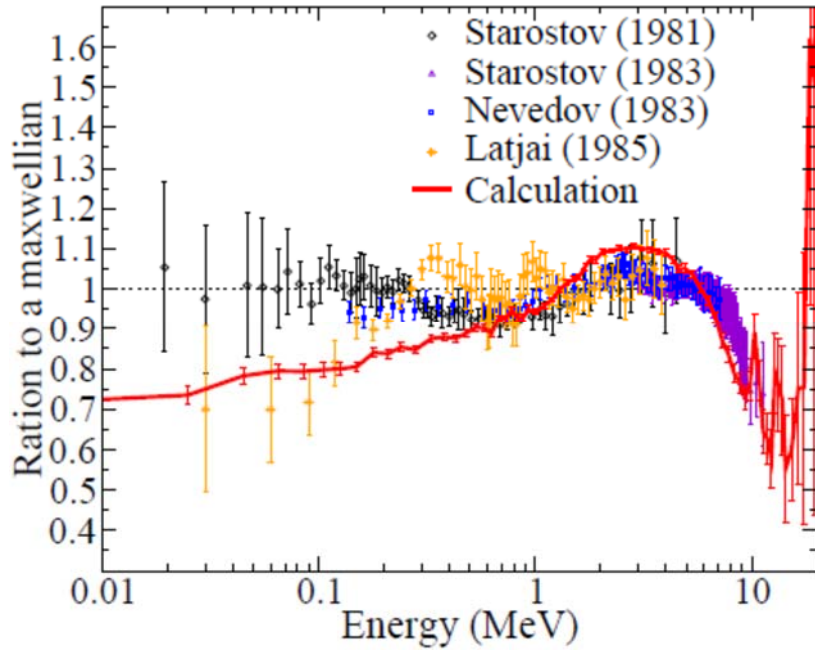
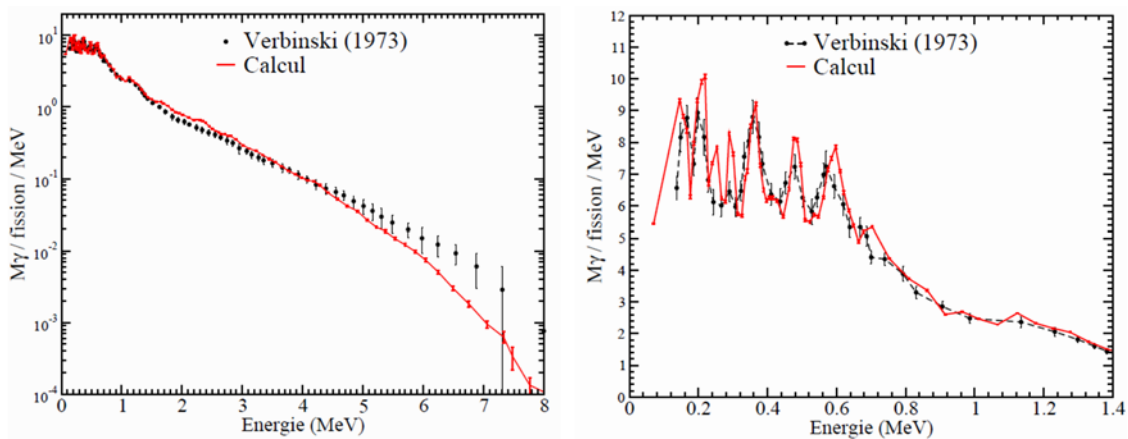


Figure 5: PFNS for $^{239}\text{Pu}+n_{\text{th}}$

Comparison between Verbinski, Weber and Sund (1973) data and the FIFRELIN calculation (Regnier, 2013)

Left: whole energy range. Right: low-energy range highlighting the capability of the code to reproduce the structures.



function models was reported in Regnier (2013). The structures observed at low energies can be reproduced with a good agreement. The influence of fission modes (Brosa terminology) on the prompt fission neutron spectrum was studied and results were reported in Serot, Litaize and Regnier (2013).

A coupling has been initiated between the FIFRELIN and CONRAD codes in order to generate covariance matrices associated with prompt fission spectra presented in this first section. This is under construction. For the time being we have started to generate covariances associated with PFNS from the usual analytical models. This is described hereafter.

Covariance matrices

The parameters of three PFNS models (Maxwell, Watt and Madland-Nix) were adjusted to experimental data in order to produce variance-covariance matrices. Details of the calculation and results can be found in Berge, *et al.* (2013). The general methodology to obtain matrices with marginalisation techniques is briefly reminded hereafter. Details (related to cross-sections) can be found elsewhere (Habert, 2009; Habert, *et al.*, 2010; Archier, 2011; De Saint Jean, 2010). If we note M_x^{stat} the covariance matrix of model parameters after minimisation, G_x the derivatives of the spectrum relative to the model parameters, G_0 the derivatives of the spectrum relative to the “nuisance” parameters (normalisation for instance) and M_0 the covariance matrix of the nuisance parameters, then the final posterior covariance matrix after minimisation and marginalisation can be written as:

$$M_x^{marg} = M_x^{stat} + \left(G_x^t \cdot G_x\right)^{-1} \cdot G_x^t \cdot G_0 \cdot M_0 \cdot G_0^t \cdot G_x \cdot \left(G_x^t \cdot G_x\right)^{-1} \quad (1)$$

The uncertainty of the prior values were fixed to 10%. The posterior values with corresponding uncertainties without and with marginalisation of 5% uncertainty on the normalisation are presented in Table 1. The adjusted PFNS is shown in Figure 6 with its

Table 1: Maxwell, Watt and Madland-Nix model parameters for $^{235}\text{U}+n_{th}$ PFNS uncertainty estimation without marginalisation of the normalisation (posterior value in light black) and with a 5% uncertainty on the normalisation marginalised (posterior uncertainty in bold)

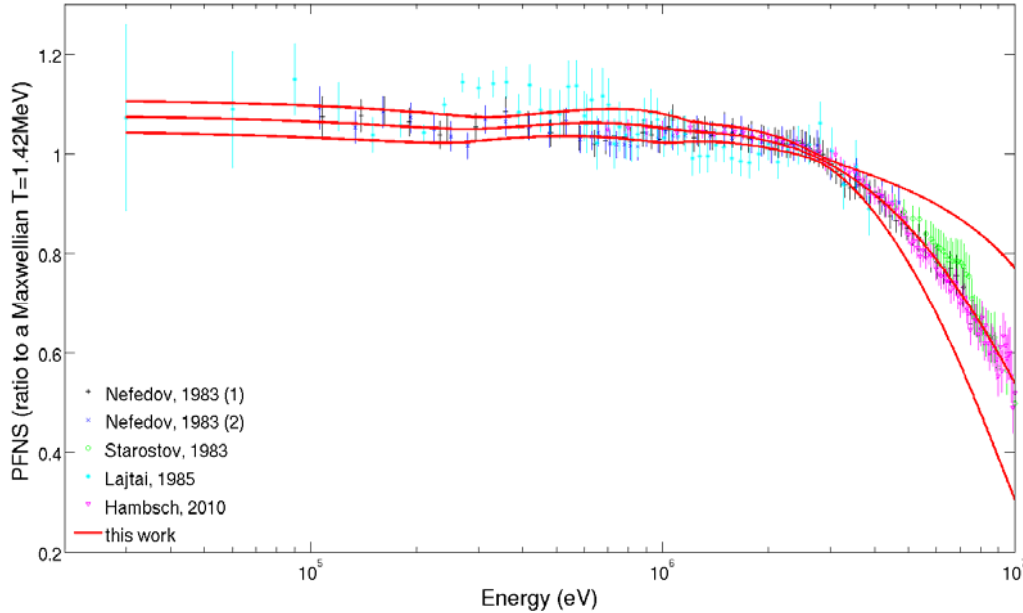
The experimental data used are those from Starostov, Nefedov and Boytzov (1983), Lajtai, *et al.* (1985), Hamsch and Kornilov (n.d.), and Nefedov, Starostov and Boytzov (1983)

Model	Parameters	Prior (MeV)	Posterior (MeV)
Maxwell	T	$1.32 \pm 10\%$	$1.31 \pm 0.1\%$ $\pm 2.4\%$
Watt	T_w	$0.90 \pm 10\%$	$1.03 \pm 0.6\%$ $\pm 11.0\%$
	E_w	$0.78 \pm 10\%$	$0.44 \pm 2.3\%$ $\pm 24.7\%$
Madland-Nix	T	$1.01 \pm 10\%$	$0.96 \pm 1.6\%$ $\pm 18.5\%$
	E_f^L	$1.07 \pm 10\%$	$1.12 \pm 4.0\%$ $\pm 23.9\%$
	E_f^H	$0.50 \pm 10\%$	$0.25 \pm 2.5\%$ $\pm 24.9\%$

Figure 6: Ratio to a Maxwellian of the prompt fission neutron spectrum for $^{235}\text{U}+n_{\text{th}}$

Band width uncertainty obtained after minimisation and marginalisation of 5% uncertainty in the normalisation

The experimental data used are those from Starostov, Nefedov and Boytzov (1983), Lajtai, *et al.* (1985), Hamsch and Kornilov (n.d.), and Nefedov, Starostov and Boytzov (1983)



error band obtained by minimising the chi-square between different experimental data (Starostov, Nefedov and Boytzov, 1983; Lajtai, *et al.*, 1985; Hamsch and Kornilov, n.d.; Nefedov, Starostov and Boytzov, 1983) and a Madland-Nix functional (with marginalisation). The corresponding correlation matrix is shown in Figure 7, as well as the matrices obtained with Maxwell and Watt functionals (without marginalisation). Figure 8 shows the same matrices but with marginalisation. The structures appearing if only statistical uncertainties are accounted for are washed out by marginalising the uncertainty on the normalisation. It might be not straightforward to use normalisation as the key parameter for the marginalisation (ongoing analysis to use a more reliable experimental parameter such as detection efficiency). Nevertheless it allows to reproduce the necessary strong correlation due to the inner spectrum normalisation and to obtain more realistic final uncertainties compared to adjustment with only statistical uncertainties.

Figure 7: Correlation matrices without marginalisation of the normalisation uncertainty for $^{235}\text{U}+n_{\text{th}}$

Maxwell (left), Watt (centre) and Madland-Nix (right)

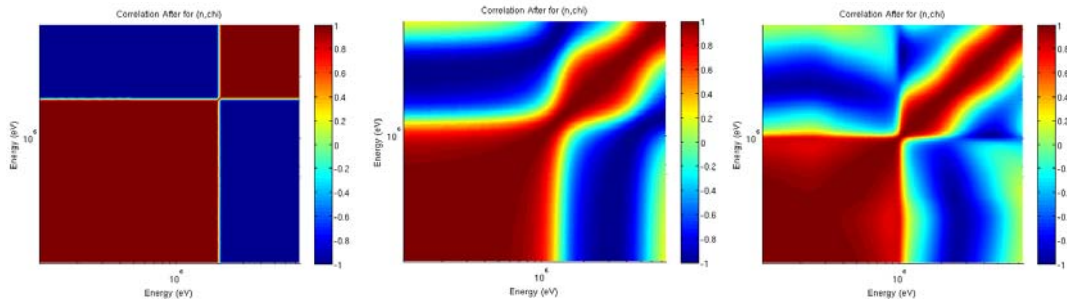
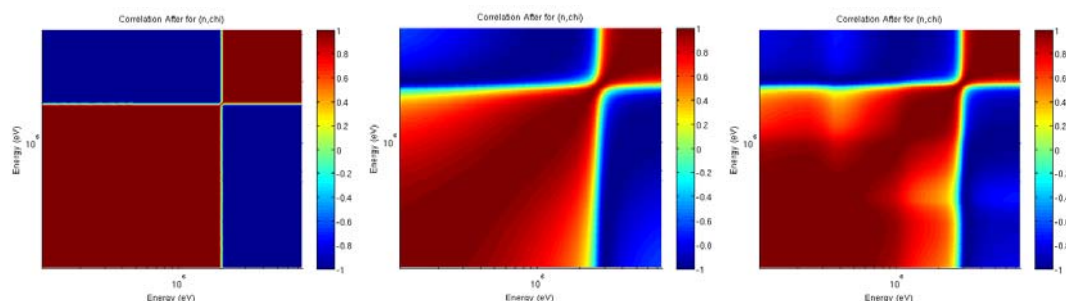


Figure 8: Correlation matrices with marginalisation of 5% of the normalisation uncertainty for $^{235}\text{U}+n_{\text{th}}$

Maxwell (left), Watt (centre) and Madland-Nix (right)



Conclusion

This paper briefly described the ongoing work performed at CEA Cadarache around prompt fission spectra. A Monte Carlo simulation of the fission fragment de-excitation based on Weisskopf or Hauser-Feshbach approaches was first performed with the FIFRELIN code in order to produce neutron- and gamma-related fission observables in a single consistent run. On the other hand, prompt fission neutron spectrum model parameters were adjusted to experimental data in order to produce variance-covariance matrices. A marginalisation technique, already used for cross-sections in the recent past, was used to take into account experimental parameters such as normalisation in the generation of the covariance matrices. In the future it is planned to improve the models implemented in FIFRELIN and couple the code to CONRAD in order to generate these matrices by using a more sophisticated PFNS model.

References

- Archier, P. (2011), “Contribution à l’Amélioration des Données Nucléaires Neutroniques du Sodium pour le Calcul des Réacteurs de Génération IV”, PhD thesis, Université de Grenoble.
- Becvar, F. (1998), “Simulation of Gamma Cascades in Complex Nuclei with Emphasis on Assessment of Uncertainties of Cascade-Related Quantities”, *Nucl. Instrum. and Methods in Physics Research A*, 417, p. 434.
- Berge, L., *et al.* (2013), “Generation of Covariance Matrices for Prompt Fission Neutron Spectra”, JEF/DOC 1529, OECD/NEA, Paris.
- Capote, R., *et al.* (2009), “RIPL3: Reference Input Parameter Library for Calculation of Nuclear Reactions and Nuclear Data Evaluations”, *Nucl. Data Sheets*, 110, 12, pp. 3107-3214.
- De Saint Jean, C., *et al.* (2007), “Status of CONRAD, a Nuclear Reaction Analysis Tool”, *Proc. of Int. Conf. on Nuclear Data for Sci. and Techn.*, Nice, France, p. 251.

- De Saint Jean, C., *et al.* (2010), “A Monte Carlo Approach to Nuclear Model Parameter Uncertainties Propagation”, *Nucl. Sci. Eng.*, 161, pp. 363-370.
- Gilbert, A. and A.G.W. Cameron (1965), “A Composite Nuclear-Level Density Formula with Shell Corrections”, *Can. J. Phys.*, 43, 8, pp. 1446-1496.
- Habert, B. (2009), “Estimation des Incertitudes dans l'Évaluation des Sections Efficaces de Réactions Nucléaires”, PhD thesis, Université de Grenoble.
- Habert, B., *et al.* (2010), “Retroactive Generation of Covariance Matrix of Nuclear Model Parameters Using Marginalization Techniques”, *Nucl. Sci. Eng.*, 166, 3, pp. 276-287.
- Hambusch, F.-J. and N. Kornilov (n.d.), private communication.
- Hauser, W. and H. Feshbach (1952), “The Inelastic Scattering of Neutrons”, *Phys. Rev.*, 87, 2, pp. 366-373.
- Koning, A.J. and J.-P. Delaroche (2003), “Local and Global Nucleon Optical Models from 1 keV to 200 MeV”, *Nucl. Phys. A*, 713, pp. 231-310.
- Koning, A.J., S. Hilaire and M.C. Duijvestijn (2007), “Talys 1.0”, *Proc. of Int. Conf. on Nucl. Data*, 22-27 April 2007, Nice, France, p. 211.
- Lajtai, A., *et al.* (1985), “Prompt Neutron Spectra for Energy Range 30 keV-4 MeV from Fission of ^{233}U , ^{235}U and ^{239}Pu Induced by Thermal Neutrons”, *Proc. of Int. Conf. on Nucl. Data for Basic and Appl. Sci.*, 1, p. 613.
- Litaize, O. and O. Serot (2010), “Investigation of Phenomenological Models for the Monte Carlo Simulation of the Prompt Fission Neutron and Gamma Emission”, *Phys. Rev. C*, 82, p. 054616.
- Litaize, O., D. Regnier and O. Serot, (2013), “Prompt Fission Gamma Spectra and Multiplicities for Various Fissioning Systems”, forthcoming in *Phys. Proc.* 2014.
- Litaize, O., *et al.* (2013), “Investigation of $^{238}\text{U}(n,f)$ Fission Observables”, *Proc. of Int. Conf. on Nucl. Data*, Manhattan, NY, United States, 4-8 March 2013, forthcoming in *Nucl. Data Sheets*.
- Madland, D.G. and J. Nix (1982), “New Calculation of Prompt Fission Neutron Spectra and Average Prompt Neutron Multiplicities”, *Nucl. Sci. Eng.*, 81, p. 213.
- Nefedov, V.N., B.I. Starostov and A.A. Boytsov (1983), “High Precision Spectra Measurements for Neutrons Arising from the Fission of ^{252}Cf , ^{233}U , ^{235}U , ^{239}Pu in the Energy Range 0.04-5 MeV”, *Proc. of Conf. on Neutron Physics*, Vol. 2, p. 285, Kiev, USSR. EXFOR entries: 40871007 and 40871008.
- Oberstedt, A., *et al.* (2013), “Improved Values for the Characteristics of Prompt Fission Gamma-Ray Spectra from the Reaction $^{235}\text{U}(n_{th},f)$ ”, *Phys. Rev. C*, 87, p. 051602.
- Peelle, R.W. and F.C. Maienschein (1971), “Spectrum of Photons Emitted in Coincidence with Fission of ^{235}U by Thermal Neutrons”, *Phys. Rev. C*, 3, 1, pp. 373-390.
- Regnier, D. (2013), “Contribution à l'Étude des Gammas Prompts de Fission”, PhD thesis, Université de Grenoble.
- Regnier, D., O. Litaize and O. Serot (2013a), “A Monte Carlo Simulation of Prompt Gamma Emission from Fission Fragments”, *EPJ Web of Conferences*, 42, *Proc. of Int. Workshop on Nucl. Data Eval. for Reactor Appli. (WONDER-2012)*, Aix-en-Provence, France, O. Serot, *et al.* (eds.), p. 04003.
- Regnier, D., O. Litaize and O. Serot (2013b), “Preliminary Results of a Full Hauser-Feshbach Simulation of the Prompt Neutron and Gamma Emission from Fission Fragments”, *Phys. Proc.*, 47, p. 47.

- Serot, O., O. Litaize and D. Regnier. (2013), “Influence of Fission Modes on Fission Observables for ^{239}Pu (n_{th},f) Reaction”, forthcoming in *Phys. Proc.* 2014.
- Starostov, B.I., A.F. Semenov and V.N. Nefedov (1981), *Measurement of Prompt Neutron Spectra for ^{233}U , ^{235}U and ^{239}Pu Thermal-Neutron-Induced Fission in the 0.01-5 MeV Energy Region and for ^{252}Cf Spontaneous Fission in the 0.01-10 MeV Region*, Report INDC-CCP-0164, International Atomic Energy Agency, Vienna, Austria.
- Starostov, B.I., V.N. Nefedov and A.A. Boytzov (1983), “High Precision Prompt Neutron Spectra Measurement for Neutrons from ^{252}Cf , ^{233}U , ^{235}U , ^{239}Pu Fission in the Energy Range 2-11 MeV”, *Proc. of Conf. on Neutron Physics*, Vol. 2, p. 290, Kiev (USSR).
- Verbinski, V.V., H. Weber and R.E. Sund (1973), “Prompt Gamma Rays from $^{235}\text{U}(n,f)$, $^{239}\text{Pu}(n,f)$, and Spontaneous Fission of ^{252}Cf ”, *Phys. Rev. C*, 7 (3), p. 1173.
- Watt, B.E. (1952), “Energy Spectrum of Neutrons from thermal Fission of ^{235}U ”, *Phys. Rev.*, 87, p. 6.
- Weisskopf, V. (1937), “Statistics and Nuclear Reactions”, *Phys. Rev.*, 52, p. 295.
- Yufeng, J. (1989), “Experimental Study of the Prompt Neutron Spectrum of ^{235}U Fission Induced by Thermal Neutrons”, *Chin. J. Nucl. Phys.*, 11, 4, p. 47.

Characteristics of prompt fission gamma-ray emission – Experimental results and predictions

Andreas Oberstedt,^a Robert Billnert,^{a,b} Stephan Oberstedt^b

^aFundamental Fysik, Chalmers Tekniska Högskola
Göteborg, Sweden

^bEuropean Commission, Joint Research Centre
Institute for Reference Materials and Measurements
Geel, Belgium

Abstract

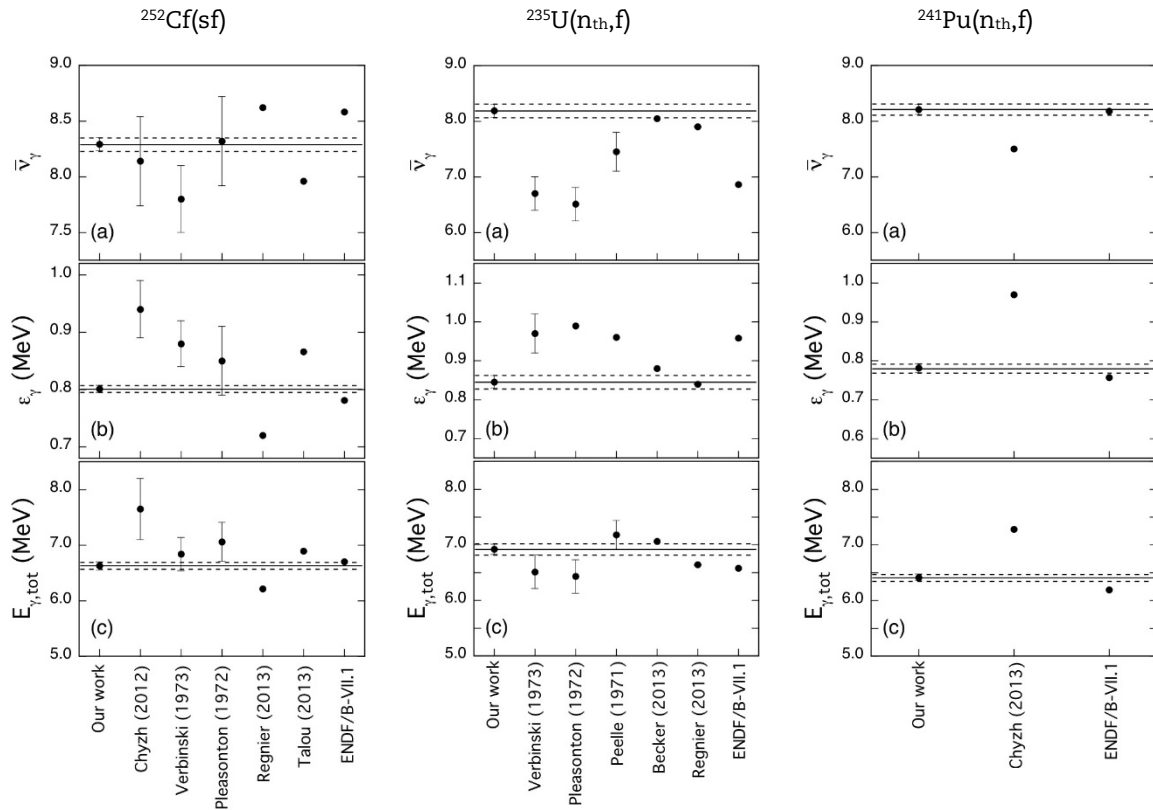
Systematics from 2001, describing prompt fission gamma-ray spectra (PFGS) characteristics as function of mass and atomic number of the fissioning system, has been revisited and parameters have been revised based on recent experimental results. Although originally expressed for spontaneous and thermal neutron-induced fission, validity for fast neutrons was assumed and applied to predict PFGS characteristics for the reaction $n + ^{238}\text{U}$ up to incident neutron energies of $E_n = 20$ MeV. The results from this work are in good agreement with corresponding results from both model calculations and experiments.

Introduction

A bit more than a decade ago an evaluation of prompt fission gamma-ray spectra (PFGS) was presented by Valentine (2001), trying to describe the average total gamma-ray energy released in fission as well as the average energy per emitted gamma-ray as functions of mass and atomic number, A and Z , of the fissioning system. From both characteristic properties, even the average gamma-ray multiplicity was deduced. Based on experimental data available back then for $^{233}\text{U}(n_{\text{th}},f)$, $^{235}\text{U}(n_{\text{th}},f)$, $^{239}\text{Pu}(n_{\text{th}},f)$ and $^{252}\text{Cf}(sf)$, A - and Z -dependencies were found “by trial and error” (see the work mentioned above for references). Although without any physical significance, the description given there offers the possibility to estimate average properties of PFGS for fissioning systems, which are difficult or virtually impossible to access experimentally.

However, in recent years the measurement of PFGS has undergone a renaissance, motivated by requests for new, precise values especially for gamma-ray multiplicities and average photon energy release per fission in the thermal neutron-induced fission of ^{235}U and ^{239}Pu (OECD/NEA, 2006). Basically two experimental groups have been involved in the gathering of new data. A collaboration involving IRMM/Chalmers/Budapest, represented by Billnert, *et al.* (2013a) and Oberstedt, *et al.* (n.d.), has reported results from $^{252}\text{Cf}(sf)$, $^{235}\text{U}(n_{\text{th}},f)$ and $^{241}\text{Pu}(n_{\text{th}},f)$ (Oberstedt, *et al.*, 2013; Billnert, *et al.*, n.d., 2013b), while another one between Los Alamos/Livermore, represented by Chyzh, *et al.* (2012, 2013) and Ullmann, *et al.* (2013), reported on $^{252}\text{Cf}(sf)$ and $^{235}\text{U}(n,f)$, $^{239,241}\text{Pu}(n,f)$. A comparison of all results for the PFGS properties from $^{235}\text{U}(n_{\text{th}},f)$, $^{241}\text{Pu}(n_{\text{th}},f)$ and $^{252}\text{Cf}(sf)$, also given in the publications by Oberstedt, *et al.* (n.d., 2013) and Billnert, *et al.* (n.d., 2013b), is shown in Figure 1. Depicted are: *i*) the average photon multiplicity; *ii*) the mean photon energy per fission; *iii*) the total

Figure 1: Overview of both experimental and theoretical results for PFGS characteristics for different fissioning systems



released photon energy. The values from our work, averaged over results obtained with different detectors, are compared to other experimental results from the early 1970s and from the recent work by the Los Alamos/Livermore collaboration (Chyzh, *et al.*, 2012, 2013; Ullmann, *et al.*, 2013). Also shown are results from recent calculations with different Monte Carlo Hauser-Feshbach codes by Litaize and Serot (2010), Regnier, Litaize and Serot (2013), Talou, Kawano and Stetcu (2013), and Becker, *et al.* (2013), respectively, as well as data from ENDF/B-VII.1 (CSEWG, 2011). The results from the calculations were provided by Regnier (2013) and Talou (2013). The full drawn and dashed lines in Figure 1 represent the averaged values from our work and their uncertainties, respectively, and are shown to make comparison with the other data easier. Obviously, Figure 1 exhibits deviations, which will be discussed later, but which motivate an investigation of the influence of the recent measurements on the evaluation by Valentine (2001). This will be done in the following section. Since that evaluation was performed for thermal neutron-induced and spontaneous fission, and, hence, the systematics that is based upon it may be assumed to be valid for those fissioning systems, the excitation energy ranges from zero to the neutron separation energy. Below we extend the revised systematics to fast neutron-induced fission and apply it to the system $n + ^{238}\text{U}$, which is highly relevant for fast reactor applications and one of the six important isotopes in the focus of the Collaborative International Evaluated Library Organisation (CIELO) Pilot Project of the OECD/NEA (n.d.). The predicted PFGS characteristics for this system up to 20 MeV incident neutron energy are then compared to results from theoretical calculations and recent measurements.

Revised systematics for PFGS characteristics

According to Valentine (2001), the average total γ -ray energy released in fission $E_{\gamma,tot}$ is depending linearly on the prompt fission neutron multiplicity $\bar{\nu}_n$, which is based on the study published by Nifenecker, *et al.* (1972). However, the latter cited work was extended from the spontaneous fission of ²⁵²Cf to other fissioning systems by including a dependence from both their mass and atomic numbers, A and Z, respectively. The suggested description for $E_{\gamma,tot}(\bar{\nu}_n, Z, A)$ in MeV is of the form:

$$E_{\gamma,tot}(\bar{\nu}_n, Z, A) = \varphi(Z, A) \times \bar{\nu}_n + 4.0 \quad (1)$$

with:

$$\varphi(Z, A) = a_0 + a_1 \times Z^2 A^{1/2} \quad (2)$$

The parameters a_0 and a_1 were determined by a least-squares fit to experimental data, while the values for $\bar{\nu}_n$ had been taken from experiments (Valentine, 2001). The average energy per emitted γ -ray ε_γ was assumed to be independent from $\bar{\nu}_n$ and depending on A and Z according to:

$$\varepsilon_\gamma(Z, A) = b_0 + b_1 \times Z^{1/3} A^{-1} \quad (3)$$

Here too, the parameters b_0 and b_1 were determined by a fit to experimental results. A relation for the average prompt fission γ -ray multiplicity $\bar{\nu}_\gamma$ may then be inferred by dividing Eq. (1) with Eq. (3) and using Eq. (2). Although different functions may be used to approximate $\bar{\nu}_\gamma(\bar{\nu}_n, Z, A)$, we have chosen:

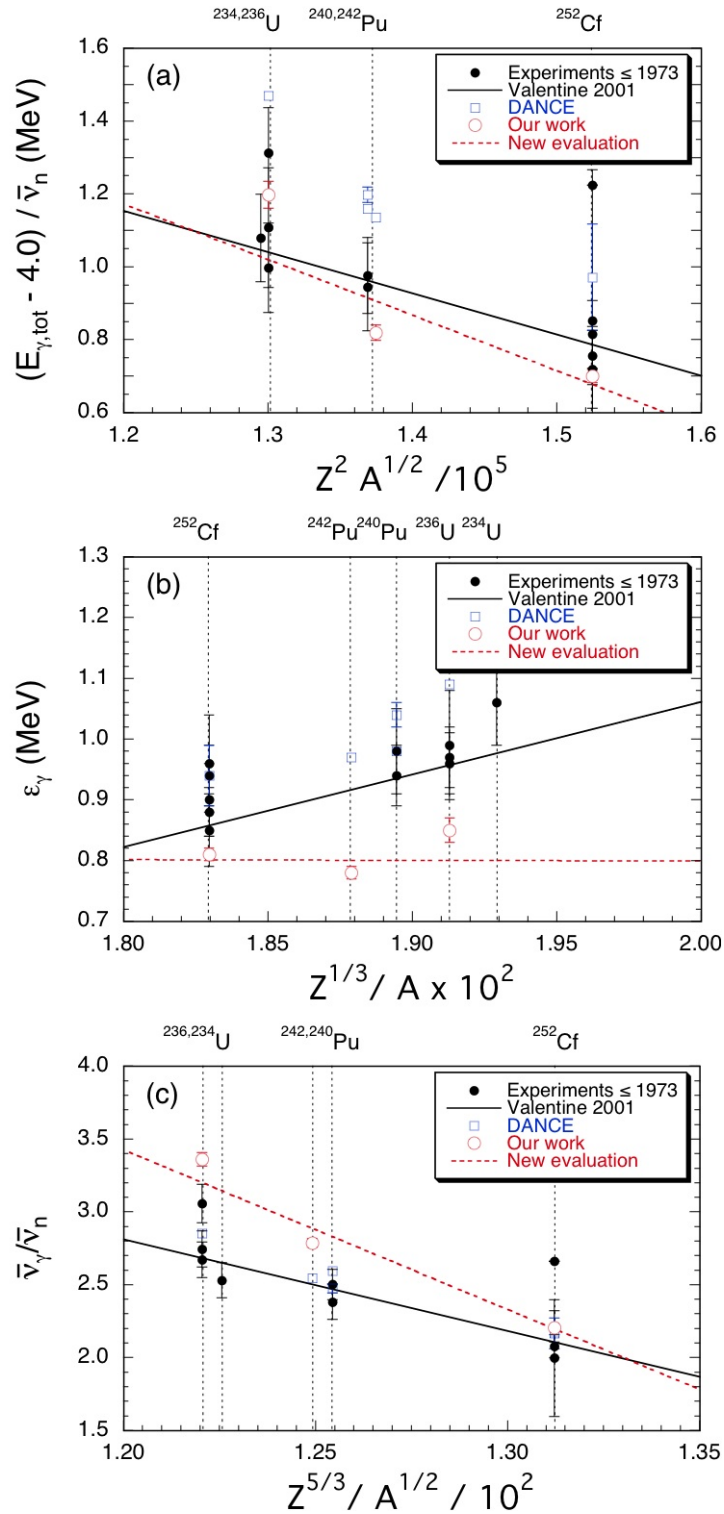
$$\bar{\nu}_\gamma(\bar{\nu}_n, Z, A) = (c_0 + c_1 \times Z^{5/3} A^{-1/2}) \times \bar{\nu}_n \quad (4)$$

in order to present experimental values graphically. Figure 2 gives an overview of all experimental results for: *i*) $E_{\gamma,tot}(\bar{\nu}_n, Z, A)$; *ii*) $\varepsilon_\gamma(Z, A)$; *iii*) $\bar{\nu}_\gamma(\bar{\nu}_n, Z, A)$ in accordance with the above equations. The full drawn (black) lines correspond to the evaluation by Valentine (2001), based on experimental results that were reported until 1973 (see references in Valentine, 2001), denoted by full drawn (black) circles. The (blue) open squares indicate the results obtained by the Los Alamos/Livermore collaboration (Chyzh, *et al.*, 2012, 2013; Ullmann, *et al.*, 2013) using the DANCE detector system, see Heil, *et al.* (2001). Our results (Billnert, *et al.*, n.d., 2013a, 2013b; Oberstedt, *et al.*, n.d., 2013) are shown as (red) open circles. The values for $\bar{\nu}_n$ were taken as given by Valentine (2001). Due to the obvious discrepancies between the historical and the recently obtained experimental data, a new evaluation seems to be reasonable on the basis of these new results. However, even those exhibit considerable differences depending on by which experimental group they were obtained. The reason for that has been understood as absorption effects in the DANCE system for γ -rays with energies below 500 keV, leading to lower γ -ray multiplicities and an overestimation of the average total γ -ray energy, see Billnert, *et al.* (2013a) for details.

This may be seen in Figure 1 for both ²⁵²Cf(sf) and ²⁴¹Pu(n_{th},f). Hence, those values are maybe not quite reliable and are therefore not included in a new evaluation, whose result is depicted by (red) dashed lines in Figure 2. They were obtained by least-squares fits, weighted with the uncertainties, to our experimental results for ²³⁵U(n_{th},f), ²⁴¹Pu(n_{th},f) and ²⁵²Cf(sf), leading to the following description of the average total γ -ray energy released in fission in MeV:

$$E_{\gamma,tot}(\bar{\nu}_n, Z, A) = \left[(3.00 \pm 0.22) - (1.53 \pm 0.15) \times 10^{-5} \times Z^2 A^{1/2} \right] \times \bar{\nu}_n + 4.0 \quad (5)$$

Figure 2: Overview of experimental results for the average total γ -ray energy released in fission (top), the average energy per photon (middle) and prompt fission γ -ray multiplicity (bottom) as function of A and Z for different fissioning systems, together with the results from evaluations by Valentine (2001) (solid black line) and from this work (dashed red line)



and the average energy per photon in MeV:

$$\varepsilon_\gamma(Z, A) = (0.82 \pm 0.42) - (0.01 \pm 0.22) \times 10^2 \times Z^{1/3} A^{-1} \quad (6)$$

while the average prompt fission γ -ray multiplicity may be approximated by:

$$\bar{\nu}_\gamma(\bar{\nu}_n, Z, A) = \left[(16.6 \pm 0.5) - (11.0 \pm 0.4) \times 10^{-2} \times Z^{5/3} A^{-1/2} \right] \times \bar{\nu}_n \quad (7)$$

Although the fit parameters are afflicted with considerable uncertainties, basically due to the fact that only few experimental data could have been considered for the new evaluation, the differences compared to the one by Valentine (2001) are quite obvious. In particular, our results predict an average γ -ray energy that is practically the same for all fissioning systems. Of course, this has to be subject to further experimental studies, which then have to be included in the systematics presented here. For the time being, we emanate from the equations presented above to predict PFGS properties for the system $n + ^{238}\text{U}$.

The system $n + ^{238}\text{U}$ at $E_n \leq 20$ MeV

From the systematics of PFGS characteristics presented in the previous section it should be possible to interpolate to any fissioning system. The only apparent energy dependence is an implicit one, hidden in the prompt fission neutron multiplicity. If this one is known, there is no obvious reason why the validity of these systematics should be restricted to spontaneous or thermal neutron-induced fission. Hence, in the following we apply the systematics to fission induced by fast neutrons on ^{238}U in the energy range from 0 to 20 MeV. According to Madland (2006), the energy dependence of the prompt fission neutron multiplicity is a linear one and the most recent data may probably be found in the evaluated library ENDF/B-VII.1 (CSEWG, 2011). However, in the considered energy range channels for multi-chance fission may be open, leading to the emission of pre-fission neutrons. Since these neutrons are not emitted from fission fragments but the compound system, they do not contribute to the de-excitation of the fragments in competition with prompt γ -ray emission. However, as shown by Chen and Liu (2011), they are included in the numbers given in the evaluated files. Hence, pre-fission neutrons have to be assessed and subtracted in order to obtain proper values to be used in the systematics above. This will be done below.

As already shown by Nifenecker, *et al.* (1972) for $^{252}\text{Cf}(\text{sf})$, the total γ -ray energy released in fission (and the γ -ray multiplicity) is increasing linearly with the average number of neutrons emitted per fission, i.e. $\bar{\nu}_n$. The same behaviour may be inferred from the work of Madland (2006) for $^{235}\text{U}(\text{n},\text{f})$ and $^{238}\text{U}(\text{n},\text{f})$, where a linear increase of both total γ -ray energy and average prompt neutron multiplicity with incident neutron energy is reported. Chen and Liu (2011), however, showed for the neutron-induced fission of ^{235}U that this is only true as long as the (n,f) channel is considered. Hence, for neutron energies above the neutron separation energy of the compound system, the channels for second, third, etc., fission, i.e. (n,nf), (n,2nf) and so on, may be open and the neutrons emitted prior to fission of the corresponding residual compound systems have to be subtracted from the total number of prompt fission neutrons. For the system $n + ^{238}\text{U}$, the threshold for the (n,nf) channel is at $E_n = S_n(^{239}\text{U}) = 4.807$ MeV, while the (n,2nf) channel becomes possible above $E_n = S_{2n}(^{239}\text{U}) = 10.959$ MeV and the (n,3nf) channel above $E_n = S_{3n}(^{239}\text{U}) = 16.085$ MeV. The neutron separation energies S_n were calculated from a mass table. Hence, for a given incident neutron energy, several fissioning systems ($^{239}\text{U}^*$, $^{238}\text{U}^*$, $^{237}\text{U}^*$, ...) are possible, depending on the threshold conditions mentioned before.

For a neutron with given E_n captured by a ^{238}U nucleus, one obtains an excitation energy E_x of the compound system $A_{\text{CN}} = 239$, which may be expressed as:

$$E_x(A_{CN}) = S_n(A_{CN}) + E_n = aT^2 \quad (8)$$

where T denotes the nuclear temperature of A_{CN} and the level density parameter $a = A_{CN}/7.524 \text{ MeV}^{-1}$ was adopted from Chen and Liu (2011). When a neutron is emitted from A_{CN} , its average kinetic energy is given by $\langle E_n \rangle = 3/2 T$, which may be calculated from the excitation energy $E_x(A_{CN})$. Here, a Maxwell evaporation spectrum is assumed. This leaves the residual system $A_{CN} - 1$ in an excited state, whose average excitation energy corresponds to a situation, where a nucleus with $A_{CN} - 2$ has absorbed a neutron of incident energy E_n . Hence:

$$E_x(A_{CN} - 1) = S_n(A_{CN} - 1) + E_n = E_x(A_{CN}) - S_n(A_{CN}) - \langle E_n \rangle = a' T'^2 \quad (9)$$

Again, a neutron may be emitted, this time with an average energy $\langle E_n \rangle = 3/2 T'$, where A_{CN} is replaced by $A_{CN} - 1$ in a' . Consequently, after further neutron emission remains a compound system $A_{CN} - 2$ with:

$$E_x(A_{CN} - 2) = S_n(A_{CN} - 2) + E_n'' = E_x(A_{CN} - 1) - S_n(A_{CN} - 1) - \langle E_n'' \rangle = a'' T''^2 \quad (10)$$

corresponding to a nucleus with $A_{CN} - 3$ after absorbing a neutron of energy E_n'' . After another neutron emission with $\langle E_n'' \rangle$, this procedure may be extended to higher fission channels. The total average prompt fission neutron multiplicity $\bar{\nu}_n^{239}(E_n)$ for the system $n + ^{238}\text{U}$ at a given energy E_n , as given in evaluated libraries, may then be decomposed into contributions from the different fission channels:

$$\bar{\nu}_n^{239}(E_n) = \bar{\nu}_{(n,f)}^{239}(E_n) + \bar{\nu}_{(n,nf)}^{239}(E_n) + \bar{\nu}_{(n,2nf)}^{239}(E_n) + \dots \quad (11)$$

Considering the fact that $\bar{\nu}_n$ contains both pre-fission neutrons $\bar{\nu}_{pre}$ and neutrons actually emitted from fission fragments $\bar{\nu}_{ff}$ according to:

$$\bar{\nu}_n = \bar{\nu}_{pre} + \bar{\nu}_{ff} \quad (12)$$

the individual contributions in Eq. (11) for $n + ^{238}\text{U}$ may be related to the multiplicities for the first chance fission of the different fissioning systems at the corresponding energies and weighted with the probabilities for each fission channel, given by the ratio of the cross-sections for each fission channel and the total cross-section:

$$\bar{\nu}_{(n,f)}^{239}(E_n) = (\bar{\nu}_{ff}^{239}(E_n) + 0) \times \frac{\sigma_{(n,f)}^{239}(E_n)}{\sigma_{fission}^{239}(E_n)} \quad (13)$$

$$\bar{\nu}_{(n,nf)}^{239}(E_n) = (\bar{\nu}_{ff}^{238}(E_n) + 0) \times \frac{\sigma_{(n,nf)}^{239}(E_n)}{\sigma_{fission}^{239}(E_n)} \quad (14)$$

$$\bar{\nu}_{(n,2nf)}^{239}(E_n) = (\bar{\nu}_{ff}^{237}(E_n) + 0) \times \frac{\sigma_{(n,2nf)}^{239}(E_n)}{\sigma_{fission}^{239}(E_n)} \quad (15)$$

In the range considered in this work, only first, second and third chance fission play a major role, since the onset of fourth chance fission is at about $E_n = 18 \text{ MeV}$. The prompt fission neutron multiplicities for $n + ^{238}\text{U}$, $n + ^{237}\text{U}$ and $n + ^{236}\text{U}$ (denoted by $\bar{\nu}_n^{239}$, $\bar{\nu}_n^{238}$ and $\bar{\nu}_n^{237}$, respectively) were taken from ENDF/B-VII.1 (CSEWG, 2011). The figures 0, 1 and 2 in Eqs. (13)-(15) denote the number of emitted neutrons prior to fission (i.e. pre-fission neutrons) in case of first, second and third chance fission, respectively. The values for

$\sigma_{fission}^{239}(E_n)$ were also taken from ENDF/B-VII.1 (CSEWG, 2011), while the contributions from the individual fission channels were estimated recursively. At the onset of second chance fission, a $1/\sqrt{E}$ dependence, motivated by the general energy dependence of cross-sections for neutron-induced reactions as given in textbooks, was adjusted to the total fission cross-section in order to describe the component for first chance fission. This component was then subtracted from the total fission cross-section and the result was treated in the same way to find the component for second chance fission. The remaining component was then assumed to correspond to third chance fission. We have chosen this procedure for two reasons: *i)* cross-section data sets for the fission of $n + ^{238}\text{U}$ in the different evaluated libraries show quite deviating values, in particular for the second chance fission in ENDF/B-VII.1 (CSEWG, 2011) and JENDL-4.0 (Shibata, *et al.*, 2011); *ii)* we were aiming at finding a technique that may be applied to nuclei, for which no evaluated data are available. This technique was tested for the multi-chance fission of $n + ^{233}\text{Pa}$ by Vladuca, *et al.* (2004), where the different fission channels were calculated with excellent agreement with calculations. A similar decomposition has also been performed for the total fission cross-section of $n + ^{237}\text{U}$, though this is not really necessary for the fast neutron-induced fission of ²³⁶U, since the maximum energy for $\langle E_n' \rangle$ considered here is just around the threshold for second chance fission. Hence, the real number of prompt neutrons per fission emitted from the fragments is given by:

$$\bar{v}_{ff}^{237}(E_n') = \bar{v}_n^{237}(E_n') \quad (16)$$

Using this result, the equivalent value $\bar{v}_{ff}^{238}(E_n')$ may be determined by:

$$\bar{v}_{ff}^{238}(E_n) = \left[\bar{v}_n^{238}(E_n) \times \sigma_{fission}^{238}(E_n) - (\bar{v}_n^{237}(E_n') + 1) \times \sigma_{(n,nf)}^{238}(E_n) \right] / \sigma_{(n,f)}^{238}(E_n) \quad (17)$$

where the cross-sections were determined according to the procedure described above. Combining Eqs. (11) and (13)-(15) and using the results for $\bar{v}_{ff}^{237}(E_n')$ and $\bar{v}_{ff}^{238}(E_n')$ according to Eqs. (16) and (17), $\bar{v}_{ff}^{239}(E_n)$ is determined by:

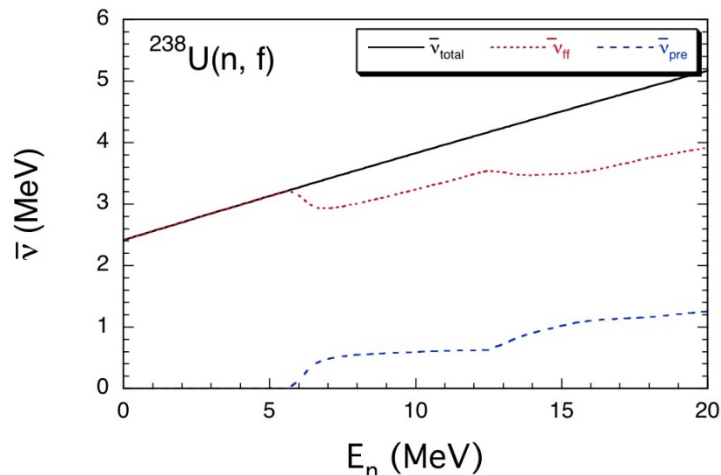
$$\bar{v}_{ff}^{239}(E_n) = \left[\bar{v}_n^{239}(E_n) \times \sigma_{fission}^{239}(E_n) - (\bar{v}_n^{238}(E_n') + 1) \right] / \left[-(\bar{v}_n^{237}(E_n') + 2) \times \sigma_{(n,2nf)}^{239}(E_n) \right] / \sigma_{(n,f)}^{239}(E_n) \quad (18)$$

Summarising the results from Eqs. (16)-(18), the total average number of prompt neutrons $\bar{v}_{ff}(E_n)$ emitted by fragments per multiple chance fission of $n + ^{238}\text{U}$ may be calculated according to:

$$\bar{v}_{ff}(E_n) = \left[\bar{v}_{ff}^{239}(E_n) \times \sigma_{(n,f)}^{239}(E_n) + \bar{v}_{ff}^{238}(E_n) \times \sigma_{(n,nf)}^{239}(E_n) \right] / \sigma_{fission}^{239}(E_n) \quad (19)$$

We would like to remind on the relations between E_n , E_n' and E_n'' given by Eqs. (8), (9) and (10). The result for $E_n = 0$ to 20 MeV is shown in Figure 3 as a (red) dotted line, together with the average total prompt fission multiplicity from ENDF/B-VII.1 (solid line) (CSEWG, 2011). The pre-fission neutron multiplicity \bar{v}_{pre} , given by the difference of both, is shown as well as a dashed line. Again, we would like to emphasise that only the prompt neutrons emitted from fission fragments are competing with prompt fission γ -ray emission in the de-excitation of fission fragments. Below we apply our findings thus far to predict PFGS properties.

Figure 3: Decomposition of the total prompt fission neutron multiplicity for $n + ^{238}\text{U}$ as given in ENDF/B-VII.1 (solid black line) (CSEWG, 2011) into components from neutrons actually emitted by fission fragments (dotted red line) and those evaporated prior to fission (dashed blue line)



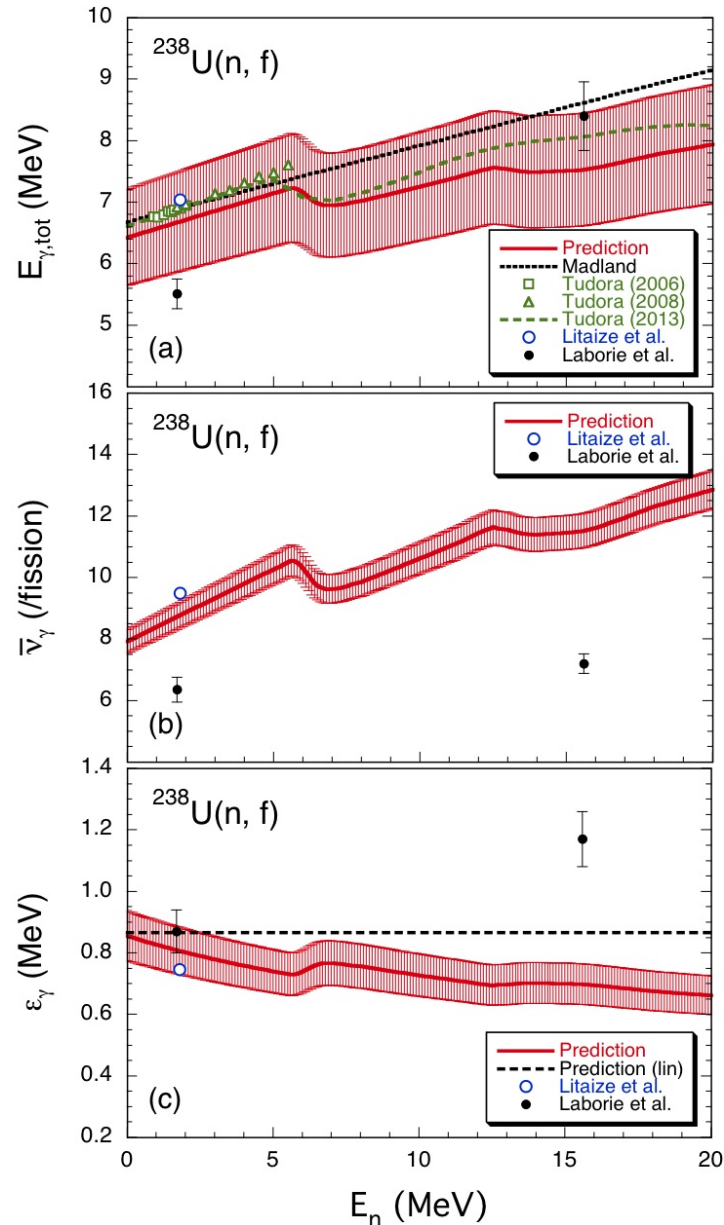
Results and conclusions

From the revised systematics presented above and the results for the prompt neutron multiplicity from the fission fragments obtained in the previous section, PFGS properties were inferred for $n + ^{238}\text{U}$. The results are summarised in Figure 4, where our work is denoted as prediction. The upper part shows the average total γ -ray energy released in fission as a function of incident neutron energy [Figure 4(a)].

Our result (solid red line) is denoted as a prediction and shown together with a linear fit to an empirical approach from Madland (2006) (dotted black line). The result of a FIFRELIN (Regnier, Litaize and Serot, 2013) calculation at $E_n = 1.8$ MeV was recently presented by Litaize, *et al.* (2013), here indicated by a (blue) open circle. The (green) squares and triangles represent results from calculations by Tudora (2013b) in the framework of the point-by-point model (for details see e.g. Tudora (2013a) and references therein). The (green) dashed line indicates results from the most recent calculations based on the same model, however with model parameters used in the work by Tudora, Hamsch and Oberstedt (2012). Preliminary experimental results from Laborie (2013) are also shown as full black circles for $E_n = 1.7$ and 15.6 MeV, earlier announced by Laborie, Belier and Taieb (2012). Our result agrees obviously very well with the different model calculations, even the kinks at the thresholds for second and third chance fission are in agreement with the latest calculations by Tudora. This behaviour is not reflected by the data from Madland (2006), which indicates that the evaporation of neutrons prior to fission had not been corrected for. These kinks also appear in our predictions for the average prompt fission γ -ray multiplicity and the average γ -ray energy per fission, both as a function of incident neutron energy as depicted in Figures 4(b) and (c), respectively. Here, the absolute values are confirmed by the calculations by Litaize, *et al.* (2013) (ε_γ was calculated from $E_{r,tot}$ and $\bar{\nu}_\gamma$). The only experimental results available for comparison are the preliminary ones from Laborie (2013), which however deviate among each other much more than expected. In Figure 4(c), the (black) dashed line indicates a constant value for the average γ -ray energy, according to Eq. (3), which contains no $\bar{\nu}_n$ and, hence, no energy dependence. The solid (red) line exhibits kinks and is the result of dividing the total γ -ray energy with the average prompt fission γ -ray multiplicity. Which description is to be preferred here cannot be judged thus far.

Figure 4: PFGS characteristics for $n + ^{238}\text{U}$ as function of incident neutron energy: (a) average total γ -ray energy released in fission; (b) average prompt fission γ -ray multiplicity; (c) average γ -ray energy per fission

The predictions from this work are shown as solid (red) lines and compared to calculations from Tudora (2013) and Litaize (2013), a linear approximation from Madland (2006) and preliminary experimental results from Laborie (2013)



We have shown that the systematics, which was originally performed by Valentine (2001) for thermal neutron-induced and spontaneous fission, may as well be applied to fission induced by fast neutrons as long as the corresponding prompt fission neutron multiplicities are known and correctly used. This implies that pre-fission neutrons must be subtracted from the total average prompt fission multiplicities, when the de-excitation of fission fragments is considered. The results from our predictions, with respect to the shape of the curves, are supported by observations for the systems $n + ^{232}\text{Th}$, $n + ^{235}\text{U}$ and

$n + ^{237}\text{Np}$, as reported by Fréhaut (1988). Our predictions build on reasonable assumptions, which in principle may be transferred to any fissioning system. So far they suffer from considerable uncertainties, basically from the fits of the systematics. However, more reliable data included in the systematics will certainly reduce the uncertainties of the fit parameters and, hence, of the predictions. For $n + ^{238}\text{U}$ new experimental results are under way. New measurements at $E_n = 1.7$ MeV and 5.2 MeV were performed by Laborie (2013) and are currently being analysed. First results for the energy region $E_n = 0.7$ -4.0 MeV, from an experiment performed at the new LICORNE facility of IPN Orsay, described by Lebois, *et al.* (2014) and Wilson, *et al.* (2013), were recently presented by Lebois, *et al.* (2013). Correction factors for the absorption of low-energy γ -rays, affecting the data obtained by the Los Alamos/Livermore group, will be presented soon, which means that a broader basis will soon be provided for a revised systematics of PFGS properties and thus predictions with higher precision. This and a more detailed description of this work will soon be given elsewhere (Oberstedt, Billnert and Oberstedt, 2014).

Acknowledgements

One of the authors (R.B.) is indebted to the European Commission for providing a PhD fellowship at EC-JRC IRMM, during which part of this work was carried out.

References

- Becker, B., *et al.* (2013), *Phys. Rev. C*, 87, 014617.
- Billnert, R., *et al.* (n.d.), forthcoming in *Phys. Rev. C*.
- Billnert, R., *et al.* (2013a), *Phys. Rev. C*, 87, 024601.
- Billnert, R., *et al.* (2013b), *Proc. of GAMMA-2 Scientific Workshop on the Emission of Prompt γ -rays in Fission and Related Topics*, Sremski Karlovci, Serbia, 24-26 September 2013, forthcoming in *Phys. Proc.*
- Chen, Yong-Jing and Liu, Ting-Jin (2011), *Chin. Phys. C*, 35 (4), 344.
- Chyzh, A., *et al.* (2012), *Phys. Rev. C*, 85, 021601 (R).
- Chyzh, A., *et al.* (2013), *Phys. Rev. C*, 87, 034620.
- CSEWG (Cross Section Evaluation Working Group) (2011), “ENDF/B-VII.1 Evaluated Nuclear Data File”, accessed 4 June 2014, www.nndc.bnl.gov/exfor/endl02.jsp.
- Fréhaut, J. (1988), *Proceedings of a Consultants Meeting on Physics of Neutron Emission in Fission*, Mito City, Japan, 24-27 May 1988, IAEA INDC(NDS)-220, 99.
- Heil, M., *et al.* (2001), *Nucl. Instr. and Meth. A*, 459, 229.
- Laborie, J-M. (2013), private communication.
- Laborie, J-M., G. Belier and J. Taieb (2012), *Phys. Proc.*, 31, 13.

- Lebois, M., *et al.* (2013), *Proc. of GAMMA-2 Scientific Workshop on the Emission of Prompt γ -Rays in Fission and Related Topics*, Sremski Karlovsci, Serbia, 24-26 September 2013, forthcoming in *Phys. Proc.*
- Lebois, M., *et al.* (2014), *Nucl. Instr. and Meth. A*, 735, 145.
- Litaize, O. and O. Serot (2010), *Phys. Rev. C*, 82, 054616.
- Litaize, O., *et al.* (2013), *Proceedings of ND2013*, New York, United States, 4-8 March 2013, forthcoming in *Nucl. Data Sheets*.
- Madland, D.G. (2006), *Nucl. Phys. A*, 772, 113.
- Nifenecker, H., *et al.* (1972), *Nucl. Phys. A*, 189, 285.
- Oberstedt, A., *et al.* (n.d.), forthcoming in *Phys. Rev. C*.
- Oberstedt, A., *et al.* (2013), *Phys. Rev. C*, 87, 051602 (R).
- Oberstedt, A., R. Billnert and S. Oberstedt (2014), forthcoming in *Phys. Rev. C*.
- OECD/NEA (n.d.), "Collaborative International Evaluated Library Organisation Pilot Project: WPEC Subgroup 40 (SG40) – CIELO Pilot Project", webpage on OECD/NEA website, OECD/NEA, Paris, accessed 4 June 2014, www.oecd-nea.org/science/wpec/sg40-cielo.
- OECD/NEA (2006), *Nuclear Data High Priority Request List*, Req. ID: H.3, H.4, OECD/NEA, Paris, accessed 21 June 2014, www.oecd-nea.org/dbdata/hprl/hprlview.pl?ID=421 and www.oecd-nea.org/dbdata/hprl/hprlview.pl?ID=422.
- Regnier, D. (2013), private communication.
- Regnier, D., O. Litaize and O. Serot (2013), *Phys. Proc.*, 47, 47.
- Shibata, K., *et al.* (2011), "JENDL-4.0: A New Library for Nuclear Science and Engineering", *J. Nucl. Sci. Technol.*, 48 (1), 1-30; see also JENDL-4.0 Evaluated Nuclear Data Files, accessed 19 June 2014, www.nndc.bnl.gov/exfor/endlf02.jsp.
- Talou, P. (2013), private communication.
- Talou, P., T. Kawano and I. Stetcu (2013), *Phys. Proc.*, 47, 39.
- Tudora, A. (2013a), *Ann. Nucl. Energy*, 53, 507.
- Tudora, A. (2013b), private communication.
- Tudora, A., F-J. Hamsch and S. Oberstedt (2012), *Nucl. Phys. A*, 890-891, 77.
- Ullmann, J.L., *et al.* (2013), *Phys. Rev. C*, 87, 044607.
- Valentine, T.E. (2001), *Ann. Nucl. Energy*, 28, 191.
- Vladuca, G., *et al.* (2004), *Nucl. Phys. A*, 740, 3.
- Wilson, J.N., *et al.* (2013), *Proc. of GAMMA-2 Scientific Workshop on the Emission of Prompt γ -Rays in Fission and Related Topics*, Sremski Karlovsci, Serbia, 24-26 September 2013, forthcoming in *Phys. Proc.*

Preliminary results on $^{238}\text{U}(n,f)$ prompt fission neutron energy spectra at 2, 5.2 and 15 MeV measured using a p-terphenyl scintillator

Alix Sardet,^a Thierry Granier,^a Benoit Laurent,^a Andreas Oberstedt,^{a,b} Cyril Varignon^a

^aCommissariat à l'Énergie Atomique (CEA), DAM, Ile-de-France, Arpajon, France

^bFundamental Physics, Chalmers University of Technology, Göteborg, Sweden

Abstract

In connection with the international co-ordinated research programme aiming at improving the adequacy and quality of prompt fission neutron energy spectra, launched in 2009 by the IAEA (Capote, et al., 2009), measurements on $^{238}\text{U}(n,f)$ were performed at the 4 MV Van de Graaff accelerator facility of the CEA/DAM in Bruyères-le-Châtel. The data were acquired using the new digital acquisition system FASTER, currently being developed by LPC Caen (2013). We present results on the characterisation of the detector in use, a coaxial p-terphenyl scintillator chosen for its excellent neutron- γ discrimination properties (Lovchikova, et al., 2004; Matei, et al., 2012), and show first results from measurements of the reaction $^{238}\text{U}(n,f)$ at 2, 5.2 and 15 MeV incident neutron energies.

Introduction

Among nuclear data needed for nuclear reactor design, prompt fission neutron energy spectra occupy a key position. They are essential for reliable predictions of nuclear criticality calculations for conventional reactors, fast neutron-induced systems as well as for non-proliferation applications. However, experimental data, on which theoretical models and evaluations are adjusted, are scarce and present strong discrepancies, especially in the low-energy range (< 1 MeV). In connection with the co-ordinated research programme launched by the IAEA in 2009 (Capote, et al.), the CEA/DAM/DIF is taking part in measurements campaigns on some of the major and minor actinides such as ^{235}U , ^{238}U or ^{237}Np . Measurements were performed using an organic crystal scintillator of doped p-terphenyl which, according to Lovchikova, et al. (2004) and Matei, et al. (2012), provides excellent neutron- γ discrimination properties as well as a good detection efficiency below 1 MeV. In this paper we report on the main results of the characterisation of this detector and present preliminary prompt neutron energy spectra obtained for the fission of ^{238}U induced by 2, 5.2 and 15 MeV neutrons.

Experimental details

In this section, we present the experimental tools, the set-up and the data acquisition system in use. Measurements were performed using the time-of-flight (TOF) technique.

Digital data acquisition system FASTER

Signals were processed and recorded using the digital data acquisition system FASTER (Fast Acquisition System for Nuclear Research), currently being developed at the LPC Caen (2013). This system through dedicated functions, such as ADC and QDC loaded on field-programmable gate arrays (FPGA) enables a real-time treatment of signals, so as to store only the relevant information (CFD timing, charges, etc.), with very low dead time (about 0%). All settings are directly defined on the acquisition computer using a graphical user interface. Each channel triggers independently and all recorded events are assigned a time stamp. Therefore, coincidences can be investigated off-line. Moreover, during the experiment, it is possible to monitor the expected TOF spectrum.

Fission chamber

Fission trigger was given using a so-called fission chamber. About 14 g of ^{238}U were deposited on 100 parallel electrodes contained in a cylinder of 10 cm diameter. This cylinder was filled with ionisation gas P10 (10% methane, 90% argon) at a pressure of 5 bars. The electrodes are grouped within the chamber into five signal outputs. For this experiment, we used only two outputs corresponding to about a 5 g spread on 40 electrodes. When an event (α -decay or fission) occurs, the gas is ionised, thus generating an electric signal which, after a pre-amplification stage, is sent to the FASTER system. By analysing the amplitude of the generated pulse, it is possible to select only fission events in the reconstruction of the TOF spectrum.

P-terphenyl neutron detector

Measurements were performed using a coaxial crystal of doped p-terphenyl optically coupled to a photomultiplier (Photonis XP53X2). The crystal is a cylinder of 75 mm diameter for a 50 mm length placed in an aluminium housing. This detector was chosen as it exhibits excellent neutron- γ discrimination properties as well as a good light output in the low-energy range (below 1 MeV), which is of utmost interest for prompt fission neutron spectra (PFNS) measurements. An extensive characterisation work (Sardet, *et al.*, n.d.), whose main results are listed below, was performed on this detector.

Timing resolution

Coincident γ -rays emitted by ^{60}Co (1 174 and 1 332 keV) were investigated using the p-terphenyl neutron detector and two fast response detectors (LaBr₃:Ce), placed at about 25 cm from the source and 120° from one another (Oberstedt, *et al.*, 2012). As the square of the coincidence timing resolution is equal to the sum of the squares of the intrinsic timing resolution of the detectors, intrinsic timing resolution of all detectors can be extracted. Results are presented in Table 1. The intrinsic timing resolution of the p-terphenyl is similar to that of a classic organic liquid scintillator (e.g. NE213-equivalent BC501A), which was determined using the same procedure.

Table 1: Intrinsic timing resolutions measured using γ - γ coincidences from ^{60}Co

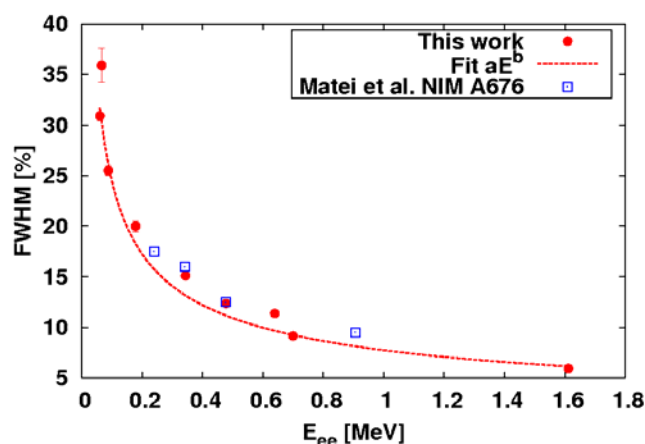
See text for details

Detector	FWHM (ps)
P-terphenyl	477 ± 12
LaBr ₃ :Ce-1	368 ± 15
LaBr ₃ :Ce-2	387 ± 15
BC501-A	475 ± 15

Deposited energy resolution

The deposited energy resolution presented in Figure 1 was measured using γ -sources in the energy range 59.5 to 1 836 keV. For an electron equivalent energy of 477.65 keV_{ee} (^{137}Cs), the obtained energy resolution is of about 12%. Data were fitted using a power function aE^b giving $a = (7.90 \pm 0.04) \text{ MeV}^{-b}$ and $b = (0.487 \pm 0.002)$. Results are in agreement with what was previously measured by Matei, *et al.* and reflect the expected \sqrt{E} dependence. This measurement also serves for the energy calibration of the system. A correspondence between the charge Q (result of signal integration) and the electron equivalent energy E_{ee} can be obtained which suggests that this detector presents slight non-linearity effects in the low-energy range.

Figure 1: Deposited energy resolution of the p-terphenyl neutron detector determined using γ -sources



Neutron response

Neutron response of the detector was characterised using an active scintillating target of $^{252}\text{Cf}(\text{sf})$ where the actinide is dissolved into an organic liquid scintillator (Belier, *et al.*, 2012). This kind of target presents a very high detection efficiency ($\sim 100\%$) and excellent pulse shape discrimination (PSD) (Leo, 1987) properties. A time-of-flight measurement was performed above a 3-m-deep pit so as to minimise any contribution from the environment (scattered neutrons and γ -rays). The active scintillating target provided the start of the TOF measurement. Two organic scintillators (the p-terphenyl crystal and a liquid BC501A) provided the stop. A sketch of the experimental set-up is presented in Figure 2. The BC501A, which was previously calibrated at the PTB,¹ served as a cross-check for our method and results.

In order to retain only neutron events in the organic scintillators, PSD was performed by integrating the waveforms over different time windows. For low values of the total charge (i.e. low energies), neutron and γ regions overlap. The limit of discrimination is estimated to be at around 500 keV neutron energy, as indicated by the red dashed line in Figure 3, in the case of the p-terphenyl neutron detector.

To calibrate the neutron response of the detector, we studied the charge distribution of the recoil proton (Q) for several incident neutron energies. This was performed using the ^{252}Cf measurement and plotting the charge spectrum conditioned by the TOF-calculated incident neutron energy for several energies. The edge of the distribution corresponds to

1. Physikalisch – Technische Bundesanstalt (Germany).

the maximum recoil proton energy (E_p), and therefore to the incident neutron energy. Knowing from the previous γ -sources measurements the relation between Q and E_{ee} , we obtain the so-called light output function, presented in Figure 4. This curve presents the expected behaviour, apart from a saturation effect that seems to appear above 7 MeV.

Figure 2: Sketch of the experimental set-up for the $^{252}\text{Cf}(\text{sf})$ TOF measurement

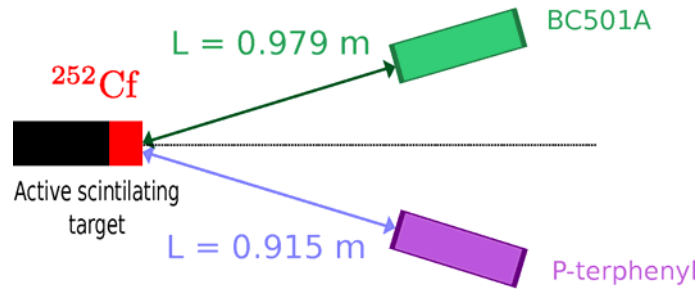


Figure 3: Pulse shape discrimination for an organic crystal of doped p-terphenyl

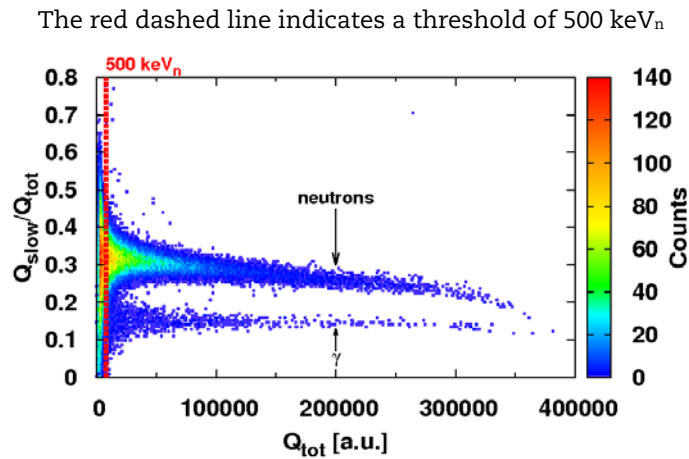
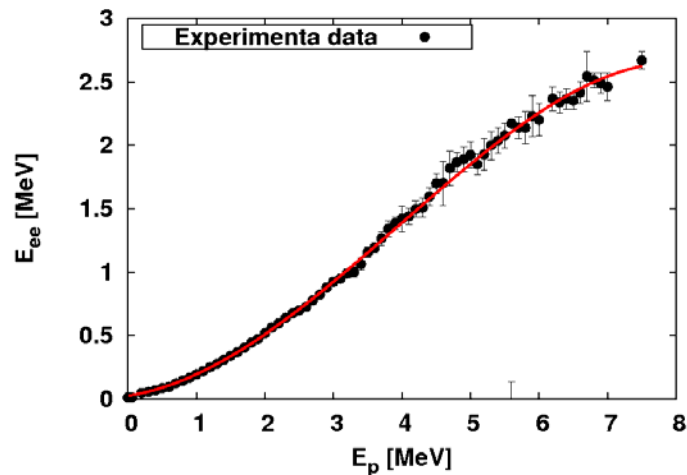


Figure 4: Light output function of a $75 \times 50 \text{ mm}^2$ p-terphenyl neutron detector obtained using γ -sources and a $^{252}\text{Cf}(\text{sf})$ active scintillating target

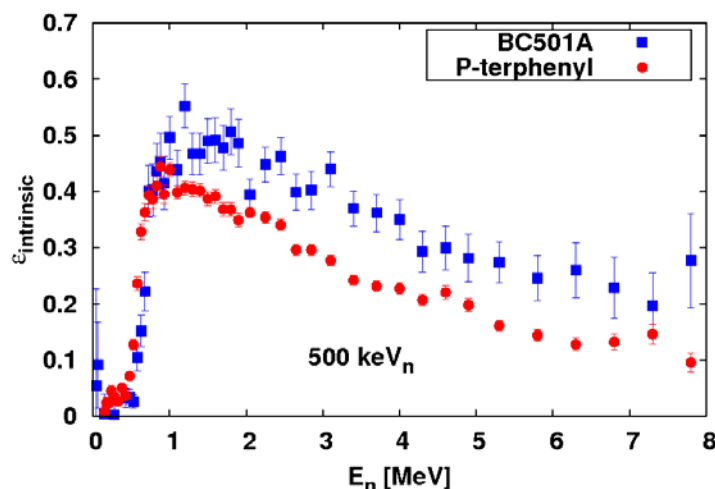
See text for details



The measured PFNS for $^{252}\text{Cf}(\text{sf})$ also served for the determination of the neutron intrinsic efficiency of the detector. The ratio of the measured spectrum to the standard recommended by the IAEA (Mannhart, 1989) gives the intrinsic efficiency curve presented in Figure 5 which is compared to that of a BC501A obtained for the same neutron energy threshold of 500 keV. The curves show that, unlike in Matei, *et al.* (2012), the intrinsic efficiency of the p-terphenyl is lower than that of a NE213-equivalent detector. However, it was previously reported (Hamsch, n.d.) that all p-terphenyl detectors may not show completely equivalent properties.

Figure 5: Neutron intrinsic efficiency of a p-terphenyl detector compared to that of a BC501A for a 500 keV_n threshold

See text for details



Prompt fission neutron energy spectra measurements

Experimental set-up for the measurements on ^{238}U at the CEA in Bruyères-le-Châtel

Quasi mono-energetic neutrons of 2, 5.2 and 15 MeV were produced, respectively through $\text{T}(\text{p},\text{n})^3\text{He}$, $\text{D}(\text{d},\text{n})^3\text{He}$ and $\text{T}(\text{d},\text{n})^4\text{He}$ reactions, and irradiated the fission chamber containing the ^{238}U . Neutrons emitted during the fission process were detected using the p-terphenyl neutron detector placed in a shielding cone at relatively 90° from the accelerator beam line and about 1 m from the fission chamber. The shielding cone, made of lead and paraffin, served as a protection against room return (scattered neutrons and γ -rays). A shadow bar was also placed between the neutron production target and the detector in order to shield the latter from the neutrons produced by the accelerator. A sketch of this set-up is shown in Figure 6 for the measurement of $^{238}\text{U}(\text{n}_{5.2\text{ MeV}},\text{f})$ PFNS.

Data treatment

As ^{238}U decays by emitting α -particles, a threshold is placed on fission chamber signals so as to select only those related to fission events. Coincidences are then investigated with events recorded by the p-terphenyl neutron detector. Since this detector is sensitive to both neutrons and γ -rays, PSD is performed (see Figure 3) and only the neutron TOF component is retained. The resulting TOF spectrum (see Figure 7) presents three different regions: remains of the prompt fission γ -peak ($\sim 6\%$), a flat time-independent background noise (corresponding to scattered neutrons and γ -rays) and a neutron lump. The remaining

Figure 6: Sketch of the experimental set-up for the measure of the energy spectrum of prompt neutrons emitted during the fission of ^{238}U induced by 5.2 MeV neutrons

Incident neutrons were produced through the strongly anisotropic $\text{D}(d,n)^3\text{He}$ reaction whose emission lobe is represented in purple

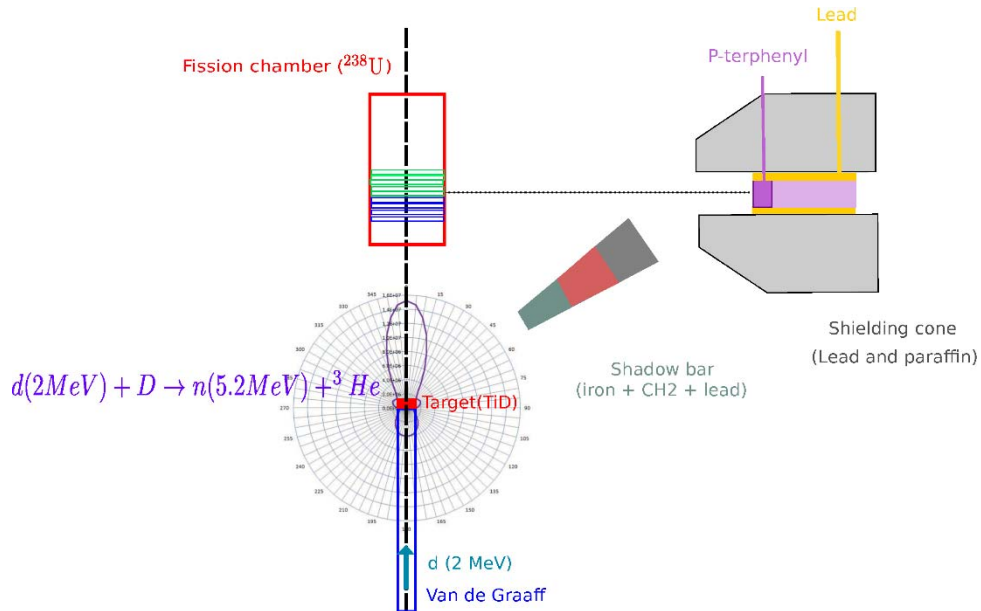
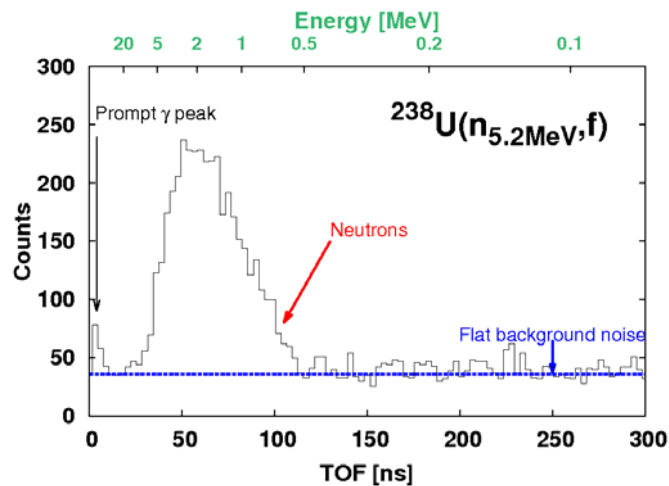


Figure 7: Neutron time-of-flight spectrum after neutron- γ discrimination for the fission of ^{238}U induced by 5.2 MeV neutrons

See text for details



constant background is subtracted off and the obtained TOF spectrum is converted bin by bin into energy. It is then normalised to the number of fissions and corrected for the neutron detection efficiency. The latter has two components: a geometric acceptance, function of the solid angle, which was in the order of $(2.73 \pm 0.29) \cdot 10^{-4}$, and an intrinsic component (see Figure 5), which was determined by using a $^{252}\text{Cf}(sf)$ source.

Preliminary results and discussion

The corrected spectra are then compared to previous measurements available in the EXFOR database and to ENDF/B-VII and JEFF-3.1.2 evaluations. These results are presented for the fission of ^{238}U induced by 2, 5.2 and 15 MeV neutrons in Figures 8, 9 and 10. These energies correspond respectively to the end of the opening of the first chance fission, right before the opening of the second chance fission and the opening of the third chance fission.

At 2 MeV, our data (represented by the blue dots in Figure 8) show a fair agreement with the ENDF (black full line) and JEFF (red dashed line) evaluations. The discrepancies below 1 MeV can be explained by distortions caused by the environment and which are not

Figure 8: Prompt fission neutron energy spectrum for the fission of ^{238}U induced by 2 MeV neutrons

See text for details

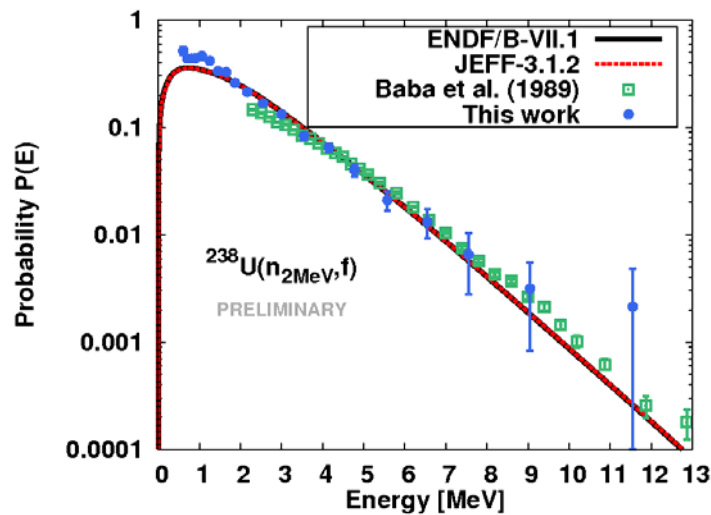
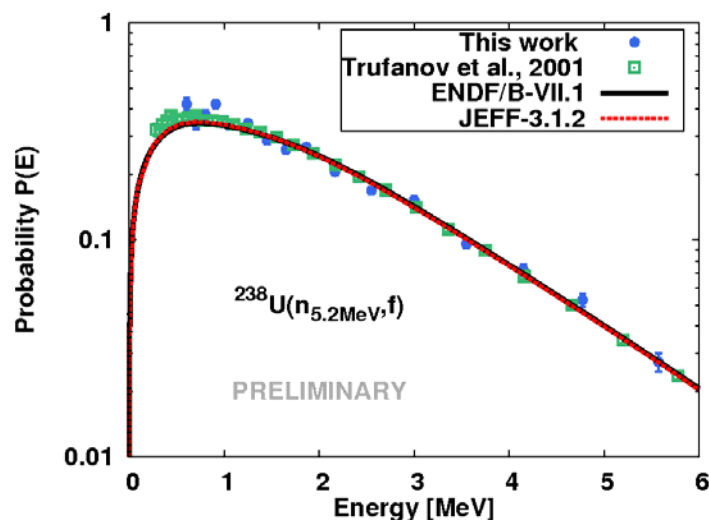


Figure 9: Prompt fission neutron energy spectrum for the fission of ^{238}U induced by 5.2 MeV neutrons

See text for details



yet taken into account in the applied efficiency correction. Nevertheless, this measurement tends to confirm the shape of the spectrum available in the data libraries, which proves to be rather different than what was obtained in 1989 by Baba, *et al.* By fitting a Maxwellian between 0.8 and 6 MeV, nuclear temperatures can be extracted (see Table 2). The obtained 1.50 MeV shows a much harder spectrum than the 1.18 MeV previously measured.

In Figure 9 (measurement at 5.2 MeV), the blue dots representing our work show an overall agreement with both evaluations and the previously performed measurement. The extracted nuclear temperature is slightly lower than what can be extracted from the Trufanov data.

The measurement at 15 MeV (see Figure 10) presents very low statistic, however, the shape above 2 MeV is in fair agreement with evaluations and previous measurements. The extracted nuclear temperature (by fitting only between 1 and 6 MeV) is compatible with those obtained from earlier measurements.

Overall, our data present a fair agreement with the major nuclear data libraries even though quite strong discrepancies are obtained below 1 MeV. They should subside once corrections for distortion caused by shielding and room-return are taken into account.

Figure 10: Prompt fission neutron energy spectrum for the fission of ^{238}U induced by 15 MeV neutrons

See text for details

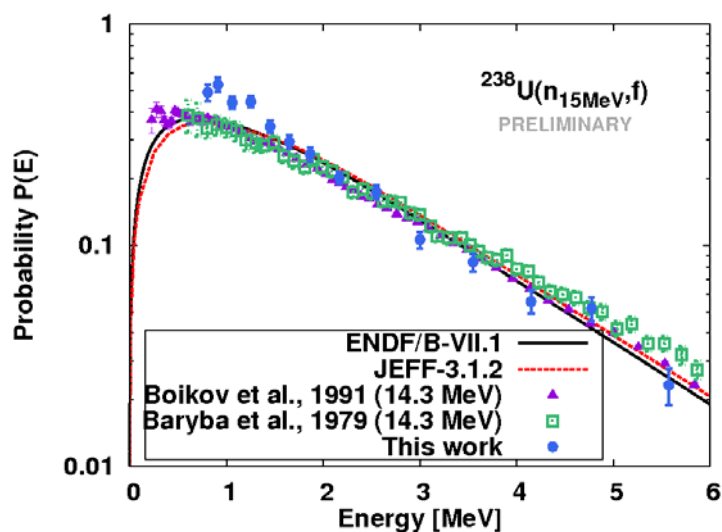


Table 2: Nuclear temperatures of ^{238}U PFNS extracted by fitting a Maxwellian between 0.8 and 6 MeV on experimental data sets for several incident neutron energies

Incident neutron energy [MeV]	Data set	Nuclear temperature [MeV]
2	This work	1.50 ± 0.13
	Baba, <i>et al.</i>	1.18 ± 0.01
5.2	This work	1.23 ± 0.05
	Trufanov, <i>et al.</i>	1.34 ± 0.01
15	This work	1.15 ± 0.07
	Baryba, <i>et al.</i>	1.23 ± 0.04

Conclusion

We have fully characterised the neutron detector in use (doped crystal of p-terphenyl) and the results we obtained were slightly disappointing compared to what was previously reported (Matei, *et al.*, 2012). However, it would seem this type of detector presents crystal-dependant properties (Hamsch, n.d.). Nevertheless, very encouraging results were obtained in terms of PFNS for the fission of ^{238}U . Despite discrepancies in the low-energy range (below 1 MeV), our measurements present a fair agreement with the evaluations and previous measurements apart at 2 MeV where they tend to show that data available in EXFOR are not reliable. Some corrections remain to be applied for each of these measurements, namely distortions caused by the environment, which will be assessed by performing MCNP simulations. In December 2013, a measurement for the fission ^{238}U induced by 1.5 MeV neutrons (opening of the first chance fission) will complete this work on prompt fission neutron energy spectra for the fissioning system ^{238}U . Upcoming activities also include analysing the data recorded at the JRC-IRMM in Geel for the fission of ^{235}U and ^{237}Np induced by 500 keV neutrons and performing other measurements on other actinides, namely ^{235}U and ^{239}Pu .

References

- Belier, G. *et al.* (2012), "Characterization and Development of an Active Scintillating Target for Nuclear Reaction Studies on Actinides", *Nucl. Instr. and Meth. A*, 664, pp. 341-346.
- Capote, R., *et al.* (2009), *Consultants Meeting on Prompt Fission Neutron Spectra of Major Actinides, Summary Report*, IAEA-INDC International Nuclear Data Committee, INDIC(NDS)-0541, International Atomic Energy Agency, Vienna.
- Hamsch, F-J (n.d.), private communication.
- Leo, W.R. (1987), *Techniques for Nuclear and Particle Physics Experiments*, Springer-Verlag, ISBN 0-387-17386-2.
- Lovchikova, G. *et al.* (2004), "Spectra and Mean Energies of Prompt Neutrons from ^{238}U Fission Induced by Primary Neutrons of Energy in the region $E_n < 20$ MeV", *Physics of Atomic Nuclei*, 67, pp. 1246-1263.
- LPC Caen (2013), FASTER website, accessed 21 June 2014, <http://faster.in2p3.fr>.
- Mannhart, W. (1989), "Status of the Cf-252 Fission Neutron Spectrum Evaluation with Regard to Recent Experiments", *Physics of Neutron Emission in Fission*, H.D. Lemmel (ed.), IAEA, INDIC(NDS)-220, 305-336, IAEA, Vienna.
- Matei, C., *et al.* (2012), "Proton Light Output Function and Neutron Efficiency of a p-Terphenyl Detector Using a ^{252}Cf Source", *Nucl. Instr. and Meth. A*, 679, pp. 135-139.
- Oberstedt, A., *et al.* (2012), "Identification of Prompt Fission γ -Rays with Lanthanum-Chloride Scintillation Detectors", *Nucl. Instr. and Meth. A*, 668, pp. 14-20.
- Sardet, A., *et al.* (n.d.), forthcoming.

Scintillation neutron detector with dynamic threshold

N. Kornilov, T. Massey, S. Grimes

Department of Physics and Astronomy, Ohio University
Athens, OH, United States

Abstract

Scintillation neutron detectors with hydrogen are a common tool for neutron spectroscopy. They provide good time resolution, neutron-gamma discrimination and high efficiency of neutron counting. The real open problems connected with application of these detectors are in the energy range >10 MeV. There are no standard neutron spectra known with high accuracy for this energy range. Therefore, traditional methods for experimental investigation of the efficiency function fail for these neutrons. The Monte Carlo simulation cannot provide reasonable accuracy due to unknown characteristics of the reactions for charged particle production (p , α and so on, light output, reaction cross-sections). The application of fission chamber with fissile material as a neutron detector did not help to solve the problem.

We may avoid many problems if we use the traditional neutron detector with non-traditional data analysis. In this report we give main relations, and demonstrate the method for Cf-source. Experimental detector efficiency is compared with MC simulation.

Introduction

The total characterisation of neutron detector can be realised if the property of the neutron source is known. Standard neutron source on the basis of ^{252}Cf with timing of fission fragments was used in Kornilov, *et al.* (2009). All neutron detector characteristics (efficiency, light output for protons, pulse height resolution, and response function versus input neutron energy) were investigated with high accuracy.

^{252}Cf is a standard neutron source very useful for practical applications. The only problem is the “high-energy limit”. Neutrons with energy >10 MeV have very low intensity, and this energy range is practically unavailable for experimental research.

Reaction of (n,p) scattering, which is the main process in hydrogen neutron detector, is the standard. This fact stimulated the Monte Carlo simulation of neutron interaction with detector and estimation of its efficiency. However, there are some obstacles for realisation of these calculations with high accuracy. The contribution of (n, α)($Q = -5.7$ MeV) reaction at neutron energy >10 MeV relative to (n,p) scattering is $\sim 10\%$. The alpha particle produces a small pulse height just near the detector threshold or less. The light output for the alpha particle is unknown. The second problem is the scattering in the detector environment. The estimation of the intensity of this process and neutron angular energy distribution is a rather difficult task. Thus the extrapolation of the MC calculation to neutron energy ~ 20 MeV can be done with accuracy not less than $\sim 10\%$, or even higher.

This big, old problem stimulated several directions for investigation. Neutrons from symmetric reactions [for example ${}^6\text{Li}({}^6\text{Li},n)$, $Q = 9.449$ MeV] have the same yield, and energies for symmetric angle in CMS (by definition). Due to proper selection of ion energy and Q-value, neutron will cover wide energy range in LS according to reaction kinematic. So, if you will start from low energy where the efficiency can be measured relative to ^{252}Cf , we may reach ~20 MeV energy, and solve this problem.

However, the yield of the neutrons with excitation of ground state and first levels is very small, and did not allow to realise this good idea (Kornilov, *et al.*, 2014).

Meadows (1991), Massey, *et al.* (1988), and Di Lullo, Mossey and Grimes (2008) changed the direction to reach the main goal – increase the accuracy of neutron efficiency estimation. They used an ionisation fission chamber as a neutron detector. The obvious advantage of this method is connected with high accuracy for efficiency calculation using a very simple relation. The disadvantage is very long experimental runs.

Kornilov, Massey and Grimes (2013) concluded that until now the data spread for neutron standard fields [$\text{Be}(d,n)$, $\text{B}(d,n)$ and $\text{Al}(n,n)$] has been very high (~20%), and do not allow us to use these neutron sources for detector calibration.

We do not see any experimental methods to measure neutron detector efficiency in the energy range up to 20 MeV with high accuracy. Can we suggest a new idea, realise a new method to increase accuracy for a calculating procedure? Is it possible to connect the advantage of using a fission chamber as a neutron detector (accurate calculation of the detector efficiency in whole energy range <20 MeV), and traditional hydrogen scintillation detector (high absolute efficiency)? We try to answer these questions in the present report.

Special selection of the detector's events

The detector consists of an NE213 scintillator with a diameter of 12.7 cm and a depth of 5.08 cm. The scintillator is coupled with an RCA 4522 photomultiplier tube with a 12.7 cm diameter photocathode (Randers-Pehrson, *et al.*, 1983).

Modern techniques allow us to collect all detected events in list mode. Thus each event is available for off-line analysis. For realisation of this method we should have the following information for each event: time-of-flight (TOF), pulse height (PH) and pulse shape (PS). After traditional neutron-gamma selection we may analyse only neutron events.

The response function for 8 MeV neutrons produced with $\text{D}(d,n)$ reaction is shown in Figure 1.

The calculation was made with a code developed in PTB (NRESP) (Dietze and Klein, 1982), and modified in Kornilov, *et al.* (2009). An additional selection requires the following information: PH_0 , PH_{\min} and PH_{\max} .

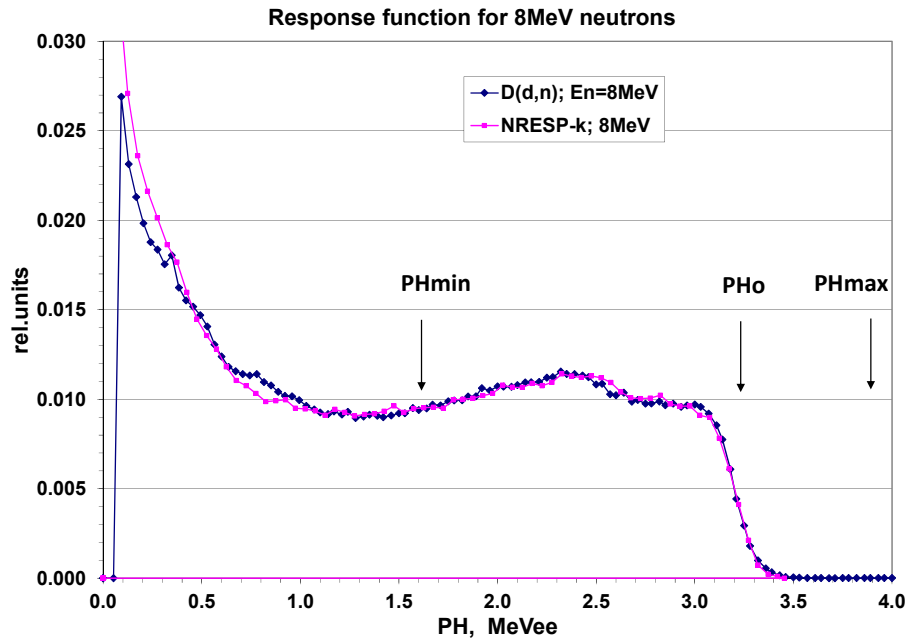
PH_0 is the highest proton energy for the selected neutron energy. $PH_0 = L(E)$, where $L(E)$ is proton light output. We also incorporate $PH_{\min} = E \cdot \cos(\theta)^2$, and $PH_{\max} = PH_0 + 3 \cdot \sigma(PH_0)$. The angle θ may be selected in such way as to remove all unwonted events. In this analysis we used $\theta = 45^\circ$.

The selection of events for each neutron energy was made with the simple equation:

$$PH_{\min} < L < PH_{\max} \quad (1)$$

Functions $L(E)$, and $\sigma(L)$ are very important and should be measured for each detector. Both dependences were measured with “white” neutron spectrum from reaction $\text{B}(d,n)$ in thick target, $E_d = 7.44$ MeV, angle of neutron emission 60° . It is important to highlight that we do not need information about spectrum shape. The high neutron yield at high energy is the only request for reaction selection.

Figure 1: Experimental and calculated RF (pulse height distribution) for “monoenergetic neutrons”

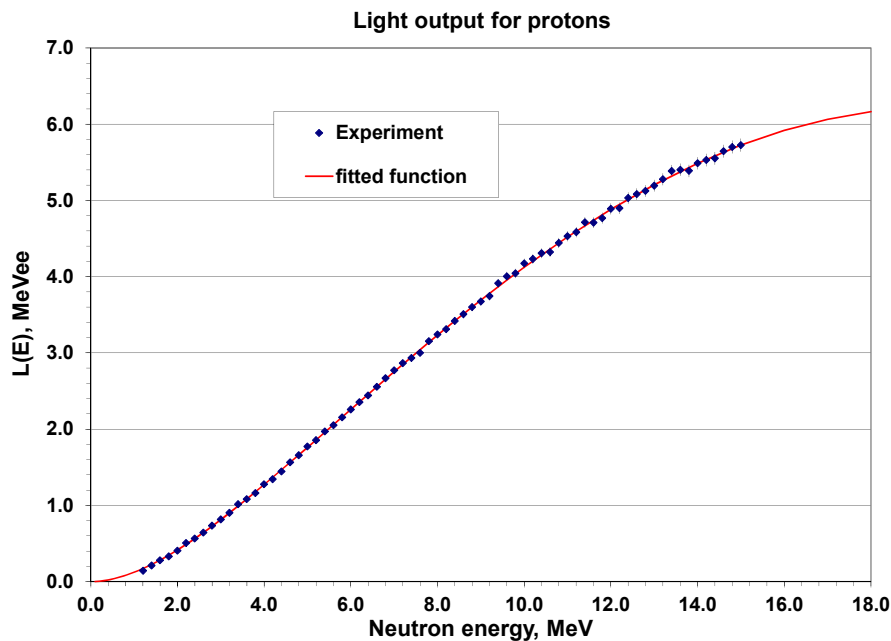


The light output data were fitted with Eq. (2) (Kornilov, *et al.*, 2009):

$$L(E) = (a_0 + a_1 * E) \frac{E^2}{E + E_0} \quad (2)$$

where a_0 , a_1 and E_0 are fitted parameters. The a_1 parameter is connected with the non-linearity of electron pulses (saturation in PM tube).

Figure 2: Experimental and calculated light output $L(E)$ dependences



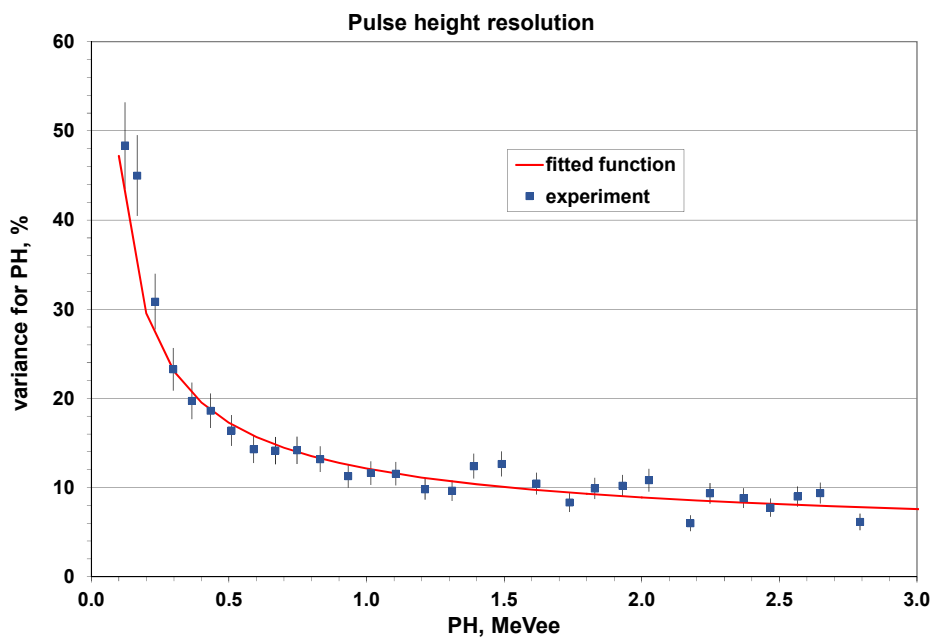
Pulse height resolution function was measured in the same experiment, and was described by Eq. (3):

$$\sigma = L \left(\alpha^2 + \frac{\beta^2}{L} + \left(\frac{\gamma}{L} \right)^2 \right)^{0.5} \quad (3)$$

where $\alpha = 0.04$, $\beta = 0.11$, $\gamma = 0.10$.

Experimental and calculated resolution functions are given in Figure 3.

Figure 3: Experimental and calculated resolution functions



Experimental and calculated efficiencies

The absolute efficiency NE213 detector was measured with ^{252}Cf neutron source (Kornilov, *et al.*, 2009). Fission fragment count rate was 2.28×10^4 1/s, total time resolution 2.4 ns, flight path 4.108 m. Time channel width was 0.209 ns (4 096 channels). Run time was ~100 h. Effect count rate ~1 1/s, and total background ~120 1/s.

The MC simulation was realised with code NEFF7-DYTH modified from NEFF7 (Dietze and Klein, 1982). It is interesting to realise how new selection changes traditional TOF distributions.

The TOF spectra with neutron-gamma selection are given in Figure 4 This spectra were collected with following conditions: $\cos(\theta) = 0.1$, $PH_{\max} = 20$ MeV_{ee}. Thus, the spectra have traditional shapes.

The selection condition $\cos(\theta) = 0.1$ and $PH_{\max} = PH_0 + 3 \cdot \sigma(PH_0)$ change results very much. Time-independent background as in Figure 4 was transformed to time-dependent function (Figure 5) at low-energy range.

The working selection $\cos(\theta) = 0.707$ and $PH_{\max} = PH_0 + 3 \cdot \sigma(PH_0)$ changed very much as did the high energetic part of TOF distribution (Figure 6). Background was reduced (practically concealed) in comparison with data in Figure 4.

Figure 4: TOF distributions without an additional selection

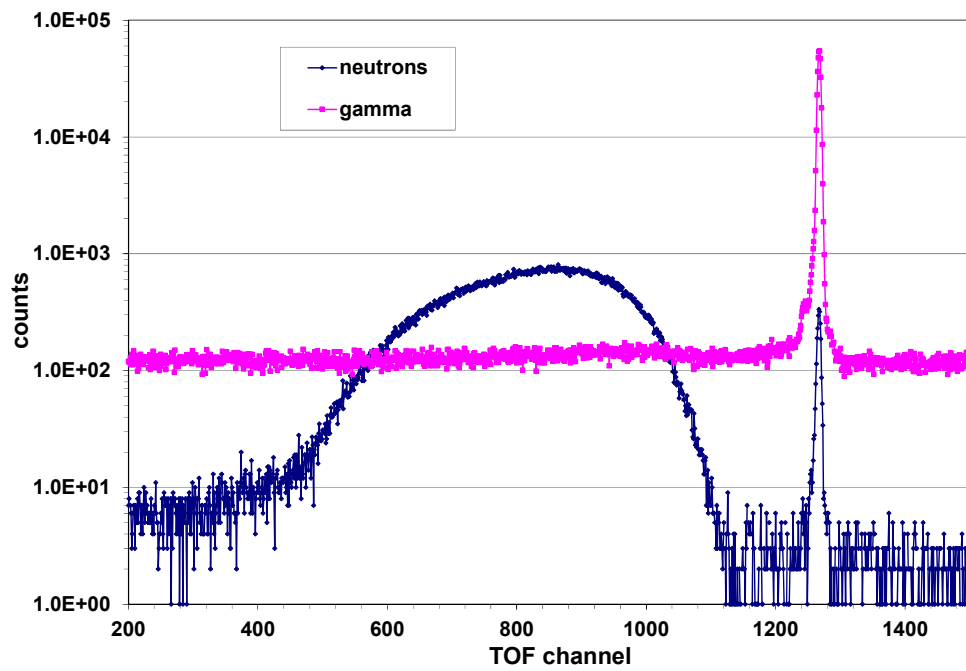


Figure 5: Selection for high-energy limit

$$\cos(\theta) = 0.1, PH_{\max} = PH_0 + 3\sigma(PH_0)$$

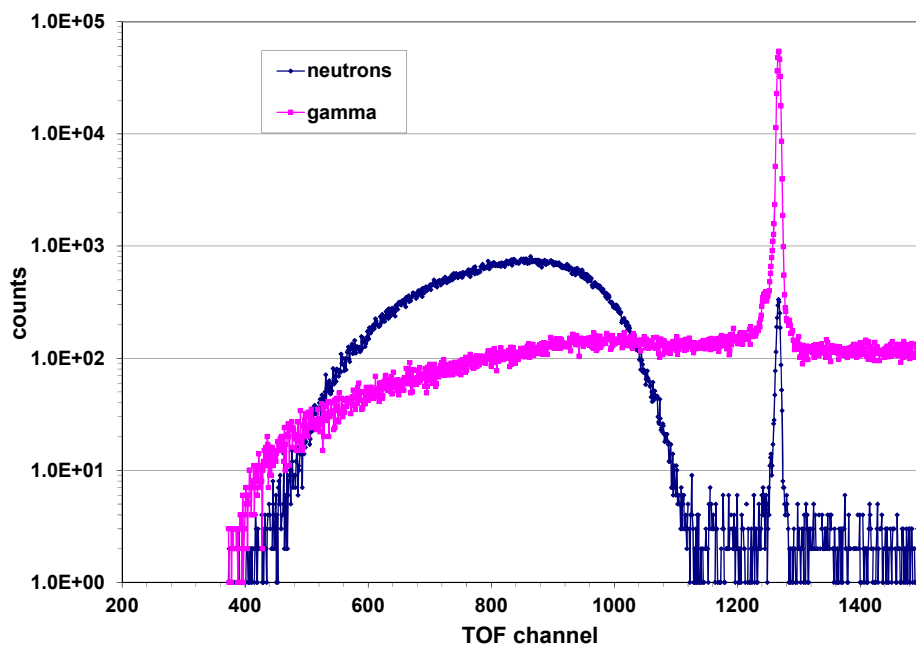
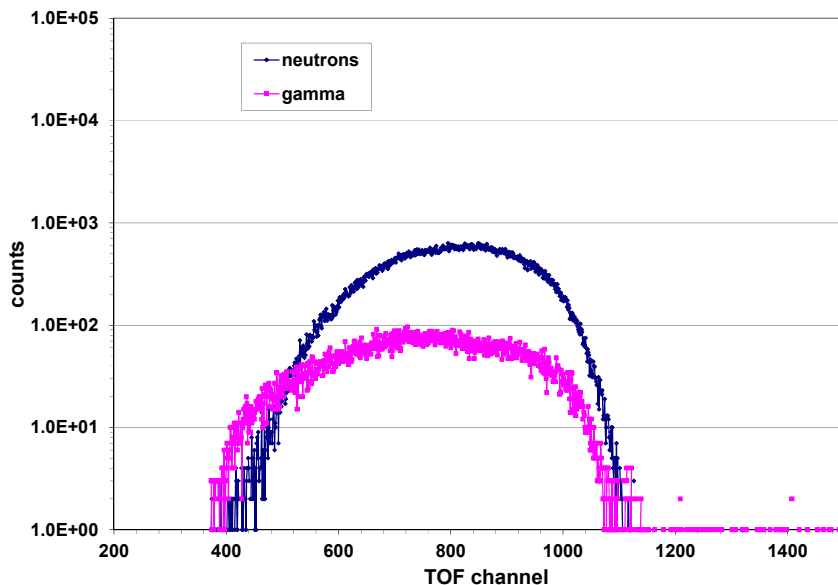


Figure 6: TOF spectra for working selection

$$\cos(\theta) = 0.707, PH_{\max} = PH_0 + 3 \cdot \sigma(PH_0)$$

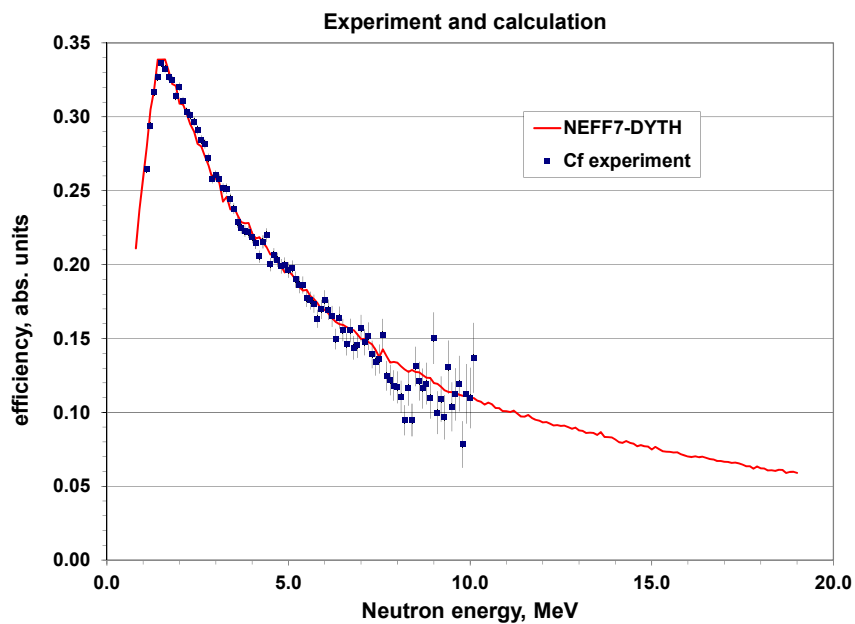


Experimental and calculated efficiency are shown in Figure 7. The average ratio is $R = E/C = 1.012 \pm 0.004$ for energy range 1.3-6 MeV. So, MC simulation reproduces the energy dependence and absolute value with high accuracy.

The resolution function is a very important parameter for MC simulation in the energy range $E_n < 2$ MeV. Calculated results are very sensitive to absolute value and energy dependence $\sigma(L)$.

Figure 7: Experimental and calculated efficiencies with dynamic threshold

MC simulation was multiplied with factor 1.012



Conclusions

- A method of dynamic threshold was developed for the NE213 detector and was investigated with a ²⁵²Cf neutron source. “A dynamically biased neutron detector” was realised in 1971 (Brandenberger and Grandy) for background reduction in TOF experiments. Our realisation and motivation are quite different. It should be emphasised that successful realisation of this method is not possible without an experimental light output function for a particular detector.
- The unique peculiarity of this method is that its application removes events connected with the (n,α) reaction in an organic scintillator. This allow to increase an accuracy for extrapolation of calculated data in the high-energy range 10-20 MeV.
- This method also reduces time-independent background, the contribution of neutron scattering on the detector environment and time resolution.
- In the whole energy range <20 MeV only one reaction (n,p)-scattering is responsible for formation of the detector efficiency after application of the dynamic threshold. It seems that the contribution of multiple scattering inside the detector, and interaction with the detector environment are much reduced. In the energy range <8 MeV the agreement between experimental and calculated results is perfect. Hence, we may expect that extrapolation to the energy range 10-20 MeV may also be done with high accuracy. However, detailed investigation of the uncertainties in the whole energy range is an important direction for future activities.
- This method is very useful for experimental investigations of inelastic neutron scattering on Fe, ²³⁸U nuclei at the incident energies 6-8 MeV, and ~14 MeV.

References

- Brandenberger, J.D. and T.B.Grandy (1971), *NIM*, 93, 495-508.
- Dietze, G. and H. Klein (1982), *Nucl. Instr. and Meth.*, 193, 549. See also G. Dietze and H. Klein (1982), PTB-ND-22, *Physikalisch-Technische Bundesanstalt*.
- Di Lullo, A.R., T. Mossey and S. Grimes (2008), *NSE*, 159, 349.
- Kornilov, N.V., *et al.* (2009), “Total Characterisation of Neutron Detector with Cf Source and a New Light Output Determination”, *NIMPR*, A (589), 222-233.
- Kornilov, N.V., *et al.* (2014), “New Method for Measurement of Neutron Detector Efficiency Up to 20 MeV”, *ND2013 Conference*, New York, United States, forthcoming.
- Kornilov, N.V., T. Massey and S. Grimes (2013), “Standard Neutron Sources for High Energies (Current Problem, How to Increase an Accuracy)”, *1st Meeting CRP on IRDFF Validation*, IAEA, Vienna, accessed 21 June 2014, <https://www-nds.iaea.org/publications/indc/indc-nds-0639.pdf>.
- Massey, T.N., *et al.* (1988), *NSE*, 129, 175.
- Meadows, J.W. (1991), ANL/NDM 124, Argonne National Laboratory, Argonne, IL.
- Randers-Pehrson, G., *et al.* (1983), *Nucl. Instr. and Meth.*, 215, 433-436.

General Interest – Part 1

Chair: M. Dunn

What is the proper evaluation method: Some basic considerations

Helmut Leeb, Georg Schnabel, Thomas Srdinko
Atominstytut, Technische Universität Wien
Vienna, Austria

Abstract

Recent developments and applications demand for an extension of the energy range and the inclusion of reliable uncertainty information in nuclear data libraries. Due to the scarcity of neutron-induced reaction data beyond 20 MeV the extension of the energy range up to at least 150 MeV is not trivial because the corresponding nuclear data evaluations depend heavily on nuclear models and proper evaluation methods are still under discussion. Restricting to evaluation techniques based on Bayesian statistics the influence of the a priori knowledge on the final result of the evaluation is considered. The study clearly indicates the need to account properly for the deficiencies of the nuclear model. Concerning the covariance matrices it is argued that they depend not only on the model, but also on the method of generation and an additional consent is required for the comparison of different evaluations of the same data sets.

Introduction

The availability of evaluated nuclear data of high quality is an important prerequisite for the development of novel nuclear technologies, construction of nuclear installations, determination of safety measures as well as medical and industrial applications. Hence there is a world wide effort to obtain consolidated data sets (i.e. cross-sections, spectra, etc.) which represent our best knowledge of observables relevant for the user community. For many key observables accurate and complete measurements have been performed or are planned. Including the new measurements an update of the consolidated data sets must be performed taking consistently into account all available previous data sets as well as the *a priori* knowledge usually expressed in terms of nuclear models and theory constraints. The consolidation process is usually denoted as nuclear data evaluation and provides a consistent set of values of observables as well as uncertainty estimates. Well known examples of such evaluations are the set of consistent fundamental constants (Mohr, Taylor and Newell, 2012) and the consolidated particle data (Beringer, *et al.*, 2012). In principle such an evaluation step is required for any scientific conclusion from experiment, but frequently one considers dedicated experiments with an almost unique interpretation where the evaluation step is trivial.

In this contribution we focus on nuclear data evaluation, which provides an extended set of nuclear cross-section data and spectra consistent with available experimental data and satisfying all basic principles (e.g. sum rules, unitarity, ...). As mentioned above there is a wide community of users in industry, medicine and science. Fuelled by recent developments in nuclear technology and accelerator applications there is a demand for an increased energy range (at least up to 150 MeV) and the inclusion of uncertainty information in nuclear data libraries. The latter is also driven by questions of optimisation

and consequently by economics. The extension of the energy range is not trivial because of the scarcity of experimental data sets at incident neutron energies beyond 20 MeV. Hence a corresponding evaluation relies heavily on the prior and thus on the nuclear model used. Despite the world-wide effort to develop proper methods for evaluations which rely heavily on nuclear models the problem is still not solved. A recent status review of the developed evaluation procedures is given in Bauge, *et al.* (2010). Among these the Bayesian techniques are most promising because they properly account for *a priori* knowledge in a natural way. Though the procedures are well defined, the meaning of the resulting uncertainty information in terms of probability is not fully clarified. Thus no established criteria are available for comparison and quality assessment at present.

In the following we study the properties of Bayesian evaluation techniques considering a specific example in order to obtain a deeper insight in the properties of the evaluation with regard to mean values and uncertainties. Therefore we briefly revisit the basics of Bayesian evaluation techniques in the next section. Specifically, for the example of a simple evaluation of some neutron-induced reaction channels of ^{181}Ta a careful analysis of mean values and covariance matrices is performed. This study clearly indicates the need to account for the deficiencies of models in nuclear data evaluations. In the subsequent section, *Open problems of nuclear data evaluation*, the impact of model defects as defined in Koning, Hilaire and Duijvestijn (2008) is discussed and open problems in covariance matrices are addressed. In the final section concluding remarks are given.

Bayesian evaluation techniques

Concept

It is the primary goal of nuclear data evaluation to provide the best knowledge of a given set of observables σ based on available measurements and *a priori* knowledge. The latter is of mathematical and/or physics nature and is an inherent feature of the involved nuclear models depending on a set of parameters \mathbf{x} .

Bayesian statistics is generally accepted as the proper means for a consistent combination of measured data and *a priori* knowledge. It is based on two simple principles, i.e.:

$$\textit{The sum rule:} \quad p(\mathbf{x}|M) + p(\bar{\mathbf{x}}|M) = 0 \quad (1)$$

$$\textit{The product rule:} \quad p(\mathbf{x}|\sigma M)p(\sigma|M) = p(\sigma|\mathbf{x}M)p(\mathbf{x}|M) \quad (2)$$

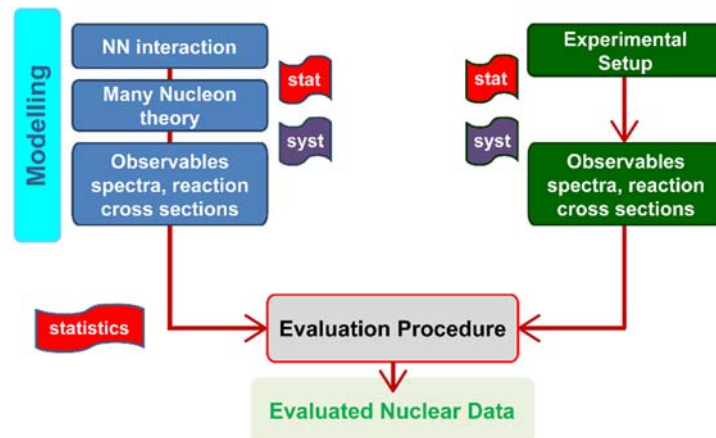
where $p(a|B)$ denotes a conditional probability density function (pdf) that an event a takes place if the condition B is true. Here, M refers to the specific nuclear model chosen. The basis of nuclear data evaluation is Bayes theorem:

$$p(\mathbf{x}|\sigma M) = C \cdot p(\sigma|\mathbf{x}M)p(\mathbf{x}|M) \quad (3)$$

which is a consequence of Eq. (2). It combines *a priori* knowledge given in terms of the prior pdf $p(\mathbf{x}|M)$ with experimental knowledge via the likelihood function $p(\sigma|\mathbf{x}M)$. The quantity C is a normalisation constant. Eq. (3) is the basic relation of Bayesian evaluation methods [see e.g. Bauge, *et al.* (2010)].

In the following we will use the so-called “Full Bayesian Evaluation Technique” (Leeb, Neudecker and Srdinko, 2008) for our considerations. As shown in Figure 1, a Bayesian evaluation procedure has two types of input, i.e. *i)* the experimental data and their uncertainties; *ii)* the *a priori* knowledge which is given in terms of nuclear models. Both informations are associated with probability density functions and determine via Eq. (3) the *a posteriori* pdf which in turn gives the mean values and the covariance matrices in the evaluation step.

Figure 1: General scheme of an evaluation procedure based on Bayesian statistics



Both the experimental data as well as the prior are subject to statistical uncertainties and therefore the evaluation in terms of Bayesian statistics is best suited. In addition systematic errors occur which are of non-statistical nature and require a special treatment (Leeb, Neudecker and Srdinko, 2008).

Properties of the evaluation

In order to reveal the generic properties of a Bayesian evaluation technique we study a simplified evaluation restricted to the total and differential elastic scattering cross-sections of neutrons incident on ^{181}Ta . The prior is generated by default calculations with TALYS-1.4 (Koning, Hilaire and Duijvestijn, 2008) and depends, apart from the compound-elastic contribution, only on the optical potential. The statistical uncertainties are generated by random variation of the parameters of the optical model. Actually a Monte Carlo technique is applied assuming a uniform distribution between physically reasonable defined boundaries. At first glance this seems to be an *ad hoc* procedure and a maximum entropy based method (Leeb and Pigni, 2006) should be more appropriate. However, it turned out that the prior is mainly affected by the selected boundaries of the parameters, while the probability density functions of the parameters are of minor importance. Experimental total cross-sections (Finlay, *et al.*, 1993) and differential elastic cross-sections (Smith, 2005) with properly estimated covariance matrices have been used for the evaluation. For the evaluation procedure we choose a reasonable mesh in energy $\{E_i\}$ and represent the angle integrated cross-sections $\sigma_c(E)$ with the help of spline functions. For the differential cross-section we choose the representation:

$$\frac{d\sigma}{d\Omega} = \sum_{\lambda} \alpha_{\lambda}(E) P_{\lambda}(\cos \vartheta) \quad (4)$$

where $P_{\lambda}(\cos \vartheta)$ are Legendre polynomials and $\alpha_{\lambda}(E)$ are coefficient functions which again are described by spline functions using the same energy mesh. It is important to remark that in this representation the values of $\sigma_c(E)$ and $\alpha_{\lambda}(E)$ at the mesh points $\{E_i\}$ act as the parameters of our “model” in the evaluation. Since a multivariate normal distribution is imposed for the cross-sections at the mesh points, sum rules are exactly maintained there. For a sufficiently dense grid this will also be true in good approximation in between the mesh points. The Bayesian evaluation procedure has been performed in its linearised version as outlined in Leeb, Neudecker and Srdinko (2008).

The results of this simple evaluation are displayed in Figures 2 and 3. In Figure 2 the prior of the differential elastic cross-section of n- ^{181}Ta and the corresponding evaluated data at $E=4.51$ MeV are shown. It is evident from Figure 2 that the evaluation

Figure 2: Comparison of experimental differential elastic n-¹⁸¹Ta cross-section of Smith (2005) at E = 4.51 MeV with (a) the prior cross-section and its uncertainty band and (b) the evaluated differential cross-section

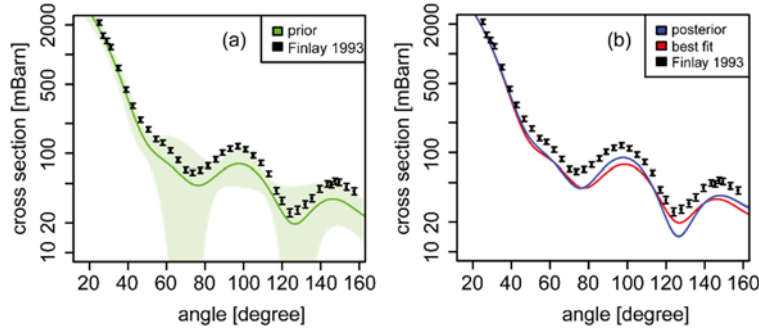
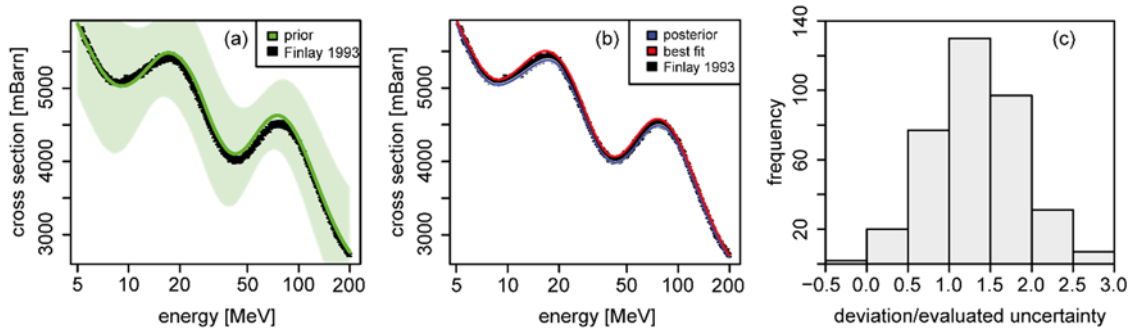


Figure 3: Experimental total n-¹⁸¹Ta cross-section (Finlay, *et al.*, 1993) compared with (a) the prior and (b) the evaluated cross-section; (c) deviation: evaluated from experimental one



underestimates the cross-section. The same is also found at other energies. There arises the question whether this behaviour is a specific feature of angle-differential data. Therefore we also took a closer look at the total cross-section shown in Figure 3. At first glance the evaluated total cross-section agrees extremely well with the experimental values. A more quantitative analysis given in the histogram, part (c) of Figure 3, reveals again a small but systematic underestimation of the total cross-section by the evaluation.

Hence the problem of systematic deviation of the evaluated cross-section from the mean of experimental data appears to be a general one and is not a specific feature of certain observables. In addition for both observables the evaluation leads to unrealistically small error bands. These observations jeopardise the usefulness of any evaluation and require a more careful analysis. With regard to a compact presentation we restrict the analysis here to the total cross-section.

In a first step we performed a principal component analysis of the prior covariance matrix of total cross-section uncertainties. The ordered eigenvalues, i.e. the variances in direction of the principal axes, are shown in Figure 4. In Figure 5 the 12 most important normalised eigenvectors $\phi_i(E)$ are displayed which reproduce the covariance matrix of total cross-section uncertainties better than 0.3%. From this consideration it is obvious that the evaluated total cross-section must be a superposition of the eigenvectors. In particular the mean value of the total cross-section of the prior is given by:

$$\sigma_{tot}(E) = \sum_{i=1}^K a_i \phi_i(E) \tag{5}$$

where K is the number of mesh points in energy. In Table 1 the coefficients a_i and their standard deviation are listed. For a model prior which gives a fair description of the experimental data the first 16 eigenstates will constitute the dominant contribution and uncertainty bands comparable to experimental capabilities will emerge. If the model prior significantly deviates from the experimental data the evaluated cross-section will be mainly composed of eigenstates with small variances. Therefore the covariance matrix of the evaluated total cross-section uncertainties will have unrealistically small variances. Consequently, these unrealistically small error bands reflect the deficiencies of the model and are not an indication of excellent knowledge of the observables.

The problem can be easily illustrated by a schematic example. Let us assume a model which allows constant energy-independent cross-sections denoted with $\mathbf{x}_{\text{prior}}$. The corresponding prior covariance matrix of cross-section uncertainties A_{prior} is of rank 1 with one eigenvector associated with a non-zero eigenvalue $n\delta_{\text{mod}}^2$, where n is the number of mesh points and δ_{mod}^2 is the variance at every mesh point. Furthermore we assume a set of experimental data \mathbf{y}_{exp} which exhibit an energy dependence and are

Figure 4: Eigenvalues of the prior covariance matrix (see text)

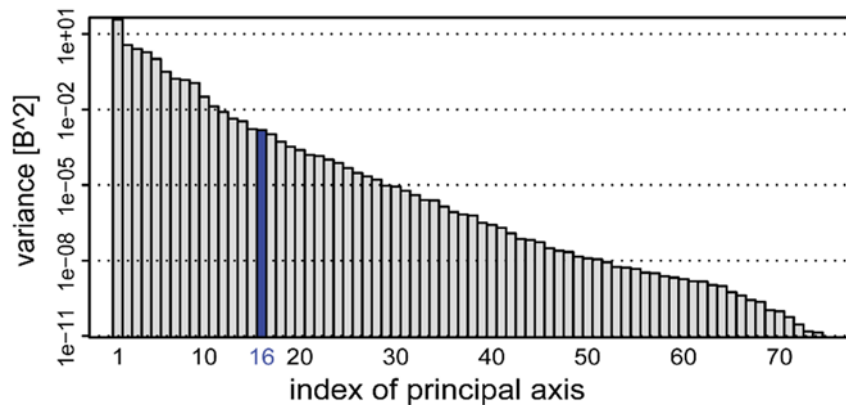


Figure 5: The first 12 normalised eigenvectors of the prior covariance matrix of total cross-section uncertainties

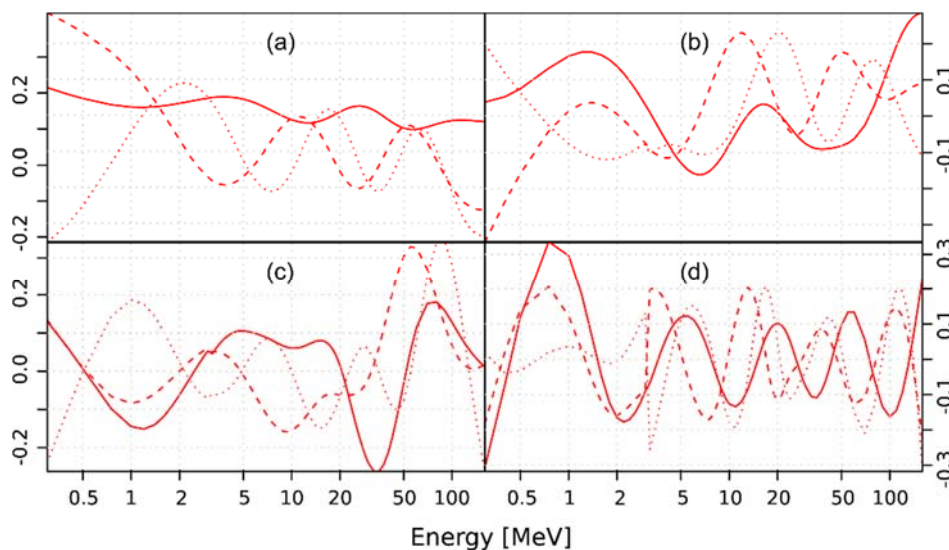


Table 1: Coefficients a_i and standard deviation Δa_i for the first 12 eigenvectors

“EV No.” (eigenvector number), “Line type” and “Part” (a), (b), (c) and (d) refer to Figure 5

Line type	Part (a)			Part (b)		
	EV No.	a_i (barn)	Δa_i (barn)	EV No.	a_i (barn)	Δa_i (barn)
Solid	1	48.669	6.122	4	1.415	1.377
Dashed	2	6.147	1.928	5	5.077	1.012
Dotted	3	1.378	1.599	6	0.752	0.564
Line type	Part (c)			Part (d)		
	EV No.	a_i (barn)	Δa_i (barn)	EV No.	a_i (barn)	Δa_i (barn)
Solid	7	1.112	0.411	10	0.165	0.180
Dashed	8	0.773	0.389	11	0.107	0.116
Dotted	9	0.665	0.336	12	0.041	0.090

given at the same mesh points as the model. The experimental covariance matrix B_{ij} may include a statistical error Δ_{stat}^2 and an overall normalisation error Δ_{syst}^2 affecting every experimental value:

$$B_{ij} = \Delta_{stat}^2 \delta_{ij} + \Delta_{syst}^2 \quad (6)$$

The corresponding sensitivity matrix is the identity. Thus the linearised update can be performed in closed form and yields the *a posteriori* covariance matrix:

$$A_{post} = \frac{1}{1 + \frac{n\delta_{mod}^2}{\Delta_{stat}^2 + n\Delta_{syst}^2}} A_{prior} = \frac{\delta_{mod}^2}{1 + \frac{n\delta_{mod}^2}{\Delta_{stat}^2 + n\Delta_{syst}^2}} \begin{pmatrix} 1 & 1 & \dots & 1 & 1 \\ 1 & 1 & & 1 & 1 \\ \vdots & & \ddots & & \vdots \\ 1 & 1 & & 1 & 1 \\ 1 & 1 & \dots & 1 & 1 \end{pmatrix} \quad (7)$$

This toy model shows several characteristic features. The posterior covariance matrix is completely determined by the uncertainty estimates of the model and the experiment. The mean value of the prior and the experimental value do not enter into the posterior covariance matrix. For vanishing systematic errors and $\delta_{mod} \gg \Delta_{stat}$ all elements of the posterior covariance matrix are Δ_{stat}^2/n and thus much smaller than the experimental uncertainties. For vanishing statistical error and $\delta_{mod} \gg \Delta_{syst}$ the evaluated uncertainty is approximately given by Δ_{syst} of the experiment. For an increasing number of experimental data the influence of the statistical error on the evaluated uncertainties vanishes.

Open problems of nuclear data evaluation

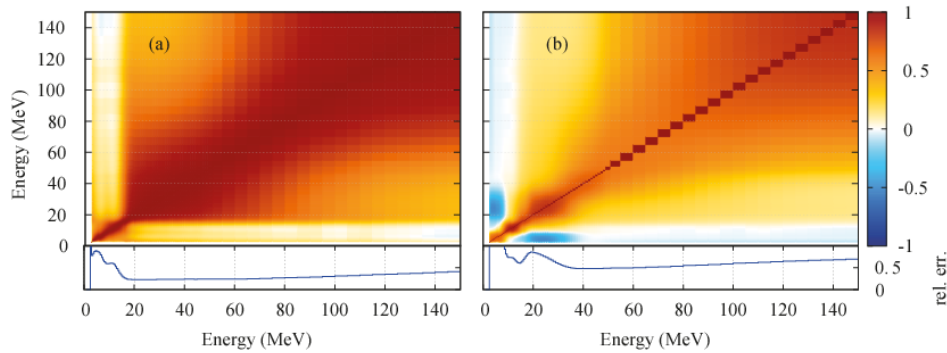
Accounting for model deficiencies

The considerations in the previous section clearly demonstrate the importance to account for deficiencies of the nuclear model in the evaluation procedure. In nuclear physics the occurrence of deficient descriptions is obvious because we deal with a many-body problem which cannot be solved in its full complexity. Hence nuclear models have been set up which describe part of the effects sufficiently well, while other aspects are not reproduced at all. A first systematic formulation of a covariance matrix associated

with model defects was given in Leeb, Neudecker and Srdinko (2008). An alternative procedure for model defects is used by Trkov, *et al.* (2011). The method of Leeb, Neudecker and Srdinko (2008) is based on a systematic comparison of experimental reaction data of neighbouring nuclei with model calculations. In this procedure it is inherently assumed that the model is equally well suited for these nuclei and reliable estimates of the deviations can be obtained. In Figure 6 a typical prior covariance matrix without and with model defects is shown for the $^{55}\text{Mn}(n,p)$ reaction cross-section uncertainties. The most important effect of model deficiencies on covariance matrices is obviously the reduction of correlations. Having this in mind we have repeated the simplified evaluation of $n\text{-}^{181}\text{Ta}$ with a non-correlated prior keeping only the diagonal elements. As expected we found in this case agreement of the evaluated cross-sections with the experimental data and the uncertainty bands remained in the order of the systematic errors of the experiments. Recently a more sophisticated study (Neudecker, Capote and Leeb, 2013) on $^{55}\text{Mn}(n,2n)$ reactions was presented which clearly demonstrates that the inclusion of model defects is essential to obtain reasonable error bars of the evaluated cross-sections. Apart from the success of available formulations to account for model deficiencies their use in complete evaluations is still questionable because violations of sum rules and unitarity may occur.

Figure 6: Correlation matrix and relative errors of the $^{55}\text{Mn}(n,p)$ cross-section

(a) Parameter uncertainties only, (b) model deficiencies included



Covariance matrices associated with modelling

The covariance matrices for experimental cross-section uncertainties are well defined by means of statistics. However the situation is more intriguing if we determine the covariance matrix starting from a nuclear model. This is easily seen, if we assume linear error propagation in the vicinity of the best set of parameters \mathbf{p} :

$$A_{x,x'} = \langle \Delta\sigma(x)\Delta\sigma(x') \rangle = \sum_{i,j=1}^N \frac{\partial\sigma(x,\mathbf{p})}{\partial p_i} \langle \Delta p_i \Delta p_j \rangle \frac{\partial\sigma(x,\mathbf{p})}{\partial p_j} \quad (8)$$

Here, it is assumed that the nuclear model depends on N parameters p_1, p_2, \dots, p_N and x and x' are values of the independent variable, e.g. the energy. At present the priors are usually generated by uncorrelated variation of the parameters p_i . However, one may use any other correlation of the parameters and obtain a different covariance matrix. This situation is not satisfactory with regard to comparison of evaluations and in particular for applications. Therefore additional criteria would be useful to classify evaluations.

The previous question is not trivial and depends on the quality of the model with regard to physics. Let us assume that we know for a given observable $y(x)$ the true physics description $y(x) = f(x,\mathbf{p})$, where \mathbf{p} are N parameters and x is the independent variable, e.g. the energy. In general the physics description is very involved and therefore

we prefer to use a model description $y(x) = g(x, \mathbf{q})$ which depends on M parameters \mathbf{q} and is easier to evaluate. On a given mesh $\{x\}$ the model yields the same values of the observable as the complete physics description. Introducing parameter covariance matrices and associated sensitivity matrices:

$$F_{i,j} = \langle \Delta p_i \Delta p_j \rangle, S_{i,j} = \frac{\partial f(x_i, \mathbf{p})}{\partial p_j} \text{ and } G_{i,j} = \langle \Delta q_i \Delta q_j \rangle, R_{i,j} = \frac{\partial g(x_i, \mathbf{q})}{\partial q_j} \quad (9)$$

one obtains the covariance $A^{\text{phy}} = S F S^T$ and $A^{\text{mod}} = R G R^T$ for the physics and the model description, respectively. Requiring that both covariance matrices are equal, $A^{\text{phy}} = A^{\text{mod}}$, and assuming a diagonal matrix F implies different correlations of the model parameters. In particular if the model space is larger than the physics dependences the matrix G must contain dependences. In the case that the model space is too small, the model parameter covariance matrix G is a projection of F . Hence the quality of the model has also an impact on the proper covariance matrix.

Conclusions

It has been the primary goal of this contribution to reveal basic features of a Bayesian evaluation process. In particular we have shown in an example that the evaluation based on the generation of prior covariance matrices via parameter variation may yield questionable results with respect to mean values and uncertainties. This is also true if within the model a perfect description of the experimental data is in principle possible but unlikely. Especially the variances of the evaluation may result unrealistically small. This is not a failure of the Bayesian approach, but reflects the fact that the evaluated covariance matrices are always obtained for a specific model as indicated by the symbol M in Eq. (3). Our considerations clearly indicate the necessity to account for model deficiencies in the evaluation process. These model deficiencies lead to reduced correlations of the covariance matrices. The use of available formulations of model deficiencies is very promising, but still has the drawback that basic features, e.g. sum rules, are violated in complete evaluations. Therefore work is in progress to find better formulations which solve this problem.

In addition we pointed out that the generation of covariance matrices from nuclear models are not uniquely defined. Additional criteria are needed to classify evaluations with respect to their uncertainties. It is also argued that the quality of the model has to be taken into account in these considerations.

In summary for the quality of an evaluation strongly based on nuclear models it is important to use the best available physics description. Thus model deficiencies will become small, but are still required to accomplish reliable evaluations. In fact nuclear data evaluation is a challenge for both experimental and theory research. In this context the CIELO project is an important initiative which will provide not only better evaluations for selected nuclei, but also deeper insight into their physics.

Acknowledgements

Work has been supported by EURATOM via the specific grant of the Fusion for Energy Partnership Agreement F4E-FPA-168. The views and opinions expressed herein do not necessarily reflect those of the European Commission.

References

- Bauge, E., *et al.* (2011), *Covariance Data in the Fast Neutron Region*, International Evaluation Co-operation, Vol. 24, NEA/NSC/WPEC/DOC/(2010)427, OECD/NEA, Paris.
- Beringer, J. *et al.* (2012), “Review of Particle Physics”, *Phys. Rev. D*, 86, 010001.
- Finlay, R.W., *et al.* (1993), “Neutron Total Cross Sections at Intermediate Energies”, *Phys. Rev. C*, 47, pp. 237-247.
- Koning, A.J., S. Hilaire and M.C. Duijvestijn (2008), “TALYS-1.0”, *Proceedings of the International Conference on Nuclear Data for Science and Technology*, Nice, France, 22-27 April 2007, O. Bersillon, *et al.* (eds.), EDP Sciences, pp. 211-214.
- Leeb, H., D. Neudecker and T. Srdinko (2008), “Consistent Procedure for Nuclear Data Evaluation Based on Modelling”, *Nucl. Data Sheets*, 109, pp. 2762-2767.
- Leeb, H. and M.T. Pigni (2006), “Basic Statistics and Consistent Covariances for Nuclear Data Files”, *Proceedings of the Workshop on Perspectives of Nuclear Data in the Next Decade*, Bruyères-le-Châtel, France, E. Bauge (ed.), NEA No. 6121, OECD/NEA, Paris, pp. 235-242.
- Mohr, P.J., B.N. Taylor and D.B. Newell (2012), “CODATA Recommended Values of the Fundamental Physical Constants: 2010”, *Rev. Mod. Phys.*, 84, pp. 1527-1605.
- Neudecker, D., R. Capote and H. Leeb (2013), “Impact of Model Defect and Experimental Uncertainties on Evaluated Output”, *Nucl. Instr. Meth. A*, 723, pp. 163-172.
- Smith, A.B. (2005), “Fast Neutrons Incident on Rotors: Tantalum”, *Annals of Nuclear Energy*, 32, pp. 1926-1952.
- Trkov, A., *et al.* (2011), “Covariances of Evaluated Nuclear Cross Section Data for ^{232}Th , $^{180,182,183,184,186}\text{W}$ and ^{55}Mn ”, *Nuclear Data Sheets*, 112, pp. 3098-3119.

Data mining the EXFOR database

David Brown,^a John Hirdt,^b Michal Herman^a

^aNational Nuclear Data Center, Brookhaven National Laboratory, Upton, NY, United States

^bSaint Joseph's College, Patchogue, NY, United States

Abstract

The EXFOR database contains the largest collection of experimental nuclear reaction data available as well as this data's bibliographic information and experimental details. We created an undirected graph from the EXFOR datasets with graph nodes representing single observables and graph links representing the connections of various types between these observables. This graph is an abstract representation of the connections in EXFOR, similar to graphs of social networks, authorship networks, etc. Analysing this abstract graph, we are able to address very specific questions such as: i) What observables are being used as reference measurements by the experimental community? ii) Are these observables given the attention needed by various standards organisations? iii) Are there classes of observables that are not connected to these reference measurements? In addressing these questions, we propose several (mostly cross-section) observables that should be evaluated and made into reaction reference standards.

Introduction

The EXFOR nuclear experimental database provides the data which underpins nearly all evaluated neutron and charged particle evaluations in the ENDF-formatted nuclear data library (e.g. ENDF/B, JEFF, JENDL, ...). Therefore, EXFOR is in many ways the “mother library” which leads to the data used in all applications in nuclear power, security, nuclear medicine, etc. The EXFOR database includes a complete compilation of experimental neutron-induced data, a selected compilation of charged-particle-induced data, a selected compilation of photon-induced reaction data, and assorted high-energy and heavy-ion reaction data. The EXFOR library is the most comprehensive collection of experimental nuclear data available so it is the best place to look for an overview of what the applied and basic experimental community feels are valuable experimental reactions and quantities.

The basic unit of EXFOR is an ENTRY. An entry corresponds to one experiment and contains the numerical data along with the related bibliographic information and a brief description of the experimental method. An entry is typically divided in several subentries (SUBENT) containing the various data tables resulting from the experiment. Each SUBENT contains within it a REACTION field which encodes what reaction was studied [e.g. $^1\text{H}(n,\text{el})$] and what quantity was measured (e.g. cross-section). A SUBENT may also contain a MONITOR field which encodes a second well-characterised reaction and quantity used to reduce or eliminate systematic experimental errors. Often the measured data encoded in the REACTION field is measured relative to the reaction/quantity encoded in the MONITOR field. There is usually a straightforward mapping between the reactions/quantities measured in EXFOR and the evaluated reactions/quantities stored in the ENDF libraries.

Several specific reaction/quantities are important enough, usually because of one or more specific applications, that the nuclear data community has elevated them to the level of an international reference standard. Carlson, *et al.* (2009), Mughabghab (2006) and Oblozinsky (2001) provide details of the well-known neutron-induced, charged-particle and photonuclear standard reaction/quantities. There is also a new standards-level effort just beginning known as the CIELO pilot project (Chadwick, *et al.*, 2013), which promises to entire generate standards-level evaluations, including all reactions/quantities needs for the ENDF-formatted libraries for neutron-induced reactions on ^1H , ^{16}O , ^{56}Fe , ^{235}U , ^{238}U and ^{239}Pu .

In this work, we take a somewhat abstract view of the EXFOR database and generate an undirected graph describing all the connections between reactions/quantities in the EXFOR database. From just these connections, we can infer what reactions/quantities the nuclear data community collectively (and somewhat unconsciously) views as important. This set of reactions/quantities does not exactly match our previous expectations. We will provide a series of recommendations for reactions/quantities that should also be elevated to the level of the standards in Carlson, *et al.* (2009), Mughabghab (2006), Oblozinsky (2001) and Chadwick, *et al.* (2013) and possibly included in a follow-up CIELO project.











Building the graph

As each EXFOR SUBENT corresponds to one measured data set and each SUBENT contains exactly one REACTION field, we will focus on the REACTION fields. Each SUBENT may also contain a MONITOR field which we also note. Both REACTION and MONITOR fields have essentially the same format and contain much the same information. The MONITOR field may also contain other free-text information detailing how the monitor was used and we ignore this information. An example of a simple measurement is:

$$(1\text{-H-1(N,TOT),,SIG,,MXW}) \quad (1)$$

This REACTION field tells us that the $^1\text{H}(n,\text{tot})$ Maxwellian (MXW) averaged cross-section (SIG) was measured in the associated SUBENT. In our graph, we consider each of these elementary reaction/quantities in REACTION or MONITOR fields to be nodes. Table 1 lists all of the types of nodes. In this table, the nodes are coloured by whether they correspond to one of the standards in the various standards efforts (Carlson, *et al.*, 2009; Mughabghab, 2006; Oblozinsky, 2001; Chadwick, *et al.*, 2013).

Table 1: Types of nodes

Description	Example
Regular node	
CIELO isotope	
ENDF/B-VII.1 standards	
Standards proposed at IAEA Technical Meeting, July 2013	
Standards proposed in the past/proposed by us	 
Mughabghab, S.F., <i>Atlas of Neutron Resonances</i>	
Diagnostic radioisotopes and monitor reactions	
Isomer target	
Elemental target	

The nodes in our graph are connected by edges. Types of edges considered are listed in Table 2. By far the most common type of edge in our graph is the MONITOR-REACTION connection. However, the EXFOR format provides several other connections between elementary nodes. REACTION and MONITOR fields may also contain mathematical relations, e.g.:

$$(3\text{-LI-6(N,T)2-HE-4,,SIG,,SPA)/(92-U-235(N,F),,SIG,,SPA) \quad (2)$$

Here, this field tells us that the ratio of $6\text{Li}(n,t)$ and $^{235}\text{U}(n,f)$ spectrum averaged cross-sections was measured. Any relation using +, -, *, /, //, = are allowed in the REACTION and MONITOR fields. EXFOR also allows what we call “isomer math”:

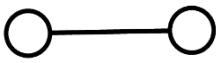



$$(72\text{-HF-177(N,G)72-HF-178-M/T,,SIG/RAT) \quad (3)$$

Here, what was measured was the ratio of $^{177}\text{Hf}(n,g)^{178\text{m}}\text{Hf}$ cross-section to the total of $^{177}\text{Hf}(n,g)^{178\text{m}}\text{Hf}$ and $^{177}\text{Hf}(n,g)^{178\text{g}}\text{Hf}$ cross-sections. There are several other EXFOR quantities which have special meanings and are actually simply mathematical relations:

- ALF: capture-to-fission ratio;
- ETA: average neutron yield per non-elastic event for n-induced reactions;
- RI: resonance integral;
- NON, INEL, SCT: all obey sum rules.

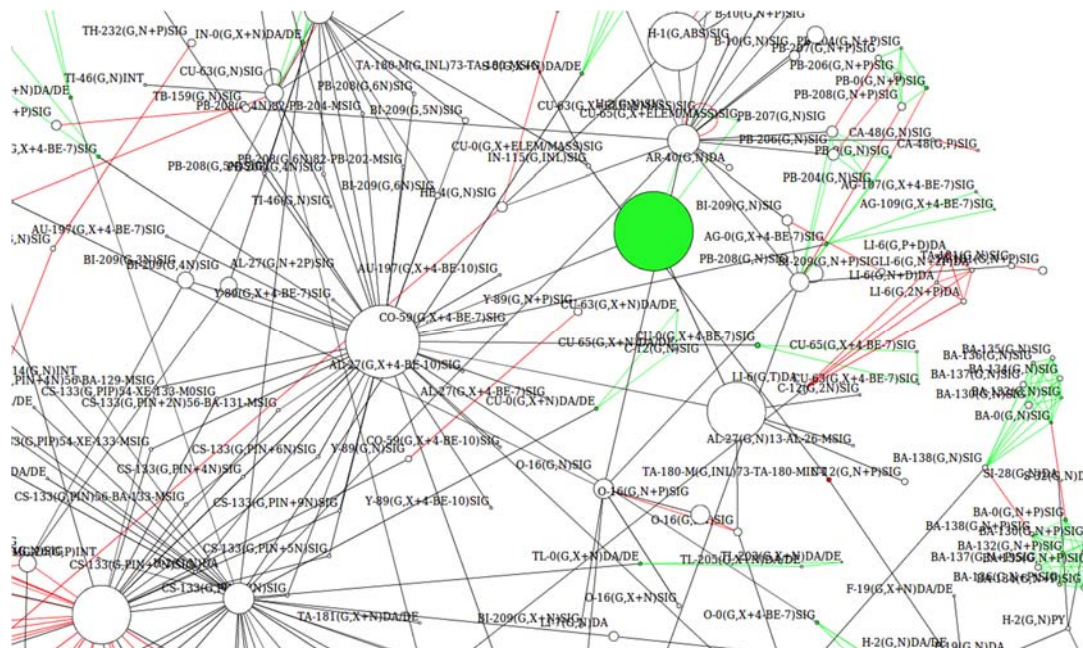
We also consider all reactions/quantities covered by the CIELO pilot project and link all reaction/quantities corresponding to a CIELO isotope. Finally, as an element is an abundance weighted sum of the isotopes that make up the element, we link any reaction/quantity on an elemental target to the corresponding isotopic reaction/quantities.

Table 2: Types of edges

Edge type	Description	Example
MONITOR	Typically a, well characterised reaction used to reduce or eliminate systematic experimental errors.	
Mathematical relation (e.g. “isomer math”; sum rules; math is REACTION string; ALF, ETA, etc.)	Connections representing a simple ratio or a more complex mathematical equation.	
Neutron standards/CIELO	All evaluated simultaneously and therefore are linked.	
Elemental	Data on an elemental target is connected to every stable isotope of the element for the same measurement.	

We used the x4i code (Brown, 2011) to read the EXFOR database and parse the REACTION and MONITOR strings. We then built up the undirected graph within x4i and stored the resulting graph in a graphml formatted file. The full graph has 87 925 nodes and 276 852 edges. We then studied this graph with the NetworkX (Hagberg, *et al.*, 2013) and graph-tool (Peixoto, 2013) codes. With graph-tool, we were able to visualise portions of the graph and this is shown in Figure 1. The final graph is too large and fully connected to visualise with currently available tools. Unfortunately, we were not able to visualise the portion of the graph that contains the majority of the standards and CIELO nodes.

Figure 1: A portion of the second-largest cluster in the graph



Analysing the graph

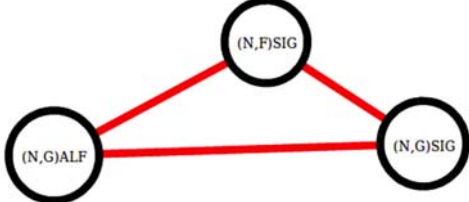
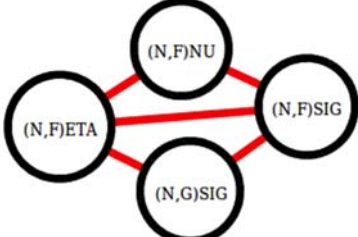
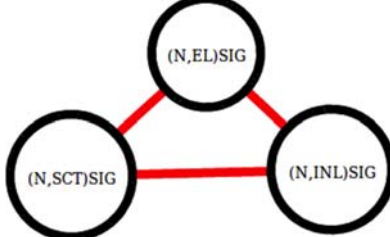
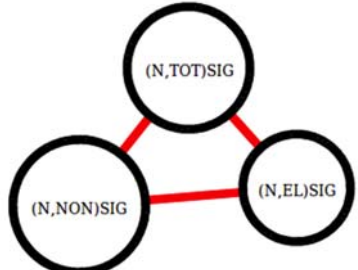

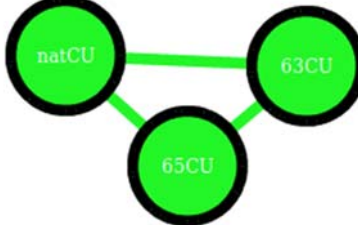
Gross features of the graph

The graph is not fully connected and the probability that any two nodes connected is $7.162e-05$. There are 23 196 isolated nodes. These nodes correspond to experiments that purport to be absolute measurements. Aside from these nodes, the graph is arranged in series of clusters. Figure 1 is a close-up of the second-largest cluster, containing 488 nodes, 977 edges and mostly photonuclear data. The largest cluster contains 35 410 nodes, including all of our standards nodes and is clearly less than half of all nodes in the graph. Two other large clusters of note are the third largest with 164 nodes, 460 edges and thick-target yield data, and the fourth largest with 149 nodes, 294 edges and charged pion scattering. We wonder if all of the disconnected nodes and clusters are as disconnected as our simple analysis implies. Also, if they are, should they really remain disconnected? A reaction/quantity pinned to a standard is often in better shape than an absolute measurement.

There are many repeating patterns in our graph. In graph theory literature these patterns are known as motifs. We tabulate the motifs in our graph in Table 3. In all cases, they correspond to clusters of nodes we imposed on the graph either to encode the special EXFOR quantities or elemental data.

We also note that our graph has several self-loops. These are cases where a node connects to itself. This is caused by a bug in our graph generation code and will be removed before final publication. These self-loops are small in number and do not affect our central results.

Table 3: Reoccurring motifs in the graph

EXFOR quantity	Definition	Example
ALF	σ_γ/σ_f	
ETA	$\bar{\nu}\sigma_f/(\sigma_\gamma + \sigma_f)$	
SCT	$\sigma_{el} + \sigma_{inel}$	
NON	$\sigma_{tot} + \sigma_{el}$	
RI	$\int_0^\infty dE \frac{\sigma(E)}{E}$	
Elemental	$\sum_i \omega_f \sigma_i(E)$	

Discerning the important nodes

We now discuss which nodes are most important. There are several ways we could rank the elementary reaction/quantities by importance and the most obvious is just counting the number of measurements of each reaction/quantity. We could also rank the elementary reaction/quantities by number of connections to an elementary reaction/quantity. The number of connections to a node is known as the node degree. In Table 4, we list the most important nodes' rank ordered by degree. Interestingly, the top four nodes by degree or number of measurements are the same, although the rank order is different. Also interesting is the fact that seven of the top twenty reactions/quantities are not addressed by any standards effort.

Table 4: Top twenty nodes in graph ranked by degree

Node	# measurements	Degree	Note
$^{27}\text{Al}(p,X+^{22}\text{Na}): \sigma$	3 806	2 276	IAEA charged-particle monitor
$^{27}\text{Al}(p,X+^{24}\text{Na}): \sigma$	3 626	2 122	IAEA charged-particle monitor
$^{27}\text{Al}(p,n+3p): \sigma$	2 316	1 535	
$^{27}\text{Al}(n,\alpha): \sigma$	5 049	1 281	
$^1\text{H}(n,\text{el}): \sigma$	2 903	1 207	ENDF neutron standard/CIELO
$^{197}\text{Au}(n,\gamma): \sigma$	4 106	1 073	ENDF/ <i>Atlas</i> neutron standard
$^1\text{H}(n,\text{el}): d\sigma/d\Omega$	2 601	953	ENDF neutron standard/CIELO
$^{56}\text{Fe}(n,p)^{56}\text{Mn}: \sigma$	2 272	833	CIELO
$^{235}\text{U}(n,f): \sigma$	3 707	774	ENDF neutron standard/CIELO
$^{93}\text{Nb}(n,2n)^{92}\text{mNb}: \sigma$	2 465	710	
$^{\text{nat}}\text{Cu}(p,X+^{65}\text{Zn}): \sigma$	1 899	627	IAEA charged-particle monitor
$^{27}\text{Al}(^{12}\text{C},X+^{24}\text{Na}): \sigma$	1 060	610	
$^{\text{nat}}\text{Mo}(p,X+^{96}\text{Tc}): \sigma$	1 109	600	
$^{\text{nat}}\text{Mo}(p,X+^{97}\text{Ru}): \sigma$	547	594	
$^{59}\text{Co}(n,\gamma): \sigma$	1 332	578	<i>Atlas</i> neutron standard
$^{27}\text{Al}(n,p)^{27}\text{Mg}: \sigma$	1 902	544	
$^{238}\text{U}(n,f): \sigma$	1 394	511	ENDF neutron standard/CIELO
$^{27}\text{Al}(d,X+^{24}\text{Na}): \sigma$	990	507	IAEA charged-particle monitor
$^{197}\text{Au}(n,\gamma): \text{RI}$	1 961	440	ENDF/ <i>Atlas</i> neutron standard
$^{10}\text{B}(n,\alpha): \sigma$	860	432	ENDF neutron standard

We attempted to confirm this with several other measure of node importance including node centrality, betweenness and eigenvalue centrality (Brown, 2011; Hagberg, *et al.*, 2013). All of these measures fail for our graph because the graph is too large. All of these measures rely on performing complex linear algebra on the adjacency matrix of the graph. The adjacency matrix is the matrix that one constructs by associating each node with a column/row. For node i , the adjacency matrix A_{ij} is defined as $A_{ij} = 1$ if node i is connected to node j and 0 otherwise. The adjacency matrix is a $87\,925 \times 87\,925$ sparse matrix for our graph, and is a challenge for most off-the-shelf linear algebra packages.

There is one measure, Google's PageRank (Brown, 2011; Hagberg, *et al.*, 2013), which can be used on our graph. PageRank is an iterative process to determine what the probability is that a given node is connected. The exact algorithm is given in many places and is implemented in the codes we used for our analysis (Brown, 2011; Hagberg, *et al.*, 2013). This algorithm is robust and simple and can work on graphs as large as the entire Internet. When using PageRank, we confirm the importance of the Al, Mo and Nb reactions/quantities noted in Table 4.

Conclusion

It is clear from the analysis of our graph that the following reaction/quantities have outsized importance and they are not considered in any standards effort:

- Aluminium reaction/quantities:
 - $n+^{27}\text{Al}$: (n, α), (n,p) cross-sections;
 - $p+^{27}\text{Al}$: (n,n+3p) cross-section and ^{22}Na and ^{24}Na production cross-sections;
 - $^{12}\text{C}+^{27}\text{Al}$: ^{24}Na production cross-section.
- Molybdenum and niobium also very important structural materials:
 - $n+^{93}\text{Nb}$: $^{93}\text{Nb}(n,2n)^{92\text{m}}\text{Nb}$ cross-section;
 - $p+^{\text{nat}}\text{Mo}$: ^{96}Tc and ^{97}Ru production cross-section.

We recommend that at the very least that ^{27}Al , ^{93}Nb and all of the Mo isotopes be considered as a target material in any CIELO follow-up project.

Acknowledgements

The work at Brookhaven National Laboratory was sponsored by the Office of Nuclear Physics, Office of Science of the United States Department of Energy under contract No. DE-AC02-98CH10886 with Brookhaven Science Associates, LLC. This project was supported in part by the United States Department of Energy, Office of Science, Office of Workforce Development for Teachers and Scientists (WDTS) under the Science Undergraduate Laboratory Internships Program (SULI).

References

- Brown, D.A., (2011), "x4i: The EXFOR interface", <https://ndclx4.bnl.gov/gf/project/x4i>.
- Carlson, A.D., *et al.* (2009), "International Evaluation of Neutron Cross Section Standards", *Nucl. Data Sheets*, 110.12, pp. 3215-3324.
- Chadwick, M.B., *et al.* (2013), "CIELO: A Future Collaborative International Evaluated Library", *Proc. of the International Conference of Nuclear Data for Science and Technology (ND2013)*.
- Hagberg, A., *et al.* (2013), "NetworkX version 1.8", <http://networkx.github.io>.

Mughabghab, S.F. (2006), *Atlas of Neutron Resonances*, Elsevier Science.

Oblozinsky, P. (2001), *Charged Particle Cross-Section Database for Medical Radioisotope Production: Diagnostic Radioisotopes and Monitor Reactions*, IAEA-TECDOC-1211, International Atomic Energy Agency (IAEA), Vienna, accessed 5 June 2014, www-nds.iaea.org/medical.

Peixoto, T.P. (2013), “graph-tool version 2.2.26”, <http://graph-tool.skewed.de>.

General Interest – Part 2

Chair: P. Schillebeeckx

Fission measurements at the n_TOF facility with a PPAC detection set-up

C. Paradela,^{a,*} L. Audouin,^b I. Durán,^a E. Leal-Cidoncha,^a
L.S. Leong,^b D. Tarrío,^{a,c} L. Tassan-Got,^b n_TOF Collaboration

^aUniversidad de Santiago de Compostela, Santiago de Compostela, Spain

^bCentre National de la Recherche Scientifique/IN2P3, IPN, Orsay, France

^cDepartment of Physics and Astronomy, Uppsala University, Uppsala, Sweden

Abstract

Over the past years, fission cross-section data have been measured at the CERN n_TOF facility by using two different detection set-ups based on parallel plate avalanche counters (PPAC). The current set-up also provides the full fission fragment angular distribution which improves the accuracy of the fission cross-section measured.

Introduction

The n_TOF facility at CERN (Guerrero, *et al.*, 2013) is a unique facility providing an intense neutron flux in the wide energy range from thermal to GeV neutrons. During the past decade an extensive experimental campaign has been developed at the CERN n_TOF facility with the aim of improving the existing nuclear data required for the development of future nuclear reactors and nuclear waste incineration.

In particular, fission measurements have been performed with three different types of detectors: a classical ionisation chamber (Calviani, *et al.*, 2008), MicroMegas detector (Andriamonje, *et al.*, 2011) and parallel plate avalanche counters (PPAC) (Paradela, *et al.*, 2011a). The results obtained with the PPAC-based detection set-up, mainly focused on the isotopes related with the thorium fuel cycle, are reviewed in this work.

Characteristics of the detection set-up

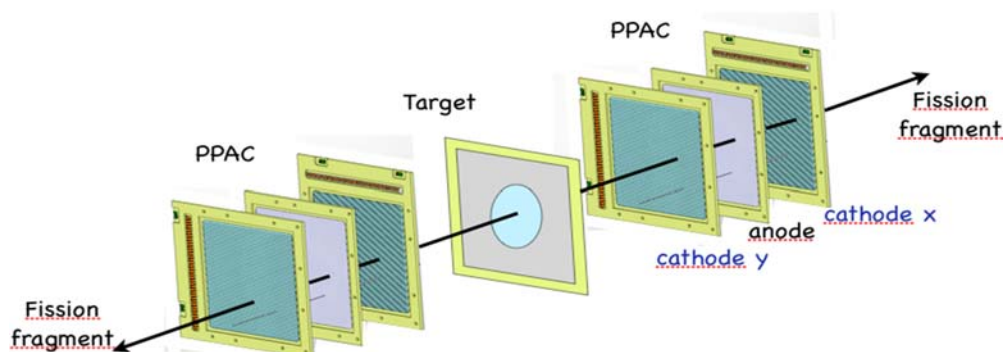
PPAC are gas detectors usually used for tracking relativistic heavy ion beams in radioactive beam facilities such as GSI (Stelzer, 1976) or RIKEN (Kumagai, *et al.*, 2001). n_TOF PPAC are very thin detectors having only a few layers of aluminised Mylar resulting in a minimum amount of scattered neutrons. The low pressure gas (4 mbar of C₃F₈) and the small gap thickness (3 mm) result in high reduced electric fields, producing a very fast signal collected in the central anode. In addition, two stripped cathodes with delay line read-outs provide the position where the fragment hits.

In our set-up, each target is flanked by two PPAC, as shown in Figure 1. Thus, both fission fragments are detected in time coincidence and the trajectory can be reconstructed.

* Current position: EC-JRC-IRMM, Geel, Belgium.

Figure 1: Schematic picture of two PPAC sandwiching the fission target

The separation between the detector layers has been magnified to better observe the details



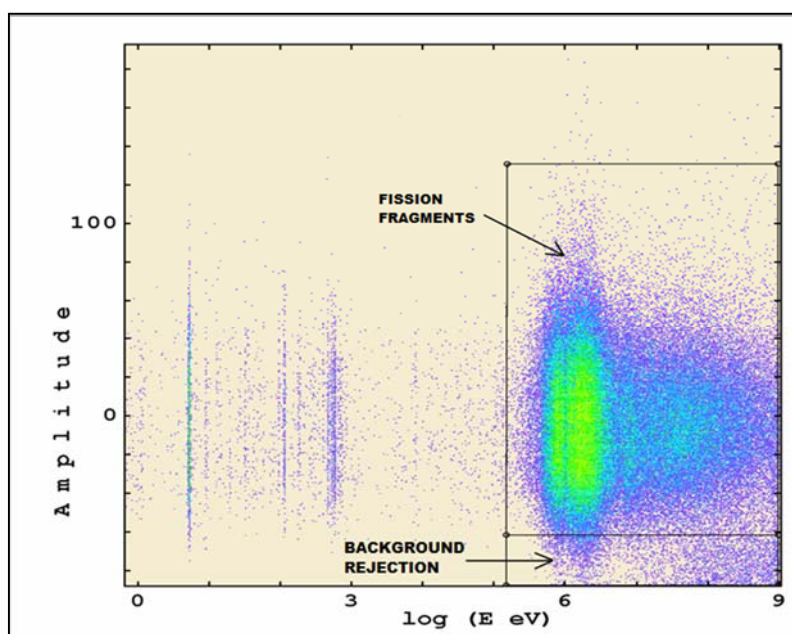
The targets and their backings must also be very thin in order to detect both fragments with the higher efficiency. To provide accurate cross-sections, target masses and other characteristics such as homogeneity, impurities or oxygen content in the sample are carefully characterised by alpha counting and the Rutherford Backscattering (RBS) method.

Data analysis

The coincidence method is extremely powerful in order to discriminate the fission events from the background coming from the samples' radioactivity or from the spallation reactions produced by high-energy neutrons in the different set-up layers. As can be observed in Figure 2, most of the low amplitude signals related with these background events disappear when the coincidence between the two next detectors is required.

Figure 2: Discrimination of fission events after applying the coincidence method

Low signal amplitude signals due to ^{234}U sample activity and spallation reactions are strongly rejected



In addition, both amplitude signals are also registered so that they can be combined for a further selection of fission events, rejecting most of the random coincidences occurring for the shortest time-of-flights.

On the other hand, trajectory reconstruction of the fission fragments is obtained from the time difference between each couple of cathode signals. We can obtain the horizontal and the vertical position using both detector cathodes and, therefore, the trajectory is determined assuming back-to-back emission of the fragments. At high neutron energies (>20 MeV) some corrections are required to take into account the nucleus recoil due to the linear momentum transfer from the neutron. This information not only provides the emission angle, but also the emission position in the target, which allows us to study the beam profile evolution with the energy.

The angular acceptance of the set-up is dominated by the larger absorption of the fission fragments for increasing angles; in the former PPAC configuration it was limited to less than 60° with respect to the beam axis. Therefore, the full angular distribution for the fission fragments could not be covered. To obtain the cross-section, this angular dependence of the efficiency must be corrected taking into account the anisotropic emission of the fission fragments which strongly depends on the target nucleus and the neutron energy. In Paradela, *et al.* (2010) and Tarrío, *et al.* (2011), the anisotropy of each isotope has been obtained from the experimental data base EXFOR (NNDC, 2009) for each isotope, extrapolating at high energies where no data were available.

Results during n_TOF Phase I

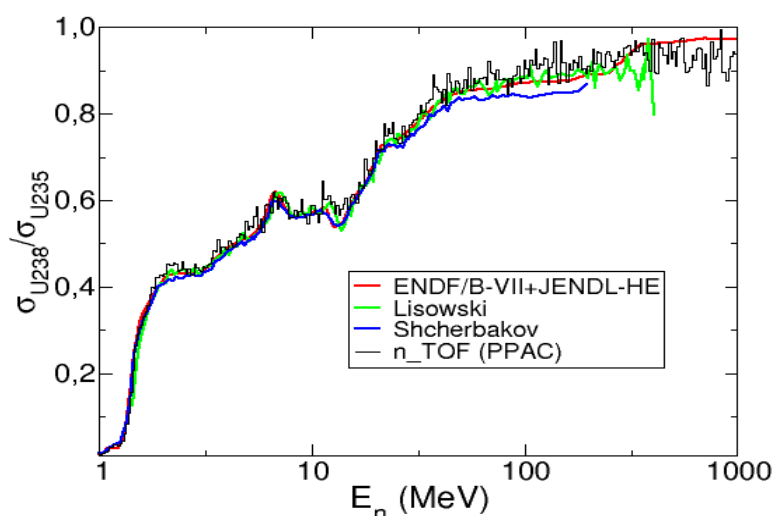
During fission campaigns at 2002 and 2003 up to eight different isotopes were measured with this experimental set-up, including ^{234}U , ^{233}U , ^{237}Np , ^{232}Th , ^{209}Bi and $^{\text{nat}}\text{Pb}$ in addition to the reference samples ^{235}U and ^{238}U . The results obtained for the involved cross-section has been published in different proceedings and regular publications (Audouin, *et al.*, 2007; Paradela, *et al.*, 2010; Tarrío, *et al.*, 2011). An overall agreement within the reported uncertainties was found with current evaluations in the overlapping energy range, except for the ^{237}Np case. In addition, the energy range of existing data could be extended up to 1 GeV. For the ^{237}Np , a higher cross-section of 5-7% was reported for energies above 1 MeV. This discrepancy was really unexpected because this isotope was supposed well measured and used as a secondary reference in other experiments.

A revision about this topic was tackled in our contribution to the Nuclear Data Conference in 2010 (Paradela, *et al.*, 2011b), concluding that high-precision measurements performed by Lisowski, *et al.* (1998) and Tovesson and Hill (2007) were normalised on the basis of Meadows (1983) data for ^{237}Np , in which the target mass estimation was not optimised with the alpha counting method, recommended by the author himself. On the other hand, most of other measurements such as those performed with 14 MeV monoenergetic beams or with the surrogate method were compatible with our results. Additional work was dedicated to investigate the impact of changing this fission cross on integral experiments (Leong, *et al.*, 2013).

More recently, experimental data obtained at IRMM for the ^{230}Pu and ^{232}Pu using ^{237}Np as a secondary reference have shown a better agreement with the evaluations if they are normalised by using n_TOF data (Salvador, *et al.*, 2014).

Furthermore, by using the reference samples included in our set-up, it is possible to provide the cross-section ratio between ^{238}U and ^{235}U , which relates two standard fission cross-sections in the fast neutron energy region. However, the situation at energies above 20 MeV is not clear mainly due to the existence of two discrepant sets of data. The n_TOF ratio is closer to the results reported by Lisowski, *et al.* (1998), and higher than those provided by Shcherbakov, *et al.* (2002).

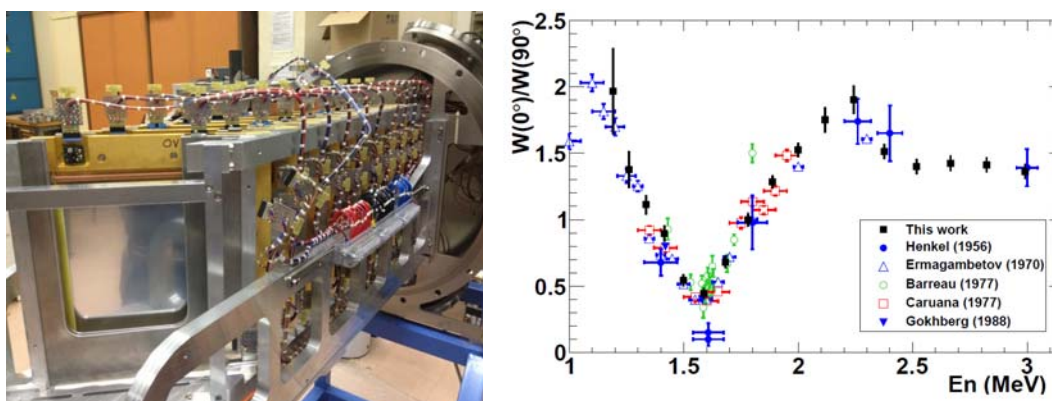
Figure 3: Ratio of ^{238}U and ^{235}U cross-section obtained at n_TOF Phase I, compared to evaluation and existing experimental data



Results of the n_TOF Phase II set-up

In order to overcome the limitation in the angular acceptance, a modified PPAC set-up was implemented for the n_TOF Phase II measurements. By tilting the PPAC and the targets by 45° with respect to the neutron beam axis, it is possible to access the full angular distribution measuring emission angles between 0° and 90° with respect to the beam axis. The efficiency of the new set-up has been studied by using GEANT4 simulations that show a similar efficiency response of about 50%. In addition, these measurements were taken without zero suppression, so that no signal threshold is used to register the data. This will allow reducing the uncertainty related with different threshold behaviour in the detectors, which amounted to 3% in the previous measurements.

Figure 4: Picture of the PPAC set-up used at n_TOF Phase II (left); results for the anisotropy parameter obtained for the ^{232}Th in the threshold region (right)



This set-up has been successfully employed during 2010 and 2011 fission campaigns in order to measure the fission fragment angular distribution (FFAD) of the ^{232}Th . A detailed description of the set-up and the analysis method, together with anisotropy results in the fission threshold region are reported in Tarrío, *et al.* (2013). Because of the lower statistics available for the rest of the isotopes included in the set-up, ^{237}Np , ^{238}U and ^{235}U , only

coarse results for their FFAD in the fast and intermediate neutron energies are available. They will be improved with the data taken in the 2012 campaign, focused on ^{234}U isotopes and currently under analysis. Preliminary results were already presented in the Final ERINDA Workshop at CERN. These two experiments will clarify the fission fragment anisotropic behaviour for the neutron-induced fission beyond 20 MeV.

Conclusions and perspectives

The usefulness of the PPAC detection set-up used at the CERN n_TOF facility in order to study fission reactions has been proven over a wide energy range, from eV to GeV. Phase II upgrading allows us to measure important observables of these reactions such as the energy dependence of the cross-section and the fission fragment angular distribution. Moreover, complete characterisation of the sample masses and the target characteristics provides an accurate value of the cross-section, based on the recommended standards. The data obtained for most of the measured isotopes have already been published and reported to the EXFOR database.

Because of the improvements in the Phase II set-up and the availability of FFAD information for each measured isotope, we are confident about providing more accurate cross-sections from n_TOF data, by reducing the uncertainty of several corrections.

Finally, comparison of the results that will be obtained in the various n_TOF campaigns for the ratio between the reference isotopes ^{238}U and ^{235}U will provide a consistent bunch of data that will serve to improve and extend knowledge of these priority isotopes.

Acknowledgements

This work was partially supported by the EC under contract No. FIKW-CT-2000-00107.

References

- Andriamonje, S., *et al.* (2011), “A Transparent Detector for n_TOF Neutron Beam Monitoring”, *J. Korean Phys. Soc.*, 59, pp. 1597-1600.
- Audouin, L., *et al.* (2007), “Neutron-Induced Fission Cross Section Measurements at n_TOF”, *Proc. of International Conference on Nuclear Data for Science and Technology*, Nice, France, EDP Sciences, pp. 421-424.
- Calviani, M., *et al.* (2008), “A Fast Fission Ionization Chamber for Fission Measurements at n_TOF”, *Nucl. Instrum. Meth. A*, 594, pp. 220-227.
- Guerrero, C., *et al.* (2013), “Performance of the Neutron Time-of-Flight n_TOF at CERN”, *Eur. Phys. Journal A*, 49-2, p. 27.
- Kumagai, H., *et al.* (2001), “Delay-Line PPAC for High-Energy Light Ions”, *Nucl. Instrum. Meth.*, 164, pp. 477-490.
- Leong, L.S., *et al.* (2013), “Criticality Experiments for Validation of Cross Sections”, *Annals of Nucl. Energy*, 54, pp. 36-42.

- Lisowski, P., *et al.* (1998), *Proc. of Conference on Nuclear Data for Science and Technology*, Mito, Japan, pp. 97.
- Meadows, J.W., (1983), “The Fission Cross Section of ^{237}Np Relative to ^{235}U from 0.1 to 9.4”, *Nucl. Sci. Eng.*, 85, pp. 271.
- NNDC (National Nuclear Data Center) (2009), “Experimental Nuclear Reaction Data (EXFOR)”, Brookhaven, NY, United States.
- Paradela, C., *et al.* (2010), “Neutron-Induced Fission Cross Section of ^{234}U and ^{237}Np Measured at the CERN Neutron Time-of-Flight (n_TOF) facility”, *Phys. Rev. C*, 82, 034601.
- Paradela, C., *et al.* (2011a) “Fission Measurements with PPAC Detectors Using a Coincidence Technique”, *Proc. of 2nd International Conference on Advancements in Nuclear Instrumentation Measurement Methods and their Applications (ANIMMA)*.
- Paradela, C., *et al.* (2011b), “ ^{237}Np Cross Section: New Data and Present Status”, *J. Korean Phys. Soc.*, 59, pp. 1908-1911.
- Salvador, P., *et al.* (2014), these proceedings.
- Shcherbakov, O., *et al.* (2002), *J. Nucl. Sci. Tech.*, Suppl. 2, 230.
- Stelzer, H. (1976), “A Large Area Parallel Plate Avalanche Counter”, *Nucl. Instrum. Meth.*, 133, pp. 409.
- Tarrío, D., *et al.* (2011), “Neutron-Induced Fission Cross Section of $^{\text{nat}}\text{Pb}$ and ^{209}Bi from Threshold to 1 GeV: An Improved Parametrization”, *Phys. Rev. C*, 83, 044620.
- Tarrío, D., *et al.* (2013), *Nucl. Instr. Meth.*, submitted.
- Tovesson, F. and T. Hill (2007), “Neutron Induced Fission Cross Section of ^{237}Np from 100 keV to 200 MeV”, *Phys Rev. C*, 75, 034610.

Measurement of the neutron-induced fission cross-section of $^{240,242}\text{Pu}$

P. Salvador-Castiñeira,^{a,b} F-J. Hambsch,^a T. Bryś,^a S. Oberstedt,^a C. Pretel^b, M. Vidali^a

^aEuropean Commission, JRC-IRMM, Geel, Belgium

^bInstitute of Energy Technologies, Technical University of Catalonia, Barcelona, Spain

Abstract

Fast spectrum neutron-induced fission cross-section data for transuranic isotopes are in high demand in the nuclear data community. In particular, highly accurate data are needed for the new Generation-IV nuclear applications. The aim is to obtain precise neutron-induced fission cross-sections for ^{240}Pu and ^{242}Pu . In this context accurate data on spontaneous fission half-lives have also been measured. To minimise the total uncertainty on the fission cross-sections the detector efficiency has been studied in detail. Both isotopes have been measured using a twin Frisch-grid ionisation chamber (TFGIC) due to its superiority compared to other detector systems in view of radiation hardness, $2 \times 2\pi$ solid angle coverage and very good energy resolution.

Introduction

In a recent assessment of target accuracies and uncertainties the OECD Nuclear Energy Agency (NEA) highlighted the need for improved nuclear data to be used in model calculations for innovative reactor systems (GEN-IV) (Salvatores, 2008). In this paper the neutron-induced fission cross-sections of $^{240,242}\text{Pu}$ have been identified as of highest priority for fast neutron spectrum reactors. Their target uncertainties are very stringent and are requested to be 1-2% for ^{240}Pu and 3-5% for ^{242}Pu from current uncertainties of 6% and 20%, respectively.

In the framework of the Accurate Nuclear Data for Nuclear Energy Sustainability (ANDES) collaboration, several actinides are being studied, among them $^{240,242}\text{Pu}$. Different experimental methods are being used to determine their neutron-induced fission cross-section. For the first time the new digital data acquisition technique has been applied for cross-section measurements. Using digital electronics and storing the full waveform opens up new analysis possibilities not available using regular analogue electronics.

This report gives an overview of the present status of the experiment in terms of newly determined spontaneous fission half-lives for both $^{240,242}\text{Pu}$ and the resulting preliminary fission cross-sections.

Experimental set-up

A twin Frisch-grid ionisation chamber (TFGIC) has been chosen as fission fragment (FF) detector. Its characteristics (radiation resistance, solid angle of nearly $2 \times 2\pi$ and good

energy resolution) made this type of detector the excellent choice for performing direct kinematics fission experiments.

A schematic representation of the set-up is presented in Figure 1. Since the two samples used in this study have a thick backing, allowing to detect just one FF, they were placed in back-to-back geometry. The TFGIC was filled with P10 (90% Ar + 10% CH₄) as counting gas at a pressure of 1 052 mbar with a constant flow of ~50 ml/min. The cathode-grid distance was 31 mm and the grid-anode distance was 6 mm, allowing the FF to be fully stopped within the space between the cathode and the grid. The cathode was common for the two samples and was set at a high voltage (HV) of -1.5 kV, while the two anodes were set at 1 kV. Both grids were grounded. Grids and anodes were connected to charge-sensitive pre-amplifiers, and the output was fed into a 12 bit 100 MHz waveform digitiser (WFD). The cathode was connected to a current-sensitive pre-amplifier. The output signal was split, one signal was fed into the WFD and the other was treated with a timing filter amplifier (TFA) and a constant fraction discriminator (CFD) resulting the trigger signal for all the WFD.

The Pu samples used in this experiment were produced by the so-called molecular plating technique in the target preparation laboratory of the JRC-IRMM. Due to the short α half-life of the ²⁴⁰Pu, 6 561 yr (0.1%), the sample has a total mass of only 92.9 μ g (0.4%) with an α -activity of 0.8 MBq (0.4%). The ²⁴²Pu has an α half-life longer than 105 yr, for this reason more material could be deposited on top of the disk, being its mass of 671 μ g (0.9%) and its α -activity of 0.1 MBq (0.3%). The main contribution on the mass uncertainty of ²⁴²Pu is due to its α half-life and its uncertainty, 3.75×10^5 yr (0.5%). The activity of both samples was determined by defined solid angle α -particle counting. The purity of the samples is higher than 99.8% and their atomic abundances were measured by mass spectrometry. The main characteristics of the ^{240,242}Pu samples are summarised in Table 1 (Sibbens, *et al.*, 2013).

The experiments were performed at the Van de Graaf (VdG) accelerator at JRC-IRMM. The neutron-producing reactions used were ⁷Li(p,n)⁷Be and T(p,n)³He, giving a neutron energy range from 0.2 MeV to 3 MeV. The reference samples used are described in Table 2.

Figure 1

(a) Schematic drawing of a twin Frisch-grid ionisation chamber (TFGIC) with a reference sample in one side and a sample under study in the other

(b) Scheme of the electronics for one chamber side

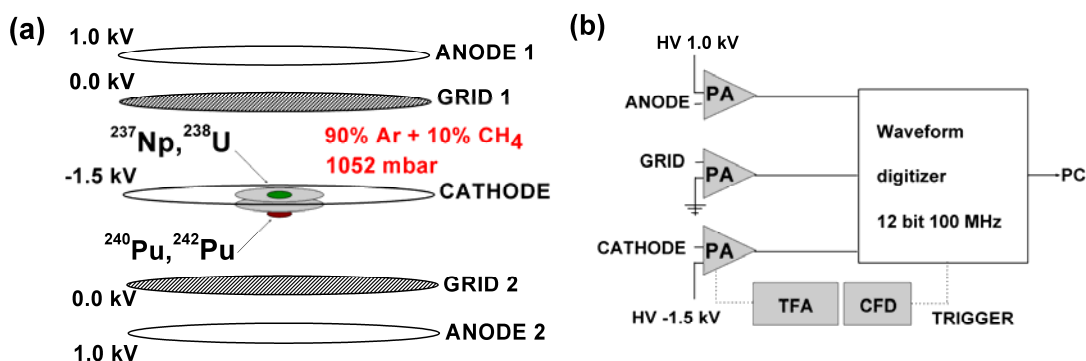


Table 1: Main characteristics of the $^{240,242}\text{Pu}$ samples

All the uncertainties are expanded with a coverage factor $k = 1$;
the expanded uncertainty of the sample purity has a coverage factor of $k = 2$

	^{240}Pu	^{242}Pu
Method	Molecular plating	Molecular plating
Chemical composition (assumed)	$\text{Pu}(\text{OH})_4$	$\text{Pu}(\text{OH})_4$
Total mass (μg) (calculated)	119.22 (0.4%)	859.54 (0.9%)
Total area density ($\mu\text{g}/\text{cm}^2$) (calculated)	16.9 (0.4%)	122 (0.8%)
Backing	Aluminium	Aluminium
Mass (μg)	92.9 (0.4%)	671 (0.9%)
Areal density ($\mu\text{g}/\text{cm}^2$)	13.19 (0.4%)	95.3 (0.8%)
α -activity (MBq)	0.780 (0.4%)	0.0984 (0.3%)
Purity	99.8915(18)%	99.96518(45)%

Source: Sibbens, *et al.* (2013).

Table 2: Main characteristics of the secondary standards used

	^{237}Np	^{238}U
Mass (μg)	391.3 (0.3%)	614 (0.5%)
Areal density ($\mu\text{g}/\text{cm}^2$)	308.1	86.9
α -activity (Bq)	10168 (0.1%)	7.64 (0.5%)

Source: Pommé (2012).

Data analysis

Several corrections have been applied to the raw anode and grid signals: α pile-up correction, grid inefficiency, etc. A detailed description is given in (Salvador-Castiñeira, *et al.*, 2013). To determine the detection efficiency of the ionisation chamber the procedure described by Budtz-Jørgensen and Knitter (1984) has been used based on the following equation to determine the total number of emitted FF (N_{cos}):

$$N_{\text{cos}} = A + \Delta A \quad (1)$$

with A being the integral of the cosine distribution and ΔA the missing part related with the thickness of the sample [Figure 2(a)]. To extract the sample loss the anode PH distribution (N_{PH}) must be considered and extrapolated down to 0 (ΔN_{PH}) to account for FF emitted but not detected due to the high electronic threshold requested not to trigger on α events [Figure 2(b)]. The experimental efficiency due to sample loss (ϵ_{exp}) will then be calculated as:

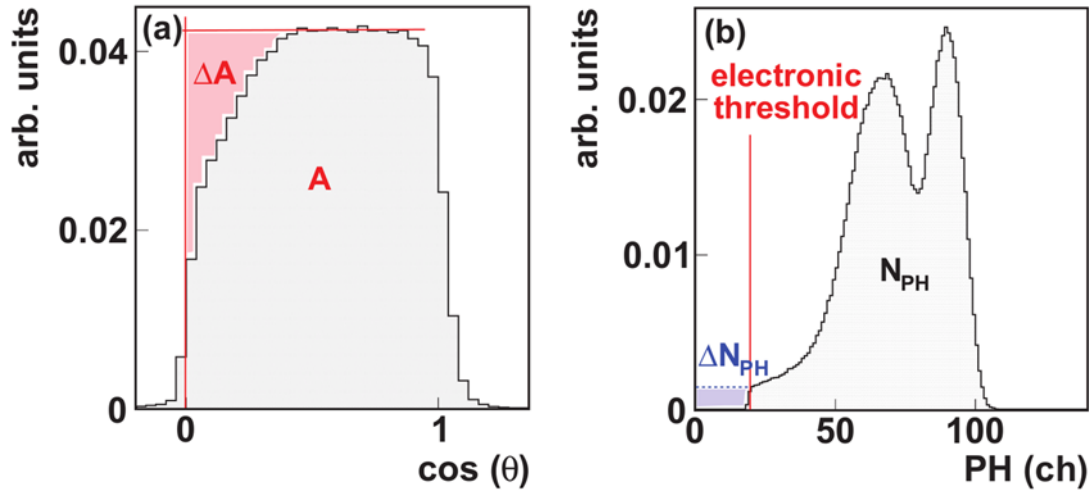
$$\epsilon_{\text{exp}} = \frac{N_{PH} + \Delta N_{PH}}{N_{\text{cos}}} = \frac{N_{2\pi}}{N_{\text{cos}}} \quad (2)$$

During the analysis of the P10 data we found a strong correlation between the degradation of the cosine distribution and the α -activity of the sample, obtaining a lower efficiency for the thinner but more active target (^{240}Pu) and a higher one for the thicker

Figure 2

(a) Angular distribution for ^{242}Pu . The FF loss inside the sample is visible at low $\cos \theta$ values. By determining the integral of the distribution and ΔA (the missing part of the distribution) one can obtain the sample loss.

(b) PH distribution for ^{242}Pu and determination of counts under the electronic threshold



but less active target (^{242}Pu). Improving the signal rise time by using CH_4 as counting gas, which has a drift velocity two times higher than P10 (Knoll, 2000), the results on the efficiency calculation of the ionisation chamber also improved, getting closer to what should be expected with theoretical calculations. To verify the efficiency results obtained with the different analysis methods, theoretical calculations using SRIM (Ziegler, Biersack and Ziegler, 2008) stopping power ranges and Geant4 simulations (2014) have been performed as well.

The theoretical calculation has been done as presented by Salvador-Castiñeira, *et al.* (2013). Properties for two typical FF have been used. The loss inside the sample can be calculated as:

$$\Delta_{sample} = \frac{t}{2R_{sample}} = \frac{t}{2} \sum_i \frac{W_i}{R_i} \quad (3)$$

with t as the thickness of the sample, R_i the range of isotope i and W_i the weight fraction of isotope i in the sample.

Simulations with Geant4 have been performed with a FF kinetic energy distribution obtained with the GEF code (Schmidt and Jurado, n.d.). The transmitted FF from the sample to the counting gas were obtained from the simulations.

Spontaneous fission half-life

The SF half-life has been calculated using:

$$T_{1/2,SF} = \frac{\%^j\text{Pu}}{A_j} \cdot \frac{1}{\left(\frac{C_{SF}}{t \cdot \epsilon_j \cdot \ln 2 \cdot m_{Pu} \cdot N_A} - \sum_i^n \frac{\%^i\text{Pu}}{A_i \cdot T_{1/2,SF}(i)} \right)} \quad (4)$$

where $\%Pu$ is the purity of the sample, A_j its atomic mass, C_{SF} the counts detected, ϵ_j the detection efficiency, m_{Pu} the sample mass, N_A the Avogadro's number and $\sum_i^n \frac{\%^i Pu}{A_i \cdot T_{1/2,SF}(i)}$ the contribution from the other isotopes contained in the sample.

Several measurements have been performed with each sample. Figure 3 summarises in a graph the resulting $T_{1/2,SF}$ values. Run 1 for ^{240}Pu and 1-5 for ^{242}Pu were performed with P10 as counting gas, while runs 2-3 for ^{240}Pu and 6-7 for ^{242}Pu with CH_4 . Each run contains several individual data sets with up to 250 000 fission events using P10 and up to 1 500 000 events using CH_4 . All labelled runs are performed using a different electronic threshold. The error bars in the plot describe the statistical and the systematic uncertainties, the thick horizontal line is an eye guide for the weighted average of our data and the dotted lines are the final uncertainties (systematic and statistical) expressed with 1σ . The bullet symbols represent previous experimental results, the highlighted literature value is a weighted average of a subset of the literature data made by Holden and Hoffman (2000) and using the same data by reference Chechev (2005)/LNHB (n.d.). Table 3 lists the present uncertainty budget and Table 4 lists the weighted average of our experimental data together with the weighted average of the literature values by Holden and Hoffman (2000) and the same weighted average calculated by Chechev (2005)/LNHB (n.d.).

Figure 3: SF half-life results for ^{240}Pu (a) and ^{242}Pu (b) (stars) compared with some literature values (bullets), their weighted average calculated by Holden and Hoffman (2000) and the weighted average calculated by Chechev (2005)/LNHB (n.d.)

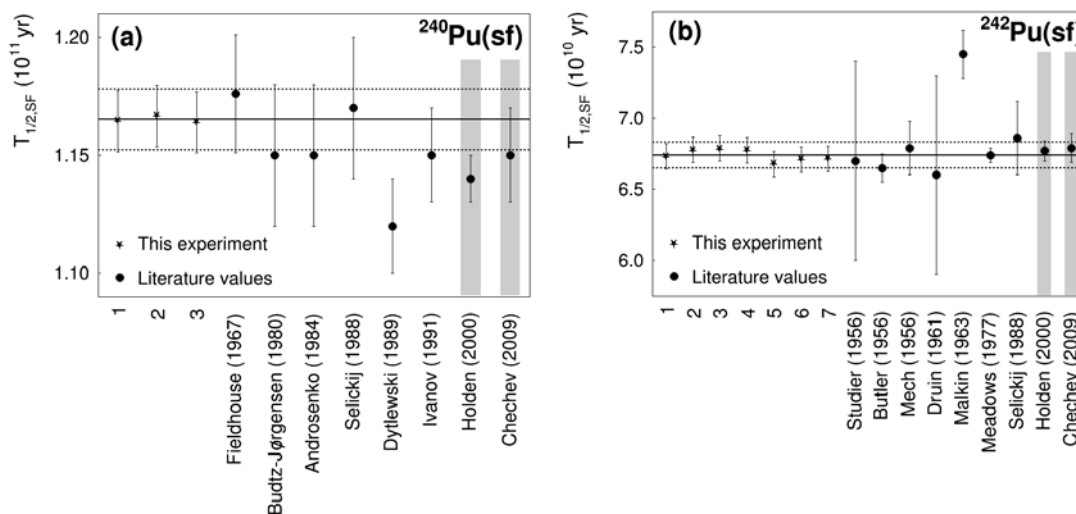


Table 3: Summary of the uncertainties corresponding to the SF half-life ($T_{1/2,SF}$) for $^{240,242}\text{Pu}$

Uncertainty source	^{240}Pu	^{242}Pu
Statistical	0.13%	< 0.1%
Mass	0.4%	0.9%
Sample efficiency	1%	1%
Sample purity	< 0.001%	< 0.001%
Dead time acquisition system	< 0.07%	< 0.12%
Total (systematic and statistical)	1.1%	1.3%

Table 4: Summary of the SF half-life ($T_{1/2,SF}$) for $^{240,242}\text{Pu}$

The experimental uncertainties presented are both the statistical and systematic. The weighted average of literature values presented by Holden and Hoffman (2000) and that calculated by Chechev (2005)/LNHB (n.d.) using the same literature data.

$T_{1/2,SF}$ (yr)	^{240}Pu	^{242}Pu
Holden and Hoffman (2000)	1.14×10^{11} (0.9%)	6.77×10^{10} (1.0%)
Chechev (2005)/LNHB (n.d.)	1.15×10^{11} (1.7%)	6.79×10^{10} (1.4%)
This experiment	1.165×10^{11} (1.1%)	6.74×10^{10} (1.3%)

Our results are in agreement with the literature values for ^{242}Pu . Nevertheless, and using exactly the same method, the ^{240}Pu SF half-life is slightly higher than some of the literature values. This could be explained by the high α -activity of the sample. By having a more precise discrimination of α -particle signals our count rate might have been lower than in previous experiments done with analogue electronics, thus obtaining a higher SF half-life value. More details are given in Salvador-Castiñeira, *et al.* (2013).

Fission cross-sections

Measurements have been performed at the Van de Graaff facility of the JRC-IRMM. Several campaigns have been done for the two plutonium isotopes using the two different standards. The neutron-producing reactions used were $^7\text{Li}(p,n)^7\text{Be}$ for neutron energies between 0.2 MeV and 1.8 MeV and using $^{237}\text{Np}(n,f)$ as a reference; and $\text{T}(p,n)^3\text{He}$ for neutron energies between 1.8 and 3 MeV and using $^{238}\text{U}(n,f)$ as a reference. Based on the newly determined half-lives and efficiency determination of the ionisation chamber the fission cross-sections have been calculated for both ^{240}Pu and ^{242}Pu according to the following equation:

$$\sigma_{Pu}(E_0) = \left[\frac{N_{ref}}{N_{Pu}} \cdot \frac{(C_{Pu}/\epsilon_{Pu} - C_{SF})}{C_{ref}/\epsilon_{ref}} - \sum_i P_i \frac{\sigma_i(E_0)}{\sigma_{ref}(E_0)} \right] \cdot \left(\frac{\phi_0^{ref}}{\phi_0^{Pu}} \cdot \sigma_{ref}(E_0) + \frac{\phi_1^{ref}}{\phi_0^{Pu}} \cdot \sigma_{ref}(E_1) \right) - \frac{\phi_1^{Pu}}{\phi_0^{Pu}} \cdot \sigma_{Pu}(E_1) \quad (5)$$

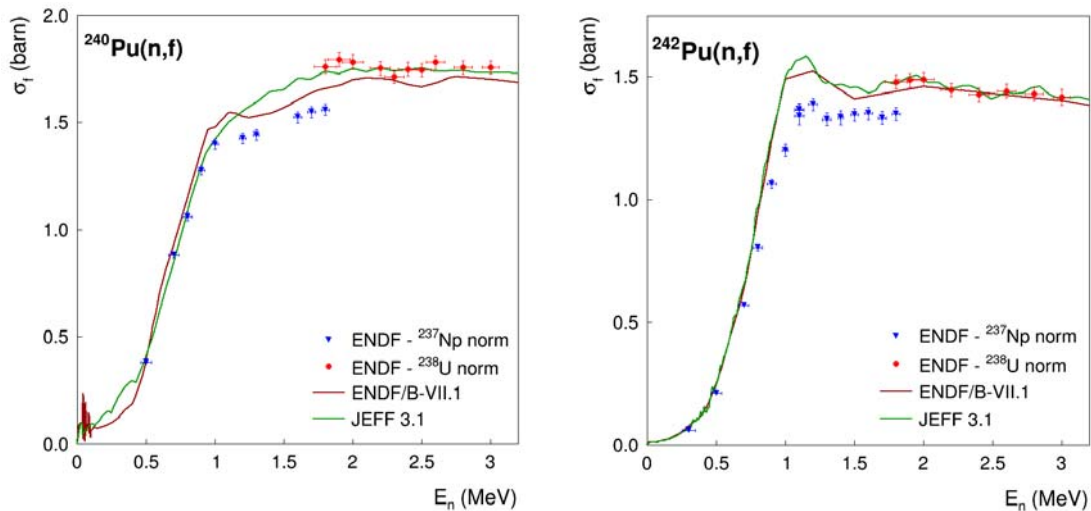
where E_0 and E_1 refer to the ground state and the first excited state of the $^7\text{Li}(p,n)^7\text{Be}$ reaction, respectively; ϕ_0 is the flux related to the ground state of the Li reaction and ϕ_1 to the excited state of the same reaction; N_i are the number of atoms in the sample i , C_i are the number of counts detected from the sample i , C_{SF} are the number of spontaneous fission counts from the plutonium sample, ϵ_i is the transmission probability of a fission fragment (FF) to leave the sample and enter into the counting gas, $\sum_i P_i \frac{\sigma_i(E_0)}{\sigma_{ref}(E_0)}$ is the

contribution on the plutonium fission counts from the impurities of the sample and $\sigma_{ref}(E_i)$ is the cross-section from the reference isotope. When the $\text{T}(p,n)^3\text{He}$ reaction was used, thus the ^{238}U sample, Eq. (5) was simplified since the neutron-producing reaction gave a quasi-monoenergetic beam. The excited state of the Li reaction grows its influence with the increasing neutron energy; being about 8% of the total neutron flux at 1.8 MeV (ground state energy).

The provisional results are given in Figure 4, for ^{240}Pu and for ^{242}Pu .

Figure 4: Neutron-induced fission cross-section of ^{240}Pu (left) and ^{242}Pu (right)

The triangles represent our data taken relative to the ENDF/B-VII.1 ^{237}Np evaluation; while the bullets are data taken relative to the ENDF/B-VII.1 ^{238}U evaluation



Two different normalisations have been performed. At first, the data were normalised to the ENDF/B.VII.1 evaluation (Chadwick, *et al.*, 2011) for the two reference isotopes (^{237}Np – blue symbols; ^{238}U – red symbols). A clear discrepancy between the data relative to the ^{237}Np evaluation and the ^{238}U evaluation is observed. The difference at the overlapping incident neutron energy point (at 1.8 MeV) amounts to about 13% in both cases. The data for both ^{240}Pu and ^{242}Pu measured relative to the ^{238}U fission cross-section is in agreement with the JEFF-3.1 evaluation. The threshold for ^{240}Pu is very well reproduced and also agrees best with the JEFF-3.1 evaluation. There is a distinct difference above threshold for both Pu isotopes if the ^{237}Np ENDF/B-VII.1 evaluation is used.

The uncertainty calculation includes the contribution of the sample mass, the uncertainties on half-life and isotope content, statistics and efficiency. When normalising to ^{238}U the uncertainty budget considered includes, in addition, the uncertainty of the reference cross-section; in that particular case the value is around 0.7% in the considered energy range. The uncertainty that should be considered when using the cross-section of ^{237}Np as a reference amounts from 3.5 to 5% from 0.2 MeV up to 1.8 MeV. In the case of ^{237}Np , this source of uncertainty is not yet added in the present results.

Recently, new values for the neutron-induced fission cross-section for ^{237}Np were published by Paradela, *et al.* (2010), these data were around 5% higher in value than the current evaluations (see Figure 5). By normalising our ^{237}Np data to Paradela, *et al.* (2010), the green symbols would be obtained in Figure 6. Then in case of ^{240}Pu the new results would be much better in agreement with the ENDF/B-VII.1 evaluation over the whole energy range covered by the ^{237}Np reference. For ^{242}Pu however, both the threshold and above threshold values are still too small compared to the ENDF/B-VII.1 evaluation. The difference in the overlap region to the ^{238}U reference data is in both cases still 5-8%.

Conclusions

The neutron-induced fission cross-section has been measured for $^{240,242}\text{Pu}$ at the Van de Graaff facility of the JRC-IRMM. The energy range studied has been between 0.2 MeV and 3 MeV neutron incoming energy. Two different secondary standards have been used: ^{237}Np and ^{238}U . The results obtained at the overlap neutron energy region for the two standards used (1.8 MeV) do not agree within uncertainties. The preliminary

results presented in Figures 2-4 neither agree with each other nor with evaluations. All points to a too-small ^{237}Np fission cross-section. New measurement of this cross-section by Paradela, *et al.* (2010) are 5% larger compared to the present evaluation but are still too small to make the match in the overlap region between the two standards.

Figure 5

Left: Ratio of the neutron-induced fission cross-section of ^{237}Np and the ^{235}U ; three groups of data are distinguished

Right: Neutron-induced fission cross-section of ^{237}Np ; the latest evaluations are shown together with data from Paradela, *et al.* (2010) and Jiacoletti, Brown and Olson (1972)

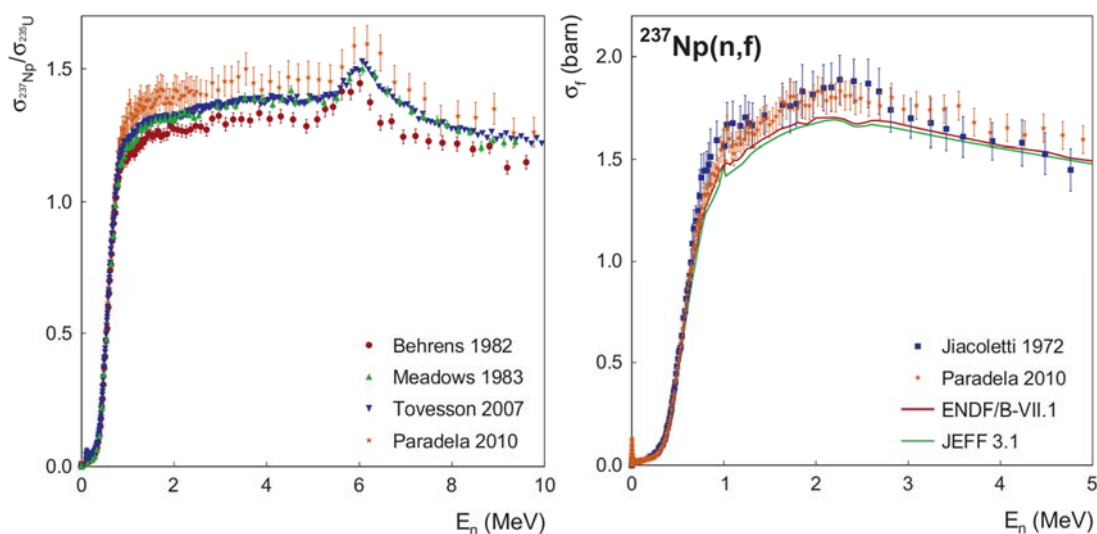
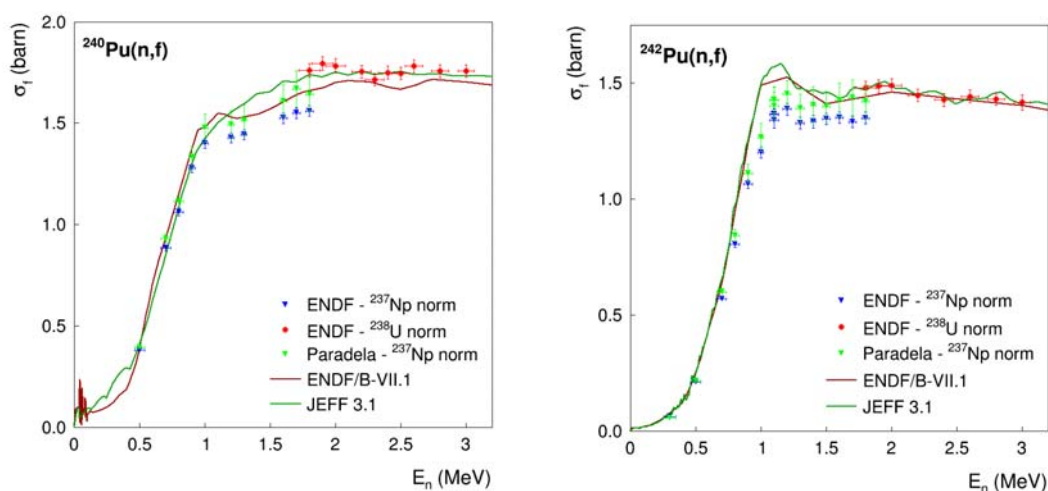


Figure 6: Neutron-induced fission cross-section of ^{240}Pu (left) and ^{242}Pu (right)

The blue triangles represent our data taken relative to the ENDF/B-VII.1 ^{237}Np evaluation, while the bullets are data taken relative to the ENDF/B-VII.1 ^{238}U evaluation; a new normalisation of the ^{237}Np data is presented relative to the new cross-section values of Paradela, *et al.* (2010)



Acknowledgements

One of the authors (P.S-C.) acknowledges financial support from the ANDES collaboration (contract No. FP7-249671).

References

- Budtz-Jørgensen, C. and H-H. Knitter (1984), *Nucl. Sci. Eng.*, 86, pp. 10-21.
- Chadwick, M.B., *et al.* (2011), “ENDF/B-VII.1 Nuclear Data for Science and Technology: Cross Sections, Covariances, Fission Product Yields and Decay Data”, *Nucl. Data Sheets*, 112, p. 2887.
- Chechev, V.P. (2005), *Proc. Intern. Conf. Nuclear Data for Science and Technology*, Santa Fe, New Mexico, 26 September-1 October 2004, R.C. Haight, *et al.* (eds.), Vol. 1, p. 91, AIP Conf. Proc., 769.
- Geant4 (2014), Geant4 website, accessed 23 June 2014, <http://geant4.web.cern.ch/geant4/>.
- Holden, N.E. and D.C. Hoffman (2000), *Pure Appl. Chem.*, 72, pp. 1525-1562.
- Jiacoletti, R.J., W.K. Brown and H.G. Olson (1972), *Fission Cross Sections of ^{237}Np from 20 eV to 7 MeV Determined from a Nuclear-Explosive Experiment*, Los Alamos National Laboratory (LANL), Los Alamos, NM, United States.
- Knoll, G.F. (2000), *Radiation Detection and Measurement*, John Wiley and Sons, Inc., New York, United States, 3rd edition.
- LNHB (Laboratoire National Henri Becquerel) (n.d.), “Recommended Data” webpage on LNHB website, accessed 23 June 2014, www.nucleide.org/DDEP_WG/DDEPdata_by_Z.htm.
- Paradela, C., *et al.* (2010), “Neutron-Induced Fission Cross Section of ^{234}U and ^{237}Np Measured at the CERN Neutron Time-of-Flight (n_TOF) Facility”, *Physical Review C*, 82 (3), 034601.
- Pommé, S. (2012), private communication.
- Salvador-Castiñeira, P., *et al.* (2013), “Highly Accurate Measurements of the Spontaneous Fission Half-Life of $^{240,242}\text{Pu}$ ”, forthcoming in *Phys. Rev. C*.
- Salvatores, M. (2008), *Uncertainty and Target Accuracy Assessment for Innovative Systems Using Recent Covariance Data Evaluations*, NEA/WPEC-26, OECD/NEA, Paris.
- Schmidt, K-H. and B. Jurado (n.d.), “GEF-code Version 2012/2.7”, webpage on Centre d’Etudes Nucléaires de Bordeaux Gradignan (CENBG) website, accessed 23 June 2014, www.cenbg.in2p3.fr/-GEF-.
- Sibbens, G., *et al.* (2013), “Preparation of ^{240}Pu and ^{242}Pu Targets to Improve Cross Section Measurements for Advanced Reactors and Fuel Cycles”, *J. Rad. Nucl. Chem.*, 297:DOI 10.1007/s10967-013-2669-6.
- Ziegler, J.F., J.P. Biersack and M.D. Ziegler (2008), *SRIM – The Stopping and Range of Ions in Matter*, SRIM Co., Chester, MD, United States, ISBN 0-9654207-1-X, www.srim.org.

Sensitivity analysis of the nuclear data for MYRRHA reactor modelling

Alexey Stankovskiy,^a Gert Van den Eynde,^a
Oscar Cabellos,^b Carlos J. Diez,^b Peter Schillebeeckx,^c Jan Heyse^c
^aSCK•CEN, Mol, Belgium
^bUniversidad Politécnica de Madrid, Madrid, Spain
^cEuropean Commission, JRC-IRMM, Geel, Belgium

Abstract

A global sensitivity analysis of effective neutron multiplication factor k_{eff} to the change of nuclear data library revealed that JEFF-3.2T2 neutron-induced evaluated data library produces closer results to ENDF/B-VII.1 than does JEFF-3.1.2. The analysis of contributions of individual evaluations into k_{eff} sensitivity allowed establishing the priority list of nuclides for which uncertainties on nuclear data must be improved.

Detailed sensitivity analysis has been performed for two nuclides from this list, ^{56}Fe and ^{238}Pu . The analysis was based on a detailed survey of the evaluations and experimental data. To track the origin of the differences in the evaluations and their impact on k_{eff} , the reaction cross-sections and multiplicities in one evaluation have been substituted by the corresponding data from other evaluations.

Introduction

The Multi-Purpose Hybrid Research Reactor for High-Tech Applications (MYRRHA) research reactor is being designed at SCK•CEN, Belgium. This flexible facility will operate in both critical (at nominal power 100 MWth) and subcritical operation modes (at ~70 MWth). The latter one represents an accelerator-driven system (ADS), where neutrons driving the subcritical MOX-fuelled core are originated from the lead-bismuth eutectic (LBE) spallation target bombarded by a 600 MeV proton beam with intensity up to ~3 mA from a superconducting linear accelerator. The design characteristics of MYRRHA are determined by the international needs in terms of flexible fast spectrum irradiation capabilities, ADS demonstration and the targeted applications catalogue for this facility. As a direct consequence of the desired high flux levels [$\sim 3 \times 10^{15}$ n/(cm²s)], and hence high-power density, a compact core is needed, and therefore the central hole in the core which houses the spallation target should be of limited dimensions. This required high cooling efficiency which is provided by the LBE, thanks to its low melting temperature which allows the primary systems to function at rather low temperatures. A pool-type system has been chosen to profit from the thermal inertia provided by a large coolant volume (OECD/NEA, 2009). The neutronics design of MYRRHA is a challenging task since the huge amount of heavy metal coolant, the highly enriched mixed-oxide (MOX) fuel and the presence of high-energy neutrons in the subcritical operation mode require accurate knowledge of safety parameters such as an effective neutron multiplication

factor k_{eff} , reactivity coefficients, etc. The calculation of these characteristics heavily relies on the nuclear data which thus must be accurate enough to ensure acceptable uncertainties on calculated neutronic parameters. The Belgian licensing authorities require that safety-related neutronics calculations of MYRRHA must be performed with the selected, validated and approved nuclear data set. A primary step towards the creation and validation of such data set is the nuclear data sensitivity and uncertainty analysis with respect to MYRRHA. The sensitivity of effective neutron multiplication factor of MYRRHA critical core to the nuclear data has been thoroughly studied and the results are reported below. The priorities on the dedicated differential and integral experiments targeting to reduce key nuclear data uncertainties are discussed.

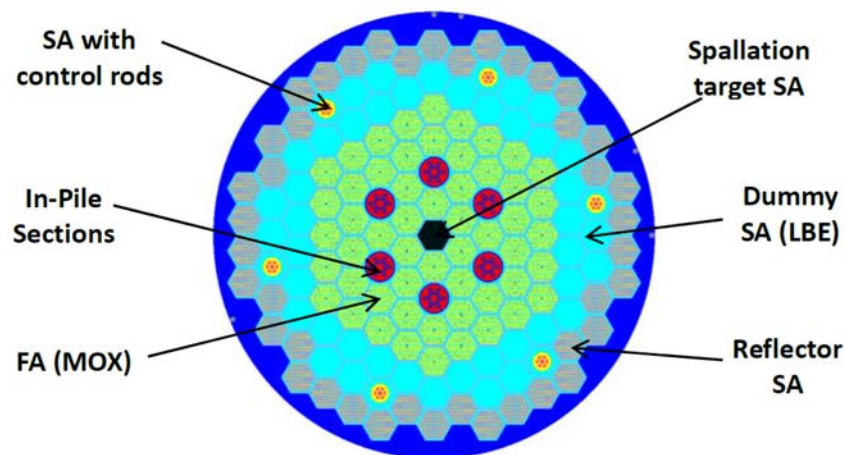
Sensitivity analysis of general purpose neutron induced data

The neutronics calculations of the MYRRHA critical and subcritical cores are carried out at SCK•CEN with the general purpose radiation transport code MCNPX (Pelowitz, 2008) which has nowadays almost no alternates when dealing with ADS-related problems. Since this code relies heavily on the general and special purpose neutron data, several evaluated neutron-induced data libraries of last generation have been processed at SCK•CEN for various nuclear temperatures, including neutron-induced data from ENDF/B-VII.1 (Chadwick, *et al.*, 2011) and JEFF-3.1.2 (Santamarina, *et al.*, 2009). The test version of the JEFF-3.2 library, JEFF-3.2T2, has been added to this list (OECD/NEA, 2012). The libraries have been processed by the ALEPH-DLG code (Haeck and Verboomen, 2005) which automatizes evaluated data processing with the NJOY code (MacFarlane and Muir, 1994) and performs quality assurance of produced transport libraries suitable for MCNPX.

As a result, three neutron-induced data libraries in ACE format have been generated for the set of 22 nuclear temperatures from 300 to 2 100 K (Stankovskiy, 2012).

The subcritical core configuration has been chosen for this study. It is targeted to operate at $k_{\text{eff}} \sim 0.95$ and is composed of 58 MOX-fuelled assemblies surrounding LBE spallation target subassembly (SA). The core also hosts several in-pile sections dedicated for the materials testing. The MCNPX geometry model is shown in Figure 1.

Figure 1: Subcritical core layout



To identify the most problematic nuclides from the viewpoint of nuclear data quality, nuclear data sensitivity analysis has been performed. It has become customary in nuclear data sensitivity studies to calculate the sensitivity of integral parameters to the arbitrary variation of nuclear data. Prior to this, the sensitivity of effective neutron multiplication factor k_{eff} to the choice of nuclear data library has been investigated.

Table 1 lists the effective neutron multiplication factors calculated for subcritical core with three neutron-induced point-wise data libraries: ENDF/B-VII.1, JEFF-3.1.2 and JEFF-3.2T2. ENDF/B-VII.1 was treated as a reference library so that the deviations of results obtained with the JEFF libraries were calculated as:

$$\Delta = \frac{k_{endfb} - k_{jeff}}{k_{endfb}} (\%) \quad (1)$$

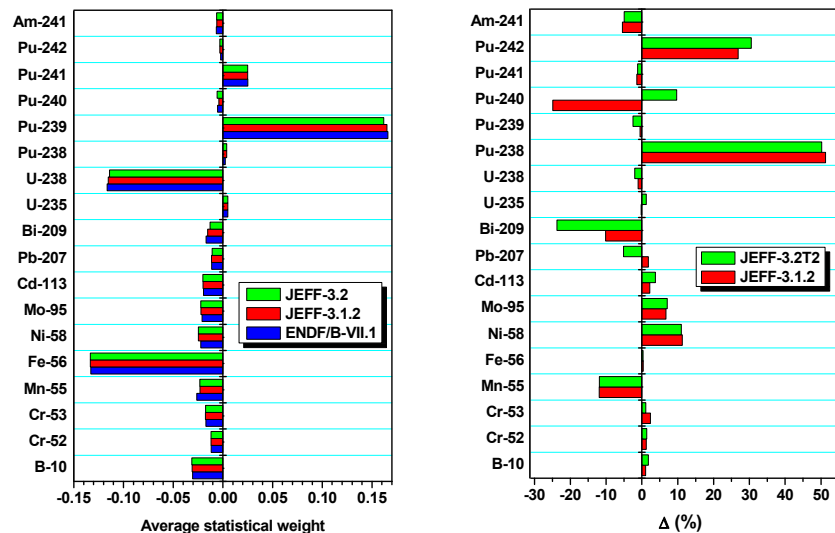
where k is the neutronics parameter under investigation (k_{eff} in Table 1).

Table 1: Effective neutron multiplication factor calculated with different libraries

Library	k_{eff} (std. dev.)	Difference (pcm)	$\Delta(\%)$
ENDF/B-VII.1	0.95911 (0.00004)	–	–
JEFF-3.1.2	0.96301 (0.00005)	390	0.41
JEFF-3.2T2	0.96091 (0.00004)	180	0.19

The deviation of JEFF-3.1.2 from ENDF/B-VII.1 does not exceed 0.5% and is even less for the test version of the JEFF-3.2 library. Both the ENDF/B and JEFF libraries tend to converge, however, JEFF libraries overestimate k_{eff} compared to ENDF/B-VII.1. The net neutron production by each nuclide calculated as differences between neutron statistical weights of production [by fission and (n,xn) reactions] and loss (capture) is plotted in Figure 2. This figure helps to identify the main contributors to the general neutronic behaviour of the reactor.

Figure 2: Net neutron production on selected nuclides (a) and deviations of JEFF libraries from ENDF/B-VII.1 (b)

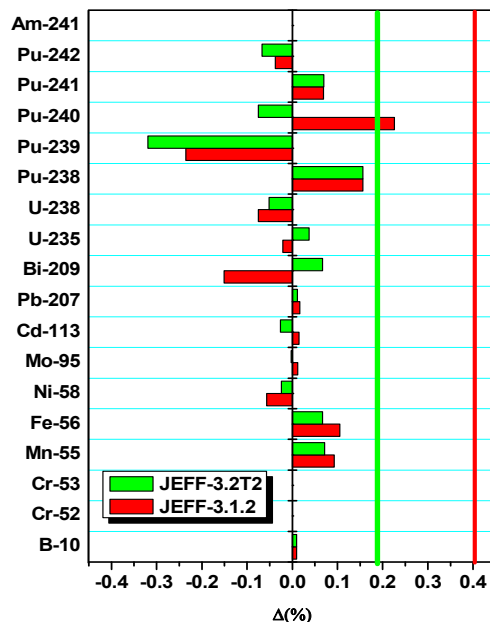


As it is seen from Figure 2(a) the majority of neutrons is generated by fissions of ^{239}Pu . The positive contributions into the net neutron production are also given by $^{238,241}\text{Pu}$ and ^{235}U . Major neutron absorbers are ^{238}U , ^{56}Fe and other nuclides composing structural steels. LBE nuclides do not significantly change the net neutron production. However, Figure 2(b), which shows the deviations of JEFF-3.1.2 and JEFF-3.2T2 from ENDF/B-VII.1, indicates that data for ^{239}Pu , ^{238}U and ^{56}Fe are less uncertain than even plutonium isotopes and ^{209}Bi . For instance, net neutron production on ^{238}Pu is rather small (but positive). However, the

differences between the JEFF and ENDF/B-VII.1 libraries reach 50%. The sensitivity of the effective neutron multiplication factor to the evaluated data file choice for a particular nuclide has been studied by substituting the reference ENDF/B-VII.1 data for this nuclide with data taken from JEFF-3.1.2 or JEFF-3.2T2. The differences in k_{eff} caused by this data substitution are shown in Figure 3. The strong underestimation of k_{eff} (compared to the reference ENDF/B-VII.1 case) is observed for ^{239}Pu with both JEFF-3.1.2 and JEFF-3.2T2. The new evaluated file proposed for JEFF-3.2 has an even higher impact due to reduced fission cross-section, because, as is seen from Figure 2, the net neutron production is lower than in other evaluations. However, this 0.3% underestimation does not change the global picture when ENDF/B-VII.1 is substituted by JEFF libraries. This global difference, as demonstrated by Figures 2 and 3, is governed by the combined effect of other plutonium isotopes, ^{56}Fe and ^{55}Mn . For instance, the JEFF-3.2T2 evaluation results in higher neutron absorption by ^{240}Pu than JEFF-3.1.2 with ENDF/B-VII.1 data in between. As a result, k_{eff} is highly sensitive to this, even small, difference.

Figure 3: Sensitivity Δ_i of k_{eff} to the change of nuclear data for a particular nuclide

Horizontal lines show the differences in k_{eff} obtained with global library change: from ENDF/B-VII.1 to JEFF-3.1.2 (red line) and to JEFF-3.2T2 (green line)



It is also interesting to note that differences in net neutron behaviour of ^{56}Fe between evaluations are rather small, while k_{eff} has a remarkable increase when substituting the ENDF/B-VII.1 evaluation with JEFF. This immediately shows that elastic and inelastic scattering cross-sections of ^{56}Fe together play a more important role than neutron capture. Figures 2 and 3 give an indication of which data has higher integrated sensitivity coefficients without performing separate calculations of these coefficients. The uncertainty levels on the data can also be predicted when analysing these figures. Indeed, rather large positive differences in neutron production on ^{238}Pu provoke a significant increase in k_{eff} (by 0.15%). This means that fission cross-section and average neutron release per fission event are rather uncertain.

Sensitivity and uncertainty analysis performed for a previous model of MYRRHA, XT-ADS (Sugawara, *et al.*, 2011) resulted in the priority list of uncertainties which have to be improved by setting up dedicated integral and differential experiments. For the current design, which differs from XT-ADS by fuel enrichment, fuel assembly design, etc.,

the neutron spectrum remains almost the same; the priority list has not been changed significantly. One can only add ^{55}Mn neutron capture cross-section, ^{56}Fe elastic and inelastic scattering cross-sections and change the sequence in descending order of importance:

- ^{239}Pu neutron capture and fission neutron yields;
- ^{238}Pu fission, capture and (n,2n) cross-sections;
- ^{240}Pu fission neutron yield;
- ^{241}Pu fission and elastic scattering cross-sections;
- ^{56}Fe neutron capture, elastic and inelastic scattering cross-sections;
- ^{55}Mn neutron capture cross-section;
- ^{209}Bi neutron capture and (n,2n) cross-sections.

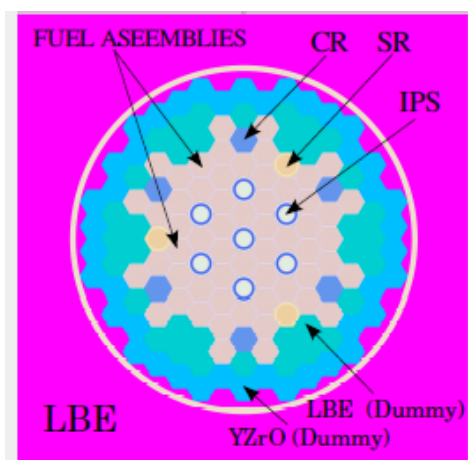
To confirm the results of this sensitivity analysis, detailed sensitivity and uncertainty analysis for the current MYRRHA design has been launched in the framework of the EC FP7 CHANDA project. Some preliminary results are reported below.

Sensitivity profiles

A detailed sensitivity analysis of k_{eff} to the neutron cross-section data has been performed using the SCALE-6.1 code suite (ORNL, 2011). The calculation sequence included KENO-VI Monte Carlo forward and adjoint transport calculations followed by the calculation of sensitivity coefficients by the SAMS module. SAMS calculates the sensitivity coefficients to every cross-section involved in the transport calculations as well as to the fission neutron multiplicity ($\bar{\nu}$) and the fission spectrum (χ).

A model of a critical MYRRHA core with 57 fresh fuel assemblies has been used for KENO-VI calculations. The number of assemblies in this case is less than for the subcritical core reported in the previous section because higher Pu content in MOX has been used here. The core layout is shown in Figure 4. The fuel assemblies are modelled in detail, while the rest of the elements (in-pile sections for material testing, subassemblies with control and safety rods, dummy assemblies and reflector assemblies) is represented as homogenised hexagonal cells. The control rods are extracted from the core giving an initial reactivity excess of $\sim 5\,000$ pcm.

Figure 4: Model of MYRRHA critical core with 57 fresh fuel assemblies implemented in the KENO-VI code of the SCALE-6.1 package



In this sensitivity analysis the following values have been obtained:

- Sensitivity coefficients, $\frac{\partial k_{eff}}{k_{eff}} / \frac{\partial \sigma_i}{\sigma_i}$ which reflect the changes in k_{eff} with the variation of the energy group cross-section. The energy dependence of the sensitivity coefficients of the same reaction forms the sensitivity profile.
- Integrated sensitivity coefficients (ISC) as results of sensitivity profiles integration over energy. They are used to rank the reactions according to their importance for k_{eff} .

Table 2 lists the reactions influencing the criticality calculations of the MYRRHA core. Besides reactions on Pu and U isotopes, the elastic scattering of neutrons on ^{209}Bi could have a significant impact on k_{eff} . In general, this list of the 12 most important reactions corresponds to the list drawn up in the previous section. The exceptions are ^{56}Fe and ^{238}Pu , which certainly influence the criticality calculations but the integrated sensitivity coefficients on these isotopes are rather small. Hence, a deeper investigation of nuclear data for these isotopes is required. That is why these coefficients, three most important for each isotope, are also listed in Table 2 (highlighted in grey).

The comparison of nuclear data evaluations for ^{56}Fe and ^{238}Pu is presented below.

**Table 2: Integrated sensitivity coefficients (ISC)
sorted in decreasing order of ISC absolute value**

The three largest ISC of ^{56}Fe and ^{238}Pu are highlighted in light and dark grey, accordingly

Isotope	Reaction	ISC	Std. dev. (1σ), %
^{239}Pu	$\bar{\nu}$	0.6969	0.01
^{239}Pu	(n,f)	0.4779	0.01
^{241}Pu	$\bar{\nu}$	0.1035	0.01
^{238}U	(n, γ)	-0.1023	0.02
^{240}Pu	$\bar{\nu}$	0.08256	0.01
^{241}Pu	(n,f)	0.07122	0.01
^{238}U	$\bar{\nu}$	0.06128	0.02
^{239}Pu	(n, γ)	-0.05764	0.03
^{240}Pu	(n,f)	0.05577	0.02
^{209}Bi	(n,n)	0.05039	0.30
^{238}U	(n,f)	0.03767	0.04
^{240}Pu	(n, γ)	-0.02564	0.03
^{56}Fe	(n,n)	0.02215	1.28
^{56}Fe	(n, γ)	-0.01409	0.02
^{56}Fe	(n,n')	-0.00733	0.96
^{238}Pu	$\bar{\nu}$	0.01961	0.01
^{238}Pu	(n,f)	0.01347	0.01
^{238}Pu	(n, γ)	-0.00351	0.04

Impact of nuclear data evaluations for ^{56}Fe on MYRRHA criticality calculations

Evaluations from three major nuclear data libraries have been compared:

- The ENDF/B-VII.1 evaluation is based on the older data taken from ENDF/B-VI.1 (Chadwick, *et al.*, 1999).
- JENDL-4.0 data (Shibata, *et al.*, 2011) were taken from JENDL-3.3 (Shibata, *et al.*, 2002) with some reaction cross-sections recalculated for JENDL-4.0.
- The JEFF-3.1.2 evaluation was copied from EFF-3.1 (Hogenbirk, *et al.*, 1995).

Below 850 eV neutron capture and elastic scattering cross-sections are written by means of resonance parameters in all three evaluations. But ENDF/B-VI.1 and JENDL-4.0 provide a background cross-section for (n,γ) which is added to the cross-section calculated with the resonance parameters. On the other hand, EFF-3.1 provides more resonances for which at least two, at 423.1 and 446.0 keV, are not referred in the literature. The inelastic scattering cross-section is given with more detail in the EFF-3.1 evaluation, where more excited levels are represented compared to JENDL-4.0 and ENDF/B-VI.1. The impact of the above differences is shown in Table 3. The JEFF-3.1.2 and ENDF/B-VII.1 evaluations have been compared. Taking the JEFF-3.1.2 file for ^{56}Fe as reference (and using the JEFF-3.1.2 library for other nuclides), the inelastic scattering and neutron capture cross-sections were replaced in this file by the corresponding cross-section data from ENDF/B-VII.1 evaluation, and the impact on k_{eff} was studied.

Table 3: Impact of modifications in the ^{56}Fe file

^{56}Fe file	Modified part	k_{eff}	Δk_{eff} (pcm)
JEFF-3.1.2	–	1.05374±0.00008	–
ENDF/B-VII.1	–	1.05224±0.00008	-150
JEFF-3.1.2	(n,n')	1.05343±0.00007	-31
JEFF-3.1.2	(n, γ)	1.05275±0.00008	-99

The difference in neutron capture cross-section covers almost two-thirds of the difference observed in the results of criticality calculations done with two ^{56}Fe evaluations. The background cross-section provided in ENDF/B-VII.1 is responsible for this effect.

Impact of nuclear data evaluations for ^{238}Pu on MYRRHA criticality calculations

The analysis of three evaluations for ^{238}Pu reveals that:

- For ENDF/B-VII.1, a new evaluation was performed in September 2010. It takes the resonance parameters from JENDL-4.0.
- For JENDL-4.0, a completely new evaluation was released in January 2010.
- JEFF-3.1.2 takes the evaluation from JENDL-3.2 (Nakagawa, *et al.*, 1995), but in the unresolved resonance region the BROND-2.2 (Blokhin, *et al.*, 1994) evaluation is used.

The main differences in neutron capture and fission cross-sections are observed in the unresolved resonance region (URR), where the BROND-2.2 evaluation uses the resonance parameters to calculate the cross-section, while JENDL-4.0 provides cross-section values stored in MF=3, MT=18 and MT=102 (Trkov, *et al.*, 2012). The differences in fission neutron multiplicities can be grouped as less than 1% at the energies up to 1 MeV, and less than 5% from 1 to 20 MeV. The impact of these differences on the criticality calculations is shown in Table 4. The same methodology as for ^{56}Fe was applied.

Table 4: Impact of modifications in the ^{238}Pu file

^{238}Pu file	Modified part	k_{eff}	Δk_{eff} (pcm)
JEFF-3.1.2	–	1.05363±0.00008	–
ENDF/B-VII.1	–	1.05178±0.00008	-185
JEFF-3.1.2	$\bar{\nu}$	1.05378±0.00007	+15
JEFF-3.1.2	(n,f)	1.05201±0.00008	-162
JEFF-3.1.2	(n, γ)	1.05319±0.00008	-44

The difference in the fission cross-section is the most important for the MYRRHA criticality calculations. In the energy range between 0.5 and 150 keV, where BROND-2.2 data is used in JEFF-3.1.2, the cross-section runs higher than in the JENDL-4.0 evaluation.

Conclusions

Detailed sensitivity analysis of effective neutron multiplication factor to the change of nuclear data evaluation has been performed. It allowed creating a priority list of nuclides for further, deeper analysis. It has been shown that the test version of the JEFF-3.2 library gives closer results to ENDF/B-VII.1 than JEFF-3.1.2. With this tendency of libraries to converge, however, the open issue is to assess the uncertainties on the cross-sections and fission multiplicities.

The importance of the ^{56}Fe and ^{238}Pu reactions has been demonstrated. The main differences between evaluations and their impact on the criticality calculations for the MYRRHA neutronic model have been studied. For ^{56}Fe , the most relevant difference between evaluations comes from the background cross-section for radiative neutron capture reaction. It is given in the ENDF/B-VII.1 evaluation and is omitted in JEFF-3.1.2. A better description of the resonance range would improve the ENDF/B-VII.1 or JENDL-4.0 evaluations. For ^{238}Pu , the JEFF-3.1.2 file takes the unresolved resonance parameters from BROND-2.2, which overestimates neutron-induced fission cross-section and causes a large difference in the criticality calculations. A new evaluation for ^{238}Pu is highly recommended for future releases of the JEFF library. The comparison of nuclear data evaluations reported here for ^{56}Fe and ^{238}Pu will be extended in the framework of the EC FP7 CHANDA project on the other nuclides and reactions identified in this study.

References

- Blokhin, A.I., *et al.* (1994), “Current Status of Russian Evaluated Neutron Data Libraries”, *Proc. Conf. Nucl. Data and Techn.*, Gatlinburg, TN, ORNL, Vol. II, p. 695.
- Chadwick, M.B., *et al.* (1999), LA-UR-99-1222, Los Alamos National Laboratory (LANL), Los Alamos, NM, United States.
- Chadwick, M.B., *et al.* (2011), “ENDF/B-VII.1 Nuclear Data for Science and Technology: Cross Sections, Covariances, Fission Product Yields and Decay Data”, *Nucl. Data Sheets*, 112, pp. 2887-2996.

- Haeck, W. and B. Verboomen (2005), *ALEPH-DLG (Data Library Generator) – Creating a General Purpose Validated Application Library for MCNP(X) and ALEPH*, Report SCK•CEN-BLG-1002, SCK•CEN, Mol, Belgium.
- Hogenbirk, A., *et al.* (1995), “Validation of the EFF-3.0 Evaluation for Fe-56”, EFF-DOC-382.
- MacFarlane, R.E. and D.W. Muir (1994), *The NJOY Nuclear Data Processing System, Version 91*, LA-12740-M, Los Alamos National Laboratory (LANL), Los Alamos, NM, United States.
- Nakagawa, T., *et al.* (1995), “Japanese Evaluated Nuclear Data Library, Version 3 Revision-2; JENDL-3.2”, *J. Nucl. Sci. Technol.*, 32, p. 1259.
- OECD/NEA (Organisation for Economic Co-operation and Development/Nuclear Energy Agency) (2009), *Independent Evaluation of the MYRRHA Project*, NEA No. 6881, OECD/NEA, Paris.
- OECD/NEA (2012), “JEFF-3.2T2”, NEA Data Bank webpage “JEFF and EFF projects”, OECD/NEA, Paris, accessed 6 June 2014, www.oecd-nea.org/dbdata/jeff.
- ORNL (Oak Ridge National laboratory) (2011), *SCALE: A Modular Code System for Performing Standardized Computer Analyses for Licensing Evaluation*, ORNL/TM-2005/39, ORNL, Oak Ridge, TN, United States.
- Pelowitz, D.B. (ed.) (2008), *MCNPX User’s Manual*, Version 2.6.0, LA-CP-07-1473, Los Alamos National Laboratory (LANL), Los Alamos, NM, United States.
- Santamarina, A., *et al.* (2009), *The JEFF-3.1.1 Nuclear Data Library*, JEFF Report 22, NEA No. 6807, OECD/NEA, Paris.
- Shibata, K., *et al.* (2011), “JENDL-4.0: A New Library for Nuclear Science and Engineering”, *J. Nucl. Sci. Technol.*, 48 (1), pp. 1-30.
- Shibata, K., *et al.* (2002), “Japanese Evaluated Nuclear Data Library Version 3 Revision-3: JENDL-3.3”, *J. Nucl. Sci. Technol.*, 39, p. 1125.
- Stankovskiy, A. (2012), *Processing of the JEFF-3.1.1, JEFF-3.1.2 and ENDF/B-VII.1 Neutron Cross Section Data into Multi-Temperature Continuous Energy Monte Carlo Radiation Transport Libraries*, Report SCK•CEN/1684326, SCK•CEN, Mol, Belgium.
- Sugawara, T., *et al.* (2011), “Nuclear Data Sensitivity/Uncertainty Analysis for XT-ADS”, *Ann. Nucl. Energy*, 38, pp. 1098-1108.
- Trkov, A., *et al.* (2012), *ENDF-6 Formats Manual*, Report BNL-90365-2009 Rev. 2, Brookhaven National Laboratory, Upton, NY, United States.

General Interest – Part 3

Chair: Z. Ge

Application of a Bayesian/generalised least-squares method to generate correlations between independent neutron fission yield data

L. Fiorito,^{a,b} C. Díez,^c O. Cabellos,^{c,d} A. Stankovskiy,^a G. Van den Eynde,^a P.E. Labeau^b

^aInstitute for Advanced Nuclear Systems, SCK•CEN, Mol, Belgium

^bUniversité Libre de Bruxelles (ULB), Brussels, Belgium

^cDpto. de Ingeniería Nuclear, Escuela Técnica Superior de Ingenieros Industriales
Universidad Politécnica de Madrid (UPM), Madrid, Spain

^dInstituto de Fusión Nuclear, Escuela Técnica Superior de Ingenieros Industriales
Universidad Politécnica de Madrid (UPM), Madrid, Spain

Abstract

Fission product yields are fundamental parameters for several nuclear engineering calculations and in particular for burn-up/activation problems. The impact of their uncertainties was widely studied in the past and evaluations were released, although still incomplete. Recently, the nuclear community expressed the need for full fission yield covariance matrices to produce inventory calculation results that take into account the complete uncertainty data.

In this work, we studied and applied a Bayesian/generalised least-squares method for covariance generation, and compared the generated uncertainties to the original data stored in the JEFF-3.1.2 library. Then, we focused on the effect of fission yield covariance information on fission pulse decay heat results for thermal fission of ²³⁵U. Calculations were carried out using different codes (ACAB and ALEPH-2) after introducing the new covariance values. Results were compared with those obtained with the uncertainty data currently provided by the library. The uncertainty quantification was performed with the Monte Carlo sampling technique. Indeed, correlations between fission yields strongly affect the statistics of decay heat.

Introduction

Nowadays, any engineering calculation performed in the nuclear field should be accompanied by an uncertainty analysis. In such an analysis, different sources of uncertainties are taken into account. Works such as those performed under the UAM project (Ivanov, *et al.*, 2013) treat nuclear data as a source of uncertainty, in particular cross-section data for which uncertainties given in the form of covariance matrices are already provided in the major nuclear data libraries. Meanwhile, fission yield uncertainties were often neglected or treated shallowly, because their effects were considered of second order compared to cross-sections (Garcia-Herranz, *et al.*, 2010).

However, the Working Party on International Nuclear Data Evaluation Co-operation (WPEC) – a party dedicated to assessing the needs of nuclear data improvement – raised new interest on fission yield data within its Subgroup 37 (SG37), with the goal of developing

“Improved fission product yield evaluation methodologies” (Mills, 2013), not only in order to quantify the impact of such uncertainties, but also to provide a proper set of variances and correlation matrices.

In addition, fission yield data are of critical importance in decay heat applications (Katakura, 2012). The calculation of the decay heat and of its uncertainty has a deep impact on a series of industrial challenges like the design of emergency cooling systems, the design of transport waste casks and storage facilities or the cooling time that is needed before maintenance. The uncertainty on decay heat stems from the propagation of variance and covariance values of the nuclear data. Individual fission yield uncertainties, where no correlation is taken, are regarded as the main contributors to the fission pulse decay heat uncertainty (Diez, Cabellos and Martinez, 2011). However, the use of covariance data may have a huge impact on the final result.

The aim of this study was to analyse and apply a Bayesian/generalised least-squares (GLS) method for the generation of fission yield data covariances. Then, we assessed the impact of the correlations on fission pulse decay heat (FPDH) calculations for ^{235}U thermal fission, after generating covariance matrices using the JEFF-3.1.2 library (Kellet, Bersillon and Mills, 2009) The uncertainty quantification (UQ) was performed with the Monte Carlo sampling method.

Description of fission yields

Fission yields (FY) characterise the probability of a particular nuclide or mass to be formed after fission. Accurate FY measurements and/or predictions, as well as the knowledge of the carried uncertainties, are essential to many applications in nuclear technology. The widely used general-purpose evaluated nuclear data library JEFF-3.1.2 provides these data in the ENDF-6 format (CSEWG, 2013) along with their uncertainties as standard deviation. To date, no correlation between FY is supplied in such a library, but several institutions/projects are devoting all their energies to developing methodologies to generate full covariance matrices.

There exist different definitions of FY, as outlined below.

The independent fission yield (IFY), $y(A,Z,I)$, is defined as the number of atoms of nuclide with mass A , charge Z and isomeric state I produced directly from one fission after the emission of prompt neutrons, but before the emission of delayed neutrons. Several coefficients need to be known for each fissioning system to calculate IFY, but even those chains with the highest coverage of measured data do not provide values for all the parameters. It is indeed necessary to resort to semi-empirical models and interpolation/extrapolation methods.

The cumulative fission yield (CFY) $C(A,Z,I)$ is the total number of atoms of nuclide with mass number A , charge Z and isomeric state I produced over all time after one single fission. That is, the total number of atoms of that nuclide generated both through one single direct fission and radioactive decay of all the precursors. CFY have a strong relationship with fission products decay chains, which means that they can be calculated from IFY and decay data branching fractions using the so-called “Q-matrix” approach (James, Mills and Weaver, 1991), represented by Eq. (1):

$$C_j = \sum_i Q_{ji} Y_i \quad (1)$$

where Q_{ji} are the decay branching ratios from isotope i to j . Therefore, the Q-matrix is the matrix of the decay branching ratios that steers fission products toward stable nuclides.

The chain fission yield (ChFY) $Ch(A)$ is defined as the sum of cumulative yields of the last stable or long-lived chain members with same mass A and is obtained in classical mass spectrometric measurements of long-lived and stable end products of mass chains.

The term “chain yield” has been commonly used to describe both the sum of cumulative yields of the last stable or long-lived chain members, and the isobaric sum of independent yields [mass fission yields (MFY) $Y(A)$]:

$$Y(A) = \sum_i y_i \quad (2)$$

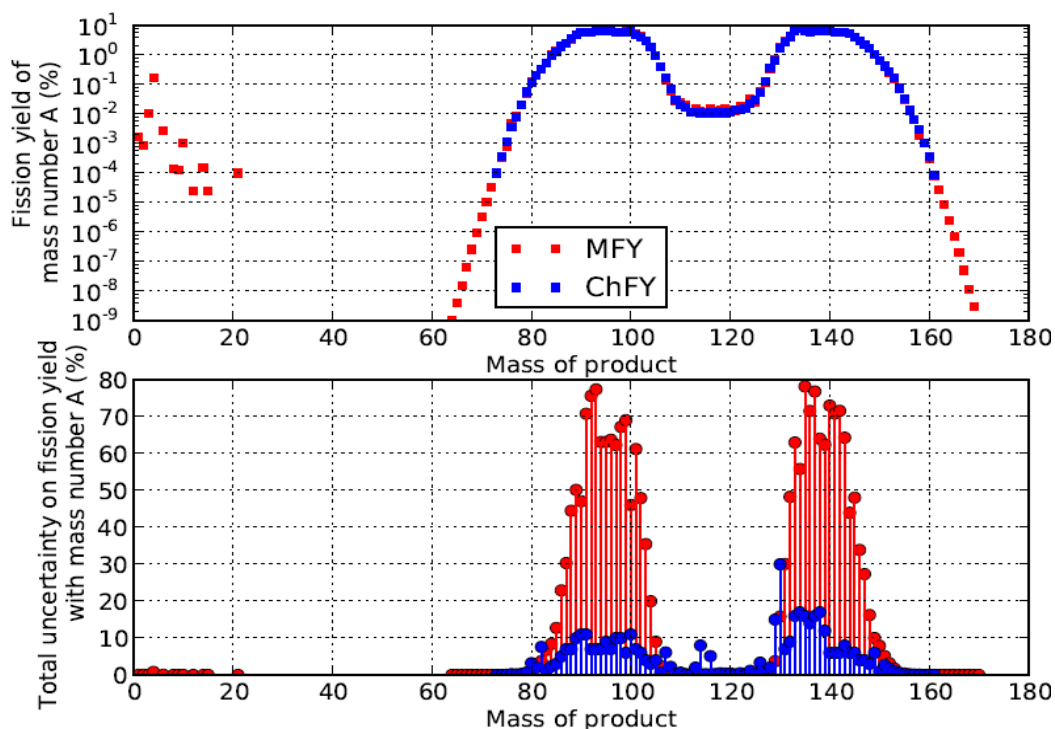
The two definitions, even if slightly, may differ by a few per cent as the second does not include the contribution of delayed-neutron emission (Mills, 1995). However, for the purpose of this work, ChFY and MFY are treated indistinctly.

Figure 1 shows that the evaluated MFY (or ChFY) stored in the libraries are in good agreement with those calculated with Eq. (2). However, the associated uncertainties show discrepancies. Uncertainties on the total MFY are calculated by means of simple propagation through the sum of IFY, assuming no correlation between different IFY belonging to the same chain [Eq. (3)]:

$$\Delta Y(A) = \sqrt{\sum_i (\Delta y_i)^2} \quad (3)$$

The gap between calculated and evaluated MFY uncertainties may arise from the lack of correlations between IFY, highlighted in Eq. (3). Since a similar behaviour also occurred in the calculation of CFY uncertainties, the implementation of a covariance matrix generation method appears as an urgent need.

Figure 1: Evaluated and calculated mass yield distribution and uncertainties for ^{235}U thermal fission products from the JEFF-3.1.2 database



Bayesian/generalised least-squares method

Great efforts have been committed to developing methodologies for correlation generation (full covariance matrices) for IFY data. Katakura (2012), followed by Kawano and Chadwick (2013), proposed a Bayesian/generalised least-squares (GLS) method, where the IFY covariance matrix is updated with information on the chain yields. These proposals, together with a variation in which the IFY covariance matrix is updated with CFY uncertainties, are described and reported hereunder.

The Bayesian/generalised least-squares (GLS) method is an adjustment technique which states that the information on some prior system parameters can be improved with the addition of new knowledge – new data – (e.g. experimental or evaluated response values η), for which relationships between data and parameters are established [Eq. (4)]. These relationships, or constraints, must be linearised in the form:

$$y - y_a = S(\theta - \theta_a) \quad (4)$$

where θ are the parameters of the system, θ_a the prior estimates of θ , y the responses of the constraining equation, y_a the responses of the constraining equation to the prior estimates θ_a and S are the sensitivity coefficients of the response $y - y_a$ to the parameters $\theta - \theta_a$. It was assumed that no correlation existed between the prior and the new information. Then, further information η could be introduced in order to derive refined values for the parameters θ , with all the available uncertainty information properly incorporated into the formalism. The updating process is represented by Eqs. (5) and (6):

$$\theta - \theta_a = V_a S^t (S V_a S^t + V)^{-1} (\eta - y_a) \quad (5)$$

$$V_s = V_a - V_a S^t (S V_a S^t + V)^{-1} S V_a \quad (6)$$

where V_a is the covariance matrix of the prior estimates of the parameters θ_a , V is the covariance matrix of the introduced data fitting the constraining system η , and V_s is the updated covariance matrix of the system parameters (θ). Superscript t refers to the transpose of a vector or a matrix.

It has already been proposed to update the covariance matrix with the evaluated MFY variance information. In such a case, S becomes the array of sensitivity coefficients of MFY to IFY, η the evaluated MFY introduced in the system and y_a the MFY calculated with the prior IFY (θ_a) in Eq. (4), that is, summing up all the yields belonging to the same chain. V_a and V are the variance matrices of the prior θ_a and of the experimental MFY, respectively.

A new proposal introduced in this current paper and developed by the authors is the use of the CFY evaluated data to update the variance matrix of the IFY. Then, η becomes the evaluated CFY with variance matrix V , y_a is the array of CFY calculated with Eq. (4), where θ_a is the vector of prior IFY and V_a its variance matrix. Here, the Q-matrix equation [Eq. (1)] is the linear constraining system and S are the sensitivity coefficients of IFY to CFY.

Uncertainty quantification on FPDH calculations

FY data and uncertainties have a major role in fission pulse decay heat (FPDH) calculations and correlations may significantly influence the decay heat uncertainty. In such cases, uncertainty quantification (UQ) studies come to hand to assess this impact. Here, we generated covariance data by means of the Bayesian/GLS method previously

described, using uncertainties from the JEFF-3.1.2 database. The UQ on the FPDH calculation for ^{235}U thermal fission follows.

The fission pulse decay heat is the heat generated by the radioactive decay after a single atom of a specific material fissions. Accurate calculations of such values assume a capital importance in reactor operation strategies as the residual heat, which inevitably follows the reactor shutdown, is one of the most important parameters for reactor safety. FPDH was calculated for a thermal fission event of ^{235}U : radioactive decay and fission yield data were taken from the library, whereas cross-sections do not take part in this kind of calculation. The time evolution of radioactive material subject to pure decay is described by the system of ordinary differential equations (ODE) in Eq. (7):

$$\frac{dN_i}{dt} = -\lambda_i N_i + \sum_j \lambda_j \beta_{ji} N_j \quad i = 1, \dots, M \quad (7)$$

where λ are the decay constants, N_i the concentrations of isotopes involved in the calculation, β_{ji} is the branching ratio which indicates the decay mode and the fraction of decays that converts isotope j into i , and M is a finite integer, that is, the size of the system. The initial composition, $N(t=0)$, is the same FY distribution given in the library for ^{235}U thermal fission.

The decay heat is calculated with Eq. (8), with the isotopic inventory being followed throughout the whole cooling time:

$$DH = \sum_i DH_i = \sum_i \lambda_i N_i \left(\sum_j \beta_{ij} E_j \right) \quad (8)$$

Here, E_j is the average released energy for the corresponding decay model given by the β_{ij} branching ratio.

Two codes were used to perform these calculations:

- ACAB (Sanz, Cabellos and Garcia-Herranz, 2008) is an activation/transmutation code that solves the general nuclear transmutation chains for multi-dimensional neutron flux distributions. Its ODE solver is based upon the ORIGEN algorithm (Isotalo and Aarnio, 2011), which uses a truncated Taylor series expansion of the exponential matrix, from which all the short-lived nuclides are removed and handled separately with the Gauss-Seidel iterative method under an assumption of secular equilibrium.
- ALEPH (Van den Eynde, *et al.*, 2013) is a general-purpose burn-up code created and developed at the SCK•CEN Belgian Nuclear Research Centre. Its new release ALEPH-2 has decay heat and FPDH calculation capabilities and resorts to the highly accurate Runge-Kutta method RADAU5 (Hairer and Wanner, 1980), as an inherent routine, to solve the system of depletion equations.

We carried out a Monte Carlo sampling to quantify the impact of IFY uncertainties on FPDH. One thousand i.i.d. random samples from normal probability density functions (PDF) granted the convergence of the mean and standard deviation of the IFY. Best-estimate and uncertainty values stored in JEFF-3.1.2 represented the mean and standard deviation of the PDF, respectively. Since small IFY generally carry high uncertainties, the random sampling of a negative value is likely to happen. When it occurred, such random samples were set to zero. Then, a small bias could be expected from the use of truncated normal PDF, still negligible for decay heat calculation purposes.

For each draw, a full FPDH calculation was performed and 1 000 different response functions were retrieved. Then, through a statistical analysis of the response functions, it was possible to gather information such as PDF, mean and standard deviation of the FPDH.

Results and discussion

Plots and results of FPDH calculations for ^{235}U thermal fission with UQ are presented here. Monte Carlo sampling is performed with 1 000 samples to guarantee the convergence of IFY means and standard deviations. Full simulations are carried out using both ACAB and ALEPH codes, making sure to keep full consistency on all the data treated in the system. A list of the performed calculation is presented as follows:

- I. Total FPDH calculation with variance matrix without correlations (JEFF-3.1.2 + no corr.).
- II. Total FPDH calculation with correlation matrix generated with Bayesian/GLS method and mass chain yield information [JEFF-3.1.2 + COV(ChFY)].
- III. Total FPDH calculation with correlation matrix generated with Bayesian/GLS method and cumulative yield information [JEFF-3.1.2 + COV(CFY)].
- IV. Total FPDH calculation with correlation matrix generated with Bayesian/GLS method and cumulative yield information; we allowed only for the diagonal terms of the matrix [JEFF-3.1.2 + COV(CFY), only diag.].

To guarantee coherence in the calculations, all the simulated values have been compared with Tobias' (1989) compiled data.

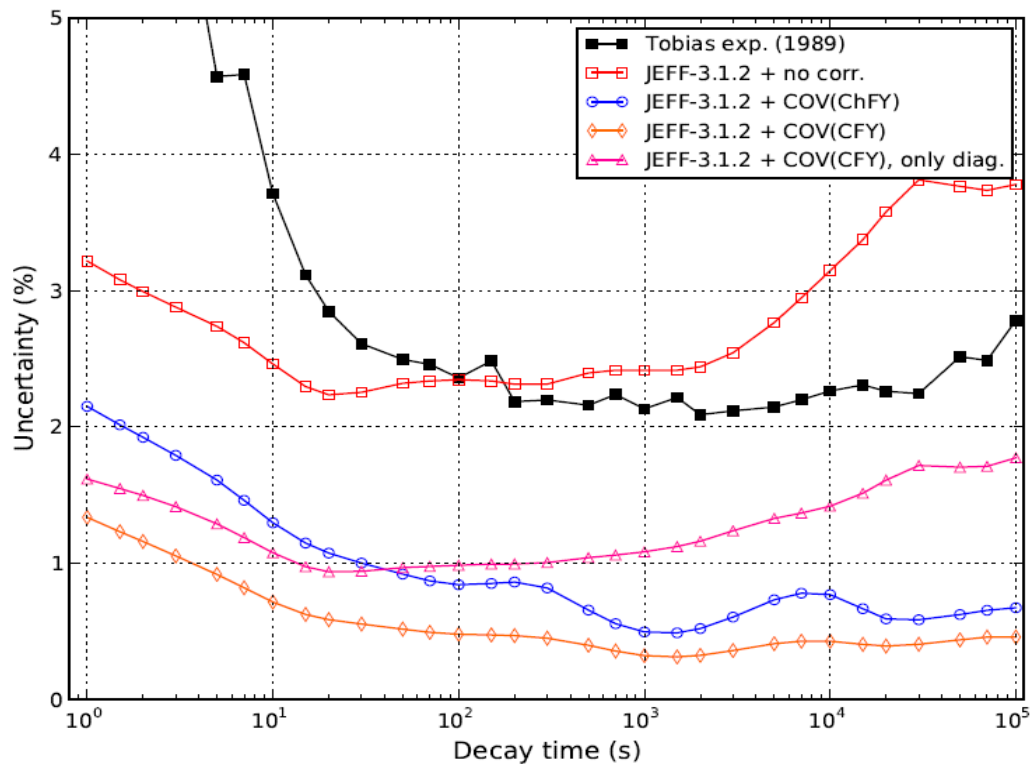
As expected, for pure decay systems, the discrepancy related to the use of different codes – ACAB or ALEPH – is negligible in FPDH calculations.

Results obtained with data from the JEFF-3.1.2 library are reported in Figure 2. Uncertainties, in the form of relative standard deviations, are plotted as functions of the decay time and sketched together with Tobias' experimental uncertainties (black line). The red curve (squares) is calculated using non-correlated fission yields (I). The blue curve (circles) corresponds to calculation II, where information on evaluated mass fission yields is introduced from the IAEA (1974). The orange line (diamonds) shows results for calculation III.

The full covariance matrices for IFY contribute to strongly reducing the uncertainty on decay heat. A glance at Eq. (6) immediately explains this behaviour; evaluated uncertainties in the right-hand term of the equation cut down the diagonal terms of the FY covariance matrix. This effect is more enhanced when the new data introduced in the system carry uncertainties that are smaller than the prior parameters. This happens because the piece of information introduced in the system in order to update the prior IFY data is more powerful when the variance of the new data is much smaller than that of the calculated observables, so that the evaluated new data are dominant. Strong variance reductions also occur when the uncertainty of a single parameter (IFY) has a very high sensitivity to the constraining system in Eq. (4). Hence, most of the uncertainty is removed from the diagonal to be reintroduced as negative correlation between IFY. Small adjusted uncertainties of IFY inevitably contribute to reduce the uncertainty on FPDH, as well. However, reduced IFY variances are not the only contributors to this effect.

FPDH in the purple line (triangles) is obtained using the Bayesian/GLS method with CFY evaluated data, this time with off-diagonal terms of the IFY covariance matrix cancelled out (IV); only the contribution of the main diagonal is taken into account. The purple curve has a shape similar to the red line, that is, when IFY are not correlated, but the uncertainty suffers a sharp reduction.

However, such a reduction is not sufficient to justify the uncertainty values obtained with IV, which means that not only adjusted diagonal terms (variances), but also correlations between IFY affect the uncertainty of the decay heat introducing negative contributions.

Figure 2: Uncertainty (%) of thermal FPDH for ^{235}U calculated with JEFF-3.1.2

Conclusion

Fission yields are catalogued amongst the sources of uncertainties in the widely-used nuclear data library JEFF-3.1.2, however the lack of correlations impacts on the reliability and consistency of the library itself and its use for practical applications. A Bayesian/generalised least-squares method was applied to generate covariance matrices for independent fission yields. We performed our study on the ^{235}U thermal IFY stored in the JEFF-3.1.2 database, introducing evaluated CFY and MFY data. Then, we tested the effect of such correlations on a fission pulse decay heat problem.

The implementation of Bayesian/generalised least-squares method provided negative correlations between IFY and simultaneously reduced the IFY variance values. Correlations on IFY levelled off the discrepancies on evaluated and calculated fission yields, thus justifying the covariance generation methodology. The uncertainty quantification of FPDH results proved that the use of non-correlated IFY overestimates the decay heat uncertainty.

Acknowledgements

The research leading to these results has received funding from the FP7-EURATOM-FISSION-2009: Project ANDES/249671. Part of the project was sponsored in the framework of a collaboration between ULB and SCK•CEN. Also, this work is partially supported by the Spanish Ministry of Education with an FPU grant (AP2009-1801) for second author C. Díez). The authors want also to thank I.C. Gauld (ORNL), M.T. Pigni (ORNL), T. Kawano (LANL) and R.W. Mills (NNL) for fruitful advice.

References

- CSEWG (2013), *ENDF-6 Formats Manual. Data Formats and Procedures for the Evaluated Nuclear Data Files ENDF/B-VI and ENDF/B-VII*, ENDF-102 BNL-90365-2009 Rev. 2, Brookhaven National Laboratory, Upton, NY, United States.
- Díez, C., O. Cabellos and J. Martinez (2011), “Propagation of Nuclear Data Uncertainties in Fuel Cycle Calculations Using Monte Carlo Technique”, *Proc. of the Conference M&C 2011*, Rio de Janeiro, Brazil.
- Garcia-Herranz, N., *et al.* (2010), “Nuclear Data Requirements for the ADS Conceptual Design EFIT: Uncertainty and Sensitivity Study”, *Annals of Nuclear Energy*, 37, pp. 1570-1579.
- Hairer, E. and G. Wanner (1980), *Solving Ordinary Differential Equations II: Stiff and Differential-Algebraic Problems*, Springer-Verlag, Berlin, Heidelberg, New York.
- Isotalo, A. and P. Aarnio (2011), “Comparison of Depletion Algorithms for Large Systems of Nuclides”, *Annals of Nuclear Energy*, 38, pp. 261-268.
- Ivanov, K., *et al.* (2013), *Benchmarks for Uncertainty Analysis in Modelling (UAM) for the Design, Operation and Safety Analysis of LWRs*, NEA/NSC/DOC(2013)7, OECD/NEA, Paris.
- James, M., R. Mills and D. Weaver (1991), *A New Evaluation of Fission Product Yields and the Production of a New Library (UKFY2) of Independent and Cumulative Yields. Part I. Methods and Outline of the Evaluation*, Technical Report AEA-TRS-1015.
- Katakura, J. (2012), *JENDL FP Decay Data File 2011 and Fission Yields Data File 2011*, JAEA, Japan.
- Kawano, T. and M.B. Chadwick (2013), *FPY Data Evaluation for ENDF/BVII.1*, Working Party on International Evaluation Co-operation, Subgroup 37, OECD/NEA, Paris.
- Kellet, M., O. Bersillon and R. Mills (2009), *The JEFF-3.1/-3.1.1 Radioactive Decay Data and Fission Yields Sub-libraries*, NEA No. 6287, OECD/NEA, Paris.
- Mills, R. (1995), *Fission Product Yield Evaluation*, thesis, University of Birmingham, Birmingham, United Kingdom.
- Mills, R. (2013), “WPEC Subgroup 37 Description”, WPEC – Subgroup 37, OECD/NEA, Paris.
- Sanz, J., O. Cabellos and N. Garcia-Herranz (2008), *ACAB Inventory Code for Nuclear Applications: User’s Manual V*, Madrid, Spain.
- Tobias, A. (1989), *Derivation of Decay Heat Benchmarks for ^{235}U and ^{239}Pu by a Least Squares Fit to Measured Data*, CEGB report RD/B/6210/R89.
- Van den Eynde, G., *et al.* (2013), “Development and Validation of ALEPH-2 Monte Carlo Burnup Code”, *Proc. of the Conference M&C 2013*, Sun Valley, ID, United States, pp. 2566-2577.

Effect of fission yield libraries on the irradiated fuel composition in Monte Carlo depletion calculations

E. Mitenkova, N. Novikov

Nuclear Safety Institute of Russian Academy of Sciences
Moscow, Russia

Abstract

Improving the prediction of radiation parameters and reliability of fuel behaviour under different irradiation modes is particularly relevant for new fuel compositions, including recycled nuclear fuel. For fast reactors there is a strong dependence of nuclide accumulations on the nuclear data libraries. The effect of fission yield libraries on irradiated fuel is studied in MONTEBURNS-MCNP5-ORIGEN2 calculations of sodium fast reactors. Fission yield libraries are generated for sodium fast reactors with MOX fuel, using ENDF/B-VII.0, JEFF3.1, original library FY_Koldobsky, and GEFY 3.3 as sources. The transport libraries are generated from ENDF/B-VII.0 and JEFF-3.1. Analysis of irradiated MOX fuel using different fission yield libraries demonstrates the considerable spread in concentrations of fission products. The discrepancies in concentrations of inert gases being ~25%, up to 5 times for stable and long-life nuclides, and up to 10 orders of magnitude for short-lived nuclides.

Introduction

Improving the prediction of radiation parameters and reliability of fuel behaviour under different irradiation modes is particularly relevant for new fuel compositions and recycled nuclear fuel in closed fuel cycles. The accurate depletion calculations are the base while assessing the radiation characteristics of irradiated fuel. The requirements to the accuracy of calculated nuclide accumulations are very different when solving nuclear safety problems such as the radioanalysis of irradiated fuel and estimations of dose rates, simulation of emergency situations in reactor systems (e.g. residual heat analysis within the specified time and emergency heat removal), in thermochemistry for diffusion analysis in irradiated fuel (gaseous and pore diffusion in fuel swelling, the yield of fission gases under the fuel cladding), etc.

Accurate depletion calculations use the full base of fission products and take into account the changes of neutron spectra and one-group cross-sections (for reactions, involved in the transmutation) under different modes of irradiation. For fast reactors the numerous calculations confirm strong dependence of nuclide accumulations on the fission yield library used. In accurate depletion calculations the concentrations of accumulated fission products depend primarily on FY libraries and cross-sections $\sigma_{n,\gamma}$ and $\sigma_{n,2n}$, involved in radioactive-transformation series.

The effect of fission yield libraries on irradiated fuel composition is studied in MONTEBURNS-MCNP5-ORIGEN2 calculations of sodium fast reactors. Fission yield (FY) libraries are generated for sodium fast reactors with MOX fuel, using ENDF/B-VII.0

(FY_B-VII), JEFF-3.1 (FY_JEFF), original library FY_Koldobsky (FY_KLD) and GEFY 3.3 (FY_GEF) as sources. The transport libraries are generated from ENDF/B-VII.0 and JEFF-3.1 source files. In ENDF/B source files the yields of fission products are traditionally presented for the thermal point 0.0253 eV, “average” point 0.4 MeV (or 0.5 MeV) and high-energy point 14 MeV. The three-group energy grid representation causes the ambiguous compilation of FY libraries for the meaningful energy range of fast reactors. The modern versions of original library FY_Koldobsky, GEFY, TENDL contain data for more detailed grids in intermediate and fast energy ranges (Table 1).

Table 1: Energy grid kE in fission yield sources

Source	kE , MeV	FP nuclides	Comment
ENDF/B-VII	2.53 10 ⁻⁸ , 0.5, 14.0	1 321	Ti (Z=22)
FY_Koldobsky	2.53 10 ⁻⁸ , 0.5, 1.0, 2.5, 5.0, 7.5, 10.0, 14.0	820	No data for ²³⁵ U, from Cr (Z=24)
JENDL-4	2.53 10 ⁻⁸ , 1.0, 14.0	1 241	From V (Z=23), Light el.
JEFF-3.1	2.53 10 ⁻⁸ , 0.4, 14.0	1 355	No data for ²³⁹ Pu, ²⁴¹ Pu at $E = 14$ MeV, from Ca (Z=20), Light el.
GEFY 3.3	2.53 10 ⁻⁸ , 0.4, 1, 2, 3, 4, 5, 6, 7, 8, 9, 10, 11, 12, 13, 14, 15, 16, 17, 18, 19, 20	907	Mn (Z=25)
TENDL-2010	2.53 10 ⁻⁸ , 1.0 10 ⁻⁶ , 1.0 10 ⁻⁴ , 0.5, 1.0, 14.0	1 772	Ar (Z=18)

In this paper we present the results of irradiated fuel analysis when using codes MONTEBURNS-MCNP5-ORIGEN2 with the FY_B-VII, FY_JEFF, FY_KLD and FY_GEF libraries. Analysis of irradiated MOX fuel demonstrates the considerable spread in concentrations of fission products. The discrepancies in concentrations of inert gases being ~25%, up to 5 times for some stable and long-lived nuclides (e.g. isotopes of antimony and cadmium), and up to 10 orders of magnitude for short-lived nuclides.

Fission yield library generation

The generation of fission yield library is the important stage of preparing the nuclear database, used for depletion calculation in the codes MONTEBURNS-MCNP-ORIGEN (Mitenkova and Novikov, 2011; Blokhin, Mitenkova and Koldobsky, 2011).

Fission yield libraries can be generated for reactor systems with averaged neutron spectrums or using a specific neutron spectra in key areas of the core. For main actinides the FP_i data (index indicates the i^{th} fission product) are accumulated for kE . The different ENDF/B source files contain from about 800 up to 1 800 fission products. For each energy range kE the sum $\sum_i FP_i({}^kE) = 200$.

For main actinides the average fission yield $\langle FP_i \rangle$ of i^{th} nuclide can be calculated either by the neutron spectrum or by fission rate. We use the second method, because it takes into account the fissile properties in the specific area or in the whole core. The average fission yield $\langle FP_i \rangle$ is defined as:

$$\langle FP_i \rangle = \sum_k C_k * FP_i({}^kE)$$

where weight factors $C_k \left(\sum_k C_k = 1 \right)$ approximate the fission distributions in specific areas:

$$C_k = \int_{k-1E}^{kE} dE_n \Phi(E_n) \sigma_f(E_n) \Big/ \int_0^{E_{max}} dE_n \Phi(E_n) \sigma_f(E_n) \quad (k \geq 1)$$

The average fission yield $\langle FP_i \rangle$ is calculated as:

$$\langle FP_i \rangle = C_1 * FP_i(^1E) + \sum_{k \geq 2} C_k * [FP_i(^{k-1}E) + FP_i(^kE)] / 2$$

Comparative analysis of fission product yield for main actinides

Figure 1: Mass fission product distribution in ^{239}Pu

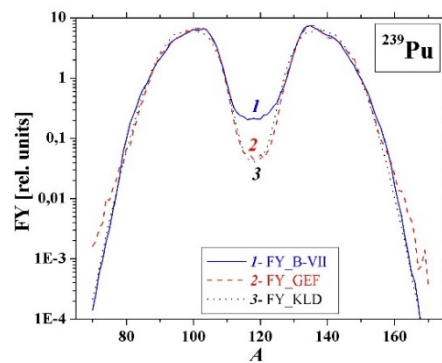


Figure 2: Differences in fission product distribution according to the nucleus charge (Z) in ^{239}Pu

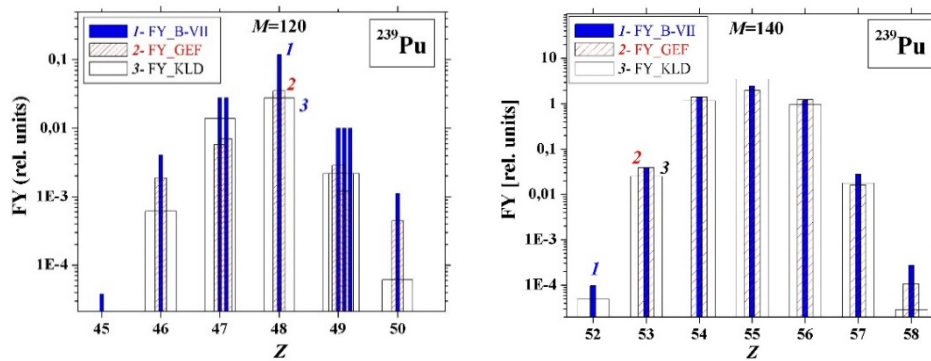


Figure 3: Mass fission product distribution in ^{238}U

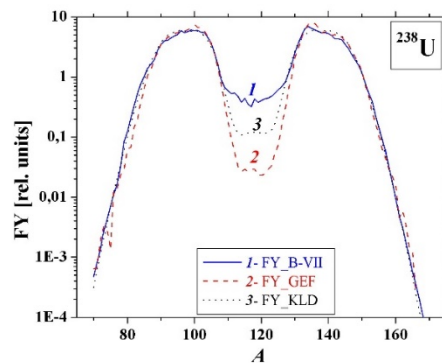


Figure 4: Differences in fission product distribution according to the nucleus charge (Z) in ^{238}U

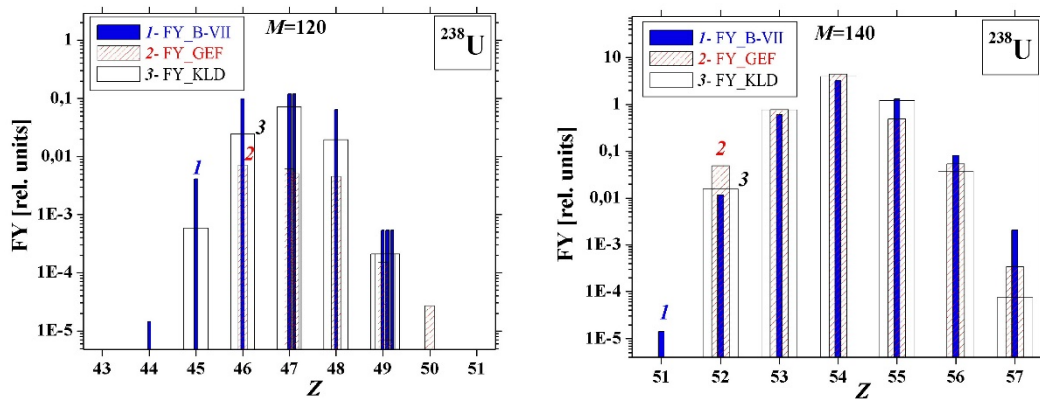


Figure 5: Independent fission yield of isotopes Kr, Xe, Cs in ^{239}Pu

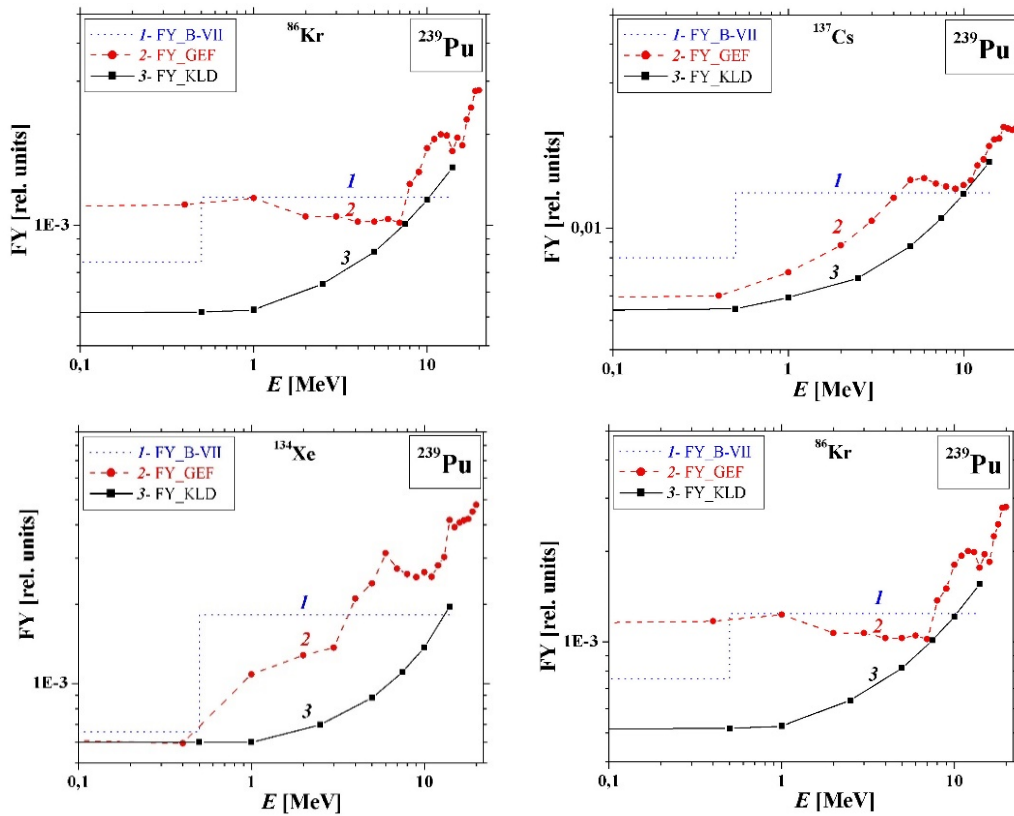
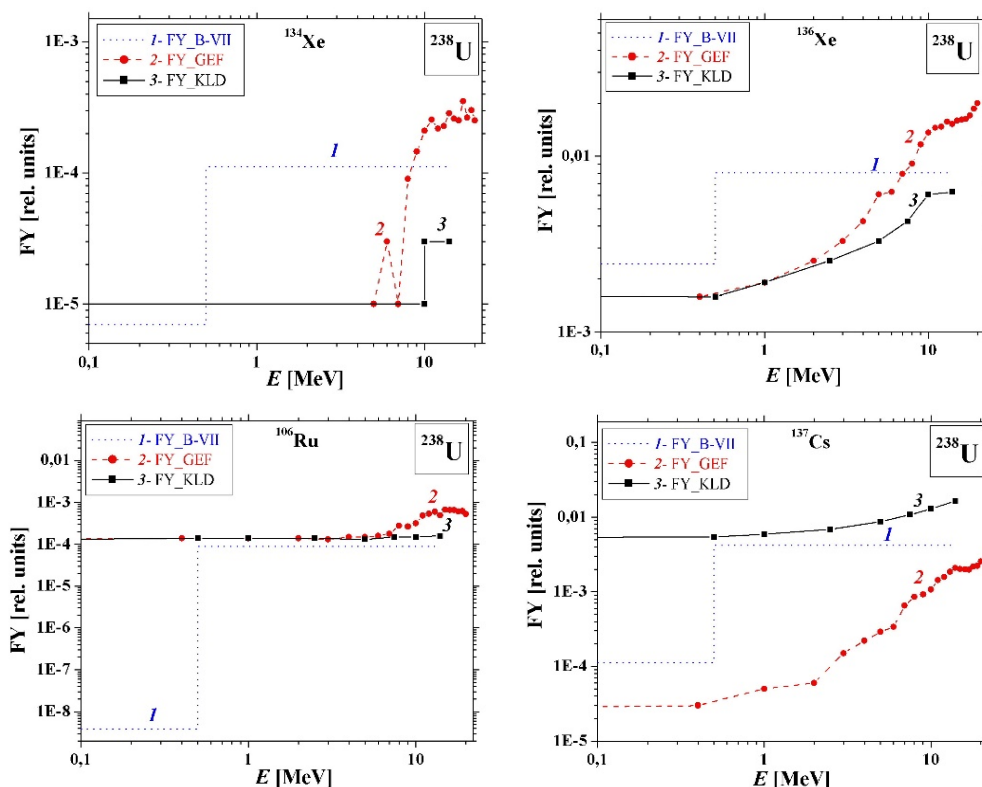
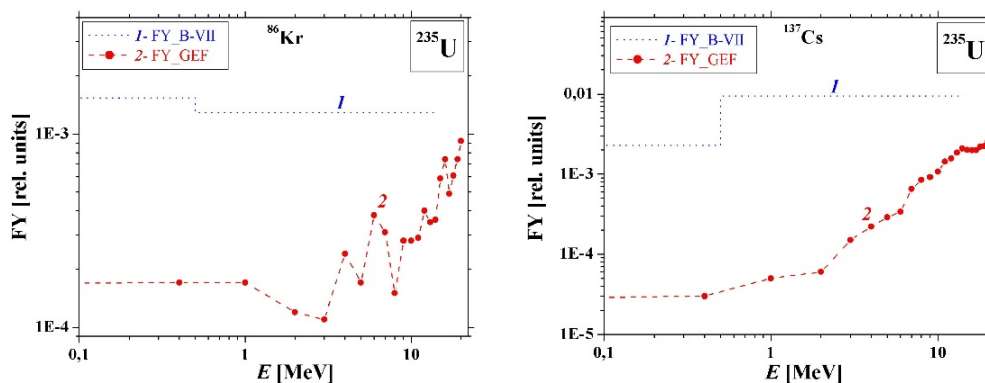


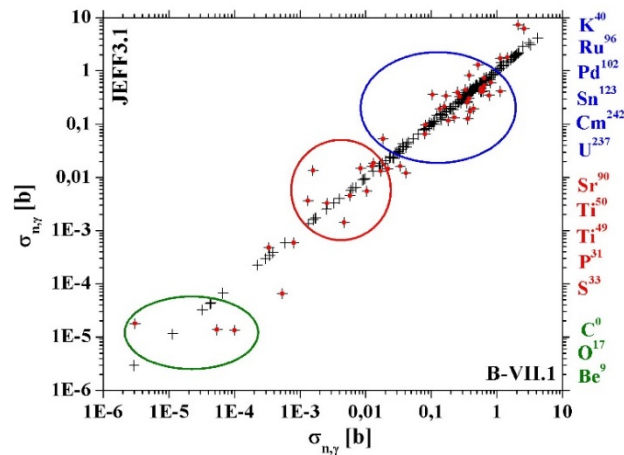
Figure 6: Independent fission yield of isotopes Ru, Xe, Cs in ^{238}U Figure 7: Independent fission yield of isotopes Kr, Cs in ^{235}U 

One-group constants in depletion calculations

The noticeable differences of one-group constants are observed when using different transport nuclear data libraries in depletion calculations (Figure 8). At the same time the discrepancies of one-group constants when using different FY libraries is very small because of negligible spectrum changes. When using libraries FY_JEFF, FY_KLD and FY_GEF (and the same transport library) the one-group fission cross-sections (n,f) and radiation capture cross-sections (n,γ) differ by 2 and 10%, respectively.

Figure 8: One-group cross-sections $\sigma_{n,\gamma}$ of fission products in MOX fuel under ENDF/B-VII.0 and JEFF-3.3 transport libraries

A diagonal corresponds to the identical data



Radionuclide accumulation in irradiated MOX fuel of sodium fast reactor

Kr and Xe accumulation in MOX fuel

For development of improved thermo-mechanical codes more accurate accumulation data of volatile fission products, noble gases, hydrogen and helium are needed. The simulation of microstructure evolution (porosity changes, transport of fission products, yield of noble gases, etc.) require the reliable data of nuclide accumulations under different conditions of irradiation, providing high burn-up. Comparative Kr and Xe accumulations are shown in Tables 2 and 3. The differences of 25 and 16% in Kr and Xe demonstrate the considerable dependence on the fission yield library used.

The gas accumulations from calculations with different FY libraries are compared with the results when using the library FY_B-VII. The most significant differences of fission gas accumulations are in ^1H and Kr, ~12 and ~25% using FY_JEF and FY_GEF, respectively. With increasing burn-up, the discrepancies are changing in ^1H and are practically unchanged in He, Kr and Xe.

Table 2: Kr and Xe accumulation in MOX fuel (5.0% h.a.)

Nuclide	Fission yield library				Maximum difference, %
	FY_B-VII	FY_GEF	FY_JEFF	FY_KLD	
$^{83}\text{Kr}/\text{Kr}$	0.182	0.137	0.176	0.154	~25
$^{84}\text{Kr}/\text{Kr}$	0.256	0.245	0.257	0.252	~5
$^{85}\text{Kr}/\text{Kr}$	0.080	0.070	0.074	0.075	~8
$^{86}\text{Kr}/\text{Kr}$	0.480	0.547	0.491	0.517	~13
$^{131}\text{Xe}/\text{Xe}$	0.156	0.146	0.155	0.170	~14
$^{132}\text{Xe}/\text{Xe}$	0.225	0.210	0.219	0.226	~7
$^{134}\text{Xe}/\text{Xe}$	0.314	0.315	0.311	0.284	~10
$^{136}\text{Xe}/\text{Xe}$	0.294	0.321	0.306	0.309	~8
Kr, g/cm ³ * 10 ⁻³	3.185	2.409	3.152	2.870	~25
Xe, g/cm ³ *10 ⁻²	6.025	6.242	6.107	5.233	~16

Table 3: Ratios of fission gas accumulation in irradiated MOX fuel

Burn-up = 5.0% h.a.			
Nuclide	FY_GEF/FY_B-VII	FY_JEFF/FY_B-VII	FY_KLD/FY_B-VII
¹ H	0.97	0.88	0.90
⁴ He	1.00	1.23	1.00
Kr	0.76	0.99	0.90
Xe	1.04	1.01	0.87
Burn-up = 10.3% h.a.			
¹ H	1.02	0.99	1.04
⁴ He	1.01	1.22	1.00
Burn-up = 20.8% h.a.			
¹ H	1.0	1.16	0.99
⁴ He	1.0	1.21	1.0

Stable and long-life nuclide accumulation in MOX fuel

Very different nuclide accumulation ratios relative to the library FY_B-VII (both greater and less unity) are shown in Table 4. For library FY_GEF the differences are more than 15% in ⁹⁰Sr, ¹²⁷I, ¹⁵⁴Eu, ~50-60% in ⁷⁹Se, ¹⁶¹Dy, ¹¹²Cd. The discrepancies of accumulations overdraw five times for some isotopes of Br, Cd, Sb (Table 5). As a whole while using the library FY_JEFF the differences are less than for library FY_GEF, with the peak difference being more than three times for isotopes of Cd and Sb.

Table 4: Ratios of stable and long-life nuclide accumulation in MOX fuel (5.0% h.a.)

Nuclide	Half-life (year)	FY_GEF/FY_B-VII	FY_JEFF/FY_B-VII	FY_KLD/FY_B-VII
⁷⁹ Se	~10 ⁵	0.60	0.80	0.70
⁸² Se	–	0.50	0.98	0.68
⁸⁵ Rb	–	0.65	0.94	0.87
⁸⁷ Rb	~10 ¹⁰	0.88	0.98	1.05
⁹⁰ Sr	~30	1.15	0.98	1.21
⁹⁹ Tc	~10 ⁵	1.02	1.02	1.09
¹⁰⁴ Ru	–	1.02	1.04	0.83
¹⁰⁶ Ru	~1	0.93	0.99	0.81
¹¹² Cd	–	0.53	0.42	0.72
¹²⁸ Te	~10 ²⁴	1.07	0.88	1.45
¹³⁰ Te	~10 ²⁴	0.94	1.06	1.09
¹²⁷ I	–	0.85	0.74	1.35
¹³³ Cs	–	0.93	1.05	0.81
¹³⁴ Cs	~2	0.91	1.04	0.79
¹³⁵ Cs	~10 ⁶	1.01	1.01	0.80
¹³⁷ Cs	~30	1.09	1.03	1.01

Table 4: Ratios of stable and long-life nuclide accumulation in MOX fuel (5.0% h.a.) (cont.)

Nuclide	Half-life (year)	FY_GEF/FY_B-VII	FY_JEFF/FY_B-VII	FY_KLD/FY_B-VII
¹³⁹ La	–	0.92	1.05	1.12
¹⁵⁴ Eu	~10	0.82	0.96	0.82
¹⁵⁵ Eu	~5	0.73	0.90	0.69
¹⁶¹ Dy	–	1.56	0.77	0.72
Discrepancies >100%				
⁸¹ Br	–	0.41	0.89	0.61
¹¹³ Cd	~10 ¹⁶	0.34	0.48	0.52
¹¹⁴ Cd	~10 ¹⁸	0.27	0.37	0.39
¹¹⁶ Cd	~10 ¹⁹	0.22	0.43	0.27
¹²¹ Sb	–	0.16	0.44	0.26
¹²³ Sb	–	0.18	0.32	0.40
¹²⁵ Sb	~3	0.41	0.43	0.80

Short-life nuclide accumulation in MOX fuel

The ratios of short-life nuclide accumulation with $1 \text{ min} < T_{1/2} < 1 \text{ h}$ are shown in Table 5. The accumulation of some nuclides differ by more than 3 000 times.

Table 5: Ratios of short-life nuclide accumulation in MOX fuel (5.0% h.a.)

Nuclide	Half-life (min)	FY_GEF/FY_B-VII	FY_JEFF/FY_B-VII	FY_KLD/FY_B-VII
⁸¹ Se	~20	0.42	0.88	0.61
^{81m} Se	~1	0.20	0.62	0.45
⁸⁰ Br	~20	0.03	0.41	0.06
^{84m} Br	~6	0.07	0.54	0.62
^{102m} Te	~5	0.06	0.35	0.55
¹⁰⁶ Ag	~24	0.0003	0.0003	0.0002
¹¹⁵ Ag	~20	0.14	0.22	0.28
¹¹⁸ Cd	~50	0.18	0.42	0.23
¹¹⁹ Cd	~3	0.07	0.16	0.25
^{112m} In	~21	0.04	0.05	0.06
^{123m} Sn	~40	0.18	0.33	0.42
^{129m} Sn	~7	2.4	1.5	1.5
^{135m} Cs	~53	0.23	0.44	0.42
¹⁶² Gd	~8	2.8	0.72	0.23
¹⁶³ Tb	~20	4.0	0.75	0.92
¹⁶⁴ Tb	~3	4.2	0.68	0.94
¹⁶⁷ Dy	~6	3.61	0.49	1.06
¹⁶⁸ Dy	~9	6.06	0.66	1.66

Nuclides as indicators

The isotopes of ^{137}Cs and ^{106}Ru can be used for estimation of fuel burn-up. In many studies, including the nuclear material assay, the burn-up is determined on the basis of ^{145}Nd distribution or the sum of stable neodymium isotopes (^{142}Nd , ^{143}Nd , ^{144}Nd , ^{145}Nd , ^{146}Nd , ^{148}Nd and ^{150}Nd). For aged spent fuel ^{154}Eu can be used for burn-up estimation.

The discrepancies of neodymium isotope ratios for various FY libraries are shown in Figure 9. The per cent difference of calculated fission products is determined by:

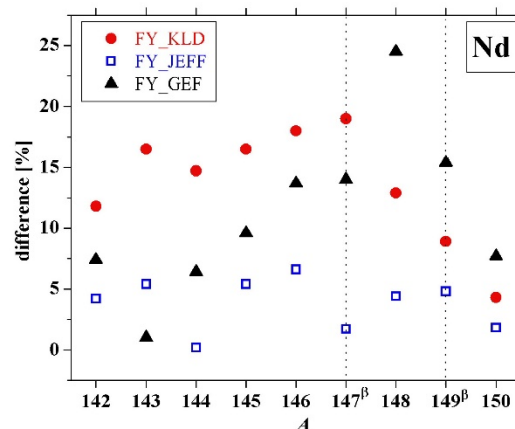
$$\text{Difference} = \frac{|FY_LIB - FY_BVII|}{FY_BVII} * 100\%$$

where FY_LIB is the analysed library.

At the same time the total neodymium concentrations are differed by 5, 16 and 9% for libraries FY_JEFF, FY_KLD and FY_GEF, respectively.

It should be also noted that in fast reactors the concentrations of fission products have significant sensitivity to the FY libraries, generated from the single data source for different fuels. Only while replacing the FY library generated from ENDF/B-VII for UO_2 fuel by the library for MOX fuel are there significant differences of accumulation for some individual nuclides. The ^1H concentrations are increased by 8%, and for the individual isotopes of Br, Se, Rb, Gd, Eu and some others the concentrations are changed more than two times.

Figure 9: Discrepancies of calculated neodymium ratios in MOX fuel (10.3% h.a.)



Conclusion

The considerable spread in concentrations of fission products is observed in depletion calculations while using codes MONTEBURNS-MCNP5-ORIGEN2 with fission yield libraries, generated on the base of ENDF/B-VII, JEFF-3.1, GEFY 3.3 and original library FY_Koldobsky. In depletion calculations of MOX-fuelled sodium fast reactors the spread in concentrations of inert gases being ~25%, up to 5 times for stable and long-life nuclides, up to 4 000 times for short-life nuclides with half-life more than 5 minutes, and up to 10 orders of magnitude for nuclides with half-life less than 10 seconds.

The lack of full-core benchmarks and difficulties in obtaining the experimental data complicate estimation of the final nuclide accumulations, taking into account the considerable discrepancies while using different nuclear data libraries.

For accurate depletion calculations it is reasonable to define something as benchmark technology by including the specifications of compulsory steps for these calculations. Then, taking into account the expected accuracy of the task being solved, the analysis results of calculations using the benchmark technology allow specifying final values. Perhaps for key fission products the final accumulations of nuclides, e.g. in the form of a range, would be more preferable for accurate simulation of fuel behaviour than single values.

References

- Blokhin, A.I., E.F. Mitenkova and A.B. Koldobsky (2011), “Fission Yield Library Effect on Effective Multiplication Factor at Deep Fuel Burn-up”, *J. Nuc. Physics and Engineering*, 2, pp. 72-79.
- Mitenkova, E.F. and N.V. Novikov (2011), “Fission Yield Library Effect on Accurate Calculations of Irradiated Fuel Composition in Sodium Fast Reactor”, *J. Atomic Energy*, 111, pp. 99-108.

Comparative sensitivity study of some criticality safety benchmark experiments using JEFF-3.1.2, JEFF-3.2T and ENDF/B-VII.1

Timothée Kooyman,^b Nadia Messaoudi^a

^aSCK•CEN, Mol, Belgium

^bUniversité Paris Sud, Orsay, France

Abstract

A sensitivity study on a set of evaluated criticality benchmarks with two versions of the JEFF nuclear data library, namely JEFF-3.1.2 and JEFF-3.2T, and ENDF/B-VII.1 was performed using MCNP(X) 2.6.0. As these benchmarks serve to estimate the upper safety limit for criticality risk analysis at SCK•CEN the sensitivity of their results to nuclear data is an important parameter to assess. Several nuclides were identified as being responsible for an evident change in the effective multiplication factor k_{eff} : ^{235}U , ^{239}Pu , ^{240}Pu , ^{54}Fe , ^{56}Fe , ^{57}Fe and ^{208}Pb . A high sensitivity was found to the fission cross-section of all the fissile material in the study. Additionally, a smaller sensitivity to inelastic and capture cross-section of ^{235}U and ^{240}Pu was also found. Sensitivity to the scattering law for non-fissile material was postulated. The biggest change in the k_{eff} due to non-fissile material was due to ^{208}Pb evaluation (± 700 pcm), followed by ^{56}Fe (± 360 pcm) for both versions of the JEFF library. Changes due to ^{235}U (± 300 pcm) and Pu isotopes (± 120 pcm for ^{239}Pu and ± 80 pcm for ^{240}Pu) were found only with JEFF-3.1.2. ^{238}U was found to have no effect on the k_{eff} . Significant improvements were identified between the two versions of the JEFF library. No further differences were found between the JEFF-3.2T and the ENDF/B-VII.1 calculations involving ^{235}U or Pu.

Introduction

SCK•CEN is performing criticality safety studies for its internal and external partners. To perform the technical assessments requested for the different studies, SCK•CEN is using validated computational tools and nuclear data libraries such as MCNP(X) calculations and JEFF and ENDF data libraries. In this work, several criticality experiments benchmarks which were deemed representative of the work carried out at SCK•CEN in terms of neutron spectra and material used were selected and the related calculations were run using various nuclear data libraries. The results were then analysed to assess the sensitivity of their results to nuclear data, which is an important parameter to establish as these benchmarks are used to estimate the upper safety limit for criticality risk analysis.

Methodology used for the benchmark calculations

Experiments were selected in OECD/NEA (2010) so as to cover a broad range of experimental configurations with highly-enriched uranium (HEU) and plutonium as fissile materials, both in oxide and metallic form. Reflectors included steel, water, lead and organics compounds. A comprehensive list of the selected experiments is given in

Appendix 1. A strong emphasis was put on the fast neutron spectrum. The input file for each selected experiment was taken from OECD/NEA (2010) and modified to make use of the nuclear data libraries used for this work, namely: JEFF-3.1.2 (Santamarina, *et al.*, 2009), JEFF-3.2T (Stankovsky, n.d.) and ENDF/B-VII.1 (Chadwick, M.B., *et al.*, 2011). Each calculation was run with 350 cycles of 10 000 particles, 50 of which were skipped before beginning tally accumulation. For the reaction rates tallies, 550 cycles of 300 000 particles were done, 50 of which being skipped.

The effective multiplication factor for each of the experiments was computed using MCNP(X) 2.6.0 (Pelowitz, *et al.*, 2008) and each of the aforementioned nuclear data libraries. The k_{eff} was then compared to the benchmark value provided in OECD/NEA (2010). If the calculated values were too different from the benchmark value, typically more than 500 pcm, the experiment was not used for the sensitivity analysis. If not, the calculation was run again after replacing the cross-section data of a given element from the ENDF file by the one from another library and leaving all the other cross-sections unchanged. This allowed us to know the total effect of the difference in the evaluation of the cross-section of this element between the libraries. This was done for the main elements present in the experimental set-up, mainly the fissile isotopes and the reflector/moderator material.

Once the elements responsible for the difference in the calculated values were identified, the calculations were run again after replacing the cross-section data of a single isotope from the previously identified elements from the ENDF file by the one from another library. This allowed us to ascertain the precise effect due to the evaluation of a given isotope. For the evaluated nuclei triggering a change greater than 80 pcm, the calculations were run again while tallying reaction rates for fission, capture, elastic and inelastic scattering. Using the neutron flux, the different microscopic cross-sections were then computed and compared. Physical hypotheses on the reason why the calculated values were different were then made according to the differences observed between the cross-sections. Finally, these hypotheses were tried using the perturbation tool provided in MCNP-2.6.0. These comparisons were made between all of the three nuclear data libraries used.

Results

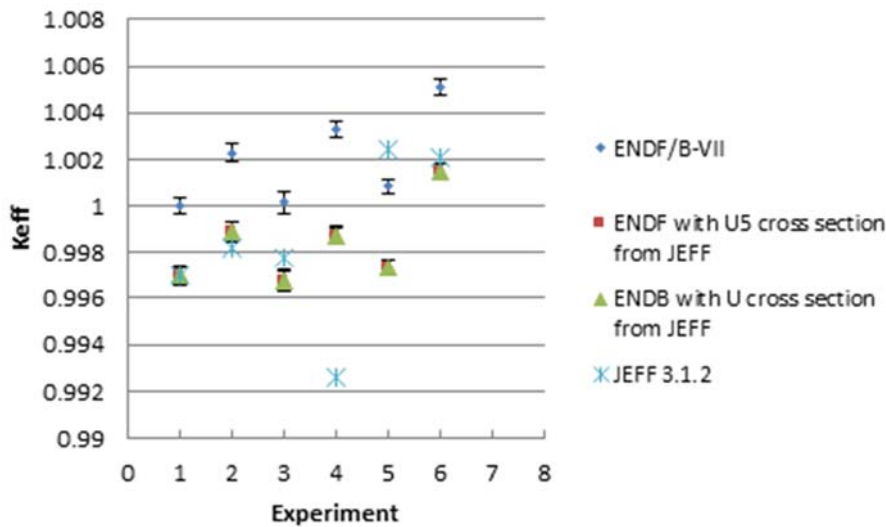
Uranium-235

At thermal energies, there were no differences between the results from the various calculations. For fast neutrons, ^{235}U was responsible for an increase of 350 pcm on average to the calculated value obtained using JEFF-3.1.2 compared to the value obtained using ENDF/B-VII.1, as is shown in Figure 1. This is not true for Experiments 4 and 5 because of the presence of additional material such as lead or iron which also have an effect on the k_{eff} . No significant differences were found between the results of ENDF and JEFF-3.2T, which is consistent with the re-evaluation of the ^{235}U fission cross-section in JEFF-3.2T compared to the previous version. On average, the JEFF-3.2T value was 250 pcm higher than the JEFF-3.1.2 value. This is consistent with the fact that the ^{235}U evaluation has been changed in the new JEFF-3.2T version.

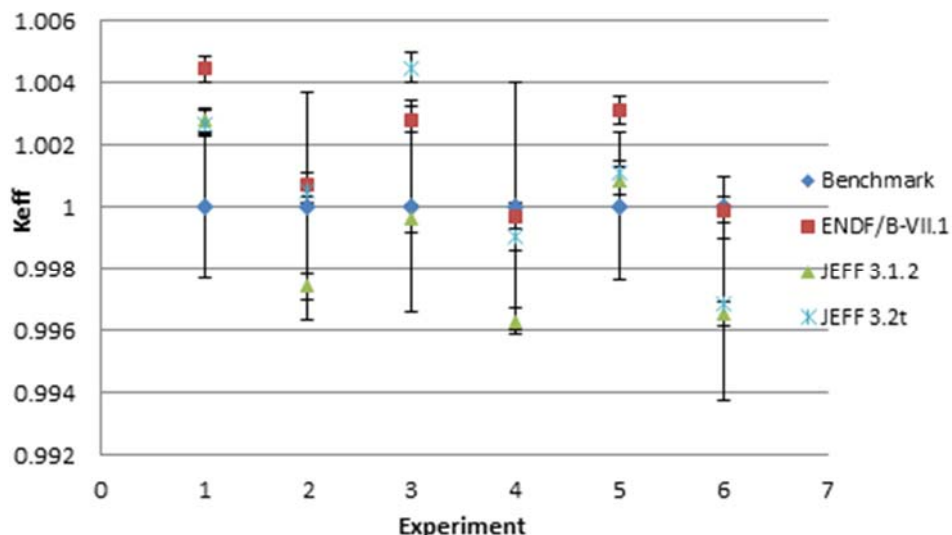
Using the tallied cross-sections, it was possible to discern that there was a high dependency to the fission cross-section of ^{235}U and to its inelastic scattering cross-section, both in the fission neutron energy range. Between 1 and 11 MeV, a 2% increase of the JEFF-3.1.2 fission cross-section led to a change of +674 pcm in the k_{eff} , while a decrease of 5% in the inelastic scattering cross-section led to a decrease of 330 pcm in the k_{eff} .

Plutonium-239 & -241

Only experiments with plutonium and fast neutrons were used. ^{239}Pu and ^{240}Pu were found to trigger changes in the calculated values. ^{239}Pu led to an increase of 120 pcm on average for the ENDF value with regard to the JEFF-3.1.2 value. ^{240}Pu was similarly

Figure 1: Difference in k_{eff} between ENDF with ^{235}U vs. from JEFF-3.1.2 and ENDF only

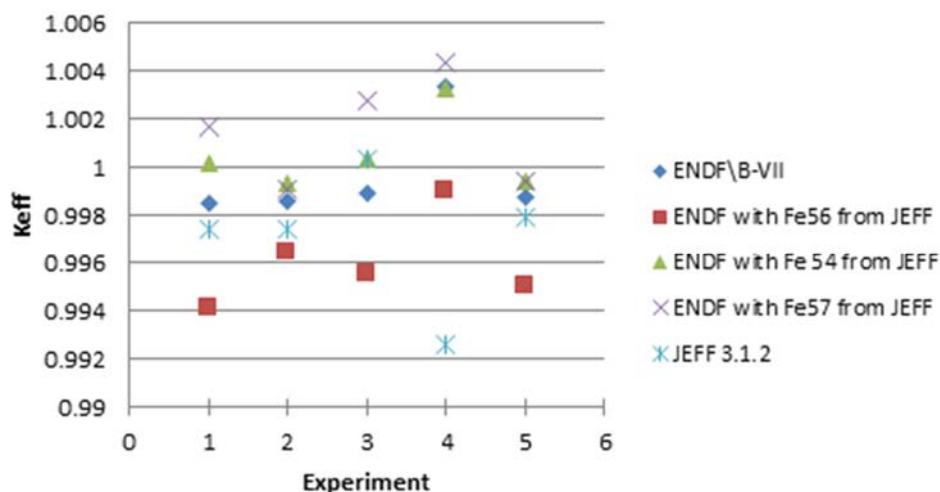
responsible for a decrease of 80 pcm on average. However, for JEFF-3.2T, no clear pattern could have been found between the results obtained with this library and the two others. This is consistent with the fact that the data for plutonium have been re-evaluated in the new version of the JEFF library. The specific reaction cross-section responsible for the change seems to be the fission cross-section for ^{239}Pu , a change of 1% in this cross-section at fission neutron energies being responsible for a change of 116 pcm in the k_{eff} . For ^{240}Pu , the fission cross-section between 100 keV and 1 MeV is one and a half smaller in JEFF-3.1.2 than in ENDF, leading to an approximate change of -174 pcm in the effective multiplication factor. Additionally, capture cross-section evaluations seem to have a smaller effect for these two nuclei but this cannot be confirmed as the MCNP perturbation tool is not reliable for changes of more than 20-30% in the cross-section.

Figure 2: K_{eff} for different nuclear data libraries and plutonium experiments with fast spectrum

Fe-54, -56, -57

Only experiments with iron and fast neutron spectrum were used. The three most common isotopes from iron, namely ^{54}Fe , ^{56}Fe and ^{57}Fe were found to cause differences between the calculated values. Overall, the sum of these differences tends not to be significant. ^{54}Fe caused a decrease of 80 pcm of either the JEFF-3.1.2 or JEFF-3.2T value compared to ENDF/B-VII.1. ^{56}Fe similarly caused an increase of 360 pcm and ^{57}Fe a decrease of 180 pcm on average, as shown in Figure 3. The similarity in results between the two versions of the JEFF library is consistent with the fact that the iron data have not been re-evaluated in JEFF-3.2T.

Using the tallied cross-section and MCNP perturbation tool, no explanation could have been found for the reason of the change. However, for iron, only the capture and scattering interactions matters, and the MCNP tool only modifies the scattering cross-section but not the scattering law. Hence, the most probable hypothesis is that there is a strong sensitivity to the scattering law, either inelastic or elastic. However, it is not possible to clearly determine which one is responsible for the change.

Figure 3: K_{eff} to sensitivity to iron isotopes**Lead-208**

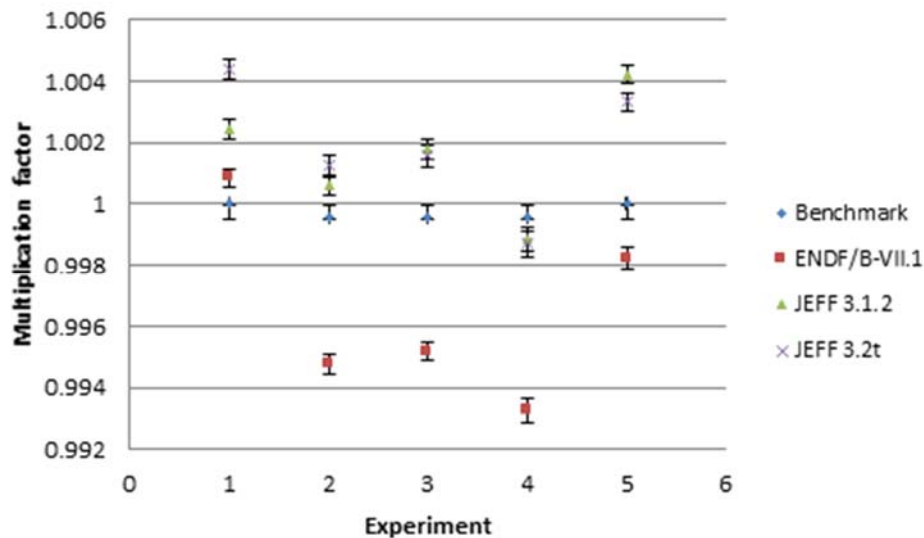
Only experiments with lead and fast neutron spectrum were used. Only the ^{208}Pb isotope of lead was found to cause important differences between the calculated values, as is shown in Table 1. Yet, it accounted for changes up to 1 000 pcm between the

Table 1: Comparative effect of each lead isotope on the k_{eff}

All changes in pcm	HMF-27	PMF-35	HMF-64.1	HMF-64.2	HMF-64.3
Difference JEFF-ENDF	158	600	584	659	557
Change due to ^{204}Pb	0	0	0	0	13
Change due to ^{206}Pb	27	33	57	79	64
Change due to ^{207}Pb	70	39	64	67	32
Change due to ^{208}Pb	417	713	998	996	980
Overall change due to Pb	418	723	1 001	978	1 017

ENDF/B-VII.1 calculations and the JEFF-3.1.2 calculations with an average of 700 pcm, as is shown in Figure 4. This difference is slightly smaller for JEFF-3.2T, with an average of 520 pcm. Although the various nuclear data library cross-section evaluations presented some differences, no explanation could have been found using the perturbation tool from MNCP(X), as was the case for iron. The same explanation than before is then postulated. This is consistent with results obtained by Iwamoto (2013), which showed a high sensitivity to the scattering angle cosine mean value of ^{208}Pb for the VENUS-F core.

Figure 4: K_{eff} for different nuclear data libraries and lead experiments with fast spectrum



Summary and conclusion

A sensitivity analysis was carried out on several criticality safety benchmark experiments using MCNP(X)-2.6.0 and three nuclear data libraries: ENDF/B-VII.1, JEFF-3.1.2 and JEFF3.2T. Several sensitivities were found, mostly to the fission cross-sections for fissile material, namely ^{235}U , ^{239}Pu and ^{240}Pu . Additional effects were seen due to capture cross-sections of these nuclides. For non-fissile nuclides, important differences between the various calculations were found to be caused by the different data of lead and iron, with lead being responsible for the biggest change between two calculations, around 700 pcm between the ENDF results and the JEFF-3.1.2 result on the average. No explanation could have been found for this difference, but it is postulated that there is an important sensitivity to the mean value of the scattering angle cosine of neutrons on lead and iron. Additional research on this topic may be interesting to see if this hypothesis can be confirmed.

Acknowledgements

Thanks to Nadia Messaoudi for being my internship mentor at SCK•CEN and to Gert Van den Eynde for replacing her by the end of my internship.

References

- Chadwick, M.B., *et al.* (2011), “ENDF/B-VII.1 Nuclear Data for Science and Technology: Cross Sections, Covariances, Fission Product Yields and Decay Data”, *Nuclear Data Sheets*, 2887-2996.
- Iwamoto, H. (2013) *Uncertainty and Sensitivity Study of the Venus-F Core*, Internal Report, SCK•CEN, Mol, Belgium.
- OECD/NEA (Organisation for Economic Co-operation and Development/Nuclear Energy Agency) (2010), *International Handbook of Evaluated Criticality Safety Experiments*, OECD/NEA, Paris.
- Pelowitz, *et al.* (2008), *MCNP(X) 2.6.0 User's Manual*, Los Alamos National Laboratory (LANL), Los Alamos, NM, United States.
- Santamarina, A., *et al.* (2009), *The JEFF-3.1.1 Nuclear Data Library*, OECD/NEA, Paris.
- Stankovsky, Alexey (n.d.), personal communication.

Annex 1: Experiments used for each case and multiplication factor value

Table A.1: Experiments used for calculations on uranium and fast neutrons

Nº	Exp	k_{exp}	Δk_{exp}	k_{jeff}	Δk_{jeff}	k_{endf}	Δk_{endf}	Description
1	HEU-MET-FAST-001	1.00000	0.00100	0.99697	0.00041	1.00000	0.00035	Bare sphere
2	HEU-MET-FAST-004	1.00200	0.00000	0.99816	0.00043	1.00229	0.0004	Water reflected sphere
3	HEU-MET-FAST-011	0.99890	0.00150	0.99774	0.00043	1.00014	0.00046	Polyethylene reflected sphere
4	HEU-MET-FAST-013	0.999	0.0015	0.99256	0.00036	1.00332	0.00035	Steel reflected sphere
5	HEU-MET-FAST-027	1.00000	0.00250	1.00243	0.00031	1.00085	0.00032	Lead reflected sphere
6	HEU-MET-FAST-061	0.9998	0.0025	1.00204	0.00039	1.0051	0.00035	Cylindrical assembly with graphite

Table A.2: Experiments used for calculations on lead and fast neutrons

Nº	Exp	k_{exp}	Δk_{exp}	k_{jeff}	Δk_{jeff}	k_{endf}	Δk_{endf}	Description
1	HEU-MET-FAST-027	1.00000	0.00250	1.00243	0.00031	1.00085	0.00032	Lead reflected sphere
2	HEU-MET-FAST-064,1	0.99960	0.00080	1.00061	0.00033	0.99477	0.00032	Lead reflected cylinder
3	HEU-MET-FAST-064,2	0.99960	0.00100	1.00177	0.00032	0.99518	0.00032	Lead reflected cylinder
4	HEU-MET-FAST-064,3	0.99960	0.00090	0.99883	0.00039	0.99326	0.00039	Lead reflected cylinder
5	PU-MET-FAST-035	1.00000	0.00160	1.00423	0.00031	0.99823	0.00034	Lead reflected sphere

Table A.3: Experiments used for calculations on plutonium and fast neutrons

N°	Exp	k_{exp}	Δk_{exp}	k_{jeff}	Δk_{jeff}	k_{endf}	Δk_{endf}	Description
1	PU-MET-FAST-031	1.00000	0.0023	1.00279	0.00040	1.00444	0.00042	Polyethylene reflected sphere
2	PU-MET-FAST-037 Case 5	1.00000	0.00370	0.99739	0.00039	1.00074	0.00039	Flooded array of cylinders
3	PU-MET-FAST-037 Case 10	1.00000	0.00340	0.99964	0.00045	1.00281	0.00043	Flooded array of cylinders
4	PU-MET-FAST-037 Case 12	1.00000	0.00400	0.99627	0.00043	0.99970	0.00043	Flooded array of cylinders
5	Pu-MET-FAST-027	1.00000	0.0024	1.00086	0.00046	1.0031	0.00046	Polyethylene reflected sphere
6	PU-MET-FAST-011	1.00000	0.00100	0.99652	0.00040	0.99990	0.00043	Water reflected sphere

Table A.4: Experiments used for calculations on iron and fast neutrons

N°	Exp	k_{exp}	Δk_{exp}	k_{jeff}	Δk_{jeff}	k_{endf}	Δk_{endf}	Description
1	PU-MET-FAST-026	1.00000	0.00260	0.99742	0.00036	0.99853	0.00036	Steel reflected sphere
2	PU-MET-FAST-025	1.00000	0.0022	0.99746	0.00035	0.99861	0.00038	Steel reflected sphere
3	PU-MET-FAST-028	1.00000	0.00240	1.00033	0.00035	0.99896	0.00038	Steel reflected sphere
4	HEU-MET-FAST-013	0.999	0.0015	0.99256	0.00036	1.00332	0.00035	Steel reflected sphere
5	PU-MET-FAST-032	1.00000	0.0022	0.99791	0.00037	0.99878	0.00035	Steel reflected sphere

Table A.5: Experiments used for calculations on thermal neutrons and uranium

N°	Exp	k_{exp}	Δk_{exp}	k_{jeff}	Δk_{jeff}	k_{endf}	Δk_{endf}	Description
1	HEU-MET-THERM-032.1	0.9976	0.00100	1.00342	0.00031	1.00257	0.00032	Polyethylene reflected array
2	HEU-MET-THERM-032.2	1.0055	0.00100	1.00297	0.00030	1.00215	0.00030	Polyethylene reflected array
3	HEU-MET-THERM-018	1.00380	0.00410	0.99923	0.00025	0.99938	0.00024	Polyethylene reflected with concrete
4	HEU-MET-THERM-031	1.0037	0.00240	1.00915	0.00034	1.00836	0.00033	Polyethylene reflected array

Appendix 1: Final Programme

*Workshop on Nuclear Measurements, Evaluations and Applications (NEMEA-7)
Collaborative International Evaluated Library Organisation (CIELO)
5-8 November 2013 • Geel, Belgium*

Tuesday, 5 November

Session 1 Introduction

A.J.M. Plompen

Opening

M.B. Chadwick

CIELO goals and timeline

Session 2 ^1H and ^{16}O

Chair: T. Fukahori

G.M. Hale

Status and plans for ^1H and ^{16}O evaluations by R-matrix analyses of the NN and ^{17}O systems/Why the uncertainties from least-squares R-matrix analyses are so small

A.J.M. Plompen

The status of data for ^{16}O and the programme of work for CIELO

S. Kopecky

Low-energy scattering and cross-section data

S. Kunieda

Estimation of neutron cross-sections for ^{16}O up to 5.2 MeV through R-matrix analysis

V. Khryachkov

Status and future plans of $^{16}\text{O}(n,\alpha)^{13}\text{C}$ reaction cross-section investigation at IPPE

C.R. Lubitz

Neutron cross-sections for ^{16}O

P.K. Romano

Critical benchmark results for a modified ^{16}O evaluation

Session 3 ^{56}Fe

Chair: R. Jacqmin

L. Leal, T. Ivanova

Overview of the resonance evaluations for ^{16}O , ^{56}Fe

M. Herman, D. Brown

Fe-isotopes evaluation within the CIELO project

O. Iwamoto

Review of nuclear data of ^{56}Fe in JENDL-4.0

J.R. Vanhoy

Differential cross-section measurements at the University of Kentucky –
Adventures in analysis

Y. Danon

CIELO (Fe) related nuclear data measurements at the Gaertner LINAC Center
at RPI

Monitor: A.J.M. Plompen – Wrap-up discussion on ^1H , ^{16}O , ^{56}Fe

Wednesday, 6 November

Session 4 The Big Three – ^{235}U , ^{238}U , ^{239}Pu – Part 1

Chair: M.B. Chadwick

Y. Danon

CIELO (U) related nuclear data measurements at the Gaertner LINAC Center
at RPI

P. Romain

BRC neutron evaluations of actinides with the TALYS code

R. Capote

Evaluation of neutron-induced reactions on ^{238}U nucleus

T. Kawano

Status of ^{239}Pu evaluations

O. Iwamoto

Review of nuclear data of major actinides JENDL-4.0

P. Schillebeeckx

Status of evaluated data for neutron induced reactions on ^{238}U in the
resonance region

**Monitor: M.B. Chadwick – Wrap-up discussion on evaluations for the
big three**

Session 4 The Big Three – ^{235}U , ^{238}U , ^{239}Pu – Part 2

Chair: M. Herman

L. Leal, G. Noguère

Overview of the resonance evaluations for ^{235}U , including α ratio in the fast
energy range

G. Noguère, L. Leal

Overview of the resonance evaluations for ^{239}Pu

A. Bacquias

^{235}U and ^{238}U (n,xn gamma) cross-sections

T.J. Wright

High-precision measurement of the $^{238}\text{U}(n,\gamma)$ cross-section with the total
absorption calorimeter (TAC) at n_TOF, CERN

A. Wallner

Neutron-induced reactions on U and Th – A new approach via AMS

I.J. Thompson

Coupled-channels effects in optical potentials for deformed nuclei, and in semi-direct mechanisms for neutron capture

C. De Saint Jean

Covariances on ^{239}Pu , ^{238}U and ^{235}U neutron cross-sections with CONRAD code: From physical to integral experiment constraints

Monitor: T. Kawano – Wrap-up discussion on experiments and evaluations for the big three

Thursday, 7 November

Session 4 The Big Three – ^{235}U , ^{238}U , ^{239}Pu – Part 3

Chair: E. Bauge

R. Capote

Evaluation of prompt fission neutron spectra for major actinides

O. Litaize

Investigation of prompt fission neutron and gamma spectra with their covariance matrices – Application to $^{239}\text{Pu}+n_{\text{th}}$, $^{238}\text{U}+n_{1.8\text{MeV}}$ and $^{235}\text{U}+n_{\text{th}}$

A. Oberstedt

Characteristics of prompt fission gamma-ray emission – Experimental results and predictions

A. Sardet

Characterisation of a paraterphenyl neutron detector and preliminary results on $^{238}\text{U}(n,f)$ prompt fission neutron energy spectra at 2, 5.2 and 15 MeV

N. Kornilov

Scintillation neutron detector with dynamic threshold

Monitor: R. Capote – Wrap-up discussion on the big three PFNS/PFGS

Session 5 General Interest – Part 1

Chair: M. Dunn

M. Herman

Consistent data assimilation

H. Leeb

What is the proper evaluation method: Some basic considerations

D. Brown

Data mining the EXFOR database

B. Becker

Evaluation of neutron-induced reaction cross-sections for ^{197}Au in the resonance region

Session 5 General Interest – Part 2

Chair: P. Schillebeeckx

S. Kopecky

Resonance parameters from neutron-induced total and capture cross-section measurements on ^{241}Am at GELINA

D. Cano-Ott

Measurement of the ^{241}Am capture cross-section at the n_TOF facility at GERN

C. Paradela

Fission cross-sections measured at n_TOF with PPAC

P. Salvador

Measurement of the neutron-induced fission cross-section of $^{240,242}\text{Pu}$

A. Stankovskiy

Sensitivity analysis of the nuclear data for MYRRHA reactor modelling

Friday, 8 November

Session 5 General Interest – Part 3

Chair: Z. Ge

L. Fiorito

Fission yield covariance generation and uncertainty propagation through fission pulse decay heat calculation

E. Mitenkova

Effect of fission yield libraries on the irradiated fuel composition in Monte Carlo depletion calculations

N. Messaoudi

Comparative sensitivity study of some criticality safety benchmark experiments using JEFF-3.1.2, JEFF-3.2T and ENDF/B-VII.1

Monitors: E. Dupont, A.J.M. Plompen – Round table discussion on CIELO and international collaboration

Perspectives from evaluation projects, international organisations and participants

Appendix 2: List of Participants

Australia

WALLNER, A. Australian National University

Austria

LEEB, H. TU Wien (Technische Universität Wien),
ATI (Institute of Atomic and Subatomic Physics)

Belgium

FIORITO, L. SCK•CEN (Belgian Nuclear Research Centre)
MESSAOUDI, N. SCK•CEN (Belgian Nuclear Research Centre)
STANKOVSKIY, A. SCK•CEN (Belgian Nuclear Research Centre),
Institute for Advanced Nuclear Systems

China

GE, Z. China Nuclear Data Centre

Czech Republic

CHUDOBA, P. NPI (National Physics Institute) Řež
MAJERLE, M. NPI (National Physics Institute) Řež
NOVAK, J. NPI (National Physics Institute) Řež
SIMECKOVA, E. NPI (National Physics Institute) Řež

France

BACQUIAS, A. CNRS (Centre Nationale de la Recherche Scientifique)/
IN2P3
BAUGE, E. CEA (Commissariat à l'Énergie Atomique) DIF, DPTA/SPN
CAPDEVIELLE, O. IPHC (Institut Pluridisciplinaire Hubert Curien)/DRS
DE SAINT JEAN, C. CEA (Commissariat à l'Énergie Atomique)
DESSAGNE, P. IPHC (Institut Pluridisciplinaire Hubert Curien)/DRS
HENNING, G. IPHC (Institut Pluridisciplinaire Hubert Curien)/DRS
IVANOV, E. IRSN (Institut de Radioprotection et de Sûreté Nucléaire)

IVANOVA, T.	IRSN (Institut de Radioprotection et de Sûreté Nucléaire)
JACQMIN, R.	CEA (Commissariat à l'Énergie Atomique)
KERVENO, M.	IPHC (Institut Pluridisciplinaire Hubert Curien)/DRS
NOGUERE, G.	CEA (Commissariat à l'Énergie Atomique)/DEN
ROMAIN, P.	CEA (Commissariat à l'Énergie Atomique)/DPTA/SPN
SARDET, A.	CEA (Commissariat à l'Énergie Atomique)/DAM

Japan

FUKAHORI, T.	JAEA (Japan Atomic Energy Agency)
IWAMOTO, O.	JAEA (Japan Atomic Energy Agency)
KUNIEDA, S.	JAEA (Japan Atomic Energy Agency)

Russian Federation

KHRYACHKOV, V.	IPPE (Institute for Physics and Power Engineering)
MITENKOVA, E.	Nuclear Safety Institute of Russian Academy of Sciences

Slovenia

TRKOV, A.	IJS (Jožef Stefan Institute)
GASPER, Ž.	IJS (Jožef Stefan Institute)

Spain

CANO OTT, D.	CIEMAT (Centro de Investigaciones Energéticas, Medioambientales y Tecnológicas)
MENDOZA, E.	CIEMAT (Centro de Investigaciones Energéticas, Medioambientales y Tecnológicas)

Sweden

OBERSTEDT, A.	Fundamental Fysik
---------------	-------------------

United Kingdom

WRIGHT, T.	University of Manchester, School of Physics and Astronomy
------------	--

United States

BROWN, D.	BNL (Brookhaven National Laboratory)
CHADWICK, M.B.	LANL (Los Alamos National Laboratory)
DANON, Y.	Gaerttner LINAC Center

DUNN, M.	ORNL (Oak Ridge National Laboratory)
GUBER, K.H.	ORNL (Oak Ridge National Laboratory)
HALE, G.M.	LANL (Los Alamos National Laboratory)
HERMAN, M.W.	NNDC (National Nuclear Data Center)
KAWANO, T.	LANL (Los Alamos National Laboratory)
KORNILOV, N.	Ohio University
LEAL, L.C.	ORNL (Oak Ridge National Laboratory)
LUBITZ, C.R.	KAPL (Knolls Atomic Power Laboratory)
ROMANO, P.	KAPL (Knolls Atomic Power Laboratory)
THOMPSON, I.	LLNL (Lawrence Livermore National Laboratory)
VANHOY, J.	United States Naval Academy, Department of Physics

International Organisations

BECKER, B.	EC (European Commission)/JRC (Joint Research Centre)/IRMM (Inst. for Reference Materials and Measurements), Belgium
BEVILACQUA, R.	EC (European Commission)/JRC (Joint Research Centre)/IRMM (Inst. for Reference Materials and Measurements), Belgium
DUPONT, E.	OECD (Organisation for Economic Co-operation and Development)/NEA (Nuclear Energy Agency), France
GÖÖK, A.	EC (European Commission)/JRC (Joint Research Centre)/IRMM (Inst. for Reference Materials and Measurements), Belgium
KOPECKY, S.	EC (European Commission)/JRC (Joint Research Centre)/IRMM (Inst. for Reference Materials and Measurements), Belgium
LEICHTLE, D.	Fusion for Energy (Spain)
OBERSTEDT, S.	EC (European Commission)/JRC (Joint Research Centre)/IRMM (Inst. for Reference Materials and Measurements), Belgium
PARADELA, C.	EC (European Commission)/JRC (Joint Research Centre)/IRMM (Inst. for Reference Materials and Measurements), Belgium
PLOMPEN, A.	EC (European Commission)/JRC (Joint Research Centre)/IRMM (Inst. for Reference Materials and Measurements), Belgium
SALVADOR-CASTIÑEIRA, P.	EC (European Commission)/JRC (Joint Research Centre)/IRMM (Inst. for Reference Materials and Measurements), Belgium
SCHILLEBEECKX, P.	EC (European Commission)/JRC (Joint Research Centre)/IRMM (Inst. for Reference Materials and Measurements), Belgium

